



SPIDER VENOMS AND CHRONIC PAIN –

**Developing Novel Pharmacological Tools from
the Spider Venoms to Target P2X4 in Microglia**

Lučka Bibič

Faculty of Science

School of Pharmacy

Ph.D.

January 2020

Thesis submitted to the School of Pharmacy, University of East Anglia, in fulfilment of the requirement for the degree of Doctor of Philosophy.

"I wonder," said Frodo, "But I don't know. And that's the way of a real tale."

– J.R.R. Tolkien, The Lord of the Rings

Intellectual Property and Publication Statements

The candidate confirms that the work submitted is her own, except where work which has formed part of co-authored publications has been included. The contributions of the candidate to this work has been explicitly indicated below.

The Chapter 1 on “No Pain, All Gain” was adapted from various sources, including from our review article on the subjects, which was published in 2017: “P2X4 receptor function in the nervous system and current breakthroughs in pharmacology,” Stokes L., Layhadi J. A., Bibic L., Dhuna K., and Fountain S.J., *Frontiers of Pharmacology*. 2017, 8, 291. The contribution of LB (the candidate) were to co-write the corresponding section of the review and produced the related figures.

The work described in Chapter 3 on “Development of high-throughput fluorescent-based screens to accelerate discovery of P2X inhibitors from animal venoms” formed the basis for a research article published in 2019 as “Development of high-throughput fluorescent-based screens to accelerate discovery of P2X inhibitors from animal venoms,” Bibic L., Herzig V., King G. F., and Stokes L., *Journal of Natural Products*. 2019, 82.9., p.2559-2567. The contribution of LB (the candidate) were to conduct the experiments, analyse the data, prepare the figures, co-write the initial manuscript draft and edit the final drafts.

Chapters 4 and 5 are based on a manuscript with a running title of “Discovery of a novel spider toxin that selectively inhibits P2X4 receptor,” Bibic L., et al. and is currently in preparation.

Part of the study described in Chapter 6 found its home as a research paper titled ‘Bug Off Pain: educational virtual reality game on spider venoms and chronic pain for public engagement,’ Bibic L.*, Druskis J., Walpole S., Angulo J., and Stokes L., *Journal of Chemical Education*. 2019, 96, 7, 1486-1490. The contribution of LB (the candidate) were to direct the program of research, designed the game, produced the educational videos, prepared the figures, initiated, wrote, and edited the article.

The candidate (LB) owns, together with the University of East Anglia, a copyright protection of the virtual reality game Bug Off Pain©.

The copy of the thesis has been supplied on condition that anyone who consults it is understood to recognise that its copyright rests with the author and that use of any information derived there must be in accordance with current UK Copyright Law. In addition, any quotation or extract must include full attribution.

© 2020 University of East Anglia and Lucka Bibic

Publication Record List

Peer-reviewed publications (academic):

1. **Bibic, L.**, Stokes L., Revisiting the idea that amyloid- β peptide acts as an agonist for P2X7. *In review*.
2. Stokes L., Bidula S., **Bibic L.**, Allum E., "To inhibit or enhance? Is there a benefit to positive allosteric modulation of P2X receptors?" *In review*.
3. **Bibic, L.**, Herzig V., King G., Stokes L., 2019. Development of high-throughput fluorescent-based screens to accelerate discovery of P2X inhibitors from animal venoms. *J Nat Prod.* 82, 9, 2559-2567. DOI: 10.1021/acs.jnatprod.9b00410
4. **Bibic, L.***, Druskis J., Walpole S., Angulo J., and Stokes L., 2019. "Bug Off Pain: educational virtual reality game on spider venoms and chronic pain for public engagement." *J Chem Educ.* 96, 7, 1486-1490. DOI: 10.1021/acs.jchemed.8b00905 (*corresponding author)
5. Cook, A.B.* and **Bibic L.***, 2019. Macromolecules, actually: from Plastics to DNA." *Front Young Minds.* 7:126. DOI: 10.3389/frym.2019.00126 (*co-corresponding author)
6. Botta J., **Bibic L.**, Howell L.A., McCormick P.J., 2019. Staple peptides for the G-protein coupled dimers. *J Biol Chem.* Ahead of print. DOI: 10.1074/jbc.RA119.009160
7. Blasco-Benito et al. Therapeutic targeting of HER2-CB2 heteromers in HER-2 positive breast cancer. 2019. *Proc Natl Acad Sci.* 116.9: 3863-3872. DOI: 10.1073/pnas.1815034116
8. Dhuna, K., Felgate, M., Bidula, S.M., Walpole, S., **Bibic, L.**, Cromer, B.A., Angulo, J., Sanderson, J., Stebbing, M.J. and Stokes, L., 2019. Ginsenosides act as positive modulators of P2X4 receptors. *Mol. Pharmacol.* 95(2), pp.210-221. DOI: 10.1124/mol.118.113696
9. Moreno, E., Mireia M., Chiarlone A., Puigdemívol M., **Bibic L.**, Howell L.A., et al. Singular location and signaling profile of adenosine A_{2A}-Cannabinoid CB₁ receptor heteromers in the dorsal striatum. 2018. *Nat Neuropsychopharmacology.* 43.5, 964. DOI: 10.1038/npp.2017.12
10. Stokes L., Layhadi J. A., **Bibic L.**, Dhuna K., and Fountain S.J. 2017. P2X4 receptor function in the nervous system and current breakthroughs in pharmacology. *Front Pharmacol.* 8, 291. DOI: 10.3389/fphar.2017.00291
11. Busnelli M., Kleinau G., Muttenthaler M., Stoev S., Manning M., **Bibic L.**, Howell L. A., et al. 2016. Design and characterization of superpotent bivalent ligands targeting oxytocin receptor dimers via a channel-like structure. *J Med Chem.* 59.15, 7152-7166. DOI: 10.1021/acs.jmedchem.6b00564

Other academic publications:

12. **Bibic, L.*** 2018. Learning to lead. *Science*. 361: 6407. DOI: 10.1126/science.361.6407.1158 (Working Life article, *corresponding author)
13. **Bibic, L.** 2018. "Sustainable Electrochemical Functionalization of Alkenes". *J. Am. Chem. Soc.* 140: 48. DOI: 10.1021/jacs.8b12638 (Spotlight feature)
14. **Bibic, L.** 2019. Common Metals, Cheaper Catalysts in Fuel Cells". *J. Am. Chem. Soc.* 141: 4. DOI: 10.1021/jacs.9b00602 (Spotlight feature)
15. **Bibic, L.** 2019. Small but Mighty: Clickable Fluorescent Probe for Bioimaging. *J. Am. Chem. Soc.* 141: 7. DOI: 10.1021/jacs.9b01585 (Spotlight feature)
16. **Bibic, L.** 2019. "Spongy yet Sturdy: MOF Harvests Water from Air". *J. Am. Chem. Soc.* 141: 12 DOI: 10.1021/jacs.9b02969 (Spotlight feature)
17. **Bibic, L.** 2019. "Playing with Fire Recovers an Unusual Carbon Compound". *J. Am. Chem. Soc.* 141: 15. DOI: 10.1021/jacs.9b03757 (Spotlight feature)
18. **Bibic, L.** 2019. "Getting a Grip on Protein–Protein Interactions". *J. Am. Chem. Soc.* 141: 20. DOI: 10.1021/jacs.9b05138 (Spotlight feature)
19. **Bibic, L.** 2019. "Triangular Prism Sorts Natural Products". *J. Am. Chem. Soc.* 141: 22. DOI: 10.1021/jacs.9b05712 (Spotlight feature)
20. **Bibic, L.** 2019. "Lighting the Way for Photonic Devices". *J. Am. Chem. Soc.* 141: 34. DOI: 10.1021/jacs.9b09008 (Spotlight feature)
21. **Bibic, L.** 2019. "Under Pressure: Analyzing Amyloid-Beta Peptides as They Fold". *J. Am. Chem. Soc.* 141: 37. DOI: 10.1021/jacs.9b09762 (Spotlight feature)
22. **Bibic L.** 2019. "Pushing the Triple-Phase Boundary for Fuel Cells". *J. Am. Chem. Soc.* 141: 48. DOI: 10.1021/jacs.9b12613 (Spotlight feature)

Conference Abstracts, Presentations, Travel Awards and a Peer-Review

- 1. Discovery of a small molecule toxin with inhibitory activity at human P2X4 ion channel.** Oral presentation at the “Pharmacology 2019” conference (Edinburgh, UK, December 2019) and at the “Venoms and Toxins 2019” meeting (Oxford, UK, August 2019).
- 2. Bug Off Pain: Educational VR game about spider venoms and chronic pain for public engagement.** Invited speaker for the Gamification: Pedagogy and Practice (Norwich, UK, May 2019) and BISON Conference (Norwich, UK, November 2018). Oral presentations.
- 3. No Pain, All Gain: Discovery of a novel spider toxin that selectively inhibits hP2X4 Receptor.** Poster presentation at the 156th National meeting (Boston, USA, August 2018). Part of CAS Future Leaders Award.
- 4. Bug Off Pain: Probing P2X Channels with Animal Venoms.** Oral presentation at the Purines 2018 (Foz do Iguacu, Brazil, June 2018). Awarded with UEA Pharmacy travel grant (£1000). Poster and flash presentation at the Gordon Research Conference "Venom evolution, structure and biomedical application" (Vermont, USA, August 2018). Awarded with the travel grants from RSC and the Biochemical Society (£1000).
- 5. Disruption of G-protein coupled receptor dimers by cell-penetrating interference peptides *in vitro*.** Poster and flash presentation at the XXIV EFMC International Symposium on Medicinal Chemistry (EFMC-ISMC 2016, Manchester, UK, 2016). Awarded with the Royal Society Travel Grant (£500).
- 6. It takes two to tango and one to dip: Disruption of GPCR heteromers by cell-penetrating peptides.** Poster presentation at the Peptide and Protein Science Group RSC (Durham, UK, November 2015) and at the GPCRS: Beyond Structure towards Therapy (Prato, Italy, September 2015).
- 7. Invitation to undertake a peer-review as offered by the *Journal of Chemical Education*** (June 2019)
– accepted

Awards

The list of awards and a certificate obtained during my doctoral studies include:

- **Honours certificate in Writing in the Sciences by Stanford University (2019)** – Credential ID K266YN4V5PB8, grade: 95.6%.
- **International CAS Future Leaders Award (2018)** – a leadership program organized by Chemical Abstract Service (CAS) and American Chemical Society (ACS) that recognize the top postgraduate and postdoctoral students in chemical sciences.
- **UEA Engagement Award (2018)** – a university-based award that recognizes outreach efforts to the local community.
- **Presentation Award “Best 3-minute thesis” (2017)** at the UEA, School of Pharmacy’s Research Day.
- **Winners of the Biotechnology YES2017 (2017)** entrepreneurship competition and People’s Choice Awards. Best start-up business plan branded as CryoThaw Heart. Finalist pitch at the GlaxoSmith Kline (GSK) at Stevenage (UK). Best Biotechnology pitch for the venture capitalists and judges at the finals in the Royal Society (London, UK). Sharing the award with the CryoThaw team.

Abstract

Today, one in five adults experience chronic pain and this figure increases for those over 65 years old. However, frustration is mounting over the inadequate treatment for chronic neuropathic pain since its symptoms are challenging to treat and often resistant to opioids. Processing of pain signals relies on the activities of ion channels with the microglial P2X4 receptor being an important player. Animal venoms play an essential role in drug discovery as they contain a rich source of bioactive molecules evolutionarily fine-tuned to target ion channels such as P2X receptors. First, we have established and validated several fluorescent-based high throughput screening assays for assessing the activity of venom toxins at P2X receptors. Second, a diverse selection of 180 crude venoms has been screened against human P2X4 in HEK293 and 1321N21 cells, resulting in several venoms containing inhibitors against hP2X4. Two of them, LK-601 and LK-729, were confirmed to be structurally uncharacterized acylpolyamines, which potently inhibited hP2X4 with the apparent IC_{50} values between 1.1 – 4.5 μ M, however only LK-601 showed a relatively high level of selectivity over hP2X3, hP2X7 and NMDA 1a/2a. Species differences were evident with no effect at rat P2X4, however, blocking the mouse P2X4. Using LK-601 as a structural guide, the fragment-based screening was carried out and five smaller toxin analogues chemically synthesized. One of them, LA-3, was found to block the hP2X4 (IC_{50} of 9.7 – 18.6 μ M) and showed selectivity to hP2X4 over hP2X3, hP2X7 and rP2X4 with a modest inhibition at mP2X4. Due to the differential sensitivity of LA-3 to block P2X4 orthologues, the potential binding site were identified, and the validation showed that two crucial amino acid residues, D220 and N238, might be involved in LA-3 binding to hP2X4; however, more experiments are needed to confirm that effect fully. In summary, we discovered a novel toxin from a spider venom with inhibitory activity at human P2X4 ion channels that shows selectivity at hP2X4 over other P2X receptors. Further characterization and validation are required to understand whether these novel compounds could be useful as analgesics.

Contents

INTELLECTUAL PROPERTY AND PUBLICATION STATEMENTS	4
PUBLICATION RECORD LIST	6
CONFERENCE ABSTRACTS, PRESENTATIONS, TRAVEL AWARDS AND A PEER-REVIEW	8
AWARDS	9
ABSTRACT	10
CONTENTS	11
LIST OF FIGURES.....	14
LIST OF TABLES	16
ACKNOWLEDGEMENTS	17
ABBREVIATIONS	19
~ CHAPTER ONE ~	24
1. NO PAIN, ALL GAIN: TACKLING CHRONIC PAIN USING VENOM TOXINS	25
1.1. PAIN MECHANISMS	26
1.1.1. NOCICEPTIVE PAIN	27
1.1.2. INFLAMMATORY PAIN	30
1.1.3. NEUROPATHIC PAIN	31
1.1.4. PATHOLOGICAL ROLE OF NON-NEURONAL CELLS IN CHRONIC PAIN	32
1.1.4.1. <i>Monocytes and Macrophages</i>	33
1.1.4.2. <i>T Lymphocytes, Keratinocytes and Bone Marrow Stem Cells</i>	33
1.1.4.3. <i>Cancer Cells</i>	34
1.1.4.4. <i>Glial Cells</i>	34
1.1.5. EXPRESSION OF NEUROTRANSMITTER RECEPTORS ON MICROGLIA	36
1.1.5.1. <i>Activated Microglia Contributes to Pathological Pain</i>	38
1.1.6. PURINERGIC RECEPTORS	41
1.1.6.1. <i>P2X1</i>	42
1.1.6.2. <i>P2X2</i>	42
1.1.6.3. <i>P2X3</i>	43
1.1.6.4. <i>P2X4</i>	43
1.1.6.5. <i>P2X7</i>	43
1.1.7. PHARMACOLOGY OF P2X4	45
1.2. ANIMAL VENOMS: A RICH SOURCE OF NOVEL ION CHANNEL-TARGETED COMPOUNDS	48
1.2.1. ION CHANNELS AS DRUG TARGETS IN CHRONIC PAIN	48
1.2.2. <i>Spider Venom Toxins</i>	50
1.2.3. <i>Polyamines and Acylpolyamines</i>	52
1.2.4. <i>Spider-Venom Peptides as Pharmacological Tools and Potential Therapeutic Leads</i>	53
1.2.5. <i>Isolation, Characterization, Production and Structure Determination of the Toxins</i>	55
1.3. MOTIVATION AND OBJECTIVES OF THE THESIS	56
~ CHAPTER TWO ~	58

2. MATERIALS AND METHODS.....	59
2.1. MATERIALS.....	59
2.2. CELL CULTURES.....	66
2.3. ESTABLISHMENT OF STABLE CELL LINES	67
2.4. TRANSIENT TRANSFECTION.....	68
2.5. FLOW CYTOMETRY	68
2.6. CA ²⁺ MEASUREMENTS (FURA-2 AM)	69
2.7. FLIPR CA-6 ASSAY.....	69
2.8. YO-PRO-1 ASSAY	70
2.9. ISOLATION AND PURIFICATION OF VENOM FRACTIONS USING RP-HPLC.....	70
2.10. MASS ANALYSIS OF VENOM FRACTIONS AND PURE TOXINS AND SOFTWARE AIDS.....	71
2.11. MOLECULAR FORMULAE DETERMINATION BY MS-FINDER	72
2.12. VALIDATION METHODS FOR THE HP2X4-SPECIFIC ASSAY DEVELOPMENT	72
2.13. CELL VIABILITY ALAMAR BLUE ASSAY	73
2.14. LDH RELEASE ASSAY	74
2.15. AMINO ACID SEQUENCING.....	74
2.16. STRUCTURAL ELUCIDATION OF THE TOXINS BY NUCLEAR MAGNETIC RESONANCE	74
2.17. CHEMICAL SYNTHESIS OF SMALL MOLECULES AND NMR	75
2.18. DOCKING STUDIES.....	79
2.19. MUTAGENESIS.....	80
2.20. EVALUATION OF VR GAME BUG OFF PAIN©.....	81
2.21. DATA ANALYSIS	86
~ CHAPTER THREE ~	88
DEVELOPMENT OF HIGH-THROUGHPUT FLUORESCENT-BASED SCREENS FOR THE RAPID DISCOVERY OF NOVEL ANIMAL TOXIN HITS AGAINST P2X RECEPTORS	88
3.1. INTRODUCTION.....	89
3.2. RESULTS AND DISCUSSION	90
3.2.1. <i>Assay Design</i>	90
3.2.2. <i>Assay Optimization</i>	93
3.2.3. <i>Screen of Animal Venoms Against hp2X4</i>	97
3.2.4. <i>Fractionation of Crude Venom Hits</i>	99
3.2.5. <i>Assay Hit Identification and Validation</i>	101
3.2.6. <i>Assay Specificity</i>	105
3.2.7. <i>Assay Reproducibility</i>	106
3.2.8. <i>Assay Variability</i>	108
3.3. CONCLUSIONS	110
~ CHAPTER FOUR ~	116
DISCOVERY OF A SMALL MOLECULAR TOXIN FROM SPIDER VENOM THAT SELECTIVELY INHIBITS HP2X4 RECEPTOR.....	116
4.1. INTRODUCTION.....	117
4.1.1. <i>Small Molecule Toxins in Animal Venoms</i>	117
4.1.2. <i>Identification and Structural Characterization of Small Molecular Toxins in the Animal Venoms</i> ..	119
4.2. RESULTS AND DISCUSSION	121
4.2.1. <i>Screening Crude Animal Venoms for hp2X Modulators</i>	121
4.2.2. <i>Activity-Guided Fractionation of the Spider Venoms Against 1321N1-hp2X4</i>	130
4.2.3. <i>Purification and Mass Analysis of Fraction Hits Against hp2X4</i>	137

4.2.4.	<i>Effects of LK-601 and LK-729 against hP2X4 and Related Targets</i>	147
4.2.5.	<i>Structural Elucidation of LK-601 and LK-729</i>	153
4.3.	CONCLUSIONS	157
~ CHAPTER FIVE ~		163
SYNTHESIS, STRUCTURE-ACTIVITY RELATIONSHIP AND EVALUATION OF LK-601 ANALOGUE LA-3, A NOVEL HP2X4 ANTAGONIST		163
5.1.	INTRODUCTION	164
5.1.1.	<i>Importance of Structure-Activity Relationship of Natural Products</i>	164
5.1.2.	<i>Animal Toxins as a Template to Lead Selection</i>	165
5.1.3.	<i>Chemical Synthesis of Acylpolyamine Toxins Derived from Spider Venoms</i>	165
5.1.4.	<i>Biological Effects of Polyamines and Acylpolyamines</i>	167
5.2.	RESULTS AND DISCUSSION	170
5.2.1.	<i>Investigating the Nature of Structure-Activity Relationship in LK-601</i>	171
5.2.2.	<i>Chemical Synthesis of LK-601 Analogues</i>	188
5.1.1.	<i>In Vitro Evaluation of LK-601 Analogues</i>	191
5.1.1.	<i>Ligand Docking and Prediction of Binding Mode to hP2X4 of LA-3</i>	195
5.1.2.	<i>Structural Basis for the Pharmacological Properties of LA-3</i>	201
5.2.	CONCLUSIONS	205
~ CHAPTER SIX ~		209
BUG OFF PAIN©: AN EDUCATIONAL VIRTUAL REALITY GAME ON SPIDER VENOMS AND CHRONIC PAIN FOR PUBLIC ENGAGEMENT		209
6.1.	INTRODUCTION	210
6.1.1.	<i>Science Communication</i>	210
6.1.2.	<i>Digitalization in Science Education</i>	211
6.1.3.	<i>A Science of Games</i>	212
6.1.4.	<i>Virtual Reality as an Interactive Learning Environment</i>	213
6.2.	RESULTS AND DISCUSSION	214
6.2.1.	<i>The Game</i>	214
6.2.2.	<i>Evaluation of General Public Opinion about Bug Off Pain</i>	220
6.2.3.	<i>Evaluation of VR-based Learning by Use of Bug Off Pain Among High School Students</i>	223
6.3.	CONCLUSIONS	228
~ CHAPTER SEVEN ~		231
GENERAL CONCLUSION AND FUTURE DIRECTIONS		231
7.1.	GENERAL CONCLUSION	232
7.2.	FUTURE DIRECTIONS	236
REFERENCES		239
SUPPORTING INFORMATION		273

List of Figures

FIGURE 1.1. NOCICEPTION	28
FIGURE 1.2. NON-NEURONAL CELLS INTERACT WITH THE NOCICEPTORS	32
FIGURE 1.3. P2X4 PURINORECEPTOR SIGNALLING IN CHRONIC PAIN	40
FIGURE 1.4. PURINERGIC SIGNALLING PATHWAYS IN CHRONIC PAIN	42
FIGURE 1.5. P2X4 RECEPTOR STRUCTURE BASED ON PDB ID 4DW1	44
FIGURE 1.6. P2X4 ANTAGONISTS	46
FIGURE 1.7. FOUR DIFFERENT TYPES OF POLYAMINES.	52
FIGURE 1.8. THE STRUCTURE OF JORO SPIDER TOXIN.	53
FIGURE 1.9. MASS DISTRIBUTION OF SPIDER VENOM PEPTIDES.	54
FIGURE 2.1. PRINTED SURVEY ADMINISTRATED TO COLLECT THE PLAYER’S OPINIONS AND FEEDBACK ABOUT BUG OFF PAIN.	82
FIGURE 2.2. PRE- AND POST-TEST QUESTIONNAIRE.	85
FIGURE 2.3. QR CODE FOR BUG OFF PAIN.	86
FIGURE 3.1. HIGH-THROUGHPUT SCREEN OF CRUDE VENOMS AGAINST P2X RECEPTORS	91
FIGURE 3.2. VALIDATION OF THE STABLE CELL LINES EXPRESSING HP2X4 FOR HTS	94
FIGURE 3.3. VALIDATION OF THE STABLE CELL LINE EXPRESSING HP2X7 FOR HTS	95
FIGURE 3.4. VALIDATION OF THE STABLE CELL LINE EXPRESSING HP2X3 FOR HTS.	95
FIGURE 3.5. SCREEN OF CRUDE VENOMS AGAINST 1321N1-HP2X4 AND HEK293-HP2X4	98
FIGURE 3.6. REPRESENTATIVE RP-HPLC CHROMATOGRAMS FROM VARIOUS VENOMOUS ANIMALS	100
FIGURE 3.7. SCREENING OF <i>N. CHROMATUS</i> VENOM FRACTIONS	102
FIGURE 3.8. NONSPECIFIC Ca ²⁺ RESPONSES ON 1321N1 CELLS	104
FIGURE 3.9. ASSAY SPECIFICITY	106
FIGURE 4.1. GENERAL STRUCTURE OF SPIDER ACYLPOLYAMINE.	117
FIGURE 4.2. STRUCTURES OF SOME OF THE MOST CHARACTERIZED ACYLPOLYAMINES	119
FIGURE 4.3. A CONCENTRATION-DEPENDENT SCREEN OF CRUDE CONE SNAIL VENOMS AGAINST HP2X4 AND HP2X7	123
FIGURE 4.4. A CONCENTRATION-DEPENDENT SCREEN OF CONE SNAIL CRUDE VENOMS AGAINST HP2X3	124
FIGURE 4.5. A CONCENTRATION-DEPENDENT SCREEN OF CONE SNAIL FRACTIONS AGAINST HP2X3	125
FIGURE 4.6. CRUDE SPIDER VENOM SCREEN	126
FIGURE 4.7. REPRESENTATION OF THE CRUDE VENOM <i>L. KLUGI</i> SCREEN AGAINST HEK293-HP2X4 CELL LINE	128
FIGURE 4.8. NON-SPECIFIC EFFECTS OF CRUDE VENOMS ON 1321N1-HP2X4 (FURA-2)	129
FIGURE 4.9. HPLC CHROMATOGRAMS FROM DIFFERENT SPIDER VENOMS	130
FIGURE 4.10. HPLC CHROMATOGRAMS FROM DIFFERENT SPIDER VENOMS	131
FIGURE 4.11. SCREENING OF VARIOUS SPIDER VENOM FRACTIONS AGAINST 1321N1-HP2X4	133
FIGURE 4.12. SCREENING OF VARIOUS SPIDER VENOM FRACTIONS AGAINST 1321N1-HP2X4	134
FIGURE 4.13. SCREENING OF <i>E. MURINUS</i> AGAINST 1321N1-HP2X4 WITH FURA-2 DYE	135
FIGURE 4.14. VALIDATION OF SPIDER VENOM FRACTIONS FROM <i>L. KLUGI</i> AGAINST HEK293-HP2X4	136
FIGURE 4.15. PURIFICATION AND MASS SPECTROSCOPY CONFIRMATION OF LK-601 AND LK-729 FROM <i>L. KLUGI</i>	139
FIGURE 4.16. HPLC CHROMATOGRAMS SHOW THE INSTABILITY OF THE TOXIN HITS	141
FIGURE 4.17. ELUTING LC-MS PROFILES AND ESI-MS/MS OF THE [M+H] ⁺ IONS OF LK-601 AND LK-729	142
FIGURE 4.18. MASS SPECTROSCOPY OF SMALL INHIBITORY TOXINS.	144
FIGURE 4.19. AN EXAMPLE OF GRAPHICAL USER INTERFACE OF MS-FINDER SOFTWARE CALCULATIONS FOR LK-601.	146
FIGURE 4.20. PHARMACOLOGICAL EFFECTS OF LK-601 AND LK-729 ON HP2X4	148
FIGURE 4.21. SELECTIVITY ASSAYS OF LK-601 AND LK-729 AMONG P2X AND NMDA SUBTYPES.	149
FIGURE 4.22. EFFECT OF LK-601 IN A NATIVE MICROGLIAL MODEL.	151

FIGURE 4.23. SELECTIVITY ASSAYS OF LK-601 AND LK-729 AMONG P2X4 SPECIES.....	152
FIGURE 4.24. NMR-SPECTROSCOPIC ANALYSIS OF LK-601 BY 800 MHZ NMR.	154
FIGURE 4.25. NMR-SPECTROSCOPIC ANALYSIS OF LK-729 BY 800 MHZ NMR	155
FIGURE 4.26. INSTABILITY ISSUES WITH LK-601 AND LK-729 AS SEEN BY THE NMR-SPECTROSCOPIC ANALYSIS.	157
FIGURE 5.1. STRUCTURE OF MR44.	165
FIGURE 5.2. STRUCTURES OF NPTX-9, NPTX-11, AGEL-489, ARG-636 AND JSTX-3.	167
FIGURE 5.3. STRUCTURES OF PHTX-83, PHTX-56, PHTX-12, PHTX-343 AND PHTX-433.	170
FIGURE 5.4. APPLICATION OF POLYAMINES PRIOR TO 10 mM ATP APPLICATION IN TWO STABLE CELL LINES.	171
FIGURE 5.5. CHEMICAL STRUCTURES OF EIGHT INDOLE-LIKE COMPOUNDS THAT WERE SCREENING IN OUR PRELIMINARY ASSAYS.....	172
FIGURE 5.6. APPLICATION OF SIMPLE INDOL-BASED COMPOUNDS PRIOR TO 10 mM ATP APPLICATION IN TWO STABLE CELL LINES.....	173
FIGURE 5.7. STRUCTURE OF SMARTS	174
FIGURE 5.8. APPLICATION OF THE COMPOUNDS (1513, 329271, 13964, 16892 AND 17812) IN HEK293-HP2X4	176
FIGURE 5.9. APPLICATION OF THE COMPOUNDS (17815, 63799, 113928 AND 135831) IN HEK293-HP2X4.....	177
FIGURE 5.10. APPLICATION OF THE COMPOUNDS (1969, 339919, 369856, 608048 AND 673655) IN HEK293-HP2X4	178
FIGURE 5.11. APPLICATION OF THE COMPOUNDS (1513, 329271, 13964, 16892, 17812 AND 17815) IN 1321N1-HP2X4	179
FIGURE 5.12. INTERFERENCE ASSAYS.	180
FIGURE 5.13. APPLICATION OF THE COMPOUNDS (63799, 113928, 135831 AND 1969) IN 1321N1-HP2X4.....	181
FIGURE 5.14. SELECTED INDOLE-LIKE “HIT” COMPOUNDS FROM THE NCI-DTP LIBRARY.	182
FIGURE 5.15. DOSE-DEPENDENT INHIBITION OF 1513	183
FIGURE 5.16. DOSE-DEPENDENT INHIBITION OF 13964	183
FIGURE 5.17. DOSE-DEPENDENT INHIBITION OF 135831.	184
FIGURE 5.18. DOSE-DEPENDENT INHIBITION OF 1969	185
FIGURE 5.19. HITS AND OTHER INDOLE-LIKE COMPOUNDS THAT DID NOT SHOW PROMISED AS THE HITS (“NO HITS”)......	186
FIGURE 5.20. THE CHEMICAL STRUCTURE OF ARGIOPININ-1.	187
FIGURE 5.21. EVALUATING THE EFFECTS OF ARGIOPININ-1 ON 1321N1-HP2X4 CELL LINE	188
FIGURE 5.22. REACTION OUTLINE FOR THE CHEMICAL SYNTHESIS OF LUCAS ANALOGUES (LA).	189
FIGURE 5.23. STRUCTURES OF LUCAS ANALOGUES (LA)	190
FIGURE 5.24. HPLC CHROMATOGRAM OF TOXIN ANALOGUES.....	191
FIGURE 5.25. EFFECTS OF LK-601 ANALOGUES.	192
FIGURE 5.26. EFFECTS OF LK-601-INSPIRED ANALOGUE LA-3.....	194
FIGURE 5.27. ALIGNMENT OF THE AMINO ACID SEQUENCES	196
FIGURE 5.28. MODEL OF A SINGLE HUMAN P2X4 SUBUNIT IN SURFACE VIEW (A) AND RIBBON VIEW (B).	197
FIGURE 5.29. MODELLING OF THE LA IN HUMAN P2X4	199
FIGURE 5.30. MODELLING OF THE LA-3 IN MOUSE P2X4.....	200
FIGURE 5.31. EFFECT OF DIFFERENT MUTANT VARIANTS OF HP2X4 AND RP2X4 ON ATP RESPONSIVENESS.....	202
FIGURE 5.32. THE INHIBITORY EFFECT OF LA-3 ON DIFFERENT MUTANT VARIANTS OF HP2X4 AND RP2X4.....	203
FIGURE 6.1. THE GRAPHICAL ABSTRACT OF VR GAME BUG OFF PAIN	215
FIGURE 6.2. THE MODEL OF OUR ACADEMY THEATRE IN THE VR ENVIRONMENT FOR BUG OFF PAIN.	215
FIGURE 6.3. VR ENVIRONMENT BEFORE THE FIRST MOVIE CLIP	216
FIGURE 6.4. TWO ENVIRONMENTS OF BUG OFF PAIN	217
FIGURE 6.5. 3D-MOVIE THAT ALLOWS THE PLAYER TO TRAVEL INSIDE THE BRAIN.	218
FIGURE 6.6. REPRESENTATION OF ONE SPECIFIC TARGET (PURINERGIC RECEPTOR P2X4) IN THE BRAIN (PDB: 4DW1).	218
FIGURE 6.7. VR ENVIRONMENT WITH THE TARGET ON THE STAGE	219
FIGURE 6.8. QR CODE FOR BUG OFF PAIN.....	219
FIGURE 6.9. PRINTED SURVEY.....	220
FIGURE 6.10. THE SURVEY	221
FIGURE 6.11. PRE- AND POST-TEST QUESTIONNAIRE	224

FIGURE S1. NMR SPECTRA OF THE ACTIVATED ESTERS (INTERMEDIATES) AND THE FINAL PRODUCTS (LK-601 ANALOGUES)	281
FIGURE S2. PEPTIDE F25 PURIFICATION AND MASS ESTIMATION.	289
FIGURE S3. PEPTIDE F25 MASS DETERMINATION AND IDENTIFICATION	290
FIGURE S4. A CONCENTRATION-RESPONSE CURVE OF F25 ON 1321N1-HP2X4 (FURA-2) CELL LINE	292
FIGURE S5. ESI-MS FOR 1H-INDOLE-3-CARBOXYLIC ACID, 4-NITROPHENYL ESTER.....	292
FIGURE S6. ESI-MS FOR 1H-INDOLE-3-CARBOXAMIDE	293
FIGURE S7. ESI-MS FOR 1H-INDOLE-3-ACETIC ACID	294
FIGURE S8. ESI-MS FOR 1H-INDOLE-3-ACETAMIDE	294
FIGURE S9. ESI-MS FOR 1H-INDOLE-2-CARBOXYLIC ACID	295
FIGURE S10. ESI-MS FOR 1H-INDOLE-2-CARBOXAMIDE	295

List of Tables

TABLE 2.1. LIST OF SPECIES OF ANIMAL VENOMS USED AND TESTED IN OUR ASSAYS.	60
TABLE 2.2. LIST OF PRIMERS FOR THEIR RESPECTIVE MUTATION AS PURCHASED FROM SIGMA ALDRICH.	80
TABLE 3.1. IC ₅₀ VALUES OF KNOWN P2X INHIBITORS	96
TABLE 3.2. ASSAY VARIABILITY BETWEEN RUNS ON 1321N1-HP2X4.....	108
TABLE 3.3. ASSAY VARIABILITY BETWEEN RUNS ON HEK293-HP2X4	109
TABLE 3.4. ASSAY VARIABILITY BETWEEN RUNS ON HEK293-HP2X7	109
TABLE 4.1. ANIMAL VENOMS THAT WERE SCREENED FOR HP2X MODULATORS.	122
TABLE 4.2. SV1, SV8, SV9 AND SV10 DEMONSTRATED DOSE-DEPENDENT INHIBITION OF HP2X4.....	127
TABLE 4.3. RP-HPLC RETENTION TIMES OF THE FRACTIONATED TOXIN HITS FROM VARIOUS SPIDER VENOMS	132
TABLE 4.4. MOST INTENSE <i>m/z</i> RATIOS OF THE INHIBITING FRACTIONS ACCURATELY DETERMINED BY THE LC-MS SPECTRUM.....	138
TABLE 4.5. FRAGMENT IONS <i>m/z</i> OF LK-601 AND LK-729 OBTAINED BY MS/MS.	143
TABLE 5.1. A SET OF 14 COMPOUNDS FROM THE NCI-DTP LIBRARY COMPOUND SET.....	175
TABLE 5.2. SUMMARY OF AMINO ACID SUBSTITUTIONS.....	201
TABLE 5.3. SUMMARY OF % OF P2X4 INHIBITION BY LA-3 (10 μM).	204
TABLE 6.1. LEARNING OBJECTIVES RELATED WITH THE CONTENTS AND CHARACTERISTICS OF BUG OFF PAIN APPLICATION.	216
TABLE 6.2. COMPARISON OF PUPILS' AVERAGE SCORES BY INSTRUCTIONAL METHOD	225
TABLE 6.3. COMPARATIVE STUDENT PERFORMANCE RELATIVE TO INSTRUCTIONAL METHOD	226
TABLE S1. RETENTION TIMES OF THE SPIDER VENOM FRACTIONS (RP-HPLC).....	273

Acknowledgements

Time and time again, I saw people energized by the story of venoms and chronic pain – energized, and filled with the desire to do something about it. Many of those people put that energy into helping me with my Ph.D. My gratitude goes out to everyone who devoted time, insights, knowledge, money, and heart to our project(s).

Some of these unsung heroes include – first and foremost – my Norwich family.

Mar Puigdemívol Cañadell and Gerard Callejo were my rocks - their positivity, their laughter, their “*bye Felicia*”, their determination, and their remarkable strength were an ongoing inspiration that helped me working all these years. Thank you guys for encouraging me to fight for who I want to be and taking the time to get me. Mar, thank you for showing me the importance of staying true to myself and for your drive – these have been a tremendous guide for me. I feel deeply honoured to have been part of both of your lives.

I thank Elise Wright, Remy Narozny, Oliver Cartwright and Sam Walpole for their enthusiasm, tireless support, spiderwoman costumes, Mars expeditions, running journeys, ice-cream vans, and for believing I can (and probably will) kick asses. Elise’s and Remy’s support was unwavering; I thank them for their stories and their laughter. I feel very fortunate to find friends who were (somehow) always willing to edit my drafts with amusement. Oliver and Sam are one of them – thank you guys for your trust, friendship, encouragement, seeing the value of our projects and being their backbones.

I’m grateful to Marco Maurizio Cominetti, Ryan Tinson, Hui Poh Goh, Serena Monaco, Noelia Dominguez Falcon, Ana Bermejo Martinez, Estela Perez Santamarina, Tom Leggo-Bridge, Stefan Bidula, and Valeria Gabrielli for keep me laughing and for answering my many questions. The same is true for Noe, who always sang beautiful messages for my WhatsApp repertoire, and never failed to serenade me on my birthday. My in-house editor/postdoc Stefan deserves a medal for reviewing (nearly) everything I’ve ever written, offering a brilliant feedback and teaching me new things as I grow as a writer, and a scientist.

I would like to thank my Future Leaders 2018 family. Guys, you are a continuous source of inspiration for me. Kudos to Dr Dario Cambie and Dr Alexander Cook - our discussion, prompted on the bus, has actually resulted in one of the chapters (and a cool research paper).

A special thanks goes to Dr César A. Urbina-Blanco who kept me functioning with encouraging texts and simultaneous thoughtful insights throughout my thesis writing. César, to me you are a gift!

Now, to the next thing – my scientific advisers. I feel lucky to have found Dr Leanne Stokes and Prof Mark Searcey whose mentorship was a game changer for me. Thank you for reading my detailed emails and supporting my countless little “research hobbies” and imaginary pursuits. Thank you Leanne for taking me under your wing when I navigated the complexities of my Ph.D. Mark, thank you for offering me the opportunity to come to the School of Pharmacy in the first place and work in your lab. Seriously guys, thank you; you rock.

Thanks also to other actual and virtual communities that have made a huge contribution to my learning and ultimate success in the Ph.D. process. Thank you BBSRC DTP and University of East Anglia for a grant that supported my doctoral research. My collaborators and/or colleagues, Dr Ewan John Smith, Dr Jesus Angulo, Prof Glenn King, Prof Yaroslav Khimyak, Dr Zoe Waller and Prof Dave Evans – thank you for being the scientific leaders I certainly look up to. Kudos for always cheerleading for me on Twitter (and in real life)!

As is true for many articles and stories these days, mines struggled to find their ways to press. Dozens of rejections and a few editors later, I feel extremely fortunate to have worked with Dr Nicole Camasso (JACS) and Dr Rachel Bernstein (Science). Thank you Nicole and Rachel for taking the chance on me and being patient with me. Rachel – thank you for gently pushing me out of my comfort zone. I feel humbled to find an expert source as generous with the time and editorial insights as yours. I have learnt so much from both of you!

My parents and my brothers deserve to have entire wings of this Ph.D. named after them for all the support they’ve given me over the years. My mom and dad have never faltered in their belief in me and my ambitions. My mother Renata kept me sane through pep talks, reality checks, and the gifts of wisdom. Thanks also to my brothers, Klemen and Jošt, and my sister-in-law Maruša for your grace, your support, your heart, and your compassion. You kept me happy and I consider myself to be a very lucky to have a family as such.

Last, but certainly not the least, special thanks to Špela, Laura, Cristina, Mariša, Vid, Nejc and Gloria for their adventurous spirit, authenticity, love, undying support and for being there for the long haul. You are my persons in this life. As for Gloria - thank you for being my safe haven.

Abbreviations

5-BBBD – 5-(3-Bromophenyl)-1,3-dihydro-2H-benzofuro[3,2-e]-1,4-diazepin-2-one

ADP – adenosine diphosphate

AIDS – acquired immune deficiency syndrome

AMP – adenosine monophosphate

AMPA – α -amino-3-hydroxyl-5-methyl-4-isoxazole-propionate

ArgTX – argiotoxin

ASIC – acid-sensing ion channel

ATP – adenosine triphosphate

A β – amyloid β

BDNF – brain-derived neurotrophic factor

BMSC – bone marrow stem cells

BRET – fluorescent polarization and bioluminescent resonance energy transfer

BX430 – 1-(2,6-dibromo-4-isopropyl-phenyl)-3-(3-pyridyl) urea

CCL2 – chemokine (C-C motif) ligand 2

CCR5 – chemokine (C-C motif) ligand 5

CNS – central nervous system

COSY – correlation spectroscopy

COX – cyclooxygenase

CS – cone snail

CX3CL1 – chemokine (C-X-C3 motif) receptor 1

CX43 – connexin43

CXCL1 – chemokine (C-X-C motif) ligand 1

D₂O – deuterated water

DRG – dorsal root ganglion

ERK – extracellular signal-regulated *kinase*

FAB – fast atom bombardment

FRET – fluorescent-resonance energy transfer

GABA – gamma-aminobutyric acid

GMP – good manufacturing practice

GPCR – G-protein coupled receptor

GTP – Guanosine Triphosphate

HaTx 1-2 – hanatoxins 1 and 2

HIV – human immunodeficiency virus.

HMBC – heteronuclear multiple bond correlation

HMQC – heteronuclear multiple quantum coherence

HpTx – heteropodatoxin

HTS – high-throughput screening

IFN- γ – interferon gamma

iGlu – ionotropic glutamate

iGluRs – ionotropic glutamate receptors

IL-10 – Interleukin 10

IL-18 – interleukin-18

IL-1 β – interleukin-1 β

IL-33 – interleukin-33

IL-4 – interleukin-4

ILR1 – interleukin 1 receptor-like 1

IR – infrared spectroscopy

JNK – jun N-terminal kinase

JSTX-3 – joro spider toxin

KKC2 – potassium chloride cotransporter 2

KORs – κ -opioid receptors

Kv – voltage-gated potassium channel

LC-MS – liquid chromatography-mass spectrometry

LPS – lipopolysaccharides

MAb – monoclonal antibody

MALDI-TOF – matrix assisted laser desorption ionization - time of flight

MAP – mitogen-activated protein

MAPKs – mitogen-activated protein kinases

mAU – mili-absorbance units

mGluRs – metabotropic glutamate receptors

MMP2 – metalloproteinase-2

MORs – μ -opioid receptors

MS-MS – tandem mass spectrometry

nAChR – nicotinic acetylcholine receptor

Nav – voltage-gated sodium channel

NF- κ B – nuclear factor κ B

NGF – nerve growth factor

NIST – national institute of standards and technology

NMDA – *N*-methyl-D-aspartate

NME – new medical entities

NMR – nuclear magnetic resonance.

NO – nitric oxide

NOESY – nuclear overhauser effect spectroscopy

NP-1815-PX – (5-[3-(5-thioxo-4*H*-[1,2,4]oxadiazol-3-yl)phenyl]-1*H*-naphtho[1,2-*b*][1,4]diazepine-2,4(3*H*,5*H*)-dione)

NSAIDs – non-steroidal anti-inflammatory drugs

PaTxs – phrixotoxins

PaulTx3 – phrixotoxin 3

PCR – polymerase chain reaction

PcTx1 – psalmotoxin1

PDGFR α – platelet-derived growth factor receptor α

PGE2 – prostaglandin E2

PI3K – phosphatidylinositol-3 kinase

PKA – protein kinase A

PKC – protein kinase C

PNS – peripheral nervous system

PPADS – pyridoxalphosphate-6-azophenyl-2',4'-disulfonic acid

PSB12054 – *N*-(*p*- Methylphenyl)sulfonylphenoxazine 12054

PSB12062 – *N*-(*p*- Methylphenyl)sulfonylphenoxazine 12062

PT1 – purotoxin 1

RB-2 – reactive blue 2

RNA – ribonucleic acid

RP-HPLC – reversed phase-high performance liquid chromatographic method

S/N – signal-to-noise

SAR – structure-activity relationship

SD – standard deviation

SMILE – simplified molecular-input line-entry system

SNARE – nsf (N-ethylmaleimide factor) attachment receptor

SPPS – solid phase peptide synthesis

SPS – solid-phase synthesis

SV – spider venom

TGF- β – transforming growth factor beta

TNF – tumor necrosis factor

TrkA – tropomyosin receptor kinase A

TrkB – tropomyosin receptor kinase B

TRP – transient receptor potential cation channel

TRPC – transient receptor potential cation

TRPV1 – transient receptor potential cation channel subfamily V member 1

TSP4 – thrombospondin-4

UTP – uridine-triphosphate

VEGF – vascular endothelial growth factor

VEGGR1 – vascular endothelial growth factor receptor 1

YO-PRO-1 – 4-((3-methyl-2(3H)-benzoxazolylidene)methyl)- 1-(3-(trimethylammonio)propyl)quinolinium

~CHAPTER ONE~

Introduction

Section 1.1.4 of this Chapter contributed to a review article published as:

Stokes, L., Layhadi, J.A., Bibic, L., Dhuna K. And Fountain, S.J., P2X4 receptor function in the nervous system and current breakthroughs in pharmacology. *Frontiers in Pharmacology*. **2017**, 8, p.291.

1. No Pain, All Gain: Tackling Chronic Pain Using Venom Toxins

Pain represents a necessary physiological function yet remains a significant pathological process worldwide. While exciting progress is being made in deciphering the molecular and cellular mechanisms that underlie what we ultimately interpret as pain, chronic pain still continues to be an enduring health problem. Nociceptive pain is an evolutionary protective mechanism that guards us from potentially damaging or life-threatening events, whereas long-lasting chronic pain (pain lasting >3 months) transforms this into a debilitating disease. For many patients, pain continues to produce severe distress, limiting the quality of their lives. To put things into perspective, 1.4 billion of the world's 7 billion people – 20% – currently suffer from chronic pain, a number that increases to 50% for individuals older than 65.¹⁻² Given the impact of pain, the stakes are enormous. Just at the close of 2014, the annual economic burden of chronic pain in the USA was ~\$600 billion (£10 billion in the UK),³ which exceeds the combined cost of cancer, diabetes and stroke.⁴

As chronic pain is a common medical problem, the relief of pain is an important therapeutic goal. The generally accepted forms of chronic pain are chronic inflammatory pain and neuropathic pain, the latter being induced by explicit nerve damage. However, frustration is mounting over the inadequate treatment for neuropathic pain since its symptoms are difficult to treat and often resistant to the current available treatments, including the potent analgesic effects of the opioid drugs.⁵⁻⁶ This is in stark contrast to acute and chronic inflammatory pain for which there are many effective therapies.

Current remedies for neuropathic pain have at best moderate efficacy, poor tolerability, unfavourable side-effects, and concerns over long-term safety and abuse potential as noted in a double-blind, randomised meta-analysis study by Finnerup and others.^{5, 7-9} For example, in the recent two decades, the United States has seen a dramatic increase in opioid prescriptions for chronic pain. This so called “opioid crisis”, a term coined by reporters, has been linked with the growing misuse of prescription opioids and has led to increases in deaths due to unintentional opioid overdose, as well as in the number of patients seeking treatment for opioid-misuse disorders.¹⁰⁻¹¹

Clearly, new efficacious and safe analgesic agents are needed. The field has endured one very high profile efficacy-related failure in neurokinin 1 (substance P) receptor antagonists¹² and others, such as glycine-site antagonists¹³ and Na⁺ channel blockers.¹⁴ By contrast, the synthetic conotoxin ziconotide (Prialt®) provides an example of a peptide toxin from cone snail, targeting calcium channels, which was approved in 2004 for treatment of neuropathic pain.¹⁵

Despite these highs and lows, research efforts in drug discovery programs begin with target selection, often followed by high-throughput screening and generation of lead compounds. Critically, the transmission and processing of pain signals relies on the activities of ion channels – proteins located in the plasma membrane that mediate the transport of charged ions across hydrophobic lipid membranes. These can be either sodium, calcium, potassium and chloride channels in peripheral nerve endings, as comprehensively reviewed by Waxman and Zamponi.¹⁶ In response to nerve injury, dysregulated ion channels cause neural hyperexcitability that underlies neuropathic pain.

One such ion channel is purinergic P2X4 that has been implicated in the pain processing. Thus, this section would focus on bridging the gap between the exciting progress that has been made in dissecting out the pain mechanisms involving P2X4 and how a greater and more sophisticated effort is essential in the drug discovery for new analgesics.¹⁷⁻¹⁹ Furthermore, I will provide an update on current pharmacological tools targeting P2X4 and discuss strategies of exploiting these targets with the compounds from the spider's venoms.

1.1. Pain Mechanisms

The recognition of pain as a disease and not a symptom, is not only an important part of patient understanding, but it also impacts the drug discovery field. Nowadays, pain is broadly classed as nociceptive, inflammatory and neuropathic pain. While nociceptive (acute) pain serves as a warning mechanism that is activated only by noxious stimuli, chronic pain occurs via inflammation and damage, or dysfunction of the nervous system, termed as inflammatory and neuropathic pain, respectively.^{2, 20}

1.1.1. Nociceptive Pain

Many define pain as an unpleasant sensation that takes place in a particular part of the body.² This may happen due to initial insults within the body that are capable to compromise the tissue such as temperature change, mechanical danger (pressure, touch, stretch) or other danger.

Once such damaging stimuli are detected by sensory nociceptors called C-fibers and A δ -fibers within the injured tissue, the processing of pain signals is ultimately initiated.^{2, 21} Nociceptors can be imagined as free nerve endings that have branched from the dorsal root ganglia to the dorsal horn of the spinal cord. The way they communicate with each other is by relaying messages in form of neurotransmitters such as glutamate, substance P, somatostatin and calcitonin gene-related peptide. When these neurotransmitters act on their primary receptors, they activate so-called second-order neurons that travel from the spinal cord to the thalamus via a spinothalamic tract. In turn, the third-order neurons are then activated and they carry the neuronal message to the primary sensory cortex and other brain regions where the sensation of pain is experienced (**Figure 1.1**).²¹

From the moment noxious signals are processed by nociceptors to when the pain is experienced, three steps are crucial: transduction, transmission and modulation.

a) Nociceptive transduction usually begins when the human body transform external physical or chemical stimuli into the biochemical and/or electrical signals. This usually happens in the thinly myelinated (A δ) and unmyelinated (C fibres) that are found between epidermal cells, somatosensory organs and include both the peripheral and central nervous system. For their vast amount of functions, nociceptors have four major functional components: the peripheral end that is capable of processing external events and generating the action potentials; the axon which then conducts the action potentials; the cell body and the central termini which keep the integrity of the neuron and form the synapse in the CNS, respectively.²²

There are different transduction pathways that are involved in transducing nociceptive stimuli. In response to physical stimuli, some of the key hallmarks include the activation of various ion channels, particularly voltage-gated sodium (Na_v) channels, transient receptor potential (TRP) channels and acid sensing ion channels (ASIC). Here, the opening of ion channels leads to ion flux, changes in membrane potential which facilitates the opening of additional channels. Ultimately, this results in the depolarization of the afferent nerve, producing a nociceptive signal.²²

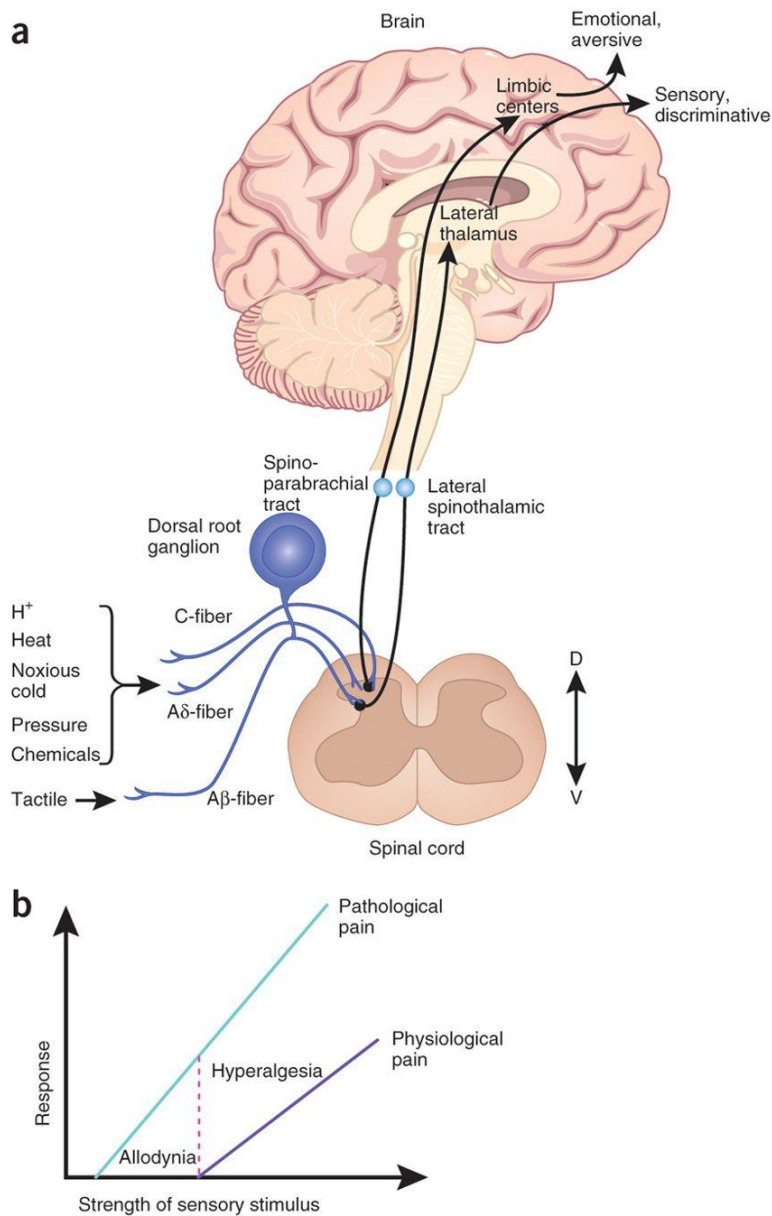


Figure 1.1. Nociception. A: A schematic representation of the pathways mediating physiological pain. Nociceptors transmit a normal acute pain to the spinal cord dorsal horn, leading to the release of pain transmitters from primary afferent terminals to laminae I, IV and V in the spinal cord dorsal horns (DRG). A β , A δ and C fibres also project to II-VI. However, in the case of tissue injury or inflammation, molecular signals (e.g., ATP, ADP, AMP, bradykinin, glutamate, substance P, serotonin, prostaglandin E₂, interleukin 1 and 6, histamine, certain protons) are released from the peripheral nerve terminals. This leads to the sensitization of the nociceptors in DRG and transmitted to the dorsal spinal cord and brain, where the experience of pain occurs. **B:** Manifestation of chronic pain. Figure adapted from Rohini Kuner.²³

- b) Transmission is the next aspect in processing the damaging events. Here, the neuronal information from the periphery is transmitted via A δ - and C-fibres to the thalamus via the spinal cord up to the cortex. While C-fibres tend to respond to mechanical, thermal and chemical stimuli, A δ -fibres react to high-intensity mechanical stimulation and chemical inputs. Once these afferent fibres reach the second-order neurons, the message gets transmitted via spinothalamic tract to the thalamus where the synapses with the third-order neurons are formed and the message is conveyed to the sensory cortex. When the nociceptors terminate in the dorsal horn in the spinal cord, they transmit the signal from periphery by releasing neurotransmitters which, in turn, react with their primary receptors. For example, glutamate and substance P interact with ion channels such as N-methyl-D-aspartate (NMDA)-type and non-NMDA excitatory amino acid receptors, and tachykinin receptor family (GPCRs), respectively.^{20, 23-24}
- c) Modulation is the last and most critical step in the pain processing. Not only it explains why individual responses to the similar painful stimuli may differ, but also why the activation of pain neurons and sensory experience of pain sometimes do not coincide. Probably most importantly, pain modulation elucidates the clinical mechanisms that underlie analgesia. Here, the nervous system responds to the noxious stimuli which can result in either boost (excitatory) or reduction (inhibition) of the transmission of pain impulses.²⁵ This processing of damaging events to higher centres is modified by descending modulatory pain pathways that allow the release of inhibitory neurotransmitters such as endogenous opioids, serotonin, noradrenaline, gamma-aminobutyric acid (GABA), neurotensin, acetylcholine and oxytocin. Although the term “pain modulation” is usually perceived to have an exclusively analgesic connotation, pain modulation can actually lead to both analgesia and hyperanalgesia. As an example – opiates are capable of both; decreasing and increasing the experience of nociception. This example may be further highlighted by a fact that when Watanabe et al.²⁶ gave a small dose of morphine to rats, that relieved the symptoms of pain; however, high doses of the same drug led to painful responses in these animals.²⁶ Thus, opioids can cause recipients to increase as well as decrease the experience of pain.

1.1.2. Inflammatory Pain

This acute pain pathway is usually triggered to induce an adaptive and protective response that helps prevent further tissue damage. Here, we have two kinds of pain: first pain is usually sharp, precisely located, and produces a reflex phasic contraction, and then is second pain – intense, poorly located, prolonged, and creates a reflex tonic contraction. While a stimulus for the first pain may be heat or a pin prick, and is mediated by the fast-conducting A δ -fibres, the second pain comes as a response to a tissue damage which is mediated by C-fibres. However, when injury or inflammation is prolonged, the same nociceptor function might be substantially modified, which sets up changes in the responsiveness in the CNS and sensitize the neurons in the spinal cord, leading to pain of a more chronic nature.^{21, 27} While a nociceptive (acute) pain is a part of the rapid body's defence system, chronic pain serves no known biological function. Pain is classified as "chronic pain" when the symptoms last for longer than 3 months, or when it is associated with a pathological condition that does not heal.²⁸

There are two types of chronic pain: inflammatory and neuropathic pain. Whereas inflammatory pain arises from tissue injury and the subsequent inflammatory response, neuropathic pain is usually caused by spinal cord injury, stroke or multiple sclerosis.²⁹ In both cases, there is change in the balancing excitatory and inhibitory influences within the spinal cord which results in the three fundamental characteristics of chronic pain: hyperalgesia, allodynia, and spontaneous pain. For instance, stimuli that were normally painless can produce pain (allodynia), and noxious stimuli become both exaggerated and prolonged (hyperalgesia).⁷

At the peripheral level, inflammation leads to the release of inflammatory mediators from injured and inflammatory cells. These stimuli include but are not limited to kinins, amines, prostaglandins, growth factors, chemokines and cytokines, proteases, protons and ATP, which together make up an "inflammatory soup." These ingredients first evoke and then sensitize the nociceptors, reducing the threshold for action potential generation and therefore increase responsiveness. As a consequence of the change in the chemical milieu, nociceptors change; they not only detect only the noxious stimuli but also innocuous inputs.

These inflammatory components accomplish this by binding on their respective receptors and produce intracellular signalling that include various targets such as TRPV1 channels, voltage-gated sodium channels Na_v1.7 – Na_v1.9, ASICs, TrkA, P2Y, B1/B2, ILR1 and effector proteins as PKC, PKA, PI3K, and the MAP kinases ERK and p38. Targeting these receptors might be a useful approach for treatment of inflammatory pain.

However, more frequently prescribed drugs for inflammatory pain are non-steroidal anti-inflammatory drugs (NSAIDs) which act as the non-selective inhibitors of COX enzymes (aspirin, ibuprofen). While this inhibition reduces the formation of prostaglandins, and thus leads to an antihyperalgesic effect, the clinical use of such drugs is hampered by serious gastrointestinal side effects.³⁰ To circumvent these issues, the COX-2 inhibitors as well as nitric oxide-releasing derivatives of NSAIDs³¹ potentially provide some means to reduce these damaging effects, however, long-term studies are still in process.³²

1.1.3. Neuropathic Pain

Neuropathic pain is a more maladaptive pain that typically results from damage to the nervous system. Such symptoms are challenging to treat and often resistant to existing treatments, including opioid drugs.⁷ Due to their central activity, these agents are notorious for producing serious adverse effects, including respiratory depression, sedation, euphoria, dependence, and addiction. These effects are especially concerning as they may lead to opioid abuse and opioid—related deaths have risen to epidemic proportions in the United States. Importantly, neuropathic pain is mechanistically unrelated to inflammatory pain where the altered chemical events are in play. Thus, it has to be treated differently.

Ultimately, the burden of neuropathic pain is associated with the imbalances between excitatory and inhibitory somatosensory signalling, altered functions of ion channels and the ways the pain sensitization is modulated in both, the central nervous system (CNS) and peripheral nervous system (PNS). Although there have been numerous definitions used, the most recent points out that neuropathic pain is caused by lesions or defects in either CNS or PNS. While central neuropathic pain is caused by spinal cord injuries and multiple sclerosis, peripheral injuries involve A δ - and C-fibres. Altered sensory fibres impact the transmission of sensory signals that travel up to the cortex hence the pain can be a consequence of diabetes, HIV infection, leprosy, amputation, nerve compression, nerve trauma, “channelopathies” (ion channel dysfunctionalities), chemotherapy and stroke.

Now, chronic pain is being considered among the most devastating and difficult to treat conditions. Due to alterations in CNS and PNS, the patients display a distinct set of symptoms. This includes the pain resulting from non-painful stimuli (allodynia) and severe burning sensations (hyperalgesia), all of which respond poorly to current pharmacological treatment. However, just recently it was suggested that these symptoms not only come as a result of plastic alterations in neurons but also the cells that surround them, known as glial cells.³³⁻³⁴

Here the pioneering results from the Garrison's team³³ suggested that astrocytes and microglia, collectively referred to as glia, can participate in the pathogenesis of pain, and that, crucially, glial activation might be a cause for neuropathic pain.³³

1.1.4. Pathological Role of Non-Neuronal Cells in Chronic Pain

Garrison's results³³⁻³⁴ first came as a surprise, as so far the scientific community thought that chronic pain was only a matter of neurons. Now, we know that several non-neuronal cells such as immune, glial, epithelial, cancer and even bacterial cells influence the pain sensation. These cells achieve this by interacting with nociceptors in either CNS or PNS compartments. Similarly to neurons, the non-neuronal cells release chemical substances that modulate the pain sensation. Since that happens in the proximity of nociceptors, this might either promote or reduce pain depend on the mechanism involved. In the following paragraphs, pain modulation by monocytes, macrophages, T lymphocytes, keratinocytes, stem, cancer and glial cells will be described (**Figure 1.2**).

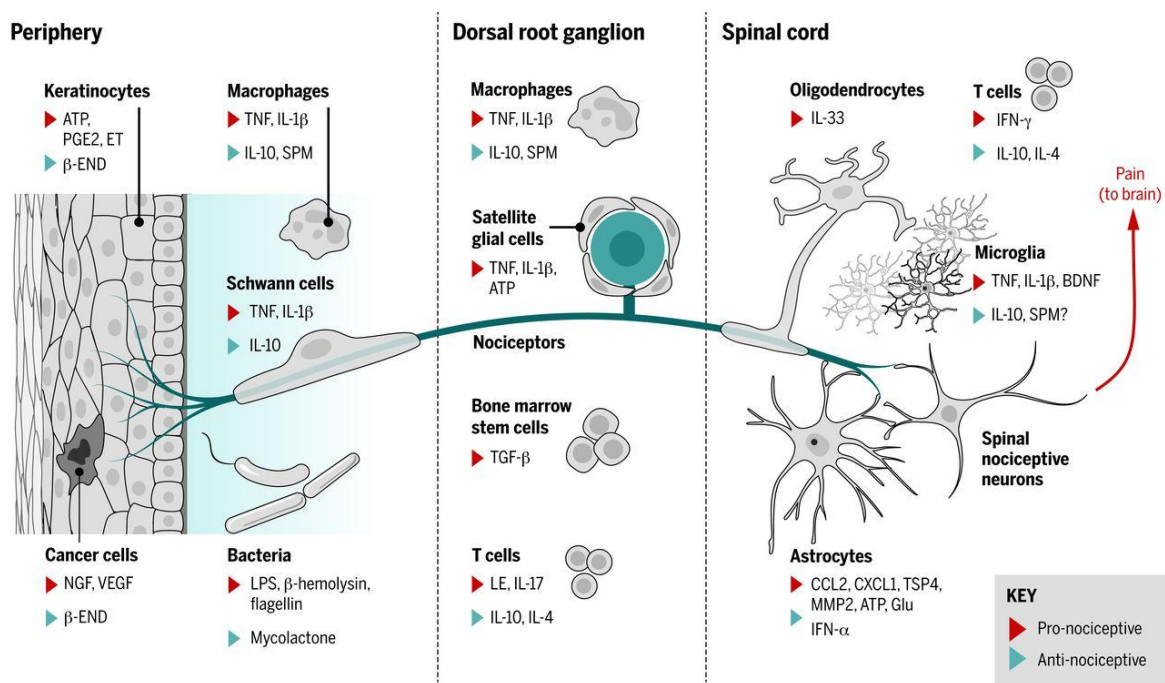


Figure 1.2. Non-neuronal cells interact with the nociceptors. Here you can see how keratinocytes, macrophages, Schwann cells, cancer and bacteria cells at the periphery; macrophages, satellite glial cells, bone marrow stem cells and T cells at the dorsal root ganglion; and oligodendrocytes, T cells, microglia and astrocytes at the spinal cord produce both pro-nociceptive (red) and anti-nociceptive (green) modulators. These include ATP, IL-10, IL-4, IL-33, TNF, PGE2, VEGF, NGF, IFN-γ, TNF-α, BDNF, CCL2, CXCL1, MMP2, Glu and TSP4 which then bind to their respective targets on the nociceptors which in turn effect their sensitivity and excitability (Figure adapted from Ji and colleagues³⁵).

1.1.4.1. Monocytes and Macrophages

In the peripheral system, monocytes and macrophages usually initiate pain through the release of proinflammatory mediators such as tumour necrosis factor (TNF) and interleukin-1 β (IL-1 β). Although there is no evidence that these cytokines have a direct effect on nociceptors, their main contribution is the involvement in production of agents such as prostaglandins, bradykinin, and extracellular protons, also known as “inflammatory soup”. While some of these components can produce thermal hyperalgesia via activation of downstream intracellular signalling pathways through TRVP1 channel, others (extracellular protons and lipids) can function as direct positive modulators of these channels.³⁶⁻³⁷ However, there are some cases that contradict this; while Old *et al.*³⁸ demonstrated that in a chemotherapy-induced neuropathic pain model, monocytes elicit pain indirectly by acting on TRPA1, Peng and co-workers³⁹ showed that in a mouse model of neuropathic pain, deletion of peripheral monocytes did not abolish pain.³⁹

1.1.4.2. T Lymphocytes, Keratinocytes and Bone Marrow Stem Cells

After nerve injury, T cells are abundantly found in the DRG neurons where they release proalgesic mediators, resulting in mechanical allodynia.⁴⁰⁻⁴¹ On the other hand, some other authors suggested this role of T cells is limited only to female mice while male mice seems to depend on microglial signalling.⁴²

Keratinocytes can be found in the epidermis where they reside nearby nociceptors and produce proalgesic mediators such as ATP, IL-1 β , prostaglandin E2 (PGE2), endothelin, and nerve growth factor (NGF).⁴³ One such example is sunburn. Before the sunburn settles, the experience of sun is pleasant since the keratinocytes keep releasing the β -endorphins (endogenous opioid peptides).⁴⁴ However, with the sun overexposure, keratinocytes release endothelin that elicit pain via the activation of TRPV4.⁴⁵

Bone Marrow Stem Cells (BMSCs) elicit many beneficial effects that result in tissue regeneration. Usually they achieve that by secreting growth factors (transforming growth factor- β 1) as a potent anti-inflammatory mediator. Many researchers in the field have shown that either a systemic or local injection of BMSCs inhibits neuropathic pain caused by a peripheral nerve injury.⁴⁶⁻⁴⁷

1.1.4.3. Cancer Cells

Since cancer cells secrete many mediators, including protons, bradykinin, prostaglandins and endothelins, these chemicals activate nociceptors surrounding these abnormal cells. Subsequently, cancer cells release NGF and vascular endothelial growth factor (VEGF), promoting nociceptor excitability and pain hypersensitivity via activation of VEGFR1.⁴⁸ Some other mediators such as TGF- β , secreted by rat mammary gland carcinoma also promote bone cancer pain.⁴⁹ Furthermore, Yang⁵⁰ has shown that, as a result of increased ATP release, P2X7 receptors in spinal microglia are upregulated in bone cancer environment. As a result, mediators such as IL-18 via p38 MAP kinase pathway are released. Interestingly, the same authors showed that by blocking P2X7/IL-18/p38 MAP pathway resulted in reduced bone cancer pain in female rats as a consequence of suppression of hyperactivity in the spinal neurons. However, further studies that would test sex-dependant modulation of microglial signalling in both males and female pain models as well as in the different phases of chronic pain, are necessary.⁵⁰

1.1.4.4. Glial Cells

Since there are many different targets and cellular pathways contributing to the progression of the pain pathology at different times, such a concept required researchers to seek for a “missing link”.⁵¹ One of such was found almost 20 years ago. At that time, the main view was that neuropathic pain following a peripheral nerve injury was the direct result of alterations in neurons and neuronal function in the nervous system.^{2, 20, 52-53} Since then, although not disputed that neurons are essentially involved in neuropathic pain, it is clear that a neuron-centric view to understand pain is an oversimplification and does not justify the diverse network of cell types within the central nervous system.⁵⁴ This came as a response to mounting evidence that glia-neuron interactions are critical in establishing and maintaining neuropathic pain states, and particularly, it is the influence of microglia (the nervous system’s resident immune cells) that is critical.⁵⁵⁻⁵⁶

Although glia have a number of housekeeping functions that are essential for healthy neuronal communication, they also exert neuroprotective effect and serve as immunoresponsive cells.⁵⁴ This realization came as a response to a rapidly growing body of evidence that the activation of microglia contributes to neuropathic pain after nerve injury by releasing the classic immune signals such as ATP, cytokines and chemokines.⁵⁷⁻⁶² In parallel, overexpression of purinergic receptors, namely P2X4, P2X7 and P2Y12, and CX3CL1 has been demonstrated in spinal microglia after nerve injury.⁵⁸⁻⁵⁹

Once these receptors are activated, that results in downstream signalling via p38 mitogen-activated protein (MAP) kinase triggering the release of TNF- α , IL-1 β , IL-18, BDNF, COX and PGE2. These modulators ultimately fine-tune the pain transmission pathways to the cortex.⁶³

Apart from microglia, other glial cells – astrocytes – perform a vast array of functions from neurotransmitter recycling to modulation of synaptic transmission. Some examples include up-regulating CXCL13 in spinal cord neurons and releasing CCR5 to potentiate neuropathic pain after nerve injury;⁶⁴ up-regulation of CX43 leads to release of cytokines that enhance excitatory synaptic transmission in the spinal cord;⁶⁵ and up-regulation of thrombospondin-4 (TSP-4) by astrocytes which promotes chronic pain after a nerve injury.⁶⁶⁻⁶⁷

The last cells that are part of glial group are oligodendrocytes. In a model of nerve injury, oligodendrocytes release IL-33 that modulate the pain hypersensitivity via MAP kinases and nuclear factor κ B (NF- κ B).⁶⁸ Another study confirmed similar results, and pointing out to another factor (platelet-derived growth factor receptor α -PDGFR α) as an important oligodendrocytes-derived mediator in chronic pain.⁶⁹

A few years after those initial findings, Mogil's group⁷⁰ reported that testosterone might act as a control switch for pain pathways. Interestingly, only early in pregnancy, mice seemed to shift from a female-associated, microglia-independent mechanism of pain sensitization, to a more typically male-related one that is linked to microglia. And when the scientists applied testosterone to castrated males, or to females, the pain routes diverted to a microglial-dependent pathway.⁷⁰

But immune cells and hormones don't seem to fully explain pain differences. For instance, Domeier's group⁷¹ has found that women might have a genetic predisposition to chronic pain. Specifically, they investigated a suite of RNA molecules in the vascular system that are elevated in females who experience chronic neck, shoulder or back pain. Interestingly, many of these RNA molecules are encoded by genes on the X chromosome.⁷¹ This may be critical information to have since it would help to develop useful medicines that can be used specifically in females. Since then, the researchers continued to find evidence consolidating the importance of microglia - and the cell's receptors - in male mice experiencing pain. Alongside this phenomenon, some new players have now entered the game.

1.1.5. Expression of Neurotransmitter Receptors on Microglia

After tissue damage, many cells, notably macrophages, neutrophils, and mast cells are recruited and release many inflammatory mediators, including; glutamate, TNF α , IL-1 β , IL-6, NO, bradykinin, NGF, and protons. They can act directly on nociceptors or indirectly through the release of other mediators.^{57, 72-74} These endogenous signals activate a few receptors such as ionotropic (iGluRs) and metabotropic glutamate receptors (mGluRs), GABA_B, purinergic, adenosine, cholinergic, adrenergic, dopaminergic, opioid and cannabinoid receptors.

While iGluRs modulate TNF α release, mGluRs can alter between a neuroprotective and neurotoxic type of microglia phenotype. For example, stimulation of mGluR2 with amyloid β (A β) or chromogranin A peptides, all found in Alzheimer's plaques, involve TNF α and glutamate release that trigger neuronal caspase-3-activation which, in turn, fuel microglial neurotoxicity.⁷⁵⁻⁷⁷ Interestingly, this neurotoxicity can be prevented by activation of mGluR3, suggesting that these type of receptors might act as potential neuroprotective targets.⁷⁸

In addition to iGluR3, another receptors that can reduce the neurotoxicity of activated microglia are agents acting on microglial GABA_B receptors and on cannabinoid CB₂ receptors which stimulation by A β ₁₋₄₀ peptide results in neuroprotection.⁷⁹⁻⁸⁰ Other G-protein coupled receptors that exert anti-inflammatory effects are microglial opioid receptors namely κ - opioid receptors (KORs) and μ -opioid receptors (MORs). While MOR3 activation inhibits microglial chemotaxis and migration, KORs agonists inhibit HIV-1 expression in microglial cell cultures suggesting these pathways to have therapeutic potential in HIV-1 encephalopathy.⁸¹⁻⁸²

Other targets within the GPCRs family of receptors include beta-adrenergic and dopaminergic receptors. While beta-adrenergic agonists suppress microglial proliferation,⁸³ alpha-adrenergic ones such as noradrenaline, reduce microglial activation which in turn modulate microglial inflammatory responses via loss of noradrenergic neurons.⁸⁴ This has implications in Alzheimer and Parkinson's diseases where the loss of control of microglial reactivity is an important hallmark. Along the same lines, the stimulation of cholinergic receptors also seem to promote anti-inflammatory and neuroprotective responses. Independent research from Shytle,⁸⁵ De Simone⁸⁶ and Suzuki⁸⁷ has shown that the microglial activation induced by LPS, IFN- γ or HIV-1 modulate microglial activation via COX-2 and PGE₂, a pathway associated with HIV-associated dementia.

However, while all these targets might show a promising therapeutic potential among HIV-1, Alzheimer's and Parkinson's patients, microglial activation is also implied in chronic pain pathways with the purinergic receptor family as a critical component.^{18, 60, 63, 88-89} Here, we distinguish between P1 and P2 families of receptors.⁹⁰⁻⁹¹ While the activation of P1 or adenosine receptors is more linked to neuroprotection,^{76, 92} the P2 family (P2Xs and P2Ys) has broader impact on microglia. For example, P2Y receptors control the movement of microglia, phagocytosis,⁹³ fine-tunes the release of cytokines and are implicated in treatment for stroke.⁹⁴ On the other hand, P2X superfamily comprises seven subunits (P2X1-P2X7) that share a common topology, but differ in their pharmacological and functional characteristics.¹⁹ Various subtypes are involved in particular functions depending on their distribution and biophysical features, extensively reviewed by North⁹⁵ and Burnstock et al.⁹⁶ These differences present an opportunity for tissue-specific inhibition of one receptor subtype with no functional alteration of others.

Among purinergic P2X family of receptors, two of them – P2X4 and P2X7 are also expressed on microglia. They belong to the family of nonselective P2X cation channels with high Ca²⁺ permeability which, at its most fundamental level, opens in response to the binding of extracellular ATP and triggers transmembrane fluxes of selected ions.⁹⁷ While activation of the P2X7 channel leads to TNF α release and superoxide production, both resulting in microglia activation, P2X4 receptors are upregulated on microglia only during nerve injury.⁹⁸ By activating P2X4 receptors, a brain-derived neurotrophic factor (BDNF) is released, which produces a disinhibitory increase in pain-transmitting nociceptive neurons in the spinal dorsal horn.¹⁷ Strikingly, it was shown that removal of P2X4 receptors prevents the development of mechanical allodynia following the activation of spinal microglia.^{60, 99} This is, in turn, critical for the rewiring that underlies the perception of mild tactile stimuli as noxious. This suggests that P2X4 receptors on microglia might open exciting new avenues for either CNS-related diseases such as neuropathic pain, as well as for diseases such as diabetes and AIDS that affect more peripheral nerve functions.^{60, 100-101}

Yet, as much as it would be comfortable to think that one target might take the pain away, much of the variability in chronic pain and analgesic response is also heritable and sex-specific. After decades of assuming that pain processing is equivalent in both sexes, Sorge and colleagues⁴² showed that chronic pain seems to manifest differently in male and female mice. Their studies suggest that microglia signalling is sex-dependant with p38 inhibitors reducing neuropathic pain in males, but not in female

mice.⁴² No matter how these researchers blocked microglia, this eliminated the pain hypersensitivity in males alone.

That doesn't mean that females were immune to pain, but only that they don't appear to use microglia to become hypersensitive to touch. This suggests that future pain medications should be tailored to individuals and identifies some key factors to consider.

1.1.5.1. Activated Microglia Contributes to Pathological Pain

Importance of pro-inflammatory molecules in the induction of neuropathic pain has led researchers to prevent the binding of these compounds to their receptors. For example, nerve-induced plasticity in the dorsal horn comes as a response of activated intracellular events such as protein kinases, responsible for transcriptional- and posttranscriptional modifications of proteins on the cell membrane.¹⁰² However, the molecular basis by which nerve injury develops tactile allodynia have remained largely unknown. It was thus essential to identify the molecular changes that lead to tactile allodynia in an effort to both understand its mechanisms and develop new therapies.⁵⁶

Soon, various research groups started reporting on mitogen-activated protein kinases (MAPKs), a family of intracellular molecules that are crucial players in chronic pain pathology and consist of extracellular-signal-regulated kinase (ERK, p44/44 MAPK), p38 and JNK.¹⁰³⁻¹⁰⁵ At about the same time, Tsuda et al.¹⁰⁵ reported that development of allodynia following nerve injury involved activated p38 MAPK in microglia. Additionally, blocking p38 MAPK resulted in abolishment of allodynia in their animal models.¹⁰⁵⁻¹⁰⁶ Following that paper, Zhuang and colleagues¹⁰⁶ reported another pathway between MAPK and ERK. In the case of peripheral injury, MAPK-ERK activation in neurons, microglia and astrocytes contribute to allodynia and the inhibition of ERK activation reduced neuropathic pain-like behaviour.¹⁰⁶

All these studies provided clues on which intracellular signalling pathways in microglia might be crucial for allodynia to occur. However, there was still a gap in knowledge regarding how glial cells in the spinal cord are activated and which message is conveyed from neurons to glia after the occurrence of peripheral nerve injury. Until then it hadn't been known that one of the most abundant neurotransmitters in our sensory nervous system – ATP – is released from damaged neurons, and directly acts as a source of stimuli for the astrocytes and glia.¹⁰⁷⁻¹⁰⁸

That gap was then addressed in the pioneering work of Coull et al.¹⁰⁹ where they demonstrated that ATP-stimulated microglia disrupts the inhibitory control of lamina I neurons in the dorsal horn of the spinal cord, leading to a collapse of their transmembrane anion gradient.

This altered gradient then stimulates an inversion of inhibitory GABA currents that are responsible for mechanical allodynia after peripheral nerve injury. Furthermore, the group identified a neuronal protein – called BDNF – as a critical microglial-neuron signalling molecule.⁶³ By blocking BDNF release with interfering RNA before ATP-stimulation, they managed to reduce allodynia.

At about the same time, findings about two ionotropic P2X receptors and metabotropic P2Y in glial cells have gained much interest. The deletion or antagonism of one of them, P2X7, reduced neuropathic pain behaviours in mice¹¹⁰⁻¹¹¹ while P2Y12 was not only found to be upregulated in microglia, but this same increase contributed to the neuropathic pain through the p38 MAPK pathway.¹¹² Similarly, P2X4, was also found to be upregulated in spinal microglia and its blockage decreased neuropathic pain.⁶⁰ However, the molecular mechanism underlying neuropathic pain via P2X4 was tricky to crack.

Soon, the researchers decided to embark on this challenge. They asked whether the activation of P2X4 may also lead to release of BDNF from microglia. Just two years later, Trang et al.¹¹³ demonstrated that in the case of a nerve injury, the influx of Ca^{2+} via ATP-stimulated P2X4 activates p38-MAPK which is required for SNARE-dependant release of BDNF. Here, SNARE stands for Soluble Nsf (N-ethylmaleimide factor) Attachment REceptor. This leads to BDNF-activated TrkB receptors and modifies E_{anion} by downregulating the $\text{K}^+ \text{Cl}^-$ cotransporter KKC2 (K-Cl as potassium Chloride Cotransporter 2), resulting in aberrant nociceptive output that is a hallmark of chronic pain.⁶³ Normally, activation of GABA_A receptors leads to an influx of chloride anions, Cl^- , causing hyperpolarization (inhibition). In this case, the anion flux shifts from inward to outward (E_{anion}) and it becomes negative with regard to the resting membrane potential of the neuron (V_{res}). However, since E_{anion} is now positive with respect to V_{rest} , GABA_A – activation allows an efflux of anions depolarizing the lamina I neurons (**Figure 1.3**).^{63, 113} All these findings pointed to microglia being a powerful modulator of pain after nerve injury and offered a completely new treatment approach, one that is essential in this age of the “opioid crisis”.

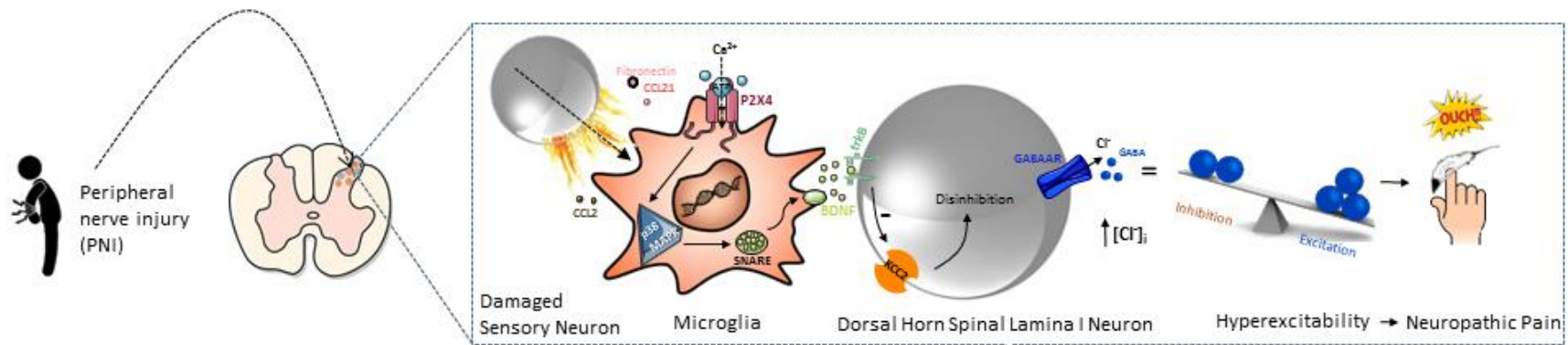


Figure 1.3. P2X4 purinoreceptor signalling in chronic pain. Peripheral nerve injury (PNI) activates microglia in the dorsal horn of the spinal cord. This causes the upregulation of P2X4R expression which is modulated by fibronectin and chemokine ligand 21 (CCL21). CCL2 signalling supports P2X4R trafficking up to the microglial surface. Influx of Ca^{2+} through ATP-stimulated P2X4 activates p38-MAPK and drives the synthesis and SNARE-dependent release of brain-derived neurotrophic factor (BDNF). After BDNF is released, it acts on its cognate receptor, TrkB which consequently downregulates potassium-chloride cotransporter KCC2 expression in dorsal horn spinal lamina I neurons. In turn, intracellular $[\text{Cl}^-]_i$ is increased, which results in the collapse of transmembrane anion gradient in dorsal horn, inducing the depolarization of these neurons. The altered chloride gradient causes the key transmitter GABA to switch its effects from inhibition to excitation. The resultant hyperexcitability in the dorsal horn could underlie the increased sensitivity that is a feature of neuropathic pain.¹¹⁴

1.1.6. Purinergic Receptors

The first suggestion that ATP could be a mediator of nociception came from the work of Pamela Holton¹¹⁵⁻¹¹⁷ in the 50's and it took researchers 30 years to firmly establish extracellular ATP could evoke pain sensation in human and subsequently define the concept of purinergic transmission. Burnstock¹¹⁸ was the first to distinguish purinergic P1 and P2 receptors based on their ligand preference. While the P1 group is activated by adenosine, P2 receptors prefer ATP. Soon after that, the P1 classification was replaced by A, as the research community realized that the preferred agonist for P1 is adenosine (A) rather than ATP. For the P2 group, Burnstock proposed the terms P2X and P2Y, on account of agonist and antagonist selectivity in a variety of tissues.¹¹⁸⁻¹²⁰

At about the same time it was found out that direct application of ATP can cause depolarization of both sensory and spinal neurons via the opening of a ligand-gated ion channel and that ATP acts as a fast excitatory neurotransmitter in central and enteric nervous system.¹²⁰ However, it was only with molecular identification of different purinergic receptors that it became more clear that P2X targets were ligand-gated ion channels and P2Y targets were G protein-coupled receptors.¹¹⁸ Since then, our understanding of P2X has reached a whole new level.

Now we know that P2X channels are typically stimulated by ATP, much less stimulated by ADP, and not activated at all by other similar molecules such as AMP, adenosine, GTP or UTP (**Figure 1.4**). As ion channels, the permeation pathway selectively prefers cations over anions: after ATP application, the channel opens within a few milliseconds, and closes within tens of milliseconds once ATP application is stopped.¹²¹ Ionic currents through homomeric P2X1 and P2X3 channels drop during the application of ATP within tens or hundreds of milliseconds; for P2X4 and P2X2 channels, this drop is seen in seconds or tens of seconds; and for P2X7 channels, a little decline in the currents even over a few minutes could be observed. P2X receptors show complex gating behaviour in which the conduction pathway dilates during several seconds of ATP stimulation from a pore that typically allows only the permeation of small cations (Na^+ , K^+ , Ca^{2+}) to one that lets the passage of larger cations (N-methyl-D-glucamine) and dyes such as 4-((3-methyl-2(3H)-benzoxazolylidene)methyl)- 1-(3-(trimethylammonio) propyl) quinolinium (YO-PRO-1) and ethidium.¹²²⁻¹²³

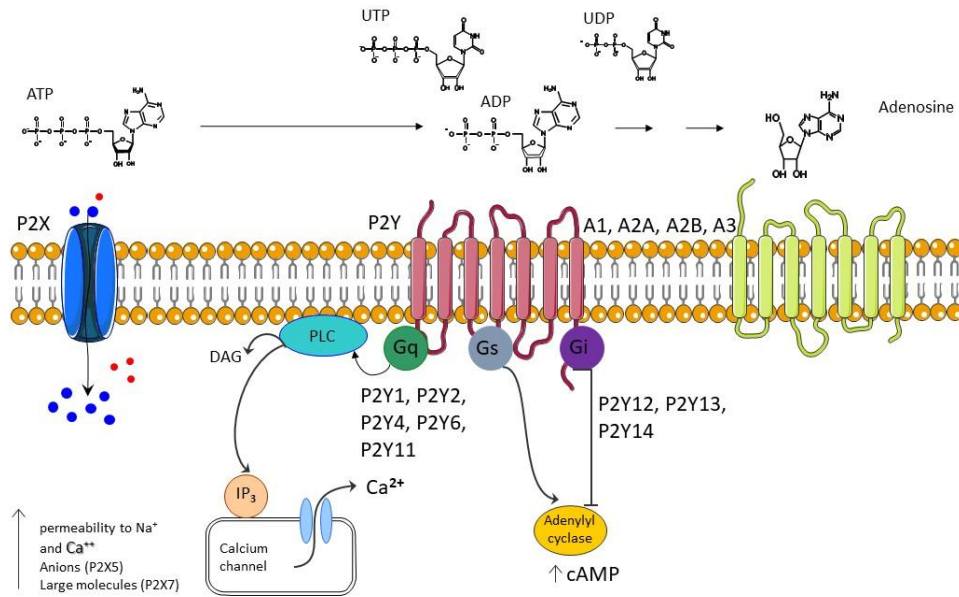


Figure 1.4. Purinergic signalling pathways in chronic pain. Here you can see how nucleotides mediate signalling effect through a series of ionotropic P2X receptors and metabotropic P2Y receptors, which are classified by their affinities towards ATP, ADP and other putative nucleotide and nucleotide-sugar agonists (UTP, UDP).

1.1.6.1. P2X1

Not only are P2X1 receptors expressed in smooth muscles such as arteries, but also in neuronal and glial cells where their inhibition display neuroprotective effects after stroke, thrombosis, and ischemic injury and Parkinson's disease, respectively.¹²⁴⁻¹²⁵ These antagonists include mostly suramin and its derivatives such as competitive antagonist NF449 which displays a nanomolar potency at P2X1 and high selectivity.¹²⁶⁻¹²⁷ Another modulator for P2X1 is RO-1 with low micromolar potency and relatively good selectivity profile when probed against hP2X2, hP2X3 and hP2X2/3.¹²⁸⁻¹²⁹

1.1.6.2. P2X2

P2X2 receptors are found across central and peripheral nervous system, including on many non-neuronal cells where they can form homo- and heterotrimeric channels with P2X3 receptors.¹³⁰ So far, antagonism of P2X2 channels include therapeutic interventions for pain with PPADS, Reactive Blue 2 (RB-2), TNP-ATP and suramin being relatively potent, however, non-selective inhibitors.¹³¹

Some of the suramin and RB2 derivatives such as NF770 and PSB-10211, respectively, showed a potent and selective action towards P2X2, both with a competitive mode of action.¹³²⁻¹³³

1.1.6.3. P2X3

P2X3 receptors forms both, homomeric and heterotrimeric channels usually dimerizing with P2X2, all of which are found on neurons in the central nervous system. Since P2X3 channels have been widely implicated in chronic pain, epilepsy and sleep disorders,¹³⁴ a search for a potent and selective antagonist has been extensively pursued with more than 50 patents filed. Some examples include a competitive inhibitor A-317491 and others allosteric modulators discovered by Roche: RO-3, RO-4 and RO-51, all of which show low nanomolar potency and good selectivity profile versus other P2Xs.¹³⁵ Notably, RO-4 showed a good bioavailability and was thus modified, yielding RO-51, with superior pharmacokinetics properties.¹³⁶ Apart from small molecules, the heptapeptide spinorphin was shown to act as potent (IC₅₀ value of 8.3 pM) allosteric antagonist at P2X3, however, its selectivity profile hasn't been extensively studied.¹³⁷ Recently, however, a potent and selective modulator of the P2X3, purotoxin 1 (PT1) was isolated from spider venom and reported as a promising lead peptide for the development of analgesics inhibiting P2X3 receptors.¹³⁸

1.1.6.4. P2X4

P2X4 receptors are widely expressed in both, the central nervous system and the periphery such as microglia and on endothelial cells. Some potential therapeutic indications include spinal cord injury, epilepsy, stroke, multiple sclerosis, Parkinson's and Alzheimer's disease.^{17, 60, 139-140} A variety of modulators have been developed towards P2X4s - this will be discussed in the next subsection.

1.1.6.5. P2X7

P2X7 expression is upregulated on macrophages, mast cells, microglial cells and oligodendrocytes where P2X7R has been shown as a promising target for a vast number of pathologies. These range from chronic pain, neuroinflammatory diseases, multiple sclerosis, neurodegenerative disorders, cerebral ischemia, brain and spinal cord injury to cancer, depression, anxiety and bipolar disorders.^{124, 141-143} Thus, it comes to no surprise that much effort has been put in the development of selective P2X7 antagonists. Some of the examples include A438079, A740003, A804598, A839977, AZ1060612, AZ11645373, GW791343, GSK1482160, JNJ-47865567 and JNJ-42253432 as reviewed by Baudelet and others.¹⁴⁴⁻¹⁴⁸ All of them show potency in the low nanomolar concentration range and high selectivity among other P2X subtypes. Furthermore, a few clinical investigations have been carried out with P2X7 antagonists, namely AZD9056 and CE-224,535, however, unsuccessfully.¹⁴⁹⁻¹⁵⁰

While it's clear that many new pharmacological tools to study P2X receptors are available now, the quest for developing a potent, yet, selective ligand continues. Although X-ray structures for P2X4 exist (**Figure 1.5**), there is scarce structural information about ligand recognition in this class of purinergic receptors. Moreover, there are currently no ligands that would be species-selective for this class of receptors.¹⁵¹

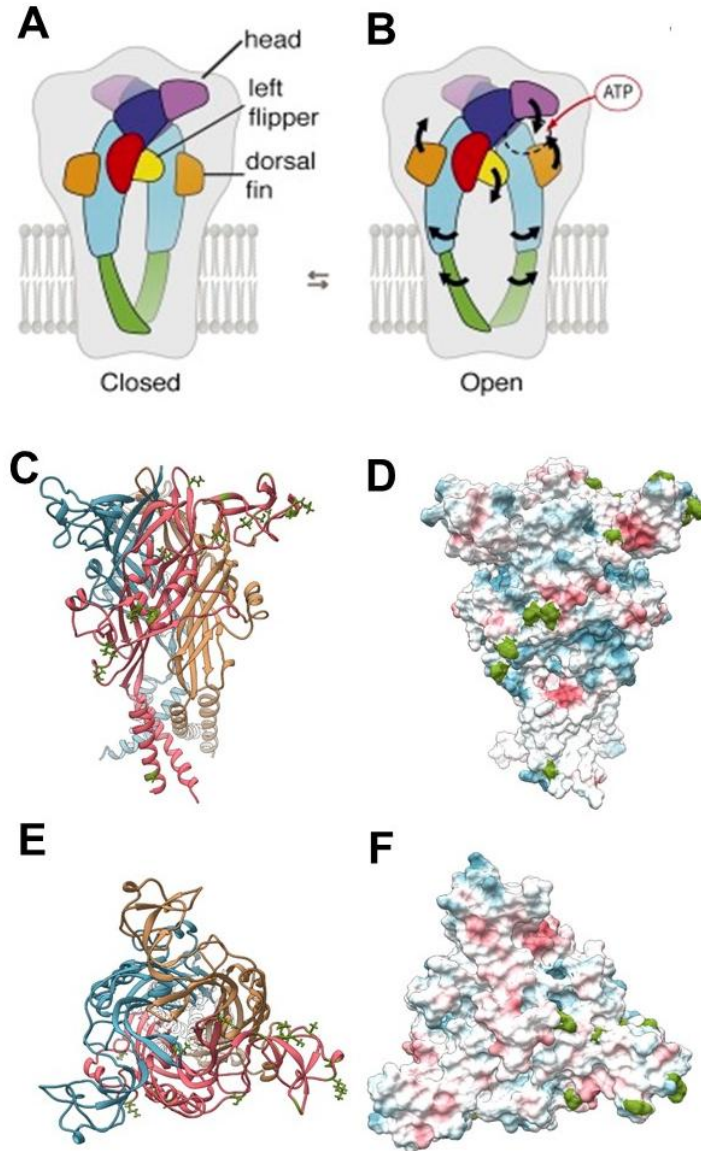


Figure 1.5. P2X4 receptor structure based on PDB ID 4DW1. **A:** A two dolphin-shaped subunits are shown. **B:** The arrows direction show the ATP binding. This is related with the upward movement of dorsal fin (*orange*), head's downward movement (*purple*) and a retraction of the left flipper (*yellow*). **C,D:** Stereoview of the homology model of the human P2X4 based on the homotrimeric zebrafish P2X4 that is seen parallel to the cell membrane. Each subunit is represented in different colour. The green spots represent potential binding sites. **E, F:** Stereoview of the homology model of the human P2X4 based on the homotrimeric zebrafish P2X4 that is viewed from the extracellular side of the membrane. Figures that are shown on A, B are taken from North *et al.*¹⁵²

1.1.7. Pharmacology of P2X4

In seeking to understand the gap between the current pain mechanisms and pharmacological tools targeting P2X4, we have to recognize that pinpointing native P2X4 channel responses within intact preparations, for example brain slices, has been recognized as difficult. First, no selective P2X4 agonists for use in rodents are reported, making it challenging to detect P2X4 receptor-expressing cells based on function.¹⁵³ This is even more complicated by the fact that ivermectin, acting as a potent allosteric modulator at P2X4,¹⁵⁴⁻¹⁵⁶ has actions on other receptors as well and that pose limitations in its usefulness as a selective P2X4 probe in multicellular preparations.¹⁵⁷ Second, the brain cells expressing P2X4 are sparse, making it trickier to achieve targeted electrophysiological recordings.¹⁵⁸

On the other hand, while the majority of the commercially available P2X4 antibodies target intracellular epitopes and may not be specific enough to be useful in live tissues, a recent study from Williams and colleagues¹⁵⁹ found an anti-P2X4 mAb IgG#151-LO that has a high selectivity for human P2X4. Furthermore, that same mAb produces a complete and potent block of the ion channel current. Interestingly, site-directed mutagenesis revealed that inhibitory mAbs binds to the head domain of P2X4 and that systematic delivery of an anti-P2X4 mAb showed analgesia in a mouse model of neuropathic pain.¹⁵⁹

A few serotonin reuptake inhibitors were studied against P2X4 such as paroxetine and amitriptyline. While paroxetine showed anti-allodynic effects with its potency in a low micromolar range at both, rat and human P2X4,¹⁶⁰ amitriptyline (clinically used for treating neuropathic pain) inhibited P2X4 only weakly.¹⁶¹ Another drug, N,N-diisopropyl carbamazepine, also displayed a low micromolar potency at human P2X4, but was less potent at rat and mouse. Additionally, this same compound did not display any preferential selectivity towards P2X4 when assayed against P2X1 and P2X3.¹⁶²

Other P2X4 inhibitors include a large polysulfonated compound suramin and pyridoxalphosphate-6-azophenyl-2',4'-disulfonic acid (PPADS), however, acting as the broad P2X antagonists. Despite some promising attempts to decipher the structural hallmarks within P2X4 channel in order to yield the more selective PPADS analogues,¹⁶³ their poor selectivity against other P2Xs still remains an ongoing issue and hampers their therapeutic potential.

Other compounds that have made the list as P2X4 antagonists are 5-BDBD,¹⁶⁴ BX430,^{153, 165} PSB12054, PSB12062¹⁶⁶ and NP-1815-PX (**Figure 1.6**).¹⁶⁷

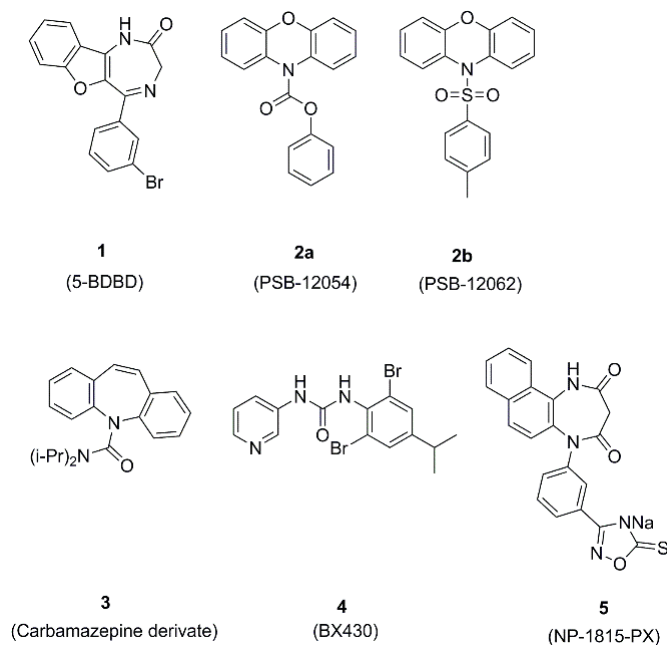


Figure 1.6. P2X4 antagonists.

However, the potency of 5-BDBD to inhibit P2X4 was similar to TNP-ATP, a nonselective P2X antagonist (IC_{50} ranges between 1 – 10 μ M among different labs) and its selectivity against other P2X receptors is described in the patent which experimental details are not available.¹⁶⁸ Although 5-BDBD showed a competitive mechanism, the very low water solubility has hindered any further clinical investigation.¹⁶⁹ A similar water solubility problem was noted with PSB12054 which exhibited an IC_{50} of 0.189 μ M at hP2X4 with similar potency at rat and mouse P2X4. Despite being the most potent antagonist at hP2X4, showing between 30- and 50-fold selectivity for hP2X4 versus the hP2X1, hP2X2, hP2X3 and hP2X7, its high lipophilicity remains an on-going issue for the oral drug delivery chemists.

A more water soluble analogue is PSB12062 which was developed as noncompetitive antagonist with submicromolar potency (IC_{50} 1.38 μ M and 0.54 μ M, respectively) and show selective inhibition of P2X4 when compared to other P2Xs. However, while PSB12062 exhibits effects at rat and mouse P2X4 (IC_{50} 0.928 μ M and 1.76 μ M, respectively), BX430 – another P2X4 antagonist – displayed no effect on rat and mouse P2X4. On top of that, its low water solubility hinders its use in many experimental conditions. Until 2016 no P2X4-selective inhibitor that would display high potency, an acceptable water solubility, decent selectivity, and analgesic effect in rodent chronic pain models has been identified. Then, NP-1815-PX was discovered.¹⁷⁰

NP-1815-PX has a slightly improved solubility and can inhibit rodent and human P2X4 with high potency and selectivity. Moreover, that same compound was the first P2X4 that exhibited anti-allodynic effects in female mice chronic pain models, without any alterations in acute physiological pain responses. This not only supported the hypothesis that microglial P2X4 could be a potential target for treating chronic pain but also highlighted NP-1815-PX as a therapeutically beneficial antagonist.¹⁷⁰ Despite all these highs, the authors note that NP-1815-PX is not suitable for oral delivery and that an intrathecal regime has to be employed for *in vivo* studies.

Just recently, Beswick and colleagues¹⁷¹ undertook a fragment-base pharmacological screening of a few hundred compounds. After coupling their method with computational modelling, clustering and SAR selection, they identified 80 hits that showed an inhibition effect on P2X4. From that group, 20 compounds were capable of inhibiting P2X4 with >50% inhibition in fluorescence-based assays, however, the team was unable to validate these results in electrophysiological assays. Their study highlight the challenge of identifying P2X4 ligands and suggest using a variety of complimentary approaches to confirm ligand activity at this receptor.¹⁷¹

The same authors also note that - so far - only two molecular entities have entered the clinical development: NC600 and Bayer's unnamed P2X4 antagonist.¹⁷¹ It would be interesting to see how these results could be translated to human patients.

1.2. Animal Venoms: a Rich Source of Novel Ion Channel-Targeted Compounds

As discussed before, the receptors responsible for transmitting pain information include G-protein coupled receptors (GPCRs), ion channels (voltage or ligand gated) and tyrosine kinase receptors. In this section, I would focus on targeting ion channels with animal venoms in general and then draw your attention to the ligand-gated ion channels, with purinergic P2X4 in particular.

1.2.1. Ion Channels as Drug Targets in Chronic Pain

Ion channels are membrane proteins that allow the flow of ions across biological membranes. Since the membrane consists of phospholipids with its hydrophobic and low dielectric barrier, hydrophilic and charged molecules find it challenging to pass through this electrical insulator. Ion channels have been equipped with a pore structure that forms a high conducting, hydrophilic pathway across the membrane. This pore structure, or the channel, helps to catalyse the movement of charged molecules across a low dielectric medium and can be either open or closed. An external modulator can induce a conformational change between closed and open state, which is known as gating.¹⁷²

According to which chemicals or physical modulators control ion channel's gating activity, we classify channels into different groups:

- Voltage gated channels (Na_v 1.7, Na_v 1.8, Na_v 1.9, K_v , TREK, TRAAK, ASIC, Ca_v , Ca-activated Cl^- and TRP channels)
- Ligand gated (nAChRs, GABA-A, glycine, serotonin, NMDA, AMPA, Kainate, P2X)
- Others (second messenger gated channels nucleotides, G-proteins, mechanosensitive channels, membrane curvature, gap junctions, porins)

The major difference between the two major groups – voltage and ligand gated channels is that the voltage gated channels open in response to voltage (when the cell gets depolarised or hyperpolarised), whereas ligand gated channels open in response to a ligand binding to them.¹⁷² In response to nerve injury, dysregulated voltage-gated ion channels cause enhanced neuronal excitability and alter pain signalling by primary afferent fibres.

By targeting the mechanisms that shape the firing properties of primary afferent fibres that play pivotal functional role in chronic pain pharmacology, poises voltage-gated ion channels as attractive targets.¹⁷³⁻

174

In the neuropathic pain field, the sodium-gated (Na_v) ion channels are of particular interest. They are classified into nine different isoforms with $\text{Na}_v1.3$, $\text{Na}_v1.7$, $\text{Na}_v1.8$ and $\text{Na}_v1.9$ being considered as valid targets for pain pharmacotherapy, with an extreme focus on $\text{Na}_v1.7$. This is mainly due to a dramatic discovery in 2006 where James Cox and Geoff Woods¹⁷⁵ showed that loss-of-function recessive mutations in $\text{Na}_v1.7$ resulted in inherited inability to experience pain.¹⁷⁵ Since their genetic study has established a very strong validation for the efficacy to reduce both inflammatory and neuropathic pain, an intense interest in developing inhibitors for $\text{Na}_v1.7$ followed. Soon, hundreds of patent applications were filed and clinical trials attempted.¹⁷⁶ Importantly, all these channels have been initially categorized using tetrotoxin (TTX). The TTX-sensitive channels are primarily found in mammalian brain and skeletal muscle ($\text{Na}_v1.1 - \text{Na}_v1.3$, $\text{Na}_v1.4$, $\text{Na}_v1.6$, $\text{Na}_v1.7$) and the TTX-resistant receptors are either located in heart ($\text{Na}_v1.5$) or sensory neurons in peripheral ganglia ($\text{Na}_v1.8$ and $\text{Na}_v1.9$).¹⁷⁷⁻¹⁷⁸

Toxins from scorpions, sea anemone, cone snails and spiders have significantly contributed to the understanding of the pharmacology of sodium channels and their physiological role in the nervous system. So far, animal kingdom-derived toxins act as sodium channel prolongers, activators and blockers. These toxins might come from spiders (δ -atracotoxins, δ -palutoxins, μ -agatoxins, hainatoxin-I, protoxin-II), cone snails (δ -conotoxins, μ -conotoxins, κ -conotoxins), scorpions (α -toxins, β -toxins, Cn-11) and sea anemone's short inhibitory toxins.¹⁷⁹ For example, peptides from the spider venoms such as JZTX-I and -III, δ -atracotoxins Ar1 and Hv1, Magi4 and -5, hainantoxin-IV, ceratoxins (CcoTx1-2) and phrixotoxin 3 (PaulTx3)^{177, 180-181} are some of the peptide modulators of the sodium channels with PaulTx3 as the most potent one (IC_{50} of 0.6 nM against $\text{Na}_v1.2$).

While the toxins acting on $\text{Na}_v1.8$ and $\text{Na}_v1.9$ might reduce neuropathic pain, the bitter irony is that they only provide limited relief due to inhibiting multiple Na_v channels isoforms. These toxins as well as other sodium channel blockers were proved to be effective analgesics, however, a critical problem is their lack of specificity.¹⁸² For example, ProTx-I and -II not only showed $\text{Na}_v1.8$ inhibition,¹⁸³ they also demonstrated inhibition against potassium and calcium channels. This non-specificity not only results in reduced efficacy but also in dose-limiting side effects since these peptide toxins might induce an autoimmune response. Tailoring more specific inhibitors has been a holy grail of pain research and the hunt for a selective blocker of these specific sodium channels still continues.¹⁸⁰

Another important voltage-gated regulators are potassium and calcium channels. Unlike other animal peptide toxins from the snakes, bees, scorpions or sea anemones blocking K_v1 or K_v3 channels, toxins from the spider venoms with the selective affinities towards K_v2 and/or K_v4 are very useful for the development of cardiac drugs. For instance, hanatoxins 1 and 2 (HaTx 1-2), heteropodatoxins (HpTx 1-3), phrixotoxins (PaTxs) and others (HmTx1-2, ScTx1, TLTx1) serve as interesting tools for characterization of potassium channels in cardiac physiology.¹⁸⁴ Apart from potassium channels, spider peptide toxins such as ω -agatoxins (AgalA-IVA), SNX-482 or -325, GSTxSIA, Huwentoxin-I and -X, DW13.3, ω -PTx-IIA, PTx3-6, and MYIIA demonstrated to be modulators of non L- and N- type of Ca^{2+} channels, respectively. The latest, MYIIA was found in the venom of the cone snails *Conus magnus* and later approved by FDA as a drug against chronic pain (ziconotide).¹⁸¹

Another group of voltage-insensitive cation channels permeable to sodium that are involved in the pain pathway are acid-sensing ion channels (ASICs). While many small molecule ASIC modulators were discovered, their low potency and poor selectivity make them less ideal probes in studying these channels. On the other hand, extensive screening of venoms in search of new modulators that target ASICs yielded toxins from spiders, sea anemones and snakes. After the first ASIC-modulating toxin called Psalmotoxin1 (PcTx1) from *Psalmopoeus camberidgei* tarantula was described,¹⁸⁵ others from spiders (Hm3a, Hi1a), sea anemones (APETx-2, PhcrTx1) and snakes (mambalgin-1, -2 and -3, MitTx, α -DTx) followed. Due to their effectiveness, lack of toxicity and fairly good selectivity profile, these toxins overcome the limitations of the small ASIC modulators, provide a better understanding of their pharmacological functions and might have valuable therapeutic value as well.

Other peptides from the animal venoms demonstrated to act on either glutamate receptors (PhTx3-4), or purinergic P2X3 receptors (PT-1)¹³⁸ all of which are associated with nociception. Although the transmembrane topologies of P2X receptors are similar to ASIC, the primary amino acid sequences, folding of ECT domains and quaternary architecture are entirely different. As there is little investigation whether spider venom contains peptide modulators of other P2X receptors, including P2X4, it would be interesting to probe these channels with different spider venoms.^{181, 186}

1.2.2. Spider Venom Toxins

Natural products have a storied past as drug leads. For example, it was estimated that ~50% of all drugs in clinical use are of natural product origin.¹⁸⁷

For example, natural products gave rise to drugs such as penicillin and morphine, and acknowledged with the 2015 Nobel Prize in Medicine for the discovery of two revolutionary therapies based on natural compounds, Avermectin and Artemisinin.¹⁸⁸ While it is fair to assume that we have raided the traditional pharmacopoeias from cultures all around the world and screened huge collections of natural product libraries, the biological and chemical space still remain to be explored. This especially holds true for the animal venoms. For example, among countless venoms, spider venoms represent an almost infinite pharmacological landscape with a conservative estimate of 200 peptides per venom, leading to a total of 9 million spider venom peptides. So far there are >45 000 extant species of spiders, however, only 0.01% of this substantial resource has been explored. This provides a massive scope, yet to be tapped.¹⁸⁹⁻¹⁹¹ Several research groups consider animal venom toxins as a reliable natural source for discovering new medicines.¹⁹²⁻¹⁹³ A classic example of a venom-based drug is the success story of Bristol-Myers Squibb captopril. This angiotensin-converting enzyme (ACE) inhibitor originated from the poisonous Brazilian viper and has since transformed cardiovascular treatments.¹⁹⁴ While the majority of currently approved treatments have been developed from snake venoms, the advances in high-throughput screening (HTS) provide efficient drug discovery mining of venom toxins from species, which unlike snakes, yield venom in small quantities.¹⁹⁵⁻¹⁹⁷ For example, the venom repertoire of spiders are estimated to contain more than 10 million compounds available for screening.¹⁹⁵

These spider venoms comprise complex cocktails of bioactive molecules with a wide range of molecular weights (0.1 – 14 kDa) and contain a high diversity of inhibitors with high affinity and selectivity that modify the function of physiologically relevant targets such as ion channel and other cell receptors. Still, the majority of them – 88% – are ion channels modulators. For example, more than 268 modulators of ion channels are currently listed in the ArachnoServer, a database¹⁹⁸ that shows the latest snapshot of toxins from spider venom, targeting ASICs, Ca_v channels, K_v channels, Na_v channels, and transient receptor potential (TRPV1, TRPA1). But only a limited amount of studies investigated whether spider-venom peptides might target P2X channels. Recently, however, PT1 – a potent and selective antagonist of the P2X3 – was isolated from spider venom and reported to be a promising peptide for the development of antagonists towards P2X3 channels.¹³⁸ It is this evolved biodiversity that makes venom peptides an invaluable research tool, unique source of leads, and structural templates from which a new generation of drugs might be developed.^{189, 199-200}

Venoms usually comprise a mixture of protein and peptides, polyamines, acylpolyamines, salts and organic components (<1kDa), such as amino acids (GABA, glutamate, and taurine), biogenic amines (histamine), nucleosides (adenosine), nucleotides (ATP), neurotransmitters (acetylcholine)^{195, 201-202} and enzymes. Some of these enzymes include collagenase, hyaluronidase, phospholipase A₂, SMase A and various proteases. Kuhn-Nentwig and colleagues²⁰³ proposed that their main role is to degrade either the extracellular matrix or the cell membrane. With the exception of enzymes, spider-venoms also contain proteins that are smaller than 12 kDa. One of them is α -Latrotoxin which binds to the nonspecific presynaptic nerve terminal, causing a massive exocytosis of synaptic vesicles which mechanism still needs to be fully elucidated.²⁰⁴

From all of these compounds found in spider venoms, acylpolyamines and peptides represent two thirds of the dry weight of the spider venom. Furthermore, these two major classes of molecules have been previously found to target mammalian receptors and display a potential therapeutic use.

1.2.3. Polyamines and Acylpolyamines

Back in 1980 it was first reported that tarantula venoms contain four different polyamines – spermine, spermidine, putrescine, and cadaverine, with spermine as the major component (**Figure 1.7**).²⁰⁵ Now we know that several types of ion channels are influenced by these polyamines. These include: the inwardly-rectifying potassium (Kir) channels,²⁰⁶⁻²⁰⁷ glutamate receptors (NMDA, AMPA),²⁰⁸⁻²¹⁰ and kainite and transient receptor potential cation (TRPCs) receptors.^{67, 209} While intracellular polyamines modify the intrinsic gating and rectification of Kir channels by directly occupying the ion channel pore,²⁰⁶⁻²⁰⁷ extracellular polyamines stimulate NMDA receptors increasing the size of the NMDA receptor currents.²⁰⁶ On the contrary, TRPC4 and TRPC5 are strongly inhibited by intracellular polyamines, particularly spermine.⁶⁷

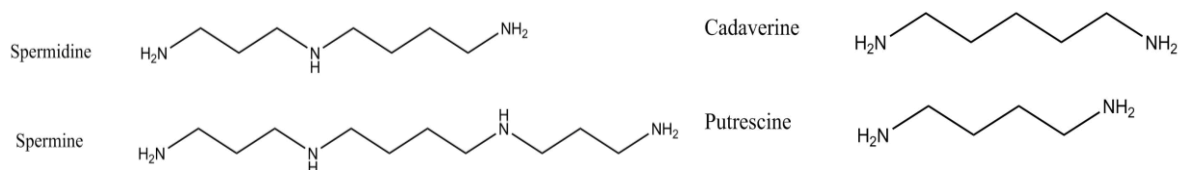


Figure 1.7. Four different types of polyamines.

While polyamines are cationic compounds with two or more primary amino groups – NH₂ –, the common structure of spider acylpolyamines contains an aromatic moiety at one end and either a primary hydrophilic amino group, or a guanidine group at the other. After acylpolyamines were first characterized from spider venom, they were found to block ligand-gated ion channels in mammalian nerve cells and found to block postsynaptic glutamate receptors in these cells (**Figure 1.8**).^{181, 211} Furthermore, Sorkin et al.²¹² found that JSTX-3 can impair allodynia via Ca²⁺-permeable AMPA receptors *in vivo*.²¹¹⁻²¹²

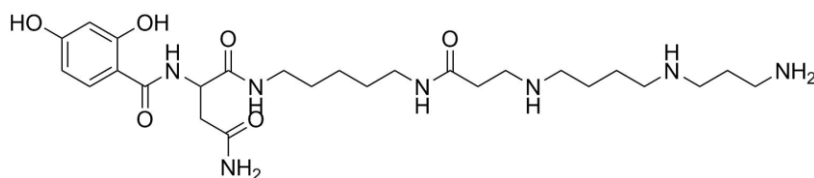


Figure 1.8. The structure of Joro spider toxin (JSTX-3).

1.2.4. Spider-Venom Peptides as Pharmacological Tools and Potential Therapeutic Leads

The journey from natural product discovery to therapy is, initially, largely focused on natural peptides. In particular, peptides found in venomous organisms are a very attractive source for drug discovery research.¹⁸⁷ That is mainly due to their nanomolar affinities which makes them not only good pharmacological tools for understanding the physiological role of the ion channels but also promising leads for the development of novel therapeutic agents.¹⁹⁶ Furthermore, their high potency in the insect nervous system renders them as probes for novel insecticide targets or genetically engineered microbial pesticides.¹⁹² Successful examples of drugs developed from venom peptides include the anti-hypertensive Captopril®, based on a venom peptide from the Brazilian viper; anti-diabetic agent *exenatide* (Byetta®) from Gila monster venom; and the painkiller *ziconotide* (Prialt®), found in the cone snail.¹⁹² Many other spider venom-derived peptides are in various stages of preclinical or clinical development.²¹³

Venomomics has therefore emerged as an attractive approach to modern drug discovery. Particularly, the high potency and specificity of many venom-derived peptides, their possibility of chemical synthesis and recombinant production, and the proteolytic stability of many disulphide-rich peptides makes them an increasingly valuable source of lead molecules.^{193, 195}

However, some spider venoms also contain small cytolytic peptides without any disulphide bridges and with high degree of cationic charge. It's been suggested that they potentiate the action of disulphide-rich neurotoxins by breaking down anatomical barriers, dissipating transmembrane ion gradient and perturbing the membrane potential across excitable cells.^{203, 214}

While a lot has been known about their mechanism of action on these channels, very little is known about the structure of spider venom peptides. Most spider venom peptides have a mass of 3.0 to 4.5 kDa (**Figure 1.9**). However, according to the Arachnoserver,¹⁹⁸ there is also a significant fraction with a mass of 6.5 to 8.5 kDa (composed of 58 to 76 amino acid residues). Nearly 90% of them conform to the single structure class, known as the inhibitor cysteine knot (ICK) motif. Here, the ICK motif is defined as an antiparallel β sheet stabilized by a cysteine knot, containing a ring formed by two disulphide bridges and the intervening sections of peptide backbone with third disulphide bond piercing the ring to create a pseudoknot. The ICK motif is what provides these peptides with exceptional chemical, thermal and biological stability; they are resistant to extremes of pH, organic solvents, high temperatures and, most importantly, proteases. For example, their half-life has been several days in human serum (which is in stark contrast with marine cone snails and scorpion demonstrated to be longer than 12 h in gastric fluids.²¹⁵ Whereas post-translational modifications-venom peptides are rare in spider-venom peptides, disulphide bonds and C-terminal amidation are frequent.²⁰³

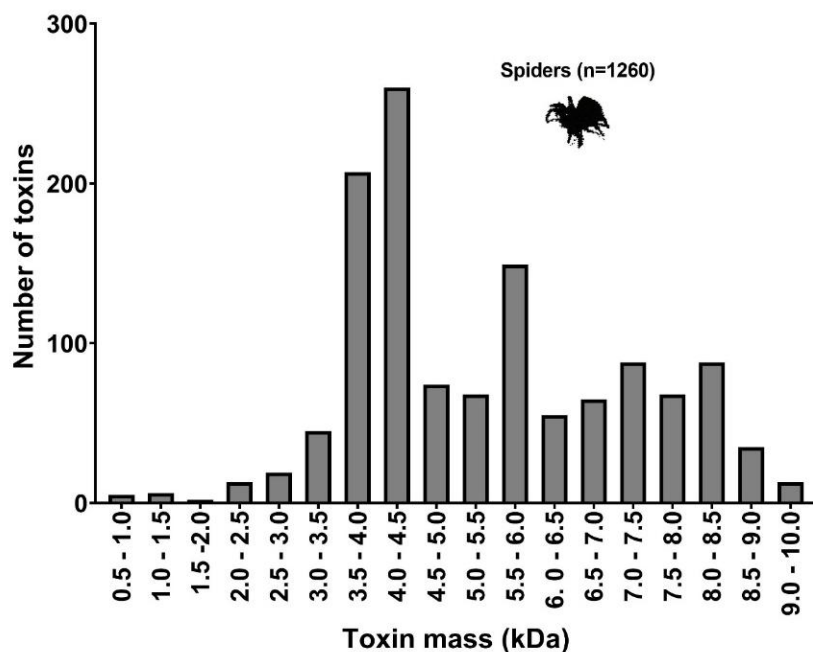


Figure 1.9. Mass distribution of spider venom peptides. All data was taken from ArachnoServer (<http://www.arachnoserver.org>). Databases were accessed on May 2019 and sorted into 500-Da bins.

1.2.5. Isolation, Characterization, Production and Structure Determination of the Toxins

Despite all the exciting progress in the field, the systematic isolation and characterization of bioactive fractions is still not straightforward. However, major advances in high-throughput screening (HTS) and structural characterizations of the venom peptides now facilitate venom-based drug discovery. Some of the HTS repertoire include more traditional assays such as electrophysiology, absorbance/fluorescence based assays, radioligand binding and ELISAs, as well as more recent developments, such as AlphaScreen and label-free, fluorescent-resonance energy transfer (FRET), fluorescent polarization and bioluminescent resonance energy transfer (BRET).¹⁹⁶

Whereas patch-clamp or voltage-clamp electrophysiology is regarded as the gold-standard assay for assessing the functional activity of ion channels, they often require a high level of expertise and are used in low-throughput format. On the other hand, fluorescent-based assays are robust and easily set up. In recent years, a fair portion of fluorescent dyes has become available for measurement of intracellular calcium, sodium, potassium and chloride ions. The fluorescent properties of these dyes can be altered by the binding of their cognate ions. For example, calcium-sensitive (Fura-2 QBT™, FLIPR® Calcium 6) dye generally give the most robust performance due to the large Ca²⁺ gradient across cells. For that same reason, Fura-2 AM can be utilized for many targets, including voltage-gated and ligand-gated ion channels as well as GPCRs.¹⁹⁶

Once an active fraction of the venom has been identified via bioassay, the isolation and characterization of the compounds is carried out. These initial steps combine RP-HPLC to separate molecules by hydrophobicity followed by ion exchange HPLC to separate by charge. Usually, these two separation are sufficient for obtaining pure peptides for amino acid sequence analysis by Edman degradation.^{183, 191, 196, 216} The molecular weight of the fractions is then analysed directly by MALDI-TOF, LC-MS or MS-MS, however, mass counts provides only limited information in regards to biological activity. Indeed, they can provide hints as to which toxin class a peptide might belong, but in order to fully exploit this, we need to know the structure of the peptide. Determination of the amino acid sequence thus enables us to produce the peptide via chemical synthesis or recombinant production. Moreover, this also provides the material for further characterization. According to Vetter *et al.*¹⁹⁶ venom peptides can be best expressed in *E.coli* (periplasmic expression) or yeast (*Pichia pastoris*) with chemical synthesis (solid-phase peptide synthesis, SPPS) coupled with native chemical ligation, serving as a backup.

Recombinant protein production is generally more time- and cost-effective than SPPS and it enables isotopic ^{13}C labelling for multidimensional NMR structural analysis.¹⁹⁶

As the direct interactions between a toxin and a channel are challenging to probe in experimental settings, the complex can be examined in atomic detail using computation methods. Rosetta is one of the most widely used and successful algorithms for *in silico* molecular modelling that was used on various peptides spider toxins. Additionally, Rosetta has recently been upgraded to model and design post-translational modifications, such as hydroxylation, sulfation, and others commonly found in venom peptides.²¹⁷

1.3. Motivation and Objectives of the Thesis

It is clear that spider venoms toxins might be used as a platform of novel compounds to probe hP2X4 function in chronic pain. With one fifth of human population suffering from chronic pain and without any suitable treatment for chronic neuropathic pain, exploring ion channels such as P2X4 with spider venom toxins might be a way to go. Since P2X4 has one of the poorest pharmacological profiles in the purinergic receptor family with only a few small molecules (5-BDBD, PSB-12062, BX-430, NP-1815-PX) targeting it, investigating new leads from spider venoms might offer the potential of mining this gap. This project will examine whether spider venoms contain small molecule and/or peptide modulators of P2X4 as well as other P2X receptors.

Research aim 1: Develop high-throughput fluorescent-based screens to accelerate discovery of P2X inhibitors from animal venoms

As part of this aim, I would attempt to design and develop three fluorescent-based high-throughput screening (HTS) cell assays that can be used to screen animal venoms against human P2X3, P2X4 and P2X7 when applied to a collections of 180 crude venoms. These HTS assays would be validated, both analytically and pharmacologically. Ideally, these *in vitro* platforms would be capable of screening multiple venoms against multiple targets, improving testing characteristics, all while minimizing the costs, specimen material, and testing time. Some of the methods that would be used here are: RP-HPLC, MALDI-TOF, fluorescent-based assays and HTS platforms.

Research aim 2: Identify the small molecules from the spider venoms that inhibit hP2X4 responses and probe their specificity towards hP2X4

Here I will try to isolate, purify and pharmacologically evaluate the toxins that may show a potential to inhibit hP2X4. Furthermore, a structural elucidation of the toxins alongside pharmacological evaluations would be carried out. To explore the specificity of the toxins, a variety of channels such hP2X3, hP2X7, NMDA 1A/2A, rP2X4, mP2X4 in different cell lines, including a mouse microglial model, would be employed. Some of the methods that would be used here are: RP-HPLC (analytical and preparative), MALDI-TOF, MS-MS, LC-MS, NMR, ChemSpider, MS-FINDER, fluorescent-based assays and HTS platforms.

Research aim 3: Chemical synthesis of the toxin's analogues, preliminary structure-activity relationship studies and evaluation of the potential binding sites on hP2X4

This aim would explore the structure-activity relationship (SAR) of the toxin that acts on the hP2X4, and the chemical synthesis of the toxin analogues would be attempted. The potential binding site of the toxins would be evaluated by the *in silico* docking and validated by mutagenesis experiments. Some of the methods that would be used here are: NMR, IR, organic synthesis, fragment-based screening, Chimera, AutoDock, PCR, site-directed mutagenesis, fluorescent-based assays and HTS platforms.

Research aim 4: Translate my research into an educational virtual reality game

I believe that science communication is essential for scientists. To develop engaging communication tools for my topic of research, I chose virtual reality (VR) as the educational tool to present, communicate, increase awareness, and educate the public, as well as the high school students, on the application of the spider venom toxins in the chronic pain illnesses. Moreover, this topic has not been pedagogically utilized in VR yet. Thus, I aimed to create Bug Off Pain© – an immersive, interactive and educational VR game as an innovative and fun approach to learning and public engagement in biochemistry. Bug Off Pain© would attempt to take the pain out of public engagement, as well as to bridge the gap between scientific and non-scientific community (general public). The design, development, and implementation of the Bug Off Pain© for both Oculus Rift (computer) and Android (mobile) platforms, and research to evaluate the game's educational benefits would be carried out. Some of the methods that would be used here are: AdobeAudition, iMovie, Unity3D, Blender, Autodesk Maya, iTween, UCSF Chimera/Pymol, Likert-type scale, pre- and post-tests.

~CHAPTER TWO~

Methodology

2. Materials and Methods

This part outlines the procedures used for developing the high-throughput fluorescent-based screens, and goes on describing the variety of assays and analytical evaluations used in toxin purification and identification. Apart from these pharmacological investigations, the methods below involve multistep organic syntheses for the generation of five small molecules and their respective identification techniques such as NMR and mass analyses. Moreover, using *in silico* docking and mutagenesis studies called for methods such as virtual screening and genetic engineering. In order to identify venom peptides, we used a variety of methods including RP-HPLC, MALDI-TOF, LC-MS, MS-MS and amino acid sequencing. On the other hand, creating a virtual reality game required the use of different techniques such as Unity3D, video productions, Likert-type based surveys and pre- and post-tests.

2.1. Materials

Lyophilized hymenopteran venoms (species reported in **Table 2.1**) were purchased from either Alphabiotoxine (Belgium) or Venomtech (UK). Cone snails venoms were supplied by BioConus (Brisbane, Australia). Some arachnid venoms were provided by Dr Volker Herzig and Professor Glenn King (Brisbane, Australia). The hP2X3 plasmid was a kind gift from Dr Lin-Hua Jiang (University of Leeds). Standard reagents for buffers and solutions were purchased from Sigma-Aldrich or Fisher Scientific unless otherwise stated. All the buffers and the solutions were made in-house, using de-ionised water filtered through a PURELAB Ultra filtration system. Any sterilisation for bacterial or mammalian cell culture was performed by autoclaving at 121°C for at least 20 min, or, where applicable, through filtration using Sterile Millex syringe filters from EMD Millipore. Media for cell culture, including DMEM 1x (Gibco, 2026849), DMEM/F12 (Gibco, 2062239), serum (FBS, Gibco, 08F5874K), 10x Trypsin-EDTA 0.5% solution (Trypsin-EDTA, Gibco, 15400-054), 0.25% Trypsin-EDTA 1x (Gibco, 2063675), DPBS (HyClone, AZF190845), Lipofectamine™ (Invitrogen, 2032921), Geneticin 50 mg/ml solution (Gibco, 202702TA), Spermine (Sigma, BCBS3256), Spermidine (Sigma, BCBS6090V), Putrescine (Sigma, BCBT6921), Cadaverine (Sigma, BCBL6699V), ATP (Sigma, SLBx3677), YO-PRO-1 Iodide (Sigma, Y3603), Staurosporine (HelloBio, HB0590), Pen Strep (Gibco, 2068817), 5-BDBD (Tocris, 3579), BX430 (Tocris, 5545), PSB12062 (Sigma, SML075), Ivermectin (Tocris, 274-536-0), 3-Indolacetic acid (Sigma, BCBX0861), AZ10606120 (Tocris, 2B/228755), Tryptan Blue (Nalgene, 648920), Hanks balanced salt

solution (HBSS, Gibco, 2003877) and Opti-MEM 1x (Gibco, 31985-062), were obtained from various suppliers. Fura-2 AM was purchased from HelloBio (HB0780), Ca-6 FLIPR Assay from Molecular Devices, and Pierce LDH Cytotoxicity Assay kit from Thermo Scientific (TK272276).

A β peptides corresponding to human A β amino acids A β ₂₅₋₃₅, A β ₃₅₋₂₅ and A β ₁₋₄₂ were purchased from GenScript (PE6871710) and prepared as 10 mM stock solutions in either water or DMSO. Goat anti-mouse Alexa IgG 488 antibody was purchased from Sigma Aldrich (Life Technologies, 1664729) and Alexa Fluoro647 Donkey anti-rabbit IgG from BioLegend (406414). The buffers were prepared with D-(+)-Glucose (BCBS1753V), HEPES (SLBW8459), Potassium Chloride (SLBH5524V), and Sodium Chloride (SZBF0350V) from Sigma.

Table 2.1. List of species of animal venoms used and tested in our assays.

ORGANISM	GENUS	SPECIES	SEX	FAMILY
centipede	Ethmostigmus	rubripes	n.d.	Scolopendridae
centipede	Scolopendra	dehaani	n.d.	Scolopendridae
centipede	Scolopendra	hardwickei	n.d.	Scolopendridae
centipede	Scolopendra	morsitans	n.d.	Scolopendridae
centipede	Scolopendra	subspinipes	n.d.	Scolopendridae
centipede	Thereuopoda	longicornis	n.d.	Scutigerae
scorpion	Androctonus	bicolor	m	Buthidae
scorpion	Hottentotta	jayakari	f	Buthidae
scorpion	Parabuthus	villosus	n.d.	Buthidae
scorpion	Nebo	yemenensis	n.d.	Scorpionidae
spider	Hadronyche	infensa	n.d.	Atracidae
spider	Hickmania	troglodytes	f	Austrochilidae
spider	Ancylometes	rufus	f	Ctenidae
spider	Ancylometes	spec.("Oyapok")	f	Ctenidae
spider	Ancylometes	spec.(Guatemala)	f	Ctenidae
spider	Phoneutria	fera	f	Ctenidae
spider	Phoneutria	nigriventer	f	Ctenidae
spider	Allocosa	obsкуроoides	f	Lycosidae

ORGANISM	GENUS	SPECIES	SEX	FAMILY
spider	Lycosidae	spec.(Australia)	f	Lycosidae
spider	Lycosidae	spec.(Papua New Guinea)	f	Lycosidae
spider	Macrothele	gigas	f	Macrothelidae
spider	Megadolomedes	australianus	f	Pisauridae
spider	Heteropoda	jugulans	f	Sparassidae
spider	Sparassidae	spec.(Indonesia)	f	Sparassidae
spider	Avicularia	juvensis	f	Theraphosidae
spider	Avicularia	purpurea	f	Theraphosidae
spider	Avicularia	spec.("amazonica")	f	Theraphosidae
spider	Avicularia	spec.("huriana")	f	Theraphosidae
spider	Avicularia	spec.("metallica")	f	Theraphosidae
spider	Avicularia	spec.("purple")	f	Theraphosidae
spider	Avicularia	variegata	f	Theraphosidae
spider	Iridopelma	hirsutum	f	Theraphosidae
spider	Ybyrapora	diversipes	f	Theraphosidae
spider	Hysterochrates	cf gigas	f	Theraphosidae
spider	Hysterochrates	ederi	f	Theraphosidae
spider	Hysterochrates	hercules	f	Theraphosidae
spider	Hysterochrates	spec.(Cameroon)	f	Theraphosidae
spider	Hysterochrates	spec.(Nigeria)	f	Theraphosidae
spider	Monocentropus	lambertoni	f	Theraphosidae
spider	Augacephalus	ezendami	f	Theraphosidae
spider	Ceratogyrus	darlingi	f	Theraphosidae
spider	Ceratogyrus	marshalli	f	Theraphosidae
spider	Ceratogyrus	sanderi	f	Theraphosidae
spider	Harpactira	cf gigas	m	Theraphosidae
spider	Harpactira	guttata	f	Theraphosidae
spider	Pterinochilus	chordatus	f	Theraphosidae
spider	Pterinochilus	lugardi	f	Theraphosidae
spider	Pterinochilus	murinus	f	Theraphosidae

ORGANISM	GENUS	SPECIES	SEX	FAMILY
spider	Chaetopelma	spec.(Libanon)	f	Theraphosidae
spider	Euthycaelus	spec.(Colombia)	f	Theraphosidae
spider	Holothele	spec.(Colombia)	f	Theraphosidae
spider	Cyriopagopus	albostriatus	f	Theraphosidae
spider	Cyriopagopus	cf longipes	f	Theraphosidae
spider	Cyriopagopus	doriae	m	Theraphosidae
spider	Cyriopagopus	hainanus	f	Theraphosidae
spider	Cyriopagopus	lividus	f	Theraphosidae
spider	Cyriopagopus	minax	f	Theraphosidae
spider	Cyriopagopus	schmidti	f	Theraphosidae
spider	Cyriopagopus	spec.("hati-hati")	f	Theraphosidae
spider	Cyriopagopus	spec.("Sumatra tiger")	f	Theraphosidae
spider	Cyriopagopus	spec.(Borneo)	f	Theraphosidae
spider	Cyriopagopus	spec.(Thailand)	f	Theraphosidae
spider	Cyriopagopus	spec.(Vietnam)	f	Theraphosidae
spider	Cyriopagopus	vonwirthi	f	Theraphosidae
spider	Lampropelma	nigerrimum	f	Theraphosidae
spider	Lampropelma	violaceopes	f	Theraphosidae
spider	Omothymus	schioedtei	f	Theraphosidae
spider	Ornithoctonus	aureotibialis	f	Theraphosidae
spider	Phormingochilus	carpenteri	f	Theraphosidae
spider	Ephebopus	cyanognathus	f	Theraphosidae
spider	Ephebopus	murinus	f	Theraphosidae
spider	Ephebopus	rufescens	f	Theraphosidae
spider	Psalmopoeus	cambridgei	f	Theraphosidae
spider	Psalmopoeus	langenbuchi	f	Theraphosidae
spider	Psalmopoeus	reduncus	f	Theraphosidae
spider	Psalmopoeus	pulcher	f	Theraphosidae
spider	Pseudoclamoris	elenae	f	Theraphosidae
spider	Tapinauchenius	cupreus	f	Theraphosidae

ORGANISM	GENUS	SPECIES	SEX	FAMILY
spider	Tapinauchenius	latipes	f	Theraphosidae
spider	Tapinauchenius	plumipes	f	Theraphosidae
spider	Tapinauchenius	sanctivincenti	f	Theraphosidae
spider	Neoholothele	fasciaaurinigra	f	Theraphosidae
spider	Schismatothele	spec.(Colombia)	f	Theraphosidae
spider	Chilobrachys	huahini	f	Theraphosidae
spider	Orphnaecus	philippinus	f	Theraphosidae
spider	Orphnaecus	spec.("treedweller")	f	Theraphosidae
spider	Phlogiellus	cf obscurus	f	Theraphosidae
spider	Poecilotheria	fasciata	f	Theraphosidae
spider	Poecilotheria	formosa	f	Theraphosidae
spider	Poecilotheria	hanumavilasumica	f	Theraphosidae
spider	Poecilotheria	metallica	f	Theraphosidae
spider	Poecilotheria	miranda	f	Theraphosidae
spider	Poecilotheria	ornata	f	Theraphosidae
spider	Poecilotheria	regalis	f	Theraphosidae
spider	Poecilotheria	rufilata	f	Theraphosidae
spider	Poecilotheria	smithi	f	Theraphosidae
spider	Poecilotheria	striata	n.d.	Theraphosidae
spider	Poecilotheria	subfusca ('lowland')	f	Theraphosidae
spider	Poecilotheria	subfusca ("highland")	f	Theraphosidae
spider	Poecilotheria	tigrinawesseli	f	Theraphosidae
spider	Poecilotheria	vittata	f	Theraphosidae
spider	Selenocosmia	arndsti	f	Theraphosidae
spider	Selenocosmia	aruana	f	Theraphosidae
spider	Selenocosmia	javanensis sumatrana	f	Theraphosidae
spider	Selenocosmia	spec.(Borneo)	f	Theraphosidae
spider	Selenocosmiinae	spec.(Papua New Guinea)	f	Theraphosidae
spider	Selenocosmiinae	spec.1 (Borneo, Indonesia)	f	Theraphosidae
spider	Selenocosmiinae	spec.2 (Borneo, Indonesia)	f	Theraphosidae

ORGANISM	GENUS	SPECIES	SEX	FAMILY
spider	Selenotholus	cf foelschei	m	Theraphosidae
spider	Heteroscodra	maculata	f	Theraphosidae
spider	Stromatopelma	calceatum	f	Theraphosidae
spider	Acanthoscurria	cf insubtilis	f	Theraphosidae
spider	Acanthoscurria	chacoana	f	Theraphosidae
spider	Acanthoscurria	geniculata	f	Theraphosidae
spider	Acanthoscurria	musculosa	f	Theraphosidae
spider	Acanthoscurria	spec.(Venezuela)	f	Theraphosidae
spider	Acanthoscurria	theraphosoides	f	Theraphosidae
spider	Aphonopelma	spec.(Panama)	f	Theraphosidae
spider	Brachypelma	albopilosum	f	Theraphosidae
spider	Brachypelma	boehmei	f	Theraphosidae
spider	Brachypelma	emilia	f	Theraphosidae
spider	Brachypelma	epicureanum	f	Theraphosidae
spider	Brachypelma	harmorii	f	Theraphosidae
spider	Brachypelma	kahlenbergi	f	Theraphosidae
spider	Brachypelma	sabulosum	f	Theraphosidae
spider	Brachypelma	verdezi	f	Theraphosidae
spider	Bumba	pulcherrimaklaasi	f	Theraphosidae
spider	Chromatopelma	cyaneopubescens	f	Theraphosidae
spider	Davus	pentaloris	f	Theraphosidae
spider	Euathlus	spec.("fire")	f	Theraphosidae
spider	Eupalaestrus	campestratus	f	Theraphosidae
spider	Grammostola	actaeon	f	Theraphosidae
spider	Grammostola	grossa	f	Theraphosidae
spider	Grammostola	iheringi	m	Theraphosidae
spider	Grammostola	porteri	f	Theraphosidae
spider	Grammostola	pulchripes	f	Theraphosidae
spider	Grammostola	rosea	f	Theraphosidae
spider	Grammostola	spec.("Chilean North")	f	Theraphosidae

ORGANISM	GENUS	SPECIES	SEX	FAMILY
spider	Homoeomma	spec.("blue")	f	Theraphosidae
spider	Lasiodora	difficilis	f	Theraphosidae
spider	Lasiodora	klugi	f	Theraphosidae
spider	Lasiodora	parahybana	f	Theraphosidae
spider	Lasiodora	striatipes	f	Theraphosidae
spider	Lasiodorides	striatus	f	Theraphosidae
spider	Nhandu	chromatus	f	Theraphosidae
spider	Nhandu	coloratovillosus	f	Theraphosidae
spider	Nhandu	tripepii	f	Theraphosidae
spider	Pamphobeteus	antinous	f	Theraphosidae
spider	Pamphobeteus	fortis	f	Theraphosidae
spider	Pamphobeteus	nigricolor	m	Theraphosidae
spider	Pamphobeteus	spec.("platyomma")	f	Theraphosidae
spider	Pamphobeteus	spec.("wuschi")	f	Theraphosidae
spider	Pamphobeteus	spec.(Icononzo, Colombia)	f	Theraphosidae
spider	Pamphobeteus	spec.(V. Restrepo, Colombia)	f	Theraphosidae
spider	Phormictopus	atrichomatus	f	Theraphosidae
spider	Phormictopus	auratus	f	Theraphosidae
spider	Phormictopus	cancerides	f	Theraphosidae
spider	Phormictopus	cautus	f	Theraphosidae
spider	Plesiopelma	spec.(Bolivia)	f	Theraphosidae
spider	Sericopelma	rubronitens	f	Theraphosidae
spider	Sericopelma	silvicola	f	Theraphosidae
spider	Sericopelma	spec.(Azuerro, Panama)	f	Theraphosidae
spider	Sericopelma	spec.(Chiriqui, Panama)	f	Theraphosidae
spider	Sericopelma	spec.(Veraguas, Panama)	f	Theraphosidae
spider	Stichoplastoris	spec.(Costa Rica)	f	Theraphosidae
spider	Theraphosa	apophysis	f	Theraphosidae
spider	Thrixopelma	spec.("lagunas")	f	Theraphosidae

ORGANISM	GENUS	SPECIES	SEX	FAMILY
spider	Xenesthis	immanis	f	Theraphosidae
spider	Xenesthis	spec.("blue")	f	Theraphosidae
spider	Xenesthis	spec.("white")	f	Theraphosidae
spider	Haploclostus	nilgirinus	f	Theraphosidae
spider	Thrigmopoeus	truculentus	f	Theraphosidae
spider	Viridasius	spec.("sylvestriformis")	f	Viridasiidae
wasp	Vespula	germanica	NA	Vespidae
wasp	Vespa	velutina	NA	Vespidae
bee	Apis	mellifera	NA	Apidae
cone snail	Conus	geographus	NA	Conidae
cone snail	Conus	textile	NA	Conidae
cone snail	Conus	striatus	NA	Conidae
cone snail	Conus	magus	NA	Conidae

2.2. Cell Cultures

Human astrocytoma 1321N1 cells stably expressing hP2X4, generated by L. Stokes, were maintained in high glucose Dulbecco's Minimal Eagle's Medium, DMEM (Bio-Whittaker) containing 10% (v/v) fetal bovine serum (FBS Gibco 16000044), 100 U/mL penicillin, 100 µg/mL streptomycin (Fisher), and 400 µg/mL G418 (Sigma). HEK293 cells stably expressing either hP2X3, hP2X4 or hP2X7, were maintained under the same condition in DMEM/F12 media (Gibco 11320033). The cells were grown for 4-5 days until 70-90% of confluency was achieved.

Once the desired confluency was reached, the cells were trypsinized with either 0.05% Trypsin-EDTA (Gibco 25300054) or 0.25% Trypsin (Gibco 25200056), centrifuged at 300 xg for 5 minutes and the supernatant was discarded.

The cells were then re-suspended in fresh media and counted with a hemacytometer using trypan blue (Sigma). Mouse microglial BV2 cell lines were maintained in similar conditions as HEK293 cells, however, without the G418 addition. These cells had to be split every 3 days since they usually reached 90-95% confluency sooner than 1321N1 or HEK293 cells. All cells were maintained at 37°C with 5% CO₂ in a humidified incubator; P2X expression remained stable for at least 25–30 passages.

2.3. Establishment of Stable Cell Lines

For generating stable 1321N1-hP2X4, 1321N1-rP2X4, 1321N1-mP2X4 and HEK293-hP2X3 stable cell lines, chemical transfection with Lipofectamine™ 2000 was used. First, the native cells (either 1321N1 or HEK293) were counted and seeded at the density of 2×10^4 in 6-well plates 24h prior to transfection.

The number of cells seeded was different among the cell lines and was calculated in respect to the 80% confluency on the day of the transfection. Since we were using Lipofectamine™ 2000, the transfection mix was prepared according to the manufacturer's protocol using a ratio of 3 μ L of Lipofectamine™ for every 1 μ g of total DNA transfected. Then, astrocytoma 1321N1 or HEK293 cells were transiently transfected with either cDNA plasmids encoding for hP2X3 or hP2X4/rP2X4/mP2X4 in 6-well plate. One day after the transfection, the cells medium was changed to either DMEM (1321N1) or DMEM/F12 (HEK293) with their positive selection geneticin (G418, 400 μ g/mL). With adding geneticin, the selection of stably transfected cells started. The neoR gene (neomycin resistance) was expressed in cells that had incorporated the desired plasmid in their genome which confer the resistance for geneticin. To remove the dead cells, the cell medium was changed every 3-4 days and, in some instances, the cells were incubated in trypsin for the duration of 5 min, combined and re-seeded. Approximately two weeks later, the non-transfected control cells (native 1321N1 or HEK293) were killed by geneticin. That ensured that only the colonies of the transfected and/or geneticin-resistant cells remained in the plate. This way, the polyclonal stable cell lines were generated. However, in order to create a monoclonal cell population, we had to utilize a standard protocol suggested by Johnston²¹⁸ and Wurm.²¹⁹ This method describes the generation of the monoclonal cell populations using limiting dilution. Following this protocol, 100 μ L medium was pre-plated in each well of the plate and 100 μ L of 4×10^5 cells/mL solution was transferred into a first well. Then a serial 1:2 dilution down the first column and a serial 1:2 dilution across the plate was performed. The same amount (100 μ L) was then carried over to the next column.

This was then repeated for each consecutive column. The cells were then incubated and the single cell wells confirmed by microscope. To ensure the desired P2X expression, G418-resistant clones were further selected according to the strength of their ATP-induced increase in intracellular calcium ($[Ca^{2+}]_i$).

Clones successfully expressing the receptor of interest were then expanded in 6-well plates and transferred to T25 tissue culture flasks. An additional experiment was conducted using flow cytometry to quantify expression of the receptor.

2.4. Transient Transfection

For NMDA 1A/2A experiments, HEK293 cells were seeded at the density of 6×10^4 per well in 2 ml of glutamine-free growth medium (Neurobasal, Gibco) in the 6-well plates 24h prior to transfection. When plating HEK293 cells, NMDA antagonists D-AP5 (100 μ M) and MK-801 (10 μ M) were used.

On the day of transfection the cells were washed with PBS and then 0.9 mL of fresh media was added. Transfection were performed using Lipofectamine™ 2000 reagent, following the manufacturer's protocol. The plasmids, whose cDNA encoded for NMDA 1A and NMDA 2A subunits, were a kind gift from Professor David Wyllie (University of Edinburgh). Eight hours after the transfection, 1.1 mL of glutamine-free growth media, supplemented with NMDA antagonists was added and the cells were maintained at 37°C with 5% CO₂ in a humidified incubator for another 16 hours. Then, the cells were incubated in trypsin (5 min), plated in the poly-D-lysine coated 96-well plates, and the Ca²⁺ measurements carried out.

2.5. Flow Cytometry

To quantify the P2X expression, cell medium was aspirated; cells were washed with PBS, trypsinized for 1 min and resuspended in PBS. Cells were then counted and diluted to $0.5 - 1 \times 10^6$ cells/ml and primary antibody of anti-human P2X4 (a kind gift from Professor F Koch-Nolte) was added (1:100 dilution). After 60 min incubation on ice in the dark room, the cells were washed with cold PBS, centrifuged and washed again prior to the addition of the secondary antibody (1:200 dilution). After the incubation on ice for 30 min, cells were washed with cold PBS and centrifuged down twice before resuspended in PBS (200 μ L). Anti-rabbit IgG-Alexa 488 was used as a secondary antibody. Instrument settings were calibrated using mock (unstained) and non-transfected cells in order to determine cellular auto-fluorescence.

All measurements were performed in 5 ml non-sterile non-pyrogenic FACS tubes using FACSCalibur with CellQuest software. Viable cells were then gated on forward and side scatter profiles. Fluorescence properties of the gated population were analysed using the FL-1 channel (FITC). Histograms were plotted and mean fluorescence intensity calculated using in-built statistics function of CellQuest.

2.6. Ca²⁺ Measurements (Fura-2 AM)

One day prior to measurements, 1321N1-hP2X4 cells were plated onto poly-D-lysine coated 96-well plates (Nunc, Fisher Scientific) at 2×10^4 cells/well. After 24 h, the cells were then loaded for 1 h at 37°C with 2 μ M Fura-2 AM (HelloBio) in Hank's Balanced Salt Solution (HBSS, Gibco). Here, Fura-2 AM is a fluorescent indicator dye for Ca²⁺ concentration and its excitation at both, 340 nm and 380 nm results in a signal intensity for the molecule both bound to Ca²⁺ and unbound.

An original stock of Fura-2 AM was first dissolved in DMSO to produce a 1 mM stock and added to the cells in its membrane permeant acetoxymethyl (AM) ester form to give a final concentration of 2 μ M. After the dye incubation, the Fura-2 AM was then removed, and the cells were incubated in 80 μ L Etocal buffer, containing (in mM): 145 NaCl, 5 KCl, 1 MgCl₂, 2 CaCl₂, 13 D-glucose, 10 HEPES; pH 7.33. Once the dye crosses the cell membrane, the ester groups undergo hydrolysis and the dye becomes trapped within the cell. Following loading the cells were pre-incubated with the antagonists such as BX430 or potentiators as ivermectin for 10 min or drugs were injected using the injector function. The [Ca²⁺]_i measurements took place on a Flexstation 3 (Molecular Devices) at 37°C. For the Fura-2 AM assay development, the injection volume was 10 μ L with 150 μ L pipette height and injection rate of 4 (~62 μ L/sec). DMSO concentration for all experiments was <0.1%. The run time was 300 sec with 3.5 sec interval and three readings per well. For microglial BV2 and BV2 P2X7-deficient cell lines, the same assay (Fura-2 AM) was used.

2.7. FLIPR Ca-6 Assay

To monitor the intracellular Ca²⁺ in either stable HEK-P2X3 or transient HEK-NMDA 1a/2a cells, the FLIPR Calcium 6 Assay Kit (Molecular Devices) was used. One day prior to measurements, the cells were plated on poly-D-lysine coated 96-well plates (Nunc, Fisher Scientific) at a concentration of 2×10^4 cells/well. After 24 h, the cells were loaded with the no-wash calcium sensitive dye Calcium 6 and incubated for 2 h prior to measurements on a Flexstation 3 (Molecular Devices) at 37°C.

For this the prepared dye was thawed and diluted 1:3 in buffer containing (in mM): 145 NaCl, 5 KCl, 0.1 CaCl₂, 13 D-glucose and 10 HEPES; pH 7.35). Intracellular calcium levels were measured at the excitation wavelength of 488 nm and emission at 520 nm, expressed as Relative Fluorescent Units (RFU). This value was baseline corrected using the fluorescence in the absence of agonist.

For the measurement of intracellular calcium release induced by agonist (α,β -methylene ATP or glutamate/glycine), a range of concentrations of antagonists (either picrotoxin-1 or MK-801/D-APS) were added to the cells 10 min before the measurements. DMSO concentration for all experiments was <0.1%.

2.8. YO-PRO-1 Assay

YO-PRO-1 uptake was carried out to estimate the time course of a so-called nonselective P2X7 pore formation, a process in which P2X7 forms a receptor-activated permeability pathway.

Once YO-PRO-1 enters cells through this pore, it binds with nucleic acids, and becomes fluorescent and thus enables an indirect measurement of P2X7 activity. This method was adapted and further optimized from Patrice et al.²²⁰ One day prior to measurements, HEK293-hP2X4 and HEK293-hP2X7 cells were plated on poly-D-lysine coated 96-well plates at 2×10^4 cells/well. After 24 h, the culture media was aspirated, and 80 μ L of YO-PRO-1 assay buffer (145 mM NaCl, 5 mM KCl, 0.1 mM CaCl_2 , 13 mM D-glucose, 10 mM HEPES; pH 7.35) containing 2 μ M YO-PRO-1 was applied. P2X7 antagonists such as AZ10606120 and JNJ47965567 were pre-incubated for 10 min before the measurements took place at 37°C using a Flexstation 3 (Molecular Devices). The run time was 300 sec with a 3.9 sec interval, 6 reads/well and medium PMT setting. Measurement parameters were as following: bottom reading, excitation wavelength (490 nm), emission wavelength (520 nm), and cut-off wavelength (515 nm).

2.9. Isolation and Purification of Venom Fractions Using RP-HPLC

Venom (1 mg) was diluted with H_2O , sterile filtered (0.22 μ m; Merck Millipore), then loaded onto an analytical C18 RP-HPLC column (Jupiter 4.6 x 250 mm, 5 μ m, 300 Å; Phenomenex, California, USA) attached to an Agilent HPLC system. Components were eluted at 1 mL/min using isocratic elution at 5% solvent B (90% ACN, 0.05% TFA in H_2O) for 5 min followed by a gradient of solvent B in solvent A (0.05% TFA in H_2O): 5–20% solvent B over 5 min; 20–40% solvent B over 40 min; 40–80% solvent B over 5 min; 80–100% over 5 min. Absorbance was measured at 214, 254 nm and 280 nm using a UV detector (Shimadzu). Individual fractions were pooled, the solvent removed, re-suspended in 200 – 500 μ L of water and lyophilized using liquid nitrogen and vacuum-induced freezing.

Once the fractions were dry, they were stored at -20°C until further studies. The fractions were checked for purity and when the purity was not sufficient ($<80\%$), they were re-suspended in $100\ \mu\text{L}$ of water, and further purified using the same RP-HPLC system before lyophilisation and storage. All solvents used were HPLC-grade.

2.10. Mass Analysis of Venom Fractions and Pure Toxins (MALDI-TOF, ESI-MS/MS, LC-MS) and Software Aids

Toxin masses were obtained using electrospray ionization mass spectrometry (ESI-MS/MS; LCMS-2020 Shimadzu, Japan) or matrix-assisted laser desorption/ionization time-of-flight mass spectroscopy (MALDI-TOF MS) using an Applied Biosystems 4700 MALDI TOF/TOF Proteomics Analyzer. The toxin fractions eluted from RP-HPLC were dissolved in $100 - 150\ \mu\text{L}$ water and $2\ \mu\text{L}$ was then mixed with $2\ \mu\text{L}$ of $10\ \text{mg/mL}$ α -cyano-4-hydroxycinnamic acid (CHCA) matrix (dissolved in 50% acetonitrile, 50% water, 0.1% TFA) to verify toxin masses. Observed masses are reported as monoisotopic m/z or average mass.

When the toxins were subjected to LC-MS for a high resolution ESI-MS/MS, all the measurements were performed on an LTQ Orbitrap XL instrument (ThermoFisher Scientific) equipped with the heated ESI Probe operated in positive ion mode. The ESI (positive ion) parameters for all compounds studied were; source voltage 5 kV, entrance capillary voltage 35 V, entrance capillary temperature 275°C , Nitrogen sheath gas flow rate 7 a.u. All the solutions were prepared in either acetonitrile or methanol and introduced into the ESI source by loop injection using 0.05% formic acid in water as the mobile phase. Then, a full MS scan was performed between m/z 50-5000 at 60,000 resolution. MS/MS of the predefined molecular ion was then performed in the linear ion trap by Collision Induced Dissociation (CID). In order to interpret the spectra, various commercially available software packages were used. These software tools tend to be fragment databases although the exact nature of the algorithms underlying these programmes has not been disclosed for intellectual property reasons. In my hands, mostly Mass Frontier, MS Fragmenter and MassBank were helpful.

2.11. Molecular Formulae Determination by MS-FINDER

For determination of molecular formulas, we used software called MS-FINDER with the text formats for both MS and MS/MS spectra. These text files include information such as precursor m/z , ion mode, mass accuracy of instrument, and precursor type.

The default parameters include the selected elements C, N, H, O; the maximum reported number was set to 50; tree depth set to 2; relative abundance cut off set to 1; the isotopic ratio tolerance together with the mass tolerance was adjusted to a combination of 1% and 1ppm; and all 14 databases were selected. Candidate hits were ranked from highest to lowest.

2.12. Validation Methods for the hP2X4-specific Assay Development (Z factor calculation)

Since we were limited to 96-well format with four controls per plate, and eight replicates each, that left the space for only eight fractions with eight replicates each. These fractions were chosen randomly, however, due to the material shortage, each fraction could only be injected eight times per plate thus different fractions had to be selected for each plate. Fractions were stored at 4°C for the duration of the study. Each prepared fraction was tested on three different days with eight replicates per plate. Eight replicates of positive control (either 10 μM for hP2X4 or 300 μM ATP for hP2X7) and negative controls (buffer, antagonist) were included on each plate. To normalize results for each fraction, we averaged signal AUC values for positive control on each plate and exposed AUC signal values as a % of a positive control signal. Normalised mean was calculated by normalising data to the control, expressed as 1.0.

First, to assess assay specificity, we examined the response evoked by commercially available hP2X4 modulators (BX430, PSB12062, IVM), together with three fractions (F8, F28, F47) from *N. chromatus* venom that were not identified as hits in our initial assay. The positive control was a hit fraction (F5) from the same venom.

Second, inter-plate and intra-plate variability were evaluated using eight venom fractions in three different experiments. Venom fractions were prepared as described above and stored at 4°C for the duration of the study. Each prepared fraction was tested on three different days, with eight replicates per plate.

Eight replicates of positive controls (ATP), eight replicates of negative controls (buffer, antagonist), and eight replicates of a positive allosteric modulator (IVM) were included on each plate. Coefficients of variation were calculated using normalized results for each fraction by expressing the venom-fraction signal as a fraction of the averaged positive control signal from the same plate. For intra-plate variability, unadjusted signal values were used to calculate variability between replicates for each fraction on a plate.

Third, the assay reproducibility was assessed using the Z' factor statistical method, which is commonly used to estimate the reproducibility and robustness of screening assays. This parameter assesses, in part, assay quality by calculating separation between positive and negative signals. Z' values of 0.5 –1.0 indicate a high level of reproducibility, whereas Z' values of 0 – 0.5 indicate a less robust assay.²²¹ The Z'-factor was calculated using the following formula:

$$Z - factor = 1 - \frac{3 \times (\sigma \text{ P2X positive} + \text{P2X negative})}{(\mu \text{ P2X positive} - \mu \text{ P2X negative})}$$

The Z' experiment was performed twice with positive and negative controls (ATP and buffer, respectively) that were used throughout the assay development. In the first experiment, 60 positive controls (ATP) and 36 negative controls (hP2X4/hP2X7 antagonist) were tested. In the second experiment, 48 positive controls (ATP) and 48 negative controls (hP2X4/hP2X7 antagonist) were tested.

2.13. Cell Viability Alamar Blue Assay

The collection of compounds were screened to assess effects on cell viability with the in-house alamar blue assay to measure cell viability. The active ingredient is resazurin, an oxidized form of redox indicator that is blue in colour and non-fluorescent.²²² When incubated with viable cells, resazurin changes colour from blue to red and becomes fluorescent.²²² By detecting either absorbance or fluorescence, we can monitor viability in real time in a reducing environment of viable cells. For the assay, the cells were plated at 2×10^5 /well and plated on poly-D-lysine coated 96-well plates (Nunc, Fisher Scientific) in a culture medium supplemented with 1% FBS. Following incubation, resazurin (0.1 mg/mL in PBS, Sigma Aldrich) was added to cells for 2h at 37°C, and the fluorescent signal was read on a Flexstation 3 plate reader ($\lambda_{exc} = 535 \text{ nm}$, $\lambda_{em} = 600 \text{ nm}$). Analyses were performed in triplicates.

2.14. LDH Release Assay

If cells get damaged, they lose their membrane integrity, releasing, among others, cytoplasmic proteins such as the lactate dehydrogenase (LDH) into the medium. Here, LDH catalyzes the conversion of lactate to pyruvate and NADH. LDH release into cell culture supernatant was quantified using a Pierce assay kit (Fisher Scientific 13454269), following the manufacturer's instructions and using cell culture medium with 1% of serum. Control cells were lysed with the lysing solution provided in the kit to harvest the total intracellular LDH. For this, cells were cultured in 96-well plates (Nunc, Fisher Scientific) and, after applying a stimulus and incubating for 24h, a 50 μ L aliquot of supernatants were determined by measuring the change in absorbance on a Flexstation 3 plate reader at 490 nm. For the data analysis, the medium average control (background) was subtracted from the average values of experimental measurements.

2.15. Amino Acid Sequencing

In order to determine the amino acid composition of the peptide within *L. klugii* F25, we sequenced this peptide using two approaches. First approach comprised the mass spectroscopy methods whereas the second approach utilized a commercial N-terminal sequencing method (Cambridge Peptides). Before sequencing, the peptide was reduced and alkylated. The disulphide bonds were reduced by incubating peptides for 15 min at 65°C in 150 mM Tris (pH 8), 1 mM EDTA and 5 mM DTT. Thiol groups were pyridylethylated using 2 μ L OF 95% 4-vinylpyridine and 10 μ L of CH₃CN; the reaction proceeded under nitrogen for 2 h in darkness at the room temperature. Samples were desalted using LC-MS, eluted as described above (Methods 2.10) and fragmentations monitored using ESI-MS/MS. To confirm these results, the N-terminal sequencing was performed by the Cambridge Peptides (commercial source).

2.16. Structural Elucidation of the Toxins by Nuclear Magnetic Resonance (NMR)

All experiments were performed at 20°C on a Bruker Avance III 800 MHz spectrometer equipped with a 5-mm TXI 800 MHz H-C/N-D-05 Z BTO probe. Small toxins (LK-729 and LK-601) were collected from RP-HPLC, freeze-dried, and prepared the next day for the NMR analysis. The toxins were dissolved in 260 μ L of D₂O and transferred in a Shigemi advanced NMR microtube assembly, matched with D₂O.

The samples were analysed by ^1H 1D excitation sculpting with water suppression, recorded with 512 scans, and by standard COSY 64 scans. However, the concentration was not sufficient to acquire ^1H - ^{13}C HSQC or 1D ^{13}C experiments.

2.17. Chemical Synthesis of Small Molecules and NMR

All chemical reagents and starting materials were of highest grade available and were used without further purification. Thin-layer chromatography analysis of crude reaction products and column chromatography were performed using Merck F254 silica gel plates and 4G/SF10 flash chromatography packing, respectively. TLC analysis used ethyl acetate:hexane (30:70) as a solvent system. The R_f values were between 0.3-0.4 for nitro-substituted products.

After all small molecules were synthesized, purification was followed either by flash column chromatography or reverse-phase chromatography (RP-HPLC) and mass spectrometry and NMR to verify the identity of all analogues. ^1H and ^{13}C NMR spectra were recorded at 400 MHz on a Bruker Avance III spectrometer. ESI+ and ESI- were run at the University of East Anglia using Bruker micrOTOF-Q ESI-MS/MS instrument with methanol as the solvent. Melting points were determined in open glass capillaries on the melting point apparatus and were uncorrected. The reaction scheme can be found in Chapter 5 (Figure 5.22).

2.16.1. Synthesis of 1H-Indole-3-carboxamide, N-[3-[[4-[(3 aminopropyl) amino] butyl]amino]propyl] also known as Lucas analogue 1 (LA-1) and its dimer Lucas analogue 2 (LA-2)

Step 1: Synthesis of 1H-Indole-3-carboxylic acid, 4-nitrophenyl ester

To the solution of 0.463 g 1H-Indole-3- carboxylic acid (2.64 mmol) in DMF (20 mL), 0.330 g (2.38 mmol) of 4-nitrophenol and 1.004 g (2.64 mmol) HATU was added. After a minute, 0.919 mL (5.28 mmol) DIPEA was added and the reaction changed colour from transparent to lightly yellow. The reaction was stirred for 24 h under nitrogen and continuously checked with above TLC method which showed the expected mixture of reagents and a product. After completion, the reaction was diluted with water, extracted 3x with DCM, washed with saturated NaCl and dried with anhydrous Na_2SO_4 . The resulting crude mixture was evaporated and purified using flash chromatography and a gradient of 30% EtOAc in hexane.

The product's fractions were collected and left for a day in a freezer to yield a white, crystalized product (0.72 g; 97 %). ESI: m/z calcd for $C_{15}H_{10}N_2O_4$ [M + H] 283.25, found 283.0535 (**Figure S5**). 1H NMR (400 MHz, $CDCl_3$) δ 9.03 (s, 1H), 8.39 – 8.23 (m, 2H), 7.78 – 7.70 (m, 1H), 7.49 – 7.41 (m, 4H), 7.38 (ddd, $J=8.2, 6.9, 1.1$ Hz, 1H), 7.23 – 7.16 (m, 1H). ^{13}C NMR (100 MHz, DMSO) δ : 158.82, 155.03, 144.97, 137.98, 126.55, 125.46, 125.36, 123.13, 122.31, 120.48, 112.61, 110.17, 79.11, 78.78, 78.46 (**Figure S1**).

Step 2: Synthesis of 1H-Indole-3-carboxamide, N-[3-[[4-[(3-aminopropyl)amino]butyl]amino]propyl]-

To the clear, homogenous solution of 25 mg 1H-Indole-3-carboxylic acid, 4-nitrophenyl ester in 15 mL methanol, 35.85 mg spermine was added dropwise at ambient temperature. After 24 h, the resulting yellow-green solution was evaporated and the crude product was suspended in 2 mL of water. Upon adjusting the pH to 4-5 by the addition of 1N HCl, a homogenous, clear solution was produced.

This was loaded onto RP-HPLC column (Jupiter 4.6 x 250 mm, 5 μ m, 300 \AA ; Phenomenex, California, USA) and components eluted at 1 mL/min using isocratic elution at 5% solvent B (90% ACN, 0.05% TFA in H_2O) for 5 min followed by a gradient of solvent B in solvent A (0.05% TFA in H_2O): 5–75% solvent B over 15 min; 75% solvent B over 5 min; and back to 5% solvent B for the last 5 min. Absorbance was measured at 214, 254 nm and 280 nm using a UV detector (Shimadzu). Three major peaks (mono, di-substituted products and 1H-Indole-3-acetic acid) were analysed by NMR and ESI and their structured and masses were verified. Mono and di-substituted products gave 22 mg (72 %) and 10 mg (23 %), respectively, of a brown powder. ESI: m/z calcd for $C_{19}H_{31}N_5O$ [M + H] 346.49, found 346.2355 (**Figure S6A**). mp for $C_{19}H_{31}N_5O$: 155 – 158°C. 1H NMR (400 MHz, MeOD) δ 7.92 – 7.83 (m, 1H), 7.68 (s, 1H), 7.25 – 7.17 (m, 1H), 7.00 – 6.89 (m, 2H), 3.30 (t, $J=6.3$ Hz, 2H), 2.84 (tt, $J=18.9, 7.8$ Hz, 10H), 1.92 – 1.70 (m, 4H), 1.64 – 1.49 (m, 4H). ^{13}C NMR (100 MHz, MeOD) δ : 169.79, 138.27, 129.49, 127.31, 123.78, 122.29, 121.79, 113.10, 111.18, 48.39, 48.19, 46.42, 45.97, 37.97, 36.74, 28.21, 25.47, 24.48, 24.39 (**Figure S1**). ESI: m/z calcd for $C_{28}H_{36}N_6O_2$ [M + H] 489.63, found 489.2634 (**Figure S6B**). mp for $C_{28}H_{36}N_6O_2$: >300°C. 1H NMR (400 MHz, MeOD) δ 8.07 – 7.99 (m, 2H), 7.83 (s, 2H), 7.39 – 7.31 (m, 2H), 7.16 – 7.02 (m, 4H), 3.51 – 3.39 (m, 4H), 3.23 (dt, $J=3.3, 1.6$ Hz, 9H), 3.16 (dd, $J=15.5, 7.5$ Hz, 1H), 3.07 – 2.91 (m, 6H), 2.81 (d, $J=16.1$ Hz, 3H), 1.97 – 1.87 (m, 2H), 1.21 (s, 1H). ^{13}C NMR (100 MHz, MeOD) δ : 175.15, 136.79, 127.01, 123.81, 121.33, 118.69, 117.94, 111.20, 108.00, 46.46, 44.54, 35.24, 32.53, 32.53, 26.24, 22.57 (**Figure S1**). IR (KBr): 722, 798, 835, 1135, 1165, 1198, 1670, 2875, 3075 cm^{-1} .

2.16.2. Synthesis of 1H-Indole-3-acetamide, N-[3-[[4-[(3-aminopropyl)amino]butyl]amino]propyl]- also known as Lucas analogue 3 (LA-3) and its dimer Lucas analogue 4 (LA-4)

Step 1: Synthesis of 1H-Indole-3-acetic acid, 4-nitrophenyl ester

To the solution of 0.7 g 1H-Indole-3-acetic acid (4 mmol) in DMF (20 mL), 0.5 g (3.6 equiv) of 4-nitrophenol and 1.365 g (4 mmol) HATU was added. After a minute, 1.25 mL (8 mmol) DIPEA was added and the reaction changed colour from transparent to lightly yellow. The reaction was stirred for 24 h under nitrogen and continuously checked with above TLC method which showed the expected mixture of reagents and a product. After completion, the reaction was diluted with water, extracted 3x with DCM, washed with Brine and dried with anhydrous Na₂SO₄. The resulting crude mixture was evaporated and purified using flash chromatography and a gradient of 30 % EtOAc in hexane. The product's fractions were collected and evaporated.

The final product yielded 0.72 g (66 %) as a white solid. ESI: m/z calcd for C₁₆H₁₂N₂O₄ [M - H] 295.28, found 295.0985 (**Figure S7**). ¹³C NMR (100 MHz, DMSO) δ: 162.12, 156.34, 145.10, 137.06, 135.12, 126.21, 125.69, 123.79, 123.49, 122.40, 113.19, 105.04, 79.83, 79.35, 79.10 (**Figure S1**). mp: 133 – 138°C.

Step 2: Synthesis of 1H-Indole-3-acetamide, N-[3-[[4-[(3-aminopropyl)amino]butyl]amino]propyl]-

To the clear, homogenous solution of 100 mg 1H-Indole-3-carboxylic acid, 4-nitrophenyl ester in 15 mL methanol, 146.4 mg spermine was added dropwise at ambient temperature. After 24 h, the resulting yellow-green solution was evaporated and the crude product was suspended in 2 mL of water. Upon adjusting the pH to 4-5 by the addition of 1N HCl, a homogenous, clear solution was produced. This was loaded onto RP-HPLC column (Jupiter 4.6 x 250 mm, 5 μm, 300 Å; Phenomenex, California, USA) and components eluted at 1 mL/min using isocratic elution at 5% solvent B (90% ACN, 0.05% TFA in H₂O) for 5 min followed by a gradient of solvent B in solvent A (0.05% TFA in H₂O): 5–75% solvent B over 15 min; 75% solvent B over 5 min; and back to 5% solvent B for the last 5 min. Three major peaks (mono, di-substituted products and 1H-Indole-3-acetic acid) were analysed by NMR and ESI and their structured and masses were verified. Mono and di-substituted products gave 81 mg (67 %) and 34 mg (19 %), respectively, as a brown solid. ESI: m/z calcd for C₂₀H₃₃N₅O [M + H] 360.52, found 360.2506 (**Figure S8A**). mp for C₂₀H₃₃N₅O: 161 – 165°C.

^1H NMR for $\text{C}_{20}\text{H}_{33}\text{N}_5\text{O}$ (400 MHz, MeOD) δ 7.24 (d, $J = 7.8$ Hz, 1H), 7.06 (d, $J = 8.1$ Hz, 1H), 6.89 (s, 1H), 6.84 – 6.77 (m, 1H), 6.76 – 6.68 (m, 1H), 3.37 (s, 2H), 3.01 – 2.94 (m, 2H), 2.77 – 2.68 (m, 4H), 2.67 – 2.59 (m, 2H), 2.46 (dt, $J = 10.9, 7.4$ Hz, 4H), 1.75 (dq, $J = 15.4, 7.7$ Hz, 2H), 1.55 – 1.44 (m, 2H), 1.43 – 1.23 (m, 4H). ^{13}C NMR (100 MHz, MeOD) δ : 176.47, 138.28, 128.55, 125.36, 122.89, 122.77, 120.26, 119.51, 112.76, 109.56, 48.25, 48.07, 46.17, 45.92, 37.91, 36.91, 33.93, 27.61, 25.44, 24.19. ESI: m/z calcd for $\text{C}_{30}\text{H}_{40}\text{N}_6\text{O}_2$ [M + H] 517.69, found 517.2922 (**Figure S8B**). mp for $\text{C}_{30}\text{H}_{40}\text{N}_6\text{O}_2$: $>300^\circ\text{C}$. ^1H NMR for $\text{C}_{30}\text{H}_{40}\text{N}_6\text{O}_2$ (400 MHz, MeOD) δ 7.62 – 7.56 (M, 2H), 7.39 (dt, $J = 8.2, 0.9$ Hz, 2H), 7.23 (d, $J = 5.0$ Hz, 2H), 7.18 – 7.10 (m, 2H), 7.09 – 7.01 (m, 2H), 3.72 (d, $J = 0.5$ Hz, 4H), 3.59 – 3.42 (M, 2H), 3.39 – 3.27 (m, 8H), 2.81 (dd, $J = 14.4, 7.3$ Hz, 4H), 2.69 (d, $J = 14.8$ Hz, 4H), 1.89 – 1.74 (m, 4H), 1.54 (dd, $J = 9.0, 5.3$ Hz, 4H). ^{13}C NMR (100 MHz, MeOD) δ : 176.71, 138.35, 128.57, 125.38, 122.88, 120.24, 119.50, 112.75, 109.55, 48.02, 46.09, 36.79, 34.08, 27.79, 24.12. (**Figure S1**). IR (KBr): 718, 802, 844, 1196, 1189, 1206, 1698, 2895, 3099 cm^{-1} .

2.16.3. 1H-Indole-2-carboxamide, N-[3-[[4-[(3-aminopropyl)amino] butyl] amino]propyl]- also known as Lucas analogue 5 (LA-5)

Step 1: Synthesis of 1H-Indole-2-carboxylic acid, 4-nitrophenyl ester

To the solution of 0.7 g 1H-Indole-2-acetic acid (4.34 mmol) in DMF (20 mL), 0.544 g (3.9 equiv) of 4-nitrophenol and 1.65 g (4.34 mmol) HATU was added. After a minute, 1.51 mL (8.68 mmol) DIPEA was added and the reaction changed colour from transparent to lightly yellow. The reaction was stirred for 24 h under nitrogen and continuously checked with above TLC method which showed the expected mixture of reagents and a product. After completion, the reaction was diluted with water, extracted 3x with DCM, washed with saturated NaCl and dried with anhydrous Na_2SO_4 . The resulting crude mixture was evaporated and purified using flash chromatography and a gradient of 30 % EtOAc in hexane. The product's fractions were collected and the solvent evaporated. The product gave 0.68 g (91 %) as a yellow solid. ESI: m/z calcd for $\text{C}_{15}\text{H}_{10}\text{N}_2\text{O}_4$ [M - H] 281.26, found 281.0846 (**Figure S9**). ^1H NMR (400 MHz, CDCl_3) δ 8.27 – 8.19 (m, 2H), 8.13 (dd, $J = 7.0, 2.2$ Hz, 1H), 7.71 – 7.63 (m, 1H), 7.42 – 7.36 (m, 1H), 7.25 (dd, $J = 3.5, 2.3$ Hz, 1H), 7.22 (dd, $J = 3.5, 1.8$ Hz, 1H), 7.20 – 7.12 (m, 1H), 4.05 (d, $J = 0.8$ Hz, 2H). ^{13}C NMR (100 MHz, CDCl_3) δ : 169.55, 168.79, 155.59, 145.31, 136.22, 127.11, 126.88, 125.24, 122.58, 120.10, 118.72, 115.62, 111.48, 107.28, 31.80 (**Figure S1**).

Step 2: Synthesis 1H-Indole-2-carboxamide, N-[3-[[4-[(3-aminopropyl)amino]butyl]amino]propyl]-

To the clear, homogenous solution of 100 mg 1H-Indole-3-acetic acid, 4-nitrophenyl ester in 15 mL methanol, 153.6 mg spermine was added dropwise at ambient temperature. After 24 h, the resulting yellow-green solution was evaporated and the crude product was suspended in 2 mL of water. Upon adjusting the pH to 4-5 by the addition of 1N HCl, a homogenous, clear solution was produced. This was loaded onto RP-HPLC column (Jupiter 4.6 x 250 mm, 5 μ m, 300 Å; Phenomenex, California, USA) and components eluted at 1 mL/min using isocratic elution at 5% solvent B (90% ACN, 0.05% TFA in H₂O) for 5 min followed by a gradient of solvent B in solvent A (0.05% TFA in H₂O): 5–75% solvent B over 15 min; 75% solvent B over 5 min; and back to 5% solvent B for the last 5 min. Two major peaks (monosubstituted product and 1H-Indole-2-carboxylic acid) were analysed by NMR and ESI and their structured and masses were verified. Only mono substituted product was obtained as a brown solid and its yield was 26 mg (85 %). ESI: m/z calcd for C₁₉H₃₁N₅O [M + H] 344.49, found 344.2810 (**Figure S10**). mp: 146 – 151°C. ¹H NMR (400 MHz, MeOD) δ 7.28 (dd, *J*= 7.2, 0.8 Hz, 1H), 7.13 (dd, *J*= 8.3, 0.9 Hz, 1H), 6.90 (ddd, *J*= 8.3, 7.0, 1.1 Hz, 1H), 6.78 (d, *J*= 0.8 Hz, 1H), 6.74 (ddd, *J*= 8.0, 7.0, 0.9 Hz, 1H), 3.20 (t, *J*= 6.4 Hz, 2H), 2.82 – 2.68 (m, 10H), 1.83 – 1.62 (m, 4H), 1.49 (dt, *J*= 7.1, 3.4 Hz, 4H). ¹³C NMR (100 MHz, MeOD) δ : 165.38, 138.53, 131.72, 129.08, 125.41, 122.95, 121.43, 113.23, 104.97, 48.37, 48.25, 46.55, 45.96, 37.93, 37.14, 27.99, 25.48, 24.41, 24.35 (**Figure S1**).

2.18. Docking Studies

The human, rat and mouse models of P2X4 in its closed state were prepared by homology modelling with MODELLER 9.18. Zebrafish P2X4 (PDB: 4DW0) was used as template and the best models obtained were further refined with Schrodinger Maestro 11, scwrl4 and GROMACS 5.1.4 and assessed for quality with propKa 3.0 and PROCHECK 3.3. The receptors were then prepared for docking with the Protein preparation Wizard of Maestro. This included assigning and adjusting bond orders and charges, adding hydrogen atoms, enhancing hydrogen bonds, deleting crystallographic waters and eliminating atomic clashes via protein minimisation. The ligands were prepared with the LigPrep module of Mestro using default parameters. The ligands LA-1, LA-2, LA-3, LA-4 and LA-5 were converted from 2D in 3D and hydrogens were added using LigPrep program to ensure the desired ligands were in a low-energy state with correct stereochemistry for its structure.

These steps included ensuring the ligands existed in appropriate ionisation states, tautomers, ring conformations, molecular weights and also the number and types of functional groups. Ligand docking required Glide to carry out the docking process using both, rigid and induced-fit docking with the default settings.

To identify ligand binding sites on the receptor models we looked at the differences in amino acid sequences between human, rat and mouse P2X4, and the binding site centre was defined based on the position of the mutated residues in the different binding hotspots we have previously identified. The ligands were docked with GLIDE and the Induced Fit procedure in Maestro. The results were rationally assessed based on the data from biological assays. The key residues of the proposed binding mode were then selected for mutagenesis studies. For graphical visualization, UCSF Chimera 1.11.2 was used.²²³

2.19. Mutagenesis

Point mutations were introduced into the wild type (WT) human P2X4 and rat P2X4 plasmid using the Stratagene Quikchange II XL site-directed mutagenesis kit (Agilent Technologies, 200521). Primers were designed and their sequence is reported in **Table 2.2**.

Table 2.2. List of primers for their respective mutation as purchased from Sigma Aldrich.

Receptor	Mutations	Forward primer	Reverse primer
hP2X4	D220A	CCTCAAGTCGTGCATTTAT <u>GCT</u> GCTAAAACAGA TCCC	GGGGATCTGTTTTAGCAGCATAAATGCACGACTTG AGG
	D220N	CCTCAAGTCGTGCATTTAT <u>AAT</u> GCTAAAACAGA TCCC	GGGGATCTGTTTTAGCATTATAAATGCACGACTTGA GG
	K222A	GCATTTATGATGCT <u>GCA</u> ACAGATCCCTTCTGCC C	GGCAGAAGGGATCTGTTGCAGCATCATAAATGC
	N238D	GGCAAATAGTGGAG <u>GAC</u> GCAGGACACAGTT TCC	GGAAACTGTGTCTGCGTCTCCACTATTTTGCC
	N238A	GGCAAATAGTGGAG <u>GCC</u> GCAGGACACAGTT CC	GGAAACTGTGTCTGCGGCTCCACTATTTTGCC
	K234A	CCATATCCGTCTTGGC <u>GCA</u> AATAGTGGAGAAC GCAGG	CCTGCGTTCTCCACTATTGCGCCAAGACGGAATATG G
rP2X4	N220D	CCTCAAATCGTGCATTTAC <u>GAT</u> GCTCAAACGGA TCCC	GGGATCCGTTTGAGCATCGTAAATGCACGATTGA GG
	D238N	GGCACAATCGTGGG <u>GAA</u> CGCGGACATAGCTT CC	GGAAGCTATGTCCC GCGTTCCCACGATTGTGCC

The PCR reaction consisted of: 5 μL of 10x reaction buffer; 20 ng of plasmid DNA template; 1.25 μL of oligonucleotide primer #1 (c=10 μM); 1.25 μL of oligonucleotide primer #2 (c=10 μM); 1 μL of dNTP mix; 3 μL of QuickSolution, and 36.5 μL ddH₂O. PCR was performed for 16-18 cycles using Pfu turbo polymerase (2.5 U/ μL) and products were digested with DpnI for 1 hour at 37°C. NEB 5-alpha competent *E.coli* cells (C2992 New England Biolabs, UK) were transformed with 5-10 μL of digested product and colonies selected following growth at 37°C for 16-24 hours. Plasmids were extracted using Qiagen miniprep and mutations verified by sequencing (Eurofins Genomics).

2.20. Evaluation of VR Game Bug Off Pain©

To protect players' confidentiality and security of their data, all data was collected anonymously. Here, evaluation of the public opinion by a Likert-type survey and VR-based learning by the use of pre- and post-tests are explained in greater detail.

2.19.1 Likert-Type Scale

Bug Off Pain was tested and evaluated at two independent events, namely Norwich Science Festival and Norwich Gaming Festival by 112 people (ages 16-74). Out of them, 78 didn't have any prior science background.

The survey with 14 statements and responses based on a Likert-type scale, was designed to collect the opinions about Bug Off Pain. Before distributing the original survey at the public engagement events we perform a test-run among 22 students at the University of East Anglia. Here, the respondents had to answer the questions such as "Does the survey or test measure what it intended to measure?" and "Is this question measurement in the survey essential to the intended measurement?" Since more than 83% participants answered "Yes" and "Yes, relevant", respectively, we concluded that our survey actually measures what it claims to and thus is deemed valid and reliable. All player feedback and opinions were acquired through either a printed (**Figure 2.1**) or electronic form (<https://goo.gl/RM99sZy>) containing 14 statements used to evaluate the game.

Statement		Strongly Disagree			Neutral				Strongly Agree		
		1	2	3	4	5	6	7	8	9	10
1	The immersive environment via VR adds to STEM engagement and motivation to learn more										
2	Bug Off Pain is an innovative approach to gamify chemistry-related subjects										
3	The game is fun, dynamic and easy to play										
4	I like to play Bug Off Pain										
5	I acquire a new knowledge about chronic pain and spider venoms										
6	Content of the Bug Off Pain is relevant and useful										
7	The design of the game is attractive and captures the attention of the player										
8	Bug Off Pain should be extended to other STEM subjects										
9	The scoring system is well in place										
10	Bug Off Pain has an easy to understand navigation (user interface)										
11	Music and voice-over is appropriate and adds to the game										
12	VR Sickness has not been experienced during the game										
13	I find this VR approach as a good alternative to public engagement and education via VR										
14	This game changes my perception of what I think about STEM-related subjects										
15	I didn't know before that science can be fun – I am more eager to study chemistry-related subjects now										

Figure 2.1. Printed survey administrated to collect the player's opinions and feedback about Bug Off Pain.

2.19.2. Pre- and Post-Test

This study compared two different types of groups – video clips and VR game Bug Off Pain. The video clips corresponding to the control group and VR game group corresponding to the experimental group. Both groups included identical learning assessments and were located in the same place (City College Norwich in Norwich, UK). Here, our hypothesis formulations were the following:

- Students from the virtual group would have significantly greater learning performance in biochemistry of spider venoms and chronic pain than students from the video clips group
- Evaluations would show that the virtual reality game have significantly greater appeal to students than video clips

The intention of this assessment was to collect quantitative data based on two questionnaires: a pre-test and a post-test. While the pre-test aimed to assess the student's knowledge before the scientific concepts were explained either by video clips or Bug Off Pain, the post-test aimed to measure, after the study, student's knowledge of the obtained scientific principles. The questionnaire had ten multiple-choice questions aimed at high school-student level (aged 17-18). Pre- and post-tests are used to model the knowledge gained from participating in a learning course. In this context, we evaluated the knowledge obtained by playing Bug Off Pain using pre- and post-test questions. Each of these questions was designed to analyze the effect of the educational role of Bug Off Pain for learning about the biochemistry of spider venoms and chronic pain. Students with a fear of spiders opted out of this study.

These studies were carried out on 44 high-school students in City College Norwich in Norwich (UK) and overseen by two teachers. The students were randomly chosen and assigned to one of the two groups - experimental group (EG) or control group (CG). The students had 30 min to respond to each test, shown in **Figure 2.2**.



“SPIDER” Exam

Pre-test and post-test for “VR Bug Off Pain” Educational Evaluation

Identification

No: X Result: _____

Class: X Date: XX/XX/XXXX

Instructions

Read each of the questions slowly and carefully and choose the letter that best describes the answer. Then, print a letter of the correct answer next to the question (on the left).

Part I: Why does it hurt?

- 1) _____ What are the two main types of pain?
 - a. Headache and back pain
 - b. Chronic and acute pain
 - c. Nausea and stomach pain

- 2) _____ Choose and answer that doesn't describe chronic pain:
 - a. It helps us survive and serves as a protective function
 - b. Rheumatoid arthritis is one form of it
 - c. When a person is experiencing this sort of pain, only one area of the brain is active

- 3) _____ What is one of the symptoms of chronic pain?
 - a. Headache
 - b. Sunburn
 - c. Heightened sensitivity to touch

Part II: How to treat pain?

- 1) _____ Choose the answer that is correct:
 - a. Local anesthetic is good when you want to treat a pain at a specific location
 - b. Opioids don't have many side effects
 - c. Ibuprofen is useful for different types of pain

- 2) _____ Can people develop addiction when taking opioids?
- Usually yes
 - No, never
- 3) _____ Chose the answer that describes some of the most common side effects of opioids:
- Stomach pain, heartburn, vomiting, constipation
 - Addiction, delusion, depression, anxiety, hostility towards others
 - Nausea, vomiting, constipation, dry mouth, sedation, dizziness, tolerance, addiction
- 4) _____ Which venom CAN NOT be used to treat chronic pain?
- Cone snail venoms
 - Spider venoms
 - Grasshopper venom
- 5) _____ What is Ziconotide?
- A drug that is used to treat chronic pain
 - Cone snail venom
 - Spider venom

Part III: Venom gang

- 1) _____ Choose the incorrect answer that describes brain cells (neurons):
- Neurons send signals with a help of neurotransmitters
 - Microglial cells are cells that surround neurons in our brains
 - Neurons and microglia are less likely to communicate between each other
- 2) _____ Chose the correct answer:
- Communication between microglia and neurons don't contribute to chronic pain
 - Proteins found on the surface of the microglial cells contribute to chronic pain
 - P2X4 is a protein and is not involved in chronic pain

Figure 2.2. Pre- and post-test questionnaire.

2.19.3. 3D Models and Software Tools

The following 3D models were adapted as CC (creative commons) from either <http://assetstore.unity.com>: spiders (22986), academy theatre (75378) and massive fantasy spider “Tarantula” (10104); <http://fre3d.com>: Lego® bricks (94903), Spiderweb (10239); <http://www.turbosquid.com>: Lightbulb (494548), Brains (833681); Neuron (277076), Microglia (374179), Cell membrane (808791). The PDB file for P2X4 was obtained from the Protein Data Bank (4DW1). The game was designed with Unity3D and several other software components such as Autodesk Maya, Blender, and iTween that are designed to support work with Unity. Modeling of proteins was conducted on either UCSF Chimera/Pymol. The generated QR is shown on the **Figure 2.3**.



Figure 2.3. QR Code for Bug Off Pain.

2.21. Data Analysis

GraphPad, v. 8.0 (GraphPad, California, USA) was used to analyse data collected from the Flexstation 3 using SoftMax Pro v5.4 software; in Softmax Pro analysis of kinetic fluorescence data the baseline was set to zero to normalise the data from multiple wells. Curve fitting was performed with Prism® (GraphPad 8.0) using nonlinear regression (least squares regression) and common sigmoidal dose response equations. Data is reported as the mean \pm SD with the experiments performed in triplicates, except where otherwise specified. For two groups, a paired samples *t*-test or Wilcoxon signed-rank test was performed. In the case of more than two groups, one-way repeated measures ANOVA was used. All data for cell viability and cytotoxicity were obtained in fluorescence units and expressed as a percentage of the negative control (culture medium). Statistically significant differences from controls are indicated by *, $p < 0.05$; **, $p < 0.01$; ***, $p < 0.001$.

For the evaluation of the VR game, we utilized the multiple comparison tests (two-way ANOVA and Wilcoxon test) between the differences in of the average number of correct answers (ANCA).

Cohen's d values were calculated by mean differences between two groups, and then divided by the pooled standard deviation. In each questionnaire (pre-test and post-test) the total of correct answers were calculated and presented as a total score ranging from 0 to 10 points. To investigate the effectiveness of either the video clips or Bug Off Pain, the repeated one-way ANOVA was used. In order to study the appeal and opinion of Bug Off Pain, the mean score of 144 answers (on the Likert scale ranged from 1-10) was calculated. Finally, in order to compare the scores between the two groups, the ANOVA was used. All of the analysis were performed using GraphPad 8.0 application with the significance level set at 0.05.

~CHAPTER THREE~

Development of High-Throughput Fluorescent-Based Screens for the Rapid Discovery of Novel Animal Toxin Hits Against P2X Receptors

This Chapter contributed to a research article published as:

Bibic L., Volker H., King G.F., Stokes L. Development of High-Throughput Fluorescent-Based Screens to Accelerate Discovery of P2X Inhibitors from Animal Venoms. *J Nat Prod* **2019**, 82.9., p.2559-2567.

3.1. Introduction

Natural products have been exploited throughout history for their medicinal properties and it is estimated that half of the top-selling drugs in the world came from natural sources.¹⁸⁷ In recent years, animal venoms have arisen as a prime source of therapeutically beneficial compounds. These include toxins from spiders,¹⁹¹ cone snails,²²⁴ snakes,²²⁵ sea anemones,²²⁶⁻²²⁷ jellyfish²²⁸ and scorpions²²⁹ – all of which have offered a diversity of inhibitors with high affinity and selectivity towards their biological targets.¹⁷⁹ However, the biochemical resources of these venomous animals has barely been explored due to a variety of biological, historical, technological, and even practical reasons.²³⁰

Fortunately, venom research can gain leverage from high-throughput 'omics techniques (genomics, transcriptomics, proteomics, and metabolomics). Together with advances in bioinformatics, these new platforms can exploit the remarkable biochemical diversity of venom pharmacopoeia in the quest for new drugs. So far, six venom-derived drugs are currently on the market.¹⁷⁹ Most of them have been developed from snakes because they yield large amounts of venom. For that reason, many venoms haven't been studied with respect to their biological targets. Thus, it is perplexing that a robust high-throughput screening (HTS) assay that could access this unexplored chemical space and determine the molecular targets of venom toxins hasn't been extensively pursued. However, a substantial advancement in HTS robotics now allows the screening of much smaller quantities of venom, allowing us to unveil the therapeutic compounds within previously unexplored venoms.²³⁰⁻²³¹

Another major bottleneck in the HTS approach is its application to investigate drug targets such as ion channels.²³² Usually, electrophysiological platforms are used for the characterisation of compound activity. While these approaches are information-rich, they are labour intensive, represent a reproducibility challenge with the cells being used, and are low-throughput.²³³ Thus, HTS-based cell assays that utilize ion flux (Ca^{2+} -sensitive), and membrane potential dyes have become integral components of ion-channel drug discovery programs.²³⁴ For example, statistical analysis of recently approved drugs suggests that HTS could indirectly provide new molecular entities.

In combination with the unrealised potential of venoms, HTS may indeed access this uncharted chemical space and potentially lead to hit identification and lead compound generation.²³⁵ Cell-based functional HTS assays are the essential requirement for the screening of ion channels. Among ligand-gated ion channels, purinergic receptors have been nearly ignored as promising drug targets for new toxins from venoms.

Only a single study from Grishin et al.¹³⁸ explored whether toxins from spider venoms are capable of targeting purinergic receptors. The team reported a potent and selective cysteine knot peptide from the venom of a wolf spider (family *Lycosidae*) against the human P2X3 receptor that is implicated in chronic pain.¹⁵¹ However, despite being published for almost a decade, the purinergic field has fallen short of identifying novel, effective, safe and well-tolerated treatments for a condition such as chronic pain. We endeavoured to develop a high-quality venom HTS screen to bridge the gap between the exciting progress in HTS development and the pursuit of P2X-targeted drugs for clinical use.²³⁶ Animal venoms may help populate the currently unexplored P2X receptor pharmacological space using an easily automated, fast, reliable, and robust platform that provides quantitative data that can be thoroughly validated data.

3.2. Results and Discussion

In this chapter, the design and development of three fluorescence-based high-throughput cell assays that selectively detect toxin hits from different animal venoms towards stably expressed purinergic receptors hP2X3, hP2X4, and hP2X7 are described. These *in vitro* platforms are capable of screening multiple venoms against multiple targets, improving testing characteristics, all while minimizing costs, specimen material requirements, and testing time. Furthermore, our assays can be applied to other natural product libraries that may yield new compounds against P2X targets and thus promote the discovery of therapeutically valuable medicines towards a range of pathologies.

3.2.1. Assay Design

In order to investigate the effect of venom toxins against P2X channels, appropriate heterologous expression systems were developed. Here, adherent 1321N1 and HEK293 cell lines were chosen because solely using the HEK293 cell line would be insufficient; HEK293 cells endogenously express high-levels of cell-surface P2Y receptors (GPCRs) which may mask P2X calcium signalling. In order to avoid this potential susceptibility to false positive hits, the 1321N1 cell line – which possesses no endogenous P2 receptors that may interfere with calcium signalling – was chosen as a suitable validation platform for our studies. Once the crude venom hits were identified in HEK293-hP2X4, a secondary screen on 1321N1-hP2X4 was carried out to validate *bona fide* hits.

Despite similar efforts towards P2X4 and P2X7 receptor screening employed by us²³⁷⁻²³⁸ or others,²³⁹ the research community still lacks a HTS that could be rigorously validated, both analytically and biochemically, when subjected to natural products such as venoms. As seen in **Figure 3.1**, a screening and fractionation workflow was developed to enable rapid exploitation of either crude venoms or semi-pure venom fractions. The general scheme involves the following steps: A) Identifying hits with cell-based *in vitro* assays using three different fluorescent dyes; B) fractionating the crude venoms and identifying the toxin hits via activity-guided fractionation; and C) validation of toxin hits. For collecting information about the calcium/dye flux, a Flexstation 3 multimode plate reader²⁴⁰ was used to capture the response kinetics of the P2X channels.

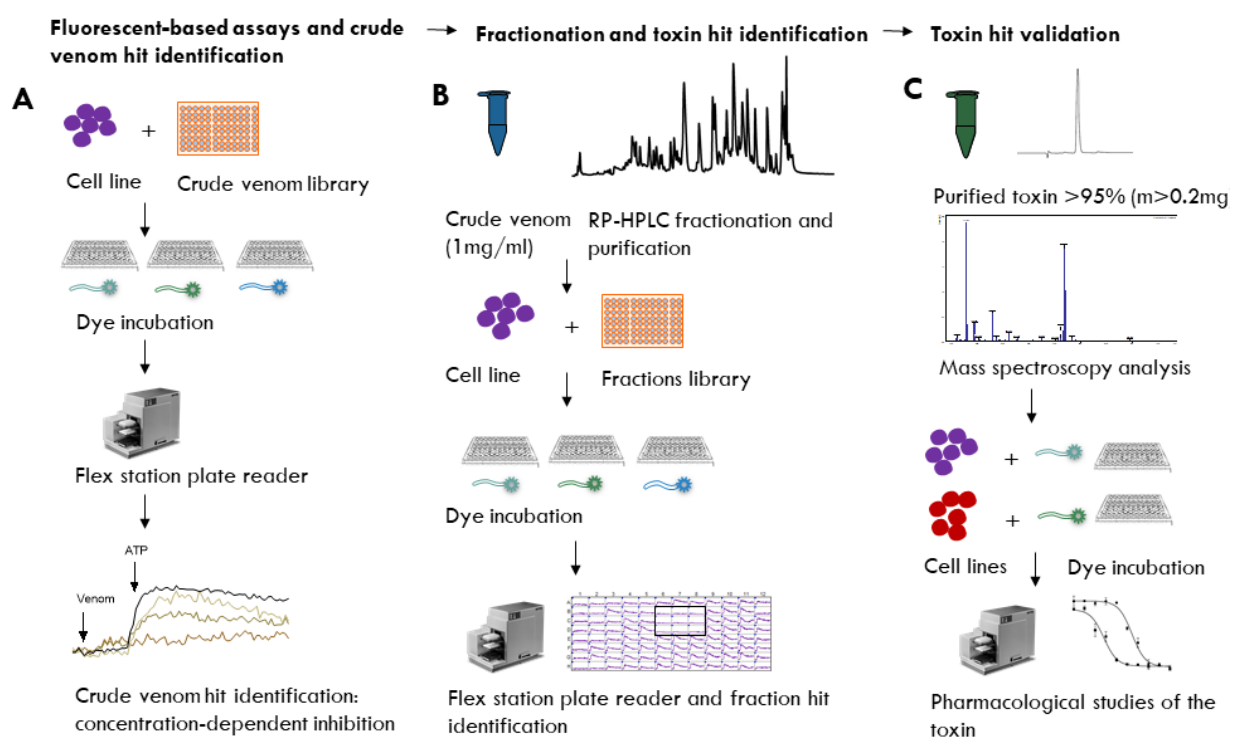


Figure 3.1. High-throughput screen of crude venoms against P2X receptors. **A:** A portion of crude venom (150 μ L at concentration of 1 g/L) is injected in triplicates into the wells of a 96-well plate. Here, three fluorescent-based dyes (Fura-2 AM, YO-PRO-1, and FLIPR Calcium-6) are used to aid the screening against 1321N1-hP2X4, HEK293-hP2X7, and HEK293-hP2X3 stable cell lines. **B:** Once the crude venom hits are identified (A), these are then fractionated using reverse-phase (RP) HPLC. After the separation of fractionated toxins, the fractions are then screened in the HTS assays against hP2X3, hP2X4 and hP2X7 receptors and hit fractions identified. **C:** RP-HPLC fractionated hits are further purified using orthogonal chromatography techniques to identify the bioactive compound, which is then analysed using mass spectroscopy techniques such as MALDI-TOF, LCMC, MS-MS. The pure (>91%) toxin hit is then subjected to pharmacological evaluation and later validation using two stable cell lines expressing the P2X receptor of interest.

Overall, this workflow was deemed to be robust and easy to implement. Since these fluorescent-based assays require the fluorescence to be measured from the bottom of the well (to reduce the background fluorescence), cells had to be firmly adhered. The signal may be compromised if the cells move or detach during venom and agonist injection, thus we developed a range of stable adherent cell lines.

Transfecting 1321N1 and HEK293 with human P2X3, P2X4 and P2X7 plasmids resulted in the following cell lines; HEK293-hP2X3; 1321N1-hP2X4; HEK293-hP2X4; and HEK293-hP2X7. Generating 1321N1-hP2X3 and 1321N1-hP2X7 stable cell lines was attempted without any measurable success. This may be due to the fact that astrocytoma 1321N1 cells are extremely challenging to transfect. Marucci and others²⁴¹ demonstrated the inability of 1321N1 cell lines to be efficiently and transiently transfected. Generating stable cell clones for use in a rigorous HTS thus posed some difficulties.

A plethora of assay formats are now commercially available to support compound screening. We restricted the assay format to a 96-well plate format to facilitate liquid handling. Literature suggests that researchers often experience significant problems with bubble-formation using a 384-well format due to the repeated wash steps, especially in a less controlled good manufacturing practice (GMP) environment.²³⁴ Prior to screening, dyes were optimised for use with HEK293-hP2X3, HEK293-hP2X4, 1321N1-hP2X4, and HEK293-hP2X7 in order to choose the ideal dye for a particular cell line. Since the YO-PRO-1 assay was already routinely used in our lab,^{237-238, 242} we utilized YO-PRO-1 for HEK293-hP2X4 and HEK293-hP2X7 experiments. However, when considering which Ca²⁺ dye to use for 1321N1-hP2X4 and HEK293-hP2X3 experiments, we had to ensure that Ca²⁺ signal responses were relatively consistent in these cell lines. Based on our observations, we selected fluorescent dyes Calcium-6 and Fura-2 AM (from now on as Fura-2) to evaluate the modulation of P2X4 and P2X3 in 1321N1 and HEK293, respectively.

By quantifying agonist ATP-induced increases in cytosolic Ca²⁺ concentrations (Fura-2 and Calcium-6) or dye uptake (YO-PRO-1), we monitored relative changes in the level of [Ca²⁺]_i or dye uptake in real-time. The fluorescence intensity of Fura-2 and Calcium-6 is proportional to the intracellular free calcium concentration in cytosol (between 0.1 – 0.2 μM at resting state) which is up to ten times less than the extracellular concentration (2 mM). In contrast, the intra- and extracellular concentrations of other ions such as K⁺, Na⁺, and Cl⁻ are not as radically different and our ability to detect these changes is low. Thus, the fluorescent dyes that are susceptible to these ions are not widely utilized. The ability of Fura-2 and Calcium 6 to bind to free intracellular calcium allowed us to monitor the influx of Ca²⁺ through their dedicated channels such as P2X targets.²⁴³ The use of a robotic system that is able to detect and measure the fluorescent signal emitted by the dyes is another important consideration.

In this study, the Flexstation 3 was the best option as it combined the functionality of a kinetic plate reader, with compatible speed, sensitivity and ratiometric output.

3.2.2. Assay Optimization

When developing the assays in 96-well format, a variety of systematic investigations in assay parameters led to the following optimal conditions that are outlined in the Chapter 2. Critically, the incubation buffers used in the Fura-2, YO-PRO-1, and Calcium-6 assays differ; the use of Fura-2 on 1321N1-hP2X4 requires a calcium-containing buffer while the buffer for YO-PRO-1 and Calcium-6 assays on HEK293-hP2X3 and HEK293-hP2X7 is devoid of Mg^{2+} ions and contains a very low concentration of Ca^{2+} ions. The variation in incubation buffer is crucial since these ions were shown to inhibit hP2X7 pore formation,²⁴⁴⁻²⁴⁵ however, extracellular Ca^{2+} ion concentration didn't seem to affect hP2X4 nor hP2X3. While facilitating protein function is critical, the real power of such *in vitro* assays lies in their HTS performance. Thus, the assay conditions were optimized to suit screening requirements. Here we had to consider two desirable outcomes – evaluation of inhibition and identification of toxin hits.

First, the pharmacological suitability of Fura-2, YO-PRO-1 or Calcium-6 assays for P2X targets on the chosen cell lines (**Figure 3.2 – 3.4**).

In order to calculate EC_{50} values in these cell lines, concentration-dependant studies were carried out with ATP in 1321N1-hP2X4 (**Figure 3.2**), HEK293-hP2X7 (**Figure 3.3**), and α,β -meATP in HEK293-hP2X3 (**Figure 3.4**). The resultant values corresponded well with the values in the literature.²⁴⁶⁻²⁴⁹ Since these *in vitro* assays must be capable of identifying inhibitors with the desired potency and mechanism of action, these EC_{50} values were used to investigate the effect of several commercially available antagonists for hP2X3 (purotoxin-1), hP2X4 (BX430, PSB12062, 5-BDBD) and hP2X7 (AZ10606120).

In order to compare all data, the normalised concentration-response curves were fitted with a sigmoidal graph and their EC_{50} and IC_{50} values determined. For 1321N1-hP2X4 cell line, the EC_{50} was found to be $1.96 \pm 0.39 \mu\text{M}$ (**Figure 3.2B**). Against 1321N1-hP2X4 (**Figure 3.2A**) the calculated IC_{50} values were found to be $0.42 \pm 1.02 \mu\text{M}$; $5.36 \pm 1.30 \mu\text{M}$ (5-BDBD); and $0.55 \pm 0.99 \mu\text{M}$ (BX430). Despite high ATP potency, 5-BDBD was unable to completely abolish ATP-evoked Ca^{2+} responses in 1321N1-hP2X4 cells. In HEK293-hP2X4 (**Figure 3.2C**) the calculated IC_{50} values were found to be $0.76 \pm 0.67 \mu\text{M}$ (PSB12062); $9.20 \pm 0.69 \mu\text{M}$ (5-BDBD); and $1.30 \pm 0.62 \mu\text{M}$ (BX430).

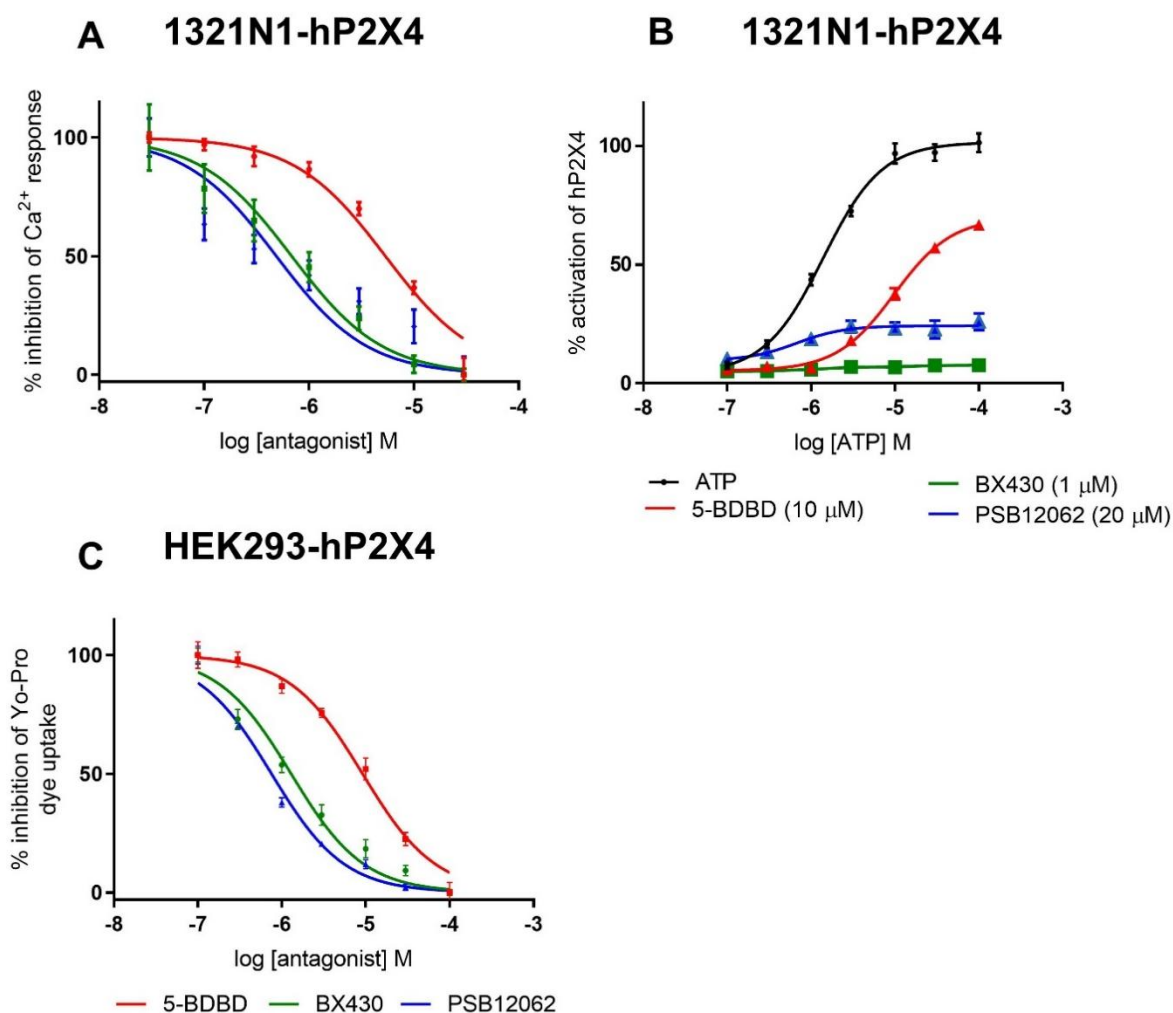


Figure 3.2. Validation of the stable cell lines expressing hP2X4 for HTS. **A, B:** Normalized concentration-response curves of commercially available hP2X4 antagonists ($n=3$) PSB12062, 5-BDBD, and BX430 using the ATP concentration of $1.6 \mu\text{M}$ (EC_{50}) on the 1321N1-hP2X4 cell line with the Fura-2 dye. **C:** Normalized concentration-response curves of commercially available hP2X4 antagonists ($n=3$) PSB12062, 5-BDBD, and BX430 using the ATP concentration of $1.6 \mu\text{M}$ (EC_{50}) on HEK293-hP2X4 with the YO-PRO-1 dye.

On HEK293-hP2X7 (**Figure 3.3**), the EC_{50} for ATP was found to be $286.6 \pm 35.4 \mu\text{M}$ (**Figure 3.3A**). This concentration was then used to determine the IC_{50} for P2X7 antagonist AZ10606120 which was calculated to be $92.0 \pm 15.8 \mu\text{M}$ (**Figure 3.3B**).

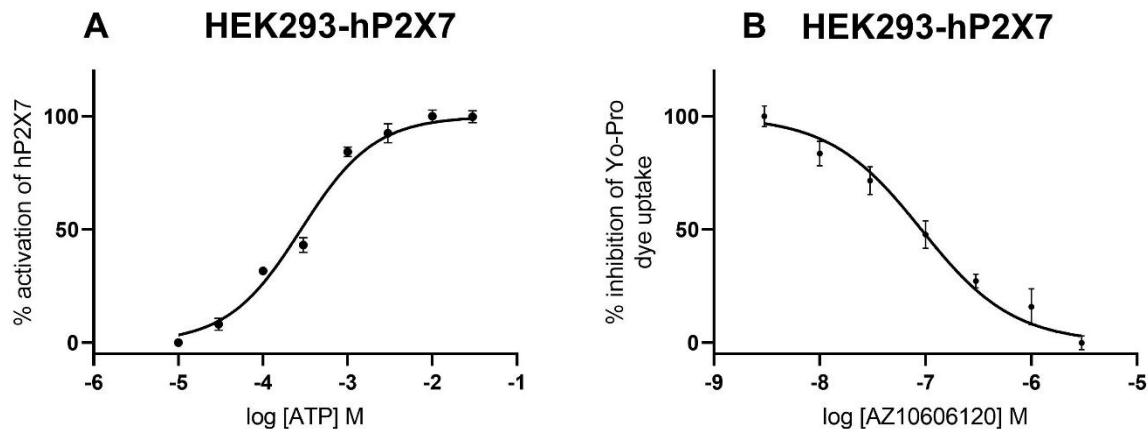


Figure 3.3. Validation of the stable cell line expressing hP2X7 for HTS. **A:** Normalized concentration-response curve of ATP on a stable HEK293-hP2X4 cell line ($n=3$) ($EC_{50} = 286.6 \pm 35.4 \mu\text{M}$). **B:** Normalized concentration-response curve of commercially available hP2X7 antagonist AZ10606120 ($n=3$) using the ATP concentration of $286 \mu\text{M}$ (EC_{50}) on HEK293-hP2X7. The experiments were carried out using YO-PRO-1 dye.

On HEK293-hP2X3 (**Figure 3.4**), we showed the calculated EC_{50} to be $15.8 \pm 2.87 \mu\text{M}$ (**Figure 3.4A**), and the IC_{50} value for purotoxin-1 (PT1) was found to be $6.26 \pm 3.56 \text{ nM}$ (**Figure 3.4B**). Once this cell line was pre-incubated with PT1 at $1 \mu\text{M}$, the α,β -meATP responses were reduced by 79% (**Figure 3.4A**).

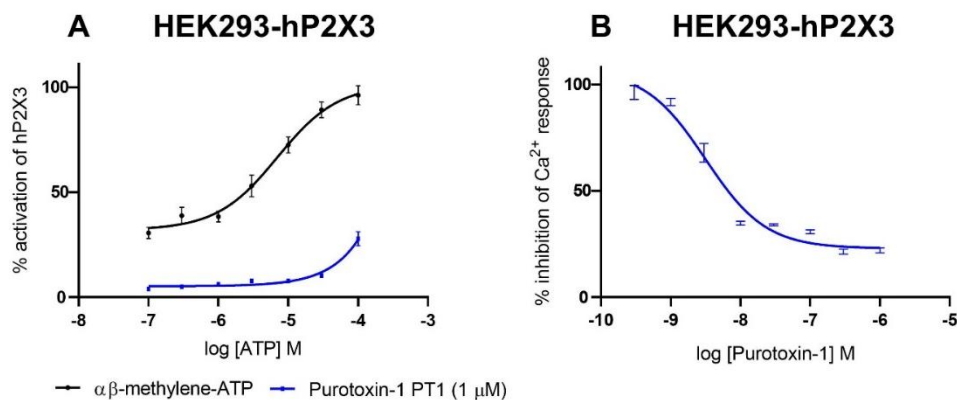


Figure 3.4. Validation of the stable cell line expressing hP2X3 for HTS. **A:** Normalized concentration-response curve (*black line*) of α,β -meATP ($EC_{50} = 15.8 \pm 2.87 \mu\text{M}$) and pre-incubation (*green line*) with $1 \mu\text{M}$ of the commercially available hP2X3 antagonist PT-1. **B:** Normalized concentration-response curve of PT1 ($n=3$) using the α,β -meATP concentration of $16 \mu\text{M}$ (EC_{50}) on HEK293-hP2X3. The experiments were carried out using Calcium 6 dye.

All the IC₅₀ literature values, except those for hP2X3, are reported in **Table 3.1**. In case of hP2X3, the IC₅₀ value for purotoxin-1 was reported as 12 nM by Kabanova and others²⁴⁶ which is two magnitudes higher than the value reported here but is still within a similar range.

Table 3.1. IC₅₀ values of known P2X inhibitors calculated using our HTS assays against 1321N1-hP2X4, HEK293-hP2X4, and HEK293-hP2X7 cell lines. *Literature values.

Inhibitor	Cell line								
	1321N1-hP2X4			HEK-hP2X4			HEK-hP2X7		
	*IC ₅₀ [μM]	IC ₅₀ [μM]	95% CI	*IC ₅₀ [μM]	IC ₅₀ [μM]	95% CI	*IC ₅₀ [μM]	IC ₅₀ [nM]	95% CI
BX430	1.56 ²⁴⁷	0.55	0.34–0.87	0.54 ¹⁵³	1.30	1.15–1.46	N.A. N.A. N.A.		
5-BDBD	N.A.	5.36	4.33–6.65	1.20 ²⁵⁰	9.20	8.36–10.01			
PSB12062	3.31 ²⁴⁷	0.42	0.25–0.73	1.38 ¹⁶⁶	0.76	0.69–0.83			
AZ10606120	N.A.			N.A.			~10.00 ²⁵¹	92.0	80.9–10.5

Based on these results, we concluded that our assays represent a good starting point for the pharmacological characterization of known drugs. That said, IC₅₀ values for the 5-BDBD, PSB12062 and AZ10606120 in HEK293-hP2X4, 1321N1-hP2X4, and HEK293-hP2X7 respectively, differed from published examples by sometimes up to 9-fold. This may be due to the independent assessment of IC₅₀ values in different laboratories and the influence of using different assays. Comparing IC₅₀ values measured under similar conditions would be ideal and as the IC₅₀ values from BX430 were the most comparable (and showed only 2-3 fold difference to the ones in the literature^{153, 251}), BX430 was chosen as the positive control for the hP2X4 assays.

For hP2X4 activation, a concentration of 10 μM ATP (rather than the EC₅₀ of 1.96 μM) was used throughout the screening. This was primarily to avoid issues with reproducibility when using the estimated EC₅₀ with 1321N1-hP2X4. Using a higher concentration of agonist (ATP) to activate stably expressed P2X4 in 1321N1 cell lines has been employed before by various groups for the discovery of novel antagonists.^{167, 252} Sometimes these cells responded poorly due to the high passage number (>20 passages) and stopped responding after the 25th passage. For that same reason, the cells were not used for any pharmacological evaluation after the 20th passage.

3.2.3. Screen of Animal Venoms Against hP2X4

Following the optimization of the screening conditions, we ventured into larger-size libraries, such as venoms, to determine assay performance. First, crude venoms were dissolved in water and diluted up to 25-fold from a 1 g/L stock solution into the 96-well assay plate. For our typical HTS crude venom screen, toxins were applied directly onto cells in a 96-well plate at 30 sec prior to application of agonist (ATP) at 100 sec. This incubation time of 70 sec was sufficient to block either P2X4 or P2X7. The fluorescent responses were monitored for a further 200 sec per well following the second application of agonist.

In total, 180 crude venoms (for details see Chapter 2) from arachnids, centipedes, hymenopterans and cone snails were arranged in standard 96-well drug plates and tested in duplicate (L. Stokes, personal communication). A subset of venoms were tested for dose dependent effects in triplicate (10 μ g, 2 μ g, 0.4 μ g per well). Usually, chemical libraries are stored in organic solvents such as EtOH or DMSO²⁵³ and cell-based assays have to be configured to avoid toxic concentrations of these solvents. Conveniently, the venoms (and later fractionated toxins) were all dissolved in low-calcium containing buffer, and thus solvent effects were mitigated. Then, 10 μ L of both crude venom and agonist were applied at 30 s and 100 sec, respectively, and fluorescent responses were measured as a function of time. Critically, while Ca²⁺ responses were measured as Fura-2 dye ratios in 1321N1-hP2X4 cells (**Figure 3.5A-B**), YO-PRO-1 dye uptake (**Figure 3.5C-D**) was measured as area under the curve in HEK293-hP2X4 cell lines.

Since the venoms are complex mixtures of hundreds of components that are found in the crude venoms in various concentrations, the exact concentration of the toxins used in the assays could not be determined. Nevertheless, the studies performed with the diluted series of crude venoms helped to distinguish venoms with higher or lower activity. Hits were then defined as crude venoms/fractions that showed concentration-dependent inhibition with at least 50% inhibition at the highest concentration (10 μ g/well), and whose activities were reproducibly validated.

While venom SV7 did not show modulation of hP2X4, a hit venom - spider venom 1 (SV1) – inhibited activity of 1321N1-hP2X4 in a dose-dependent manner with 10 μ g, 2 μ g and 0.4 μ g venom resulting in ~69%, 27%, and 4% inhibition, respectively (**Figure 3.5A**). This effect was confirmed in HEK293-hP2X4 using another dye (YO-PRO-1) and monitoring dye uptake rather than Ca²⁺ release with Fura-2 dye as used previously (**Figure 3.5C**). Notably, 10 μ g of SV1 venom yielded 69 – 80% inhibition, respectively. This is interesting because the inhibition is similar to the commercially available hP2X4 antagonist BX430 (75% inhibition at 10 μ M).

The response for each crude venom that was plotted as a function of time and is shown on **Figures 3.5B** and **Figure 3.5D** with 1321N1-hP2X4 and HEK293-hP2X4, respectively.

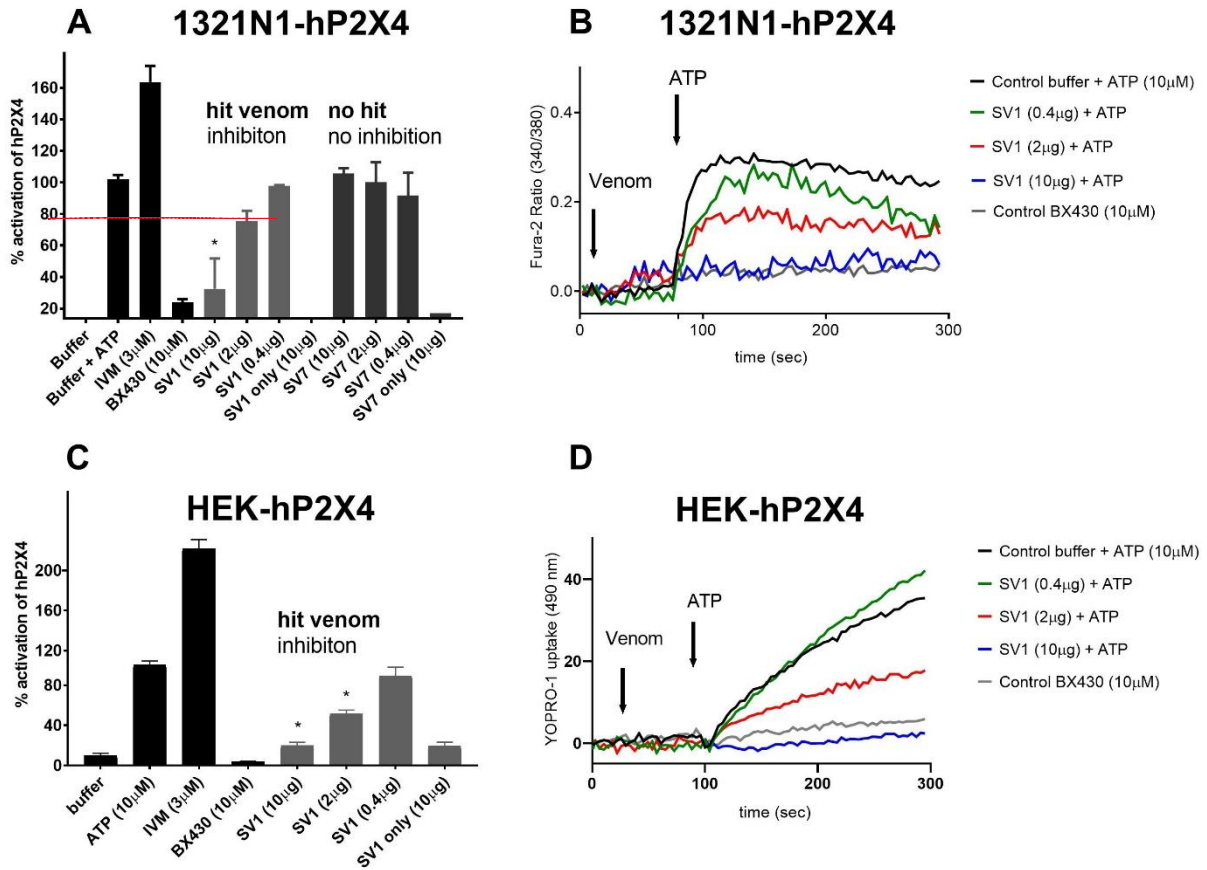


Figure 3.5. Screen of crude venoms against 1321N1-hP2X4 and HEK293-hP2X4 with Fura-2 (at 340/380 nm ratio) and YO-PRO-1 (490 nm). **A:** Representative figure showing the effect of spider venom 1 (SV1) - *Acanthoscurria brocklehursti* and SV7 - *Hickmania troglodytes* together with the controls (buffer, ATP, hP2X4-specific antagonist BX430) on 1321N1-hP2X4 and HEK293-hP2X4 cell lines. While some venoms (e.g. SV1) showed concentration-dependant inhibition of hP2X4 activity, some venoms (e.g. SV7) had no effect. To investigate whether the crude venoms have an effect on their own (data denoted as “Venom SV1/SV7 only”), they were applied alone via Flexstation 3 automated injection system without the later application of the P2X4 agonist ATP. **B:** The kinetic responses of 1321N1-hP2X4 to venom and ATP agonist are plotted. **C:** The dose-dependent inhibitory effect of SV1 was confirmed against the HEK293-hP2X4 cell line via YO-PRO-1 dye and its kinetic responses are shown (**D**). Data points represent mean \pm SD of three replicated experiments with triplicates on each plate except fraction injections.

3.2.4. Fractionation of Crude Venom Hits

Once the crude venom hits were identified, the crude mixtures were simplified through the creation of fractionated venom product libraries. This activity-guided fractionation was previously shown to enhance the identification of minor components in the assay²⁴⁰ and help confirm the fraction hits. C18 RP-HPLC approach was selected to separate components on the basis of their relative hydrophobicity. The elution of fractions was monitored via absorbance at three different wavelengths ($\lambda_1=214$ nm, $\lambda_2=254$ nm and $\lambda_3=280$ nm). Some venoms contained fractions that eluted very closely together, resulting in fractions containing multiple toxins. An additional chromatography step was required in such cases to obtain the fractions in higher purity. This was often as simple as an additional C18 RP-HPLC fractionation with a shallower gradient.

All the fractions were separated and collected based on absorbance at 214 nm (**Figure 3.6**). The chromatograms from *L. klugi* (**Figure 3.6A**), *C. geographus* (**Figure 3.6C**), *V. germanica* (**Figure 3.6D**), and *A. mellifera* (**Figure 3.6E**), are consistent with the chromatograms for these species reported in the literature.^{224, 254-256} The elution profiles varied between cross-families, but not so within-families. The number of fractions varied from 25 to 49 relative to the particular venom, and most fractions represented only a small part of the overall venom profile. However, the venom of *L. klugi* represented a unique exception since the six fractions (out of 25) appeared to account for >75% of venom toxins.

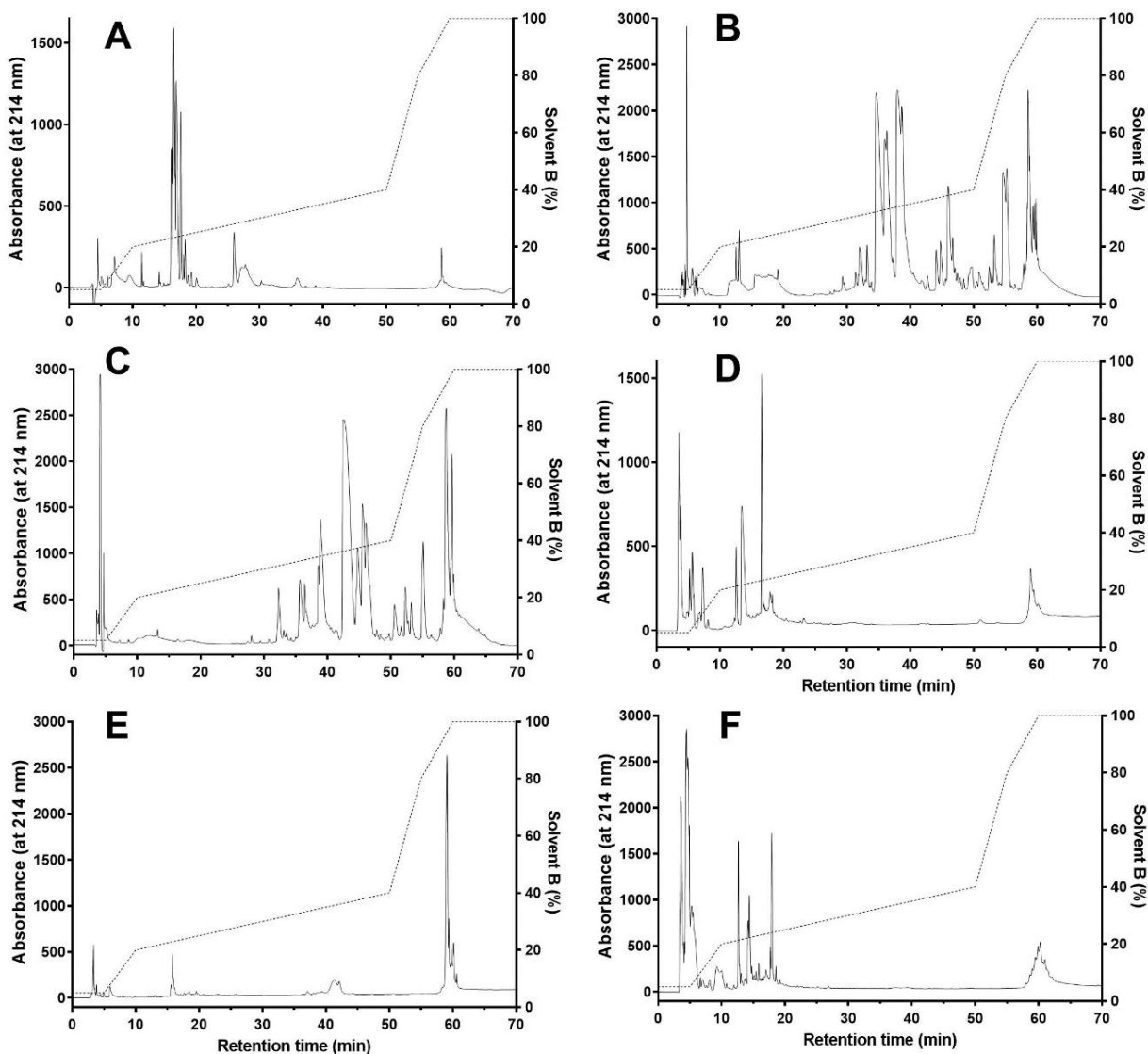


Figure 3.6. Representative RP-HPLC chromatograms displaying the fractionation of crude venoms from various venomous animals. **A:** Bahia scarlet tarantula (*Lasiodora klugi*); **B:** Brazilian tarantula (*Nhandu chromatus*); **C:** Marine cone snail (*Conus geographus*); **D:** German wasp (*Vespula germanica*); **E:** European honeybee (*Apis mellifera*); **F:** Asian hornet (*Vespa velutina nigrithorax*). Crude venoms were fractionated and purified on an analytical C18 RP-HPLC column and components eluted at a flow rate of 1 mL/min using a gradient of solvent B (90% MeCN), 0.05% trifluoroacetic acid (TFA in H₂O) in solvent A (0.05% TFA in H₂O) as indicated by the dotted lines. Absorbance was monitored at 214, 254 nm and 280 nm, however, for easier representation, only the 214 nm absorbance is plotted here.

3.2.5. Assay Hit Identification and Validation

Broach and Thorner²⁵⁷ have suggested that a well-designed HTS that delivers information on selectivity may be obtained by running a counter-screen with a target related to the protein of interest. For that reason, venom fractions were screened against hP2X3 and hP2X7 versus hP2X4 and toxins exhibiting activity against only the primary (hP2X4) receptor were targeted, as they may be more selective. Moreover, examining the range of toxins that score positively as hits may help to pinpoint the structural characteristics that are responsible for the efficacy of the toxins. Such preliminary structure-activity relationships may assist in further optimizing lead compounds and deliver information about achieving cytotoxicity requirements.

For the purpose of method validation, the inhibitory activity of fractions from *Nhandu chromatus*, followed by agonist application, was investigated in detail here. These fractions were assessed for hP2X4 inhibitory activity using the fluorescent-based bioassays developed on four stable cell lines 1321N1-hP2X4, HEK293-hP2X4, HEK293-hP2X3 and HEK293-hP2X7 (**Figure 3.7**). Crude venom from *N. chromatus* yielded 48 fractions which were initially screened using 1321N1-hP2X4 via the Ca²⁺ based Fura-2 assay (**Figure 3.7A**). These fractions were then validated on an additional cell line (HEK293-hP2X4), using another dye (YO-PRO-1) as seen on **Figure 3.7B**. Furthermore, to test for the target selectivity of the fractions, the evaluation was carried out on HEK293-hP2X3 (**Figure 3.7C**) and HEK293-hP2X7 (**Figure 3.7D**). The appropriate P2X positive and negative controls (ATP, ivermectin,²⁵⁸ buffer, hP2X4-antagonist BX430,¹⁵³ hP2X7-antagonists AZ10606120 and JNJ47965567;²⁵¹ α,β -meATP;²⁵⁹ and the hP2X3-antagonist PT1) were included in the assays.

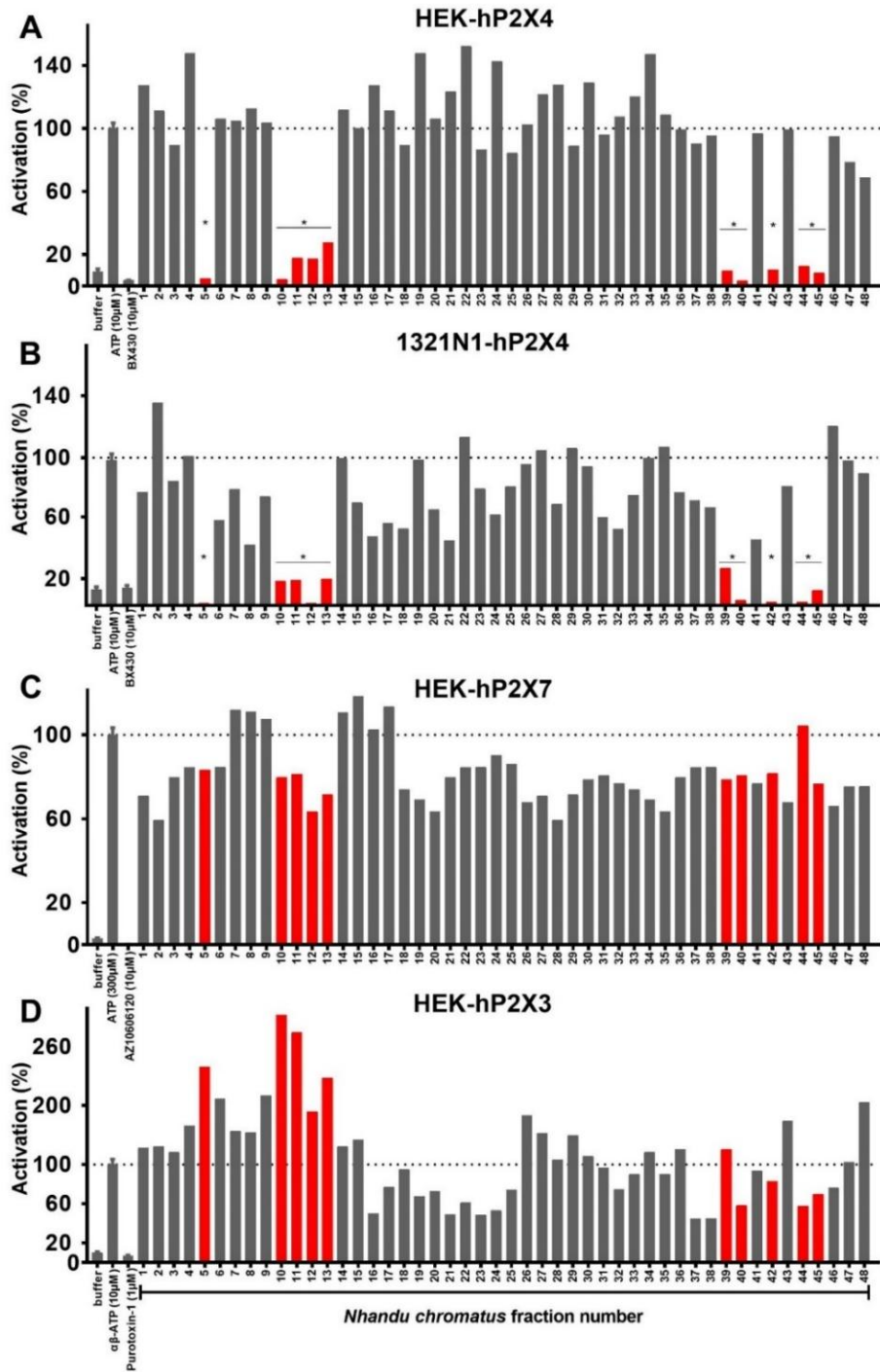


Figure 3.7. Screening of *N. chromatus* venom fractions. Here, **A)** 1321N1-hP2X4 cell line, **B)** HEK293-hP2X4 cell line, **C)** HEK293-hP2X7; and **D)** HEK293-hP2X3 cell lines were used. Fractions coloured green selectively inhibited hP2X4. The dash represents 100 % hP2X4 activity as induced by 10 μ M ATP. Data points represent the mean \pm SD of three replicated experiments, with triplicates on each plate except fraction injections. Significant differences between the positive control (ATP) and the fractions on either 1321N1-hP2X4 or HEK293-hP2X4 cell line are indicated by * ($P < 0.05$) using one-way ANOVA followed by Dunnett’s test.

By comparing the results between P2X3, P2X4 and P2X7 expressing cell lines, some noteworthy inhibitory patterns of venom fractions can be seen. For example, 10 out of 48 fractions inhibit hP2X4 by >75% (**Figure 3.7A**) in the 1321N1 cell line and nine of these 10 were also active against the HEK293-hP2X4 cell line (**Figure 3.7B**). This validation rate of 90% falls into an acceptable range for HTS assays.²⁴⁰ Furthermore, fractions F10 - F13, F40, F44 - F45 displayed <20% inhibition on hP2X7 (**Figure 3.7C**) or hP2X3 (**Figure 3.7D**); F39 and F42 did not exhibit inhibition on either of these two receptors; and F5, F44 showed a slight potentiation on hP2X3. These examples further highlighted the selectivity of our toxin hits for hP2X4. This set of assays also allowed the exclusion of several hit fractions identified using the 1321N1-hP2X4 (Fura-2) cell line since they couldn't be validated using the HEK293-hP2X4 (YO-PRO-1) cell line. We call these fractions false positive hits (e.g. F15 - F18, F21, F31 - F32).

In addition to false positive hits, the toxin fraction hits that were active against hP2X3 and hP2X7 (e.g. F16, F21 - F24, F37 - F38 and F28, F35, respectively) were omitted as non-specific hits. Generally, the entry point for any drug discovery screening is the identification of modulators with specific and potent activity against the target of interest.²⁶⁰ Thus, these initial hits from our HTS provided a valid starting point to rapidly trace pharmacologically relevant compounds.

While this establishes the fluorescent Fura-2 and YO-PRO-1 assays as effective for measuring inhibitory activity on venom fractions on 1321N1-hP2X4 and HEK293-hP2X4, respectively, there are still some limitations worth mentioning. First, some venom toxins yielded non-specific calcium responses prior to agonist application, and some wasp venoms (e.g. *V. germanica*) either interfered with the fluorescent signal generation or had cytotoxic pore-forming activity (**Figure 3.8**). As soon as these crude venoms were applied to the 1321N1-hP2X4 cells at 30 sec, they initiated a strong Ca²⁺ response (denoted as arrow "Venom" on **Figure 3.8A-C, green**) prior to injection of ATP at 100 sec. While our buffer control did not elicit any response at 30 sec (**Figure 3.8A-C, black**), the application of venom caused up to 2-fold greater calcium responses, relative to the control. Part of the observed effect might be either a presence of agonist-like toxins; highly concentrated biogenic amines (spermine, spermidine, histamine, acetylcholine, and serotonin), pore-forming and cytolytic toxins (mellitin²⁵⁶); or high concentrations of the crude venom itself. These fractions may simply modulate some endogenously expressed receptors in these cell lines such as NMDAs²⁶¹ or GPCRs, and were thus categorized as non-specific.

Critically, the majority of the fractionated compounds from *V. germanica* exhibited yellow or red colour – which is not ideal since it may present a limitation to our fluorescence-based assays.

As Simeonov and Davis²⁶² suggested, coloured compounds might display autofluorescence, absorb light itself, and thus interfere with the fluorescence assay.²⁶² Thus, we subjected these wasp fractions to the interference assay (data now shown). Unsurprisingly, the coloured fractions absorbed the excitation light within a wide range of investigated wavelengths (340 nm, 380 nm and 490 nm for Fura-2 and YO-PRO-1, respectively). This interference resulted in decreased measured fluorescent intensity of the assays using these fractions as a consequence of fluorescent quenching. Thus, we had to disregard these samples and conclude that the vast majority of the wasp venom fractions could not be used in the fluorescent assays reported here. Alternatively, a different method utilizing patch-clamp electrophysiology could be used that would not involve using the fluorescent dyes.²³¹ However, due to the time constraints, probing wasp venom fractions using a non-fluorescent technique was deemed beyond the scope of this body of work.

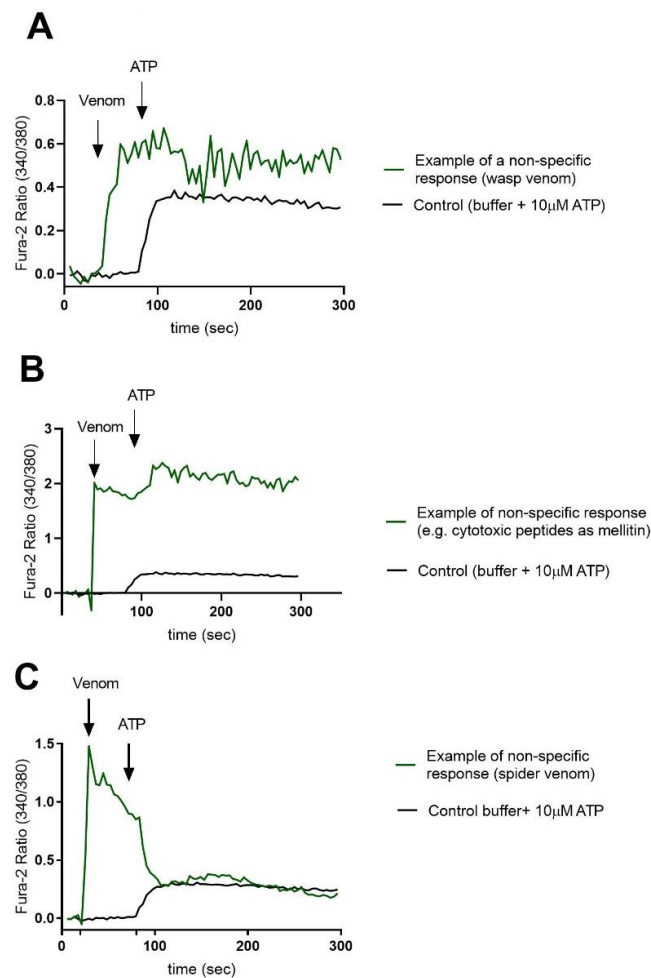


Figure 3.8. Nonspecific Ca^{2+} responses on 1321N1 cells. The experiments were carried out with Fura-2 dye from **A)** crude spider venoms **B)** wasp venom toxins, and **C)** cytotoxic and pore inducing peptides interfering with the fluorescent dye measurements.

3.2.6. Assay Specificity

Once the crude venoms and their respective venom fractions were screened and preliminary hits identified, evaluation of assay precision, reproducibility, specificity, and variability was carried out. To assess these parameters, fractions F14, F28 and F47 that had no effect on any of the studied P2X receptors were chosen as the negative controls alongside F5 that showed inhibition of hP2X4 (**Figure 3.9**). When F5 was tested on 1321N1-hP2X4 (**Figure 3.9A**) and HEK293-hP2X4 (**Figure 3.9B**), Ca²⁺ signals and YO-PRO-1 dye uptake, respectively, were similar and resulted in an up to 50-fold difference in signal when compared to the ATP control. However, against off-target hP2X7, that difference was significantly less pronounced in HEK293-hP2X7 cells (**Figure 3.9C**) where ATP control and each of the fraction (F5, F14, F24, F47) signals produced similar patterns.

Generally, the evaluation of assay specificity verified that these assays are specific for the intended measure (inhibition) and analytes (toxins), and can select the active venom constituents from a complex mixture of crude venom without positive or negative interference. In some cases, assay specificity may also be evaluated by examining a difference in fluorescence between a sample and its physiochemically similar analyte. These two compounds (fraction F5 spiked with F14/F28/F47) would be co-administered as spiked concentrations to determine the lower limit of quantification (LLOQ) and estimate the concentration at which interference is most likely to take place. Due to the scarcity of toxin material, this type of evaluation could not be realized practicably.²⁶³

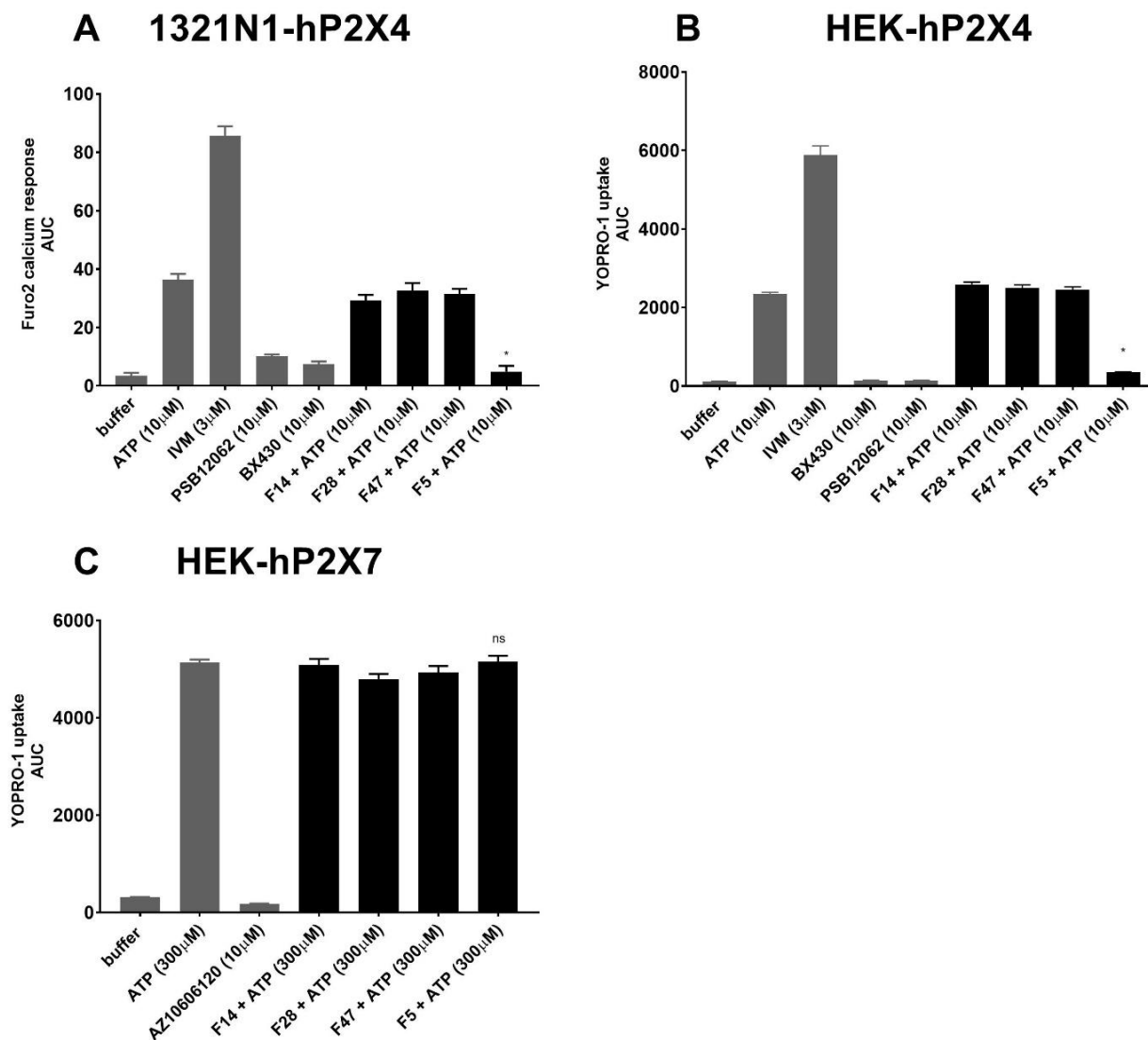


Figure 3.9. Assay specificity. A hit venom fraction (F5) was tested for a response in the **A**) Fura-2 1321N1-hP2X4, **B**) YO-PRO-1 HEK293-hP2X4 and **C**) YO-PRO-1 HEK293-hP2X7 assays, together with the commercially available compounds (BX430, PSB12062, AZ10606120, IVM) that are known modulators of hP2X4 and hP2X7, and inactive venom fractions (F14, F28, F47). Data points show the mean \pm SD of three experiments with triplicates on each plate except when stated otherwise. Significant differences between the positive control (ATP) and the fractions on either 1321N1-hP2X4 or HEK293-hP2X4 cell line are indicated by * ($P < 0.05$) using one-way ANOVA followed by Dunnett's test.

3.2.7. Assay Reproducibility

For the assay to be deemed reproducible across assay plates and different days within the compound screening program, the Z' factor is usually evaluated.

This is a standard statistical parameter for judging the quality of HTS assays and a common method for measuring assay quality per plate.^{220-221, 234} One of the strengths of the Z' factor is to consider the signal window in the assay as well as the variance between both - the high and low signals in the assay. While Z' values range from 0 to 1, many industry groups prefer to work with a Z' factor >0.6. However, a value higher than 0.4 is still considered robust enough to indicate a valid HTS.²³⁴

Some authors use signal window (SW) rather than Z' factor to assess reproducibility. Yet, when studies were carried out comparing both, SW and Z' factor, the authors²⁶⁴ point out that Z' factor can more accurately measure reproducibility. Another advantage of Z' factor is its simplicity and intuitive clarity of results which reduces the amplitude and variability in assay signals to a single parameter. Throughout the assay development, when the conditions are being constantly optimised to achieve the ideal output, Z' factor is highly suitable to fit these needs. On the basis of their²⁶⁴ and the others,^{221, 265-266} it was concluded that using Z' factor for tracking assay performance over time was sufficient for our assay settings.

To determine Z' factor we calculated the mean and standard deviation values for positive (buffer + ATP) and negative (antagonist + ATP) controls. The Z' factor was calculated using the following formula:²²¹

$$Z' = 1 - \frac{3 \times (\sigma_{\text{positive}} + \sigma_{\text{negative}})}{(\mu_{\text{positive}} - \mu_{\text{negative}})}$$

Here, σ is the standard deviation of either positive (σ_{positive}) or negative (σ_{negative}) control, and μ represents the mean of positive (μ_{positive}) negative (μ_{negative}) control. The Z' experiment was performed twice with positive and negative controls (ATP and buffer/inhibitor, respectively) that were used throughout the assay development. Similarly to Zhang,²²¹ 60 positive controls (ATP) and 36 negative controls (hP2X4/hP2X7 antagonist) were tested in the first experiment. In the second experiment, 48 positive controls (ATP) and 48 negative controls (hP2X4/hP2X7 antagonist) were tested.

As suggested by Zhang and colleagues,²²¹ the experiment was only repeated once and the averaged Z' factor, together with the coefficient of variation (CV), for experiments on 1321N1-hP2X4, HEK293-hP2X4, and HEK293-hP2X7 cell lines were as following: 0.565 ± 0.023 (CV 4.11%); 0.697 ± 0.0323 (CV 4.43%); and 0.557 ± 0.012 (CV 2.17%), respectively.

Since our Z' factor is > 0.55, this falls within the range of robust and reproducible assays and indicates that our screening assays are appropriate for HTS applications. Critically, it shows that any plate or systematic errors that may potentially affect the reproducibility of the assay are not substantial.

3.2.8. Assay Variability

In addition to Z' factor, other HTS quality parameters include intra- and inter-plate variability. Here, well-to-well (intra-plate) variability as well as plate-to-plate (inter-plate) variability on six venom fractions and two controls (ATP, antagonists) was determined. As a 96-well format limits experiment design to four controls per plate, and eight replicates each, that left the space for only eight compounds with eight replicates each. Therefore, six venom fractions and two controls were chosen. Due to the scarcity of toxin material, each fraction could only be injected eight times per plate thus different fractions had to be selected for each plate. Critically, these fractions were chosen randomly, prepared as described in Chapter 2, and stored at 4°C for the duration of the study until used. Each prepared fraction was tested on three different days with eight replicates per plate throughout one month.

For the 1321N1-hP2X4 assay (**Table 3.2**), inter-plate variability analysis resulted in a mean %CV of 9.98 (min – 6.43%, max – 13.82%, median – 8.83%). The calculated intra-plate variability was 4.47% (min – 0.84%, max – 10.26%, median – 3.01%). Since the variability distribution is rather skewed, the median may give a more realistic estimate of central value and was thus chosen as a more robust measure of data distribution relative to the mean. Signal AUC values for positive controls on each plate were averaged to normalize results for each fraction and exposed AUC signal values were calculated as a percentage of a positive control signal. Normalised mean was calculated by normalising data to the control, expressed as 1.0.

Table 3.2. Assay variability between runs on 1321N1-hP2X4. Assay variability between runs was evaluated on eight compounds: venom fractions, a negative control (10 µM BX430) and a positive control (10 µM ATP) on 1321N1-hP2X4 that were included on each plate. NC=negative control.

Fraction	Normalised Mean	%CV
NC F4	0.89	10.3
NC F7	0.97	7.3
NC F15	1.04	6.5
NC F21	0.92	2.9
NC F29	0.86	0.8
NC F34	0.85	3.2
NC F37	0.85	2.3
Control (BX430)	1.00	2.6

For the HEK293-hP2X4 assay (**Table 3.3**), inter-plate variability analysis demonstrated a mean %CV of 13.59% (min – 11.68%, max – 14.97%, median – 14.13%). The calculated intra-plate variability yielded 4.94% (min – 1.66%, max – 7.52%, median – 5.25%).

Table 3.3. Assay variability between runs on HEK293-hP2X4. Assay variability between runs was evaluated on eight compounds: venom fractions, a negative control (10 µM BX430) and a positive control (10 µM ATP) on HEK-hP2X4 that were included on each plate. NC=negative control.

Fraction	Normalised Mean	%CV
NC F6	1.12	12.9
NC F9	1.08	17.5
NC F17	1.11	14.7
NC F23	1.08	13.0
NC F31	1.11	15.0
NC F35	1.06	14.5
NC F36	0.99	14.5
Control (BX430)	1.05	16.5

The last variability calculation was carried out on HEK293-hP2X7 cell line (**Table 3.4**). Here, the inter-plate variability determination yielded a mean %CV of 14.88% (min – 12.88%, max – 17.49%, median – 14.82%). The calculated intra-plate variability was 5.22% (min – 2.61%, max – 6.07%, median – 5.68%).

Table 3.4. Assay variability between runs on HEK293-hP2X7. Assay variability between runs was evaluated on eight compounds: venom fractions, a negative control (10 µM AZ10606120) and a positive control (300 µM ATP) on HEK-hP2X7 that were included on each plate. NC=negative control.

Fraction	Normalised Mean	%CV
NC F3	1.01	14.7
NC F8	1.07	14.9
NC F16	0.99	14.4
NC F22	1.02	15.3
NC F30	0.96	11.7
NC F40	1.01	13.9
NC F41	0.96	11.8
Control (AZ10606120)	0.99	12.1

Since it would make little sense to run a cheap and easy assay that is highly variable or overly sensitive to inhibition and sample/liquid handling, as well as cell clumping, a coefficient of variation of signal and background (expressed as %CV) was measured. Generally, %CV are rarely below 5%. Even more, if the assays display %CV below 16%, is still considered a good assay with low variability.²⁶⁷

Judging from the intra- and intraplate variabilities, reported as %CV, is clear that these assays demonstrate low variability and high signal to background ratios with mean values between 5.22% – 14.88%. This data points out that the assays are stable, and relatively insensitive to variation in liquid handling, detection instruments and other random errors. As such, the false negatives and false positives may be eliminated from the dataset based on the minimal variability demonstrated by these results and characteristics.

Ideally, a suitable HTS assay would involve a method that generates sample signal that is broadly separate from background. As argued by Sue and Wui,²⁶⁶ one summary statistic, known as S/B (mean signal/mean background) may partially capture that information as a single parameter. Thus, some research groups have adapted S/B measurement rather than %CV as a measure of suitability. While S/B may be useful in early assay development to investigate the plate format or preliminary screenings, it is an incomplete indicator of assay quality. It mainly assesses the separation between signal and background, and doesn't evaluate the variability suggesting it is less appropriate for the assessment of HTS assays.

Another value that can be used to determine assay quality is variability between the pharmacological controls. Within each assay, the controls (ATP and antagonists) fell within a predefined range (%CV between 1.9 – 5.3%), and is thus deemed acceptable (**Tables 3.2 – 3.4**). Additionally, the fractions used in this study remained relatively stable (purity only dropped from >91% to >80%), as measured by RP-HPLC within one month (*data not shown*). These assessments indicate that our fluorescent-based assay provides a rapid and sensitive strategy for HTS screening of animal venoms, and imply that these sorts of assay may be adapted to other libraries of natural products as well.

3.3. Conclusions

In the last century, HTS has been the primary backbone of drug discovery within the pharmaceutical industry. However, in the last decade, it has also made its way into academic settings. This has predominantly been made possible by the development of the robust robotic systems, parallel processing and miniaturization of pharmacological assays – all of which have greatly increased the throughput while keeping costs at bay. The main aim of HTS is to rapidly and accurately screen a large quantity of diverse chemicals to identify “hits” for a specific target.

While the plating formats and number of chemical compounds per plate vary, the automated process allows screening of several hundred plates over a screening program of several weeks. Once identified hits are reproduced, a secondary screen is carried out in order to validate *bona fide* hits. Despite HTS showing promise in directly identifying drugs that received FDA approval (cyclosporine A and mevastatin), usually this is not the case. This drawback exists because HTS does not assess the design and development of a successful drug; thus, the final compound that eventually progresses through strict FDA policies, may be very different from the initial molecule from the chemical library. Rather, medicinal chemistry and pharmacological studies are required to convert a HTS-identified compound into a useful drug. Some of the HTS limitations include: bioavailability (a drug should be absorbed well after oral intake); pharmacokinetics (a drug should remain in the body for a certain time period); toxicity (the nonspecific effects of a drug should be kept at minimum); and absolute specificity (a drug should act on the desired target with minimal effect on the other physiologically-relevant targets).

It is thus not surprising that despite a current popularity of HTS programs, the number of new drugs reaching the market and being approved has declined.²⁶⁰ The literature suggests that the root of this problem may lay in assay optimization and validation.^{234-235, 268} In order to fulfil the promise of HTS, some authors suggest that improving hit specificity and sensitivity cannot be advanced by technological improvements, thus, progress in validation techniques and data analysis are crucial.²⁶⁹ This maturation in HTS programs initiated other shifts as well. For example, a greater emphasis is now placed on the quality and robustness of data, investigation of uncharted targets and novelty of screens rather than the numbers screened within the HTS environment.^{231, 235, 270}

With this consideration, unexplored ion channel targets - purinergic receptors – were probed via a robust HTS assay. Since these ion channels are Ca^{2+} permeable, the measurement of changes in intracellular concentration of these ions may be monitored by using either fluorescent-ion dyes or radiolabelled ions. The approach described in this chapter utilizes the fluorescent indicators in a cell-based 96-well format. The main reason for choosing this approach is due to the fact that fluorescent readout is widely used for Ca^{2+} channels such as P2X receptors. By monitoring the influx of Ca^{2+} ions through open channels, we can measure the relative difference in intracellular concentration of Ca^{2+} levels (usually between 100 – 1000 fold) via a range of commercially available fluorescent Ca^{2+} probes such as Fura-2, and Calcium-6 are the most widely used fluorescent dyes for purinergic receptor functional evaluation. Taking advantage of the large pore formation, a hallmark of P2X receptors, YO-PRO-1 was used to monitor the dye uptake.

Although a cell-and fluorescent-based HTS assay may initially appear daunting, it is still generally considered to be the fastest and cheapest path to hit compound identification.

Some of its limitations include inner filter effect (compounds that absorb the excitation light such as buffer, coloured compounds, biological tissues, plates, etc.), quenching (deactivation of the excited state of the fluorescent dye), auto-fluorescence (anything in the assay, except the dye, that adds fluorescence intensity at the monitoring wavelengths), light scattering (turbidity resulting from insoluble compounds in the medium) and photo bleaching (light-induced reaction such as dye oxidation that results in loss of fluorescence and ability to absorb light). All of them, except auto-fluorescence, can decrease fluorescence intensity and thus result in false positive hits.

Apart from photo bleaching, all of these interferences may originate from the venoms/toxins themselves. But of equal importance is the limitation of the assay signal to avoid perturbation by the toxin's nonspecific effects. These can usually originate from the assay components themselves and can impact HTS directly as false results, both positives and negatives. Consequently, that equates to extra testing and more money spent on cross-checking these nonspecific effects.

Two kinds of nonspecific errors can occur with these assays: "false positives" (inactive toxins against P2X targets but score as hits in the assay) and "false negatives" (active toxin against the P2X targets but fail to score as hits in the assay). While false negatives don't represent a substantial issue, pursuing false positives may result in resource and time loss. Thus, the suitable controls (ATP, buffers and commercially available antagonists in our case) and secondary screens are vital to validate the authenticity of an initial hit. This inefficiency may impact upon the assay efficiency, especially if too many false positives or negatives are generated.

Other inferential errors can be initiated by "noise" - in our case, this was sometimes a consequence of poor pipette delivery and robotic failures. Since the toxins were all prepared on the day in the water-based vehicle (buffer), the differences in toxin concentrations due to the evaporation of solvent was not substantial. Other factors that could, nevertheless, result in higher assay variation include potency differences across toxin fractions, and "edge effect" – column and row bias. If the controls are plated on the edges, this is unfortunate since these would affect the measurements of the crude venoms/toxin library of compounds as they are adjusted relative to these controls. For example, it was found that edge effect alters the detection levels on average compared to the remainder of the plate.

For example, in a 96-well plate, we observed that having eight positive controls in the first column and four negative controls on the last column was less efficient than the opposite arrangement method.²⁶⁹ Positive and negative control well locations were randomly alternated along the available edges of the plate to minimize this edge-related bias.

Other ways to circumvent these interferences with the fluorescent dyes include using other methodologies such as electrophysiology. By monitoring the direct activity of the ion channels, we would thus eliminate the fluorescent dyes that may contribute to these interferences. However, such methodologies are multi-step, require complex automation, and are low throughout. For this reason, homogenous technologies such as *in vitro* fluorescent-based cell assays, which circumvent these challenges have become more popular.²⁴⁰ Furthermore, the majority of *in vitro* HTS approaches have been miniaturized to assay volumes of 96-, 384-, and 1536-well format, with the capacity to capture temporal and spatial target activity data.²⁴⁰ Yet, for these assays to be actually utilized in large screening programs (>10⁴ compounds in the chemical library), these assays would need to be scaled-up to suit the higher-density formats such as 1536, or even 3456 well. By employing larger formats and more dedicated robotic workstations in place, the screening of larger libraries may become more tangible.

Another observed setback with the cell-based HTS assays and their controls is the variability in cell growth patterns, such as cell clumping, or buffer evaporation which may lead to different growth conditions and eventually to position-related bias. This results in the increased rates of false positives and false negatives, something which has been shown and discussed in detail already by Lundholt and others.²⁷¹ These issues were circumvented by using controls that are located randomly within plates, thus avoiding any potential row or column biases.

Other random errors that may affect measurement precision in our set of assays include inevitable influences such as equipment errors (injection dispensing difficulties), human error (compound and control preparation and handling)²⁷² or compound-related errors (stability, solubility, autofluorescence, and degradation). These factors have been circumvented by obtaining replicates, minimizing external variation due to the sample handling, and using statistical power analysis to control the number of false hits. For assays described in this chapter, replicates are defined as samples which were measured repeatedly under the same experimental conditions.

Once the technical and set-up efficiencies have been optimized, and assays carried out, data processing is a logical next step. To further investigate the assay variability, averages (e.g. mean, median) across replicate measurements were obtained. This was made possible due to replicated measurements which provided a direct estimate of variability as well as the probability of detecting true hits. Moreover, as suggested by Malo and colleagues,²⁶⁹ replicates tend to reduce the number of false negatives without – crucially – increasing the number of false positives.

Another potential challenge is that a HTS strategy relies heavily on non-robust statistics. While it is fair to calculate means and standard deviations, these are greatly influenced by putative hits and their statistical outliers. In order to circumvent these issues, more robust parameters may be adopted, such as median, Tukey's biweight function and median absolute deviation. For example, instead of Z' factor, a "normalized percent inhibition"²⁶⁹ or NPI, where the compound measurements are normalized relative to the controls can be used. This way, less measurement bias due to the positional effects (row and column bias) may be detected.²⁷³

This simply means that we divided the difference between the compound measurement (x_i) and the mean of the positive controls (c_+) by the difference between the means of the measurements on the positive and the negative controls ($c_+ - c_-$), as depicted by this equation:

$$NPI = 1 - \frac{c_+ - x_i}{c_+ - c_-}$$

Another robust analogue of Z' score is the B score. Its main advantage is being nonparametric (there are minimal assumptions in the variability distribution), more robust to statistical outliers; and there's a minimal measurement bias when it comes to the positional effects.²⁶⁹ However, given the current statistical trajectory within HTS environment, we have used Z' factor as the preferred processing method.²²¹

Once HTS data had been processed, the next step was to decide which compounds should be considered for a secondary screen. Currently, this stage is not well-defined statistically. A variety of reports suggest that these procedures are based on informal "rules of thumb" which arises as a consequence of capacity limitations. For that reason, we started to look at a raw or pre-processed measurements against crude venoms/toxin hits for each plate separately. Crude venoms/toxin fractions whose inhibitory activity deviates from the bulk of the activity measurements are identified as hits.

Although this subjective “eyeball” approach may be adequate for identifying highly active compounds, toxins with low potency ($IC_{50} > 100 \mu M$) would be challenging to reliably pinpoint in this way, and were likely missed. One way to avoid this might lie in a different processing method, for example to display hits as a percentage of the fractions with the highest measured inhibition (e.g. top 1%). On the other hand, this method is arbitrary and it may result in poor specificity and selectivity across screens. For example, the toxins whose activity exceeds a fixed “percent of control” threshold may also be considered as hits.

My experience regarding false negatives is that little can be done about them and so it is best to adopt a forward-looking perspective. While it is necessary to quantify potential false hits, deciding whether they are negligible in a particular screen or not is also of equal importance. For example, if 0.1% of our 200 venoms/toxins are truly active, a usual 2% false negative rate²⁶⁹ would represent 4 potential candidates lost. So, practically, missing an active toxin hit may matter less if related toxins are detected. While it is not ideal for a natural product hit to go completely undetected, the assay optimization required to take these hits into account could be, in academic lab setting, economically unfeasible.

The HTS reported here can be useful strategy for identifying P2X modulators from animal venoms and may provide a powerful tool in the hit generation process. In principle, arranging fractions and crude venoms into 96-well drug plates allows for rapid screening of hundreds of samples against multiple receptor targets. The reported HTS screens against P2X receptors were demonstrated to provide a reliable, sensitive, and specific method for HTS assessment of venoms and their fractions against hP2X3, hP2X4 and hP2X7. Using these assays, we first showed that this HTS strategy allowed screening of multiple targets and subsequently reduced costs. Second, a more meaningful comparison between targets at early stage of lead compound generation can be brought to our attention. Third, fractionation and further purification of venom fractions allows for the discrimination between cytolytic fractions and those with a specific effect on a particular target. Finally, the majority of validated hits against hP2X4 resulted from spider venoms. This further emphasizes the rich biochemical diversity of this class of natural products. The availability of novel and selective modulators from divergent chemical classes could be useful in understanding the pharmacological insights into P2X receptor family. Future chapters aim to isolate and characterize structurally new P2X4 inhibitors from the spider venoms with an aim of accelerating drug discovery in the purinergic field.

~CHAPTER FOUR~

Discovery of a Small Molecular Toxin from Spider Venom that Selectively Inhibits hP2X4 Receptor

This Chapter is based on a research article, currently in preparation as:

Bibic L., et al. Discovery of a Novel Spider Toxin that Selectively Inhibits P2X4 Receptor. In preparation.

4.1. Introduction

4.1.1. Small Molecule Toxins in Animal Venoms

Animal venoms contain a chemically diverse pharmacopoeia of toxins that affect both insect and mammalian targets.¹⁸¹ These range from either low molecular weight (MW) organic molecules such as acylpolyamines to ones with a greater MW such as peptides, both of which can disturb the function of invertebrate and the vertebrate targets due to their structural similarity.²⁷⁴ Together, acylpolyamines and peptides account for nearly 70% of the spider venom and represent a fertile ground for the discovery of novel therapeutic hits.²⁷⁵ While peptides exhibit molecular size smaller than 10 kDa and are usually highly hydrophobic, the molecular weight of acylpolyamines is usually less than 1 kDa. Furthermore, acylpolyamines are highly hydrophilic¹⁸¹ and share structurally similar features; a lipophilic head group (aromatic indole or phenol group) at one end, and either a primary amino, or guanidine moiety at the other (**Figure 4.1**).

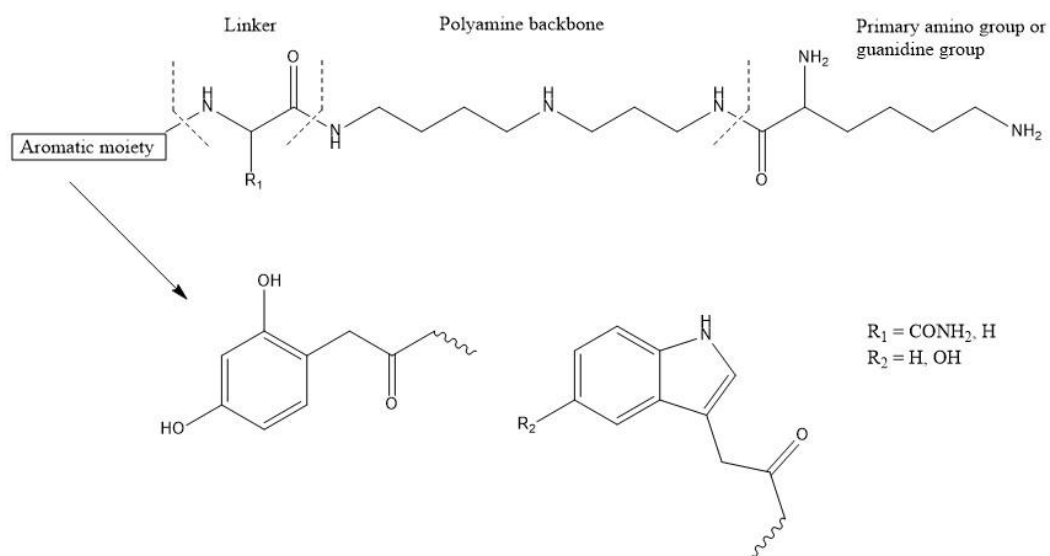


Figure 4.1. General structure of spider acylpolyamine.

Between the aromatic core and its primary amino/guanidine group, various lengths of polyamine components can be found. The link between a polyamine chain and aromatic pharmacophore can be either through an amide bond or through an amino acid linker. Usually the pharmacophore can be either a 2,4-dihydroxyphenyl- or indole-3-acetyl-group with or without a hydroxyl group in the 4- and/or 6-position.^{274, 276-277}

In the early eighties, the acylpolyamines were first characterized as metabolites from spiders and wasps which are capable of paralyzing their prey. Furthermore, their physiological action demonstrated they serve as selective blockers of postsynaptic ionotropic glutamate receptors in invertebrate neuromuscular synapses.²⁷⁸ This was unsurprising, since glutamate is the primary chemical messenger in the neuromuscular junctions of spider's prey (insects). Almost a decade later, Sheardown and colleagues²⁷⁹ showed that acylpolyamines not only block invertebrate, but also vertebrate and mammalian receptors, and may serve as promising leads for development of new therapeutics. By being open-channel blockers, they can selectively block iGlu receptors such as *N*-methyl-D-aspartate (NMDA), α -amino-3-hydroxyl-5-methyl-4-isoxazole-propionate (AMPA), and kainate receptors that play a role in the neurological disorders such as Alzheimer disease and stroke. This ultimately made the acylpolyamines the first inhibitors of such targets.²⁷⁹

However, for acylpolyamines to serve as lead structures, they had to be chemically characterized. The first structural elucidation was carried out in 1986 by Grishin and co-workers,²⁸⁰ yielding argitoxin-636 (ArgTX-636) from the orb-weaver (*Argiope*) spider. Shortly after, ArgTX-673, ArgTX-659, and others followed.²⁸¹⁻²⁸² Following these observations, the *Nephila* genus was also highlighted as a source of various acylpolyamines. Some of these are now known as JSTX-3 (Joro toxin) and NSTX-3 (neosaxitoxin).^{277, 283-287} However, it was not until a mass spectrometry was technologically advanced in the mid-nineties that rapid identification of acylpolyamines could be performed.¹⁸¹ Now, nearly 90% of all acylpolyamines have been structurally elucidated (**Figure 4.2**).²⁸⁸

As soon as the chemical synthesis of acylpolyamines became less complex, researchers started exploring their roles as labeled and photolabile cross-linked probes. The first radiolabeled acylpolyamine was based on ¹²⁵I-containing JSTX-3.²⁸⁹ Later, analogues comprising of photolabile cross-linkers were synthesized that bind to the nicotinic acetylcholine receptors.²⁹⁰⁻²⁹¹ Still, it wasn't until 2009 when the first fluorescently labeled analogue was prepared with neosaxitoxin NPTX-594 as a starting point. Not only did that analogue structurally resemble NPXT-594, but also its potency was confirmed to be equivalent to the original acylpolyamine (**Figure 4.2**).²⁸⁴

4.1.2. Identification and Structural Characterization of Small Molecular Toxins in the Animal Venoms

The first full structural identification of an acylpolyamine toxins was accomplished for argitoxin-636 (ArgTX-636), ArgTX-673, ArgTX-659, JSTX-3, NSTX-3 and other structurally related toxins.^{281-282, 286, 292} The isolation and structural elucidation of these toxins was carried out using ion exchange chromatography coupled with RP-HPLC, and ¹H-NMR with mass spectroscopy, respectively. 2D COSY spectra were used to depict the aromatic systems of the protons coupled via two or three chemical bonds. Fast atom bombardment (FAB) was used as an ionization technique to analyze the fragmentation patterns of the toxins. However, the first chemical synthesis was only achieved later for JSTX-3 and NSTX-3,^{287, 293} thus unequivocally confirming these toxins' structures (**Figure 4.2**).

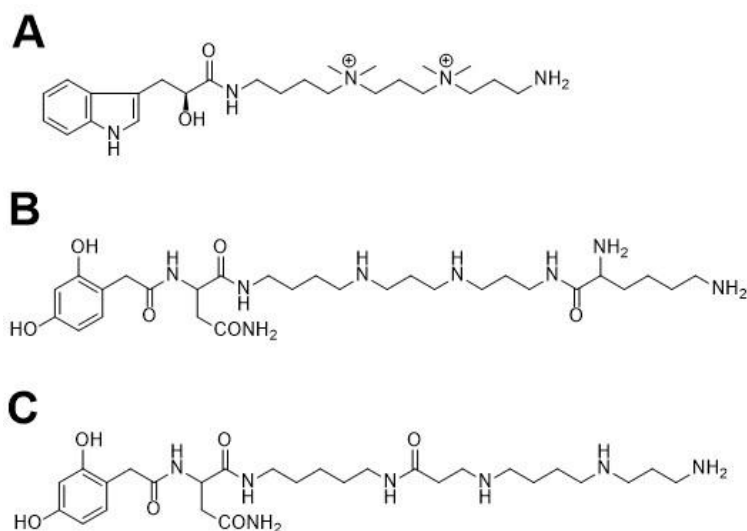


Figure 4.2. Structures of some of the most characterized acylpolyamines. Chemical structures of **A)** MG30, **B)** NPTX-594, and **C)** JSTX-3.

Later, MS methods accelerated the characterization of small molecular toxins that were present in even very small amounts, and combining MS information with one- and two-dimensional NMR spectroscopy enabled characterization of a large number of toxins from *Agelenopsis*, *Nephila* and *Nephilengys* species.²⁹⁴⁻²⁹⁶ However, some structures have not been assigned correctly (Agel-489, Agel-489a, Agel-505a)²⁹⁷⁻²⁹⁸ and later, the total synthesis of these toxins showed they had to be revised.²⁹⁹ With the large number of acylpolyamines structures available, it became necessary to classify them into categories.

Nakajima's group suggested to cluster them based on the polyamine backbone (either cadaverine- or putrescine-like) and the aromatic acetyl group (4-hydroxybenzoyl, 2,5-dihydroxybenzoyl or indolylacetyl group).^{277, 296, 300} Most significantly, some might contain amino acids and have N-hydroxylated amino groups in the polyamine backbone. Moreover, they suggested that when naming newly discovered acylpolyamines, a molecular weight should be added after the initials of the spider from which the toxin was first isolated. For example, NSTX-3 which has the molecular weight of 664 Da, and was isolated from *Nephila Maculata*, would be NM-664, although it remains NPTX-1 for historical reasons.

Not long after these first elucidations, confirmed by synthesis, acylpolyamines from a spider *Hololela curta* were confirmed. In a remarkable study, Tzouros and colleagues³⁰¹ found two different isomers of the polyamine chain that helped the researchers to build the first MS/MS template on how to accurately characterize acylpolyamines.³⁰¹ This exhaustive structural analysis using MS techniques established how spider's biosynthesize these toxins in a combinatorial manner by using only a few building blocks. In turn, this shows that the majority of minor acylpolyamines present in the venoms might not be identified yet since the spiders discarded the non-optimal toxins through evolution over time. Some authors even suggest that the production of the varied acylpolyamine mixtures in the spiders depend upon external stimuli and their purpose of injection into their prey (defense or attack).²⁷⁴

At about same time, Manov and co-workers³⁰² showed that the total synthesis efforts are not only crucial for confirming the structures of the individual toxins but also for identifying the minor components in the crude venoms. By using parallel synthesis and LC-MS/MS coupled with NMR, they were able to depict the small modifications, such as one hydroxyl group, straight after the isolation.³⁰² The other species from which the isolation of the acylpolyamines have been attempted is that of wasps. Philanthotoxin-433 (PhTX-433) is a toxin isolated from the Egyptian digger wasp³⁰³ and its structure highly resembles NPTX-622, an acylpolyamine from a spider *Nephila Maculata*. This clearly points out that both of these organisms have evolved from similar biosynthetic pathways when it comes to these acylpolyamine toxins.

Now, small molecular weight toxins from the animal venoms are mostly identified by a combination of MS/MS analysis and 2D NMR spectroscopy. Once the standard set of spectra (¹H, COSY, HSQC, HMBC and NOESY) were combined with LC-MS/MS techniques, this enabled a rapid evaluation of biological samples, however in destructive manner. Corroboration of these structures was then undertaken by a chemical synthesis of proposed structures, or even via LC-MS and NMR-monitored fractionation of the crude sample.³⁰⁴⁻³⁰⁷

However, one major limitation of using NMR is its poor sensitivity. In case of the animal venoms where we handle a very limited amount of material, this might restrict the full structural elucidation attempt of such toxins,³⁰⁸ although advances in probe design and magnetic field strength look promising.³⁰⁹

4.2. Results and Discussion

In the previous chapter, the HTS for animal venoms is reported as a reliable, automated, fast, robust and quantitative approach for detecting hP2X4 inhibitors from animal venoms. This chapter is concerned with identifying and evaluating some of the toxin hits from the cone snail and spider venoms that have been screened using our HTS method.

4.2.1. Screening Crude Animal Venoms for hP2X Modulators

Here, venoms from cone snails and spiders were tested for their blocking activities towards hP2X4, using either 1321N1-hP2X4 or HEK293-hP2X4 cell line. Other crude venoms tested were those from scorpion and centipede species, bee (*Apis mellifera*) and wasps (*Vespula germanica* and *Vespa velutina*), but these have already been mentioned in Chapter 3 (**Table 4.1**).

Table 4.1. Animal venoms that were screened for hP2X modulators.

Animal	Abbreviation	Animal venom
Cone snail	CS1	<i>Conus textile</i>
	CS2	<i>Conus imperialis</i>
	CS3	<i>Conus geographus</i>
	CS4	<i>Conus victoriae</i>
Spider	SV1	<i>Acanthoscurria brocklehursti</i>
	SV2	<i>Phormictopus cautus</i>
	SV3	<i>Ephebopus murinus</i>
	SV4	<i>Haplopelma doriae</i>
	SV5	<i>Poecilotheria regalis</i>
	SV6	<i>Cyriopagopus</i>
	SV7	<i>Hickmania troglodytes</i>
	SV8	<i>Lasiadora klugi</i>
	SV9	<i>Lasiadora parahybana</i>
	SV10	<i>Phormictopus cancerides</i>
	SV11	<i>Acanthoscurria geniculata</i>
	SV12	<i>Haplopelma albostriatum</i>
	SV13	<i>Nhandu chromatus</i>
	SV14	<i>Acanthoscurria cordubensis</i>
	SV15	<i>Poecilotheria rufilata</i>

4.2.1.1. Probing Cone Snail Venoms Against hP2X4

Conus are a group of predatory marine snails possessing venom which contains toxins that act on calcium channels, sodium channels, NMDA receptors, nicotinic acetylcholine receptors, acid sensing ion channels, voltage-gated calcium and potassium channels, and vasopressin receptors.³¹⁰ We wanted to explore the potential of cone snail venoms against the P2X receptor family. Here, we screened four crude venoms from *Conus textile* (CS1), *Conus imperialis* (CS2), *Conus geographus* (CS3) and *Conus victoriae* (CS4), using HEK293-hP2X4 cells with YO-PRO-1 dye. When comparing these responses to our positive control - agonist (10 μ M ATP) and negative control (10 μ M BX430) – the treatment with a selective antagonist followed by injection of the agonist, none of the crude *Conus* venoms demonstrated modulation of hP2X4 (**Figure 4.3A**). The activity of hP2X4 remained between 81 – 119% with no sign of a dose-dependent inhibition for 10, 2 or 0.4 μ g of crude venom. Furthermore, none of the cone snail venoms seem to have any activity on their own without the later application of ATP (denoted as “CS only”). This notion excludes the possibility of non-specific effects of *Conus* venoms on the HEK293-hP2X4 cell line.

Since no hP2X4 - related effects were displayed with *Conus* venoms, we wondered whether they might show inhibition or potentiation on other P2X receptors. However, when probing these same crude venoms against HEK293-hP2X7, a similar trend was observed – neither CS1, CS2, CS3 nor CS4 showed any significant modulation of hP2X7 as compared to the agonist alone – 200 μ M ATP (**Figure 4.3B**). The activity of hP2X7 was found to be in the range of 92 – 121 %, relative to the ATP control, without any difference between 10, 2 or 0.4 μ g of venom. Moreover, none of the venoms had an effect on their own.

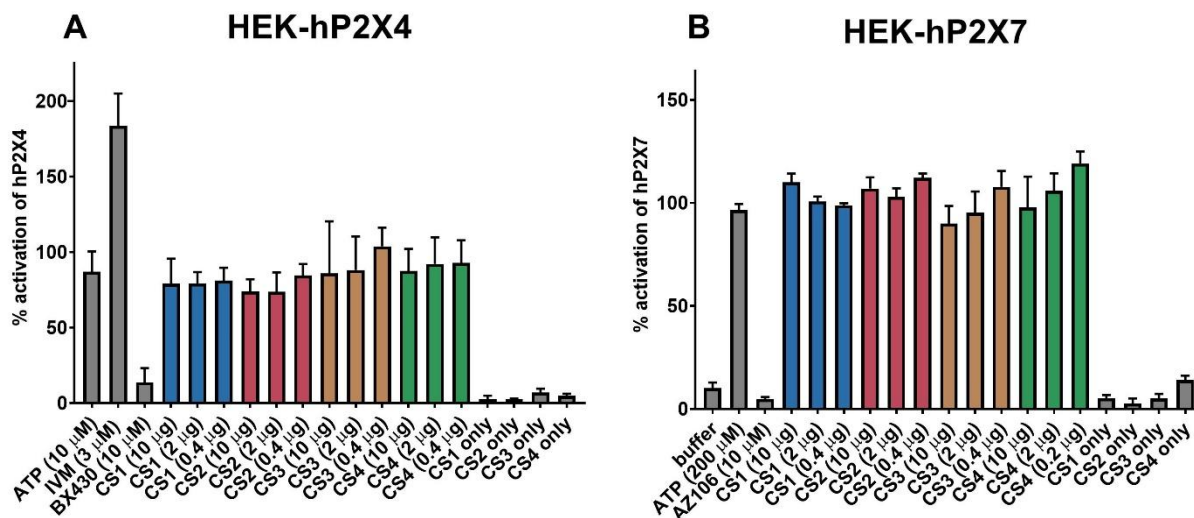


Figure 4.3. A concentration-dependent screen of crude cone snail venoms against hP2X4 and hP2X7. A fluorescent YO-PRO-1 dye uptake screen was conducted for crude *Conus textile* (CS1), *Conus imperialis* (CS2), *Conus geographus* (CS3) and *Conus victoriae* (CS4) against **A**) HEK293-hP2X4 and **B**) HEK293-hP2X7. Percentage of control (%) was calculated as the ratio between the Area Under the Curve (AUC) between YO-PRO-1 uptake (490 nm) of the experimental samples and the positive control (ATP) - denoted as 100 %. Data points represent the mean \pm SD of three replicate experiments with triplicates on each plate except fraction injections.

Then we proceeded to the final target of interest - hP2X3. In this instance, the hP2X3-specific agonist $\alpha\beta$ methylene ATP ($\alpha\beta$ -meATP) was used rather than ATP. This evaluation was carried out in the HEK293 cell line so the P2X3-specific agonist, rather than ATP, which could activate endogenously expressed P2Y receptors, was a preferred option. While CS1, CS2 and CS4 didn't display any modulation, CS3 (*C. geographus*) was found to mediate > 5-fold potentiation of the maximal $\alpha\beta$ -meATP response. This potentiation was found to be concentration-dependent ($427 \pm 14\%$, $179 \pm 39\%$, $97 \pm 42\%$ at 10, 2 and 0.4 μ g, respectively) after application of $\alpha\beta$ -meATP (**Figure 4.4A**).

When looking at the kinetics of hP2X3 responses, the shape of 10 μM $\alpha\beta\text{-meATP}$ – activated hP2X3 calcium response (**Figure 4.4B, black**) is consistent with previously reported observations.³¹¹ After the subsequent application of CS3 (10 μg) this activation increased to 5.2-fold, respectively to the magnitude of the maximal activated response of hP2X3 (**Figure 4.4B, blue**) at 110 sec. However, when only CS3 venom was injected (without a second injection of $\alpha\beta\text{-methyl ATP}$), this same venom showed non-specific responses (**Figure 4.4B, brown**) at the point of application. Due to these observations, we wondered whether the toxins in CS3 venom actually modulate hP2X3 receptor or they merely display non-specific effects in the HEK293 cells.

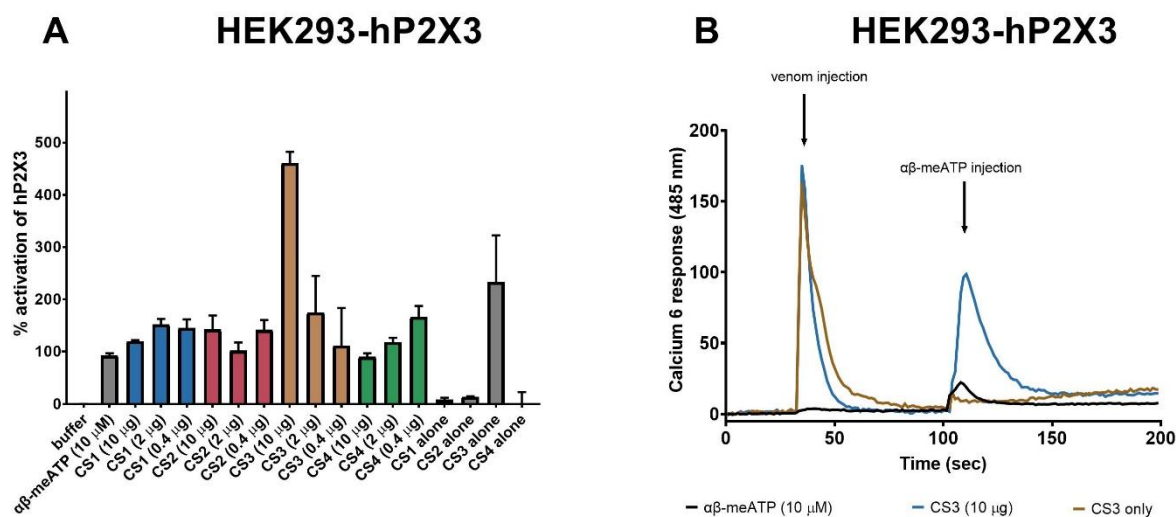


Figure 4.4. A concentration-dependent screen of cone snail crude venoms against hP2X3. **A:** A fluorescent FLIPR Ca-6 screen was conducted for crude *Conus textile* (CS1), *Conus imperialis* (CS2), *Conus geographus* (CS3) and *Conus victoriae* (CS4). **B:** The kinetic behaviour of hP2X3 response when CS3 was applied. Percentage of control (%) was calculated as the ratio between the Area Under the Curve (AUC) between Calcium 6 response (485 nm) of the experimental samples and the positive control ($\alpha\beta\text{-meATP}$) - denoted as 100%. Data points represent the mean \pm SD of three replicate experiments with triplicates on each plate except fraction injections.

To understand the effect of each toxin better, fractionation by RP-HPLC was carried out, as previously shown in Chapter 3 (Section 3.2.4). The CS3 venom yielded 20 fractions which were applied to both, HEK293-hP2X3 (**Figure 4.5A**) and HEK293 cells (**Figure 4.5B**), and effects were investigated using cells loaded with Calcium 6 dye.

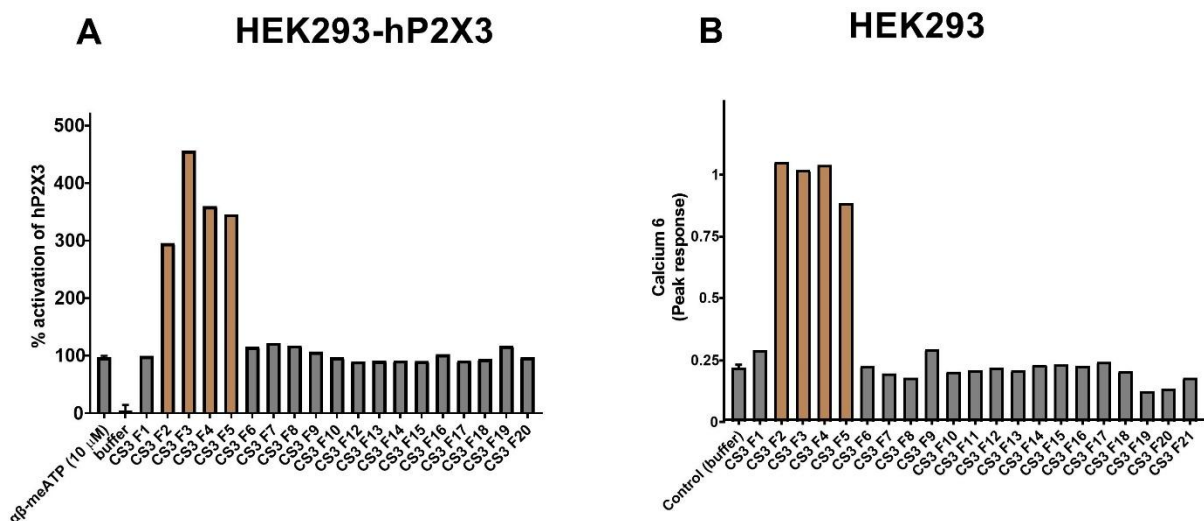


Figure 4.5. A concentration-dependent screen of cone snail fractions against hP2X3. **A:** Application of individual fractions from CS3 on HEK293-hP2X3. **B:** Application of individual fractions from CS3 on a native HEK293 cell line. Percentage of activation (%) was calculated as the ratio between the Area Under the Curve (AUC) between Calcium 6 response (485 nm) of the experimental samples and the positive control ($\alpha\beta$ -meATP) - denoted as 100 % in HEK293-hP2X3 cells. In HEK293 cell line, the peak response was used to analyse the data.

Early eluting fractions (F2-F5) displayed 3 – 4.5-fold potentiation of the $\alpha\beta$ -meATP-induced response in HEK293-hP2X3 cell line, as well as eliciting the response in native HEK293 cells. This suggests the toxins are non-specific for the hP2X3 receptor. Interestingly, this same positive modulation by CS3 was not observed in HEK293-hP2X4 nor HEK293-hP2X7. Part of the reason might lie in the fact that the different assays were used; HEK293-hP2X4 and HEK293-hP2X7 were probed with YO-PRO-1 dye uptake assays, measuring the dye uptake through the channels, while HEK293-hP2X3 and native HEK293 cells were probed using the Calcium 6 dye, measuring the calcium responses upon the toxin application. While it may be safe to say that some of the CS3 toxins (F2-F5) yield non-specific effects, investigating which endogenous receptor expressed in HEK293 cell lines is responsible for such effects might be a fruitful line of inquiry.

4.2.1.2. Probing Crude Spider Venoms Against hP2X4

The venoms of spiders are less well studied than those from cone snails. Their only similarity is at the level of individual peptides indicating that they may have independently evolved similar strategies for immobilizing prey. While the mass distribution in cone snails is skewed toward small peptides (~2.7 kDa), spiders contain both, small molecules (< 1 kDa) as well as larger peptides (~4.4 kDa).¹⁹²

Thus, in order to ascertain whether the spider venoms contain toxins that may differ in their action towards hP2X4, a screen of fifteen crude spider venoms (SV1 – SV15) was carried out (**Figure 4.6**).

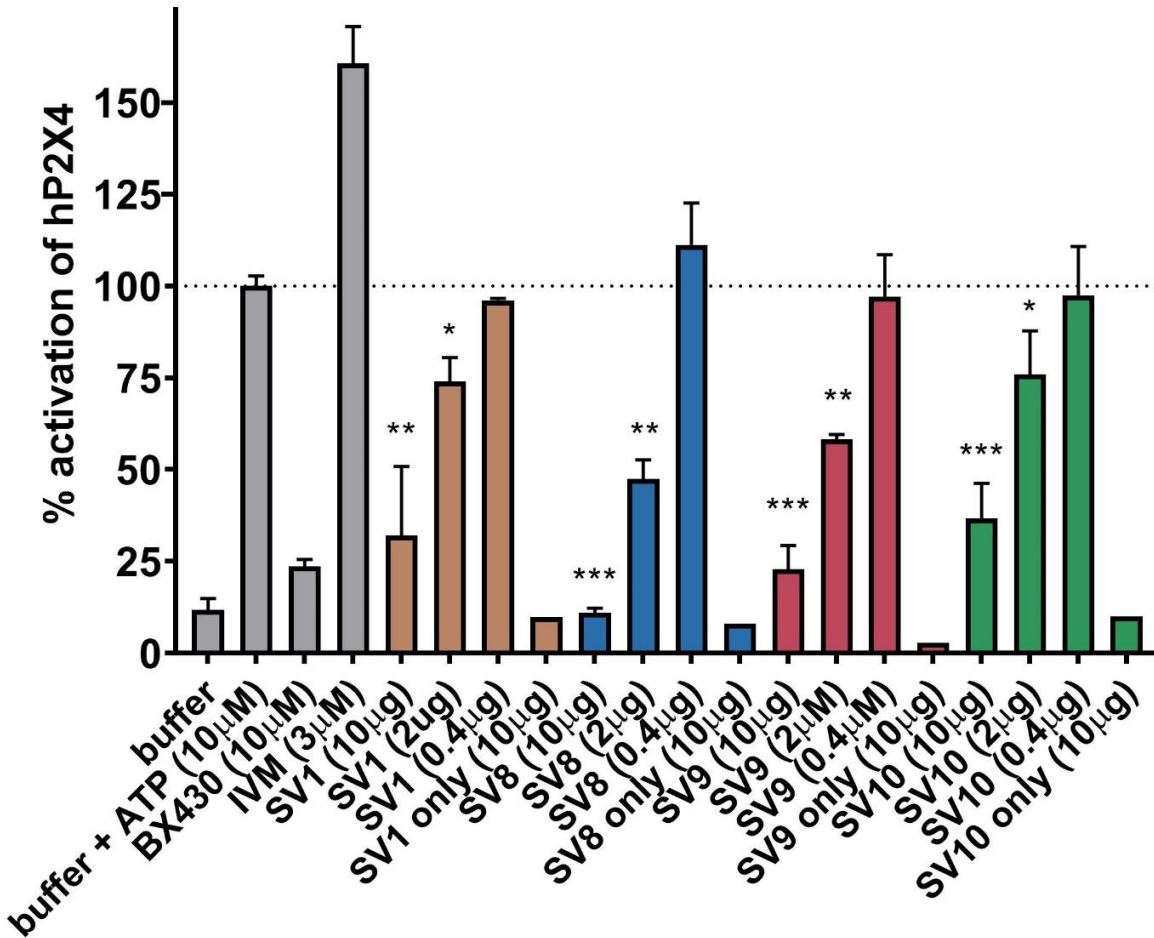


Figure 4.6. Crude spider venom screen. Here, the concentration-dependent inhibition of SV1, SV8, SV9, SV10, and controls (buffer, ATP, IVM and hP2X4-specific antagonist BX430) on 1321N1-P2X4 cells when the crude venom mass varied from 10 μg to 0.4 μg is shown. Percentage of activation (%) was calculated as the ratio between the Area Under the Curve (AUC) between Fura-2 Ratio (340/380 nm) of the experimental samples and the positive control (ATP) - denoted as 100 %. Data points represent the mean ± SD of three replicate experiments with triplicates on each plate except crude venom (“SV only”) injections. Significant differences between the control (10 μM ATP) and the venom are indicated by * (P < 0.05), ** (P < 0.01) or *** (P < 0.001) using one-way ANOVA followed by Dunnett’s test.

The crude venoms reported here were tested in triplicates using 1321N1-hP2X4 cells loaded with the Fura-2 dye. hP2X4 – mediated Ca^{2+} responses were inhibited by a range of crude spider venoms, belonging to either *Acanthoscurria brocklehursti* (SV1), *Lasiadora* (SV8 and SV9) or *Phormictopus* (SV10) family as shown in **Figure 4.6** (see above). When comparing their responses to either a positive control (10 μ M ATP) or negative control (10 μ M BX430), we found these crude venoms demonstrated dose-dependent inhibition of hP2X4 (**Table 4.2**).

Table 4.2. SV1, SV8, SV9 and SV10 demonstrated dose-dependent inhibition of hP2X4 when 10, 2 and 0.4 μ g of venom was applied.

Spider venom/mass of the crude venom	10 μ g	2 μ g	0.4 μ g
	% inhibition of hP2X4		
SV1	69 \pm 19 %	37 \pm 6 %	4 \pm 2 %
SV8	88 \pm 3 %	56 \pm 5 %	< 0 %
SV9	74 \pm 5 %	41 \pm 2 %	3 \pm 12 %
SV10	59 \pm 9 %	35 \pm 8 %	3 \pm 14 %

Among them, crude venom from *Lasiadora klugi* (SV8) demonstrated the most potent inhibition with 10 μ g, 2 μ g and 0.4 μ g yielding 88%, 56%, and 0% inhibition, respectively, when tested on 1321N1-hP2X4 cells. Then, the potency of crude venoms was as follows: *Lasiadora klugi* (SV8) > *Lasiadora parahybana* (SV9) > *Acanthoscurria brocklehursti* (SV1) > *Phormictopus cancerides* (SV10).

Since the effect of the *Lasiadora klugi* seemed promising, we wanted to verify the dose-dependent effect using another stable cell line, and another fluorescent dye (**Figure 4.7**). This led us to use HEK293-hP2X4 cells with YO-PRO-1 dye where 92%, 81%, 46% and 0% inhibition with 10 μ g, 5 μ g, 2 μ g and 0.4 μ g of crude venom *Lasiadora klugi*, respectively, was observed (**Figure 4.7A**). The kinetics of YO-PRO-1 uptake via hP2X4 is shown on the **Figure 4.7B**; notably, 10 μ g of *L. klugi* yielded greater inhibition than the commercially available hP2X4 antagonist BX430 whose inhibition was more similar to 5 μ g of *L. klugi* (86% inhibition at 10 μ M). We concluded that these results were in accordance with our previous findings on 1321N1-hP2X4 cell line, and thus, *L. klugi* - as a potential source of hP2X4 modulators - might be worth exploring further.

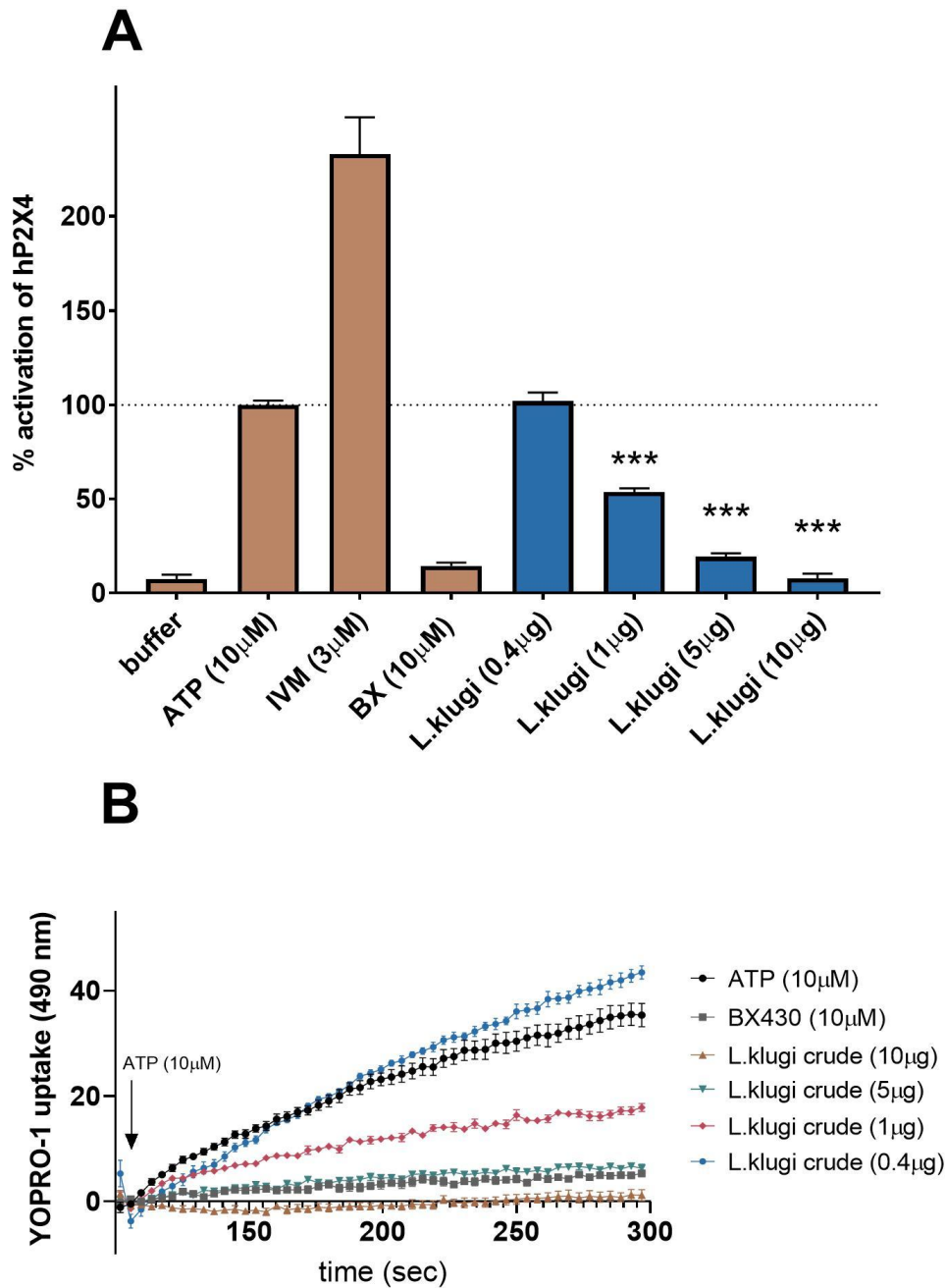


Figure 4.7. Representation of the crude venom *L. klugii* screen against HEK293-hP2X4 cell line. A: Concentration-dependent effect of *L. klugii* relative to the controls (buffer, ATP, and hP2X4-specific antagonist BX430). **B:** The kinetic responses for HEK293-hP2X4 are plotted. Percentage of activation (%) was calculated as the ratio between the Area Under the Curve (AUC) between YO-PRO-1 (490 nm) of the experimental samples and the positive control (ATP) - denoted as 100 %. Data points represent the mean \pm SD of one experiment with triplicates on each plate. Significant differences between the control (10 μ M ATP) and the venom are indicated by *** ($P < 0.001$) using one-way ANOVA followed by Dunnett's test.

However, some of the other crude venoms (*Poecilotheria sp.*, *Haplopelma sp.*, *Cyriopagopus sp.*, *Nhandu sp.*, *Hickmania sp.*, and *Ephebopus sp.*) that displayed potent inhibition in our preliminary screen on HEK293-hP2X4 (L. Stokes, personal communication), showed non-specific calcium responses on 1321N1-hP2X4 (**Figure 4.8**).

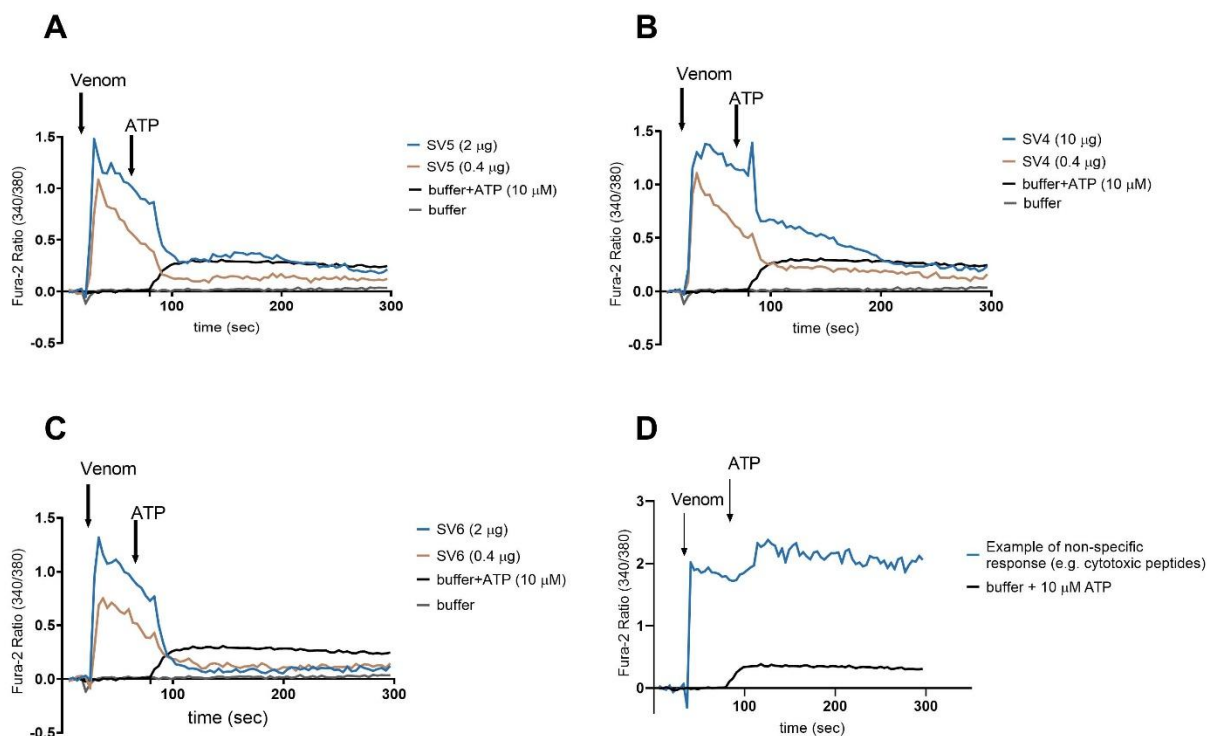


Figure 4.8. Non-specific effects of crude venoms on 1321N1-hP2X4 (Fura-2). Non-specific effects of **A)** *Poecilotheria sp.* (SV5); **B)** *Haplopelma sp.* (SV4); **C)** *Cyriopagopus sp.* (SV6); and **D)** *Acanthoscurria cordubensis* or *Acanthoscurria geniculata*. The venom was applied to the cells at 30 sec prior to the agonist (ATP) at 90 sec.

These venoms triggered non-specific Ca^{2+} signals soon after their application at 30 sec (denoted as “Venom” on **Figure 4.8A-D**, blue). While our control (buffer) did not elicit any response at 30 sec (**Figure 4.8A-D**, black), the application of venom caused nearly 1.5-fold increase in Fura-2 ratio units, relative to the control. Part of the observed effect might be either a presence of the agonist-like toxins; pore-forming and cytolytic toxins; or high concentration of the crude venom.²⁵⁶ However, this also implicates that the true effect of these venoms on hP2X4 might be masked due to presence of such toxins. Thus, in order to enhance the impact of minor components in the assay and deconvolute the crude mixtures, the fractionation of crude venoms was carried out.

4.2.2. Activity-Guided Fractionation of the Spider Venoms Against 1321N1-hP2X4

To facilitate the identification of the active components, these crude venoms were fractionated using RP-HPLC and then individual fractions tested using the 1321N1-hP2X4. However, due to the venom shortage, only eight crude spider venoms (out of fifteen initial hits that showed a potent inhibition at either 1321N1-hP2X4 or HEK293-hP2X4 regardless of the non-specific effects) from *L. klugi*, *L. parahybana*, *A. geniculata* and *A. cordubensis* (**Figure 4.9**); and *P. cancerides*, *H. albostriatum*, *E. murinus*, and *N. chromatus* (**Figure 4.10**) were subjected to semi-prep RP-HPLC.

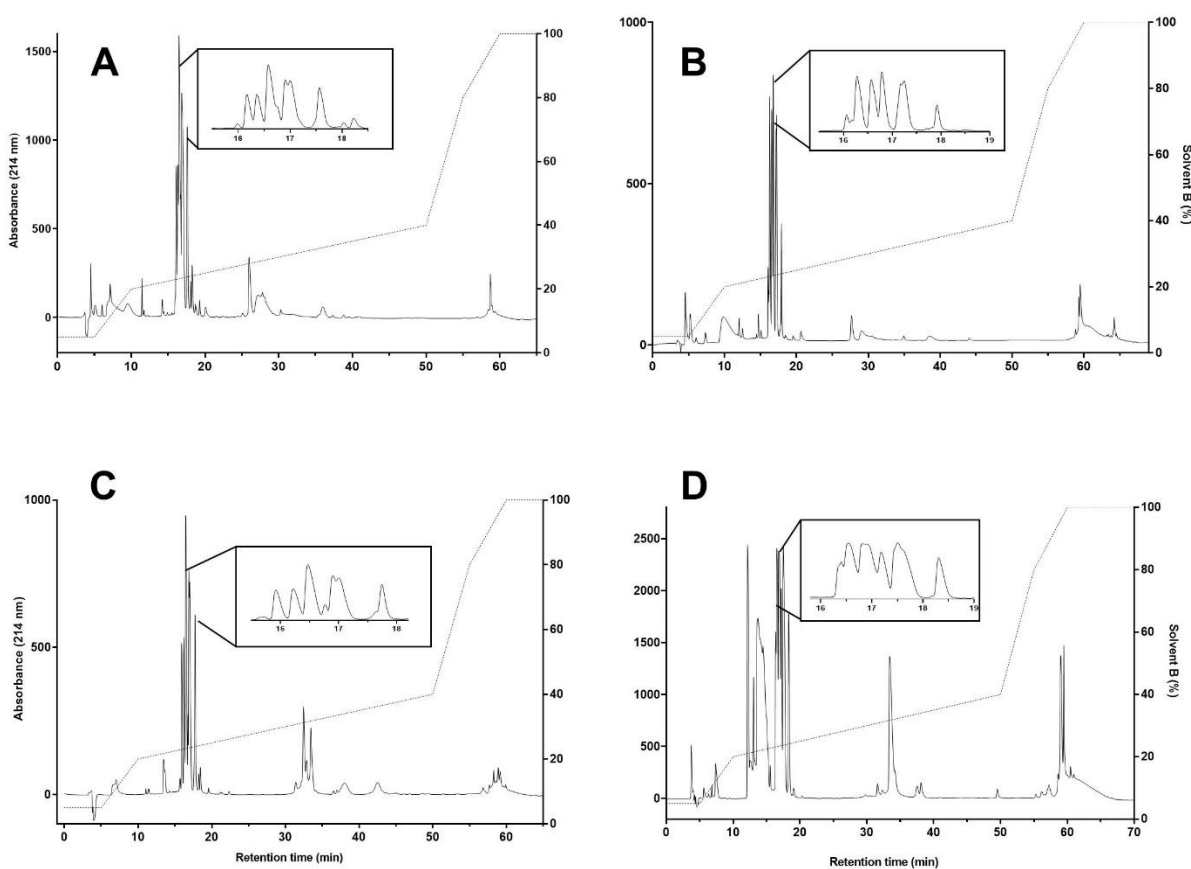


Figure 4.9. HPLC chromatograms from different spider venoms. HPLC chromatograms from tarantula **A)** *Lasiodora klugi*; **B)** *Lasiodora parahybana*; **C)** *Phormictopus cancerides*; and **D)** *Acanthoscurria cordubis*. Venoms were fractionated on an analytical C18 RP-HPLC column (Jupiter 5 μ m; Phenomenex) and components eluted at a flow rate of 1 mL/min using a gradient of solvent B (90% acetonitrile (ACN), 0.05% trifluoroacetic acid (TFA) in H₂O) in solvent A (0.05% TFA in H₂O) as indicated by the dotted lines. Absorbance was monitored at 214, 254 nm and 280 nm, but only the 214 nm absorbance is plotted here.

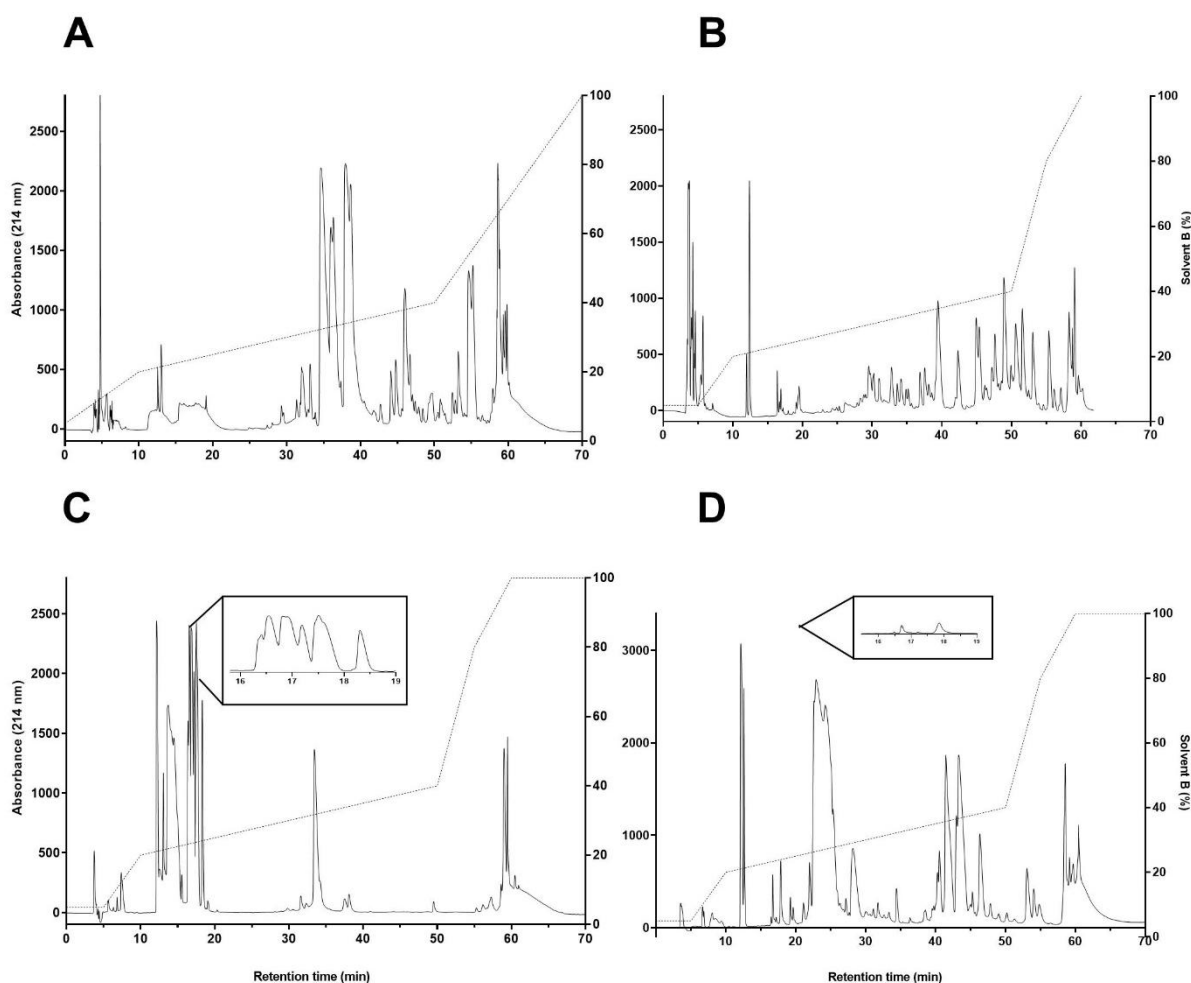


Figure 4.10. HPLC chromatograms from different spider venoms. HPLC chromatograms from **A)** *Nhandu chromatus*; **B)** *Haplopelma albostriatum**; **C)** *Acanthoscurria geniculata*; and **D)** *Epebopus murinus*. Venoms were fractionated on an analytical C18 RP-HPLC column (Jupiter 5 μ m; Phenomenex) and components eluted at a flow rate of 1 mL/min using a gradient of solvent B (90% acetonitrile (ACN), 0.05% trifluoroacetic acid (TFA) in H₂O) in solvent A (0.05% TFA in H₂O) as indicated by the dotted lines. Absorbance was monitored at 214, 254 nm and 280 nm, but only the 214 nm absorbance is plotted here. *The RP-HPLC had to be abruptly stopped at 62 min (rather than 70 min) due to the high system pressure.

The initial separation step showed between 25 - 69 eluted fractions from either of these venoms (**Table S1**, Supporting Information), which is consistent with the chromatograms for these species reported in the literature.^{253, 312-315} The comparison between the RP-HPLC chromatograms for intra-genus species showed similar elution pattern and different peak heights, suggesting potentially different concentrations of the same toxins.

In contrast, the comparison of RP-HPLC inter-genus species chromatograms indicates major differences in hydrophobic components, eluting in the range of 30 – 70% (solvent B gradient). That is expected since the hydrophobic toxins are mostly peptides with structurally varied composition among species. On the other hand, HPLC profiles from the crude hits of *Acanthoscurria*, *Lasiadora*, *Phormictopus*, but not that of *E. murinus*, exhibit similar eluting profiles between 16 – 18 min (inserts on **Figure 4.9** and **Figure 4.10**). Two other fractionated venoms - *Nhandu* and *Haplopelma* also showed some similar eluting characteristics, however, less significant than those of *Acanthoscurria*, *Lasiadora* and *Phormictopus* venom. This suggests that venoms from *Acanthoscurria*, *Lasiadora*, *Phormictopus* and potentially *Nhandu* and *Haplopelma* family may contain similar hydrophilic toxins. Thus, for now, I would like to draw your attention to the early eluting fractions (**Table 4.3**), while the late eluting fractions would be discussed later.

Table 4.3. RP-HPLC retention times of the fractionated toxin hits from various spider venoms that exhibited a similar eluting pattern.

<i>Lasiadora klugi</i>		<i>Nhandu chromatus</i>	
Fraction	Retention time (min)	Fraction	Retention time (min)
F10	16.17	F10	17.40
F11	16.34	F11	17.52
F12	16.58	F12	18.72
F13	17.00	F13	19.67
F14	17.50	-	-
<i>Lasiadora parahybana</i>		<i>Acanthoscurria cordubensis</i>	
F7	16.22	F14	15.79
F8	16.58	F15	16.08
F9	16.85	F16	16.14
F10	16.99	F17	16.57
F11	17.13	F18	16.67
F12	17.92	F19	16.67
F13	18.51	-	-
<i>Phormictopus cancerides</i>		<i>Acanthoscurria geniculata</i>	
F8	16.39	F12	16.54
F9	16.69	F13	16.81
F10	16.90	F14	16.90
<i>Haplopelma albostriatum</i>			
F7	15.34	F9	15.89
F8	15.73	-	-

The fractions were added as a primary injection to a 96-well cell plate containing 1321N-hP2X4 cells. The Fura-2 assay was carried out as previously described (Chapter 3). In our activity-guided assays, both - early and late eluting fractions from these venoms were shown to contain potent toxins that may inhibit hP2X4 (Figure 4.11 and Figure 4.12).

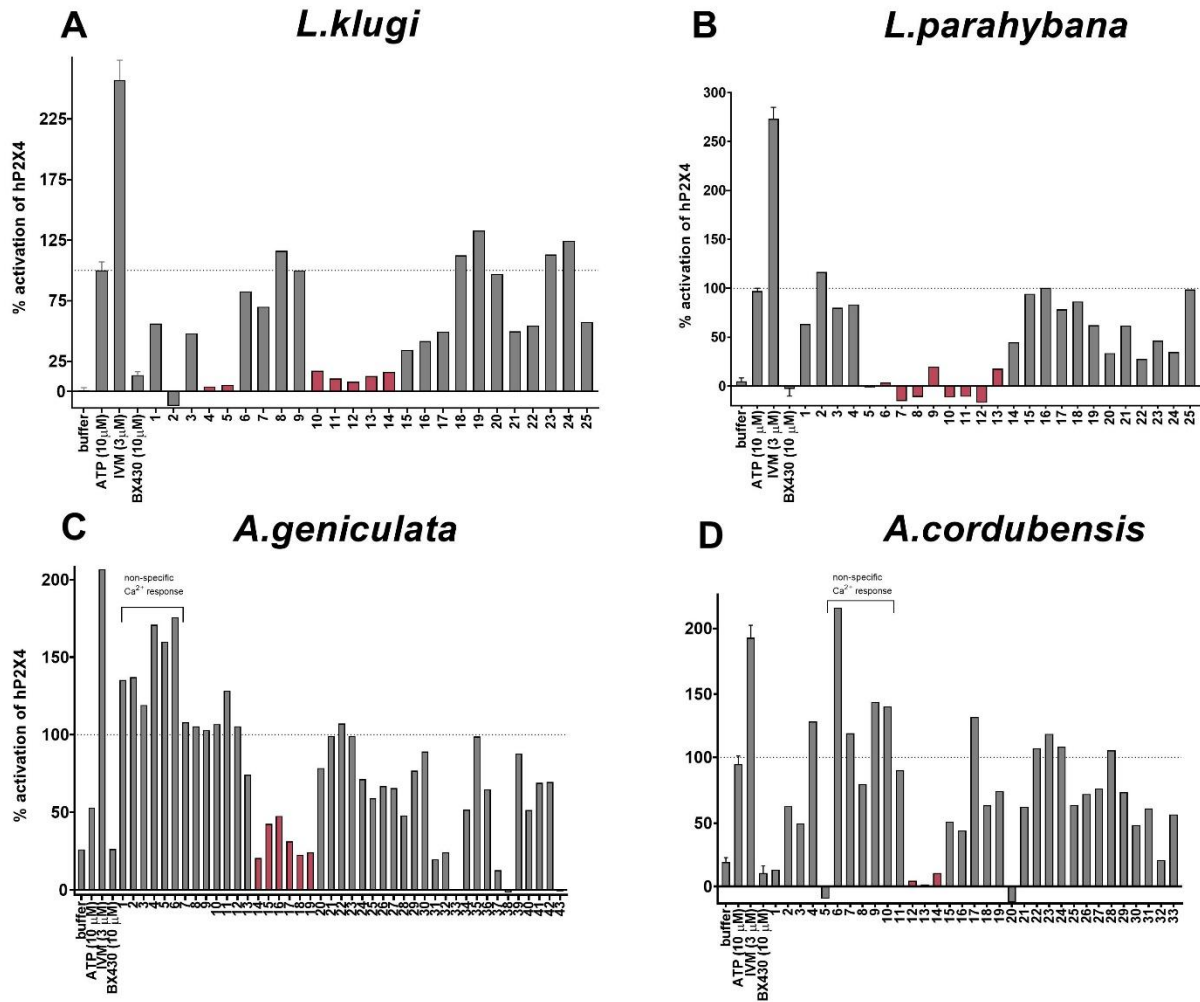


Figure 4.11. Screening of various spider venom fractions from *Acanthoscurria* and *Lasiodora* family against 1321N1-hP2X4. Using Fura-2 fluorescent dye, fractions from **A) *Lasiodora klugi***; **B) *Lasiodora parahybana***; **C) *Acanthoscurria geniculata***; and **D) *Acanthoscurria cordubensis*** were screened against 1321N1-hP2X4. Fractions coloured blue inhibited hP2X4. The dashed line represents 100% hP2X4 activity as followed by 10 μM ATP application. Data points represent the mean ± SD of three replicated experiments, with triplicates on each plate except fraction injections.

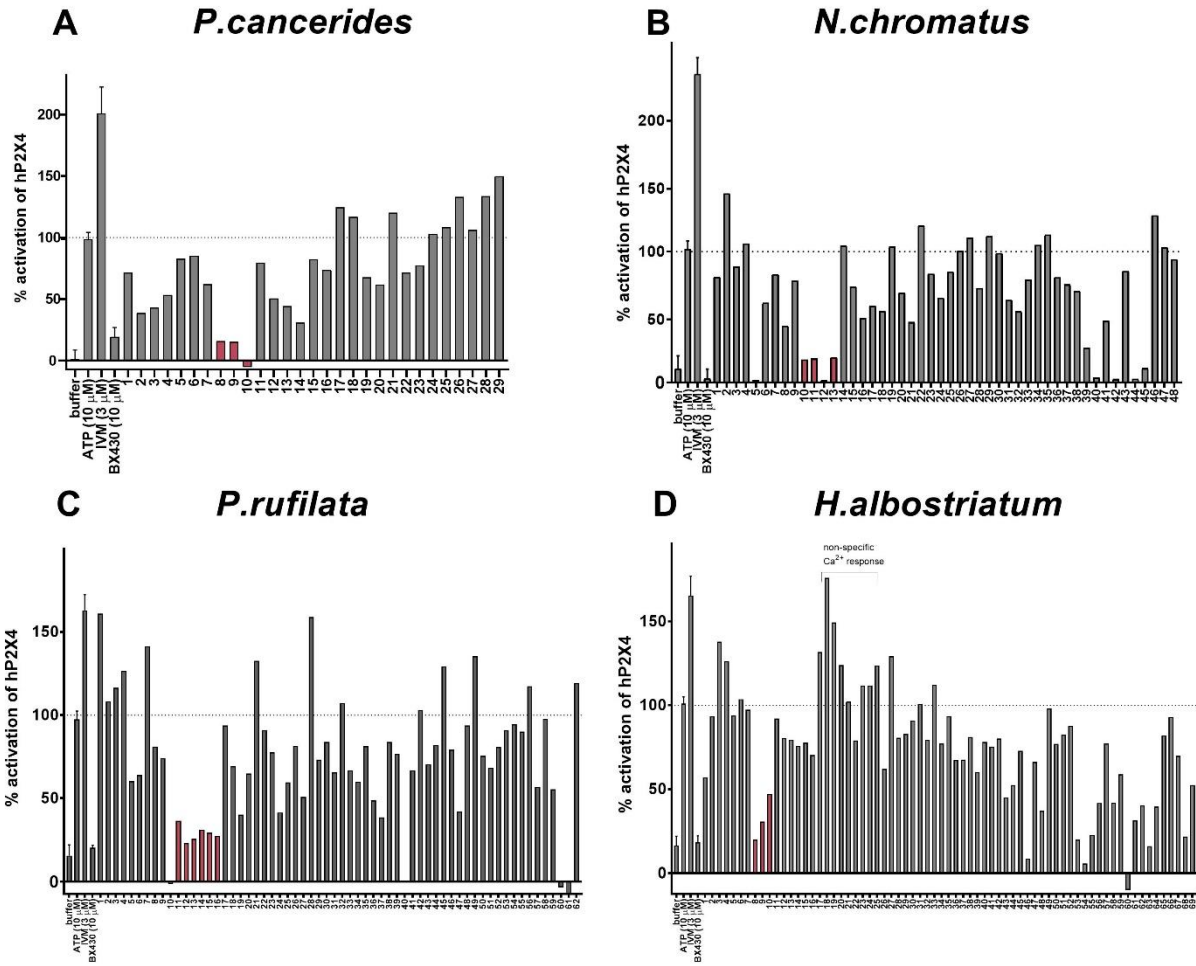


Figure 4.12. Screening of various spider venom fractions from *Phormictopus*, *Poecilotheria*, *Haplopelma* and *Nhandu* against 1321N1-hP2X4. Using Fura-2 fluorescent dye, fractions from **A)** *Phormictopus cancerides*; **B)** *Haplopelma albostriatum*; **C)** *Poecilotheria rufilata*; and **D)** *Nhandu chromatus* were screened against 1321N1-hP2X4. Fractions coloured blue inhibited hP2X4. The dash represents 100% hP2X4 activity as followed by 10 μ M ATP application. Data points represent the mean \pm SD of three replicated experiments, with triplicates on each plate except fraction injections.

As seen on the two figures above, the fractions from *L. klugi* (F2, F4, F5, F10 – F14); *L. parahybana* (F5-F13); *A. geniculata* (F12 – F14); *A. cordubensis* (F14-F19), and fractions from *P. cancerides* (F8 – F10); *H. albostriatum* (F7 – F9); *P. rufilata* (F9-F12); and *N. chromatus* (F10-F13) seemed to potently inhibit hP2X4. With the exception of two fractions of *A. cordubensis* (F16 and F17) and *P. rufilata* (F11 and F12), all these fractions showed >80% inhibition of hP2X4 relative to the positive control (10 μ M ATP).

Notably, these are the hydrophilic fractions that displayed the similar eluting HPLC pattern. However, *L. parahybana* displayed inhibition of hP2X4 across a wide range of fractions (F5-F13), suggesting the co-elution of one single hydrophilic compound throughout our RP-HPLC separation which has been previously proposed by Guette and colleagues.²⁵³ Interestingly, this inhibition wasn't observed in any of the *E. murinus* fractions (Figure 4.13).

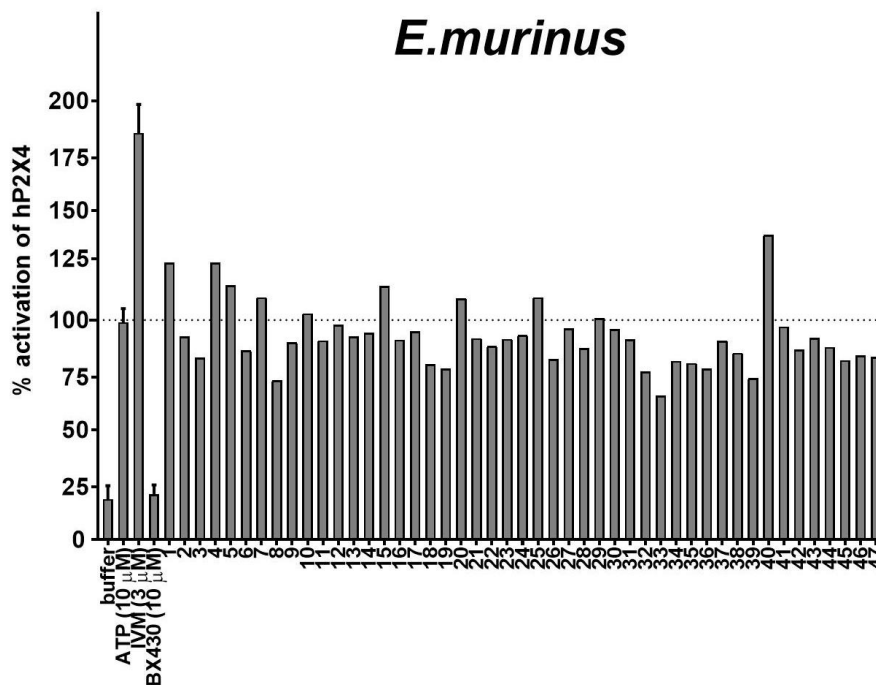


Figure 4.13. Screening of *E. murinus* against 1321N1-hP2X4 with Fura-2 dye. The dash represents 100% hP2X4 activity as followed by 10 μM ATP application. Data points represent the mean ± SD of three replicated experiments, with triplicates on each plate except fraction injections.

Although a crude venom from *E. murinus* caused a loss of ATP-induced fluorescent signal as it seemed to block the hP2X4 activity in HEK293-hP2X4 cells (L.Stokes, personal communication), this inhibition was lost upon fractionation probably due to the synergistic effects between the multiple compounds in these venoms. Laustsen³¹⁶ and others³¹⁷⁻³¹⁹ have already discussed this in several papers in both snake and spider venoms. Since the application of F8, F18, F19, F22, F23, and F39 resulted in 30 - 39% inhibition on 1321N1-hP2X4, the synergy between the different venom components targeting hP2X4 might be the case with *E. murinus* as well. Consequently, the combined effect of these individual toxins resulted in a seemingly potent block of hP2X4 when initially tested on HEK293-hP2X4. Thus, this venom served us as an adaptive control, confirming the importance of the early eluting fractions with the similar eluting pattern towards hP2X4.

However, as seen before with the cone snail venom (CS3), even though the fractions from above venoms seemed to block the ATP-induced fluorescent response via Fura-2 in the 1321N1-hP2X4, this doesn't necessarily mean they exhibit their effect through hP2X4 inhibition. Since the major limitation of fluorescent-based screens is their potential interference with the tested compounds which may result in fluorescent quenching and false positive hits,²⁶² we wanted to make sure similar inhibition could be achieved when the toxin hits would be tested on another cell line (HEK293-hP2X4), under altered screening conditions and using a different dye (YO-PRO-1).

Due to the amount of venom material provided and highest activity of early eluting fractions, toxins from *L. klugi* (found in F2, F4, F5, F10, F11, F12, F13, F14) were chosen as the main fractionated venom of interest. By using a stable HEK293-hP2X4 and YO-PRO-1 dye, the most potent fractions were shown to be F10 – F14 with all of them displaying inhibition of hP2X4 greater than 90% (**Figure 4.14A**). This data corresponds well to our previous results in the 1321N1-hP2X4 cells (> 80% inhibition) with some minor differences in the magnitude of inhibition, possibly indicating the different concentration of the individual toxins.

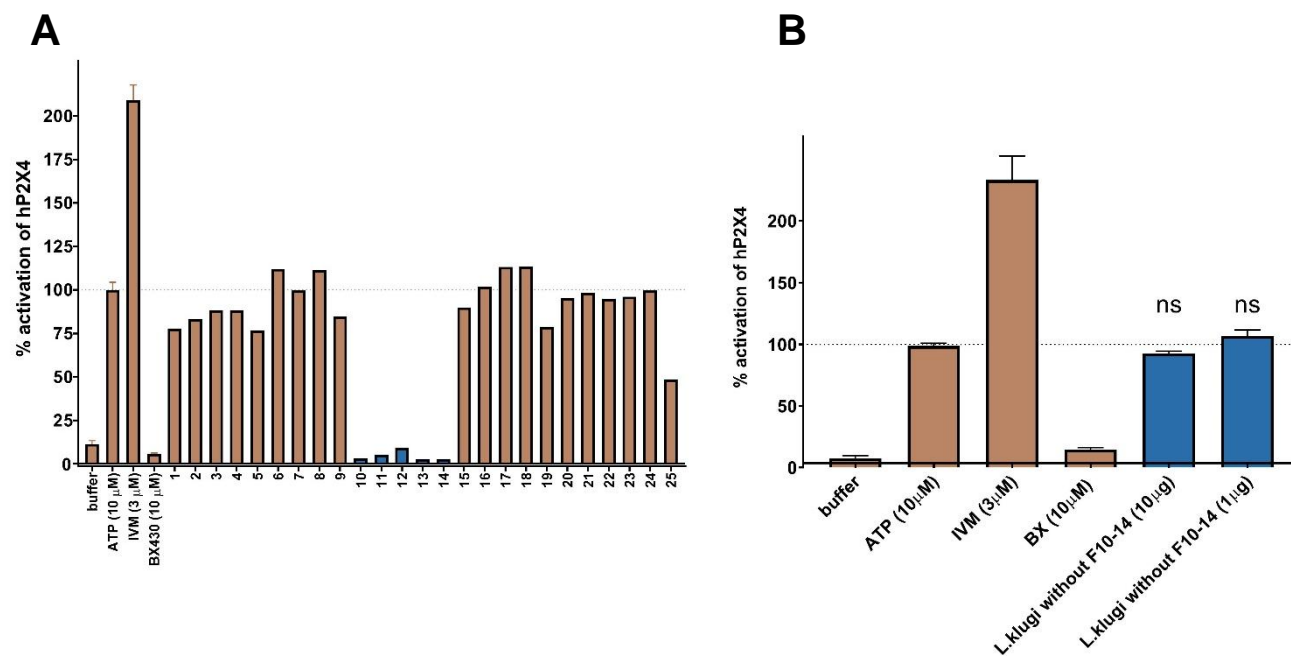


Figure 4.14. Validation of spider venom fractions from *L. klugi* against HEK293-hP2X4. **A:** Fractions coloured blue were validated as the fractions which selectively inhibited hP2X4. **B:** Using RP-HPLC, we pulled out F10-F14 and combined all the other toxins from *L. klugi* except the inhibiting fractions (F10-F14). The dash represents 100% hP2X4 activity as followed by 10 μM ATP application. Data points represent the mean ± SD of three replicated experiments, with triplicates on each plate except fraction injections.

In order to fully confirm these results and show that the dose-dependent inhibition by the crude venom *L. klugi* is due to the potent effect of fractions 10-14, we pulled out F10-F14 and combined the rest (F1-F10 and F15-F25). By applying this combined venom without the fractions 10-14 on our HEK293-hP2X4 cell line, we showed that the activity of hP2X4 was $97.4 \pm 0.6\%$ and $102.5 \pm 2.1\%$, relative to our positive control (10 μM ATP) with 10 μg and 1 μg of combined venom (denoted as “*L. klugi* without F10-14”, **Figure 4.14B**), respectively. Without fractions F10-F14, the inhibitory effect of *L. klugi* was lost regardless of the venom concentration and it became clearer that F10-F14 contained potentially interesting inhibitors of hP2X4 activity.

Furthermore, since five fractions showed similar inhibition and eluting pattern on RP-HPLC, we wondered whether these compounds contain structurally similar toxins. In order to perform a more detailed pharmacological evaluation, the desired purity ($>91\%$)³²⁰ of the hits had to be obtained, and the exact molecular weight of the toxins needed to be determined. Only when we had gained more insights into the toxins' activity was the structural elucidation of these toxins hits attempted.

4.2.3. Purification and Mass Analysis of Fraction Hits Against hP2X4

In order to estimate the molecular mass of compounds in the early eluting fractions of crude venom hits, the approximate molecular mass of fractions was approximated with MALDI-TOF, and later subjected to ESI-LC-MS/MS. In case of MALDI-TOF, approximately 1% of the pooled active peak from the initial fractionation was loaded onto a MALDI plate using the alpha-cyano-4-hydroxycinnamic acid (CHCA) matrix. However, since MALDI-TOF might give an approximate 1-2 Da mass discrepancy, a more accurate LC-MS method had to be used. Interestingly, the vast majority (92%) of the early eluting inhibiting fractions from our library of fractionated toxin hits, contained only four compounds which yielded either strong peaks, masses of either 365, 455, 601 or 729 (**Table 4.4**). Interestingly, all these toxins were present in *L. klugi* (F10-F14) and none of these masses matched any structurally known small molecules in the literature or MS-MS database.

Table 4.4. Most intense m/z ratios of the inhibiting fractions accurately determined by the LC-MS spectrum.

Spider venom / fraction	<i>L. klugi</i>	<i>L. parahybana</i>	<i>P. cancerides</i>	<i>A. geniculata</i>	<i>H. albostriatum</i>	<i>N. chromatus</i>	<i>A. cordubensis</i>	<i>P. rufilata</i>
	m/z	m/z	m/z	m/z	m/z	m/z	m/z	m/z
F2	?	-	-	-	-	-	-	-
F4	365.66	-	-	-	-	-	-	-
F5	455.15	-	-	-	-	-	-	-
F6	-	455.15	-	-	-	-	-	-
F7	-	729.35	-	-	-	-	-	-
F8	-	729.35 652.19	365.66 601.38 729.35	-	-	365.66	-	-
F9	-	291.87 601.38	291.87 601.38	-	-	220.54 601.38	-	-
F10	601.38 729.35	601.38	601.38 729.35	-	365.66	365.66 601.38 729.35	-	365.66
F11	601.73	601.38 652.19	-	-	365.66 729.35	-	-	365.66 729.35
F12	365.66 729.35	455.15 601.38	-	220.54 601.38	365.66 729.35	-	-	365.66 729.35
F13	601.73 729.35	638.47 652.19	-	365.66 729.35	729.35	-	-	601.38 365.66 729.35
F14	455.15 3194	-	-	-	-	-	220.54 601.38	220.54 601.38
F15	-	-	-	-	-	-	601.38	601.38
F16	-	-	-	-	-	-	335.56	729.35
F17	-	-	-	-	-	-	356.87	-
F18	-	-	-	-	-	-	-	-
F19	-	-	-	-	-	-	-	-

Since a reasonable amount of *L. klugi* venom was available, we then proceeded with these five fractions (F10-F14) that showed remarkable inhibition of hP2X4. In order to clarify and determine the purities of the toxins, we proceeded with the additional purification step on RP-HPLC.

This way, the toxins 601 and 729, denoted from now as LK-601 and LK-729, were confirmed to be 95.4% (m/z found at ~ 600.1) and 91.8% (m/z found at ~ 729.2) for LK-601 (**Figure 4.15A**) and LK-729, respectively (**Figure 4.15B**). MALDI-TOF was used here to help determining an approximate mass of these toxins. The purification of the toxins corresponding to 365, 455 and 3194 was attempted, however, they couldn't be purified to any measurable extent rather than for mass analysis studies.

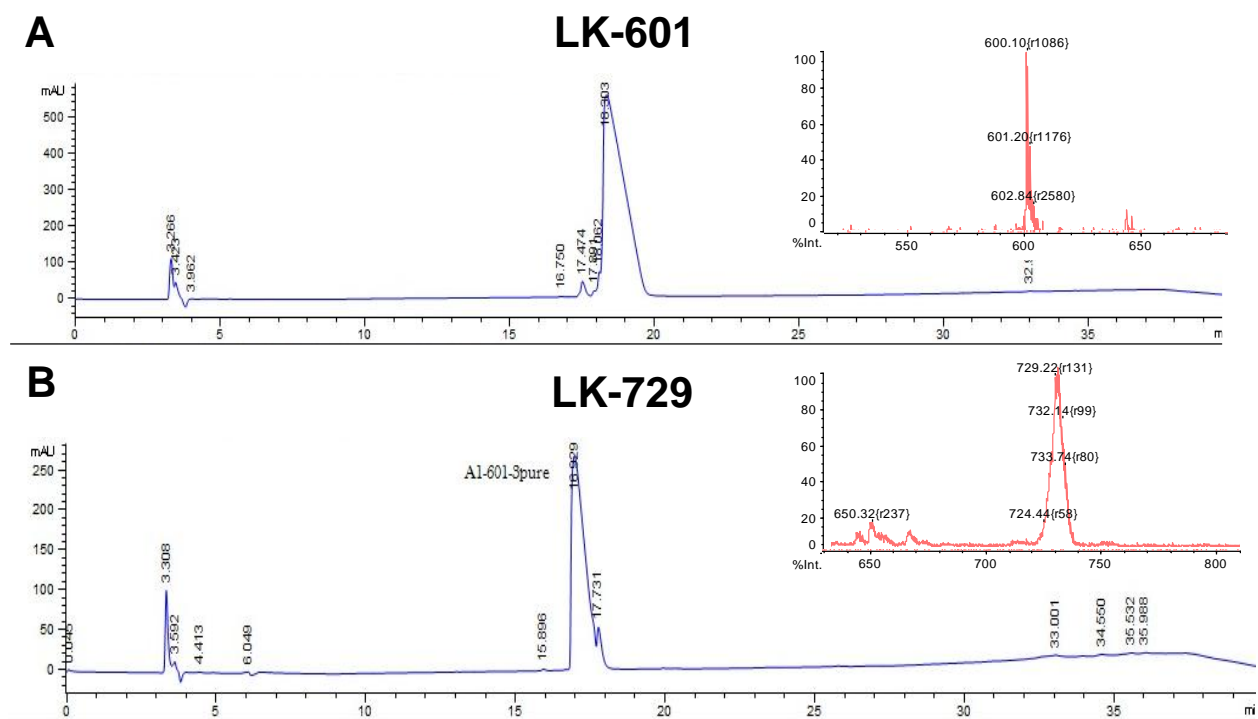


Figure 4.15. Purification and mass spectroscopy confirmation of LK-601 and LK-729 from *L. klugi*. **A:** LK-601 was purified using RP-HPLC to purity >95% and its mass estimated by MALDI-TOF (~ 600.10 m/z). **B:** LK-729 was purified using RP-HPLC to purity >91% and its mass estimated by MALDI-TOF (~ 729.22 m/z). Here, x and y axis (MALDI-TOF) represent mass per charge in Daltons (m/z , Da) and absolute intensity of signal, respectively, presented here at single wavelength of 214 nm. The x and y axis on RP-HPLC chromatograms represent the units of time (min) and the intensity of absorbance (in units of mAU, or mili-Absorbance Units), respectively.

Looking at the **Figure 4.15**, some interesting observations should also be noted. First, LK-601 and LK-729 eluted at 18.8 min (at 12% CH₃CN) and 17.5 min (at 11% CH₃CN), respectively. Rather than LK-601 and LK-729 being sharp peaks, both of them displayed a fairly broad elution, which may be due to the RP-HPLC conditions used. Since the analysis of highly hydrophilic compounds, such as LK-601 and LK-729, purification on a traditional alkyl column (C18 in our case) may be challenging due to the alkyl columns dependence on hydrophobic interactions for retention.³²¹ In order to improve the peak resolution, an optimization of HPLC conditions could be attempted, using normal phase HPLC, biphenyl columns, buffered mobile phases or higher concentration of a mobile phase modifier (TFA) rather than RP-HPLC and a C18 column.

Second, as discussed before, most venoms contain acylpolyamines and peptides. Since the RP-HPLC chromatograms indicated the toxins to be hydrophilic compounds, we hypothesised that the active fractions are likely to be acylpolyamines; linear and cyclic peptides usually elute later (> 40 min) due to their hydrophobic nature. Moreover, due to the high absorbance of the active toxins at either 214 or 280 nm, suggesting the occurrence of amide bonds or aromatic groups, respectively, this indicated that the toxins might be acylpolyamines with aromatic headgroups.³²² However, whether they contained amino acids or not, was not yet clear.

Another important observation from RP-HPLC analysis was the striking instability of these toxins (**Figure 4.16**). After three weeks, the purity of the lyophilized toxins, stored at -20°C in water, decreased to 44% as indicated by the three or five apparent peaks on RP-HPLC chromatogram with either LK-601 (**Figure 4.16A-B**) or LK-729 (**Figure 4.16C-D**), respectively. When monitoring the stability of LK-601 and LK-729 more carefully, we found out that the toxins remained stable in water for 7-10 days at -20°C, but then displayed a slow degradation. Alternatively, their instability might be also due to solvent exposure (e.g. hydrolysis) or light sensitivity. This might not only indicate degradation but rather a structural rearrangement, as noted previously by Rocha-E-Silva.³²³ When toxins were left at either room temperature or 4°C, the purity was substantially lost (<50%) after a day (data not shown). For that reason, all the pharmacological evaluations had to be carried out within a time frame of 10 days after the initial purification of the toxins.

Some of the other issues that we encountered were linked to MALDI-TOF and its poor resolution. The peaks were quite broad, thus, the signal to a given toxin may not be completely resolved from the signals of its nearest neighbours (the spacing between neighbouring peaks is more less than 1 Da).

This difficulty was then circumvented by subjecting the toxins to ESI-LC-MS/MS with an Orbitrap analyser that could permit the detection of these compounds with improved selectivity and sensitivity to confirm their exact masses for the following pharmacological studies, and reveal a better structural fingerprint.

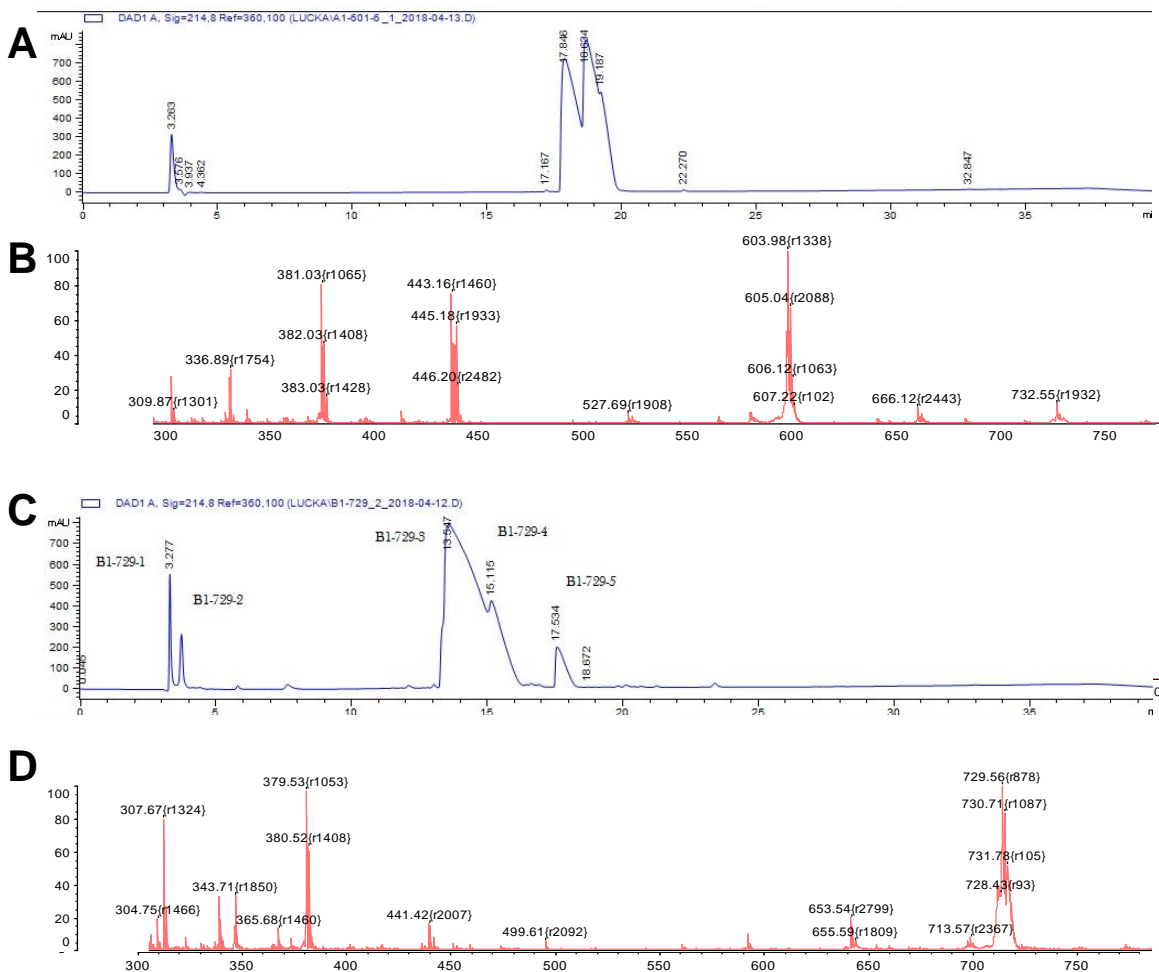


Figure 4.16. HPLC chromatograms show the instability of the toxin hits. HPLC and MALDI-TOF profiles shows **A,B)** three impurities of 601; and **C,D)** five impurities of 729 denoted as peaks with different retention times. Here, x and y axis (MALDI-TOF) represent mass per charge in Daltons (m/z , Da) and absolute intensity of signal, respectively, presented here at single wavelength of 214 nm. The x and y axis on RP-HPLC chromatograms represent the units of time (min) and the intensity of absorbance (in units of mAU, or mili-Absorbance Units), respectively.

After using LCMS QTOF-MS/MS, we could confirm previously identified reoccurring ions 366, 455, 601, 729 and 3195 as proton $[M + H]^+$ ions. The masses of these five toxins were then accurately determined as 365.2563 Da, 454.2274 Da, 600.3712 Da, 728.5026 Da and 3194.4325 Da.

Interestingly, LK-601 and LK-729 eluted similarly on LC - a broad peak between 15 and 25 min - suggesting these toxins might have similar physicochemical characteristics. To gain more insights into the structure of these toxins, we applied MS-MS fragmentation. The fragment ions m/z of LK-601 and LK-729 are shown in **Figure 4.17** and presented in **Table 4.5**.

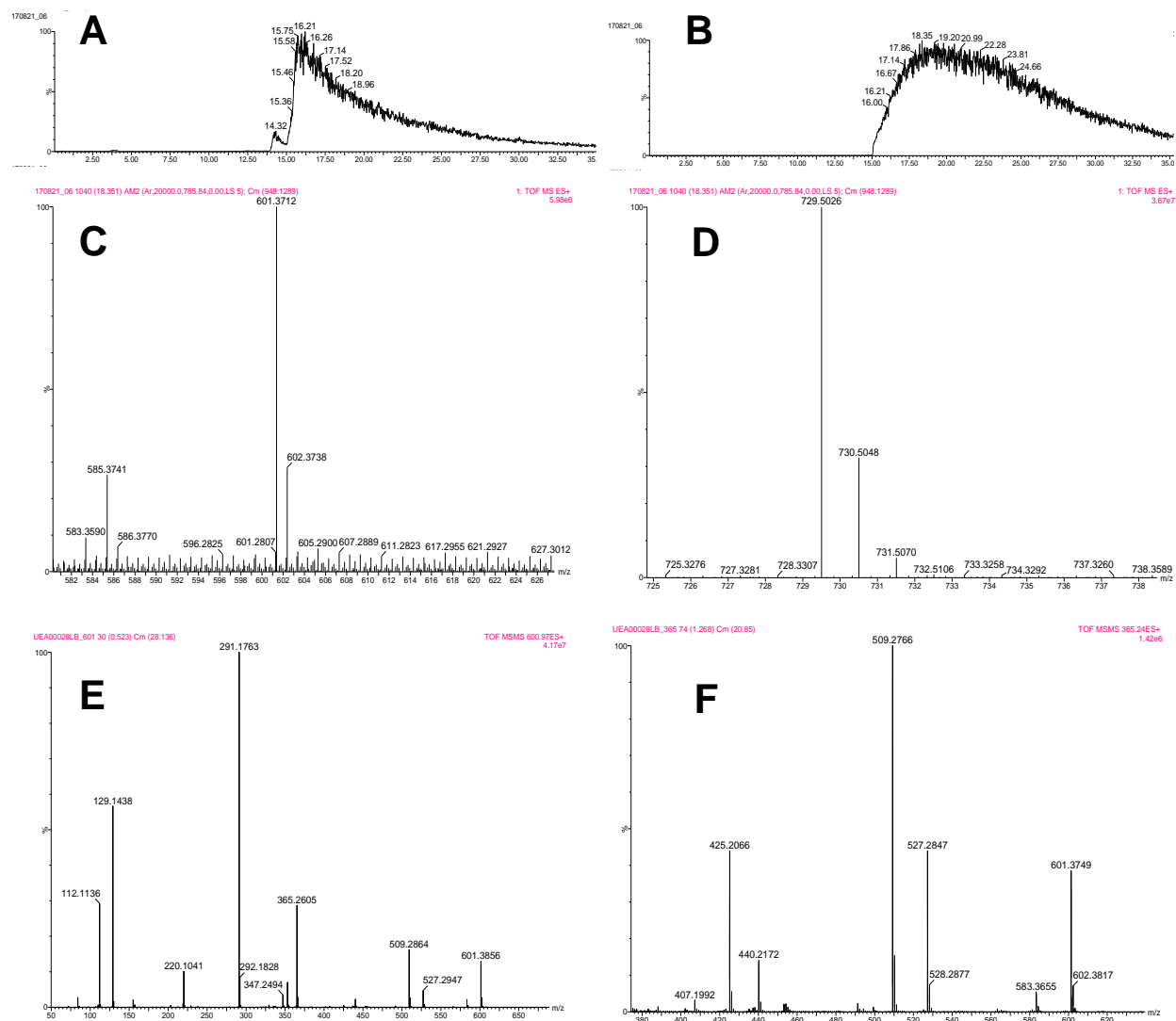


Figure 4.17. Eluting LC-MS profiles and ESI-MS/MS of the $[M+H]^+$ ions of LK-601 and LK-729. A: LC-MS profile of LK-601 and B: LK-729 showing a broad eluting peak between 15-20 % acetonitrile (solvent gradient not shown). ESI-MS accurately depicted $[M+H]^+$ ions of C: LK-601 (601.3712 Da) and D: LK-729 (729.5026 Da). The toxins were then subjected to MS/MS fragmentation which showed similar fragmentation pattern of E: LK-601 and F: LK-729 with ions at 112.1136, 129.1438, 291.1763, 365.2605, 509.2766, 527.2847 and 601.3749. Here, x and y axis (MS/MS) represent mass per charge in Daltons (m/z , Da) and absolute intensity of signal, respectively, presented here at single wavelength of 214 nm. The x and y axis on LC-MS chromatograms represent the units of time (min) and the intensity of absorbance (in units of mAU, or mili-Absorbance Units), respectively.

Table 4.5. Fragment ions m/z of LK-601 and LK-729 obtained by MS/MS.

Toxin	m/z								
365	112.1136	129.1389	220.0976	291.1689	365.2521	-	-	-	-
455	-	129.1389	220.0976	337.1550	353.1478	437.2180	455.2271	-	-
LK-601	112.1136	129.1438	220.1041	291.1763	365.2605	509.2864	527.2947	601.3856	-
LK-729	112.1136	129.1389	220.0976	291.1689	365.2521	509.2766	527.2847	601.3749	729.5060

In order to determine whether the common fragmentation pattern of 365, 600, 728 or 3194 matches the annotated spectra of known compounds in the database, we queried the National Institute of Standards and Technology (NIST), known as METLIN, as well as ChemSpider MS/MS spectral databases. Unfortunately (or fortunately), no matches with the desired fragment ions were found. Thus, it can be concluded that the toxin's structures represent a yet unidentified compound found in the spider venoms.

The fragment ions of 112.1136, 129.1438, 220.1041, 291.1763, 347.2494, 365.2605, 509.2864 and 601.3749 were recurrent in all toxins except 455, regardless of the collision energy applied, indicating that these are specific fragments originating from the structurally similar toxins. The fragment ion at 291.1763 was highly abundant even at lower collision energies, suggesting the fragmentation may be occurring at a highly labile bond such as C-N bond. Moreover, by determining a common fragmentation pattern among 365, 600, 728 and 3194, we found that while 365 is a fragment of 600, 600 is found in 728, and 728 is part of the 3194. In case of 455, the fragmentation pattern was observed only with two ions: 129.1438 and 220.1041, indicating that there might be a similarity between 455 and all the other toxin hits, however, only partial (**Figure 4.18**).

It was found before that molecules with similar structures or even of the same class can share identical fragment ions.³²⁴ Furthermore, the current literature suggests there may be a template approach for the characterization of linear polyamines.^{301, 325-326} As Tzouros and his colleagues³⁰¹ suggested, the structural identification of acylpolyamine analogues may be possible because such compounds show very unique MS fragmentation patterns. By direct correlation of these fingerprint-like signal patterns, the linear acylpolyamines could be characterized even within mixtures such as venoms.

Other authors^{277, 325-329} also had similar ideas, and even refined the analytical setups for their characterization, however, when employing their approaches to the fragmentation pattern of LK-601 or

LK-729, no indication for the structural elucidation of LK-601 and LK-729 could be found. While there were a few similarities between the fragmentation patterns of ions 112 and 129 (as in case of IndAc3334, PA3343, PA3334),³⁰¹ confirming a spermine-like chain, these approaches could not allow the identification of the aromatic ring. One possible reason for this may be the formation of a charged cyclic structure within LK-601 and/or LK-729 that would therefore limit the characterization of such structures by above methods.

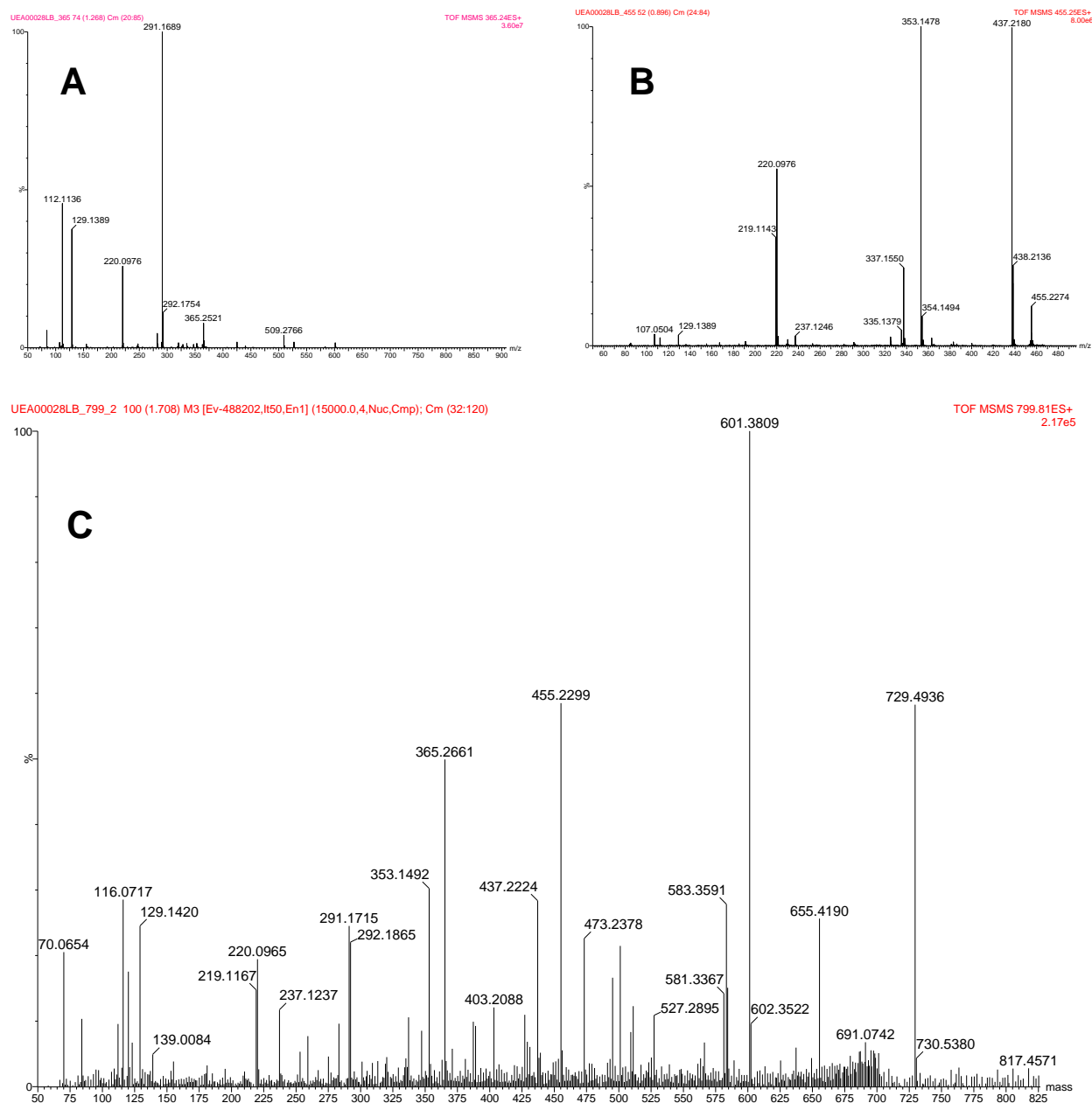


Figure 4.18. Mass spectrometry of small inhibitory toxins. ESI-MS/MS of the $[M+H]^+$ ion at m/z of **A:** LK-365/729; **B:** LK-455; and **C:** LK-3194 (low mass range fragments, deconvoluted). Here, x and y axis (MS/MS) represent mass per charge in Daltons (m/z , Da) and absolute intensity of signal, respectively.

When looking for more structural clues, a study³³⁰ conducted nearly 30 years ago captured our attention. Here, Skinner and colleagues³³⁰ confirmed the existence of toxins with the masses of 600 Da and 728 Da, but could, nevertheless, only suggest the partial structures of these toxins. Interestingly, among nearly hundreds of acylpolyamines identified so far, only 23% of them couldn't be fully elucidated to date – two of them were the toxins with masses 600 and 728 Da.²⁷⁴ Still, Skinner and his team pointed out that both, 600 and 728 contain a similar indole-derived headgroup attached to a polyamine chain, spermine-like polyamine chain and no amino acids.³³⁰ However, apart from the indole group, acylpolyamines may also contain the two para-disubstituted hydroxyphenyl ring³²² as presented earlier (**Figure 4.1**).

From our fragmentation data, two other interesting features can be noted. First, since the typical fragmentation of the parent ions don't generate any fragments that would correspond to amino acid fragmentation patterns, we can conclude that neither 365, 600, 728 and 3194 contain any amino acids and are thus amino acid depleted. This finding is in line with Skinner's³³⁰ results as well. Second, due to the high intensity ions at 112.1136 and 129.1389, and common polyamine fragmentation pattern,³⁰¹ a spermine-like chain is likely to be present in 600 and 728. However, whether the toxins have an indole or phenol ring, could not be verified by MS/MS.

To aid the structural elucidation, we then investigated how *in silico* fragmentation tools such as MS-FINDER could help us to obtain more structural information about 600 and 728. Here, MS-FINDER compares the experimental fragmentation spectrum with the theoretical spectra of all the compounds in its database and determines the possible elemental compositions.³³¹⁻³³³ Since this *in silico* fragmentation approach aims to identify "known unknowns" – compounds present in the database but without any reference spectra – the software calculates a score between the experimental spectra and the predicted spectra.³³²

However, as much as the theoretical information, such as elemental composition could be appreciated, we found that MS-FINDER held a major disadvantage for annotating "unknown unknowns" as pointed out before by Blaženковиč.³³⁴ Since the characterization of 600 and 728 has not yet been attempted, and without any MS/MS reference spectrum in the database, MS-FINDER may only predict the molecular formulae and rank based on the error rates [mDa]. A few predictions, based on our MSMS spectrum, have been put forward: C₃₅H₅₂O₈; C₂₀H₄₈N₁₂O₉; C₁₇H₁₀N₃₃O₃; C₂₁H₄₄N₁₆O₅; C₃₆H₄₈N₄O₄; C₃₂H₄₄N₁₀O₂; and C₃₇H₄₄N₈ (**Figure 4.19**).

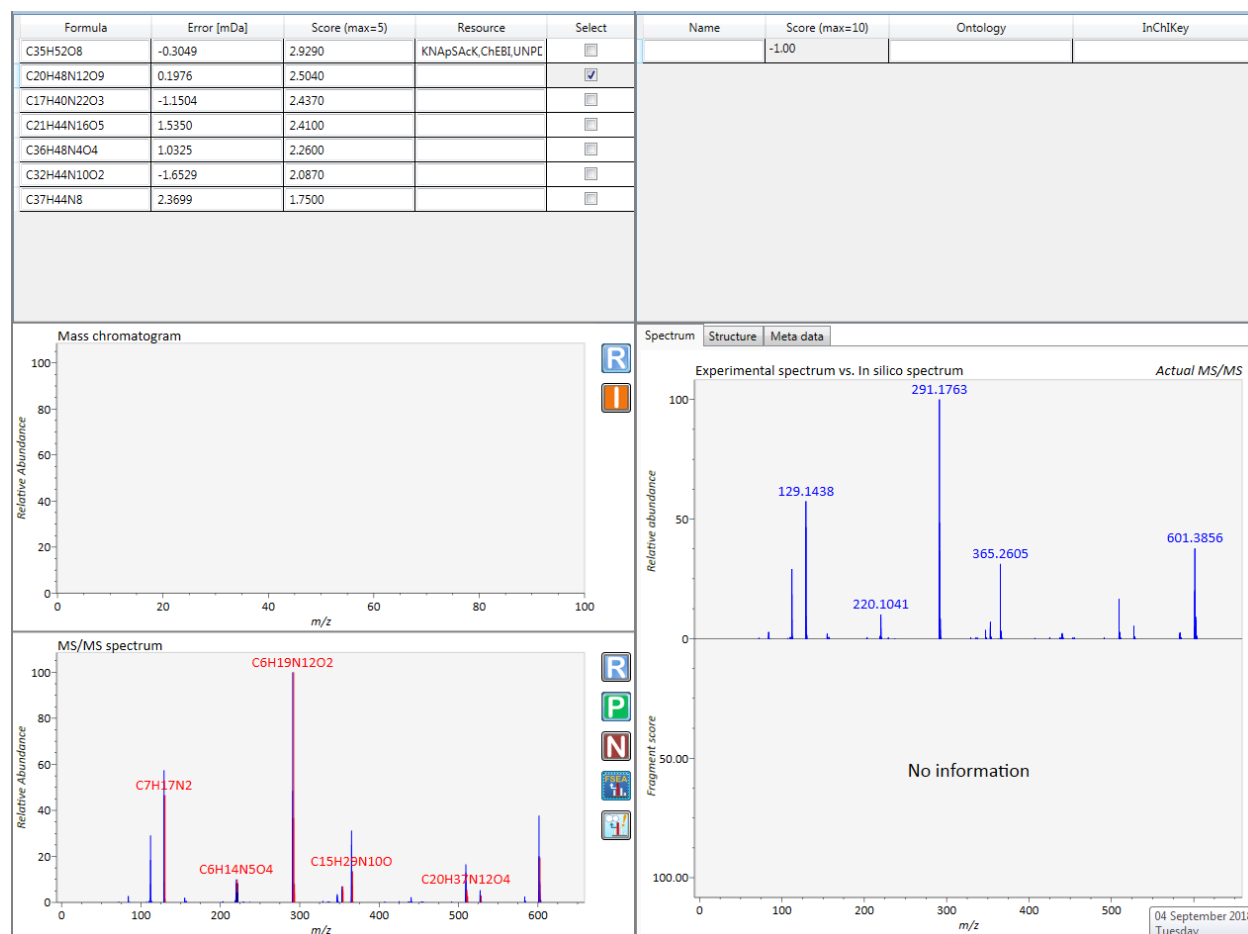


Figure 4.19. An example of graphical user interface of MS-FINDER software calculations for LK-601. The formula prediction (*top left*), database matching results (*top right*), and the result of structure elucidation together with their fragment detail (*bottom left*) and meta data (*bottom right*).

After looking at the predictions, we eliminated some of them due to the low resemblance to the acylpolyamine characteristics³⁰¹ such as the lack or the excess of the nitrogen and/or oxygen atoms (C₃₅H₅₂O₈, C₁₇H₁₀N₃₃O₃, C₂₁H₄₄N₁₆O₅, C₃₇H₄₄N₈, C₂₀H₄₈N₁₂O₉). This way, we were left with either C₃₆H₄₈N₄O₄ or C₃₂H₄₄N₁₀O₂. However, even with these two predicted molecular formulae, we could not confirm the structures as suggested by Tzourous's approach.³⁰¹

In order to observe the percentage of carbon (C), hydrogen (H) and nitrogen (N) element in the toxins, and confirm (or possibly reject) these predictions, the elemental analysis with the CHN analyser could be attempted. However, the lowest concentration that can be reliably analysed is 100 – 200 µg with the limit of detection for the pure carbon at around 10-20 µg. Since we couldn't purify the toxins in quantities greater than 50 µg, it would be unlikely we would get meaningful results.

Taken together with the destructive nature of elemental mapping, we could not afford to subject LK-601 and LK-729 to this analysis. That might also be the reason why there is no information on elemental analysis of acylpolyamines found in the literature to date. Since no additional support for the structural identity of the fragmented ions was provided, either by MS/MS databases, ChemSpider or MS-FINDER, our attention focused on LK-601 and LK-729 which could be purified in enough quantities for the pharmacological studies. With the accurate molecular weight confirmation for both toxins, we could proceed to more detailed pharmacological evaluation and ascertained the potencies, as well as specificities of LK-601 and LK-729 toward hP2X4.

4.2.4. Effects of LK-601 and LK-729 against hP2X4 and Related Targets

We assessed the potency of LK-601 and LK-729 on a ratio of Fura-2 or YO-PRO-1 fluorescence measurements of the rise of intracellular calcium levels or dye uptake, respectively, once evoked by ATP (**Figure 4.20**). LK-601 was similarly potent to LK-729, causing inhibition of hP2X4 with an IC_{50} of $1.14 \pm 2.16 \mu\text{M}$ and $1.98 \pm 1.24 \mu\text{M}$ ($4.53 \pm 2.46 \mu\text{M}$ and $2.26 \pm 1.26 \mu\text{M}$ in case of LK-729) in 1321N1-hP2X4 and HEK293-hP2X4, respectively (**Figure 4.20A-B**). By sharing similar dose-inhibition curves, this may confirm that these two toxins contain structurally similar motifs. Furthermore, it shows that the inhibition may be similar to that of a commercially available antagonist BX430 ($IC_{50} = 0.58 \pm 0.81 \mu\text{M}$ and $0.85 \pm 0.49 \mu\text{M}$ in 1321N1-hP2X4 and HEK293-hP2X4, respectively) which is a non-competitive antagonist at hP2X4.

To further investigate whether the inhibition of P2X4 activity is competitive or non-competitive, Fura-2 assays were performed in 1321N1-hP2X4 cells using different concentrations of ATP with a fixed concentration of the toxins ($10 \mu\text{M}$). Concentration-response curves gave an EC_{50} value of $1.19 \pm 0.82 \mu\text{M}$ for ATP, with a standard Hill slope (n_H) of 1 in the absence of toxins, and a reduced maximal response in the presence of $10 \mu\text{M}$ LK-601 and LK-729 (**Figure 4.20C**). The inhibitory effect of the toxins could not be overcome with increasing concentrations of ATP of up to $100 \mu\text{M}$. These two events, i.e., a shift in ATP EC_{50} and a decrease in the maximal response at saturating concentrations of ATP, indicate that LK-601 and LK-729 may be non-competitive antagonists and may be binding to an allosteric site on the P2X4 receptor channel.

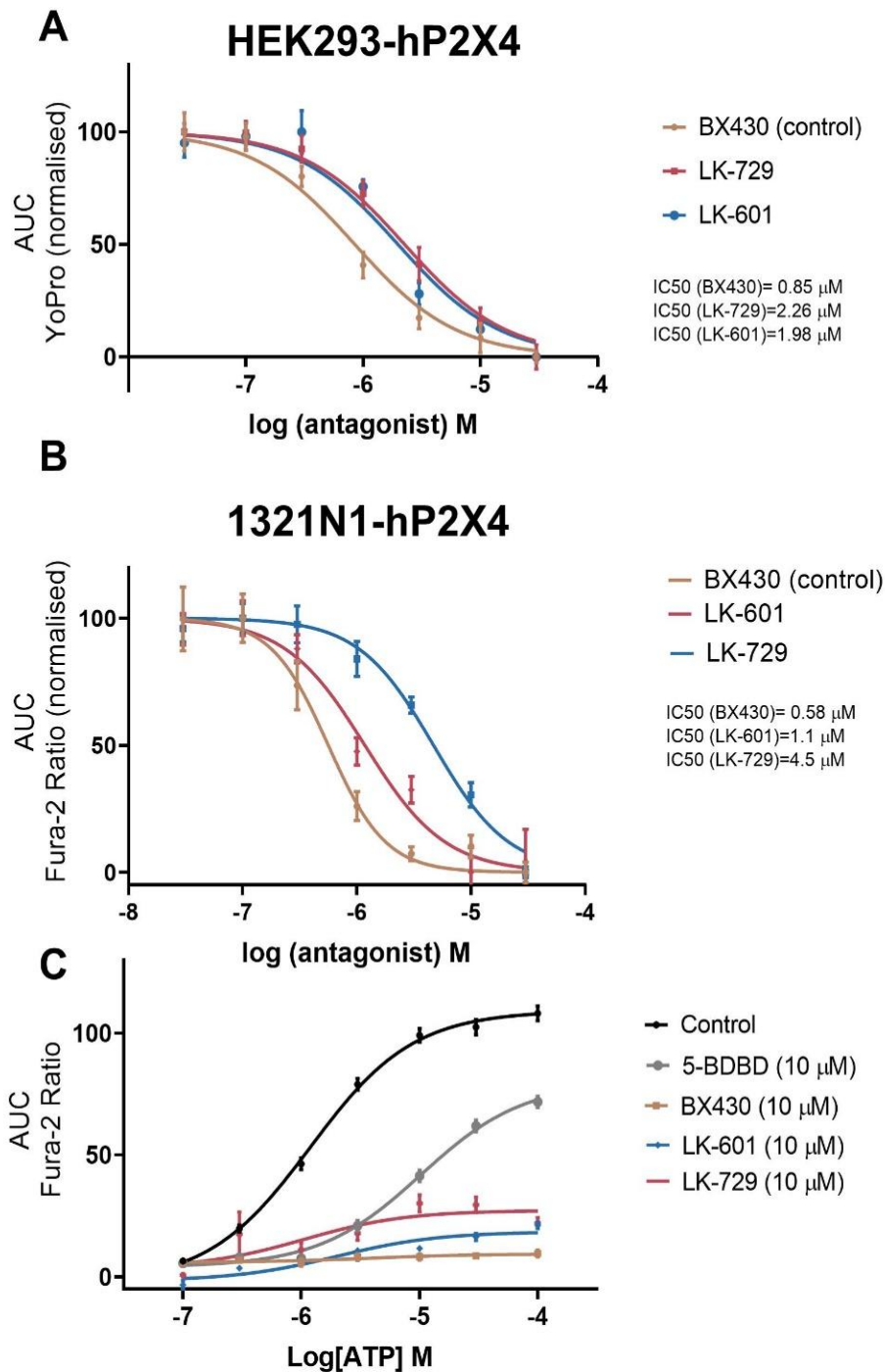


Figure 4.20. Pharmacological effects of LK-601 and LK-729 on hP2X4. **A:** Dose-dependent inhibition of LK-601 (IC₅₀ =1.98 μ M) and LK-729 (IC₅₀=2.26 μ M) on HEK293-hP2X4 cell line. **B:** The effect seen on HEK293-hP2X4 was validated with the dose-dependent inhibition of LK-601 (IC₅₀ =1.1 μ M) and LK-729 (IC₅₀=4.5 μ M) on 1321N1-hP2X4 cell line. **C:** A fixed concentration of either LK-601 or LK-729 (10 μ M) and continuous application of various concentrations of ATP revealed the toxins to be non-competitive antagonists against hP2X4. Data points represent the mean \pm SD of five replicated experiments, with triplicates on each plate.

In order to gain more functional insights in to the binding mode of LK-601 and LK-729, patch-clamping is the definitive experiment to probe hP2X4 function. Not only would it be a gold standard to confirm the potencies of LK-601 and LK-729, it could also track these effects in real time. However, due to the limited amounts of toxins and the low throughput of patch-clamping, we could not ascertain the potencies using electrophysiology. Automated patch-clamp could probably be best deployed to solve these issues and confirm the activity of toxins discovered by fluorescent assays,³³⁵ however, due to the equipment restrictions (no automated system) we could not proceed with the electrophysiology at that stage.

Still, having ascertained the potencies on hP2X4 using two fluorescent-based assays, the remaining characterization studies of LK-601 and LK-729 were focused on a variety of closely related targets (**Figure 4.21**). Both, LK-601 and LK-729 were tested in calcium influx assays at the other channels such as hP2X3, hP2X7 and NMDA 1a/2a in HEK293 cell lines. We found that neither of the toxins inhibits hP2X7 (the activity of hP2X7 remained 97.4 – 118.6% relatively to the control – 250 μ M ATP) at the conventional concentration range 3 – 30 μ M. The only discrepancy of this observation is noted with LK-729 at 30 μ M where $31.4 \pm 4\%$ inhibition was found. This might be merely due to the high concentration of the toxin rather than the dose-dependent inhibition, although higher concentrations should be tested for this effect (**Figure 4.21A**).

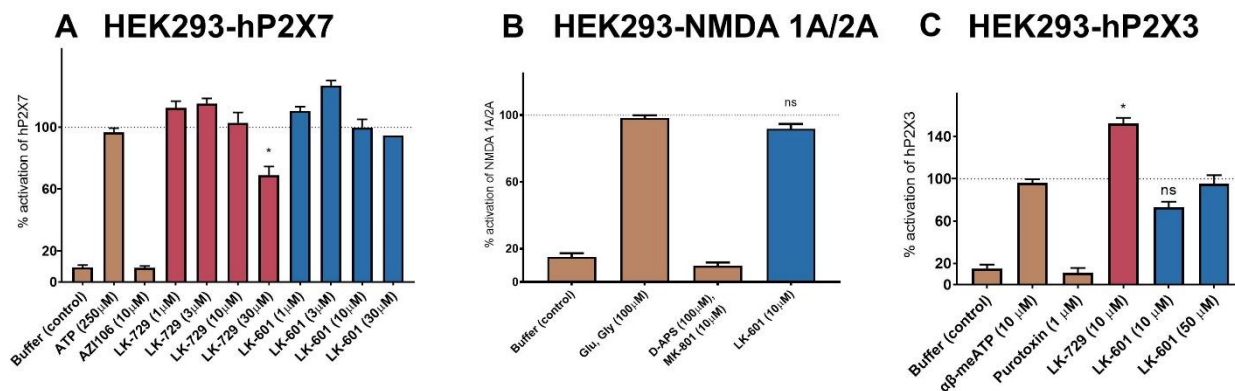


Figure 4.21. Selectivity assays of LK-601 and LK-729 among P2X and NMDA subtypes. **A:** Effects of LK-601 and LK-729 in concentration range 1 μ M – 30 μ M on HEK293-hP2X7 cell line (YO-PRO-1 uptake). **B:** Effects of LK-601 (10 μ M) on transiently transfected HEK293-NMDA 1a/2a cell line. The agonists were applied to the NMDA antagonists and LK-601, and the responses measured with Calcium 6 dye. **C:** Effects of LK-601 and LK-729 in concentration range 10 μ M – 50 μ M on HEK293-hP2X3 cell line, and the responses measured with Calcium 6 dye. Data points represent the mean \pm SD of one experiment with triplicates on each plate. Significant differences between the control (10 μ M ATP) and the venom are indicated by * ($P < 0.01$) using one-way ANOVA followed by Dunnett's test.

Since acylpolyamines have been widely reported to act as potent blockers of glutamate receptors (including NMDA),¹⁸¹ NMDA 1a/2a served as a model to probe the effects of LK-601 and LK-729 against this family of receptors. Agonists such as L-glutamate and the co-agonist L-glycine had to be used in this case, and the ability for NMDA 1a/2a to be blocked by MK801 (10 μ M) and D-AP5 (100 μ M) was confirmed prior to the application of the toxins. Interestingly, once LK-601 and LK-729 were applied, no inhibiting effect was found with either LK-601 or LK-729 at 10 μ M and the activity of NMDA 1a/2a remained 90 ± 2 % relatively to the control (**Figure 4.21B**).

In stark contrast, LK-729 was found to potentiate hP2X3 (~144%) and was thus deemed less selective for hP2X4 than LK-601 (**Figure 4.21C**). This is unfortunate since potentiating either homomeric P2X3 or the heteromeric P2X2/P2X3 would result in the sensation of painful stimuli.³³⁶⁻³³⁷ However, this potentiating effect was not observed with LK-601. Despite 10 μ M of LK-601 seeming to cause 26 ± 3 % inhibition at hP2X3, however statistically non-significant, 50 μ M of LK-601 was found to be ineffective. Thus, we shifted our main focus to LK-601 rather than to LK-729.

So far, our experiments have been done in a heterologous over-expression system of P2X4. While both models, 1321N1-hP2X4 and HEK293-hP2X4, seemed to be a good choice when looking at our target of interest, we wanted to translate these results to a model expressing endogenous P2X4. For that purpose, mouse microglial BV-2 cells were chosen. Furthermore, P2X4-dependent microglial activity is crucial for chronic pain symptoms to manifest after nerve injury.^{63, 338-339} However, one limitation with this model is that BV-2 cells express not only P2X4 but also other P2 channels and GPCR receptors that produce a Ca^{2+} increase in response to ATP. Thus, in order to selectively identify a P2X4-mediated component in the ATP-induced Ca^{2+} responses, we had to be able to distinguish P2X4 responses from other P2Ys. As suggested by Matsumuta and colleagues,¹⁶⁷ ivermectin (P2X4 positive allosteric modulator) could help us on this quest.

Initially, we demonstrated that the prior application of 3 μ M IVM clearly potentiated the 25 μ M ATP-induced Ca^{2+} responses up to 2.5-fold in BV-2 cells (**Figure 4.22**). We then investigated the inhibition of endogenous P2X4 by LK-601 in these cells. The application of LK-601 (10 μ M) suppressed the potentiation of ATP responses by IVM and the amplitude of ATP+IVM-evoked responses were inhibited by 35 ± 3 %, suggesting only P2X4 receptors in the BV-2 cell line contribute (**Figure 4.22A-B**). Furthermore, this inhibition seemed to be similar to two commercially available antagonists, PSB12062 (1 μ M) and 5-BDBD (10 μ M), which suppressed the IVM potentiation by 48 ± 5 % and 41 ± 2 %, respectively.

On the other hand, BX430 (10 μ M) did not exhibit these same effects ($9 \pm 2\%$ inhibition) in BV-2 cells. Our results were also in line with the other studies that have used 5-BDBD, PSB12062 and BX430 on mouse P2X4.^{153, 166, 250}

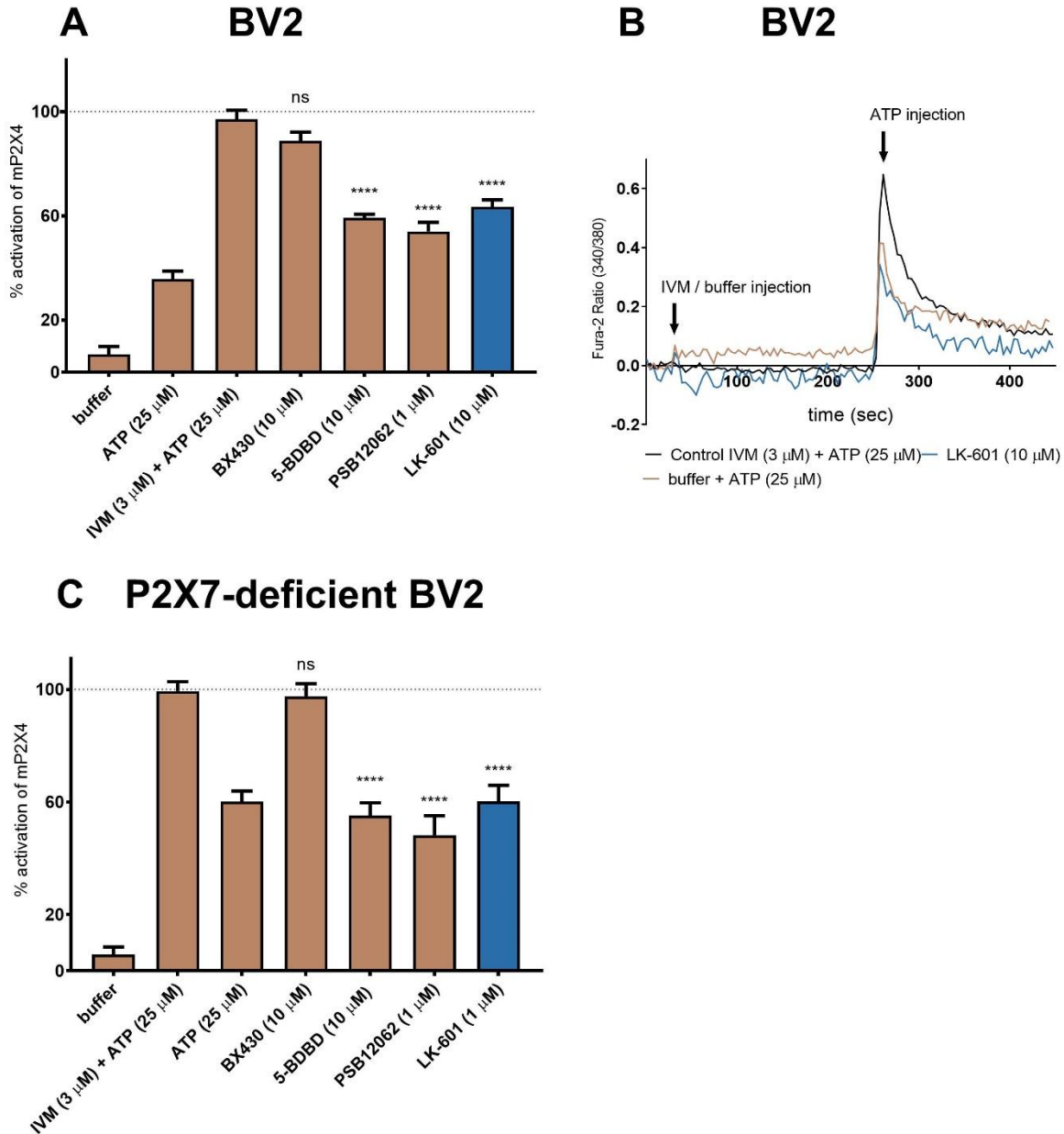


Figure 4.22. Effect of LK-601 in a native microglial model. **A:** Effects of LK-601 (10 μ M) on mouse microglial BV2 model. **B:** Kinetics of LK-601 inhibition at 10 μ M in native BV2 model. **C:** Effects of LK-601 (10 μ M) on P2X7-deficient BV2. All experiments were performed with Fura-2 dye. Data points represent the mean \pm SD of one experiment with triplicates on each plate. Significant differences between the control (IVM + ATP) and the venom are indicated by **** ($P < 0.0001$) using one-way ANOVA followed by Dunnett's test.

However, BV-2 cells are known to express both P2X4 and P2X7 receptors.³⁴⁰⁻³⁴¹ Since a P2X7-deficient BV-2 cell line was available in our lab,²³⁸ this allowed us to validate the specificity of LK-601 against P2X4 in BV-2 cells. ATP-induced calcium responses were comparable in the BV-2 and P2X7-deficient BV-2 cells and showed P2X4-like pharmacological characteristics such as potentiation by IVM and reduction in responses by P2X4 antagonists 5-BDBD, BX430 and PSB12062. LK-601 (1 μ M) gave a statistically significant inhibition of the ATP-induced calcium response ($39 \pm 5\%$) relative to the control (IVM + ATP), similar to the effects seen in the BV-2 cells ($35 \pm 3\%$) (**Figure 4.22C**). This further confirmed that the P2X7 receptor is likely not contributing to LK-601 effects observed in the mouse microglial BV2 model, and indicated a primary role for the P2X4 receptor in both cell lines.

Since the primary sequence of P2X4 subunits is highly conserved between vertebrates, from fish to primates;³⁴² we next assessed species-dependent effects of LK-601 and LK-729 on mP2X4 and rP2X4 (**Figure 4.23**). Despite our results in the BV-2 cell line showing that 10 μ M and 1 μ M of LK-601 significantly inhibits P2X4 in mouse microglia, we wanted to confirm these results in a stable 1321N1 cell line expressing mP2X4. Only after we generated the stable cell lines (1321N1-mP2X4 and 1321N1-rP2X4) and pharmacologically characterized them, we then proceeded with the screening.

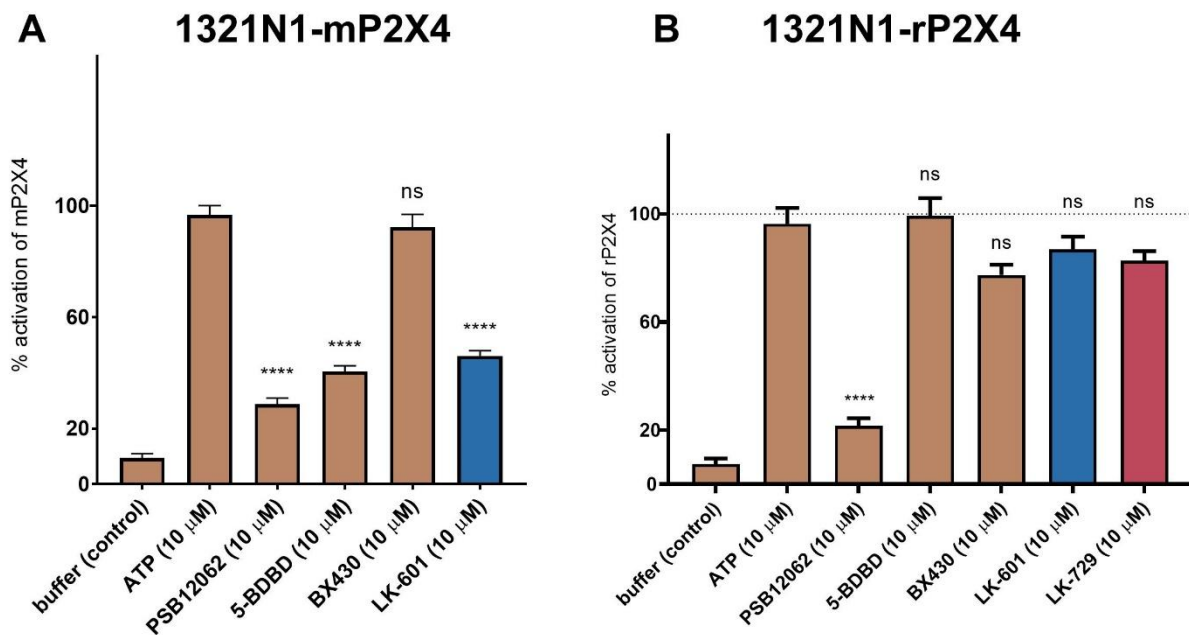


Figure 4.23. Selectivity assays of LK-601 and LK-729 among P2X4 species. **A:** Effects of LK-601 and LK-729 (10 μ M) on 1321N1-mP2X4 cell line. **B:** Effects of LK-601 (10 μ M) on 1321N1-rP2X4. All experiments were performed with Fura-2 dye. Data points represent the mean \pm SD of one experiment with triplicates on each plate. Significant differences between the control (ATP) and the venom are indicated by **** ($P < 0.0001$) using one-way ANOVA followed by Dunnett's test.

However, due to the very limited amount of LK-601 available, we could not perform the dose-inhibition studies as seen before on hP2X4. Thus, we chose 10 μM (a concentration that produced strong inhibition at hP2X4) as a concentration that could provide a reliable comparison between these species. As predicted, LK-601 inhibited mouse P2X4 in 1321N1-mP2X4 cells ($49 \pm 5\%$) (**Figure 4.23A**); however, the inhibition was nearly 1.6-fold less effective when compared to the human isoform in the same 1321N1 cell model ($79 \pm 1\%$) and 1.4-fold better than it was shown in our BV-2 model ($35 \pm 3\%$). While the comparison between our mouse P2X4 models (1321N1-mP2X4 vs BV-2) might be due to the cell line differences rather than the mode of action, the comparison between 1321N1-hP2X4 and 1321N1-mP2X4, as well as 1321N1-hP2X4 and BV-2 models clearly points out the selectivity of LK-601 for both human and mouse isoforms.

Unexpectedly, while LK-601 seemed to affect mP2X4 and hP2X4, the toxins didn't have any significant effect on rat P2X4 (82% and 94% amino acid identity with human and mouse, respectively) when applied at 10 μM (**Figure 4.23B**). Neither LK-601 nor LK-729 inhibited rP2X4 (<19 % inhibition) when tested at 10 μM , highlighting that both toxins were inactive towards rat P2X4. For comparison, the known P2X4 antagonist PSB12062 didn't show any species differences but inhibited P2X4 receptors across species ($71 \pm 4\%$ and $79 \pm 3\%$ at mouse and rat, respectively). BX430 didn't display any statistically significant inhibition on either the rat or the mouse P2X4 ($19 \pm 8\%$ and $28 \pm 5\%$ at mouse and rat, respectively) as expected.¹⁵³ Interestingly, 5-BDBD showed a similar selectivity profile as LK-601 as it blocked mP2X4 and hP2X4 but not rP2X4 ($55 \pm 3\%$ and $0 \pm 9\%$ at mouse and rat, respectively).

4.2.5. Structural Elucidation of LK-601 and LK-729

The purified toxins LK-601 and LK-729 were next subjected to NMR spectroscopic analysis. Each toxin was weighed (~ 0.1 mg), dissolved in deuterated water (D_2O), and ^1H NMR spectra were recorded. First, the toxins were probed with NMR 500Hz, but the signal-to-noise (S/N) ratio was too low to allow the accurate peak integration and extraction of J-couplings. As the concentration of both toxins, LK-601 and LK-729, was below 0.5 mg, either more material or a higher-field NMR spectrometer was required to gather structural information about these two toxins.

In an attempt to overcome this problem, both toxins were then subjected to NMR spectrometry at 800 MHz (**Figure 4.24** and **Figure 4.25**).

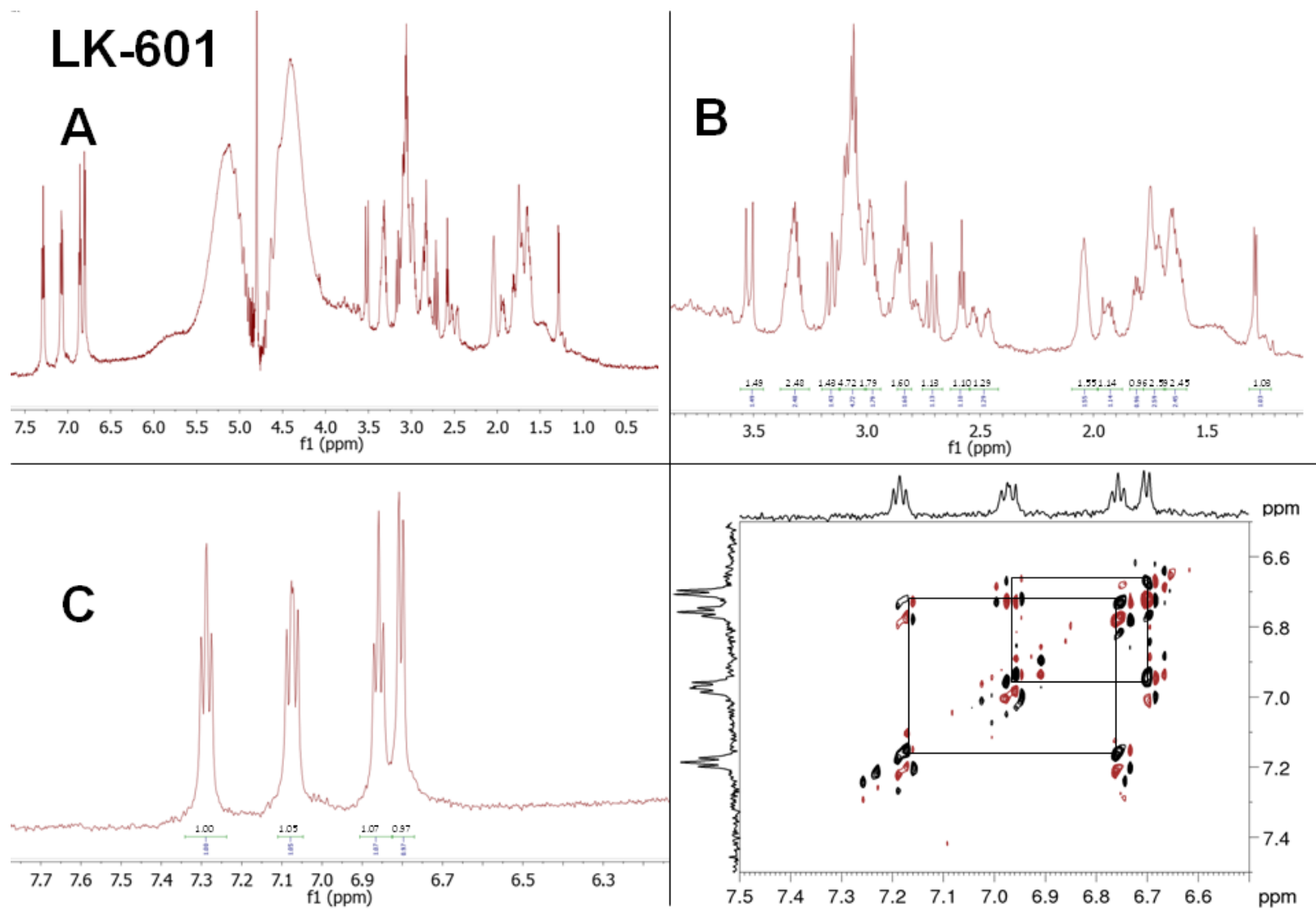


Figure 4.24. NMR-spectroscopic analysis of LK-601 by 800 MHz NMR. **A:** The full ^1H -NMR spectrum revealing a highly complex structure. **B:** ^1H -NMR signals from the aliphatic chains. **C:** ^1H -NMR signals from the aromatic region. **D:** Expansions of the corresponding COSY spectrum suggested the aromatic ring of LK-601 might have 1,2-substitution.

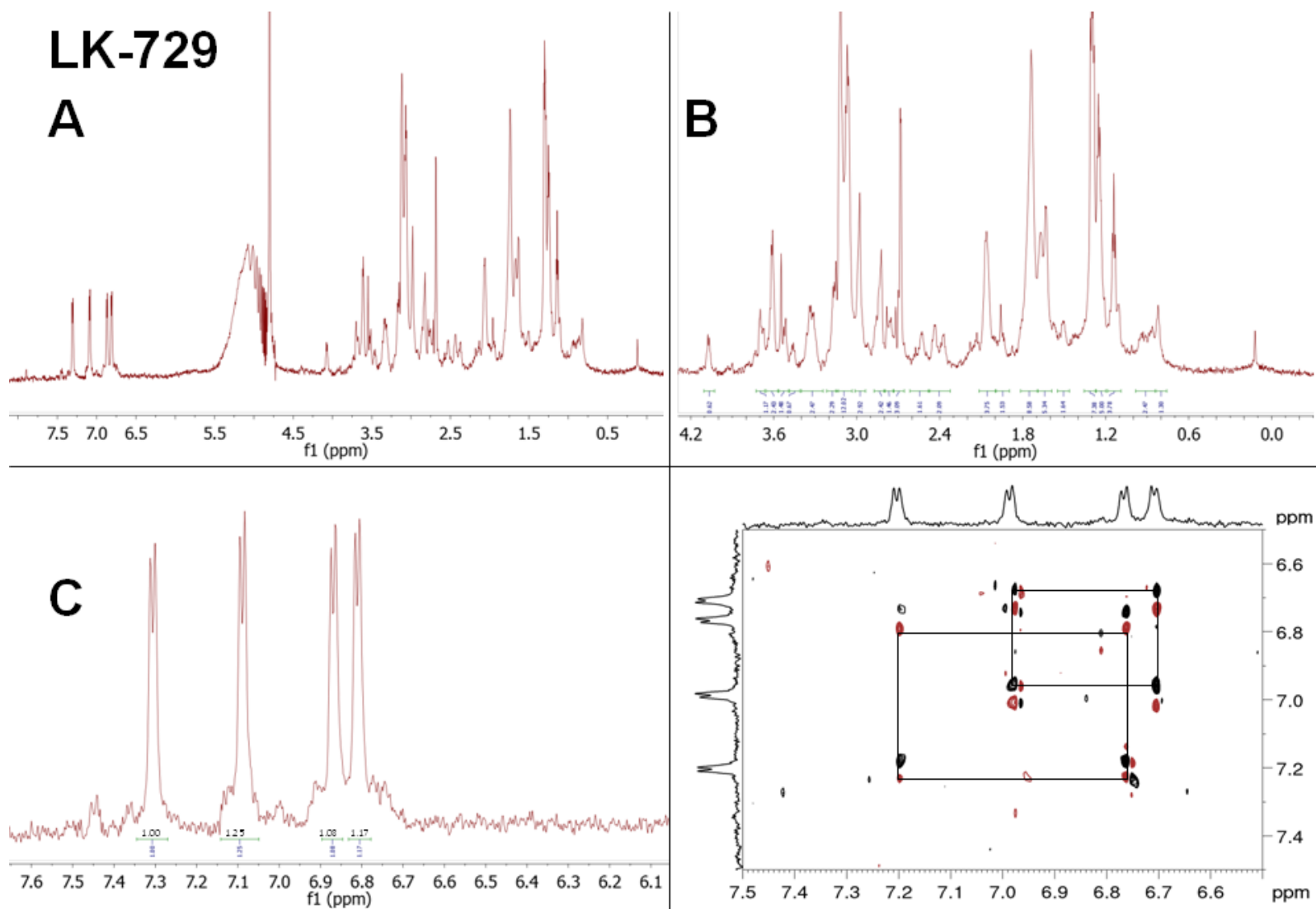


Figure 4.25. NMR-spectroscopic analysis of LK-729 by 800 MHz NMR. **A:** The full ^1H – NMR spectrum revealing a highly complex structure. **B:** ^1H – NMR signals from the aliphatic chains. **C:** ^1H – NMR signals from the aromatic group. **D:** Excerpts of the corresponding COSY spectrum suggested two aromatic rings of LK-729 with two 1,4-substitutions.

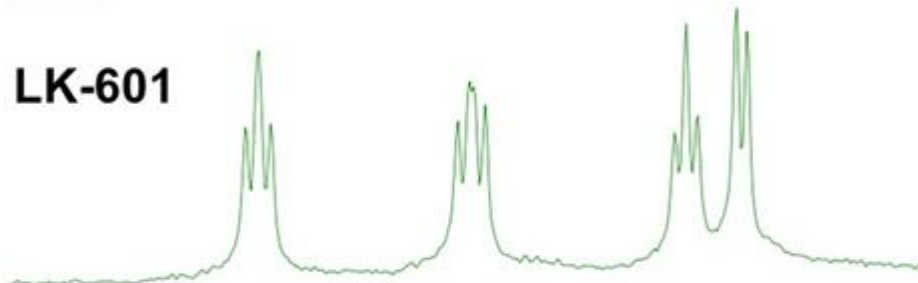
Some of the conclusions we could draw were that the signals in the aliphatic region of LK-601 (**Figure 4.24B**) and LK-729 (**Figure 4.25B**) seemed different, suggesting an aliphatic chain with different proton environments. Along similar lines, the aromatic regions were also different. For example, a splitting pattern of LK-601 (**Figure 4.24C**) seemed to have 3 triplets and a doublet while LK-729 had 4 doublets (**Figure 4.25C**). In order to obtain more information, the toxins were analysed further by using 2D NMR spectroscopy, including COSY, NOESY, HMQC, and HMBC spectra. These investigations could confirm the presence of acylpolyamines which should be simply recognized based on the typical spin systems of their aromatic head groups, whose links to the polyamine chains should be evident from the HMBC spectra. However, as much as these resulting sets of spectra could afford sufficient signal dispersion and connectivity information to assign structural fragments, we couldn't gather any valuable information about the carbon couplings. The reason being, HMQC and HMBC spectra did not yield any meaningful data, and suggest we need more material.

The only assessment that might provide some additional information about the polyamine headgroup were the COSY experiments which suggested the 1,2-substitution and two 1,4-substitutions for LK-601 and LK-729, respectively (**Figure 4.24C** and **Figure 4.25C**). Previous consultation of the literature suggested the headgroups being either indole-derived or para-disubstituted hydroxyphenyl rings.^{322, 330} Thus, we hypothesized that LK-601 may contain an indole-derived (1,2-substituted) group while LK-729 may have two para-disubstituted hydroxyphenyl (1,4-substituted) rings. Complete characterization of the connecting segments was not possible, however, because of multiple signal overlap; while the S/N here was better with 800 Mhz, the signals were still challenging to integrate due to the heterogeneity of both toxins; ¹H NMR spectra in aliphatic regions showed primarily broad, unresolved peaks, seemingly devoid of any characteristic signals representing a typical polyamine (e.g., spermine, spermidine). Furthermore, NMR spectra acquired for the period of 24h clearly pointed out to the instability of these toxins in water (**Figure 4.26**, depicted as "degradation LK-601") which made it even more difficult to determine which signals correspond to which proton. As a result, the overlap of corresponding NMR-spectroscopic signals/impurities did not permit complete characterization of individual toxins. Nevertheless, NMR-spectroscopic analysis enabled the elucidation of the general structural features of the toxins.

Degradation LK-601



LK-601



LK-729

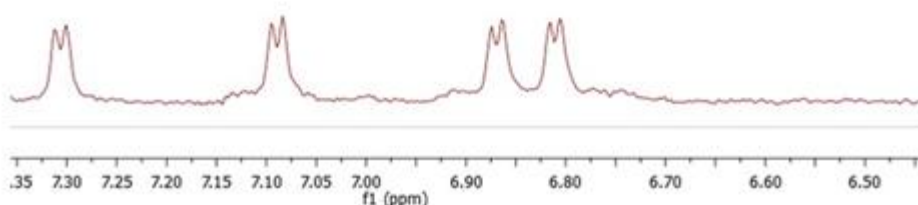


Figure 4.26. Instability issues with LK-601 and LK-729 as seen by the NMR-spectroscopic analysis.

To further elucidate the structure of the LK-601 and LK-728 toxins, more material would be required, a more efficient fractionation method should be in place, and stability of the toxins under specific conditions (temperature, solvent) should be further investigated. Additionally, for toxins of this type, structural assignments could be confirmed through NMR – spectroscopic spiking experiments using original samples of the previously identified acylpolyamines.

4.3. Conclusions

In the present chapter, we set out to investigate whether the toxins from cone snails and/or spider venoms could be found to contain novel inhibitors of hP2X4 channels. These animals, like other venomous taxa, expend their venom in both predatory and defensive contexts; they can deliver variable quantities within individual doses and from multiple glands at the particularly vulnerable region of their prey. Although it is unlikely that any P2X receptors are present in insects,³⁴² the venom of these animals may still be rich in P2X modulators.

For example, Grishin and colleagues¹³⁸ showed that Purotoxin-1, a spider venom peptide, exerted potent inhibitory action on hP2X3 receptors.¹³⁸ Since we currently lack a potent and selective antagonist of the hP2X4 channel with desirable characteristics for drug delivery,¹⁶⁷ venoms may contain clues for the design of selective hP2X4 therapeutics involved in a range of pathologies, including chronic neuropathic pain.

Firstly we examined the effects of cone snail venoms on hP2X3, hP2X4 and hP2X7 channels; however, none of the crude venoms, and later fractionated toxins, were found to inhibit these channels. The only crude venom that initially seemed to modulate hP2X3 receptor was *Conus geographus*, which exhibited potentiating effects. However, the fractionation of the venom later showed that the toxins failed to produce hP2X3-specific responses. This non-specific potentiation effect may be a consequence of either activated endogenous receptors expressed by HEK293 cells, or the toxins' ability to form pores in the membranes, thus displaying cytotoxicity²⁵⁶ in calcium-based assays.

Notably, this same non-specific effect of CS3 was not noted in HEK293-hP2X7 cells, when assessed by YO-PRO-1 dye. It would be interesting to measure the calcium effects on this cell line in order to confirm the results seen on HEK293-hP2X3. Unfortunately, there's no hP2X7-specific agonist thus we had to measure YO-PRO-1 dye uptake rather than calcium influx. All the other fractions showed similar effects on hP2X3 as its agonist, which may exclude them from being potent modulators of hP2X3.

The HEK293 cell line not only expresses P2X receptors, but also endogenous P2Y receptors, making specificity towards these receptors tougher to quantify. Therefore, the human astrocytoma cell line 1321N1 that possess no endogenous P2 receptors was used. This formed the basis of a high-throughput Fura-2 assay in which venoms, and fractionated toxins, were monitored for the ability to prevent a calcium-related fluorescent response induced by activation of the P2X channels with ATP. The inhibitory effects of the toxin hits were validated on both cell lines and any potential non-specific effects were circumvented early on. Thus, our screens were less susceptible to artefacts and false positives. The efforts were then focused towards the most potent and selective toxins able to block hP2X4.

Using this method, we screened 15 crude spider venoms that showed interesting activity against hP2X4 in our preliminary screens (L. Stokes, personal communication) by adding diluted venom to either HEK293-hP2X4 or 1321N1-hP2X4 prior to an application of 10 μ M ATP. Although a number of venoms showed non-specific activity, venoms from *A. brocklehursti*, *Lasiodora* and *Phormictopus* produced a particularly robust inhibitory effect on hP2X4 channel activated by ATP.

For example, only 5 µg of the most potent crude venom (from *Lasiadora klugi*) produced nearly complete inhibition of ATP-activated hP2X4.

To determine the inhibitory toxins within these venoms, we fractionated 9 crude venoms (*Lasiadora klugi*, *Lasiadora parahybana*, *Acanthoscurria geniculata*, *Acanthoscurria cordubensis*, *Phormictopus cancerides*, *Haplopelma albostriatum*, *Poecilotheria rufilata*, *Nhandu chromatus* and *Epebopus murinus*) using reverse-phase HPLC with water-acetonitrile gradients and tested individual fractions for activity against hP2X4. The HPLC fractionation of crude venoms resulted in the chromatograms that contain one predominant clusters of peaks. It has been previously reported that the venom components eluting between 15 and 25 min are primarily acylpolyamine toxins, whereas the toxins eluting later (> 40min) are primarily peptides.^{297, 330, 343} When these early eluting fractions were examined for activity against hP2X4, inhibitory activity was observed for the cluster of peaks corresponding to acylpolyamines with *E. murinus* serving as an adaptive control venom. This occurrence has previously been reported for acylpolyamines from spider venoms targeting TRPV1 channels³⁴⁴ so this is not a novel concept. Yet, activity against another ligand-gated ion channel (hP2X4) is.

By applying the combined crude venom without the inhibiting fractions of *L. klugi* on our HEK293-hP2X4 cell line, the inhibitory effect of the venom was lost regardless of the venom concentration. The molecular weight of the toxins was confirmed by mass spectrometric analysis, which predominately yielded masses 365.2563 Da, 454.2274 Da, 600.3712 Da, 728.5026 Da consistent with some previous observations.^{253, 330} Interestingly, the fragment ions of 112.1136, 129.1438, 220.1041, 291.1763, 347.2494, 365.2605, 509.2864 and 601.3749 were recurrent in all toxins except 454.2274, regardless of the collision energy applied, indicating that these are specific fragments originating from the structurally similar toxins. Our subsequent investigation focused on the ones with masses 600.3712 Da and 728.5026 Da because these toxins were more abundant in venoms, and thus easier to obtain in larger amounts. Both toxins eluted between 11 – 12% CH₃CN, and showed interesting activity against hP2X4. After another step of purification was performed using RP-HPLC, both toxins were obtained in purities > 91%.

To investigate the concentration dependence for inhibition by these two toxins, different concentrations of the toxins were applied to both, HEK293-hP2X4 and 1321N1-hP2X4, using two validated assays (YO-PRO-1 and Fura-2) described in the Chapter 3. This way, we discovered two novel members of hP2X4 antagonists that were found among different spider venoms species, however isolated from *Lasiadora klugi*.

These molecules were named LK-601 and LK-729 as suggested by Itagaki³²² whose nomenclature proposed to include both the molecular mass and the backbone chain subtype in the nomenclature of novel acylpolyamine toxins.³²² Both, LK-601 and LK-729 potently inhibited hP2X4 with the apparent IC₅₀ values between 1.1 – 4.5 μM, confirmed in two different cell lines and with two different sets of fluorescent-based assays.

Despite the limitation of using fluorescent-based techniques (rather than a more direct method, e.g. electrophysiology), the relationship between hP2X4 inhibition and toxin concentration (0.1 – 30 μM) could be well documented in these two cell models. Furthermore, we found no significant inhibitory effect on the other P2X subtypes (hP2X3, hP2X7), although concentrations >100 μM have not been tested. Nonetheless; LK-729 was found to potentiate hP2X3 responses. This is unfortunate since potentiating homomeric P2X3 results in the sensation of painful stimuli.³³⁶⁻³³⁷ Thus, we shifted our focus to LK-601 rather than to LK-729.

Acylpolyamines are also known to interact with ion conduction pores in potassium channels,³⁴⁵⁻³⁴⁶ cyclic nucleotide gated channels,³⁴⁷ glutamate receptor channels,^{281, 286, 344, 348-351} nicotinic acetylcholine receptor channel,³⁵² TRPM4,³⁵³ TRMP7³⁵⁴ and TRPV1.³⁴⁴ In most cases, acylpolyamines block these targets from the intracellular side of the membrane, and inhibition is strongly voltage-dependent. However, in order to ascertain whether LK-601 blocks some of these channels, we tested both toxins on NMDA 1a/2a subtype of glutamate channels. Interestingly, even though the majority of identified acylpolyamines inhibit this family of receptors,¹⁸¹ LK-601 did not have any effect on HEK293-NMDA 1a/2a. Nevertheless, we cannot exclude the possibility that LK-601 may act on other glutamate receptors such as AMPA and kainate channels. Acylpolyamines that antagonize non-NMDA glutamate receptors have been found in other spiders with JSTX-3 having subunit-specific activity on GluR1, GluR3, GluR4, and GluR1/3.³⁵⁵ Probing LK-601 towards other non-NMDA glutamate targets would help to address this gap. Still, these results suggest that LK-601 is rather selective for this type of acylpolyamines.

When looking at the species-related effects, LK-601 – while exhibiting a relatively potent inhibitory effect at hP2X4 – shows similar actions towards mP2X4 but does not block rP2X4. The effect of LK-601 on mP2X4 was also confirmed in a BV-2 microglial model. This is not an uncommon phenomenon; apart from a recently identified P2X4-selective antagonist NP-1815-PX¹⁶⁷ with high potency, no species-restricted effect and a good water solubility, other available P2X4 antagonists display similar effects to LK-601. For example, the phenylurea BX430,¹⁵³ N-substituted phenoxazine PSB12062,¹⁶⁶ and benzodiazepine derivate 5-BDBD²⁵⁰ all selectively block hP2X4 with low micromolar potency, but are less potent on rat and mouse P2X4.

Hence, in order to investigate how LK-601 might accomplish that, we needed to understand its chemical structure better. This would subsequently allow timely characterization of structure-activity relationship (SAR). Although we attempted to get a reasonable NMR signature, we rather failed to obtain a full structural elucidation of LK-601 and LK-729, and could only determine its partial structure – similarly to Skinner et al.³³⁰ thirty years ago.

Furthermore, the only other study that might reported a similar compound was from Rocha-E-Silva et al.³²³ where they isolated a small molecule VdTX-1 with a mass of 728 Da from the spider venom. They showed that their acylpolyamine may block cholinergic receptors in vertebrate nerve-muscle preparations, however, the structural elucidation could not be determined.³²³

Nevertheless, some clues could still be derived from our NMR data. The reasons for this are numerous. First, while NMR is the dominant method for determining the structure of small molecules, it suffers from low sensitivity;³⁰⁸ the quantity of material required is usually between 1 – 10 mg.³⁵⁶ A relatively good proton spectrum can be acquitted with lower amounts, however, determining carbon couplings with an acceptable resolution requires at least 1 mg of material even with 800 Mhz. Given the low amounts of isolated toxin (~0.1 mg), LK-601's striking instability in water added to the challenge, making it harder to pinpoint the structure. On the basis of that limitation, the only observations we could make were the following: 1) LK-601 and LK-729 contain a different aromatic ring with LK-601 likely to be an indole; 2) LK-729 has a longer polyamine chain than LK-601; 3) the polyamine chain very likely contains a spermine moiety.

Another aspect of the same conundrum is that MS/MS fragmentation clearly shows similar fragmentation patterns with LK-601 and LK-729 and points to 601 being a part of 729. While NMR characterization may elude to the fact that the polyamine chain is longer in LK-729, it is also evident that the head group is different (indole vs phenol). This may exclude the possibility of LK-601 being part of LK-729 or suggest rearrangement between the aromatic group of LK-601 (indole) and LK-729 (two phenols). The reasons for this inconsistency remain unclear; however, it is still conceivable that the similarity between LK-601 and LK-729 inhibiting effect is merely due to the positive charged polyamine chain rather than the aromatic systems of the toxins. Hence, all these obstacles limited the full structural characterization of LK-601 and thus, *in silico* docking studies.

Although previous studies have shown that direct NMR-spectroscopic analysis can be used to screen even crude spider venoms for the presence of sulfated nucleotides, the same authors concluded that a complete structural elucidation still requires the use of NMR in combination with mass-spectrometric analysis and synthesis.

Furthermore, they confirmed that the signal overlap in the NMR spectra of the acylated polyamines prevented a full NMR spectroscopic elucidation of the structurally novel compounds.³⁰⁸ In our case, these issues could be circumvented by either making more chemically stable analogues; having more material available which might enable faster and more comprehensive structural determination by NMR; using a superconductive NMR probe;³⁵⁷ or using other methods, rather than NMR, that don't require exposure to water (e.g. elemental analysis). However, given the destructive nature of the elemental analysis, and with limited supply of the crude venom, we could not afford to subject LK-601 to these sorts of studies. In spite of these lows, the NMR spectroscopic fingerprint revealed some structural features which provided guidance for our next pursuits.

In summary, we have isolated and characterized two acylpolyamines LK-601 and LK-729 as two novel hP2X4 antagonists with good potency and with LK-601 showing a better selectivity for hP2X4. In particular, our findings not only provided evidence for spider venoms containing inhibitors of P2X channels, but have also enabled us to ask whether the species differences in the effect of LK-601 on hP2X4 can hold a clue to the LK-601 binding site. Since the amino acid identity of rat P2X4 is 82% and 94% when compared to human and mouse, respectively, future studies would focus on obtaining more structural insights about LK-601. We would also attempt to identify a smaller fragment of LK-601 that inhibits hP2X4 with a relatively good potency, selectivity and a better stability. Thus, we proceeded with the chemical synthesis of LK-601 potential analogues, followed by the identification of the amino acids critical for the binding of LK-601 on hP2X4.

~CHAPTER FIVE~

Synthesis, Structure-Activity Relationship and Evaluation of LK-601 Analogue LA-3, a Novel hP2X4 Antagonist

This Chapter is based on a research article, currently in preparation as:

Bibic L., et al. Discovery of a Novel Spider Toxin that Selectively Inhibits P2X4 Receptor. In preparation.

5.1. Introduction

5.1.1. Importance of Structure-Activity Relationship (SAR) of Natural Products

The exploration of structure-activity relationship (SAR) is an important step in medicinal chemistry and drug design. SAR investigations might provide a chemical optimization of hits and the identification of a novel lead.^{235, 358} However, small chemical changes can also render active compounds completely or nearly inactive, or, contrarily, increase their drug-like properties, such as potency, water solubility and stability.²³⁵ It has long been established that one of the distinguishing characteristics of natural products is the molecular diversity of structurally related analogues.³⁵⁹ However, why would an organism invest in resources needed to synthesize many analogues that serve no biological function? While this might be unclear,²³⁵ Macarron and others²³⁴ suggest that the organism's need is to generate its own chemical space to optimize the activity of its own active metabolites.²³⁴ Ultimately, this suggest the organisms are doing their own structure-activity relationship (SAR) optimization.

Although selecting a lead molecule that would function as a pharmacological skeleton is poised with difficulties, various investigators have recognized that the natural product libraries, such as venoms, can be viewed as a population of structurally privileged new medical entities (NME) selected by evolutionary pressures.^{179, 191-192, 230, 310, 360} By having the characteristics of high chemical diversity and biochemical specificity, toxins from venoms are favourable as NME for drug discovery. This differentiates them from libraries of synthetic or combinatorial compounds.³⁵⁹ Although nature is a master chemist that often provides the first clues to SAR in the form of chemical analogues, not all hits generated from the natural products libraries meet the stringent criteria for potency and selectivity.³⁵⁹ Thus, preliminary SAR is essential.

Alternatively, it might be more effective to adapt approaches that combine both strategies. For example, leveraging the unique structural motifs of natural products and use it as a guidance to seek more focused libraries might yield a novel bioactive natural product scaffold with improved drug-like properties or even biological activity.²⁶⁰ One avenue for exploring SAR in this way might lead to identifying a key pharmacophore required for the activity. Once the modulation of biological response through chemical modifications is established, the hit might be declared as lead and proceeded onwards for additional optimization. This hit-to-lead approach might provide an early foundation on which the overall synthetic strategy could be developed.^{234, 260}

5.1.2. Animal Toxins as a Template to Lead Selection

A lead molecule endowed with an appropriate biophysicochemical properties as well as interesting pharmacological profile in terms of potency and selectivity, has been termed as a “universal template”.³⁶¹ In that context, polyamine toxins - a group of small molecules present in spiders and wasps – have evolved specifically as open-channel blockers of glutamate, muscarinic and nicotinic receptors for paralyzing prey, thus, they might serve as a “universal template” towards a lead selection.³⁶¹⁻³⁶⁴

However, apart from G-protein coupled receptors, this approach has also been applied to ligand-gated ion channels, such as nicotinic receptors. One of these synthetic probes, now known as MR44, proved to be one of the most promising pharmacological tool to study binding of a polyamine analogues to the nicotinic receptors (**Figure 5.1**).³⁶⁴ Thus, the ability of the polyamine backbone to hit the desired target with having low or no affinity towards the others is evident. The crucial step would be to pinpoint the highly cationic cargoes (amino groups) to anionic or aromatic sites to ensure high recognition of ion channels while abolishing affinity for other targets.

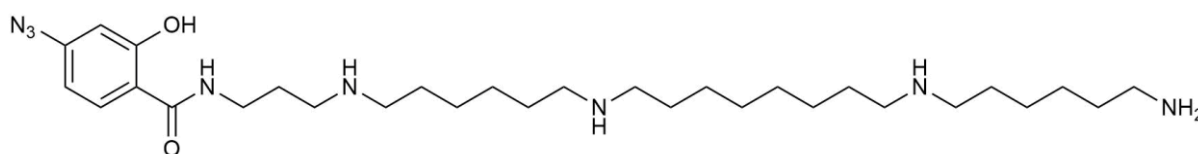


Figure 5.1. Structure of MR44.

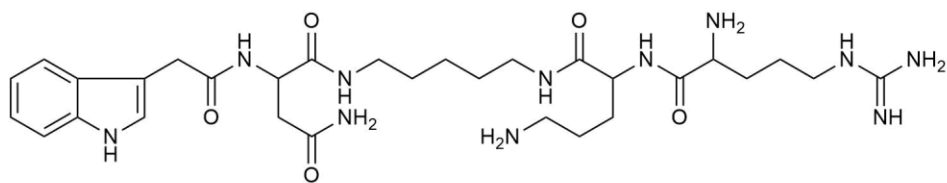
5.1.3. Chemical Synthesis of Acylpolyamine Toxins Derived from Spider Venoms

The chemical synthesis of polyamines and their derivatives were performed in solution until the nineties³⁶⁵ when Bycroft and others³⁶⁶ reported the first solid-phase synthesis (SPS) of two spider toxins, NPTX-9 and NPTX-11, with a diamine backbone(**Figure 5.2**). Since then, a great variety of methods have been introduced for the chemical synthesis of polyamine moieties.^{274, 276, 367} In particular, Fukuyama-Mitsunobu amination reaction applied SPS to yield acylpolyamine toxin analogues, although the efficiency of the reaction has dropped extensively due to the solid support.^{276, 368-373} In order to solve this issue, the same authors later devised a higher yielding strategy of a notoriously tedious acylpolyamine, Agel-489 (**Figure 5.2**). With performing Fukuyama amination steps in solution rather than on a solid support, their approach furnished this polar amino-containing natural product in 31% overall yield.^{297, 367, 374}

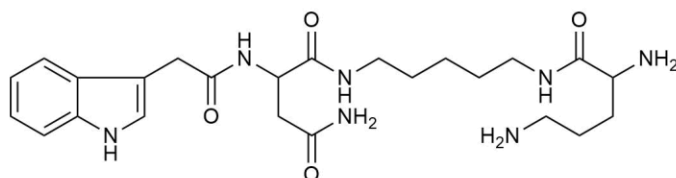
Other chemical approaches aiming for the total synthesis of the spider toxins involve adaptation of the polyamine cargo on a solid support by applying borane reduction of a trityl resin-bound tripeptide.^{303, 375} This has been since extensively used by various groups including Schultz,³⁷⁶ Jarozewski³⁶⁷ and Hall.³⁰³ Also, bidirectional SPS of the polyamines has been reported,³⁷⁷ and either N-hydroxylated polyamine units or full-length toxins (ArgTX-636) prepared (**Figure 5.2**).^{373, 378}

However, despite their desirable biological properties, the challenges of preparing acylpolyamine toxins still remain. One of them is that SPS procedures do not allow for a direct access to the large group of polyamine toxins, such as Joro toxin (JSTX-3), one of the most studied acylpolyamine toxin to date (**Figure 5.2**). This, in turn, prevents the systematic SAR studies to improve their biochemical, physical as well as pharmacological properties.³⁷⁸⁻³⁷⁹ Although some recent studies devised strategies to accelerate this,³⁷⁹ other methods, rather than SPS, might be worth considering.

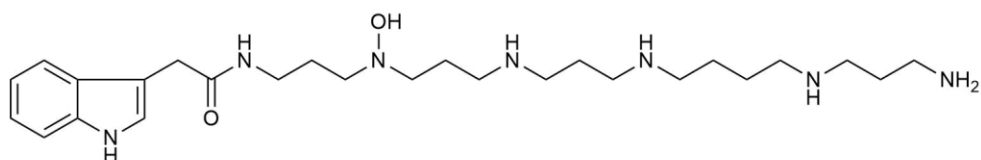
One such approach calls for selective monosubstitution of polyamines. Here, an excess of the polyamine is treated over time with the acylating reagent. Once the activated amino esters are generated by esterification between nitrophenol and the carboxylic acid of the amino acid, the resulted compounds might be coupled directly to the polyamine to yield a mixture of mono- and disubstituted products that can be fairly easily separated by RP-HPLC techniques.³⁸⁰⁻³⁸¹ The true beauty of this method is that a series of simple polyamine/amino acid conjugates can be generated, avoiding a limitation of SPS approach described earlier although the resulting yields might be a few folds lower.²⁷⁴



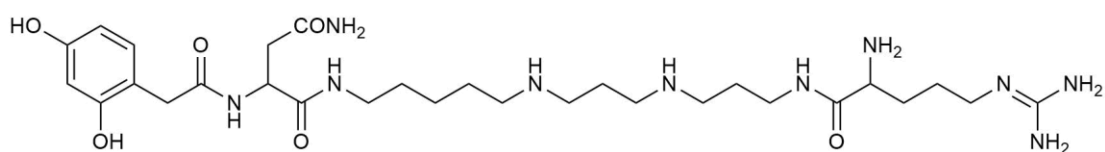
NPTX-9



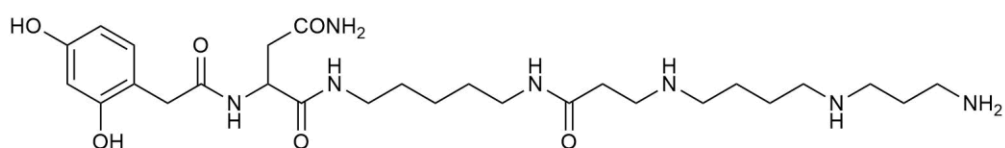
NPTX-11



Agel-489



Arg-636



JSTX-3

Figure 5.2. Structures of NPTX-9, NPTX-11, Agel-489, Arg-636 and JSTX-3.

5.1.4. Biological Effects of Polyamines and Acylpolyamines

As discussed already in Chapter 1, polyamines are polybasic aliphatic amines that are vital for protein and nucleic acid synthesis; resistance to oxidative stress; cell growth, differentiation and apoptosis; and activity of ion channels, as summarized by Anthony E. Pegg³⁸² in one of his recent reviews.

Notably, these polyamines are found in various natural products, including animal venoms.²⁹⁸ Among them, four polyamines are associated with multiple effects on AMPA³⁸³ and NMDA³⁸⁴ receptors: cadaverine, putrescine, spermidine, and spermine.³⁸⁵⁻³⁸⁶ For example, these polyamines showed either a voltage-dependent pore blockade,³⁸⁶ or an increase in the apparent affinity for the co-agonist glycine and glycine-independent potentiation,^{261, 385, 387} depends on the NMDA subunits. The latter effect of polyamines has been studied in-detail due to its remarkable subunit selectivity; only NMDAs containing the GluN2B subunit display polyamine potentiation.³⁸⁸⁻³⁸⁹ Furthermore, these polyamines (spermine in particular) were shown to bind at a subunit-subunit interface and serve to stabilize the receptor dimer assembly, defining a novel mode of how positive allosteric modulators may modulate ligand gated receptors.³⁹⁰ Other channels associated with the biological effects of polyamines are potassium (Kir), and transient receptor potential (TRP) channels. Here, polyamines act as negative allosteric modulators, able to produce either a voltage-dependent block on Kir channels,³⁴⁶ or a strong inhibition on TRP4 and -5 channels.³⁹¹

Another group of polyamines are so-called acylpolyamines, monoacylated polyamines, which have attracted most attention as pharmacological tools, illuminating both positive and negative modulators of ionotropic glutamate (iGluR) receptors, such as kainate, NMDA and AMPA. There is a vast body of clinical evidence suggesting that glutamate is involved in neurodegenerative disorders such as Huntington's, Alzheimer's and Parkinson's disease.³⁹² Thus, a discovery of a specific acylpolyamine for these channels has a potential to progress into novel treatments for neurological or psychiatric disorders.³⁹³ For example, Tikhonov³⁹⁴ identified the polyamine part of one such acylpolyamine – ArgTX-636 – to be crucial for selectivity between different NMDA- and AMPA-type subfamilies. ArgTX-636 targets NMDA subtypes with up to 100-fold differences in inhibitory potency, pointing out to its therapeutic potential in nervous diseases.

Other examples include acylpolyamines such as DACS and JSTX-3 showing neuroprotective effects in events such as prolonged hypoxia and ischemia. In particular, JSTX-3 was found to block AMPA/kainate receptors expressed in *Xenopus* oocytes, and demonstrated its action as a subunit-specific blocker on GluR1, GluR3, GluR4, and GluR1/3. Interestingly, using site-directed mutagenesis, Blaschke et al.³⁵⁵ identified a single amino acid position (glutamine in the TM2 domain) that was critical for JSTX-3 effect.³⁵⁵ While all these JSTX-3-related effects have given insights into pharmacological mechanism of iGluR in various nervous diseases, JSTX-3 was also found to specifically blocked allodynia via Ca²⁺ - permeable AMPA receptors when delivered by intrathecal injection.³⁹⁵⁻³⁹⁸

This not only suggested that AMPA receptors are important for the spinal mechanism leading to tactile allodynia in their *in vivo* injury model, but also suggest JSTX-3 as a lead compound when studying the development of spinal sensitization.

Other authors³⁹⁹ suggest that spinal sensitization effect contributing to secondary hyperalgesia (but not primary mechanical hyperalgesia) modulated by JSTX-3 requires AMPA/kainate receptors. Their data, obtained in *in vivo* rat models, demonstrated that behavior for secondary mechanical hyperalgesia may not effect the behavior for primary mechanical hyperalgesia, and can thus be separated from spontaneous pain and secondary mechanical hyperalgesia in postoperative patients. Metzger and others³⁹⁶ also showed that JSTX-3 modulates Ca^{2+} influx via AMPA/kainate receptors in the cultures of motor neurons, resulting in dendrite outgrowth that may have implications in motor neurodegenerative diseases.³⁹⁶ Nowadays, JSTX-3 is commercially available, and serves as a potent, subunit-specific blocker on iGlu receptors.

However, one of the major limitations of using acylpolyamines as potential drug candidates, is their lack of selectivity for iGluR; they block both NMDA and non-NMDA receptors. Moreover, their drug-like properties are not ideal; they possess poor physio-chemical attributes (poor chemical stability and permeability), and are usually bigger than 500 Da. In order to circumvent these effects, some synthetic analogues of acylpolyamines have been successfully synthesized. For example, in cultured hippocampal neurons, Naspn reversibly blocked kainite-activated currents in a non-competitive manner, suggesting its potent action on non-NMDA channels.²⁸³

On that note, acylpolyamines might not be only useful as potential therapeutics, but also insecticides.⁴⁰⁰ This led other group of researchers to study their SAR in a greater detail. This way, a wasp acylpolyamine philanthotoxin-433 (PhTX-433) – a nonselective antagonist at iGlu and nicotinic acetylcholine (nACh) receptors – was used to improve affinity at either iGlu (AMPA) receptors³⁶⁸ or nAChRs.⁴⁰¹ Soon, a number of analogues (PhTX-83, PhTX-56, PhTX-12 PhTX-343) followed (**Figure 5.3**).

Interestingly, while replacing one of the amino group in PhTX-433 with a methylene group renders the toxin selective for AMPA receptors (PhTX-83),³⁶⁸ changing two amino groups in PhTX-433 with two methylene groups shows a remarkable selectivity towards nAChR and potency at nanomolar concentration (PhTX-12).⁴⁰¹ Furthermore, modifications to the head group (replacing the phenol with the cyclohexylalanine) also resulted in improved selectivity towards nAChR.⁴⁰¹

P2X receptors are another class of ligand-gated ion channels, however, with barely any structural or sequence similarity to iGlu or nACTh channels. Yet, no acylpolyamine has been found that would target P2X receptor family with a reasonable potency and selectivity profile, nor any SAR attempted.

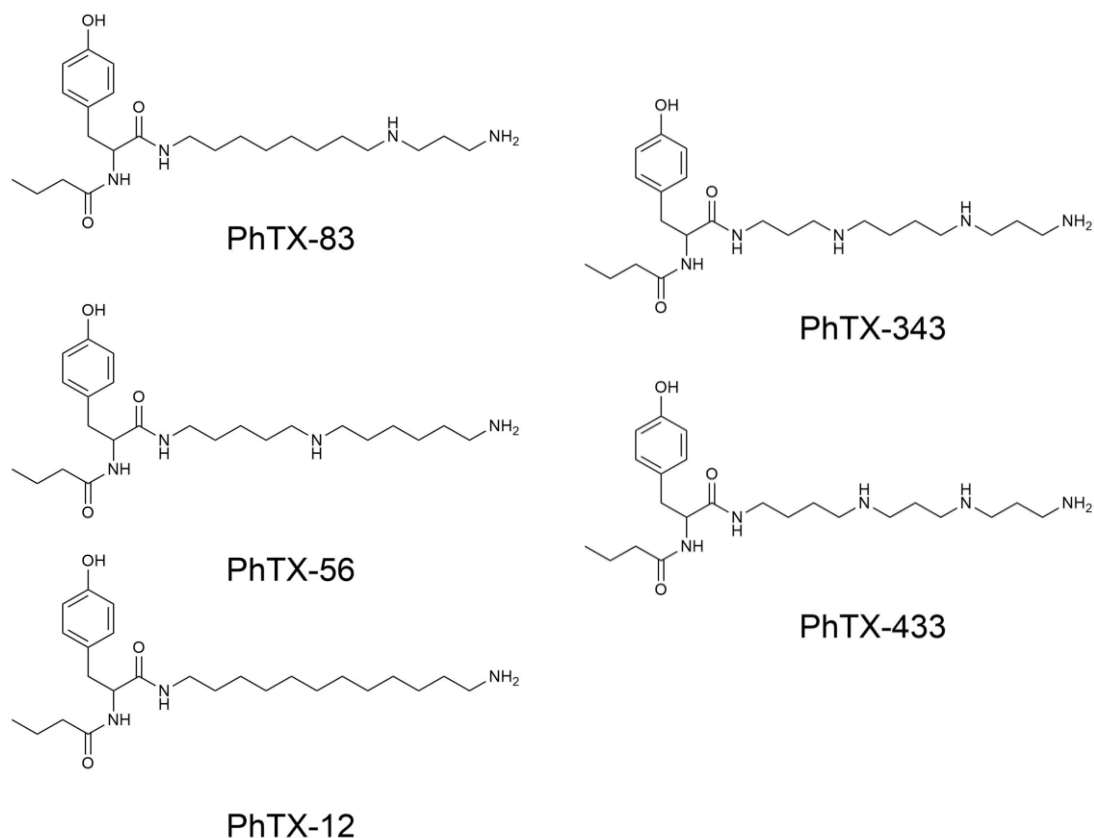


Figure 5.3. Structures of PhTX-83, PhTX-56, PhTX-12, PhTX-343 and PhTX-433.

5.2. Results and Discussion

In the previous chapter, we have isolated and characterized two acylpolyamines LK-601 and LK-729 as the novel P2X4 antagonists with good potency in low micromolar concentrations, and with LK-601 showing a better selectivity profile compared with other P2Xs. We concluded that LK-601 may not only provide evidence for spider venoms containing inhibitors of P2X channels, but also serve as a chemical template to synthesize LK-601 analogues that may yield better physicochemical and/or pharmacological properties. Thus, this Chapter will deal with SAR investigations where a variety of polyamines, indole-like compounds and a structurally similar acylpolyamine would be probed towards hP2X4 in order to ascertain functional motifs that are crucial for the LK-601 activity towards hP2X4.

We would use the obtained information as a structural guide towards synthesizing the smaller molecules that might resemble a structure of LK-601 that still retains a required potency and selectivity while avoiding some of the less appealing biochemical properties such as chemical instability of LK-601. Moreover, prediction of the amino acids that might be crucial for the binding of LK-601 and/or its structural analogues on hP2X4, would be proposed and the validation attempted.

5.2.1. Investigating the Nature of Structure-Activity Relationship in LK-601

5.2.1.1. Simple Polyamines do not Modulate hP2X4 Receptor

To ascertain whether the polyamine tail in LK-601 is responsible for the inhibitory effect on hP2X4, four polyamines (cadaverine, putrescine, spermine and spermidine) have been tested in the concentration range from 3 – 300 μM using two stable cell lines (HEK293-hP2X4 and 1321N1-hP2X4). The polyamines were applied prior to the injection of ATP (10 μM), and hP2X4 activity was then measured via Ca^{2+} influx or YO-PRO-1 dye uptake (**Figure 5.4**). We also probed the cell lines with the concentration of spermine up to 1 mM, however, these higher amounts elicit a non-specific response.

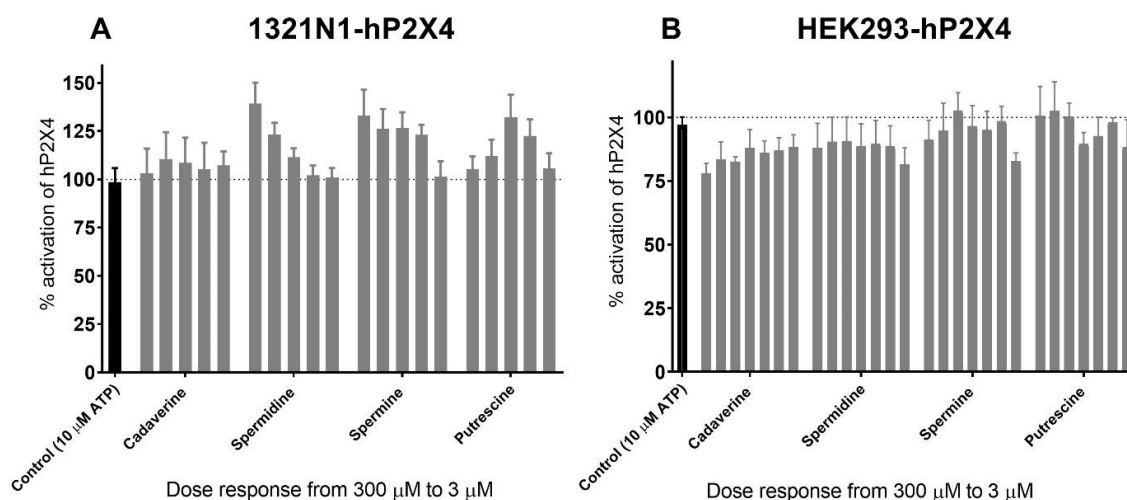


Figure 5.4. Application of polyamines prior to 10 μM ATP application in two stable cell lines. A: Application of cadaverine, spermidine, spermine and putrescine to 1321N1-hP2X4 cells (Ca^{2+} influx) in concentration range of 3 – 300 μM ($n=4$). **B:** Application of cadaverine, spermidine, spermine and putrescine to HEK-hP2X4 cells (YO-PRO-1 uptake assay) in concentration range of 300 – 3 μM ($n=4$). Data is presented as the mean \pm SD with 10 μM ATP as a control.

While neither polyamines at any given concentration showed any significant inhibitory effect on hP2X4 that could be validated by both assays (the activity of hP2X4 was found to be between 76 – 101 % and 102 – 136% in 1321N1-hP2X4 and HEK293-hP2X4, respectively), we concluded that polyamine motifs in isolation do not block hP2X4 receptor.

It first seemed that spermidine, spermine and putrescine potentiated hP2X4 at concentration >30 μM (**Figure 5.4A**); however, these effects could not be confirmed on HEK293- hP2X4 (**Figure 5.4B**). When probing the higher concentration of polyamines on a native 1321N1 cell line, we found that this potentiating effect is specific to 1321N1 cell line rather than to hP2X4 modulation (data not shown).

5.2.1.2. Indole-based Compounds Modulate hP2X4 Receptor

To test whether the indole ring may modulate the activity of hP2X4 channel, we first screened a library of indole-like compounds that we had available in-house. These included 1H-indole (**1**), 1-methylindole (**2**), 1-hydroxymethyl-1H-indole (**3**), indole-2-carboxylic acid (**4**), indole-3-carboxylic acid (**5**), 2-(1H-indol-3-yl)ethanamine or tryptamine (**6**), (2S)-2-amino-3-(1H-indol-3-yl)propanoic acid or tryptophan (**7**), and 3-(2-aminoethyl)-1H-indol-5-ol or serotonin (**8**) (**Figure 5.5**). While compound **1** was not modified from its original structure (1H-Indole), other chemicals (**2-5**) were either N-substituted (with the $-\text{CH}_3$ **2** or $-\text{CH}_2\text{OH}$ **3** group), or had modifications on the five-membered pyrrole ring ($-\text{COOH}$ on either 2'- **4** or 3' position **5**). The other three compounds were either precursors of amino acids (tryptamine **6** and serotonin **8**) or amino acids (tryptophan **7**) with both, the carboxylic and primarily amino group found on the pyrrole ring. These compounds were assigned numbers from 1 to 8 and the following *in vitro* screens were performed in blinded experiments.

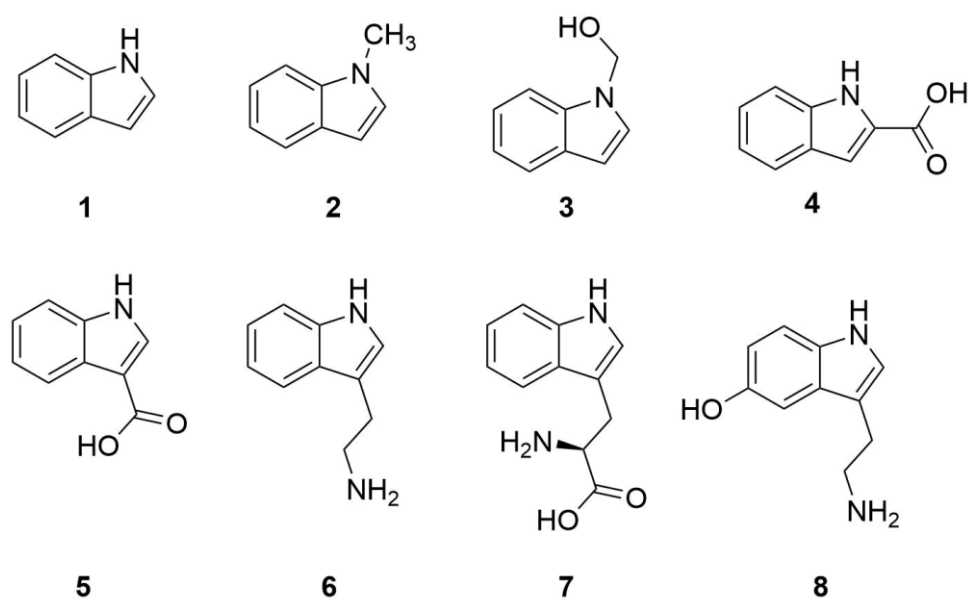


Figure 5.5. Chemical structures of eight indole-like compounds that were screening in our preliminary assays. These included 1H-Indole (**1**), 1-Methylindole (**2**), 1-Hydroxymethyl-1h-Indole (**3**), Indole-2-Carboxylic Acid (**4**), Indole-3-Carboxylic Acid (**5**), 2-(1H-Indol-3-yl)ethanamine or Tryptamine (**6**), (2S)-2-amino-3-(1H-indol-3-yl)propanoic acid or Tryptophan (**7**), and 3-(2-aminoethyl)-1H-indol-5-ol or serotonin (**8**).

These eight compounds were first screened in HEK293-hP2X4 cell line in which the inhibitory activity of the compounds was measured by YO-PRO-1 dye uptake assay. Among these compounds, only tryptamine (**6**), tryptophan (**7**) and serotonin (**8**) were identified to significantly inhibit hP2X4 with 10 μ M showing $32 \pm 5\%$, $39 \pm 6\%$ and $43 \pm 5\%$ inhibition, respectively (**Figure 5.6**). This effect has not been noted with lower concentrations (3 μ M). Interestingly, while the indole itself, N-substituted analogues or carboxylic modifications at the position 2 or 3 did not show any measurable inhibition at hP2X4 (the activity of the channel remained between 91 – 102%), the compounds with a primary amine connected to position 3 of the indole via a 2 carbon chain showed an inhibition at 10 μ M concentration, which was lost at 3 μ M. Yet, this inhibition was 4-5 times less effective than our control (BX430). The beauty of this set of results lie in the fact that we could now be more certain that LK-601 may contain an indole pharmacophore, as already suggested by 1,2-substitutions on our COSY spectrum (Chapter 4). Furthermore, it showed us that the substitution at the position 3 (-CH₂CH₂NH₂) might be essential for the inhibitory activity of LK-601 at hP2X4. Contrarily, presence of the -OH group on the position 5 of the indole and a -COOH group on the position 2 of the carbon chain does not make a difference when trying to block hP2X4 at the tested concentration of 10 μ M.

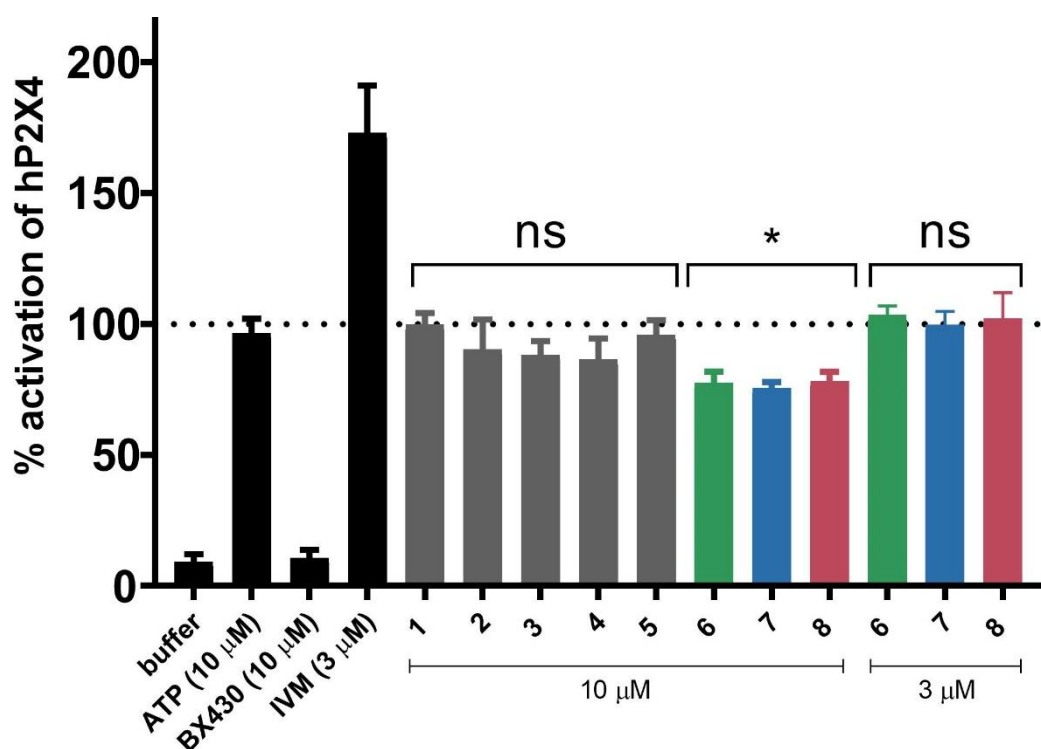


Figure 5.6. Application of simple indol-based compounds prior to 10 μ M ATP application in two stable cell lines. Application of 1H-Indole (1), 1-Methylindole (2), 1-Hydroxymethyl-1h-Indole (3), Indole-2-Carboxylic Acid (4), Indole-3-Carboxylic Acid (5), 2-(1H-Indol-3-yl)ethanamine or Tryptamine (6), (2S)-2-amino-3-(1H-indol-3-yl)propanoic acid or Tryptophan (7), and 3-(2-aminoethyl)-1H-indol-5-ol or serotonin (8) to HEK293-P2X4 cells (YO-PRO-1) at either 10 or 3 μ M concentration (n=4). Data is presented as the mean \pm SD with 10 μ M ATP as a control. Significant differences between the control (10 μ M ATP) and the venom are indicated by * (P < 0.01) using one-way ANOVA followed by Dunnett's test.

Intrigued by these results, we decided to screen a more extensive library of compounds with a hope to reveal more SAR insights and/or potential motifs of LK-601. Among many synthetic libraries available, the National Cancer Institute-Developmental Therapeutics Program (NCI-DTP) provides a diverse array of functionally relevant compounds with some great research outcomes already reported.⁴⁰² Notably, this same library contained a vast array of structurally relevant indole-like compounds for our screening purpose. On the flip side, since NCI-DTP library contained 1047 indole-like compounds, attempting to screen a library as such, called for a more systematic search. On the basis of known structural information of LK-601, and the insights we obtained with our first indole screen, we thus generated a SMARTS string of: O=C(NCCCCCCCCCCC)CC1=C[N]([H])C2=CC=CC=C12 (Figure 5.7).

O=C(NCCCCCCCCCCC)CC1=C[N]([H])C2=CC=CC=C12

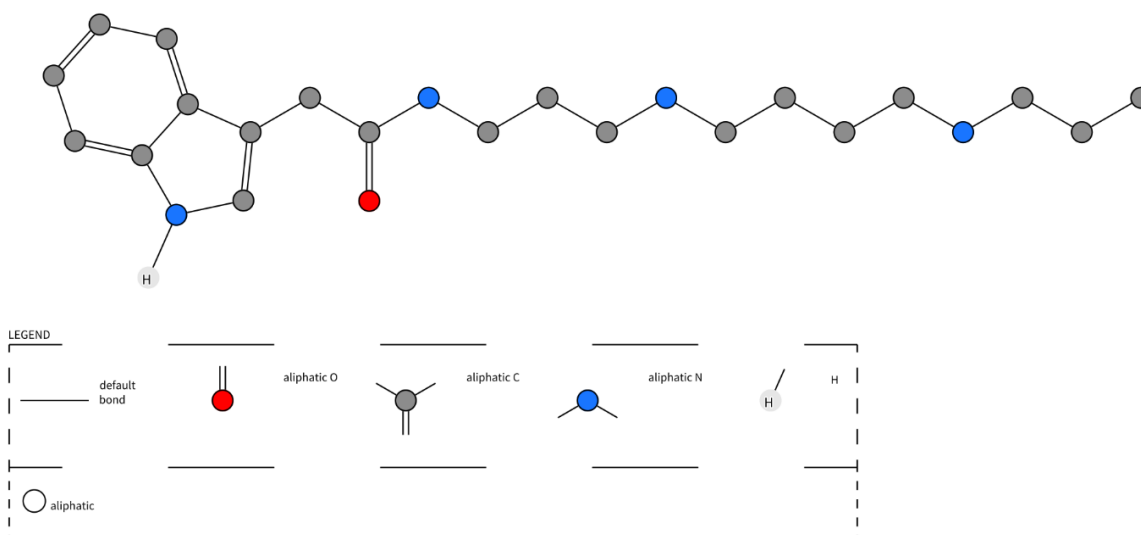


Figure 5.7. Structure of SMARTS

Once we subjected the SMARTS to the NCI-DTP library and limited the structure similarity to >90%, we were left with 22 hits (out of 1047 in total). However, only 14 compounds were available in sufficient amounts so we had to initially proceed with those (Table 5.1).

This set of 14 compounds were tested at four different concentration (0.3, 3, 30 and 100 μ M) in two different cell lines (1321N1-hP2X4, HEK293-hP2X4) with two different dyes (Fura-2 and YO-PRO-1) and with an activity cut-off at 50% inhibition for the concentration range of 30 - 100 μ M. This is two-fold higher than suggested by Hughes⁴⁰³ (cut-off at 25% inhibition at the 100 μ M), however, our aim was not to identify novel hits from the NCI-DTP library, but rather to gather some structural insights into the SAR of LK-601.

Table 5.1. A set of 14 compounds from the NCI-DTP library compound set. Each compound had an already assigned NCI-DTP number. Here, chemical names and CAS identifiers are provided.

NCI-DTP number	Chemical name	CAS identifier
329271	4,7-Methano-1H-isoindole-1,3(2H)-dione, 4,5,6,7,8,8-hexachloro-2-[[[(3-chlorophenyl)amino] carbonyl]oxy]hexahydro-	N.A.
17815	Indole-1-propionamide	21017-50-5
1513	1-nitro-3-[(2-oxo-3-indolinylidene)amino]guanidine	5347-87-5
1969	1H-Indole-3-acetamide	879-37-8
13964	Indoxyl acetate	608-08-2
16892	1H-Indole-3-methanamine	87-52-5
17812	1-(3-Indolylacetyl)hydrazine	5448-47-5
63799	1-(3-Indolylacetyl)hydrazine	5448-47-5
113928	5-Methoxy-N-acetyltryptamine	73-31-4
135831	N'-(4-chloro-2-nitrobenzylidene)-2-(1H-indol-3-yl)acetohydrazide	28558-55-6
673655	N-[2-(5-chloro-1H-indol-3-yl)ethyl]acetamide	N.A.
608048	2-(2-(1H-indol-3-yl)-2-oxoacetamido)-3-(4-hydroxyphenyl)propanoic acid	N.A.
369856	(N-(2-(3-Hydroxy-2-oxo-2,3-dihydro-1H-indol-3-yl)ethyl)-3-phenylacrylamide)	79087-89-1
339919	2-amino-N-(1-amino-3-(4-hydroxyphenyl)-1-oxopropan-2-yl)-3-(1H-indol-3-yl)propanamide hydrochloride	N.A.

In this preliminary screening, four compounds seemed to block the activity of hP2X4 when tested on HEK293-hP2X4 via YO-PRO-1 uptake. These chemicals corresponded to NCI-DTP identifiers of 1513, 13964, 135831 and 1969 (**Figures 5.8. – 5.10**). While 1513 demonstrated a concentration-dependent inhibition ($49 \pm 6\%$, $37 \pm 4\%$, $26 \pm 6\%$, and $8 \pm 5\%$ at 100, 30, 3 and 0.3 μM , respectively), and compound 13964 seemed to block the $31 \pm 3\%$ and $49 \pm 4\%$ activity of hP2X4 at 100 and 30 μM concentration, compounds 329271, 16892 and 17812 did not display any significant inhibitory effect (**Figure 5.8**). Thus, two hits (1513 and 13964) with a cut-off at 50% inhibition at either 100 or 30 μM were found.

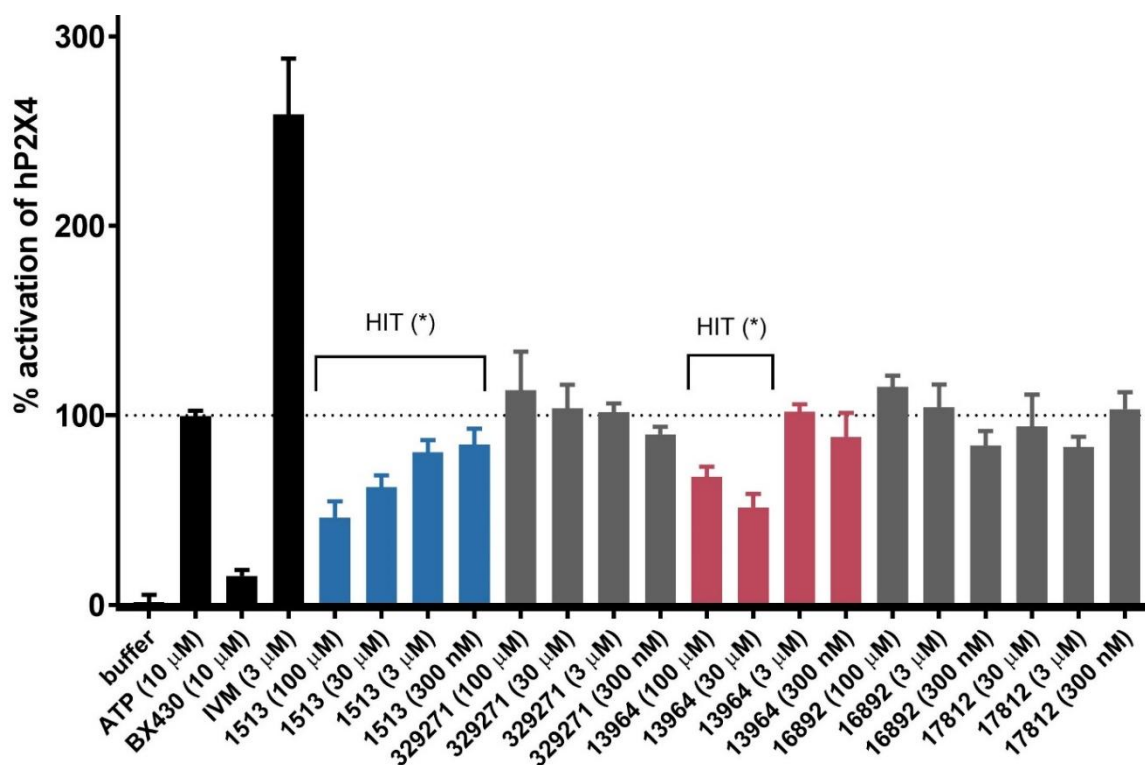


Figure 5.8. Application of the compounds (1513, 329271, 13964, 16892 and 17812) from the NCI-DTP library in HEK293-hP2X4. The compounds were pre-incubated at either 100, 30, 3 or 0.3 μM concentration (n=4). Data is presented as the mean ± SD with ATP (10 μM), IVM (3 μM) and BX430 (10 μM) as the controls. Significant differences between the control (10 μM ATP) and the venom are indicated by * (P < 0.05) using one-way ANOVA followed by Dunnett's test.

Next, we evaluated compounds 17815, 63799, 113928, and 135831. As shown in **Figure 5.9**, while 135831 demonstrated a concentration-dependent inhibition (63 ± 5%, 26 ± 4%, 25 ± 8%, and 10 ± 4% at 100, 30, 3 and 0.3 μM, respectively), compounds 17815, 63799 and 113928 did not display any significant inhibitory effect within our cut-off limit. Thus, another hit (135831) with a cut-off at 50% inhibition at either 100 μM was found.

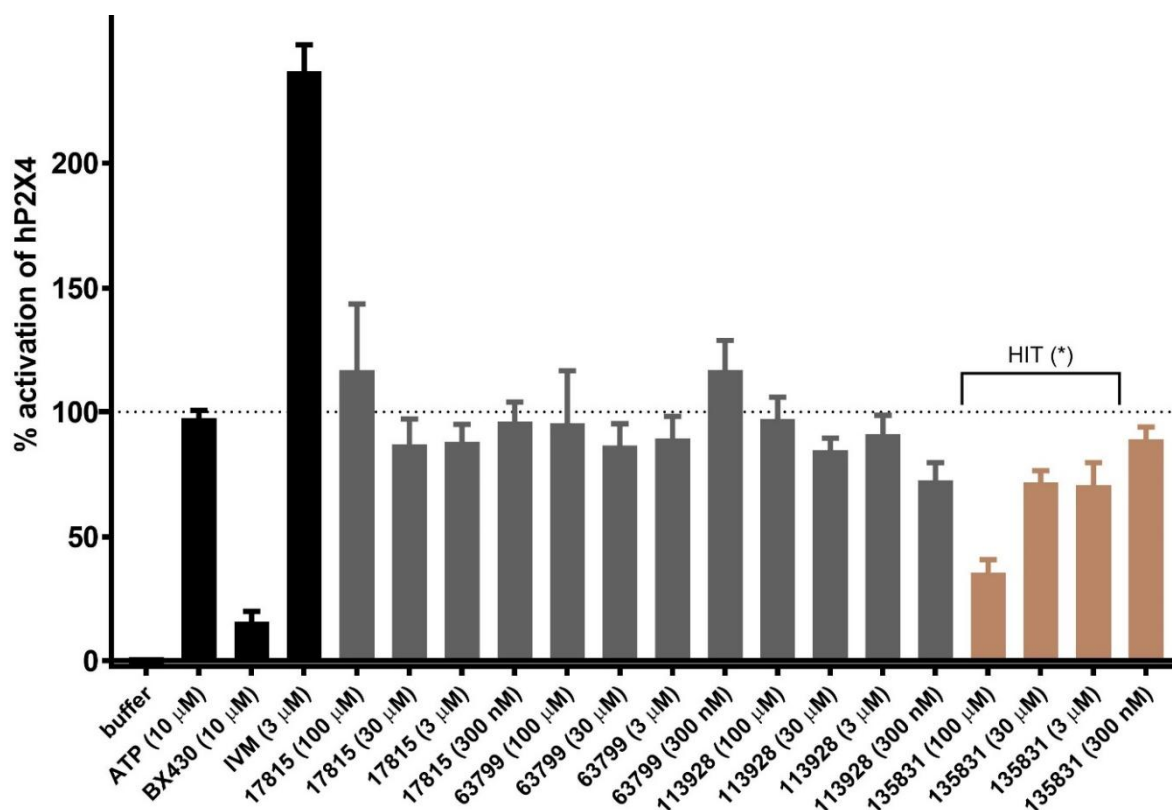


Figure 5.9. Application of the compounds (17815, 63799, 113928 and 135831) from the NCI-DTP library in HEK293-hP2X4. The compounds were pre-incubated at either 100, 30, 3 or 0.3 μ M concentration (n=4). Data is presented as the mean \pm SD with ATP (10 μ M), IVM (3 μ M) and BX430 (10 μ M) as the controls. Significant differences between the control (10 μ M ATP) and the venom are indicated by * (P < 0.05) using one-way ANOVA followed by Dunnett's test.

As the last set of experiments on HEK293-hP2X4 cell lines, we evaluated compounds 1969, 339919, 369856, 608048 and 673655. We found that while compounds 339919, 369856, 608048 and 673655 did not display any significant inhibitory effect on this cell line, 1969 demonstrated a concentration-dependent inhibition ($63 \pm 5\%$, $26 \pm 4\%$, $25 \pm 8\%$, and $10 \pm 4\%$ at 100, 30, 3 and 0.3 μ M, respectively).

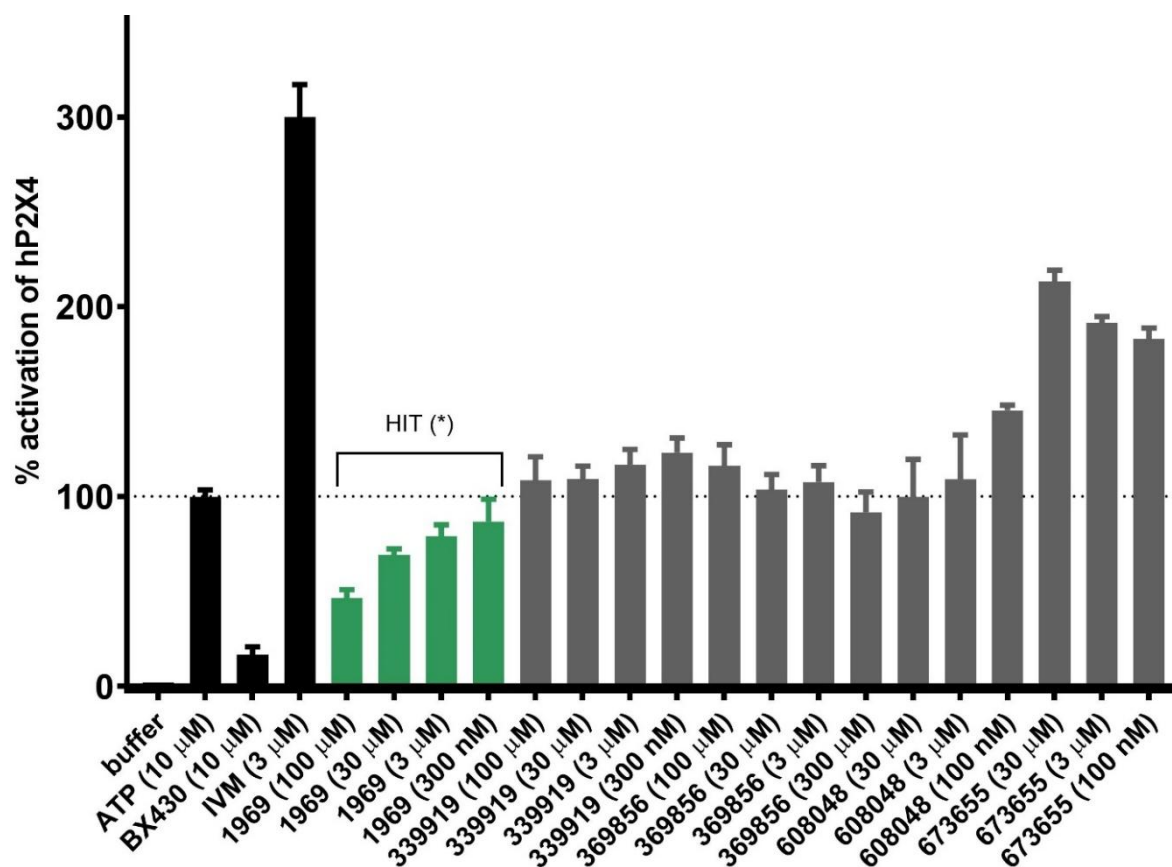


Figure 5.10. Application of the compounds (1969, 339919, 369856, 608048 and 673655) from the NCI-DTP library in HEK293-hP2X4. The compounds were pre-incubated at either 100, 30, 3 or 0.3 μ M concentration (n=4). Data is presented as the mean \pm SD with ATP (10 μ M), IVM (3 μ M) and BX430 (10 μ M) as the controls. Significant differences between the control (10 μ M ATP) and the venom are indicated by *(P < 0.05) using one-way ANOVA followed by Dunnett's test.

After an initial screen on HEK293-hP2X4 via YO-PRO-1 uptake, the identified hits were typically validated using another method. In our case, the validation was conducted with the already established Fura-2 assay on the 1321N1-hP2X4 cell line (Chapter 3). As seen on **Figure 5.11**, while compound 1513 exhibited an inhibition of $27 \pm 6\%$, $26 \pm 8\%$, and $20 \pm 10\%$ at 100, 30 and 3 μ M, respectively, one of the compounds - 16892, previously identified as hit, seemed to completely block Ca^{2+} signalling.

Since it would be very unlikely that a single compound exhibits these properties at three different concentrations, we wondered whether 16892 interferes with Fura-2 dye excitation and emission, leading to potential false positive.

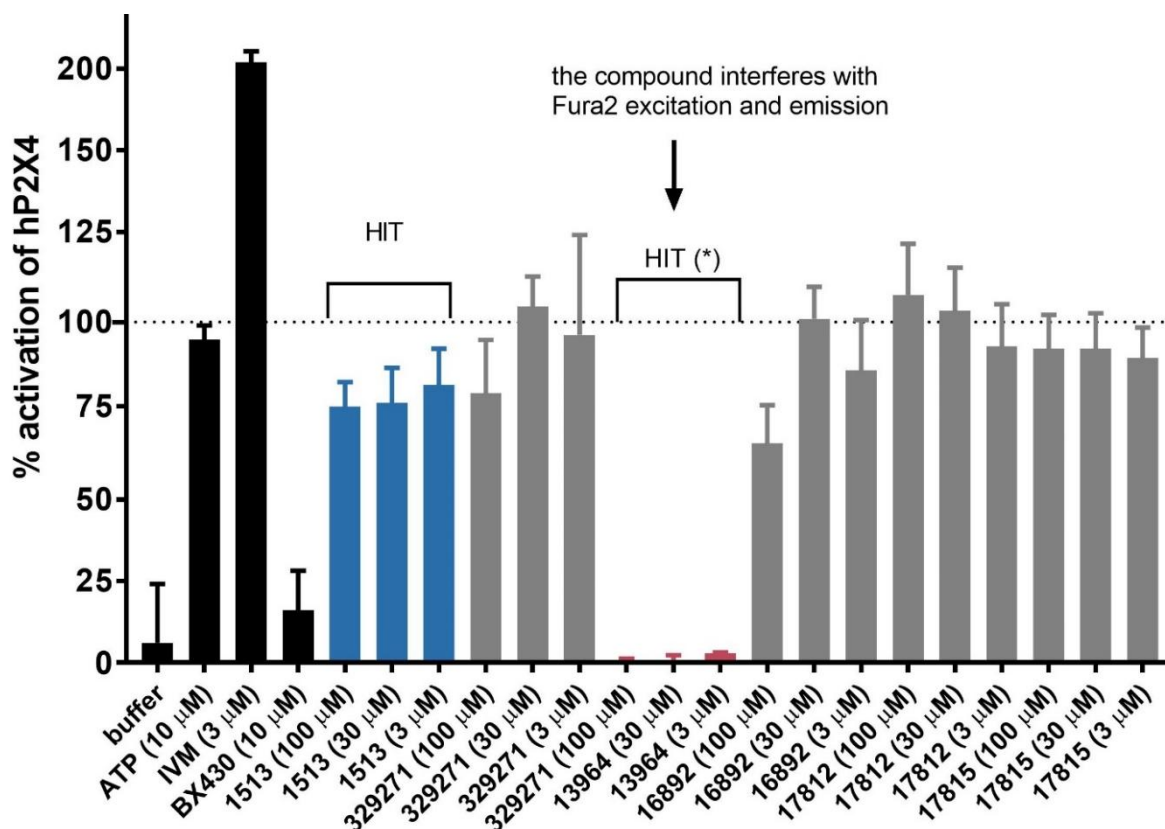


Figure 5.11. Application of the compounds (1513, 329271, 13964, 16892, 17812 and 17815) from the NCI-DTP library in 1321N1-hP2X4. The compounds were pre-incubated at either 100, 30 or 3 μM concentration (n=4). Data is presented as the mean ± SD with ATP (10 μM), IVM (3 μM) and BX430 (10 μM) as the controls. Significant differences between the control (10 μM ATP) and the venom are indicated by * (P < 0.05) using one-way ANOVA followed by Dunnett's test.

Since we wanted to confirm that 13964 interferes with Fura-2 measurements, either by quenching (absorbing either the excitation or emitted light from the dye) or autofluorescence (fluorescence of the compound in the same detection region with the dye), we conducted the interference assays with both, Fura-2 and YO-PRO-1 (**Figure 5.12**). The latter served us as the control experiment since we did not observe any assay interference in our HEK293-hP2X4 (YO-PRO-1) assay. As predicted, only 13964 was found to exhibit an autofluorescence when excited at 340 and 380 nm, which overlaps with the Fura-2 detection region (**Figure 5.12A**), but not of YO-PRO-1 region (490 nm) (**Figure 5.12B**).

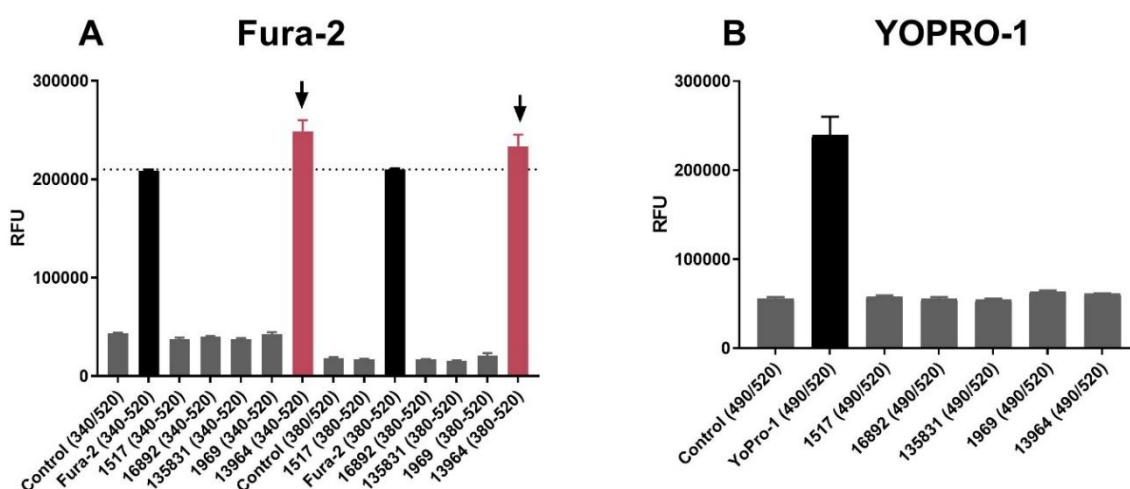


Figure 5.12. Interference Assays. Compounds 1517, 16892, 135831, 1969 and 13964, together with the buffer control were subjected to the fluorescent screen in either **A)** Fura-2 or **B)** YO-PRO-1 set of assays. RFU represents the relative fluorescent units. All samples were prepared at the same concentration, and the data are representative results from two independent experiments.

That said, the extent of interference depends on the concentration of fluorescent molecule (e.g. 13964) in the Fura-2 assay and its relative fluorescence intensity in our assay condition. Furthermore, as already noted by Simeonov and Davis,²⁶² just because 13964 is fluorescent or a quencher that does not mean that it cannot also have a relevant biological activity. It only means that having an orthogonal method (e.g. YO-PRO-1 in our case) to confirm the percent of inhibition at hP2X4 that was not prone to fluorescence interference is extremely useful. Thus, we concluded that 13964 still exhibited an interesting blocking activity at hP2X4, however, when tested on HEK293-HP2X4 via YO-PRO-1 uptake produces an assay interference.

Once the hit 1513 was validated, we evaluated the last set of compounds: 63499, 113928, 135831 and 1969. As shown in **Figure 5.13**, while 135831 and 1969 both demonstrated a concentration-dependent inhibition ($83 \pm 9\%$, $46 \pm 8\%$, $25 \pm 7\%$, and $89 \pm 11\%$, $66 \pm 1\%$, $55 \pm 4\%$ at 100, 30, 3 and 0.3 μM , respectively), other compounds (63799 and 113928) did not display any significant inhibitory effect within our cut-off limit. Thus, two other hits (135831 and 1969) were validated on 1321N1-hP2X4.

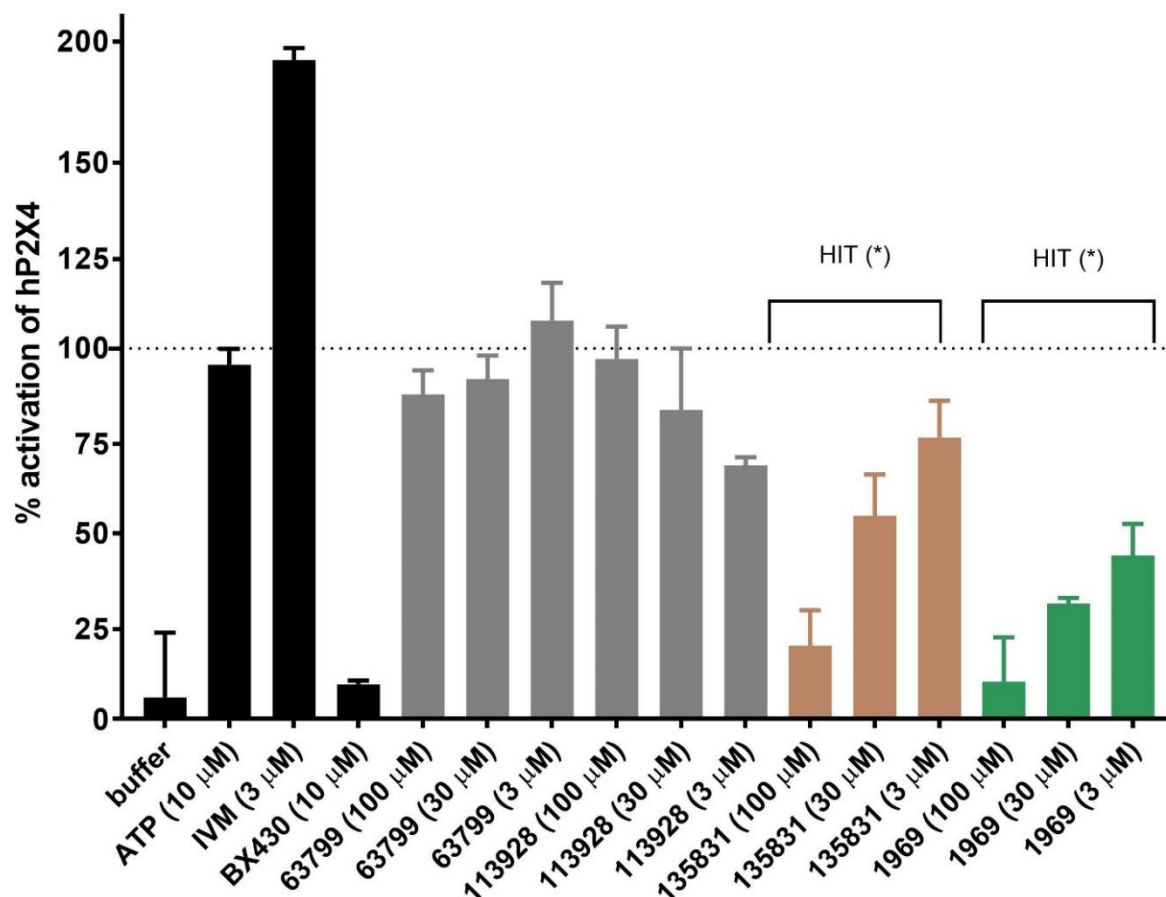


Figure 5.13. Application of the compounds (63799, 113928, 135831 and 1969) from the NCI-DTP library in 1321N1-hP2X4. The compounds were pre-incubated at either 100, 30 or 3 μ M concentration (n=4). Data is presented as the mean \pm SD with ATP (10 μ M), IVM (3 μ M) and BX430 (10 μ M) as the controls. Significant differences between the control (10 μ M ATP) and the venom are indicated by * (P < 0.05) using one-way ANOVA followed by Dunnett's test.

So far, the experiments were performed without the prior awareness of the structural information of the compounds – mainly to avoid any potential biases. However, once all the hits were confirmed, we took a careful look at their chemical structures (**Figure 5.14**). All four hits (1513, 13964, 135931, 1969) contained an indole pharmacophore and a substituted aliphatic chain at the position 3 that brings with it the hydrogen bonding ability (either donating or accepting). Longer chains might also be well tolerated (1513, 135931).

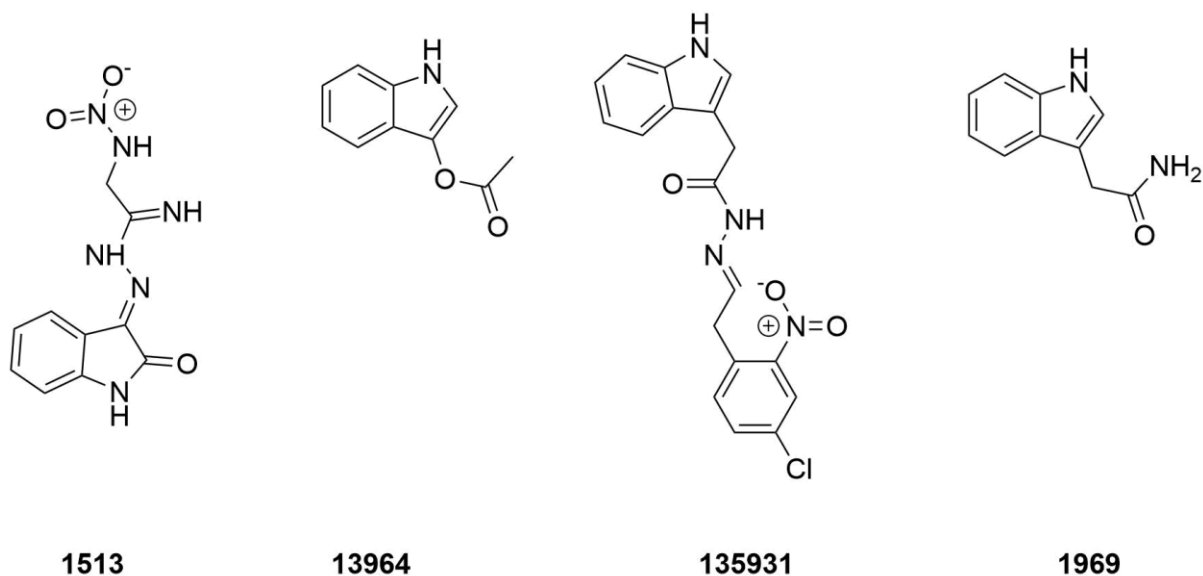


Figure 5.14. Selected indole-like “hit” compounds from the NCI-DTP library. Shown are structural examples of hits (1513, 13964, 135931 and 1969) from NCI-DTP database that showed promise in our bioassays.

When comparing the potencies of our four identified NCI-DTP hits, we noted that while on HEK293-hP2X4 the compounds were ranked as 1513 > 1969 > 13964 > 135831, this characteristic was different in 1321N1-hP2X4 cell line: 1969 > 135831 > 1513. This might merely be a consequence of a different cell line. Yet, in order to fully determine the potencies, we conducted another set of experiments; here, we aimed to determine IC_{50} of the above hits, and see whether their chemical structures might hold a clue for elucidating the structure of LK-601. Critically, we attempted to determine IC_{50} not only for hP2X4 (in HEK293-hP2X4) but also for hP2X7 (in HEK293-hP2X7). Since LK-601 was shown to inhibit hP2X4 but not hP2X7, we hypothesized that a particular structural element within the identified hits might play a role in blocking hP2X4 but not hP2X7.

First, we characterized 1513 (**Figure 5.15**), and confirmed an inhibition of $60 \pm 6\%$, $40 \pm 2\%$, and $25 \pm 4\%$ at 100, 30, and 10 μM , respectively, however, this effect was similar in HEK293-hP2X7 cell line as well ($59 \pm 4\%$, $41 \pm 5\%$, and $15 \pm 4\%$ 100, 30, and 10 μM , respectively).

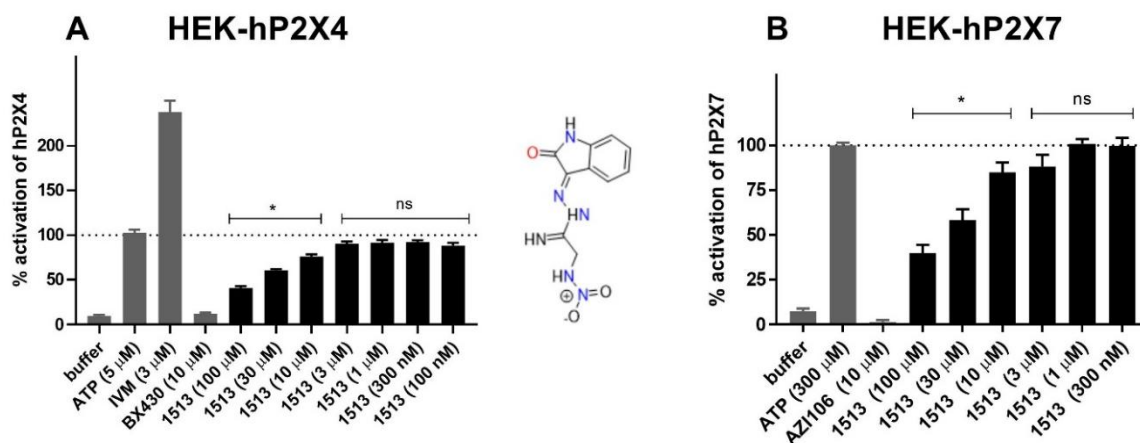


Figure 5.15. Dose-dependent inhibition of 1513. The compound 1513 was pre-incubated at either 100, 30, 3, 0.3 or 0.1 μ M concentration ($n=4$) and tested in **A**) HEK293-hP2X4 and **B**) HEK293-hP2X7. Data is presented as the mean \pm SD with ATP (10 μ M), IVM (3 μ M), BX430 (10 μ M) and ATP (300 μ M), AZ1106 (10 μ M) as the controls for P2X4 and P2X7, respectively. Significant differences between the control (10 μ M ATP or 300 μ M ATP) and the venom are indicated by * ($P < 0.05$) using one-way ANOVA followed by Dunnett's test. On the chemical structure, *blue* represents a nitrogen donor and *red* depicts an oxygen acceptor – both of which are susceptible of forming hydrogen bonds with the amino acid residues (protein/target).

Second, we characterized 13964 (**Figure 5.16**), and confirmed the hP2X4 inhibition of $52 \pm 2\%$, $38 \pm 3\%$, $33 \pm 3\%$, $29 \pm 4\%$, $25 \pm 3\%$, and $18 \pm 2\%$ at 100, 30, 10, 3, 1 and 0.3 μ M, respectively.

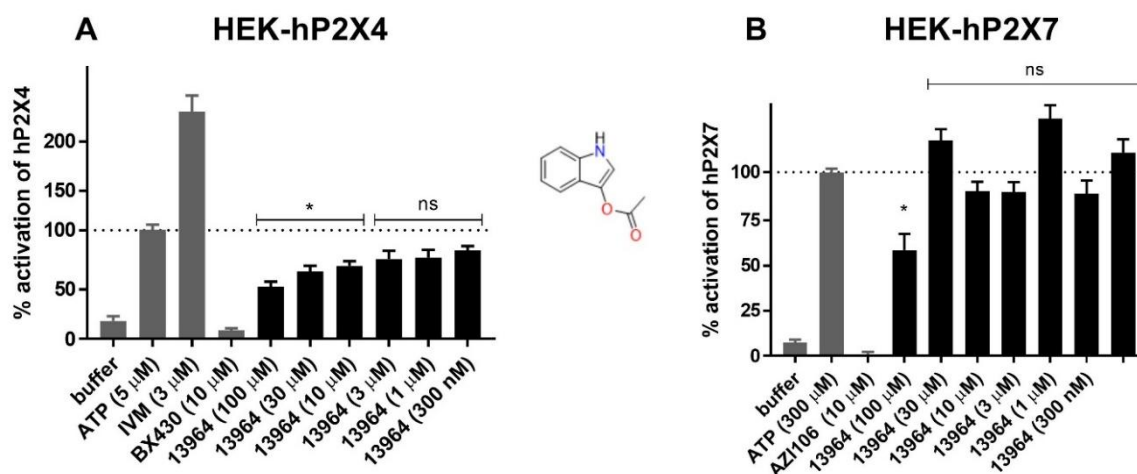


Figure 5.16. Dose-dependent inhibition of 13964. The compound 13964 was pre-incubated at either 100, 30, 3, 0.3 or 0.1 μ M concentration ($n=4$) and tested in **A**) HEK293-hP2X4 and **B**) HEK293-hP2X7. Data is presented as the mean \pm SD with ATP (10 μ M), IVM (3 μ M), BX430 (10 μ M) and ATP (300 μ M), AZ1106 (10 μ M) as the controls for P2X4 and P2X7, respectively. Significant differences between the control (10 μ M ATP or 300 μ M ATP) and the venom are indicated by * ($P < 0.05$) using one-way ANOVA followed by Dunnett's test. On the chemical structure, *blue* represents a nitrogen donor and *red* depicts an oxygen acceptor – both of which are susceptible of forming hydrogen bonds with the protein/target.

When probing the same hit on HEK293-hP2X7, an inhibition of $42 \pm 7\%$ was observed only at the relatively high concentration of $100 \mu\text{M}$. Next, we assessed 135831 (**Figure 5.17**), and confirmed the hP2X4 inhibition of $83 \pm 1\%$, $37 \pm 2\%$, $27 \pm 3\%$, $14 \pm 3\%$, $13 \pm 3\%$, and $2 \pm 1\%$ at $100, 30, 10, 3, 1$ and $0.3 \mu\text{M}$, respectively. When evaluating the same hit on HEK293-hP2X7, a striking inhibition of $96 \pm 2\%$ and $95 \pm 1\%$ was observed at 100 and $30 \mu\text{M}$ concentration with $81 \pm 5\%$, $37 \pm 3\%$ and $4 \pm 3\%$, and $5 \pm 7\%$ at $10, 3, 1$ and $0.3 \mu\text{M}$, respectively.

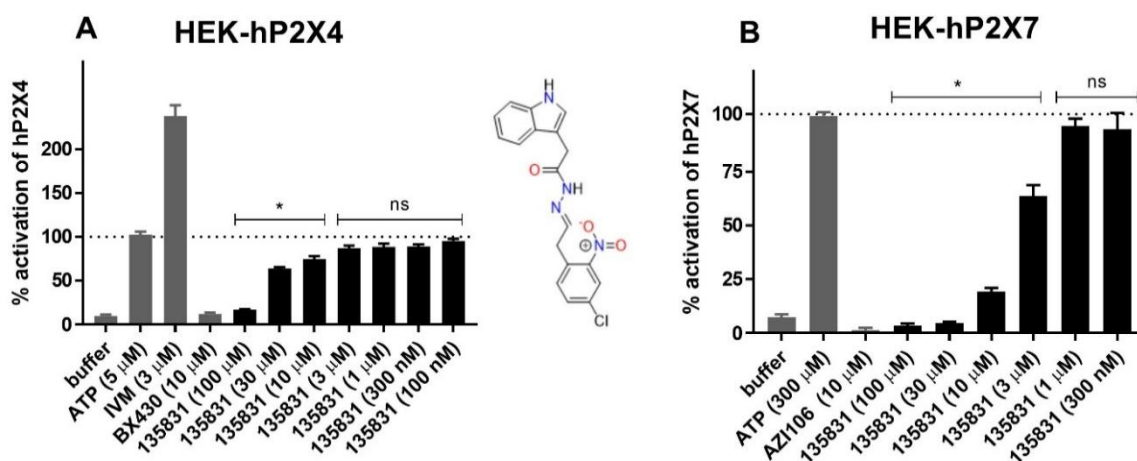


Figure 5.17. Dose-dependent inhibition of 135831. The compound 135831 was pre-incubated at either $100, 30, 3, 0.3$ or $0.1 \mu\text{M}$ concentration ($n=4$) and tested in **A)** HEK293-hP2X4 and **B)** HEK293-hP2X7. Data is presented as the mean \pm SD with ATP ($10 \mu\text{M}$), IVM ($3 \mu\text{M}$), BX430 ($10 \mu\text{M}$) and ATP ($300 \mu\text{M}$), AZ106 ($10 \mu\text{M}$) as the controls for P2X4 and P2X7, respectively. Significant differences between the control ($10 \mu\text{M}$ ATP or $300 \mu\text{M}$ ATP) and the venom are indicated by $*$ ($P < 0.05$) using one-way ANOVA followed by Dunnett's test. On the chemical structure, *blue* represents a nitrogen donor and *red* depicts an oxygen acceptor – both of which are susceptible of forming hydrogen bonds with the amino acid residues (protein/target).

Finally, the last hit – 1969 (**Figure 5.18**) was evaluated, however, we only managed to confirm the hP2X4 inhibition of $44 \pm 5\%$, $29 \pm 4\%$, and $0 \pm 11\%$ at $100, 30,$ and $10 \mu\text{M}$, respectively. However, this compound was more potent at the HEK293-hP2X7, showing the inhibition of $59 \pm 4\%$, $42 \pm 3\%$, $32 \pm 6\%$, and 23 ± 3 at $100, 30, 10$ and $3 \mu\text{M}$, respectively.

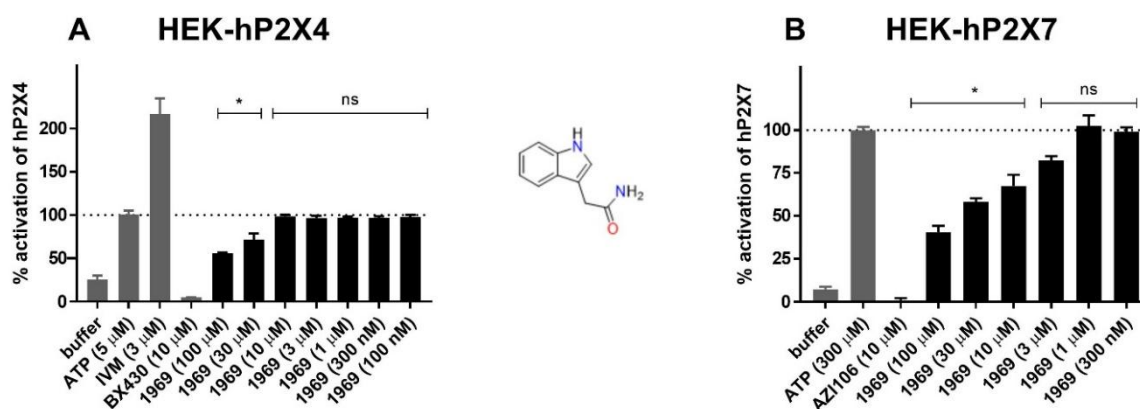


Figure 5.18. Dose-dependent inhibition of 1969. The compound 1969 was pre-incubated at either 100, 30, 3, 0.3 or 0.1 μ M concentration ($n=4$) and tested in **A**) HEK293-hP2X4 and **B**) HEK293-hP2X7. Data is presented as the mean \pm SD with ATP (10 μ M), IVM (3 μ M), BX430 (10 μ M) and ATP (300 μ M), AZ1106 (10 μ M) as the controls for P2X4 and P2X7, respectively. Significant differences between the control (10 μ M ATP or 300 μ M ATP) and the venom are indicated by * ($P < 0.05$) using one-way ANOVA followed by Dunnett's test. On the chemical structure, *blue* represents a nitrogen donor and *red* depicts an oxygen acceptor – both of which are susceptible of forming hydrogen bonds with the amino acid residues (protein/target).

Once it became apparent that the three structural elements (indole ring, the 3-substituted aliphatic (negatively and/or positively charged, and no substitution at the position 2 chain) might be important for an inhibitory activity at hP2X4, we looked at the structures of both, hits and no-hits (**Figure 5.19**), and some conclusions were made:

1. The indole group alone is not enough for the inhibitory activity at hP2X4
2. The indole ring might be replaced with another suitable aromatic group
3. The polyamine chain alone is not enough for the inhibitory activity at hP2X4
4. A hydroxyl group (-OH) at position 5 of the indole ring does not affect the hP2X4 activity, thus this substitution might be well tolerated
5. A primary amine with a two carbon spacer in position 3 of the indole is not essential for the P2X4 activity as previously thought after the first indole screening
6. Longer aliphatic side chains are well tolerated
7. An amine on the sidechain needs more than one carbon spacing from the indole

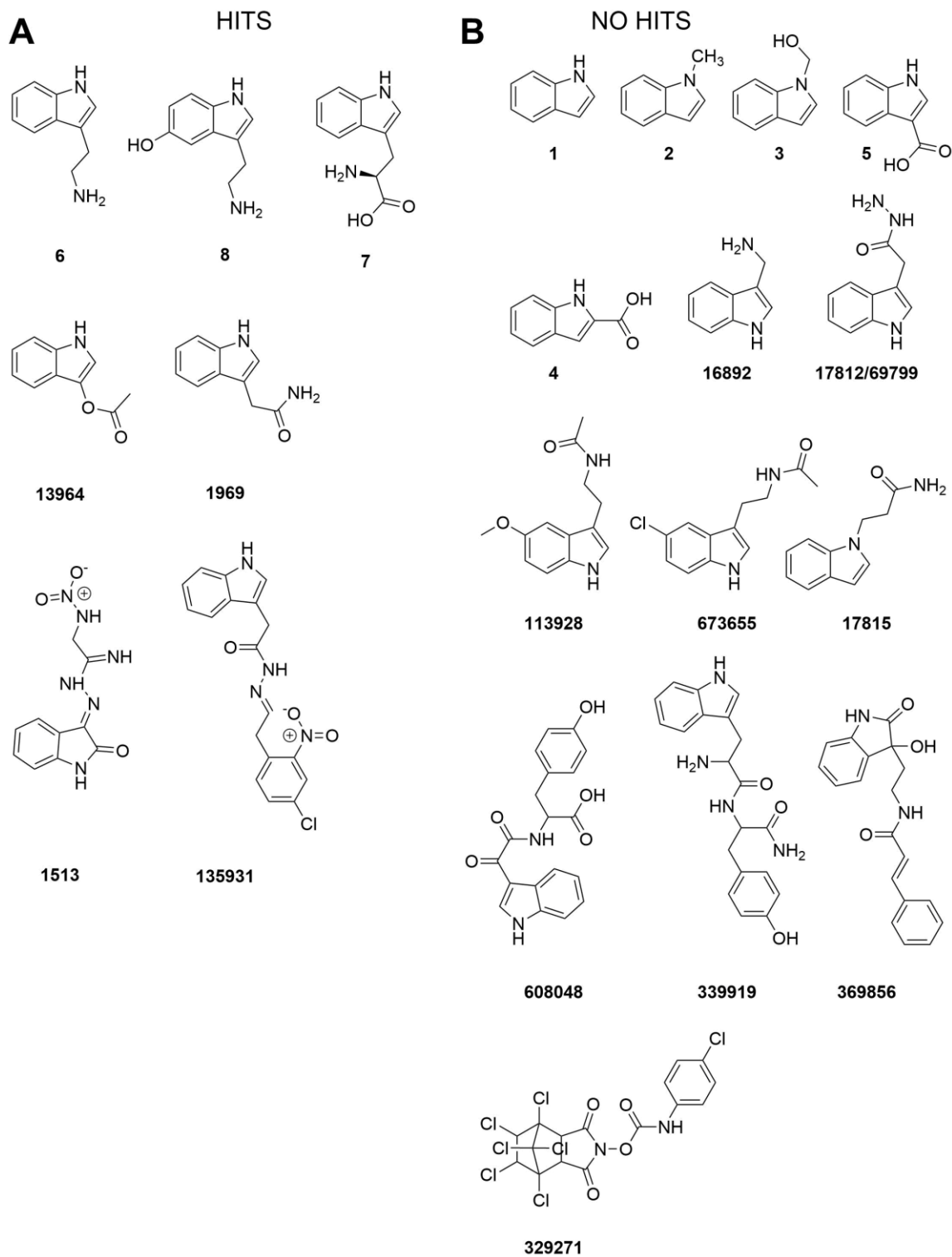


Figure 5.19. Hits and other indole-like compounds from the NCI-DTP library that did not show promised as the hits (“no hits”). Shown are structural examples of “hits” (6, 8, 7, 13964, 1969, 1513, 135931) (left) and “no-hits” (1, 2, 3, 4, 5, 17815, 16892, 17812, 69799, 329271, 113928, 673655, 608048, 369856, and 339919) that did not show any meaningful effect in our bioassays (right).

5.2.1.3. An Indole-based Acylpolyamine (Argiopinin-1) Does Not Modulate hP2X4

To find out whether the combined structural elements (1H-Indole that is acetylated with the polyamine chain on the 3 position of the indole ring) might play a role in blocking hP2X4, we tested Argiopinin-1 – an indole-based acylpolyamine initially isolated from the crude *Argiope lobate* venom (Figure 5.20).²⁸²

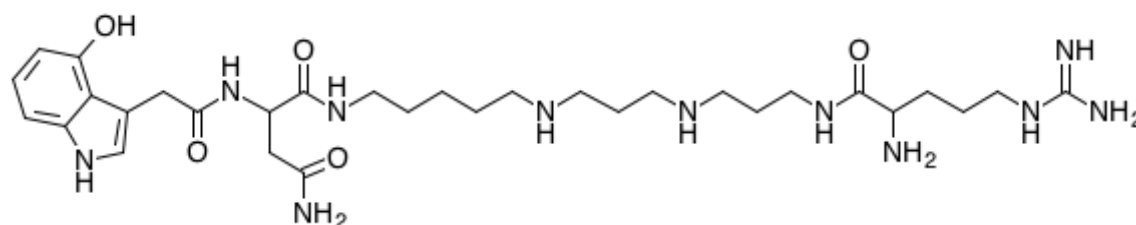


Figure 5.20. The chemical structure of Argiopinin-1.

Argiopinin-1 was demonstrated to be an antagonist of glutamate receptors, containing the 1H-Indole ring, and aliphatic polyamine chain, however, with an arginine residue and a hydroxyl residue in the chromophore. The amino acid fragment is especially important for the biological activity at the glutamate receptors with the role of hydroxyl groups still being unclear.²⁸²

Since Argiopinin-1 was shown to block (different) glutamate receptors in range of 1-10 μM , with a complete block at 10 μM ,²⁸² 10 μM was chosen to examine the effect of the toxin on hP2X4. As seen on the Figure 5.21, Argiopinin-1 was not able to block Ca^{2+} responses via hP2X4 activation by 10 μM ATP. However, a modest inhibition of $19 \pm 18\%$ was achieved, which – when statistically assessed by One-way ANOVA (Dunnet's multiple comparison test) – have not resulted as significant inhibition of hP2X4 in 1321N1-hP2X4 cells (Figure 5.21A). When examining the antagonizing ability of 10 μM Argiopinin-1 on an ATP concentration response, the toxin was not able to produce any measurable antagonism of subsequent P2X4 agonist responses (Figure 5.21B), suggesting that Argiopinin-1 does not appear to block P2X4 responses.

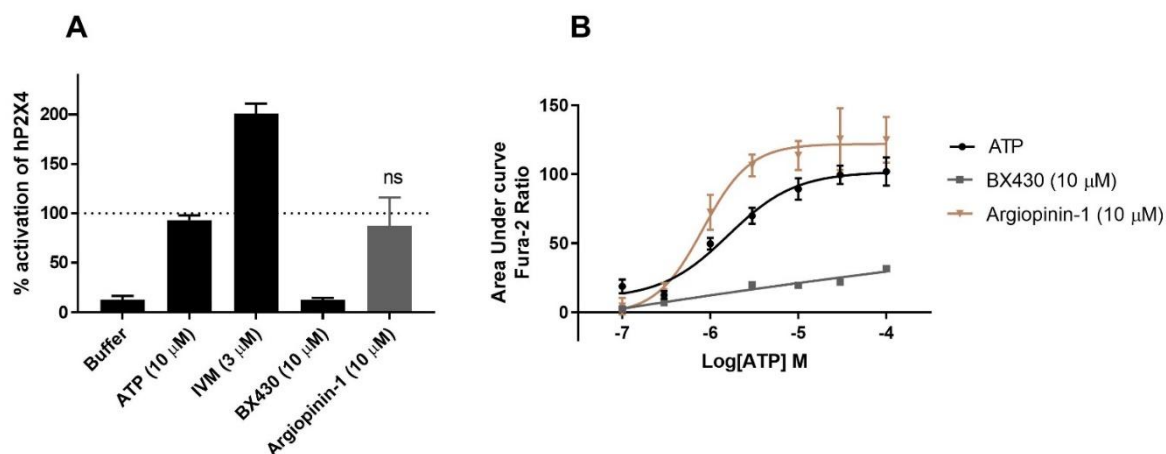


Figure 5.21. Evaluating the effects of argiopinin-1 on 1321N1-hP2X4 cell line. **A:** Pre-incubation of 1321N1-hP2X4 with 10 μ M Argiopinin-1, together with the positive (10 μ M ATP) and negative control (10 μ M BX430), as assessed with the Fura2 dye. **B:** ATP dose response when 1321N1-hP2X4 were pre-incubated with the Argiopinin-1 (10 μ M) with BX430 (10 μ M) as the control antagonist. Data is presented as the mean \pm SD with 10 μ M ATP as a control, obtained in three independent experiments ($n=3$). The dashed line represents 100% hP2X4 activity as followed by 10 μ M ATP application.

This set of results with polyamines, indole-like compounds, and finally acylpolyamine showed some apparent features: 1H-Indole with no additional substitution on the aromatic ring, and substitution with a polyamine chain on the position 3 without the additional charges (amino acid residues) might be some of the essential elements of LK-601. However, the full structure of LK-601 which would confirm these observations, and shine a light on whether LK-601 is linear or cyclic, has not been elucidated. Despite these discrepancies, we decided to proceed with the chemical synthesis of structurally similar analogues of LK-601 and hope to find a smaller, yet potent and selective, analogue against hP2X4.

5.2.2. Chemical Synthesis of LK-601 Analogues

So far, numerous reports described the synthesis of acylpolyamines using a solid-state synthesis^{274, 276, 367} as described in the introduction section of this chapter. However, this approach requires a minimum of three steps, expensive reagents, and would involve the use of suitable linkers and protecting group strategies.^{303, 404-405} Since we wanted to synthesise a number of simple acylpolyamines with a 1H-Indole pharmacophore that would be substituted on either 2 or 3 position with or without a short $-\text{CH}_2-$ linker, we had to adapt a more economical and rapid, yet effective, approach that would give us the desired molecules.

One such method, described by Krapcho,⁴⁰⁶ Blagbrough and co-workers,³⁸¹ and later improved by Burns,³⁸⁰ calls for the selective monosubstitution of the polyamines. Here, the polyamine (e.g. spermine) is treated with the acylating reagent (e.g. activated ester), thus yielding a mixture of two compounds – monosubstituted primary amide product (monomer) and its disubstituted analogue (dimer) with a higher yield of a desired monomer. In our case, 1H-Indole-3-carboxylic acid, 1H-Indole-3-acetic acid and 1H-Indole-2-carboxylic acid were used to form activated esters with 4-nitrophenol, resulting in activated 4-nitrophenyl esters. Once each activated ester was synthesized, it was then coupled directly to spermine (1 equiv) to give a mixture of mono- and disubstituted products together with the unreacted starting material (**Figure 5.22**).

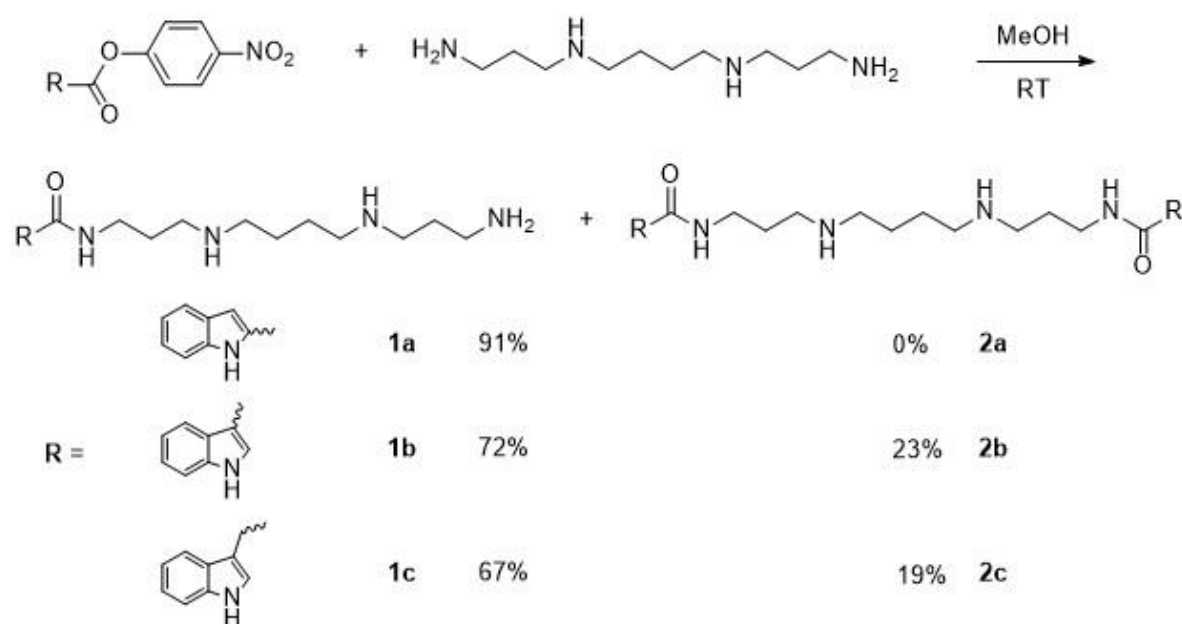


Figure 5.22. Reaction outline for the chemical synthesis of Lucas analogues (LA).

As shown in **Figure 5.22**, the compounds **1-2** were obtained in two steps. In the first step, either 1H-indole-3-carboxylic acid, 1H-indole-3-acetic acid or 1H-indole-2-carboxylic acid were esterified with a 4-nitrophenol (0.9 eq) using HATU (1 eq) and DIPEA (2 eq) as the coupling reagents in DMF over 24h at the room temperature. Then, the activated esters were used as the precursors for compounds **1-2**. By amidation of activated esters with spermine (1 eq) in methanol under nitrogen conditions at the ambient temperature, and subsequent pH adjustment with HCl, the predominantly monosubstituted **1a** (LA-1), **1b** (LA-5) and **1c** (LA-3) acylpolyamines as well as disubstituted **2b** (LA-2) and **2c** (LA-4) acylpolyamines were obtained (**Figure 5.23**).

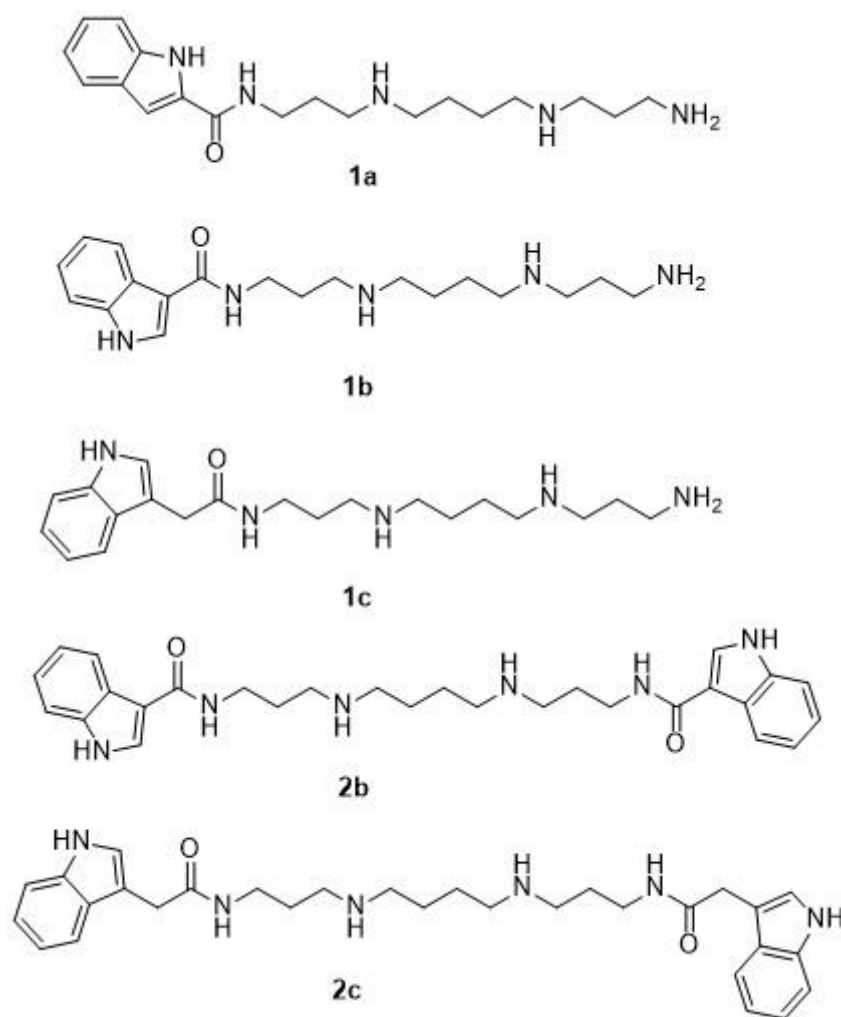


Figure 5.23. Structures of Lucas analogues (LA). **1a** represents a monomer LA-1, **1b** represents a monomer LA-5, **1c** represents a monomer LA-3, **2b** represents dimer of LA-5 denoted as LA-2, **2c** represents dimer of LA-3 denoted as LA-4.

The ratio of primary amine to activated ester was critical in order to avoid di-protection (-NH₂) and polyprotection (-NH-). The higher nucleophilicity of the secondary amines (-NH-) is masked by corresponding steric effects, thus selectivity for primary over secondary amines.^{381, 407} This way, reasonable yields of desired monosubstituted products were obtained (67 – 91%) with sufficient yields of the disubstituted products. However, **2a** was not obtained and the reason for this discrepancy are yet unclear. This crude mixture of mono- and disubstituted products were effectively separated using a preparative HPLC (**Figure 5.24**), and the purity of monomers and dimers confirmed (> 95%). All monosubstituted analogues gave satisfactory analysis by ¹H and ¹³C-NMR, HRMS by ESI(+)/ESI(-) and/or melting point determination (Supporting Information).

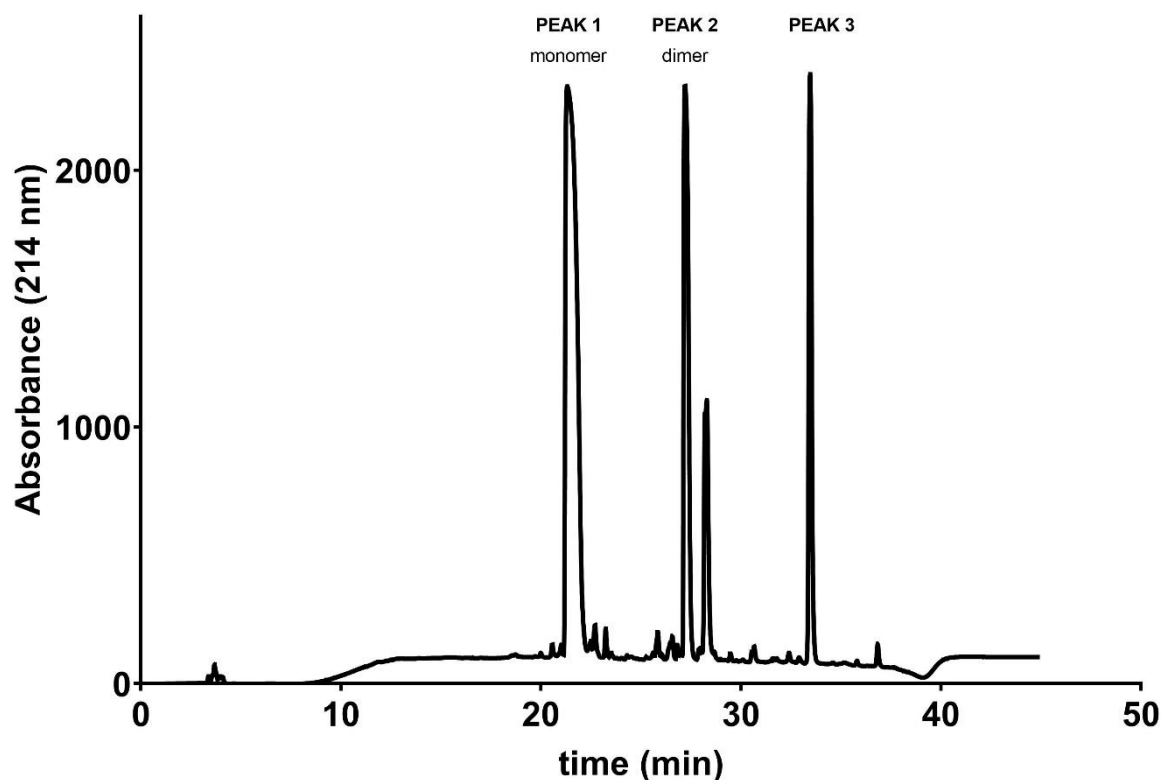


Figure 5.24. HPLC Chromatogram of toxin analogues. HPLC shows the purification of LK-601 analogues with three represented peaks. Peak 1 and 2 are denoted as monomer and dimer, respectively, while peak 3 is a starting material (*1H*-indole-3-carboxylic acid, *1H*-indole-3-acetic acid or *1H*-indole-2-carboxylic acid).

5.1.1. *In Vitro* Evaluation of LK-601 Analogues

Here, a series of 5 analogues (LA1 – LA5), structurally inspired by LK-601, were investigated with the YO-PRO-1 assay. These compounds were initially tested at 30, 10 and 1 μM for their potency to inhibit ATP-induced YO-PRO-1 uptake in either stable HEK293-hP2X4 or HEK293-hP2X7. The experiments were conducted together with the ATP control (5 μM) and BX430 (10 μM) in case of hP2X4, and ATP control (300 μM) and AZ10606120 (10 μM) in case of hP2X7. Starting material (SM) was tested subsequently (*1H*-indole-3-carboxylic acid [SM-1], *1H*-indole-3-acetic acid [SM-2] or *1H*-indole-2-carboxylic acid [SM-3]) (**Figure 5.25**).

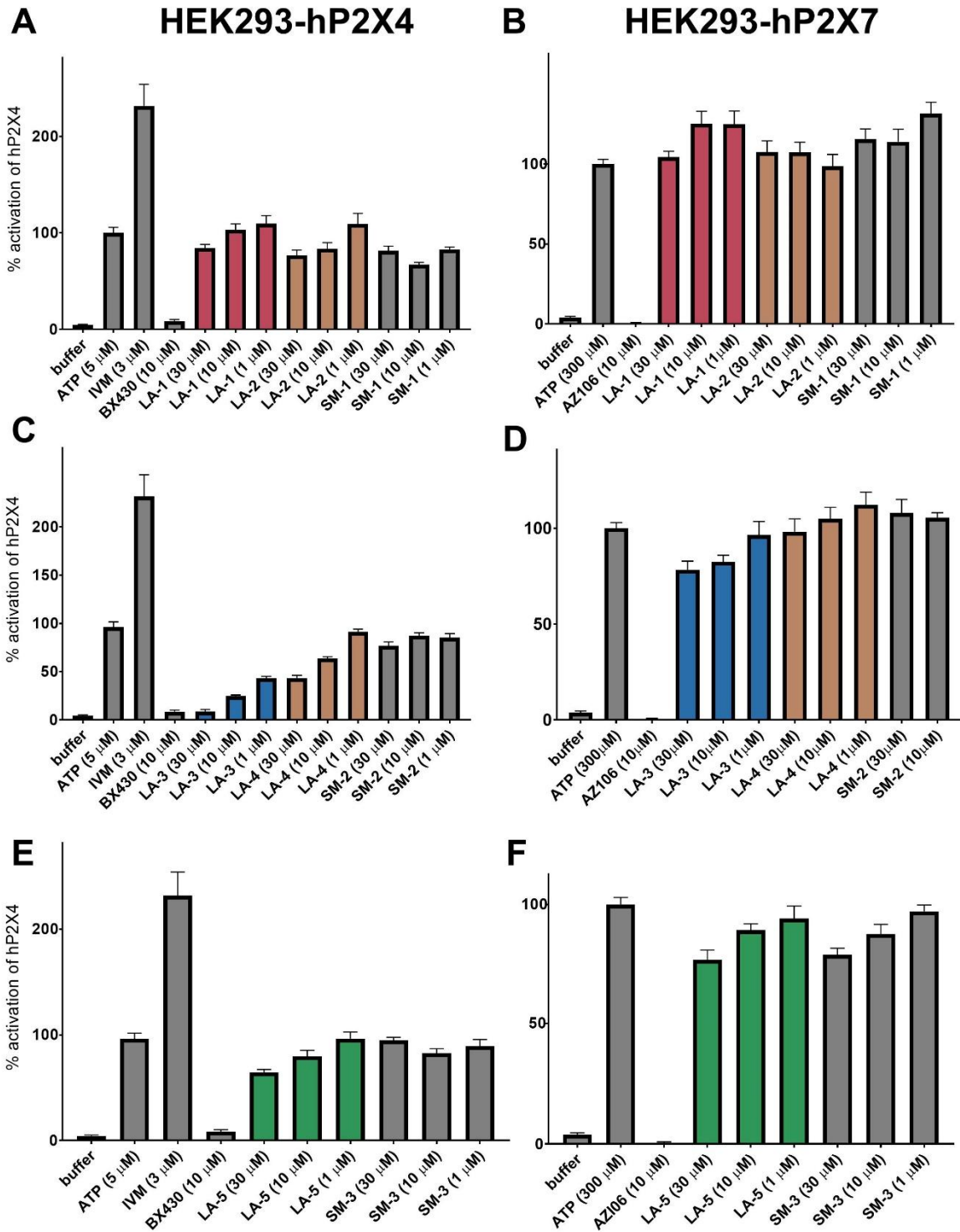


Figure 5.25. Effects of LK-601 analogues. Dose-dependent effect of **A)** LA-1 and LA-2; **B)** LA-3 and LA-4; and **C)** LA-5 on HEK293-hP2X4. Dose-dependent effect of **D)** LA-1 and LA-2; **E)** LA-3 and LA-4; and **F)** LA-5 on HEK293-hP2X7. % of activation means 100% hP2X4 activity as followed by ATP application. Data points represent the mean \pm SD of five replicated experiments. Significant differences between the control (ATP) and the venom are indicated by * ($P < 0.01$) using one-way ANOVA followed by Dunnett's test.

When testing LA-1 and LA-2 no significant dose-dependent inhibition was observed (**Figure 5.25A**), and the only (however modest) inhibition was found with LA-2 at 30 μM ($18 \pm 3\%$), yielding these analogues virtually inactive towards hP2X4. SM-1 exhibited an inhibition of hP2X4 in range of 26% when 10 μM concentration was tested. On the contrary, LA-3 exhibited an inhibition of $95 \pm 2\%$, $73 \pm 2\%$, and $53 \pm 3\%$ with 30, 10 and 1 μM , respectively.

The corresponding dimer of LA-3, LA-4, also displayed inhibition of hP2X4 with $55 \pm 4\%$, $39 \pm 3\%$ and $8 \pm 2\%$ with 30, 10 and 1 μM , respectively (**Figure 5.25B**). While 30 μM of the SM (1*H*-indole-3-acetic acid) displayed $26 \pm 2\%$ inhibition, lower concentration were found to be ineffective. The LA-5 analogue and its respective SM (1*H*-indole-3-carboxylic acid) did not show an inhibitory effect confirmed with LA-3, still, LA-5 displayed an inhibition of $32 \pm 3\%$, $13 \pm 4\%$, and $2 \pm 5\%$ with 30, 10 and 1 μM , respectively (**Figure 5.25C**). Following the hP2X4 assay, LA analogues were probed against hP2X7, however, neither of them profoundly inhibited hP2X7 in HEK293-hP2X7 cells, although LA-3 and LA-5 showed an inhibition of $27 \pm 4\%$, $23 \pm 3\%$, $1 \pm 6\%$, and $29 \pm 6\%$, $19 \pm 4\%$, $10 \pm 3\%$ with 30, 10 and 1 μM , respectively (**Figure 5.25D-F**).

Overall, the potencies of LA against hP2X4 follows as: LA3 > LA4 > LA5 >> LA1 > LA2. With LA-3 being the most potent compound (73% inhibition at 10 μM), it became clear that the short methylene (-CH₂-) linker between the indole and acetylated polyamine chain on the position 3 may be essential for the inhibitory activity of LA-3 towards hP2X4. Since only LA-3 showed potent inhibition within the concentration range of 1-30 μM , full concentration-response curves were determined and IC₅₀ values were calculated for this compound (**Figure 5.26**). An ATP concentration of 2 μM (which caused ~50% of the maximal effect as shown in Chapter 3), was used for receptor stimulation. While LA-3 exhibited an IC₅₀ value of $18.6 \pm 5.6 \mu\text{M}$ in 1321N1-hP2X4 (**Figure 5.26A**), it was found to be slightly more potent when evaluated on HEK-hP2X4 (YO-PRO-1), displaying an IC₅₀ of $9.67 \pm 0.96 \mu\text{M}$ (**Figure 5.26**).

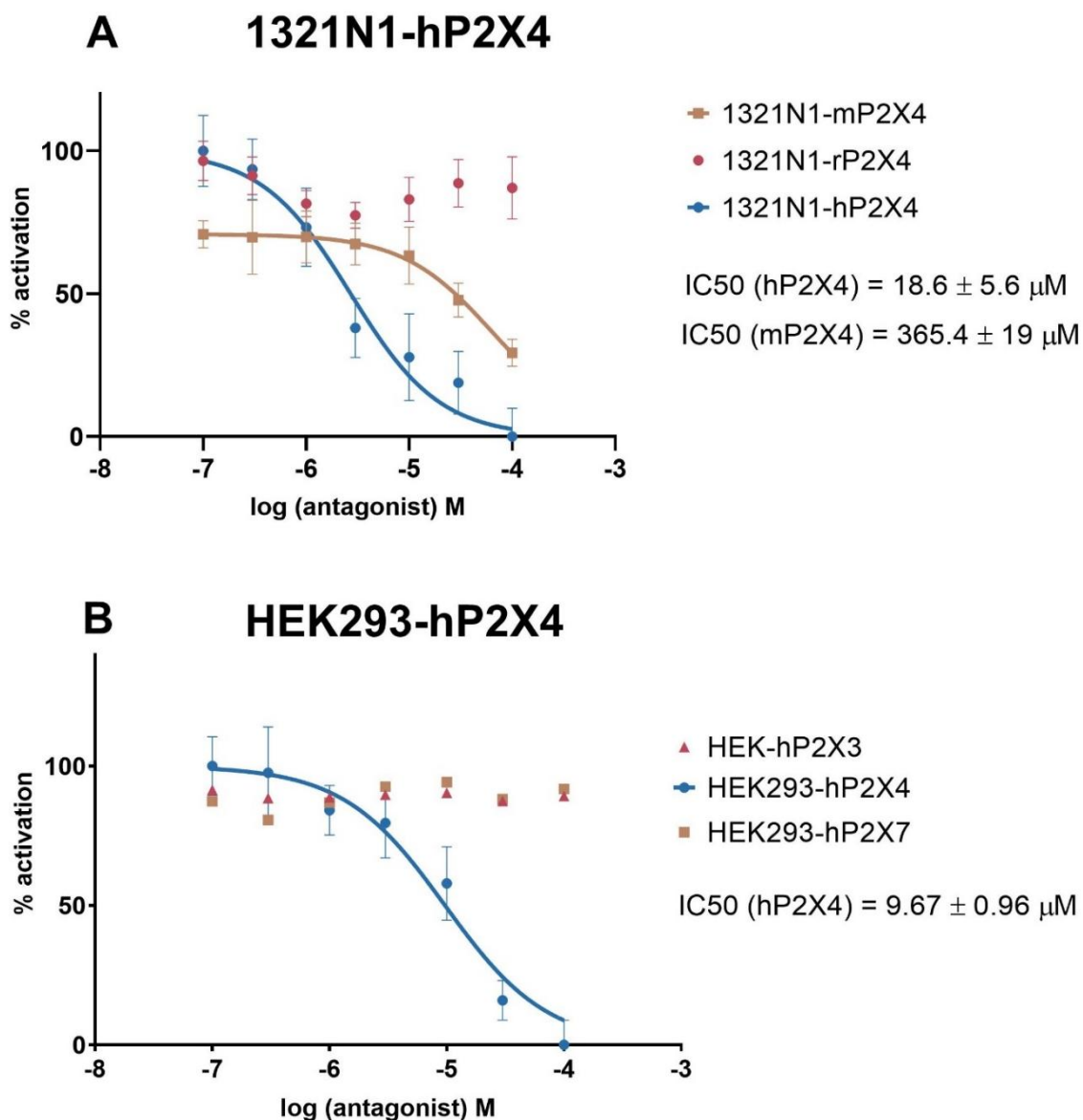


Figure 5.26. Effects of LK-601-inspired analogue LA-3. **A:** Dose-dependent inhibition of LA-3 with $IC_{50}=18.6 \mu\text{M}$ and $IC_{50}=365.4 \mu\text{M}$ on 1321N1-hP2X4 and 1321N1-mP2X4 with no effect on 1321N1-rP2X4. **B:** The effect of LA-3 seen on 1321N1-hP2X4 was validated with the dose-dependent inhibition of LA-3 on HEK293-hP2X4 ($IC_{50}=9.67 \mu\text{M}$) with no effect towards hP2X3 and hP2X7 in the same cell line.

For P2X4 receptor, large species differences between potencies at human versus rodent P2X4 have been described.^{153, 166} Thus, we investigated the sensitivity of diverse P2X4 orthologues to the inhibitory effect of LA-3 at mouse and rat P2X4 receptors, using 1321N1-mP2X4 and 1321N1-rP2X4 (Figure 5.26A) and calcium influx assays.

Despite the high similarity with human P2X4, rat P2X4 channels (87% amino acid identity) ATP-evoked calcium responses were not affected by the application of LA-3 in the concentration range 0.1 – 30 μ M.

In contrast, mouse P2X4 receptors (95% amino acid identity) displayed a modest sensitivity to LA-3 with IC_{50} being $365.4 \pm 19 \mu$ M, yielding LA-3 approximately 20-fold less potent on mouse versus human P2X4. These results not only showed that species differences may be common for P2X4 receptor antagonists, but also points out to the different binding modes of LA-3 against human/rat/mouse P2X4.

Furthermore, selectivity of the most potent analogues was assessed versus hP2X3, and hP2X7 in stably expressing HEK293 cells via YO-PRO-1 assay. As shown in **Figure 5.26B**, LA-3 displayed a good selectivity towards hP2X4 over hP2X3 and hP2X7 with virtually no inhibitory activity towards these two other P2Xs. These results indicate that LA-3 can be used as a good starting point to develop selective indole derivatives as well as antagonists for hP2X4.

5.1.1. Ligand Docking and Prediction of Binding Mode to hP2X4 of LA-3¹

Due to the differential sensitivity of LA-3 to block P2X4 orthologues, the alignment of the amino acid sequences of human/rat/mouse P2X4 was used as an approach for the identification of amino acids and/or subdomains accountable for the inhibitory effect of LA-3. Thus, we specifically looked for residues identical or similar of LA-3-sensitive human P2X4 orthologues while physicochemically different in LA-3-resistant rat orthologues (**Figure 5.27**).

Since it has been reported that polyamines, such as spermine, are highly protonated at physiological pH (85% tetracation, 15% trication), the ability for polyamine chain to interact with the carboxylate anions fixed to the backbone of a protein might offer clues about LA-3 binding pocket. However, this might be open for discussion since we don't have knowledge about how relevant these cationic interactions are on the surface where hydration plays an important role as well.

¹ The figures for this subchapter were generated by Dr Marco M.D. Cominetti.

Query	1	MAGCCSVLGSFLFEYDTPRIVLIRS	SLMNR	V	QLLILAYVIGWVFW	WEKGYQ	EIDSV	60
Sbjct	1	MAGCCSVLGSFLFEYDTPRIVLIRS	SLMNR	V	QLLILAYVIGWVFW	WEKGYQ	EIDSV	60
Query	61	VSSVTTKAGVAVTNTSQLGFRIWDVADY	V	IAQEENSLFIMINMIVTVNQ	IG	T	CPEIP	120
Sbjct	61	VSSVTTKAGVAVTNTSQLGFRIWDVADY	V	IAQEENSLFIMINMIVTVNQ	IG	T	CPEIP	120
Query	121	DKTISIFDSDANCTLGSSDTHSSGIGTGR	CVFNA	V	KTCEVAAWCPVEN	AG	VPTPAFLK	180
Sbjct	121	DKTISIFDSDANCTLGSSDTHSSGIGTGR	CVFNA	V	KTCEVAAWCPVEN	AG	VPTPAFLK	180
Query	181	AAENFTLLVKNNIWPYKFNFSKRNILPN	ITTSYLKSCIYNA	RTDPFCPI	FRLGQIV	AG		240
Sbjct	181	AAENFTLLVKNNIWPYKFNFSKRNILPN	ITTSYLKSCIYNA	RTDPFCPI	FRLGQIV	AG		240
Query	241	HSPQEMAVEGGIMGIQIKWDCNLDRAA	SL	LP	RYSFRR	LDT	RLEHN	300
Sbjct	241	HSPQEMAVEGGIMGIQIKWDCNLDRAA	SL	LP	RYSFRR	LDT	RLEHN	300
Query	301	RDLAENFQRTLTKAYGIRFDIIIVFGK	AGKFDII	IP	TMINVGS	GLALL	GVATV	360
Sbjct	301	RDLAENFQRTLTKAYGIRFDIIIVFGK	AGKFDII	IP	TMINVGS	GLALL	GVATV	360
Query	361	MKIKYYRDKKYYVEDYEQGLSGEMNQ						388
Sbjct	361	MKIKYYRDKKYYVEDYEQGLSGEMNQ						388

Figure 5.27. Alignment of the amino acid sequences of human (*first row*), mouse (*second row*) and rat (*third row*) with marked sites (S1 – S9) depicting the differences in the amino acid residues. The red lines mark the N and C-terminal, which are not available in the crystal structure of zebrafish P2X4 (pdb 4dw0).

Still; two available crystal structures of P2X4 were inspected (pdb 4DW0, 4DW1) and the structure of zebrafish P2X4 in its closed, apo state (pdb 4DW0) was selected to build the homology models of human and mouse P2X4 prior to the identification of potential LA-3 binding sites. Among nine potential binding sites (S1 – S9), S1 was particularly interesting because major differences in charged residues are present in all three orthologues (**Figure 5.28**). Furthermore, the region is involved in conformational changes upon ATP binding and subsequent channel opening.

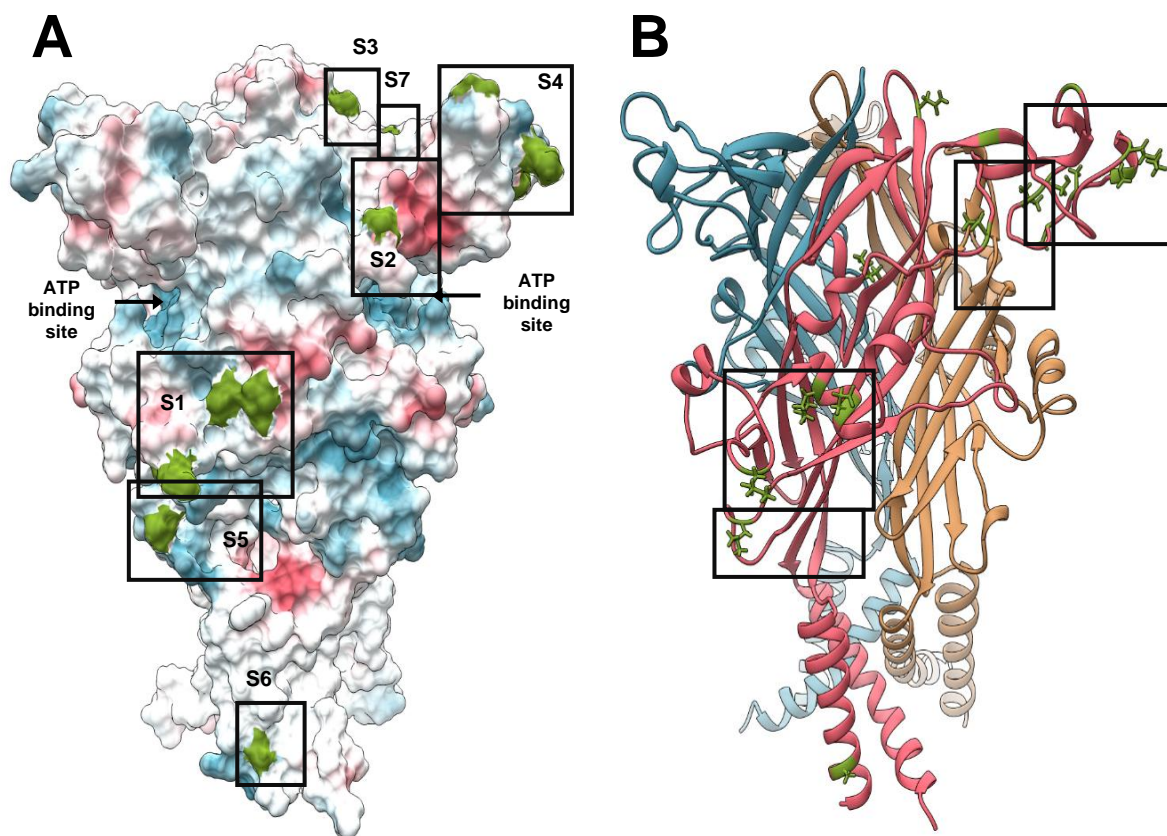


Figure 5.28. Model of a single human P2X4 subunit in surface view (A) and ribbon view (B). The spots of interest (S1 – S7) which present mutations between rat and mouse are highlighted in green. The surface displays positively charged (*blue*) and negatively charged (*red*) areas.

Other interesting spots were also S2 and S3 – while S2 is located just above the ATP binding site, S3 is not involved in known conformational changes upon channel opening. However, we attempted to dock LA1 – LA5 compounds to S2 but the only mutation which differs between rat and mouse (A199 > V199) does not appear to be relevant and could not easily explain the differences observed in the assays.

Other potential binding sites (S4 – S9) didn't involve any interesting pockets or residues that might explain the differences in binding; S4 mainly involved the mutations between hydrophobic residues while the major changes appear to be on the distal part, far from regions involved in conformational changes; S5 site contains only one different amino acid residue (His in rat P2X4 and Leu in human/mouse) with the surrounding residues being conserved in all three isoforms; S6 is a transmembrane domain with highly lipophilic amino acid residues that may be difficult for antagonist to access; S7 is distant with no conformational change in the area; S8 is part of the centre of the P2X4 which makes it inaccessible for the antagonists; and S9 is an intracellular domain for

which the structural information is not available. Thus, we focused on S1 and predicted *in silico* binding of LA1 – LA3 to human and mouse P2X4.

As seen in **Figure 5.29A-C**, LA-3 seems to wrap around the double loop constituted by residues 217 – 228 where the positively charged spermidine chain interacts with two negatively charged aspartate (D) residues (220, 224) while the carbonyl oxygen forms a hydrogen bond with the backbone hydrogen of Ala (A221), Lys (K234) and Asn (N210). The last amino group on the polyamine tail interacts with two backbone residues, namely D224 and T223. The indole group is arranged in hydrogen bond interactions with the backbone of Tyr (Y274). On the contrary, LA-5 does not maintain that same orientation and lacks some crucial interactions seen with LA-3 (**Figure 5.29D-F**). This might possibly explain the difference in activities between LA-3 and LA-5.

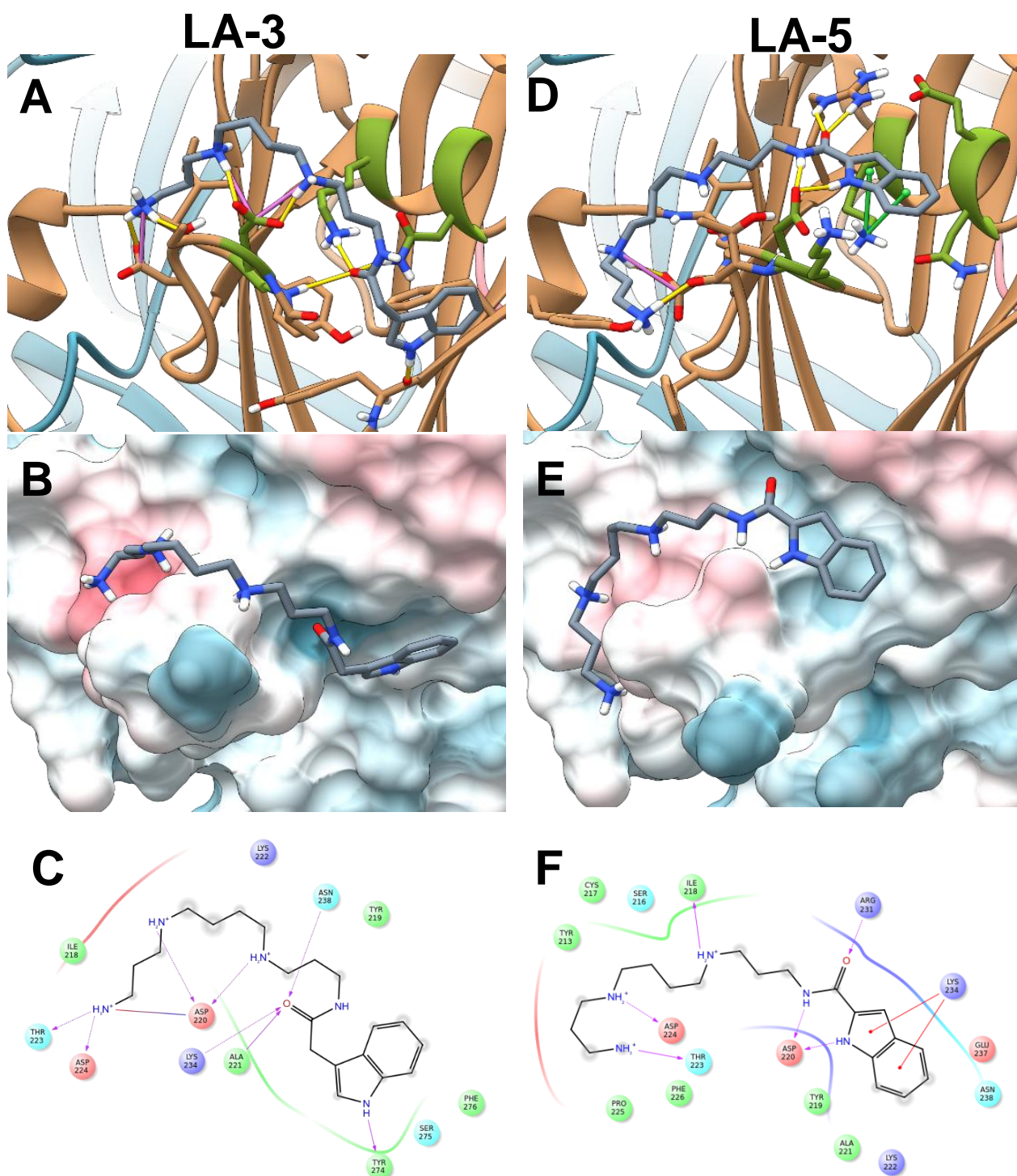


Figure 5.29. Modelling of the LA in human P2X4. Docking of the LA-3 on the homology model of human P2X4 based on X-ray crystallographic data of the zebrafish construct Δ zfp2X4(A)-GFP in its closed state (pdb code 4DW0) in either **A**) ribbon, **B**) surface or **C**) structural view. Docking of the LA-5 on the homology model of human P2X4 based on X-ray crystallographic data of the construct Δ zfp2X4(A)-GFP (pdb code 4DW0) in either **D**) ribbon, **E**) surface or **F**) structural view.

We then checked how LA-3 docks within mouse P2X4 (**Figure 5.30A-C**). While LA-3 maintains similar orientation within mouse P2X4 as in human P2X4 binding pocket, it forms only one interaction (D224) between the last amino group of polyamine tail and receptor backbone instead of two (D224, T223). It is interesting to note how an altered sequence (N220/D238 in mouse and D220/N238 in human) doesn't allow for similar interactions between the positively charged residues on the polyamine tail and protein backbone. Furthermore, this swap restrains the carbonyl oxygen that is now able to interact only with R222. However, this third mutation between human/mouse (R222 > K222) still allows the sidechain of the arginine to maintain hydrogen bonding interactions with the carbonyl oxygen and π -stacking with the indole, while the amide hydrogen interacts with the carbonyl of D238. The different position of the indole allows the hydrogen bond interaction of the indole N-H with the hydroxyl group of Y219.

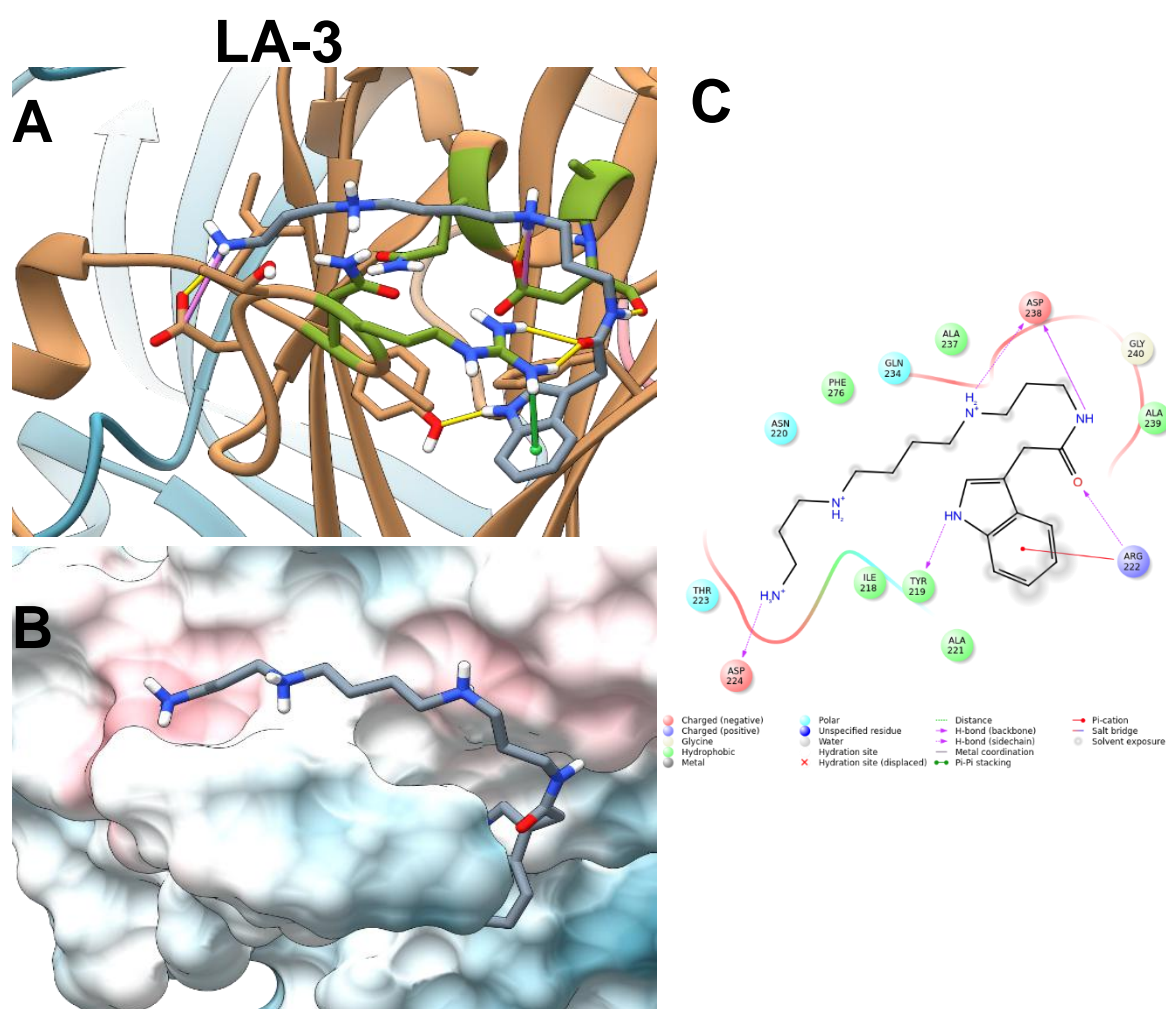


Figure 5.30. Modelling of the LA-3 in mouse P2X4. Docking of the LA-3 on the homology model of model P2X4 based on X-ray crystallographic data of the zebrafish construct Δ zfP2X4(A)-GFP in its closed state (pdb code 4DW0) in either **A**) ribbon, **B**) surface or **C**) structural view.

5.1.2. Structural Basis for the Pharmacological Properties of LA-3

To look closer into the nature of interaction between LA-3 and human P2X4, we carried out a series of systematic substitutions of human and rat P2X4 amino acids (**Table 5.2**). Since our docking studies indicated that two residues - D220 and N238 – might be the crucial players in LA-3 interaction with hP2X4, our hypothesis was that we would lose LA-3 sensitivity to hP2X4 while increase the sensitivity of rP2X4 to LA-3. Two of these residues (D220, N238) were replaced with amino acids with different side chains, such as nonpolar neutral (alanine) and either polar neutral (asparagine) or negatively charged (aspartate) in hP2X4.

Table 5.2. Summary of amino acid substitutions in our generated mutants targeting either human or rat P2X4.

Receptor	Mutations
human P2X4	D220>A
	D220>N
	K222>A
	N238>D
	N238>A
	K234>A
rat P2X4	N220>D
	D238>N

Plasmids encoding P2X4 mutants derived from human and rat P2X4 were transiently transfected in HEK293 cells and a YO-PRO-1 dye uptake assay was performed 48 h later. All mutants of human and rat P2X4 generated consistent responses evoked by 30 μ M ATP, however, the responses were lower than the wild-type P2X4. This tells us that while the mutants are fully functional and the mutations do not profoundly affect the ATP binding, S1 domain is, as predicted, involved in conformational change upon binding of ATP (**Figure 5.31**).

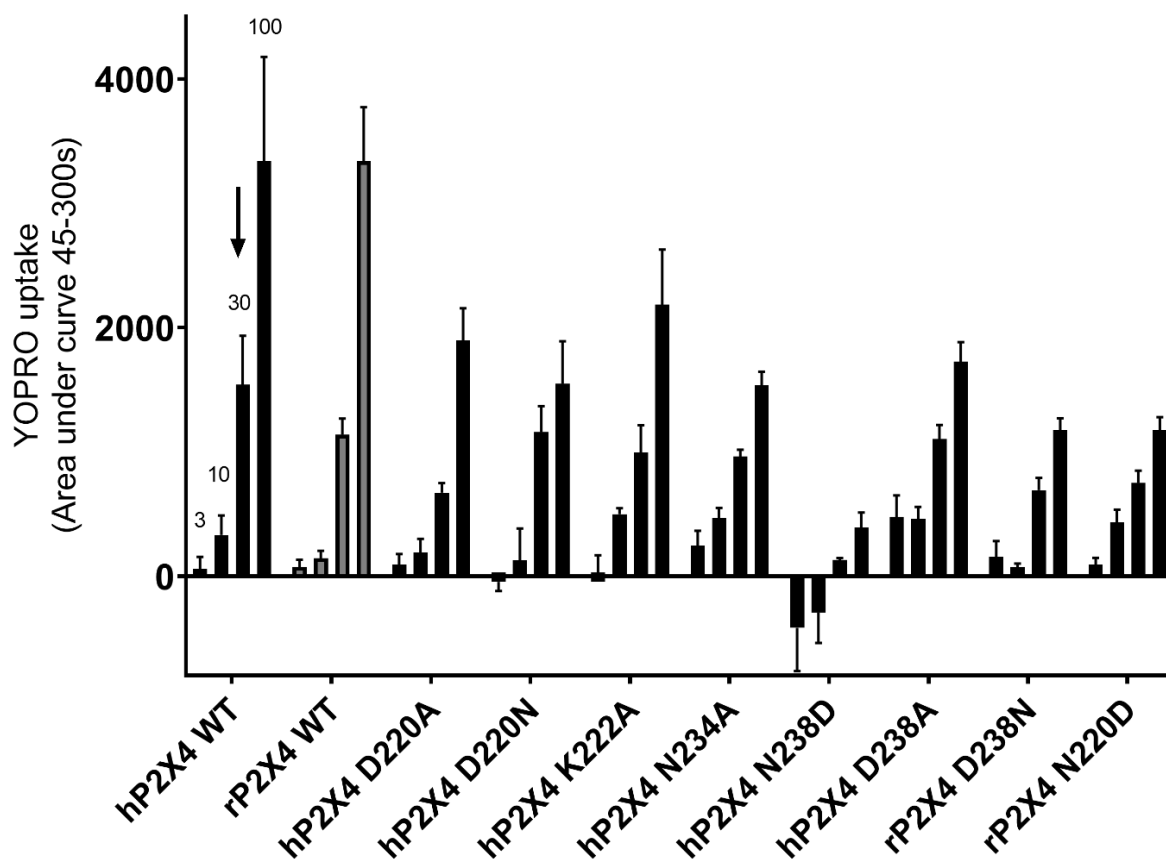


Figure 5.31. Effect of different mutant variants of hP2X4 and rP2X4 on ATP responsiveness. HEK293 cells were transiently transfected with plasmids encoding for different hP2X4 and rP2X4 mutants and stimulated with either 3, 10, 30 or 100 μ M ATP. In every group, each bar represents a single concentration of 3, 10, 30 or 100 μ M ATP and these numbers are denoted with hP2X4 WT. The arrow represents a concentration of 30 μ M where the responses were the most consistent with the WT and the mutants. Data points represent the mean \pm SD of three replicated experiments.

To monitor whether we can block the ATP-evoked response of hP2X4, the transiently transfected HEK293 cells were exposed to BX430 (10 μ M) and YO-PRO-1 dye uptake in response to ATP was measured. It has been shown that BX430 may bind to I312 in human P2X4 and that the nature of this extracellular residue in either rat or mouse P2X4 might cause the variability in the sensitivity of BX430 to block P2X4 orthologues;⁴⁰⁸ thus we chose to use BX430 as a good control inhibitor for these studies. PSB12062 was chosen for rP2X4 since it was shown by us and others that BX430 does not block rP2X4.¹⁶⁶ As shown in **Figure 5.32**, 10 μ M of BX430 managed to block >90 % of ATP-evoked responses in the hP2X4 wild type and all the mutants except in K234A (82%). In case of PSB12062, that block was noted to be 46% and 69% with D238>N and N220>D, respectively.

We observed that while LA-3 managed to block hP2X4 WT ($55 \pm 8\%$), that inhibition was less pronounced with D220>A ($22 \pm 7\%$) and N238>A ($27 \pm 10\%$) – see the summary of results in **Table 5.3**. A similar impact of replacing alanine with either asparagine (D220>N) or aspartate (N238>D) was found, however, with lower sensitivity ($32 \pm 12\%$ and $35 \pm 7\%$ of inhibition with D220N and N238D, respectively).

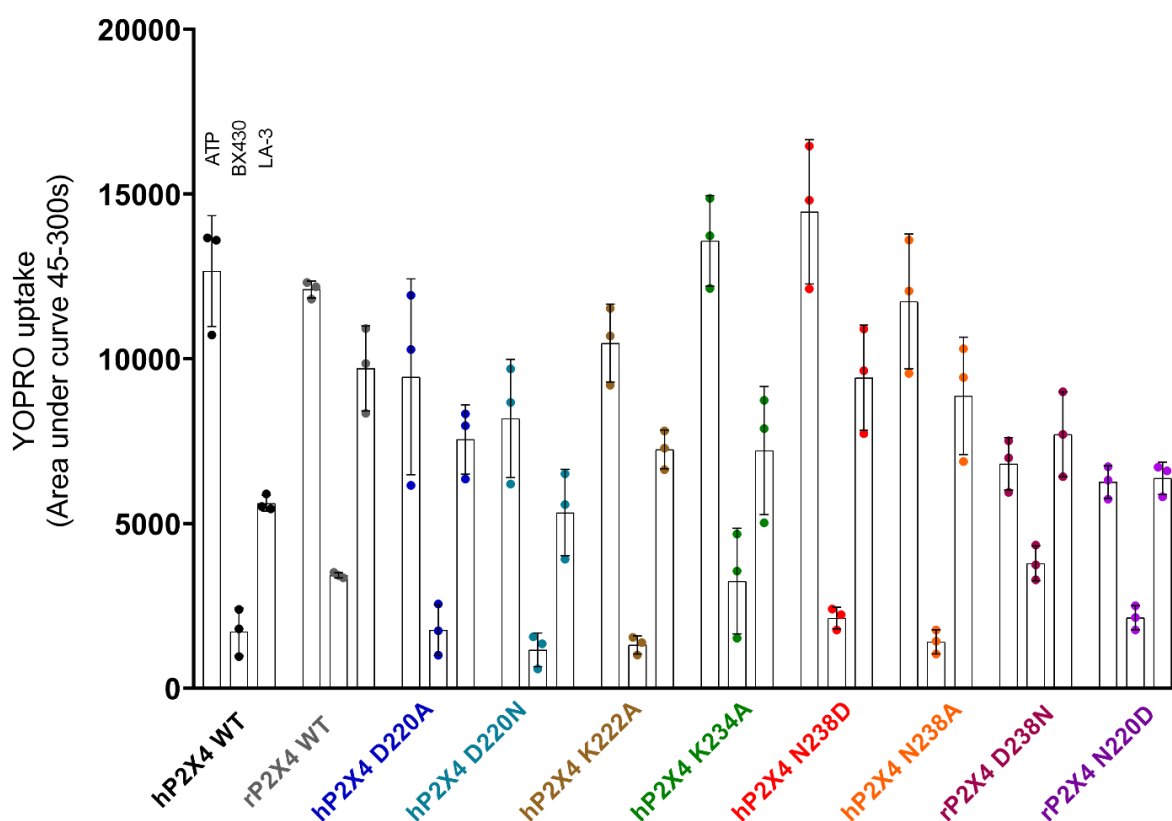


Figure 5.32. The inhibitory effect of LA-3 on different mutant variants of hP2X4 and rP2X4. HEK293 cells were transiently transfected with plasmids encoding for different hP2X4 and rP2X4 mutants and stimulated 30 μ M ATP. In every group, each bar represents either application of ATP (30 μ M), BX430/PSB12062 (10/50 μ M) or LA-3 (10 μ M). Data points represent the mean \pm SD of three replicated experiments.

The importance of the chosen amino acids substitution have been suggested before by Ase et al.⁴⁰⁸ where they noted a similar trend. Even more, they showed that while I312A, I312L and I312F result in loss of sensitivity to BX430, the mutants with aromatic side chains I312Y and I312W showed a significant potentiation of the ATP response in the presence of BX430.⁴⁰⁸ The differential impact of amino acid substitutions at one position on the sensitivity of human P2X4 to LA-3 might be demonstrated by this data.

Table 5.3. Summary of % of P2X4 inhibition by LA-3 (10 μ M).

Mutant	% of P2X4 inhibition (LA-3)
hP2X4 WT	55 \pm 8
hP2X4 D220A	22 \pm 7
hP2X4 D220N	32 \pm 12
hP2X4 K222A	30 \pm 11
hP2X4 N238D	35 \pm 7
hP2X4 N238A	27 \pm 10
hP2X4 K234A	48 \pm 11
rP2X4 WT	12 \pm 5
rP2X4 N220D	10 \pm 2
rP2X4 D238N	11 \pm 4

Two other substitutions at human P2X4, namely K222A, K234A, did not profoundly affect the sensitivity of LA-3 to inhibit hP2X4 (% inhibition was noted to be 30 \pm 11% and 48 \pm 11%) in these set of assays. Unexpectedly, substitutions at the positions 220 and 238 of rat P2X4 did not make these mutants more sensitive to LA-3. In comparison to wild type rat P2X4 (12 \pm 5% of inhibition), similar block is observed with either residues (10 \pm 2% and 11 \pm 4% at N220>D and D238>N, respectively). Nevertheless, we could not exclude the influence of different cell populations on YO-PRO-1 responses; typically, transient transfection results in cells transfected with the mutated plasmid (mutants) and non-transfected cells, however the expression levels in transiently transfected cells usually varies. This might indeed explain the variability in ATP-evoked as well as LA-3 inhibiting responses.

To mitigate this effect, we could select the P2X4-selected cells based on their antibiotic resistance and try to generate a variety of stable cell lines. In the latest scenario, the variability in ATP-evoked YO-PRO-1 responses might be reduced since the level of expression would be similar.

In summary, we report a novel antagonist of hP2X4, LA-3, which has been identified based on our fragment-based screening approach, and which guided us towards a chemical synthesis of similar toxin analogues.

LA-3 has demonstrated to inhibit hP2X4 with IC_{50} of 9.7 - 18.6 μ M and showed selectivity to hP2X4 over hP2X3, hP2X7 and rP2X4 with a modest inhibition at mP2X4 (IC_{50} = 365.4 μ M). Due to the differential sensitivity of LA-3 to block P2X4 orthologues, homology models of human, mouse and rat P2X4 were build and the potential binding site was identified. The validation of the predicted amino acid residues in binding LA-3 showed that D220 and N238 might be involved in LA-3 binding site, however, more experiments are needed to fully confirm that effect.

5.2. Conclusions

This chapter provide evidence for the existence of a smaller molecule, LA-3, based on a spider venom toxin, that is able to inhibit human P2X4 with a reasonably low potency and acceptable selectivity profile. Furthermore, by comparing the primary sequences of LA-3 sensitive and/or resistant P2X4 orthologues (mouse, rat and human P2X4), we were able to predict two residues (at position D220 and N238 in human P2X4) as the potential determinants for the inhibitory effect of LA-3. However, due to the variability of our ATP-evoked responses in the last set of experiments, we could not convincingly provide the evidence for the existence of a novel allosteric binding site for LA-3.

In the past decade, the combination of HTS and fragment-based screening, together with the untapped potential of natural products libraries, have increased hit rates for molecules of low complexity.⁴⁰⁹ Since each of these strategies might not represent a “one size fits all” solution for the problems of drug discovery against P2X targets, the combination of these approaches might explore that chemical space more effectively. That might especially hold true in our case, when limited supply of venom and instability issues with the inhibitory toxin (LK-601) prevented to get a meaningful NMR spectroscopic fingerprint, and thus achieve a full structural elucidation of such toxins.

Based on the structural hits of the LK-601, we attempted to circumvent these issues by adapting a fragment-based approach. Using four polyamines and applying a library of indole-like compounds against hP2X4, we aimed to discover structural motifs with inhibitory activity towards hP2X4.

While no polyamine has been identified as a potential fragment with the inhibitory activity against hP2X4, indole-like compounds, such as tryptamine, tryptophan and serotonin were found to significantly inhibit hP2X4 up to 43% with 10 μ M concentration.

Once it became apparent that these structural elements might hold a key to a novel pharmacophore with the ability to block hP2X4, the SMARTS algorithm was carried out, and subjected to the NCI-DTP library. After a pre-programmed cluster analysis of hits with more than 90% similarity, 22 representative compounds were suggested (out of 1047 in total, 2%).

However, only 14 compounds were available in sufficient amounts and were subjected to our biological assays. Using YO-PRO-1 assay, 4 of out of 14 compounds demonstrated a potent concentration-dependant inhibition: 1513, 1969, 13964, 135831. Their activity was confirmed using Fura-2 assay, however, the potencies were somehow different. This might merely be a consequence of using a different cell line, and different set of assay parameters.

From our structural-activity investigations we found that both the indole ring and the 3-substituted aliphatic chain seem to contribute to the overall inhibitory effect at hP2X4. On the contrary, presence of the -OH group on the position 5 of the indole and a -COOH group on the position 2 of the carbon chain does not make a difference when trying to block hP2X4. The notion that a drug with an indole moiety might modulate P2X4 is not novel,⁴¹⁰ however, a potent and selective antagonist for P2X4 with an indole pharmacophore still hasn't been reported to date. For example, Li and Fountain⁴¹⁰ have found that fluvastatin suppresses hP2X4 function, however, the authors did not report an IC₅₀ value for fluvastatin, and only showed a suppression of 10 μM fluvastatin once the cells were evoked by a relatively high concentration of agonist (100 μM). Furthermore, fluvastatin contains structural elements that do not seem to be similar to our structures.

Furthermore, just recently, Beswick et al.¹⁷¹ reported an extensive SAR of some interesting indole-like compounds (namely compound 10, 53, 58 and 108-145 in their paper). However, a visual inspection of these structures suggest that these compounds contain an indole with an additional aromatic ring (compound 10 and 108-145) or are substituted at 2 position (-CO-; -CONH-, compounds 58 and 53, respectively).¹⁷¹ While an indole might be an attractive feature, our investigations show that 3-substituted aliphatic chain seem to have a vital role in inhibiting hP2X4. Their robust fragment library series did not, unfortunately, contain any acylpolyamine-like structures. On the other hand, both – theirs and our studies – show that a struggle to identify consistent SAR is real.

Since no acylpolyamine has been reported (to date) to have an inhibitory activity at P2X channels, we wondered whether the acylpolyamine-like structure can be a general structural motif that might explain the antagonistic effect. To probe that, we used Argiopinin-1 which was previously demonstrated to be an antagonist of glutamate receptors, containing the 1H-Indole ring, and a polyamine chain.

However, when examining the antagonizing ability of 10 μM Argiopinin-1 on ATP dose response, the toxin does not appear to block P2X4 responses. That might be due to additional structural motifs, such as arginine residue and a hydroxyl residue in the chromophore group, especially as it has been shown that the amino acid fragment is important for the biological activity at the glutamate receptors²⁸² but might not be relevant for P2Xs.

To develop compounds with a reduced molecular weight that would resemble LK-601 structure, together with a desired potency, selectivity and improved stability, five analogues have been chemically synthesized. After biological evaluation against hP2X4, one of them, LA-3, has been discovered as potent and selective hP2X4 receptor antagonist. Our YO-PRO-1 and Fura-2 assays showed low micromolar level activity with IC_{50} values of $9.67 \pm 0.96 \mu\text{M}$ and $18.6 \pm 5.6 \mu\text{M}$, respectively, at human P2X4, and good selectivity versus the other P2X receptor subtypes. Thus, LA-3 may be a new starting point for the development of potent and selective P2X4 receptor antagonists, and these structural classes of compounds (acylpolyamines) might present room for further optimization with regard to affinity and improvement of their physiochemical properties.

However, LA-3 was not equally active at rat and mouse P2X4 (zero activity at rat P2X4; IC_{50} : mouse, 365.4 μM). Thus, a differential effect of LA-3 may be dependent on a specific sequence or subdomain that is not shared between these P2X4 orthologues. This has been just recently suggested before by Ase et al.⁴⁰⁸ where they showed that only a single residue located in the ectodomain of P2X4 may determine the inhibitory activity of P2X4 antagonist BX430. Moreover, they demonstrated that the nature of this residue in various P2X4 orthologues, including mouse and rat, underlies the specific resistance to the antagonistic effects of BX430. Some previous examples of species-specific pharmacology in the P2X field include P2X3 antagonist R051,⁴¹¹ P2X4 antagonists suramin and PPADS,^{248, 412} P2X7 antagonist AZ11645373⁴¹³ and positive allosteric modulator ivermectin.

Focusing on the different subdomains between rat, mouse and human P2X4, our *in silico* predictions suggested that residues at position 220, 222, 234 and 238 might be involved in LA-3 differential binding to P2X4 orthologues. Critically, two residues, aspartate and asparagine at position 220 and 238, respectively, that are swapped between human and rat (D220 and N238 in human; N220 and D238 in rat) might be essential for sub-species differences in LA-3 binding. However, once the systematic single mutations on these residues were carried out, the substitution of amino acids with different side chains (negatively charged aspartate at 220 with polar uncharged asparagine in human, and vice versa at the position 238) did still cause a minor inhibition (22 – 27%) of LA-3 at 10 μM .

This series of mutagenesis experiments might or might not exclude our hypothesis that the predicted residues are crucial for LA-3 inhibitory activity. Since aspartate and asparagine are two predicted amino acids with the charged side chains, these physiochemical properties might be required for LA-3 binding and inhibitory effects.

However, from this series of mutagenesis experiments, it might be premature to judge whether the single mutations at either D220, K222, K234 or N238 of human P2X4 render the channel insensitive to blockade by LA-3.

It remains to be elucidated whether these amino acids are actually the key players in LA-3 interaction with the human P2X4. Our future work would focus on probing whether the generation of stable cell lines of hP2X4 mutants or even a double-site mutations (D220A and N238A) might help to elucidate these effects. Furthermore, more amino acid substitutions targeting these residues in human P2X4 should be tested since a strong functional impact of replacing N220 (or N238) with alanine or asparagine/aspartate residues.

~CHAPTER SIX~

Bug Off Pain©: an Educational Virtual Reality Game on Spider Venoms and Chronic Pain for Public Engagement

This Chapter contributed to a research article published as:

Bibic, L.*, Druskis J., Walpole S., Angulo J., and Stokes L., 2019. "Bug Off Pain: educational virtual reality game on spider venoms and chronic pain for public engagement." *Journal of Chemical Education*, 96, 7, 1486-1490. (*corresponding author)

6.1. Introduction

6.1.1. Science Communication

People learn through observation and direct experience, but also by engaging in conversations with others. In fact, a defining human quality is our ability to learn from others, also known as social learning. In this context, science is an example of social learning at its best. However, not many people are trained in science. Even for those of us who are, it can be still challenging to read the literature outside of our field. For that reason we have to rely on science communication to inform, educate, share, and raise awareness of science-related topics. This way we can gather facts about issues on which we need to make decisions. Ultimately this means that science communication becomes a substitute for social learning within policymakers, scientists, educators, and research institutions.⁴¹⁴ Yet, educating the public about particular scientific topics has been ineffectual.

The underlying reason for this may be either widely publicized examples of scientific misconduct and commercialisation, like Theranos case,⁴¹⁵ or scientific malpractice. These cases are not only misleading but seriously harm the public's trust in science. Although most scientists agree that communicating science is necessary,⁴¹⁶ the participation rates still remain low.⁴¹⁷⁻⁴¹⁸ Across disciplines, scientists don't participate in public engagement activities as much. This might come down to various reasons, such as their attitude towards such activities and beliefs that they don't feel prepared to successfully interact with the public.⁴¹⁷⁻⁴¹⁹ Since science shapes the life as we know it, we need to better engage the public with scientific discoveries,⁴²⁰ and help to restore credibility within the non-scientific community.

Still, communicating science effectively often requires an unnatural act: collaboration across disciplines. Science communication practitioners might employ a different set of methodology that is more common among social scientists, and challenge norms and practises that life scientists want to adapt. Unless these two worlds fail to connect, with practitioners helping scientists to shape their communication, and scientists helping practitioners to structure the scientific information, the communication of science will suffer.⁴²¹

But sometimes the problem is broader. Haerlin and Perr⁴²² framed a question of "who is responsible for the integration of scientific discoveries and where are the scientific authorities and the editorials challenging public and corporate research strategies and perspectives?"⁴²²

For that reason, some professional societies such as the Royal Society;⁴¹⁹ funding agencies as the National Science Foundation; and publishing houses as Nature⁴²² and Science,⁴²⁰ are calling for increased dialogue between life scientists and the public. In trying to improve the participation rates and the effectiveness of science communication, a more scientific approach, might be worth trying.

For decades, the social sciences have collected a vast body of empirical evidence on how scientific outreach can be practised. The majority of these findings suggest that educating the public must be implemented with the same rigour as in science in order to effectively share findings with the public.⁴²³ Furthermore, to communicate scientific findings in a meaningful way, scientists need to adhere to effective, yet engaging, approaches.⁴²⁴ Since we live in a technological era, this quest has led educators in Science, Technology, Engineering, and Mathematics (STEM) to harness digital technology that would benefit engagement.

6.1.2. Digitalization in Science Education

There is growing evidence that people's learning preferences are undergoing a major shift. For example, since it is now common for young people to grow up with technological aids such as computer games, the preferred leisure styles, social interactions and even learning styles of such pupils have adjusted. This generation is usually referred as a "net generation";⁴²⁵ "digital natives"⁴²⁶ or "gamer generation."⁴²⁷ Thus, this new learning preference requires new ways of teaching. Csikszentmihalyi⁴²⁸ argues that the "net generation" requires new motivations that capture and hold their attention, all while still engaging them in the learning process. By combining active learning, communication of science and popular culture in an informal educational setting, an awareness of natural sciences as well as engagement might be improved. Some of these examples include "PubScience",⁴²⁹ "Reaction! Chemistry in the Movies",⁴³⁰ "Wow"⁴³¹ and "SciPop Talks".⁴³² While "SciPOP talks" and "PubScience" are the models of a successful campus outreach, "Wow" strategy uses movies and movie clips to teach chemistry.

However, using movie aids in education is not a novel concept. The earliest guidelines for using video clips to teach science were proposed in *Science in Cinema* and later updated as *Fantastic Voyages*⁴³³. These examples mainly focused on science fiction movies to teach scientific concepts in a physics course. Since then, the list of movies has expanded. Now, a vast array of movies based on true chemical narratives includes *Apollo 13* (1995) and *October Sky* (1999). These examples drove discussions concerning lithium hydroxide carbon dioxide scrubbers, rocket fuel comparison, model rocket propellants, and persistence in the face of setbacks. *Jurassic Park* (1993) was used to facilitate discussions about cloning, protein and DNA structures, genetic engineering, and scientific ethics.

Yet, none of these examples provided empirical evidence that would clearly point out to the pedagogical utilities.

It was not until 2003 that it was recognized that student understanding of science and scientists is strongly driven by movies and television cartoons, sitcoms, dramas and other out-of-school forces. During a more than a decade long search of identifying suitable movie clips for teaching and learning chemistry, Griep and others⁴³⁰⁻⁴³¹ have incorporated dozens of pedagogically useful movies into public outreach lectures. However, as much as movies provide engagement and motivation in our digital society, their learning benefits are still restricted to the two dimensional environment. Since they lack the interactive three dimensional side of it, other means of animation-mediated learning may be worth exploring.

6.1.3. A Science of Games

Alongside educational movies, computer games may add a three dimensional layer to engagement. In recent years, educational games have received increased attention from educators and researchers.⁴³⁴ In this respect, gamification (application of game design elements and mechanics to engage users and solve problems) can be an appropriate way to improve learning and enhance public interest in STEM-related subjects.⁴³⁵ Since video games are user-centered,⁴³⁵ they promote challenges, engagement, active learning, and the development of problem-solving strategies.⁴³⁵

Of course, the idea of playing to learn is not a new concept. But it was only in 2002, when an initiative known as *serious gaming* began. While usual games have a story, art and software, serious games also involve pedagogy; activities that educate and impart knowledge or skill. This addition is what makes games serious. Here, a development team usually includes scientists, communicators, subject matter experts, designers, and software developers. It was not until America's Army - a recruiting tool game - had been released, that educators and game developers started thinking how to advance game technology for educational implementations.⁴³⁶⁻⁴³⁷

Now, various research groups have explored the roles of these games in supporting pedagogical goals. Some of them resulted in games such as Chairs!;⁴³⁸ Chirality-2;⁴³⁹ and Say My Name.⁴⁴⁰ All of which have been shown to be useful instruments for learning specific strategies and acquiring chemical knowledge. But as much as this progress is valuable, it is also about investigating how these educational games may impact student academic performance. However, this type of research is not yet well established. Moreover, there's been scarce evidence of research in educational gaming and researchers still struggle for its academic credibility.⁴³⁷

This may merely be a generation-gap issue because children who have grown up since the 1980s have been exposed to video games their entire lives (“digital natives”), while older generations have not had this opportunity.⁴³⁶

Designing educational games that have a rich narrative is not an easy undertaking. HI FIVES, a joint effort of researchers in science, educators and computer scientists to improve science understanding among students, was the first one to provide a tool for teachers to design their own video games.⁴⁴¹ By generating a much higher level of positive emotional engagement and making learning more appealing, students learned to think critically about the particular topic while simultaneously gaining embedded knowledge through interacting with the environment. Furthermore, these games motivated passive students to contribute more than they usually would in a conventional learning environment.

With all that said, video games in the classroom are not a replacement for good pedagogy but merely an aid that engages students and provides avenues to learn challenging concepts in a comfortable environment.

6.1.4. Virtual Reality as an Interactive Learning Environment

At the forefront of the 21st century, gamers got a new tool to explore – virtual reality (VR). In 1997, Jayaram et al.⁴⁴² defined VR as a “synthetic or virtual environment which gives a person a sense of reality” and a feeling of being there. On this continuum, VR is an artificial environment, allowing the user to interact within that environment using special electronic devices, such as VR goggles to allow a full-immersion.⁴⁴³⁻⁴⁴⁵ This way, the user suspends their disbelief and accepts it as a real environment.

Several authors have already suggested that incorporating gaming aspects into immersive and interactive learning environments, such as VR, could be educationally beneficial. For example, Feng and others⁴⁴³ suggested it improves learning outcomes, “makes learning fun”, and offers powerful tools for “learning through doing”,⁴⁴³ as discussed in a comprehensive review.⁴⁴⁴ These researchers believe that VR has vast potential to engage, stimulate and motivate students; help to teach STEM topics such as astronomy or geology where gaining real-world first-hand experience might not be feasible; foster student’s creativity and imagination; assist students to be in charge of their learning at their own pace; and to build an authentic learning environment that suits various learning styles.

Furthermore, VR games have vast potential to reach an audience of hundreds of thousands to millions.⁴⁴⁵ Taken together with the challenges enticing the public to STEM subjects, and regaining the people's trust and appreciation in scientific matters,⁴⁴⁶ VR games may come to the rescue.^{434, 447}

So far, several works have reported remarkably successful VR methods in chemistry education and outreach such as VR-Engage;⁴⁴⁸ calorimetric titration app;⁴⁴⁹ mixed reality software;⁴⁵⁰ and others such as Water VR, Molecular Zoo and Fishtank.⁴⁵⁰ One such example, mixed reality applied in chemical outreach and education, and showed numerous pedagogical benefits. Some of the students showed better engagement, more accurate and nuanced understanding of scientific concepts, and better clarity when articulating their thoughts.⁴⁵⁰

Yet, none of these approaches tried to gamify any of the relevant research topics in VR, and evaluate them accordingly. Since the primary focus of my research is the application of spider venoms in alleviating chronic pain, I have chosen VR as an educational tool to present, communicate, increase awareness, and educate the public on this topic. Moreover, this topic has not been pedagogically utilized in VR yet. This context encouraged me to create Bug Off Pain – an educational VR game that aims to bridge the gap between scientific and non-scientific community (general public). Bug Off Pain is available for free worldwide on both Oculus Rift (computer) and Android (mobile) platforms by downloading the game or scanning its QR code. Here, the development and implementation of such a game is reported.

6.2. Results and Discussion

6.2.1. The Game

The story of Bug Off Pain includes numerous elements from theatrical movies and encourages active learning in an immersive and interactive virtual theatrical world. While navigating in the VR environment, the players have the opportunity to discover information about chronic pain, biochemistry of animal venoms and engage themselves in competitive play on both VR platforms, Oculus Rift and Google Cardboards (**Figure 6.1**).



Figure 6.1. The graphical abstract of VR game **Bug Off Pain**. The game can be played on two different platform: Oculus Rift (*left*) and Google Cardboards (*right*).

The VR environment was modeled on the existing academy theatre as a template (see Chapter 2 for more details on the 3D models) and can be seen in **Figure 6.2**. Here, the ultimate goal is to find the correct spider venom that shuts down pain signaling. However, to achieve this goal, the player has to achieve enough points through watching three VR- embedded movie clips.

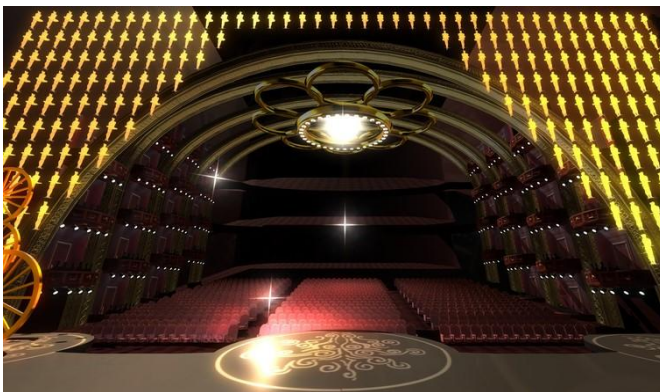


Figure 6.2. The model of our academy theatre in the VR environment for **Bug Off Pain**.

The narrative of the game includes the scientific concepts (parts) about biochemistry of spider venoms in relation to chronic pain (**Table 6.1**).

Table 6.1. Learning objectives related with the contents and characteristics of Bug Off Pain application.

Learning objects	Content of VR game Bug Off Pain
Neuroscience (chronic pain)	<ul style="list-style-type: none"> • Neuroscience of pain • Two major types of pain (acute and chronic) • Communication between neurons and microglia • Involvement of ion channels, including P2X4 in pain
Natural products (animal venoms and toxins)	<ul style="list-style-type: none"> • Chemistry of the venom (small molecules, peptides, proteins) • From venoms to drugs (drug development) • Utility of venoms in various diseases, including chronic pain
Drugs (analgesics)	<ul style="list-style-type: none"> • Current treatments for both, acute and chronic pain • The pitfalls of current treatments for chronic pain

The first part is a VR introduction about the neuroscience of pain. Here, the player has to find a screen element “play” and start watching an animated clip “Pain: Why does is hurt so much?”. This clip is incorporated into the game and introduces the player to the neuroscience of pain, both acute and chronic (**Figure 6.3A**). It includes an interactive exercise to allow players to try the navigational input device (arrows and “play and pause” elements) on the user interface (**Figure 6.3B**).

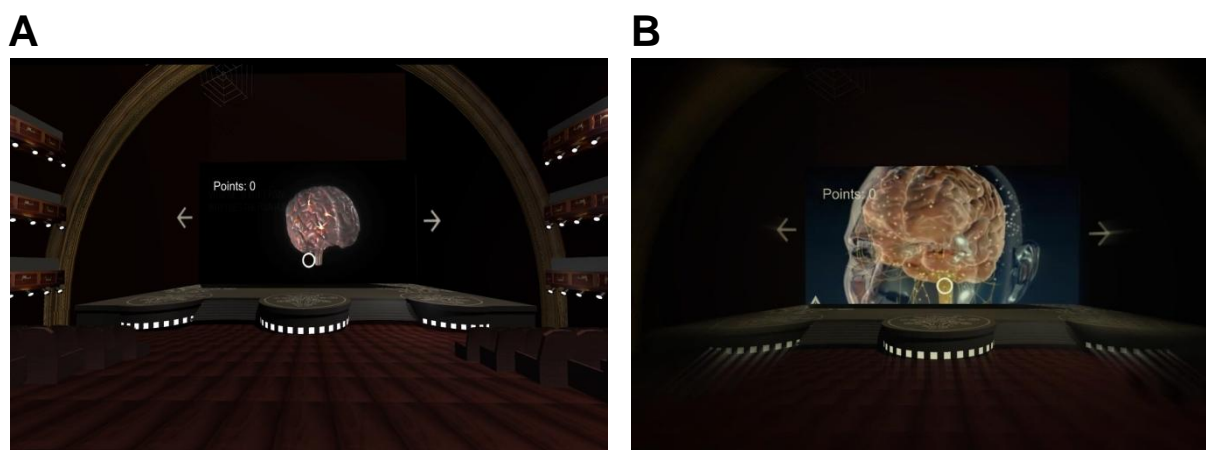
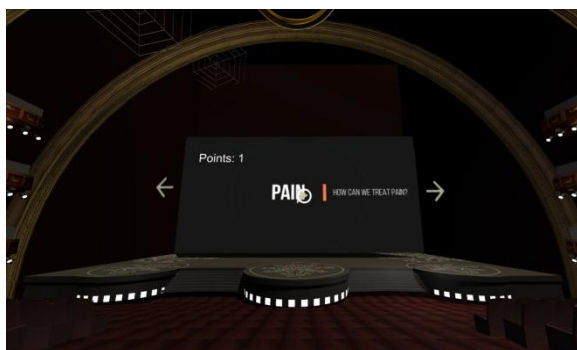


Figure 6.3. VR environment before the first movie clip. A: Model of the human brain that allows the users for immersive interaction. **B:** Close-up of the brain and nervous system as part of the first movie.

As soon as the player gets the first point (**Figure 6.4A**), a new video appears. By clicking either the left or right arrows on the user interface followed by “play”, the player starts watching another video; “How can we treat pain?”. Here, the player is familiarized with the treatment types used to help manage acute and chronic pain.

A number of options are explained, together with the pitfalls of current therapies for chronic pain such as the inadequate effects of opioid drugs. Players get to learn about different types of venomous animals such as cone snails and spiders and judge the positive and negative effects on the targets that are included in pain signaling. Moreover, by interacting with the user interface, the player gets to know more about the chemical structures of some of the major components in their venom such as small molecules, peptides, enzymes and proteins (**Figure 6.4B**). In the game, one is educated on how the chemical diversity of venoms makes them the potential candidates for chronic pain treatment. Once that video ends, the player gets the second point and moves to the final educational movie.

A



B

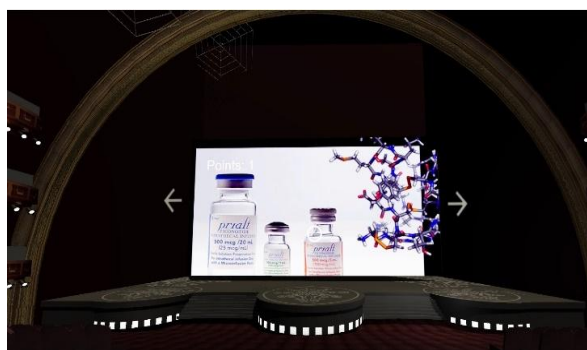


Figure 6.4. Two environments of Bug Off Pain. A, B: The end of the first movie where the player gets the first point (A) and the end of the second clip (B).

Finally, the players are transformed into a final scene: a 3D-movie (**Figure 6.5**). By listening to the voice-over narration, the player learns how different cells, such as neurons and microglia (**Figure 6.5A**) are involved in chronic pain. Furthermore, the gamers gets to familiarize themselves with the concepts such as microglia-neuron communication (**Figure 6.5B**) and roles of the microglia in chronic pain.

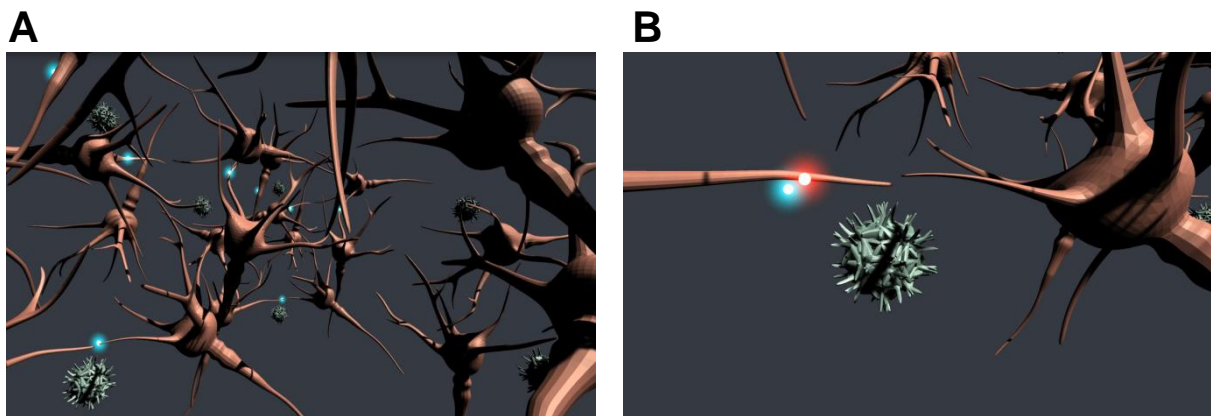


Figure 6.5. 3D-movie that allows the player to travel inside the brain. A: Depiction of neurons (*brown*) surrounded by microglia (*green*). **B:** Zoom-in to neuron-microglia communication depicted as red and blue dots.

Alongside microglia, concepts such as receptors and ion channels are explained. In particular, a 3D model of a human purinergic receptor P2X4 is introduced and its role in the pathophysiology of pain is explained (**Figure 6.6**). We modeled this target (depicted as receptor in *beige* color) together with its respective membrane (depicted as *blue dots* and *white lines* as phospholipid bilayer) and their contribution to chronic pain. This experience ends when the player gets the last (third) point.

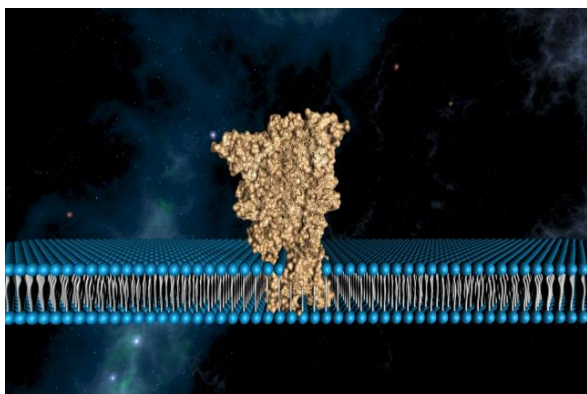


Figure 6.6. Representation of one specific target (purinergic receptor P2X4) in the brain (PDB: 4DW1).

Soon after the player collects the final point, the experience translates back to the academy theatre and that same purinergic target on **Figure 6.6** appears on the theatre's stage, together with the various spiders dropping down from the theatre ceiling.

This part includes an explanation of the scientific concept (seeking for spider venom toxins that would block the protein involved in pain pharmacology), followed by an explanation of the game rules (under what condition the spider venoms would inject the venom and how the player could probe the protein for its response to the venoms) and an interactive-gaming part (**Figure 6.7**).

To start the game, the players must click on each spider and after they split venom (represented as a building block in different colors and shapes), the gamers have to find a best way to “hit” the target on the stage. Some venom is active towards a target, and others are not. Critically, if the inactive venom is chosen, the target rejects it and the player cannot click on that spider venom. After each unsuccessful attempt, for which the player is not penalized, one has to click on another spider for the new venom to appear (**Figure 6.7A**). The players are thoroughly guided through these different stages of the game. Yet, after four failed attempts, a tarantula drops down from the ceiling and spits its venom (depicted as the *green* building block). The game ends as soon as the player drags that final venom to the purinergic receptor on the stage. That specific venom fits the target and fireworks appear (**Figure 6.7B**).

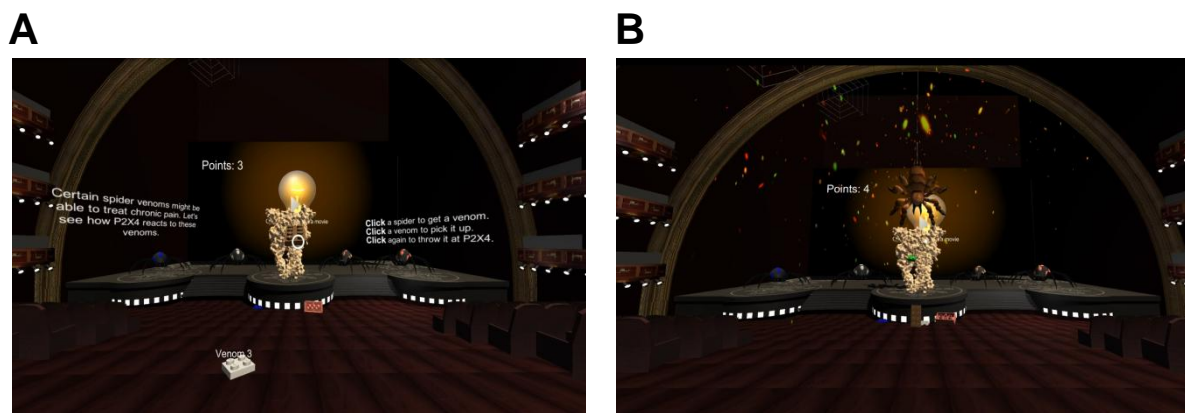


Figure 6.7. VR environment with the target on the stage. A: environment after probing the wrong venom. **B:** environment after the player finds right venom.

As soon as the game for Oculus Rift was build, we re-coded it to Android and created QR code via which the game can be downloaded (**Figure 6.8**).



Figure 6.8. QR code for Bug Off Pain.

At the end, the player can choose to see a plot summary together with an explanation of how identifying the right spider venom towards purinergic P2X targets might bring novel discoveries that patients suffering from the chronic pain might benefit from.

Soon after, the credits appear and the player can share their score and feedback to our website where we gather their feedback for our research evaluation.

6.2.2. Evaluation of General Public Opinion about Bug Off Pain

Evaluations are the most credible way of linking the developed application with reality. Here, we obtained the public opinion and evaluated feedback from the Bug Off Pain through manual or electronic forms (Figure 6.9).

Statement		Strongly Disagree			Neutral				Strongly Agree		
		1	2	3	4	5	6	7	8	9	10
1	The immersive environment via VR adds to STEM engagement and motivation to learn more										
2	Bug Off Pain is an innovative approach to gamify chemistry-related subjects										
3	The game is fun, dynamic and easy to play										
4	I like to play Bug Off Pain										
5	I acquire a new knowledge about chronic pain and spider venoms										
6	Content of the Bug Off Pain is relevant and useful										
7	The design of the game is attractive and captures the attention of the player										
8	Bug Off Pain should be extended to other STEM subjects										
9	The scoring system is well in place										
10	Bug Off Pain has an easy to understand navigation (user interface)										
11	Music and voice-over is appropriate and adds to the game										
12	VR Sickness has not been experienced during the game										
13	I find this VR approach as a good alternative to public engagement and education via VR										
14	This game changes my perception of what I think about STEM-related subjects										
15	I didn't know before that science can be fun - I am more eager to study chemistry-related subjects now										

Figure 6.9. Printed survey. This was administrated to collect the players' opinions and feedback about Bug Off Pain (electronic version can be accessed here: <https://goo.gl/RM99sZy>).

This survey contains 15 statements with responses based on a 10 point Likert-type scale (Figure 6.10). The level of agreement with the statements displayed a range from 6.02 to 10.0 among the general public (non-scientists). Some of these questions were related to the participant’s satisfaction with Bug Off Pain. These were related to: the game is fun, dynamic and easy to play; I like to play Bug Off Pain; and, the content of Bug Off Pain is relevant and useful; and the scoring system is well in place. These four questions were used as the satisfaction variables.

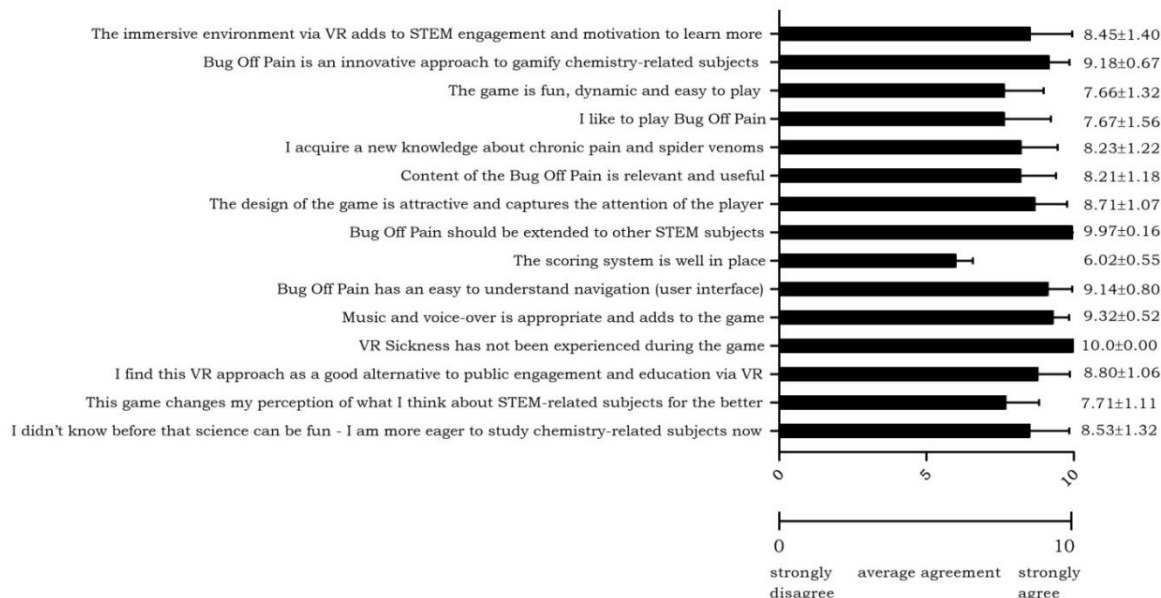


Figure 6.10. The survey. The results show the mean Likert scores together with their standard deviations for evaluators’ responses (n=144) by survey statement.

The next six questions were focused on people’s opinion about Bug Off Pain as a science communication tool and VR experience: the immersive environment via VR adds to STEM engagement and motivation to learn more; Bug Off Pain is an innovative approach to gamify chemistry-related subjects; Bug Off Pain should be extended to other STEM-subjects; VR sickness has not been experienced during the game; I find this VR approach as a good alternative to public engagement and education via VR; and, this game changes my perceptions of what I think about STEM-related subjects for the better. These six questions were used as the VR experience variables.

Other questions focused either on the design, navigation or content of the game: the design of the game is attractive; Bug Off Pain has an easy to understand navigation (user interface); music and voice-over is appropriate and adds to the game, or the potential educational benefits: I acquire a new knowledge about chronic pain and spider venoms; and, I didn’t know before that science can be fun – I am more eager to study chemistry-related subjects now. These five questions were used either as the reflective or educational variables.

Since our results suggest that the statements are closer to “strongly agree” (8-10) than to “neutral” (4-7) or even “strongly disagree” (1-3), this may predict a true trend. However, one possible limitation was that the survey respondents were self-selected. This suggests that the sample might not represent the total public population. Still, on the basis of these responses, users pointed to the game being easy to play, dynamic, fun (7.66 ± 1.32), and with an attractive (8.71 ± 1.07) and easy to understand interface (9.14 ± 0.80). Furthermore, the content is relevant (8.21 ± 1.18) and it helps the public to shift their perception about STEM-related subjects (7.71 ± 1.11). The general public would be interested in playing these types of games if these would be extended to other STEM topics (9.97 ± 0.16) since they found Bug Off Pain as a good alternative to public engagement and education via VR (8.80 ± 1.06). However, a better reward system should be in place and the scoring system should be designed better (6.02 ± 0.55).

While the motivational aspect could be improved, other game elements such as the duration of the game were taken into serious consideration. The reason for this is that a lot of VR players have reported VR-related sickness.⁴⁵¹ The evaluations showed zero VR-related sickness during the gameplay (10.0 ± 0.00) which may be due to the game duration being between 7-10 min. Other authors such as Regan⁴⁵¹ reported that symptoms of VR sickness are most pronounced at 20 min when almost half of the players reported VR sickness. This seems to be in line with these studies as well.

In the game presented by Price and others⁴⁵² an important aspect of evaluation also considered a desire to continue interacting and playing. Such a statement was not included as part of our survey, however, that implication might still be there (99% people would like to see Bug Off Pain extended to other STEM topics).

While much research in educational sciences involves measuring people’s opinions and attitudes, scales such as Likert-type scales are usually applied. For the evaluation of the public’s opinion we employed the 10-point Likert scale since these scales are easy to understand and its responses are easy to quantify when subjected to statistical analysis. Moreover, the scales with more categories are more reliable and provide more valid information. Since it doesn’t require the responders to give a concrete “yes” or “no” answer or take a stand on a specific topic, this allows the participants in our survey to respond in a degree of agreement. This accommodates neutral opinions of participants which are then easily analyzed and presented. Moreover, the participants answers were either electronically or manually obtained and are thus quick, efficient and inexpensive methods for collection of opinions about Bug Off Pain.

Despite this strong support for Likert-scales, these types of scale only gave us 5-10 options of choice, and some authors suggest that the space between each choice might not be of equal distance.⁴⁵³ As a result, it may fail to measure the real attitudes of participants. Moreover, people usually avoid the “extreme” choices even if the “extreme “(1 or 10) would be the most accurate. Another limitation of our method may be the linguists’ aspect of the statements. Specifically, since the statements are all positively worded, this doesn’t force the responders to reverse their thinking. Next time, negative statements should be included in this type of evaluation as well.⁴⁵⁴

Although the Likert scales are still a topic of debate (and taste) among educators, it is clear that the scales with more categories (such as 10-point scales) are more reliable and provide more valid information.⁴⁵⁴ After the 10-point scale was chosen, we had to ensure its reliability and validity. Before we distributed a survey at the Norwich Science Festival (where the game was officially launched), we first ran a test-run among a small panel of students at the University of East Anglia. Here, the respondents had to answer two questions in respect to the validity of the Likert-type scale. The majority (>83%) of the panel answered “Yes” and “Yes, relevant” to the questions “Does the survey measure what it intended to measure?” and “Is this question measurement in the survey essential to the intended measurement?” respectively. Thus, we have concluded that our survey measures what it claims to and this is deemed valid and reliable.

On the basis of our findings, the game Bug Off Pain is not only a good approach to public engagement via VR, but the gamification of scientific concepts such as chronic pain and biochemistry of venoms, may be seen as an alternative way to STEM outreach activities. These results are encouraging because they imply that students can also learn out-of-the-classroom at any time without demanding full control over their learning process. Yet, that does not necessarily mean that Bug Off Pain is educationally effective. To further evaluate this, we then embarked on quantifying VR-based learning influenced by the use of Bug Off Pain.

6.2.3. Evaluation of VR-based Learning by Use of Bug Off Pain Among High School Students

Several authors have pointed out that there is still a lack of research concerning how VR games might enhance learning outcomes. Since it is difficult to measure the knowledge and capability of the individual student,⁴⁵⁵ the performance on the test can be quantified.⁴⁵⁶

A study was carried out to find out whether the educational VR game Bug Off Pain may facilitate learning better than educational software without a gaming element.

Critically, the design and evaluation of Bug Off Pain was inspired by various pedagogical concepts from Kolb⁴⁵⁷ to Garder's⁴⁵⁸ theory. The purpose of all these theories is based on experiential learning, which consists of a concrete experience (feeling), a reflective observation (watching), an abstract conceptualization (thinking), and an active experience (doing). The idea that the players may learn by playing Bug Off Pain, is based on their experience. For example, players learn about the neuroscience behind chronic pain and the biochemistry of venoms by collecting rewards (points) throughout the game (concrete experience); reflecting on the game feedback after probing the wrong venoms (reflective observation); creating a concept about the chronic pain issue (abstract conceptualization); and actively experimenting with the biochemical concepts of venoms during the game (active experience).

Once these theories were considered, the evaluation was conducted by a cohort of 44 high-school students, aged 17-18. The study resulted in a controlled pretest-posttest design to analyze the educational benefit of Bug Off Pain (**Figure 6.11**). Here, the game was compared to a conventional method (video clips) without the immersion or the virtual reality environment. Indeed, these video clips are also embedded in the VR setting, however, the subjects in the control group (video clips) were not subjected to the VR nor its game elements. The tested hypothesis was: students from the virtual group would have significantly greater learning performance in biochemistry of spider venoms and chronic pain than students from the video clips group.


 <p>“SPIDER” Exam Pre-test and post-test for “VR Bug Off Pain” Educational Evaluation</p> <p>Identification No: <u> X </u> Result: _____ Class: <u> X </u> Date: <u> XX/XX/XXXX </u></p> <p>Instructions Read each of the questions slowly and carefully and choose the letter that best describes the answer. Then, print a letter of the correct answer next to the question (on the left).</p> <p>Part I: Why does it hurt?</p> <p>1) _____ What are the two main types of pain? a. Headache and back pain b. Chronic and acute pain c. Nausea and stomach pain</p> <p>2) _____ Choose an answer that doesn't describe chronic pain: a. It helps us survive and serves as a protective function b. Rheumatoid arthritis is one form of it c. When a person is experiencing this sort of pain, only one area of the brain is active</p> <p>3) _____ What is one of the symptoms of chronic pain? a. Headache b. Sunburn c. Heightened sensitivity to touch</p> <p>Part II: How to treat pain?</p> <p>1) _____ Choose the answer that is correct: a. Local anesthetic is good when you want to treat a pain at a specific location b. Opioids don't have many side effects c. Ibuprofen is useful for different types of pain</p>	<p>2) _____ Can people develop addiction when taking opioids? a. Usually yes b. No, never</p> <p>3) _____ Choose the answer that describes some of the most common side effects of opioids: a. Stomach pain, heartburn, vomiting, constipation b. Addiction, delusion, depression, anxiety, hostility towards others c. Nausea, vomiting, constipation, dry mouth, sedation, dizziness, tolerance, addiction</p> <p>4) _____ Which venom CAN NOT be used to treat chronic pain? a. Cone snail venoms b. Spider venoms c. Grasshopper venom</p> <p>5) _____ What is Ziconotide? a. A drug that is used to treat chronic pain b. Cone snail venom c. Spider venom</p> <p>Part III: Venom gang</p> <p>1) _____ Choose the incorrect answer that describes brain cells (neurons): a. Neurons send signals with a help of neurotransmitters b. Microglial cells are cells that surround neurons in our brains c. Neurons and microglia are less likely to communicate between each other</p> <p>2) _____ Choose the correct answer: a. Communication between microglia and neurons don't seem to contribute to chronic pain b. Proteins found on the surface of the microglial cells contribute to chronic pain c. P2X4 is a protein and is not involved in chronic pain</p>
---	--

Figure 6.11. Pre- and post-test questionnaire.

Once the results from the pre-test and post-test were analyzed, they showed that in all groups there was an improvement in the average number of correct answers (ANCA) in the post-test, relatively to the previous pre-test (**Table 6.2**). The analysis of the pre-test showed no major differences in the number of correct answers between the control group (3.045 ± 1.397) and experimental group (3.818 ± 0.958). This indicates that the two groups had similar background knowledge about chronic pain and animal venoms. At the same time it is clear that this score improved in both groups after the students were exposed to either video clips (5.773 ± 1.110) or VR game (8.696 ± 1.093). When calculating the average score differences, these were 2.323 and 4.878 for video clips and VR game, respectively.

These findings suggest that the students had a high level of learning (with approximately 87% of correct answers in VR group in respect to 57% in video clips group). This implies that the students improve their knowledge by utilizing both methods, yet, VR seemed to improve that performance to a greater amount. However, the study has not measured the level of understanding the explained concepts. Since some studies⁴⁵⁹⁻⁴⁶⁰ show that while the performance might be better, the level of understanding is lower. That means the students appear to understand the concepts better when using the traditional methods such as textbooks and video clips.⁴⁶¹⁻⁴⁶²

Despite this, Papastergiou⁴³⁵ and Connolly⁴⁶³ showed that digital games promote student motivation and improve their learning experience. Critically, this resulting likeability and motivation is usually not part of the traditional classroom lesson. Thus, advancing the level of scientific understanding among primary and/or high school students may result in increased interest in STEM.

Still, on the basis of this data, we can conclude that the Bug Off Pain context and the VR game itself could have been a powerful transmitter of knowledge. This is line with other studies conducted on educational benefits of VR-based games.⁴⁶¹

Table 6.2. Comparison of pupils' average scores by instructional method

Assessment ^a	Mean Scores ^a (SD) by Group, N = 22	
	Control Group: Video Clips	Experimental Group: VR Game
Pretest	3.045 (1.397)	3.818 (0.958)
Post-test	5.773 (1.110)	8.696 (1.093)
Av. Score Differences	2.323	4.878

^a The scale has a range of 1-10

As a continuation, we decided to statistically examine these results by the multiple comparison tests (two-way ANOVA and Wilcoxon test) between the relative differences of the number of correct answers (**Table 6.3**). The analysis showed a statistical difference between the pre-test and post-test in either video clips (P value 0.0001) or VR game (P value <0.0001). Lastly, the calculation of the effect size (Cohen's d value) between the post-tests (video clips vs VR game) was considered. This assessment showed the effect size to be very large ($d > 2$) based on the guidelines outlined by Cohen⁴⁶⁴ further emphasizing that the differences between these two groups is substantial. Thus, it can be concluded that the students learned some new information during both types of activities. Yet, the educational effectiveness of virtual reality, relative to video clips, resulted in a Cohen's value of 4.76 and better learning outcomes (P=0.0001).

Table 6.3. Comparative student performance relative to instructional method

Structure of analysis	P value ^b (N = 22)	Cohen's d value
Video clips (pretest vs posttest)	0.0001	2.16
VR Game (pretest vs posttest)	<0.0001	4.76
Δ video clips ^a vs Δ VR game ^a	0.0002	NA
Posttest (video clips vs VR game)	0.0001	2.65

^aRelative difference of right answers between pre- or posttest. ^bAll the p values were found to be significant (P<0.05)

This data might be further supported by a notion that 3D virtual environments allow the users to be active rather than passive participants. According to Lim,⁴⁶⁵ 3D virtual environments are characterized by two elements - immersion and interaction – with immersion being a process when awareness begins to disappear, and the engagement level increases.⁴⁶⁵ Moreover, the reward system incorporated in Bug Off Pain as a form of points and feedback allows the players a sense of control and serves as extrinsic motivation similar to when a lecturer compliments students on their good work.

Furthermore, as Lim⁴⁶⁵ noted, when too much effort is put into navigating and interacting with the material presented in a virtual world, mental resources available for the task itself diminishes. For that reason, Bug Off Pain only incorporated essential elements such as arrows, element “play”, spiders and venoms depicted as building blocks which may prevent them from exploring the VR environment as a whole. On the other hand, a recent meta-analysis study from Merchant and others⁴⁶⁶ suggested that simulations and VR worlds were effective in improving learning outcome gains.

For example, a student's performance was improved when they play the game individually rather than in a group.⁴⁶⁶ While a consensus on learning benefits of VR games has not yet been reached, the choice of the platform might add to its educational outcomes as well.

Since the game was developed on two different platforms, Oculus Rift and Google Cardboard, the evaluation was carried out only on Google Cardboard. While Oculus Rift is one of the head-mounted platforms that allows for full immersion, Google Cardboard is cut out of pieces of cardboard, folded into 3D viewer for smartphones, and is considered as an inexpensive alternative to Oculus Rift.⁴⁶⁷ Consequently, Google Cardboard as a content delivery system may offer a lower level of immersion and limited interaction compared to Oculus Rift.⁴⁶⁸ Despite these limitations, the cardboard platforms may restrict the players to only performing one virtual task thus offering better learning outcomes in respect to other VR games.⁴⁶⁵

While this data suggests that VR games, such as Bug Off Pain, facilitate learning better than traditional methods such as textbooks and video clips, other examples showed that this may not be the case. For example, the evaluation of the VR game E-junior⁴⁶⁹ showed no significant differences in the learning performance between the traditional and the virtual group. The authors suggest this may be due to the distractions of the attractiveness and complexity of the immersive environments on the children. Other authors⁴⁶⁵ also observed the correlation between immersion in the virtual world and loss of focus on their learning tasks. By engaging within a 3D space, the students failed to engage with the quests, indicating a disengagement rather than engagement. Still, this might be because of the collaborative game play rather than individual.⁴⁶⁶

However, it should be noted that E-junior didn't incorporate the narrative aspects of gaming, as Bug Off Pain did, which may one of the reasons for this distraction. According to the Malone,⁴⁷⁰ Provenzo,⁴⁷¹ Rieber,⁴⁷² and Gee,⁴⁷³ incorporating the narrative within a game design is beneficial for the learning process. First, it provides opportunities for reflection, evaluation, illustration, exemplification and inquiry.⁴⁷⁴ Second, the narrative facilitates comprehension as well as serving as a tool for navigating in VR environments.⁴⁷⁵ So far, the research in this field has been scarce, nevertheless, some of the game components may involve the mission, a cover story, roles, and scenario operations, all of which Bug Off Pain incorporated into its initial design.⁴⁷⁶

Interestingly, while the children playing E-junior reported to be more engaged and satisfied, this didn't result in better learning outcomes as it did in Bug Off Pain. On the other hand, Bug Off Pain only obtained quantitative data from its evaluation so it is difficult to compare how qualitative factors such as gender; age; school; grades; frequency of computer use and gaming; and enjoyment of computer games may influence our results.

Further, the evaluation process also gives a lot of interesting information for improving the evaluation methodology. First, it should be noted that we have not employed any surveys after the post-tests which would gather the post-test feedback such as perceived usefulness; engagement; intention to use; perceived educational value; intrinsic motivation; and enjoyment. Thus, we should employ these close-ended questions after the post-test in order to improve the application of the pedagogical value of Bug Off Pain.

It should also be noted that evaluation of the learning effectiveness should be studied further. In our study, only a declarative type of knowledge (facts) was considered. Since the learning process not only concerns facts but also procedures of how to transfer this information to other situations (strategic knowledge) and actions (procedural knowledge), these objectives should be taken into account in both short-term and long-term evaluation. This certainly might be a challenge for virtual reality gaming environments, but could be, nevertheless, an interesting point to evaluate.

Finally, Virvou and others⁴⁷⁷ suggest that if a traditional group is used as a control group in order to compare it with new technology (e.g. VR game), it assumes that the virtual technology is destined to replace traditional methods rather complementing it. In our case, Bug Off Pain is not intended as a total replacement to any current effective pedagogy. Rather, it is meant as a valuable addition to the teaching toolbox that educators can leverage to engage and educate the modern learner.

Once these practical challenges are met and overcome, this may open new opportunities for educators to apply similar concepts to their own field. Because Bug Off Pain only needs a minimum setup that includes Google Cardboard, mobile phone and internet connection, the learning activity may not be challenging.

6.3. Conclusions

Considering the increasing use of mobile applications among young people, VR games such as Bug Off Pain may have great potential as pervasive educational games. It is clear that such games allow the traditional public engagement process to become more effective when permeated with VR tools. Here, a study on the educational benefits of multi-platform, immersive and engaging VR game Bug Off Pain is presented. The game is now freely available online, and has been tested and evaluated by non-scientists (general public) and high school students.

The Bug Off Pain experience entails overcoming a series of challenges (watching video clips embedded in our game and finding a spider venom that takes down the pain) in pursuit of a goal. The player is therefore presented with some obstacles and must use his/her available game actions to create a solution that gets the player past the obstacle and further toward his/her goal. This comes from the challenge of correctly using critical thinking skills and problem-solving abilities to create a desirable outcome (finding the “perfect” venom). Apart from the problem-solving roles, another reason why Bug Off Pain may be good for pedagogy is the promotion of creativity and self-direction – all of which stand out as less-tangible, non-academic benefits. Other researchers⁴⁷⁸⁻⁴⁷⁹ continue to demonstrate that games are productive in applying, synthesizing, and thinking critically about what is learnt. However, these games might lack the necessary characteristics for successful integration into traditional learning environments such as classrooms.

Our results showed that Bug Off Pain can help public, as well as high-school students, to develop a deeper and accurate understanding of important concepts about the chemistry of venoms and chronic pain. The game’s insights showed that VR representation is an effective tool for communicating and remembering scientific ideas and solving problems – for example, a chemical structure that shows the shape of a venom peptide or other small molecules found in the venoms. Furthermore, these representations are intended to convey information to the non-scientific community and may omit the complexities in order to communicate better and educate the central idea. These findings demonstrate that the VR game Bug Off Pain is a valuable aid in science communication, education, and public engagement.

For future work, more qualitative as well as quantitative evaluations should be carried out at different schools to produce more empirical data associated with the game. While Bug Off Pain focuses on chronic pain and spider venoms, it would be interesting to apply these same concepts to a different research area. Moreover, by addressing specific aspects and evaluating them, one may improve the game before its launch. Another possible future idea would be to check long-term learning. Since Bug Off Pain only centers on short-term acquisition of knowledge, it would be interesting to determine its long-term effects.

The game itself may be enhanced as well. By adding multiplayer mode, Bug Off Pain could be more competitive or collaborative. Another challenge could be to make the VR game more dynamic and less predictable so that students may play it more often, and keep building new knowledge each time. One aspect to consider is to adapt the game to the students with different learning abilities.

While I recognize that it is daunting to convince students, teachers and lecturers that playing a VR game belongs in a lecture theatre, the intention of Bug Off Pain is merely to show the importance of emergent pedagogy of play when permeated with VR aids. While new technologies used in education must be cautiously chosen and applied so that the students not only enjoy the aesthetical features but also learn while playing, this research brings us one step closer to understanding the potential of VR technology to support and enhance learning.

~CHAPTER SEVEN~

General Conclusion and Future Directions

7.1. General Conclusion

It is clear that spider venoms might offer almost endless potential for drug discovery. That is further highlighted by the fact that evolution has redefined the biological diversity and led to the development of pharmacologically active and potent toxins that are pre-optimized for the medicinal chemist. Taken together with the fact that one fifth of human population suffers from chronic pain, and with no appropriate treatment for chronic neuropathic pain, exploring less conventional ion channels that are involved in pain processing – such as P2X4 – with spider venoms might be a fruitful line of inquiry. This project aimed to examine whether animal venoms contain pharmacologically interesting compounds for P2X4 receptor in microglia.

However, a screening of nearly 200 animal venoms towards P2X channels, called for a method that could rapidly screen our samples against multiple receptor targets. One such tool that might help us in the hit generation process is called high-throughput screening (HTS) assay. Hence, our first aim was to develop a HTS for discovering promising molecules targeting P2X channels. Notably, no HTS to detect the spider venom hits against P2X4 channel has been reported (to date), although similar efforts have focused on other P2X receptors^{239, 480} and even voltage-gated sodium channels.⁴⁸¹ This task was thus accomplished with our development of fluorescent-based screens that measure agonist-induced calcium responses (P2X3, P2X4) within cells or agonist-induced dye uptake responses (P2X7) using a Flexstation 3 plate reader. These assays were robustly tested for reproducibility (Z' factors > 0.55) and validated – both analytically and pharmacologically, as suggested by Zhang and colleagues.²²¹ We showed that our *in vitro* platforms are capable of screening multiple venoms (cone snail, scorpion, spider, bee, wasp and centipede venoms) against multiple targets (P2X3, P2X4, P2X7), all while minimizing the specimen material, testing time and costs. Furthermore, fractionation and purification of venom fractions helped us to distinguish between cytolytic (non-specific) fractions from those with a specific effect on a particular P2X target.

Our robust, fast, automated, and quantitative HTS technique resulted in potential toxin hits, both small molecules and peptides, as hit inhibitors against hP2X4. While no specific hP2X3-; hP2X4- or hP2X7-related effects were displayed with cone snail venoms, our screen with the spider venoms resulted in several inhibitors against hP2X4 in two heterologous expression systems (HEK293 and 1321N1 cells). Although we initially screened and validated 15 spider venoms, only venoms from *Acanthoscurria*, *Lasiadora* and *Phormictopus* showed a seemingly potent inhibitory effect on hP2X4 channel activated by ATP. Other crude venoms (*Haplopelma*, *Poecilotheria*, *Nhandu*, *Epebopus*) showed a non-specific activity and were thus subjected to fractionation in order to more clearly observe the effect of each fraction.

By using a combination of chromatographic and mass spectrometric techniques (RP-HPLC, ESI-LC-MS/MS, MALDI-TOF), we fractionated 9 crude venom “hits” and identified a common appearance of four inhibitory toxins, which were confirmed to be structurally uncharacterized acylpolyamines, found in a number of “hit” spider species. The molecular weight of the toxins was determined to be 365.2563 Da, 454.2274 Da, 600.3712 Da, and 728.5026 Da with the similar fragmentation ions occurring in all toxins (except 454.2274). Since 600.3712 Da and 728.5026 Da were abundant in all venoms and could be thus obtained in larger amounts, we focused our investigations on these two toxins.

Once we investigated the concentration dependence for inhibition by these two toxins, we found that both, LK-601 and LK-729, potently inhibited hP2X4 with the apparent IC_{50} values between 1.1 – 4.5 μ M, confirmed in two different cell lines and with two different sets of fluorescent-based assays. However, only one of them – LK-601 – showed an acceptable selectivity over other P2X subtypes (P2X3, P2X7) and NMDA 1a/2a receptor. Interestingly, while acylpolyamines typically antagonize glutamate receptors (such as NMDA), LK-601 and LK-729 do not exhibit these effects. Furthermore, both toxins do not seem to block rat P2X4, however, have a modest effect at mouse P2X4. This phenomenon was previously reported with BX430,^{153, 408} PSB12062¹⁶⁶ and 5-BDBD,²⁵⁰ all commercially available antagonists inhibiting hP2X4 at low sub- or micromolar concentration but being less potent on either rat or mouse P2X4 or both.

In order to better understand how LK-601 inhibits hP2X4 and mP2X4 while being inactive towards rat P2X4, we attempted a full structural elucidation using NMR techniques. However, we could only determine LK-601 partial structure which is in line with Skinner et al.³³⁰ results. The only other investigation reporting LK-601 and/or LK-729 was carried out by Rocha-E-Silva et al.³²³ in which the authors observe a remarkable light sensitivity of LK-729 toxin, which in turn prevented a full structural elucidation. In our hands, LK-601 and/or LK-729 also showed a water instability which further prevented to get a decent NMR fingerprint. Still, we managed to note down a few interesting observations: 1) LK-601 and LK-729 contain a different aromatic ring with LK-601 likely to be an indole; 2) LK-729 has a longer polyamine chain than LK-601 and contains a phenol ring; 3) the polyamine chain very likely contains a spermine moiety. Furthermore, our MS/MS data pointed out to the fact that LK-601 may be a part of LK-729. While NMR characterization may elude to the fact that the polyamine chain is longer in LK-729, it is also evident that the aromatic group is different (indole vs two phenols). This may exclude the possibility of LK-601 being part of LK-729 or suggest rearrangement between the aromatic group of LK-601 (indole) and LK-729 (two phenol groups).

Unfortunately, the reasons for this inconsistency remain unclear, but it is possible that the fragmentation similarities are due to the polyamine chain (spermine) rather than the aromatic ring.³⁰¹ In order to circumvent these issues, we aimed to explore the structure-activity relationship (SAR) of LK-601 and synthesize its analogues. Moreover, the potency differences between P2X4 orthologues (human, mouse, rat) enabled us to ask whether this might hold a clue to LK-601 binding site. Since the amino acid identity of rat P2X4 is 82% and 94% when compared to human and mouse, respectively,⁴⁰⁸ our investigations focused not only on identifying the smaller analogue of LK-601 that inhibits hP2X4 with a similar potency and selectivity, but also on pinpointing the amino acid residues that might be critical for the binding of LK-601 on hP2X4.

By using a fragment-based approach, we aimed to get more structural insights into motifs with the potential inhibitory action towards hP2X4. We concluded that while polyamines such as cadaverine, putrescine, spermidine and spermine do not seem to modulate hP2X4, indole-like compounds such as tryptamine, tryptophan and serotonin showed an interesting inhibition, when tested at 10 μM concentration – and that effect was abolished with lower concentrations.

To further validate our hypothesis, we selected 22 representative compounds from NCI-DTP library on the basis of the cluster analysis,⁴⁰² and tested 14 of them. Using two different sets of assays, 4 molecules (1513, 1969, 13964, 135831) demonstrated an interesting concentration-dependent inhibition. From these structural-activity investigations we found that both the indole ring and the 3-substituted aliphatic chain seem to contribute to the overall inhibitory effect at hP2X4. On the contrary, presence of the -OH group on the position 5 of the indole and a -COOH group on the position 2 of the carbon chain does not make a difference when trying to block hP2X4.

While one study has already reported a drug (fluvastatin) with an indole moiety that might modulate P2X4,⁴¹⁰ no acylpolyamine has been found to inhibit P2X4 channels. To develop compounds that would resemble the acylpolyamine-like structure of LK-601, and demonstrated a similar potency and selectivity, however, with improved stability, we synthesized five analogues: LA1 – LA5. One of them, LA-3, was found as a potent hP2X4 receptor antagonist (IC_{50} values between $9.67 \pm 0.96 \mu\text{M}$ and $18.6 \pm 5.6 \mu\text{M}$ in 1321N1-hP2X4 and HEK293-hP2X4, respectively) with a good selectivity over P2X3 and P2X7. However, while the molecular mass was reduced to half, the stability of LA-3 has not been improved. Despite these drawbacks, LA-3 might still be used as a new starting point for the development of potent and selective P2X4 receptor antagonists. Furthermore, these results might simply point out to the fact that there is still room for further optimization with regard to affinity and improvement of LA-3 physicochemical properties.

We then focus our efforts on trying to decipher a binding site for LA-3. Once the alignment of the sequences between human, mouse and rat was carried out, the specific sequences that are not shared between these three P2X4 orthologues were identified.

Proceeding to the *in silico* docking suggested that the following residues might be crucial in how LA-3 binds to human P2X4: D220, K222, K234 and N238. Critically, two residues, aspartate and asparagine at the position 220 and 238, respectively, that are swapped between human and rat (D220 and N238 in human; N220 and D238 in rat) might be essential for sub-species differences in LA-3 binding. The validation of the predicted amino acid residues in binding LA-3 showed that D220 and N238 might be involved in LA-3 binding site, however, more experiments are needed to fully confirm that effect.

So far, this story has seen the side of only the small molecules. But in addition to small molecular weight toxins, our HTS showed that some of the late-eluting fraction hits against hP2X4 might be peptides (Figure 4.10 – 4.11, Chapter 4). These peptide hit fractions (F) were found in spider venoms of *Lasiodora klugi* (F25), *Haplopelma albostriatum* (F46, F53-55, F60, F63, F68), *Nhandu chromatus* (F39-42, F44-45), *Acanthoscurria geniculata* (F31-33, F37-38), and *Acanthoscurria cordubensis* (F20, F32-33). Here, we would like to briefly draw your attention to our efforts on the peptide front (Supporting Information). We first focus on F25 from *Lasiodora klugi* – a peptide which we managed to obtain in purity >91 % (Figure S2A). Using MALDI-TOF technique, its monoisotopic peak was estimated to be 7756 Da (with an observed fragment ion at 3879 Da) (Figure S2B), and its accurate mass confirmed on LC-MS Orbitrap to be 7769.85 Da (Figure S3A). By subjecting peptide F25 to trypsin digestion (Figure S3B-S3D) and N-terminal sequencing (Figure S3E), we attempted to obtain its amino acid sequence.

While we confirmed its N-terminal sequence to be AEEGF, and found peptide fragments of LASSFR, GEPQCFHCECR, CMIVR, IFECVMACDIEK, GLFVTCTPGK, ALEKLASSFR and LNAELGPYALADR – similar to the previously identified U3-theraphotoxin-Lsp1a from the same spider (*Lasiodora*) – we could not align these fragments in any sensible order. By that we mean; having established its N-terminal sequenced (AEEGF) and, on the basis of U3-theraphotoxin similarity, possibly its C-terminal order (ALEKLASSFRCE), we could not overlap any other identified peptide fragments, and failed to deliver a complete sequence for F25. A reason for this might be a presence of peptide impurities that were detected by mass spectroscopy once the trypsin digestion was applied. Even though a relatively good purity of 91.26% was confirmed by RP-HPLC, gel-isolated techniques might give us a better separation and thus, less impurities.

Despite these difficulties, we still proceeded with the pharmacological evaluation of F25. However, even though F25 showed promising results in our initial HTS screen, the validation of its inhibitory effect on 1321N1-hP2X4 cell lines when tested at 5 μ M (**Figure S4**) could not be confirmed. Thus, evaluating the peptide hits might call for a more careful evaluation or even a different methodological approach.

While some promising peptide fractions in *Haplopelma albostriatum* (F46, F53-55, F60, F63, F68), *Nhandu chromatus* (F39-42, F44-45), *Acanthoscurria geniculata* (F31-33, F37-38), and *Acanthoscurria cordubensis* (F20, F32-33) were found, we have to be aware these might or might not be actual hits. In order to validate these effects, the peptide's purity should be determined not only by chromatographic (RP-HPLC) methods but also by gel-isolation techniques (polyacrylamide gels), which could be coupled by high-sensitivity nanoelectrospray mass spectroscopy for the molecular analysis of the peptides.⁴⁸² This could not only solved the purification issues observed with F25, but also material shortage.

In summary, a novel toxin from a spider venom with inhibitory activity at human P2X4 ion channels that shows selectivity at hP2X4 over other P2X receptors was discovered. In addition to small molecules, our HTS showed some potential inhibitory peptides that might block hP2X4 receptor. Further characterisation and validation is required to understand whether these novel compounds could be useful as analgesics.

7.2. Future Directions

As already suggested by Beswick et al.¹⁷¹ identifying P2X4 receptor ligands is challenging. Even though a combination of natural product libraries, high throughput and fragment-based screening, and *in silico* docking techniques were used, the other complimentary approach that would undoubtedly verify our results is electrophysiology. Apart from testing LK-601 and/or LA-3 using whole cell patch clamp, taking advantage of molecular dynamics simulation to model the docking of LA-3 on a potentially identified allosteric site (around D220 and N238) might provide more clues about the natural mode of binding rather than the "lock-and-key" theory.⁴⁰⁸ Although our *in silico* docking was performed in both, rigid and flexible modes, P2X4 was still modelled as frozen and motionless receptor which is thought to accommodate a small molecule without undergoing any conformational rearrangements.

While our results on LK-601, and later on LA-3, might indicate that these acylpolyamine-like structures, based on LK-601, provide a novel tool to study P2X4 receptors, it still remains uncertain whether these compounds can truly abolish the chronic neuropathic pain (and/or its symptoms) via P2X4 and its P2X4-BDNF-p38 MAP kinase-KCC2 cascade. Since the inhibiting effects of LA-3 are limited in rodents, one way of testing this could be using LK-601 in mouse models. Since LK-601 showed good inhibitory effects at mP2X4, mouse models with P2X4 knock-down or knock-out in the spinal cord could be used to see whether the application of LK-601 results in PNI-induced tactile allodynia.^{99, 483} This could indicate LK-601 might need P2X4 receptors to work as a potential analgesic.

An alternative approach might be to use LK-601 and/or LA-3 on activated microglia (via P2X4 inhibition) and monitor the release of BDNF – a marker that changes the transmembrane anion gradient in dorsal horn lamina I neurons via KCC2, which results in depolarization of these neurons.^{99, 113} This might further confirm that LK-601/LA-3 is able to inhibit microglial P2X4 and modulate the pathogenesis of neuropathic pain. However, to yield LK-601 in greater quantities, an optimized purification method should first be in place.

Another burning question in the field is how to develop analgesic drugs that are not limited by their side effects. For example, opioids (currently used for treating neuropathic pain) cause addiction, tolerance and hyperalgesia after chronic treatment; COX2 inhibitors produce cardiovascular defects; and antidepressant drugs (gabapentin, pregabalin) cause dizziness, drowsiness and nausea and have a limited effectiveness in some patients.^{30, 35} On the other hand, ziconotide (Prialt) is clinically effective and safe to use in patients with severe chronic pain, however, its intrathecal drug delivery is often less preferred option over oral analgesics.⁴⁸⁴ To overcome these disadvantages of current pain medicines, the research efforts have to focus on not only identifying small molecule inhibitors that might enable oral delivery, but also overcoming the drawbacks of opioids, COX2 inhibitors and antidepressants. Along these lines, even though LA-3 currently might not display potentially good pharmacokinetics characteristics, performing a more extensive SAR on LA-3 and testing whether any of its analogues can overcome the above mentioned limitations might accelerate this quest.

With the hope of designing drugs with fewer side effects, developing compounds with a good selectivity profile over one particular target brings in the promise of finding novel therapeutics for neuropathic pain that may lack side effects associated with current therapies.⁵⁹ In this work, the selectivity of LK-601 over other P2X receptor subtypes (P2X3, P2X7) and NMDA 1a/2a was tested. However, in order to assess a broader selectivity profile of LK-601 and LA-3, more targets should be evaluated.

This repertoire might include receptors such as P2X1, P2X2 and others relevant targets for acylpolyamine toxins – for example, AMPA and kainate channels as well as serotonin receptors.¹⁸¹ This could ascertain whether LK-601-like toxins might represent the “holy grail” of neuropathic pain research, developing powerful analgesic drugs devoid of the side effects linked with opioids.

Another fruitful line of inquiry might be to study acylpolyamines and P2X receptors in evolutionary terms. Since spiders prey on insects, one would expect that insects have developed purinergic targets which, in turn, acylpolyamines might target. Surprisingly, this is not the case with P2X receptors – insects are likely to be devoid of these targets.³⁴² Investigating why spiders would strategically develop acylpolyamines that target P2X receptors might give us the reason for such a functional redundancy.

Some of the possible causes, as comprehensively reviewed by Nentwig et al.,⁴⁸⁵ might involve different predators, environmental changes and diet composition. For example, a remark that *Lasiadora* species is a bird eating spider might hold a clue that could keep the evolutionary wheel turning.

References

1. Brennan, F.; Carr, D. B.; Cousins, M., Pain management: a fundamental human right. *Anesthesia & Analgesia* **2007**, 105 (1), 205-221.
2. Scholz, J.; Woolf, C. J., Can we conquer pain? *Nature Neuroscience* **2002**, 5, 1062-1067.
3. Maniadakis, N.; Gray, A. J. P., The economic burden of back pain in the UK. **2000**, 84 (1), 95-103.
4. Wolkerstorfer, A.; Handler, N.; Buschmann, H., New approaches to treating pain. *Bioorganic & Medicinal Chemistry Letters* **2016**, 26 (4), 1103-1119.
5. Attal, N.; Cruccu, G.; Baron, R. a.; Haanpää, M.; Hansson, P.; Jensen, T. S.; Nurmikko, T., EFNS guidelines on the pharmacological treatment of neuropathic pain: 2010 revision. *European Journal of Neurology* **2010**, 17 (9), 1113-88.
6. Dworkin, R. H.; O'connor, A. B.; Backonja, M.; Farrar, J. T.; Finnerup, N. B.; Jensen, T. S.; Kalso, E. A.; Loeser, J. D.; Miaskowski, C.; Nurmikko, T. J., Pharmacologic management of neuropathic pain: evidence-based recommendations. *Pain* **2007**, 132 (3), 237-251.
7. Finnerup, N. B.; Jensen, T. S., Mechanisms of disease: mechanism-based classification of neuropathic pain—a critical analysis. *Nature Clinical Practice Neurology* **2006**, 2 (2), 107-115.
8. Finnerup, N. B.; Attal, N.; Haroutounian, S.; McNicol, E.; Baron, R.; Dworkin, R. H.; Gilron, I.; Haanpää, M.; Hansson, P.; Jensen, T. S., Pharmacotherapy for neuropathic pain in adults: a systematic review and meta-analysis. *The Lancet Neurology* **2015**, 14 (2), 162-173.
9. Finnerup, N. B.; Haroutounian, S.; Kamerman, P.; Baron, R.; Bennett, D. L.; Bouhassira, D.; Cruccu, G.; Freeman, R.; Hansson, P.; Nurmikko, T., Neuropathic pain: an updated grading system for research and clinical practice. *Pain* **2016**, 157 (8), 1599.
10. Alford, D. P., Opioid prescribing for chronic pain—achieving the right balance through education. *New England Journal of Medicine* **2016**, 374 (4), 301-303.
11. Ballantyne, J. C.; Sullivan, M. D., Intensity of chronic pain—the wrong metric? *New England Journal of Medicine* **2015**, 373 (22), 2098-2099.
12. Hill, R., NK 1 (substance P) receptor antagonists—why are they not analgesic in humans? *Trends in Pharmacological Sciences* **2000**, 21 (7), 244-246.
13. Wallace, M.; Rowbotham, M.; Katz, N.; Dworkin, R.; Dotson, R.; Galer, B.; Rauck, R.; Backonja, M.; Quessy, S.; Meisner, P., A randomized, double-blind, placebo-controlled trial of a glycine antagonist in neuropathic pain. *Neurology* **2002**, 59 (11), 1694-1700.
14. Wallace, M. S.; Rowbotham, M.; Bennett, G. J.; Jensen, T. S.; Pladna, R.; Quessy, S., A multicenter, double-blind, randomized, placebo-controlled crossover evaluation of a short course of 4030W92 in patients with chronic neuropathic pain. *The Journal of Pain* **2002**, 3 (3), 227-233.
15. Li, J. W.-H.; Vederas, J. C., Drug discovery and natural products: end of an era or an endless frontier? *Science* **2009**, 325 (5937), 161-165.

16. Waxman, S. G.; Zamponi, G. W., Regulating excitability of peripheral afferents: emerging ion channel targets. *Nature Neuroscience* **2014**, 17 (2), 153-163.
17. Beggs, S.; Trang, T.; Salter, M. W., P2X4R+ microglia drive neuropathic pain. *Nature Neuroscience* **2012**, 15 (8), 1068-1073.
18. Trang, T.; Salter, M. W., P2X4 purinoceptor signaling in chronic pain. *Purinergic Signalling* **2012**, 8 (3), 621-628.
19. Hattori, M.; Gouaux, E., Molecular mechanism of ATP binding and ion channel activation in P2X receptors. *Nature* **2012**, 485 (7397), 207-212.
20. Woolf, C. J.; Salter, M. W., Neuronal plasticity: increasing the gain in pain. *Science* **2000**, 288 (5472), 1765-1768.
21. Hunt, S. P.; Mantyh, P. W., The molecular dynamics of pain control. *Nature Reviews Neuroscience* **2001**, 2 (2), 83-91.
22. McEntire, D. M.; Kirkpatrick, D. R.; Dueck, N. P.; Kerfeld, M. J.; Smith, T. A.; Nelson, T. J.; Reisbig, M. D.; Agrawal, D. K., Pain transduction: a pharmacologic perspective. *Expert Review in Clinical Pharmacology* **2016**, 9 (8), 1069-1080.
23. Kuner, R. J. N. m., Central mechanisms of pathological pain. **2010**, 16 (11), 1258.
24. Price, D. D., Psychological and neural mechanisms of the affective dimension of pain. *Science* **2000**, 288 (5472), 1769-1772.
25. Basbaum, A. I.; Bautista, D. M.; Scherrer, G.; Julius, D. J., Cellular and molecular mechanisms of pain. *Cell* **2009**, 139 (2), 267-284.
26. Watanabe, C. Mechanism of spinal pain transmission and its regulation. *Yakugaku zasshi: Journal of the Pharmaceutical Society of Japan* **2014**, 134 (12), 1301-1307.
27. Hucho, T.; Levine, J. D., Signaling pathways in sensitization: toward a nociceptor cell biology. *Neuron* **2007**, 55 (3), 365-376.
28. Treede, R.-D.; Rief, W.; Barke, A.; Aziz, Q.; Bennett, M. I.; Benoliel, R.; Cohen, M.; Evers, S.; Finnerup, N. B.; First, M. B. J., A classification of chronic pain for ICD-11. *Pain* **2015**, 156 (6), 1003.
29. Ducreux, D.; Attal, N.; Parker, F.; Bouhassira, D., Mechanisms of central neuropathic pain: a combined psychophysical and fMRI study in syringomyelia. *Brain* **2006**, 129 (4), 963-976.
30. Payne, R., Limitations of NSAIDs for pain management: toxicity or lack of efficacy? *The Journal of Pain* **2000**, 1 (3), 14-18.
31. del Soldato, P.; Sorrentino, R.; Pinto, A., NO-aspirins: a class of new anti-inflammatory and antithrombotic agents. *Trends in Pharmacological Sciences* **1999**, 20 (8), 319-323.
32. Al-Swayeh, O.; Clifford, R.; Del Soldato, P.; Moore, P. J., A comparison of the anti-inflammatory and anti-nociceptive activity of nitroaspirin and aspirin. *British Journal of Pharmacology* **2000**, 129 (2), 343-350.

33. Garrison, C.; Dougherty, P.; Kajander, K.; Carlton, S., Staining of glial fibrillary acidic protein (GFAP) in lumbar spinal cord increases following a sciatic nerve constriction injury. *Brain Research* **1991**, 565 (1), 1-7.
34. Garrison, C. J.; Dougherty, P. M.; Carlton, S. M., GFAP expression in lumbar spinal cord of naive and neuropathic rats treated with MK-801. *Experimental Neurology* **1994**, 129 (2), 237-243.
35. Ji, R.-R.; Chamesian, A.; Zhang, Y.-Q., Pain regulation by non-neuronal cells and inflammation. *Science* **2016**, 354 (6312), 572-577.
36. Caterina, M. J.; Leffler, A.; Malmberg, A. B.; Martin, W.; Trafton, J.; Petersen-Zeitz, K.; Koltzenburg, M.; Basbaum, A.; Julius, D., Impaired nociception and pain sensation in mice lacking the capsaicin receptor. *Science* **2000**, 288 (5464), 306-313.
37. Davis, J. B.; Gray, J.; Gunthorpe, M. J.; Hatcher, J. P.; Davey, P. T.; Overend, P.; Harries, M. H.; Latcham, J.; Clapham, C.; Atkinson, K., Vanilloid receptor-1 is essential for inflammatory thermal hyperalgesia. *Nature* **2000**, 405 (6783), 183.
38. Old, E. A.; Nadkarni, S.; Grist, J.; Gentry, C.; Bevan, S.; Kim, K.-W.; Mogg, A. J.; Perretti, M.; Malcangio, M., Monocytes expressing CX3CR1 orchestrate the development of vincristine-induced pain. *The Journal of Clinical Investigation* **2014**, 124 (5), 2023-2036.
39. Peng, J.; Gu, N.; Zhou, L.; Eyo, U. B.; Murugan, M.; Gan, W.-B.; Wu, L.-J., Microglia and monocytes synergistically promote the transition from acute to chronic pain after nerve injury. *Nature Communications* **2016**, 7, 12029.
40. Vicuña, L.; Strohlic, D. E.; Latremoliere, A.; Bali, K. K.; Simonetti, M.; Husainie, D.; Prokosch, S.; Riva, P.; Griffin, R. S.; Njoo, C., The serine protease inhibitor SerpinA3N attenuates neuropathic pain by inhibiting T cell-derived leukocyte elastase. *Nature Medicine* **2015**, 21 (5), 518.
41. Costigan, M.; Moss, A.; Latremoliere, A.; Johnston, C.; Verma-Gandhu, M.; Herbert, T. A.; Barrett, L.; Brenner, G. J.; Vardeh, D.; Woolf, C. J., T-cell infiltration and signaling in the adult dorsal spinal cord is a major contributor to neuropathic pain-like hypersensitivity. *Journal of Neuroscience* **2009**, 29 (46), 14415-14422.
42. Sorge, R. E.; Mapplebeck, J. C.; Rosen, S.; Beggs, S.; Taves, S.; Alexander, J. K.; Martin, L. J.; Austin, J.-S.; Sotocinal, S. G.; Chen, D., Different immune cells mediate mechanical pain hypersensitivity in male and female mice. *Nature Neuroscience* **2015**, 18 (8), 1081.
43. Baumbauer, K. M.; DeBerry, J. J.; Adelman, P. C.; Miller, R. H.; Hachisuka, J.; Lee, K. H.; Ross, S. E.; Koerber, H. R.; Davis, B. M.; Albers, K. M., Keratinocytes can modulate and directly initiate nociceptive responses. *Elife* **2015**, 4, e09674.
44. Fell, G. L.; Robinson, K. C.; Mao, J.; Woolf, C. J.; Fisher, D. E., Skin β -endorphin mediates addiction to UV light. *Cell* **2014**, 157 (7), 1527-1534.
45. Moore, C.; Cevikbas, F.; Pasolli, H. A.; Chen, Y.; Kong, W.; Kempkes, C.; Parekh, P.; Lee, S. H.; Kontchou, N.-A.; Yeh, I., UVB radiation generates sunburn pain and affects skin by activating epidermal TRPV4 ion channels and triggering endothelin-1 signaling. *Proceedings of the National Academy of Sciences* **2013**, 110 (34), E3225-E3234.

46. Guo, W.; Wang, H.; Zou, S.; Gu, M.; Watanabe, M.; Wei, F.; Dubner, R.; Huang, G. T. J.; Ren, K., Bone marrow stromal cells produce long-term pain relief in rat models of persistent pain. *Stem Cells* **2011**, 29 (8), 1294-1303.
47. Chen, G.; Park, C.-K.; Xie, R.-G.; Ji, R.-R., Intrathecal bone marrow stromal cells inhibit neuropathic pain via TGF- β secretion. *The Journal of Clinical Investigation* **2015**, 125 (8), 3226-3240.
48. Selvaraj, D.; Gangadharan, V.; Michalski, C. W.; Kurejova, M.; Stösser, S.; Srivastava, K.; Schweizerhof, M.; Waltenberger, J.; Ferrara, N.; Heppenstall, P., A functional role for VEGFR1 expressed in peripheral sensory neurons in cancer pain. *Cancer Cell* **2015**, 27 (6), 780-796.
49. Xu, Q.; Zhang, X.-M.; Duan, K.-Z.; Gu, X.-Y.; Han, M.; Liu, B.-L.; Zhao, Z.-Q.; Zhang, Y.-Q., Peripheral TGF- β 1 signaling is a critical event in bone cancer-induced hyperalgesia in rodents. *Journal of Neuroscience* **2013**, 33 (49), 19099-19111.
50. Yang, Y.; Li, H.; Li, T.-T.; Luo, H.; Gu, X.-Y.; Lü, N.; Ji, R.-R.; Zhang, Y.-Q., Delayed activation of spinal microglia contributes to the maintenance of bone cancer pain in female Wistar rats via P2X7 receptor and IL-18. *Journal of Neuroscience* **2015**, 35 (20), 7950-7963.
51. Fischer, H. P., Towards quantitative biology: integration of biological information to elucidate disease pathways and to guide drug discovery. *Biotechnology Annual Review* **2005**, 11, 1-68.
52. Woolf, C. J., Dissecting out mechanisms responsible for peripheral neuropathic pain: implications for diagnosis and therapy. *Life Sciences* **2004**, 74 (21), 2605-2610.
53. Zimmermann, M., Pathobiology of neuropathic pain. *European Journal of Pharmacology* **2001**, 429 (1), 23-37.
54. Milligan, E. D.; Watkins, L. R., Pathological and protective roles of glia in chronic pain. *Nature Reviews Neuroscience* **2009**, 10 (1), 23-36.
55. Watkins, L. R.; Maier, S. F., Glia: a novel drug discovery target for clinical pain. *Nature Reviews Drug Discovery* **2003**, 2 (12), 973-985.
56. Watkins, L. R.; Milligan, E. D.; Maier, S. F., Glial activation: a driving force for pathological pain. *Trends in Neurosciences* **2001**, 24 (8), 450-455.
57. Hanisch, U. K., Microglia as a source and target of cytokines. *Glia* **2002**, 40 (2), 140-155.
58. Denk, F.; Crow, M.; Didangelos, A.; Lopes, D. M.; McMahon, S. B., Persistent alterations in microglial enhancers in a model of chronic pain. *Cell Reports* **2016**, 15 (8), 1771-1781.
59. Grace, P. M.; Hutchinson, M. R.; Maier, S. F.; Watkins, L. R., Pathological pain and the neuroimmune interface. *Nature Reviews Immunology* **2014**, 14 (4), 217.
60. Tsuda, M.; Shigemoto-Mogami, Y.; Koizumi, S.; Mizokoshi, A.; Kohsaka, S.; Salter, M. W.; Inoue, K., P2X4 receptors induced in spinal microglia gate tactile allodynia after nerve injury. *Nature* **2003**, 424 (6950), 778-783.
61. Clark, A. K.; Yip, P. K.; Grist, J.; Gentry, C.; Staniland, A. A.; Marchand, F.; Dehvari, M.; Wotherspoon, G.; Winter, J.; Ullah, J., Inhibition of spinal microglial cathepsin S for the reversal of neuropathic pain. *Proceedings of the National Academy of Sciences* **2007**, 104 (25), 10655-10660.

62. Guan, Z.; Kuhn, J. A.; Wang, X.; Colquitt, B.; Solorzano, C.; Vaman, S.; Guan, A. K.; Evans-Reinsch, Z.; Braz, J.; Devor, M., Injured sensory neuron-derived CSF1 induces microglial proliferation and DAP12-dependent pain. *Nature Neuroscience* **2016**, 19 (1), 94.
63. Coull, J. A.; Beggs, S.; Boudreau, D.; Boivin, D.; Tsuda, M.; Inoue, K.; Gravel, C.; Salter, M. W.; De Koninck, Y., BDNF from microglia causes the shift in neuronal anion gradient underlying neuropathic pain. *Nature* **2005**, 438 (7070), 1017.
64. Jiang, B.-C.; Cao, D.-L.; Zhang, X.; Zhang, Z.-J.; He, L.-N.; Li, C.-H.; Zhang, W.-W.; Wu, X.-B.; Berta, T.; Ji, R.-R., CXCL13 drives spinal astrocyte activation and neuropathic pain via CXCR5. *The Journal of Clinical Investigation* **2016**, 126 (2), 745-761.
65. Chen, G.; Park, C.-K.; Xie, R.-G.; Berta, T.; Nedergaard, M.; Ji, R.-R., Connexin-43 induces chemokine release from spinal cord astrocytes to maintain late-phase neuropathic pain in mice. *Brain* **2014**, 137 (8), 2193-2209.
66. Kim, D.-S.; Li, K.-W.; Boroujerdi, A.; Yu, Y. P.; Zhou, C.-Y.; Deng, P.; Park, J.; Zhang, X.; Lee, J.; Corpe, M., Thrombospondin-4 contributes to spinal sensitization and neuropathic pain states. *Journal of Neuroscience* **2012**, 32 (26), 8977-8987.
67. Kim, J.; Moon, S. H.; Shin, Y.-C.; Jeon, J.-H.; Park, K. J.; Lee, K. P.; So, I., Intracellular spermine blocks TRPC4 channel via electrostatic interaction with C-terminal negative amino acids. *Pflügers Archiv-European Journal of Physiology* **2016**, 468 (4), 551-561.
68. Zarpelon, A. C.; Rodrigues, F. C.; Lopes, A. H.; Souza, G. R.; Carvalho, T. T.; Pinto, L. G.; Xu, D.; Ferreira, S. H.; Alves-Filho, J. C.; McInnes, I. B., Spinal cord oligodendrocyte-derived alarmin IL-33 mediates neuropathic pain. *The FASEB Journal* **2015**, 30 (1), 54-65.
69. Liang, L.; Zhao, J.-Y.; Gu, X.; Wu, S.; Mo, K.; Xiong, M.; Marie Lutz, B.; Bekker, A.; Tao, Y.-X., G9a inhibits CREB-triggered expression of mu opioid receptor in primary sensory neurons following peripheral nerve injury. *Molecular Pain* **2016**, 12, 1744806916682242.
70. Rosen, S.; Ham, B.; Mogil, J. S., Sex differences in neuroimmunity and pain. *Journal of Neuroscience Research* **2017**, 95 (1-2), 500-508.
71. Yu, S.; Chen, C.; Pan, Y.; Kurz, M. C.; Datner, E.; Hendry, P. L.; Velilla, M. A.; Lewandowski, C.; Pearson, C.; Domeier, R., Genes known to escape X chromosome inactivation predict co-morbid chronic musculoskeletal pain and posttraumatic stress symptom development in women following trauma exposure. *American Journal of Medical Genetics Part B: Neuropsychiatric Genetics* **2018**, 180 (6), 415-427.
72. Marchand, F.; Perretti, M.; McMahon, S. B., Role of the immune system in chronic pain. *Nature Reviews Neuroscience* **2005**, 6 (7), 521-532.
73. Allan, S. M.; Tyrrell, P. J.; Rothwell, N. J., Interleukin-1 and neuronal injury. *Nature Reviews Immunology* **2005**, 5 (8), 629-640.
74. Aronica, E.; Gorter, J.; Rozemuller, A.; Yankaya, B.; Troost, D., Activation of metabotropic glutamate receptor 3 enhances interleukin (IL)-1 β -stimulated release of IL-6 in cultured human astrocytes. *Neuroscience* **2005**, 130 (4), 927-933.

75. Taylor, D.; Diemel, L.; Cuzner, M.; Pocock, J., Activation of group II metabotropic glutamate receptors underlies microglial reactivity and neurotoxicity following stimulation with chromogranin A, a peptide up-regulated in Alzheimer's disease. *Journal of Neurochemistry* **2002**, 82 (5), 1179-1191.
76. Lee, J. Y.; Jhun, B. S.; Oh, Y. T.; Lee, J. H.; Choe, W.; Baik, H. H.; Ha, J.; Yoon, K.-S.; Kim, S. S.; Kang, I., Activation of adenosine A3 receptor suppresses lipopolysaccharide-induced TNF- α production through inhibition of PI 3-kinase/Akt and NF- κ B activation in murine BV2 microglial cells. *Neuroscience Letters* **2006**, 396 (1), 1-6.
77. Kingham, P.; Cuzner, M.; Pocock, J. J., Apoptotic pathways mobilized in microglia and neurones as a consequence of chromogranin A-induced microglial activation. *Journal of Neurochemistry* **1999**, 73 (2), 538-547.
78. Taylor, D. L.; Diemel, L. T.; Pocock, J. M. J., Activation of microglial group III metabotropic glutamate receptors protects neurons against microglial neurotoxicity. *Journal of Neuroscience* **2003**, 23 (6), 2150-2160.
79. Kuhn, S. A.; van Landeghem, F. K.; Zacharias, R.; Färber, K.; Rappert, A.; Pavlovic, S.; Hoffmann, A.; Nolte, C.; Kettenmann, H., Microglia express GABAB receptors to modulate interleukin release. *Molecular and Cellular Neuroscience* **2004**, 25 (2), 312-322.
80. Ramírez, B. G.; Blázquez, C.; del Pulgar, T. G.; Guzmán, M.; de Ceballos, M. L., Prevention of Alzheimer's disease pathology by cannabinoids: neuroprotection mediated by blockade of microglial activation. *Journal of Neuroscience* **2005**, 25 (8), 1904-1913.
81. Wallace, D. R., HIV neurotoxicity: potential therapeutic interventions. *BioMed Research International* **2006**, 65741.
82. Chao, C. C.; Hu, S.; Shark, K. B.; Sheng, W. S.; Gekker, G.; Peterson, P. K., Activation of mu opioid receptors inhibits microglial cell chemotaxis. *Journal of Pharmacology Experimental Therapeutics* **1997**, 281 (2), 998-1004.
83. Fujita, H.; Tanaka, J.; Maeda, N.; Sakanaka, M., Adrenergic agonists suppress the proliferation of microglia through β 2-adrenergic receptor. *Neuroscience Letters* **1998**, 242 (1), 37-40.
84. Heneka, M. T.; Galea, E.; Gavriluyk, V.; Dumitrescu-Ozimek, L.; Daeschner, J.; O'Banion, M. K.; Weinberg, G.; Klockgether, T.; Feinstein, D. L., Noradrenergic depletion potentiates β -amyloid-induced cortical inflammation: implications for Alzheimer's disease. *Journal of Neuroscience* **2002**, 22 (7), 2434-2442.
85. Shytle, R. D.; Mori, T.; Townsend, K.; Vendrame, M.; Sun, N.; Zeng, J.; Ehrhart, J.; Silver, A. A.; Sanberg, P. R.; Tan, J., Cholinergic modulation of microglial activation by α 7 nicotinic receptors. *Journal of Neurochemistry* **2004**, 89 (2), 337-343.
86. De Simone, R.; Ajmone-Cat, M. A.; Carnevale, D.; Minghetti, L., Activation of α 7 nicotinic acetylcholine receptor by nicotine selectively up-regulates cyclooxygenase-2 and prostaglandin E2 in rat microglial cultures. *Journal of Neuroinflammation* **2005**, 2 (1), 4.
87. Suzuki, T.; Hide, I.; Matsubara, A.; Hama, C.; Harada, K.; Miyano, K.; Andrä, M.; Matsubayashi, H.; Sakai, N.; Kohsaka, S., Microglial α 7 nicotinic acetylcholine receptors drive a phospholipase C/IP3

pathway and modulate the cell activation toward a neuroprotective role. *Journal of Neuroscience Research* **2006**, 83 (8), 1461-1470.

88. Jarvis, M. F., The neural–glial purinergic receptor ensemble in chronic pain states. *Trends in Neurosciences* **2010**, 33 (1), 48-57.

89. Ji, R.-R.; Berta, T.; Nedergaard, M., Glia and pain: is chronic pain a gliopathy? *Pain* **2013**, 154, S10-S28.

90. Nörenberg, W.; Langosch, J.; Gebicke-Haerter, P.; Illes, P., Characterization and possible function of adenosine 5'-triphosphate receptors in activated rat microglia. *British Journal of Pharmacology* **1994**, 111 (3), 942-950.

91. James, G.; Butt, A. M., P2Y and P2X purinoceptor mediated Ca²⁺ signalling in glial cell pathology in the central nervous system. *European Journal of Pharmacology* **2002**, 447 (2-3), 247-260.

92. Saura, J.; Angulo, E.; Ejarque, A.; Casadó, V.; Tusell, J. M.; Moratalla, R.; Chen, J. F.; Schwarzschild, M. A.; Lluís, C.; Franco, R., Adenosine A_{2A} receptor stimulation potentiates nitric oxide release by activated microglia. *Journal of Neurochemistry* **2005**, 95 (4), 919-929.

93. Koizumi, S.; Shigemoto-Mogami, Y.; Nasu-Tada, K.; Shinozaki, Y.; Ohsawa, K.; Tsuda, M.; Joshi, B. V.; Jacobson, K. A.; Kohsaka, S.; Inoue, K., UDP acting at P_{2Y} 6 receptors is a mediator of microglial phagocytosis. *Nature* **2007**, 446 (7139), 1091.

94. Haynes, S. E.; Hollopeter, G.; Yang, G.; Kurpius, D.; Dailey, M. E.; Gan, W.-B.; Julius, D., The P_{2Y} 12 receptor regulates microglial activation by extracellular nucleotides. *Nature Neuroscience* **2006**, 9 (12), 1512.

95. North, R. A., Molecular physiology of P_{2X} receptors. *Physiological Reviews* **2002**, 82 (4), 1013-1067.

96. Dunn, P. M.; Zhong, Y.; Burnstock, G., P_{2X} receptors in peripheral neurons. *Progress in Neurobiology* **2001**, 65 (2), 107-134.

97. Khakh, B. S.; North, R. A., Neuromodulation by extracellular ATP and P_{2X} receptors in the CNS. *Neuron* **2012**, 76 (1), 51-69.

98. Suzuki, T.; Hide, I.; Ido, K.; Kohsaka, S.; Inoue, K.; Nakata, Y., Production and release of neuroprotective tumor necrosis factor by P_{2X}7 receptor-activated microglia. *Journal of Neuroscience* **2004**, 24 (1), 1-7.

99. Ulmann, L.; Hatcher, J. P.; Hughes, J. P.; Chaumont, S.; Green, P. J.; Conquet, F.; Buell, G. N.; Reeve, A. J.; Chessell, I. P.; Rassendren, F., Up-regulation of P_{2X}4 receptors in spinal microglia after peripheral nerve injury mediates BDNF release and neuropathic pain. *Journal of Neuroscience* **2008**, 28 (44), 11263-11268.

100. Inoue, K., The function of microglia through purinergic receptors: neuropathic pain and cytokine release. *Pharmacology Therapeutics* **2006**, 109 (1-2), 210-226.

101. Pocock, J. M.; Kettenmann, H., Neurotransmitter receptors on microglia. *Trends in Neurosciences* **2007**, 30 (10), 527-535.

102. Clark, A. R.; Dean, J. L.; Saklatvala, J., Post-transcriptional regulation of gene expression by mitogen-activated protein kinase p38. *FEBS Letters* **2003**, 546 (1), 37-44.
103. Schäfers, M.; Svensson, C. I.; Sommer, C.; Sorkin, L. S., Tumor necrosis factor- α induces mechanical allodynia after spinal nerve ligation by activation of p38 MAPK in primary sensory neurons. *Journal of Neuroscience* **2003**, 23 (7), 2517-2521.
104. Svensson, C. I.; Hua, X.-Y.; Protter, A. A.; Powell, H. C.; Yaksh, T. L., Spinal p38 MAP kinase is necessary for NMDA-induced spinal PGE₂ release and thermal hyperalgesia. *Neuroreport* **2003**, 14 (8), 1153-1157.
105. Svensson, C. I.; Marsala, M.; Westerlund, A.; Calcutt, N. A.; Campana, W. M.; Freshwater, J. D.; Catalano, R.; Feng, Y.; Protter, A. A.; Scott, B., Activation of p38 mitogen-activated protein kinase in spinal microglia is a critical link in inflammation-induced spinal pain processing. *Journal of Neurochemistry* **2003**, 86 (6), 1534-1544.
106. Zhuang, Z.-Y.; Gerner, P.; Woolf, C. J.; Ji, R.-R., ERK is sequentially activated in neurons, microglia, and astrocytes by spinal nerve ligation and contributes to mechanical allodynia in this neuropathic pain model. *Pain* **2005**, 114 (1), 149-159.
107. Hanisch, U.-K.; Kettenmann, H., Microglia: active sensor and versatile effector cells in the normal and pathologic brain. *Nature Neuroscience* **2007**, 10 (11), 1387-1394.
108. Burnstock, G., Physiology and pathophysiology of purinergic neurotransmission. *Physiological Reviews* **2007**, 87 (2), 659-797.
109. Coull, J. A.; Boudreau, D.; Bachand, K.; Prescott, S. A.; Nault, F.; Sík, A.; De Koninck, P.; De Koninck, Y., Trans-synaptic shift in anion gradient in spinal lamina I neurons as a mechanism of neuropathic pain. *Nature* **2003**, 424 (6951), 938-942.
110. Chessell, I. P.; Hatcher, J. P.; Bountra, C.; Michel, A. D.; Hughes, J. P.; Green, P.; Egerton, J.; Murfin, M.; Richardson, J.; Peck, W. L., Disruption of the P2X₇ purinoceptor gene abolishes chronic inflammatory and neuropathic pain. *Pain* **2005**, 114 (3), 386-396.
111. McGaraughty, S.; Chu, K.; Namovic, M.; Donnelly-Roberts, D.; Harris, R.; Zhang, X.-F.; Shieh, C.-C.; Wismer, C.; Zhu, C.; Gauvin, D., P2X₇-related modulation of pathological nociception in rats. *Neuroscience* **2007**, 146 (4), 1817-1828.
112. Kobayashi, K.; Yamanaka, H.; Fukuoka, T.; Dai, Y.; Obata, K.; Noguchi, K., P2Y₁₂ receptor upregulation in activated microglia is a gateway of p38 signaling and neuropathic pain. *Journal of Neuroscience* **2008**, 28 (11), 2892-2902.
113. Trang, T.; Beggs, S.; Wan, X.; Salter, M. W., P2X₄-receptor-mediated synthesis and release of brain-derived neurotrophic factor in microglia is dependent on calcium and p38-mitogen-activated protein kinase activation. *Journal of Neuroscience* **2009**, 29 (11), 3518-3528.
114. Stokes, L.; Layhadi, J. A.; Bibic, L.; Dhuna, K.; Fountain, S. J., P2X₄ receptor function in the nervous system and current breakthroughs in pharmacology, *Frontiers in Pharmacology* **2017**, 8, 291.

115. Holton, F.; Holton, P., The capillary dilator substances in dry powders of spinal roots; a possible role of adenosine triphosphate in chemical transmission from nerve endings. *The Journal of Physiology* **1954**, 126 (1), 124-140.
116. Holton, P., The liberation of adenosine triphosphate on antidromic stimulation of sensory nerves. *The Journal of Physiology* **1959**, 145 (3), 494-504.
117. Holton, P., Noradrenaline in adrenal medullary tumours. *Nature* **1949**, 163 (4136), 217.
118. Abbracchio, M. P.; Burnstock, G., Purinoceptors: are there families of P2X and P2Y purinoceptors? *Pharmacology & Therapeutics* **1994**, 64 (3), 445-475.
119. Gordon, J. L., Extracellular ATP: effects, sources and fate. *Biochemical Journal* **1986**, 233 (2), 309.
120. Bodin, P.; Burnstock, G., Purinergic signalling: ATP release. *Neurochemical Research* **2001**, 26 (8), 959-969.
121. Burnstock, G., Physiopathological roles of P2X receptors in the central nervous system. *Current Medicinal Chemistry* **2015**, 22 (7), 819-844.
122. Burnstock, G., P2X ion channel receptors and inflammation. *Purinergic Signalling* **2016**, 12 (1), 59-67.
123. Burnstock, G., An introduction to the roles of purinergic signalling in neurodegeneration, neuroprotection and neuroregeneration. *Neuropharmacology* **2016**, 104, 4-17.
124. Navarro, G.; Borroto-Escuela, D. O.; Fuxe, K.; Franco, R., Purinergic signaling in Parkinson's disease. Relevance for treatment. *Neuropharmacology* **2016**, 104, 161-168.
125. Hechler, B.; Gachet, C., P2 receptors and platelet function. *Purinergic Signalling* **2011**, 7 (3), 293.
126. El-Ajouz, S.; Ray, D.; Allsopp, R.; Evans, R., Molecular basis of selective antagonism of the P2X1 receptor for ATP by NF449 and suramin: contribution of basic amino acids in the cysteine-rich loop. *British Journal of Pharmacology* **2012**, 165 (2), 390-400.
127. Kassack, M. U.; Braun, K.; Ganso, M.; Ullmann, H.; Nickel, P.; Böing, B.; Müller, G.; Lambrecht, G., Structure–activity relationships of analogues of NF449 confirm NF449 as the most potent and selective known P2X1 receptor antagonist. *European Journal of Medicinal Chemistry* **2004**, 39 (4), 345-357.
128. Ford, A. P. W.; Gever, J. R.; Nunn, P. A.; Zhong, Y.; Cefalu, J. S.; Dillon, M. P.; Cockayne, D. A., Purinoceptors as therapeutic targets for lower urinary tract dysfunction. *British Journal of Pharmacology* **2006**, 147 (S2), S132-S143.
129. Jaime-Figueroa, S.; Greenhouse, R.; Padilla, F.; Dillon, M.; Gever, J.; Ford, A., Discovery and synthesis of a novel and selective drug-like P2X1 antagonist. *Bioorganic & Medicinal Chemistry* **2005**, 15 (13), 3292-3295.
130. Gever, J. R.; Cockayne, D. A.; Dillon, M. P.; Burnstock, G.; Ford, A. P., Pharmacology of P2X channels. *Pflugers Archiv* **2006**, 452 (5), 513-537.

131. Trujillo, C. A.; Nery, A. A.; Martins, A. H. B.; Majumder, P.; Gonzalez, F. A.; Ulrich, H., Inhibition mechanism of the recombinant rat P2X2 receptor in glial cells by suramin and TNP-ATP. *Biochemistry* **2006**, 45 (1), 224-233.
132. Wolf, C.; Rosefort, C.; Fallah, G.; Kassack, M. U.; Hamacher, A.; Bodnar, M.; Wang, H.; Illes, P.; Kless, A.; Bahrenberg, G., Molecular determinants of potent P2X2 antagonism identified by functional analysis, mutagenesis, and homology docking. *Molecular Pharmacology* **2011**, 79 (4), 649-661.
133. Baqi, Y.; Hausmann, R.; Rosefort, C.; Rettinger, J. r.; Schmalzing, G. n.; Müller, C. E., Discovery of potent competitive antagonists and positive modulators of the P2X2 receptor. *Journal of Medicinal Chemistry* **2011**, 54 (3), 817-830.
134. Coddou, C.; Yan, Z.; Obsil, T.; Huidobro-Toro, J. P.; Stojilkovic, S. S., Activation and regulation of purinergic P2X receptor channels. *Pharmacological Reviews* **2011**, 63 (3), 641-683.
135. Carter, D. S.; Alam, M.; Cai, H.; Dillon, M. P.; Ford, A. P.; Gever, J. R.; Jahangir, A.; Lin, C.; Moore, A. G.; Wagner, P. J., Identification and SAR of novel diaminopyrimidines. Part 1: the discovery of RO-4, a dual P2X3/P2X2/3 antagonist for the treatment of pain. *Bioorganic & Medicinal Chemistry Letters* **2009**, 19 (6), 1628-1631.
136. Jahangir, A.; Alam, M.; Carter, D. S.; Dillon, M. P.; Du Bois, D. J.; Ford, A. P.; Gever, J. R.; Lin, C.; Wagner, P. J.; Zhai, Y., Identification and SAR of novel diaminopyrimidines. Part 2: The discovery of RO-51, a potent and selective, dual P2X3/P2X2/3 antagonist for the treatment of pain. *Bioorganic & Medicinal Chemistry Letters* **2009**, 19 (6), 1632-1635.
137. Jung, K.-Y.; Moon, H. D.; Lee, G. E.; Lim, H.-H.; Park, C.-S.; Kim, Y.-C., Structure– Activity Relationship Studies of Spinorphin as a Potent and Selective Human P2X3 Receptor Antagonist. *Journal of Medicinal Chemistry* **2007**, 50 (18), 4543-4547.
138. Grishin, E. V.; Savchenko, G. A.; Vassilevski, A. A.; Korolkova, Y. V.; Boychuk, Y. A.; Viatchenko-Karpinski, V. Y.; Nadezhdin, K. D.; Arseniev, A. S.; Pluzhnikov, K. A.; Kulyk, V. B., Novel peptide from spider venom inhibits P2X3 receptors and inflammatory pain. *Annals of Neurology* **2010**, 67 (5), 680-683.
139. Ulmann, L.; Levavasseur, F.; Avignone, E.; Peyroutou, R.; Hirbec, H.; Audinat, E.; Rassendren, F., Involvement of P2X4 receptors in hippocampal microglial activation after status epilepticus. *Glia* **2013**, 61 (8), 1306-1319.
140. Varma, R.; Chai, Y.; Troncoso, J.; Gu, J.; Xing, H.; Stojilkovic, S.; Mattson, M.; Haughey, N., Amyloid- β induces a caspase-mediated cleavage of P2X4 to promote purinotoxicity. *Neuromolecular Medicine* **2009**, 11 (2), 63-75.
141. Bartlett, R.; Stokes, L.; Sluyter, R., The P2X7 receptor channel: recent developments and the use of P2X7 antagonists in models of disease. *Pharmacological Reviews* **2014**, 66 (3), 638-675.
142. Brough, D.; Le Feuvre, R. A.; Iwakura, Y.; Rothwell, N. J., Purinergic (P2X7) receptor activation of microglia induces cell death via an interleukin-1-independent mechanism. *Molecular and Cellular Neuroscience* **2002**, 19 (2), 272-280.

143. Burnstock, G.; Di Virgilio, F., Purinergic signalling and cancer. *Purinergic Signalling* **2013**, 9 (4), 491-540.
144. Gao, M.; Wang, M.; Green, M. A.; Hutchins, G. D.; Zheng, Q.-H., Synthesis of [¹¹C] GSK1482160 as a new PET agent for targeting P2X7 receptor. *Bioorganic & Medicinal Chemistry Letters* **2015**, 25 (9), 1965-1970.
145. Baudelet, D.; Lipka, E.; Millet, R.; Ghinet, A., Involvement of the P2X7 purinergic receptor in inflammation: an update of antagonists series since 2009 and their promising therapeutic potential. *Current Medicinal Chemistry* **2015**, 22 (6), 713-729.
146. Bhattacharya, A.; Wang, Q.; Ao, H.; Shoblock, J. R.; Lord, B.; Aluisio, L.; Fraser, I.; Nepomuceno, D.; Neff, R. A.; Welty, N., Pharmacological characterization of a novel centrally permeable P2X7 receptor antagonist: JNJ-47965567. *British Journal of Pharmacology* **2013**, 170 (3), 624-640.
147. Letavic, M. A.; Lord, B.; Bischoff, F.; Hawryluk, N. A.; Pieters, S.; Rech, J. C.; Sales, Z.; Velter, A. I.; Ao, H.; Bonaventure, P., Synthesis and pharmacological characterization of two novel, brain penetrating P2X7 antagonists. *ACS Medicinal Chemistry Letters* **2013**, 4 (4), 419-422.
148. Rudolph, D. A.; Alcazar, J.; Ameriks, M. K.; Anton, A. B.; Ao, H.; Bonaventure, P.; Carruthers, N. I.; Chrovian, C. C.; De Angelis, M.; Lord, B., Novel methyl substituted 1-(5, 6-dihydro-[1, 2, 4] triazolo [4, 3-a] pyrazin-7 (8H)-yl) methanones are P2X7 antagonists. *Bioorganic & Medicinal Chemistry Letters* **2015**, 25 (16), 3157-3163.
149. Keystone, E. C.; Wang, M. M.; Layton, M.; Hollis, S.; McInnes, I. B., Clinical evaluation of the efficacy of the P2X7 purinergic receptor antagonist AZD9056 on the signs and symptoms of rheumatoid arthritis in patients with active disease despite treatment with methotrexate or sulphasalazine. *Annals of the Rheumatic Diseases* **2012**, 71 (10), 1630-1635.
150. Stock, T. C.; Bloom, B. J.; Wei, N.; Ishaq, S.; Park, W.; Wang, X.; Gupta, P.; Mebus, C. A., Efficacy and safety of CE-224,535, an antagonist of P2X7 receptor, in treatment of patients with rheumatoid arthritis inadequately controlled by methotrexate. *The Journal of Rheumatology* **2012**, 39 (4), 720-727.
151. Bernier, L. P.; Ase, A. R.; Seguela, P., P2X receptor channels in chronic pain pathways. *British Journal of Pharmacology* **2018**, 175 (12), 2219-2230.
152. North, R. A.; Jarvis, M. F., P2X receptors as drug targets. *Molecular Pharmacology* **2013**, 83 (4), 759-769.
153. Ase, A. R.; Honson, N. S.; Zaghdane, H.; Pfeifer, T. A.; Seguela, P., Identification and characterization of a selective allosteric antagonist of human P2X4 receptor channels. *Molecular Pharmacology* **2015**, 87 (4), 606-16.
154. Khakh, B. S.; Bao, X. R.; Labarca, C.; Lester, H. A., Neuronal P2X transmitter-gated cation channels change their ion selectivity in seconds. *Nature Neuroscience* **1999**, 2 (4), 322-330.
155. Khakh, B. S.; Lester, H. A., Dynamic selectivity filters in ion channels. *Neuron* **1999**, 23 (4), 653-658.

156. Khakh, B. S.; Proctor, W. R.; Dunwiddie, T. V.; Labarca, C.; Lester, H. A., Allosteric control of gating and kinetics at P2X4 receptor channels. *Journal of Neuroscience* **1999**, 19 (17), 7289-7299.
157. Zemkova, H.; Tvrdonova, V.; Bhattacharya, A.; Jindrichova, M., Allosteric modulation of ligand gated ion channels by ivermectin. *Physiological Research* **2014**, 63, S215.
158. Xu, J.; Bernstein, A. M.; Wong, A.; Lu, X.-H.; Khoja, S.; Yang, X. W.; Davies, D. L.; Micevych, P.; Sofroniew, M. V.; Khakh, B. S., P2X4 Receptor Reporter Mice: Sparse Brain Expression and Feeding-Related Presynaptic Facilitation in the Arcuate Nucleus. *Journal of Neuroscience* **2016**, 36 (34), 8902-8920.
159. Williams, W. A.; Linley, J. E.; Jones, C. A.; Shibata, Y.; Snijder, A.; Button, J.; Hatcher, J. P.; Huang, L.; Taddese, B.; Thornton, P., Antibodies binding the head domain of P2X4 inhibit channel function and reverse neuropathic pain. *Pain* **2019**, 160 (9), 1989-2003.
160. Nagata, K.; Imai, T.; Yamashita, T.; Tsuda, M.; Tozaki-Saitoh, H.; Inoue, K., Antidepressants inhibit P2X 4 receptor function: a possible involvement in neuropathic pain relief. *Molecular Pain* **2009**, 5 (1), 20.
161. Sim, J.; North, R., Amitriptyline does not block the action of ATP at human P2X4 receptor. *British Journal of Pharmacology* **2010**, 160 (1), 88-92.
162. Tian, M.; Abdelrahman, A.; Weinhausen, S.; Hinz, S.; Weyer, S.; Dosa, S.; El-Tayeb, A.; Müller, C. E., Carbamazepine derivatives with P2X4 receptor-blocking activity. *Bioorganic Medicinal Chemistry* **2014**, 22 (3), 1077-1088.
163. Buell, G.; Lewis, C.; Collo, G.; North, R.; Surprenant, A., An antagonist-insensitive P2X receptor expressed in epithelia and brain. *The EMBO Journal* **1996**, 15 (1), 55-62.
164. Balázs, B.; Dankó, T.; Kovács, G.; Köles, L.; Hediger, M. A.; Zsembery, Á., Investigation of the inhibitory effects of the benzodiazepine derivative, 5-BDBD on P2X4 purinergic receptors by two complementary methods. *Cellular Physiology and Biochemistry* **2013**, 32 (1), 11-24.
165. Ase, A. R.; Honson, N. S.; Zaghdane, H.; Pfeifer, T. A.; Séguéla, P., Identification and characterization of a selective allosteric antagonist of human P2X4 receptor channels. *Molecular Pharmacology* **2015**, 87 (4), 606-616.
166. Hernandez-Olmos, V.; Abdelrahman, A.; El-Tayeb, A.; Freudendahl, D.; Weinhausen, S.; Muller, C. E., N-substituted phenoxazine and acridone derivatives: structure-activity relationships of potent P2X4 receptor antagonists. *Journal of Medicinal Chemistry* **2012**, 55 (22), 9576-88.
167. Matsumura, Y.; Yamashita, T.; Sasaki, A.; Nakata, E.; Kohno, K.; Masuda, T.; Tozaki-Saitoh, H.; Imai, T.; Kuraishi, Y.; Tsuda, M., A novel P2X4 receptor-selective antagonist produces anti-allodynic effect in a mouse model of herpetic pain. *Scientific Reports* **2016**, 6, 32461.
168. Abdelrahman, A.; Namasivayam, V.; Hinz, S.; Schiedel, A. C.; Köse, M.; Burton, M.; El-Tayeb, A.; Gillard, M.; Bajorath, J.; de Ryck, M., Characterization of P2X4 receptor agonists and antagonists by calcium influx and radioligand binding studies. *Biochemical Pharmacology* **2017**, 125, 41-54.
169. Muller, C., Medicinal chemistry of P2X receptors: allosteric modulators. *Current Medicinal Chemistry* **2015**, 22 (7), 929-941.

170. Matsumura, Y.; Yamashita, T.; Sasaki, A.; Nakata, E.; Kohno, K.; Masuda, T.; Tozaki-Saitoh, H.; Imai, T.; Kuraishi, Y.; Tsuda, M., A novel P2X4 receptor-selective antagonist produces anti-allodynic effect in a mouse model of herpetic pain. *Scientific Reports* **2016**, *6*, 32461.
171. Beswick, P.; Wahab, B.; Honey, M. A.; Paradowski, M.; Jiang, K.; Lochner, M.; Murrell-Lagnado, R. D.; Thompson, A. J., A challenge finding P2X1 and P2X4 ligands. *Neuropharmacology* **2019**, 107674.
172. Hille, B., Ion channels of excitable membranes. Sinauer Sunderland, MA: **2001**; Vol. 507.
173. Markman, J. D.; Dworkin, R. H., Ion channel targets and treatment efficacy in neuropathic pain. *The Journal of Pain* **2006**, *7* (1), S38-S47.
174. Dib-Hajj, S. D.; Binshtok, A. M.; Cummins, T. R.; Jarvis, M. F.; Samad, T.; Zimmermann, K., Voltage-gated sodium channels in pain states: role in pathophysiology and targets for treatment. *Brain Research Reviews* **2009**, *60* (1), 65-83.
175. Cox, J. J.; Reimann, F.; Nicholas, A. K.; Thornton, G.; Roberts, E.; Springell, K.; Karbani, G.; Jafri, H.; Mannan, J.; Raashid, Y., An SCN9A channelopathy causes congenital inability to experience pain. *Nature* **2006**, *444* (7121), 894.
176. Sun, S.; J Cohen, C.; M Dehnhardt, C., Inhibitors of voltage-gated sodium channel Nav1. 7: patent applications since 2010. *Pharmaceutical Patent Analyst* **2014**, *3* (5), 509-521.
177. Klint, J. K.; Senff, S.; Rupasinghe, D. B.; Er, S. Y.; Herzig, V.; Nicholson, G. M.; King, G. F., Spider-venom peptides that target voltage-gated sodium channels: pharmacological tools and potential therapeutic leads. *Toxicon* **2012**, *60* (4), 478-491.
178. Bosmans, F.; Swartz, K. J., Targeting voltage sensors in sodium channels with spider toxins. *Trends in Pharmacological Sciences* **2010**, *31* (4), 175-182.
179. King, G. F., Venoms as a platform for human drugs: translating toxins into therapeutics. *Expert Opinion on Biological Therapy* **2011**, *11* (11), 1469-1484.
180. Kalia, J.; Milescu, M.; Salvatierra, J.; Wagner, J.; Klint, J. K.; King, G. F.; Olivera, B. M.; Bosmans, F., From foe to friend: using animal toxins to investigate ion channel function. *Journal of Molecular Biology* **2015**, *427* (1), 158-175.
181. Estrada, G.; Villegas, E.; Corzo, G., Spider venoms: a rich source of acylpolyamines and peptides as new leads for CNS drugs. *Natural Product Reports* **2007**, *24* (1), 145-161.
182. Emery, E. C.; Luiz, A. P.; Wood, J. N., Nav1. 7 and other voltage-gated sodium channels as drug targets for pain relief. *Expert Opinion on Therapeutic Targets* **2016**, *20* (8), 975-983.
183. Cardoso, F. C.; Dekan, Z.; Rosengren, K. J.; Erickson, A.; Vetter, I.; Deuis, J. R.; Herzig, V.; Alewood, P. F.; King, G. F.; Lewis, R. J., Identification and characterization of ProTx-III [μ -TRTX-Tp1a], a new voltage-gated sodium channel inhibitor from venom of the tarantula *Thrixopelma pruriens*. *Molecular Pharmacology* **2015**, *88* (2), 291-303.
184. Escoubas, P.; Diochot, S.; Célérier, M.-L.; Nakajima, T.; Lazdunski, M., Novel tarantula toxins for subtypes of voltage-dependent potassium channels in the Kv2 and Kv4 subfamilies. *Molecular Pharmacology* **2002**, *62* (1), 48-57.

185. Mazzuca, M.; Heurteaux, C.; Alloui, A.; Diochot, S.; Baron, A.; Voilley, N.; Blondeau, N.; Escoubas, P.; Gélot, A.; Cupo, A., A tarantula peptide against pain via ASIC1a channels and opioid mechanisms. *Nature Neuroscience* **2007**, 10 (8), 943-945.
186. Dutertre, S.; Lewis, R. J., Use of venom peptides to probe ion channel structure and function. *Journal of Biological Chemistry* **2010**, 285 (18), 13315-13320.
187. Paterson, I.; Anderson, E. A., The renaissance of natural products as drug candidates. *Science* **2005**, 310 (5747), 451-453.
188. Butler, M. S., The role of natural product chemistry in drug discovery. *Journal of Natural Products* **2004**, 67 (12), 2141-2153.
189. Escoubas, P.; Rash, L., Tarantulas: eight-legged pharmacists and combinatorial chemists. *Toxicon* **2004**, 43 (5), 555-574.
190. Escoubas, P.; Sollod, B.; King, G. F., Venom landscapes: mining the complexity of spider venoms via a combined cDNA and mass spectrometric approach. *Toxicon* **2006**, 47 (6), 650-663.
191. Klint, J. K.; Smith, J. J.; Vetter, I.; Rupasinghe, D. B.; Er, S. Y.; Senff, S.; Herzig, V.; Mobli, M.; Lewis, R. J.; Bosmans, F., Seven novel modulators of the analgesic target NaV1.7 uncovered using a high-throughput venom-based discovery approach. *British Journal of Pharmacology* **2015**, 172 (10), 2445-2458.
192. King, G. F.; Hardy, M. C., Spider-venom peptides: structure, pharmacology, and potential for control of insect pests. *Annual Review of Entomology* **2013**, 58, 475-496.
193. Lewis, R. J.; Garcia, M. L., Therapeutic potential of venom peptides. *Nature Reviews Drug Discovery* **2003**, 2 (10), 790-802.
194. Cushman, D. W.; Ondetti, M. A., History of the design of captopril and related inhibitors of angiotensin converting enzyme. *Hypertension* **1991**, 17 (4), 589-592.
195. Escoubas, P.; King, G. F., Venomics as a drug discovery platform. *Expert Review of Proteomics* **2009**, 6 (3), 221-224.
196. Vetter, I.; Davis, J. L.; Rash, L. D.; Anangi, R.; Mobli, M.; Alewood, P. F.; Lewis, R. J.; King, G. F., Venomics: a new paradigm for natural products-based drug discovery. *Amino Acids* **2011**, 40 (1), 15-28.
197. Liang, S., Proteome and peptidome profiling of spider venoms. *Expert Review of Proteomics* **2008**, 5 (5), 731-746.
198. Herzig, V.; Wood, D. L.; Newell, F.; Chaumeil, P.-A.; Kaas, Q.; Binford, G. J.; Nicholson, G. M.; Gorse, D.; King, G. F., ArachnoServer 2.0, an updated online resource for spider toxin sequences and structures. *Nucleic Acids Research* **2010**, D653-D657.
199. Miller, C., The charybdotoxin family of K⁺ channel-blocking peptides. *Neuron* **1995**, 15 (1), 5-10.
200. Terlau, H.; Olivera, B. M., Conus venoms: a rich source of novel ion channel-targeted peptides. *Physiological Reviews* **2004**, 84 (1), 41-68.

201. Schroeder, F. C.; Taggi, A. E.; Gronquist, M.; Malik, R. U.; Grant, J. B.; Eisner, T.; Meinwald, J., NMR-spectroscopic screening of spider venom reveals sulfated nucleosides as major components for the brown recluse and related species. *Proceedings of the National Academy of Sciences* **2008**, 105 (38), 14283-14287.
202. Vassilevski, A.; Kozlov, S.; Grishin, E., Molecular diversity of spider venom. *Biochemistry (Moscow)* **2009**, 74 (13), 1505-1534.
203. Kuhn-Nentwig, L.; Stöcklin, R.; Nentwig, W., Venom composition and strategies in spiders: is everything possible? *Advances in Insect Physiology* **2011**, 40, 1.
204. Silva, J. P.; Suckling, J.; Ushkaryov, Y., Penelope's web: using α -latrotoxin to untangle the mysteries of exocytosis. *Journal of Neurochemistry* **2009**, 111 (2), 275-290.
205. Cabbiness, S. G.; Gehrke, C. W.; Kuo, K. C.; Chan, T. K.; Hall, J. E.; Hudiburg, S. A.; Odell, G. V., Polyamines in some tarantula venoms. *Toxicon* **1980**, 18 (5-6), 681-683.
206. Kurata, H. T.; Akrouh, A.; Li, J. B.; Marton, L. J.; Nichols, C. G., Scanning the topography of polyamine blocker binding in an inwardly rectifying potassium channel. *Journal of Biological Chemistry* **2013**, 288 (9), 6591-6601.
207. Kurata, H. T.; Diraviyam, K.; Marton, L. J.; Nichols, C. G., Blocker protection by short spermine analogs: refined mapping of the spermine binding site in a Kir channel. *Biophysical Journal* **2008**, 95 (8), 3827-3839.
208. Williams, K.; Romano, C.; Molinoff, P. B., Effects of polyamines on the binding of [3H] MK-801 to the N-methyl-D-aspartate receptor: pharmacological evidence for the existence of a polyamine recognition site. *Molecular Pharmacology* **1989**, 36 (4), 575-581.
209. Bowie, D.; Mayer, M. L., Inward rectification of both AMPA and kainate subtype glutamate receptors generated by polyamine-mediated ion channel block. *Neuron* **1995**, 15 (2), 453-462.
210. Williams, K., Modulation and block of ion channels: a new biology of polyamines. *Cellular Signalling* **1997**, 9 (1), 1-13.
211. Gu, J.; Albuquerque, C.; Lee, C.; MacDermott, A., Synaptic strengthening through activation of Ca²⁺-permeable AMPA receptors. *Nature* **1996**, 381 (6585), 793.
212. Sorkin, L. S.; Yaksh, T. L.; Doom, C. M., Pain models display differential sensitivity to Ca²⁺-permeable non-NMDA glutamate receptor antagonists. *The Journal of the American Society of Anesthesiologists* **2001**, 95 (4), 965-973.
213. King, G. F., Venoms as a platform for human drugs: translating toxins into therapeutics. *Expert Opinion on Biological Therapy* **2011**, 11 (11), 1469-84.
214. Kuhn-Nentwig, L., Antimicrobial and cytolytic peptides of venomous arthropods. *Cellular and Molecular Life Sciences* **2003**, 60 (12), 2651-2668.
215. Saez, N. J.; Senff, S.; Jensen, J. E.; Er, S. Y.; Herzig, V.; Rash, L. D.; King, G. F., Spider-venom peptides as therapeutics. *Toxins* **2010**, 2 (12), 2851-2871.

216. Osteen, J. D.; Herzig, V.; Gilchrist, J.; Emrick, J. J.; Zhang, C.; Wang, X.; Castro, J.; Garcia-Caraballo, S.; Grundy, L.; Rychkov, G. Y., Selective spider toxins reveal a role for the Nav1. 1 channel in mechanical pain. *Nature* **2016**, 534 (7608), 494-499.
217. Verdes, A.; Anand, P.; Gorson, J.; Jannetti, S.; Kelly, P.; Leffler, A.; Simpson, D.; Ramrattan, G.; Holford, M., From mollusks to medicine: a venomics approach for the discovery and characterization of therapeutics from Terebridae peptide toxins. *Toxins* **2016**, 8 (4), 117.
218. St Johnston, D., The art and design of genetic screens: *Drosophila melanogaster*. *Nature Reviews Genetics* **2002**, 3 (3), 176.
219. Wurm, F. M., Production of recombinant protein therapeutics in cultivated mammalian cells. *Nature Biotechnology* **2004**, 22 (11), 1393.
220. Patrice, R.; Olivier, E.; Tanter, C.; Anaïs, W.; Dutot, M., A fast and reproducible cell-and 96-well plate-based method for the evaluation of P2X7 receptor activation using YO-PRO-1 fluorescent dye. *Journal of Biological Methods* **2017**, 4 (1), e64.
221. Zhang, J. H.; Chung, T. D.; Oldenburg, K. R., A Simple Statistical Parameter for Use in Evaluation and Validation of High Throughput Screening Assays. *Journal of Biomolecular Screening* **1999**, 4 (2), 67-73.
222. O'brien, J.; Wilson, I.; Orton, T.; Pognan, F., Investigation of the Alamar Blue (resazurin) fluorescent dye for the assessment of mammalian cell cytotoxicity. *European Journal of Biochemistry* **2000**, 267 (17), 5421-5426.
223. Pettersen, E. F.; Goddard, T. D.; Huang, C. C.; Couch, G. S.; Greenblatt, D. M.; Meng, E. C.; Ferrin, T. E., UCSF Chimera—a visualization system for exploratory research and analysis. *Journal of Computational Chemistry* **2004**, 25 (13), 1605-1612.
224. Olivera, B. M.; Rivier, J.; Clark, C.; Ramilo, C. A.; Corpuz, G. P.; Abogadie, F. C.; Mena, E. E.; Hillyard, D.; Cruz, L., Diversity of *Conus* neuropeptides. *Science* **1990**, 249 (4966), 257-263.
225. Diochot, S.; Baron, A.; Salinas, M.; Douguet, D.; Scarzello, S.; Dabert-Gay, A.-S.; Debayle, D.; Friend, V.; Alloui, A.; Lazdunski, M., Black mamba venom peptides target acid-sensing ion channels to abolish pain. *Nature* **2012**, 490 (7421), 552.
226. Diochot, S.; Schweitz, H.; Béress, L.; Lazdunski, M., Sea anemone peptides with a specific blocking activity against the fast inactivating potassium channel Kv3. 4. *Journal of Biological Chemistry* **1998**, 273 (12), 6744-6749.
227. Castañeda, O.; Harvey, A. L., Discovery and characterization of cnidarian peptide toxins that affect neuronal potassium ion channels. *Toxicon* **2009**, 54 (8), 1119-1124.
228. Jouiaei, M.; Casewell, N.; Yanagihara, A.; Nouwens, A.; Cribb, B.; Whitehead, D.; Jackson, T.; Ali, S.; Wagstaff, S.; Koludarov, I., Firing the sting: chemically induced discharge of cnidae reveals novel proteins and peptides from box jellyfish (*Chironex fleckeri*) venom. *Toxins* **2015**, 7 (3), 936-950.
229. Banerjee, S.; Gnanamani, E.; Lynch, S. R.; Zuñiga, F. Z.; Jiménez-Vargas, J. M.; Possani, L. D.; Zare, R. N., An alkaloid from scorpion venom: Chemical structure and synthesis. *Journal of Natural Products* **2018**, 81 (8), 1899-1904.

230. Holford, M.; Daly, M.; King, G. F.; Norton, R. S., Venoms to the rescue. *Science* **2018**, 361 (6405), 842-844.
231. Yu, H. B.; Li, M.; Wang, W. P.; Wang, X. L., High throughput screening technologies for ion channels. *Acta Pharmacologica Sinica* **2016**, 37 (1), 34-43.
232. Santos, R.; Ursu, O.; Gaulton, A.; Bento, A. P.; Donadi, R. S.; Bologa, C. G.; Karlsson, A.; Al-Lazikani, B.; Hersey, A.; Oprea, T. I., A comprehensive map of molecular drug targets. *Nature Reviews Drug Discovery* **2017**, 16 (1), 19.
233. Dunlop, J.; Bowlby, M.; Peri, R.; Vasilyev, D.; Arias, R., High-throughput electrophysiology: an emerging paradigm for ion-channel screening and physiology. *Nature Reviews Drug Discovery* **2008**, 7 (4), 358.
234. Macarron, R.; Banks, M. N.; Bojanic, D.; Burns, D. J.; Cirovic, D. A.; Garyantes, T.; Green, D. V.; Hertzberg, R. P.; Janzen, W. P.; Paslay, J. W., Impact of high-throughput screening in biomedical research. *Nature Reviews Drug Discovery* **2011**, 10 (3), 188.
235. Keseru, G. M.; Makara, G. M., The influence of lead discovery strategies on the properties of drug candidates. *Nature Reviews Drug Discovery* **2009**, 8 (3), 203-12.
236. Burnstock, G., Purinergic signalling: therapeutic developments. *Frontiers in Pharmacology* **2017**, 8, 661.
237. Bidula, S. M.; Cromer, B. A.; Walpole, S.; Angulo, J.; Stokes, L., Mapping a novel positive allosteric modulator binding site in the central vestibule region of human P2X7. *Scientific Reports* **2019**, 9 (1), 3231.
238. Dhuna, K.; Felgate, M.; Bidula, S. M.; Walpole, S.; Bibic, L.; Cromer, B. A.; Angulo, J.; Sanderson, J.; Stebbing, M. J.; Stokes, L., Ginsenosides act as positive modulators of P2X4 receptors. *Molecular Pharmacology* **2019**, 95 (2), 210-221.
239. Namovic, M. T.; Jarvis, M. F.; Donnelly-Roberts, D., High throughput functional assays for P2X receptors. *Current Protocols in Pharmacology* **2012**, Chapter 9, Unit 9.15.
240. Janzen, W. P., High throughput screening: methods and protocols. *Springer Science & Business Media*: **2002**.
241. Marucci, G.; Lammi, C.; Buccioni, M.; Dal Ben, D.; Lambertucci, C.; Amantini, C.; Santoni, G.; Kandhavelu, M.; Abbracchio, M. P.; Lecca, D., Comparison and optimization of transient transfection methods at human astrocytoma cell line 1321N1. *Analytical Biochemistry* **2011**, 414 (2), 300-302.
242. Helliwell, R.; ShioukHuey, C. O.; Dhuna, K.; Molero, J.; Ye, J. M.; Xue, C.; Stokes, L., Selected ginsenosides of the protopanaxdiol series are novel positive allosteric modulators of P2X7 receptors. *British Journal of Pharmacology* **2015**, 172 (13), 3326-3340.
243. Zheng, W.; Spencer, R. H.; Kiss, L. J. A.; technologies, d. d., High throughput assay technologies for ion channel drug discovery. *Assay Drug Development Technologies* **2004**, 2 (5), 543-552.
244. Surprenant, A.; Rassendren, F.; Kawashima, E.; North, R.; Buell, G., The cytolytic P2Z receptor for extracellular ATP identified as a P2X receptor (P2X7). *Science* **1996**, 272 (5262), 735-738.

245. Rassendren, F.; Buell, G. N.; Virginio, C.; Collo, G.; North, R. A.; Surprenant, A., The permeabilizing ATP receptor, P2X7 cloning and expression of a human cDNA. *Journal of Biological Chemistry* **1997**, 272 (9), 5482-5486.
246. Kabanova, N. V.; Vassilevski, A. A.; Rogachevskaja, O. A.; Bystrova, M. F.; Korolkova, Y. V.; Pluzhnikov, K. A.; Romanov, R. A.; Grishin, E. V.; Kolesnikov, S. S., Modulation of P2X3 receptors by spider toxins. *Biochimica et Biophysica Acta - Biomembranes* **2012**, 1818 (11), 2868-2875.
247. Layhadi, J. A.; Turner, J.; Crossman, D.; Fountain, S. J., ATP Evokes Ca²⁺ Responses and CXCL5 Secretion via P2X4 Receptor Activation in Human Monocyte-Derived Macrophages. *Journal of Immunology* **2018**, 200 (3), 1159-1168.
248. Jones, C.; Chessell, I.; Simon, J.; Barnard, E.; Miller, K.; Michel, A.; Humphrey, P., Functional characterization of the P2X4 receptor orthologues. *British Journal of Pharmacology* **2000**, 129 (2), 388-394.
249. Seeland, S.; Kettiger, H.; Murphy, M.; Treiber, A.; Giller, J.; Kiss, A.; Sube, R.; Krähenbühl, S.; Hafner, M.; Huwyler, J., ATP-induced cellular stress and mitochondrial toxicity in cells expressing purinergic P2X7 receptor. *Pharmacology Research Perspectives* **2015**, 3 (2), e00123.
250. Balazs, B.; Danko, T.; Kovacs, G.; Koles, L.; Hediger, M. A.; Zsembery, A., Investigation of the inhibitory effects of the benzodiazepine derivative, 5-BDBD on P2X4 purinergic receptors by two complementary methods. *Cellular Physiology and Biochemistry* **2013**, 32 (1), 11-24.
251. Allsopp, R. C.; Dayl, S.; Schmid, R.; Evans, R. J., Unique residues in the ATP gated human P2X7 receptor define a novel allosteric binding pocket for the selective antagonist AZ10606120. *Scientific Reports* **2017**, 7 (1), 725.
252. Yamashita, T.; Yamamoto, S.; Zhang, J.; Kometani, M.; Tomiyama, D.; Kohno, K.; Tozaki-Saitoh, H.; Inoue, K.; Tsuda, M., Duloxetine inhibits microglial P2X4 receptor function and alleviates neuropathic pain after peripheral nerve injury. *PLoS One* **2016**, 11 (10), e0165189.
253. Guette, C.; Legros, C.; Tournois, G.; Goyffon, M.; Célérier, M.-L., Peptide profiling by matrix-assisted laser desorption/ionisation time-of-flight mass spectrometry of the *Lasiadora parahybana* tarantula venom gland. *Toxicon* **2006**, 47 (6), 640-649.
254. Garenaux, E.; Maes, E.; Leveque, S.; Brassart, C.; Guerardel, Y., Structural characterization of complex O-linked glycans from insect-derived material. *Carbohydrate Research* **2011**, 346 (9), 1093-1104.
255. Junior, R. S. F.; Sciani, J. M.; Marques-Porto, R.; Junior, A. L.; Orsi, R. d. O.; Barraviera, B.; Pimenta, D. C., Africanized honey bee (*Apis mellifera*) venom profiling: Seasonal variation of melittin and phospholipase A2 levels. *Toxicon* **2010**, 56 (3), 355-362.
256. Lee, M. T.; Sun, T. L.; Hung, W. C.; Huang, H. W., Process of inducing pores in membranes by melittin. *Proceedings of the National Academy of Sciences* **2013**, 110 (35), 14243-8.
257. Broach, J. R.; Thorner, J., High-throughput screening for drug discovery. *Nature* **1996**, 384 (6604), 14-16.

258. Priel, A.; Silberberg, S. D., Mechanism of ivermectin facilitation of human P2X4 receptor channels. *The Journal of General Physiology* **2004**, 123 (3), 281-293.
259. Virginio, C.; Robertson, G.; Surprenant, A.; North, R. A., Trinitrophenyl-substituted nucleotides are potent antagonists selective for P2X1, P2X3, and heteromeric P2X2/3 receptors. *Molecular Pharmacology* **1998**, 53 (6), 969-973.
260. Bleicher, K. H.; Bohm, H. J.; Muller, K.; Alanine, A. I., Hit and lead generation: beyond high-throughput screening. *Nature Review Drug Discovery* **2003**, 2 (5), 369-78.
261. Lerma, J., Spermine regulates N-methyl-D-aspartate receptor desensitization. *Neuron* **1992**, 8 (2), 343-352.
262. Simeonov, A.; Davis, M. I., Interference with fluorescence and absorbance. *Assay Guidance Manual*, Eli Lilly & Company and the National Center for Advancing Translational Sciences: **2018**.
263. DeSilva, B.; Smith, W.; Weiner, R.; Kelley, M.; Smolec, J.; Lee, B.; Khan, M.; Tacey, R.; Hill, H.; Celniker, A., Recommendations for the bioanalytical method validation of ligand-binding assays to support pharmacokinetic assessments of macromolecules. *Pharmaceutical Research* **2003**, 20 (11), 1885-1900.
264. Iversen, P. W.; Eastwood, B. J.; Sittampalam, G. S.; Cox, K. L., A comparison of assay performance measures in screening assays: signal window, Z'factor, and assay variability ratio. *Journal of Biomolecular Screening* **2006**, 11 (3), 247-252.
265. Kümmel, A.; Gubler, H.; Gehin, P.; Beibel, M.; Gabriel, D.; Parker, C. N., Integration of multiple readouts into the z'factor for assay quality assessment. *Journal of Biomolecular Screening* **2010**, 15 (1), 95-101.
266. Sui, Y.; Wu, Z., Alternative statistical parameter for high-throughput screening assay quality assessment. *Journal of Biomolecular Screening* **2007**, 12 (2), 229-234.
267. Macarrón, R.; Hertzberg, R. P., Design and implementation of high throughput screening assays. *Molecular Biotechnology* **2011**, 47 (3), 270-285.
268. Macarron, R.; Banks, M. N.; Bojanic, D.; Burns, D. J.; Cirovic, D. A.; Garyantes, T.; Green, D. V.; Hertzberg, R. P.; Janzen, W. P.; Paslay, J. W.; Schopfer, U.; Sittampalam, G. S., Impact of high-throughput screening in biomedical research. *Nature Review Drug Discovery* **2011**, 10 (3), 188-95.
269. Malo, N.; Hanley, J. A.; Cerquozzi, S.; Pelletier, J.; Nadon, R., Statistical practice in high-throughput screening data analysis. *Nature Biotechnology* **2006**, (2), 167.
270. Santos, R.; Ursu, O.; Gaulton, A.; Bento, A. P.; Donadi, R. S.; Bologa, C. G.; Karlsson, A.; Al-Lazikani, B.; Hersey, A.; Oprea, T. I.; Overington, J. P., A comprehensive map of molecular drug targets. *Nature Review Drug Discovery* **2017**, 16 (1), 19-34.
271. Lundholt, B. K.; Scudder, K. M.; Pagliaro, L., A simple technique for reducing edge effect in cell-based assays. *Journal of Biomolecular Screening* **2003**, 8 (5), 566-570.
272. Gunter, B.; Brideau, C.; Pikounis, B.; Liaw, A., Statistical and graphical methods for quality control determination of high-throughput screening data. *Journal of Biomolecular Screening* **2003**, 8 (6), 624-633.

273. Brideau, C.; Gunter, B.; Pikounis, B.; Liaw, A., Improved statistical methods for hit selection in high-throughput screening. *Journal of Biomolecular Screening* **2003**, 8 (6), 634-647.
274. Olsen, C. A.; Kristensen, A. S.; Strømgaard, K., Small molecules from spiders used as chemical probes. *Angewandte Chemie International Edition* **2011**, 50 (48), 11296-11311.
275. Corzo, G.; Villegas, E.; Gómez-Lagunas, F.; Possani, L. D.; Belokoneva, O. S.; Nakajima, T., Oxyopinins, large amphipathic peptides isolated from the venom of the wolf spider *Oxyopes kitabensis* with cytolytic properties and positive insecticidal cooperativity with spider neurotoxins. *Journal of Biological Chemistry* **2002**, 277 (26), 23627-23637.
276. Strømgaard, K.; Andersen, K.; Krogsgaard-Larsen, P.; Jaroszewski, J. W., Recent advances in the medicinal chemistry of polyamine toxins. *Mini Reviews in Medicinal Chemistry* **2001**, 1 (4), 317-338.
277. Hisada, M.; Fujita, T.; Naoki, H.; Itagaki, Y.; Irie, H.; Miyashita, M.; Nakajima, T., Structures of spider toxins: Hydroxyindole-3-acetyl polyamines and a new generalized structure of type-E compounds obtained from the venom of the Joro spider, *Nephila clavata*. *Toxicon* **1998**, 36 (8), 1115-1125.
278. Abe, T.; Kawai, N.; Miwa, A., Effects of a spider toxin on the glutaminergic synapse of lobster muscle. *The Journal of Physiology* **1983**, 339 (1), 243-252.
279. Sheardown, M. J.; Nielsen, E. O.; Hansen, A. J.; Jacobsen, P.; Honore, T., 2, 3-Dihydroxy-6-nitro-7-sulfamoyl-benzo (F) quinoxaline: a neuroprotectant for cerebral ischemia. *Science* **1990**, 247 (4942), 571-574.
280. Volkova, T.; Grishin, E.; Arseniev, A.; Reshetova, O.; Onoprienko, V. *Structural Characteristic of Argiopine-Blocker of Glutamate Channels from the Venom of Spider Argiope Lobata*, Sixth European Society for Neurochemistry General Meeting in Prague, **1986**.
281. Adams, M.; Carney, R.; Enderlin, F.; Fu, E.; Jarema, M.; Li, J.; Miller, C.; Schooley, D.; Shapiro, M.; Venema, V., Structures and biological activities of three synaptic antagonists from orb weaver spider venom. *Biochemical and Biophysical Research Communications* **1987**, 148 (2), 678-683.
282. Grishin, E.; Volkova, T.; Arseniev, A., Isolation and structure analysis of components from venom of the spider *Argiope lobata*. *Toxicon* **1989**, 27 (5), 541-549.
283. Asami, T.; Kagechika, H.; Hashimoto, Y.; Shudo, K.; Miwa, A.; Kawai, N.; Nakajima, T., Acylpolyamines mimic the action of Joro spider toxin (JSTX) on crustacean muscle glutamate receptors. *Biomedical Research* **1989**, 10 (3), 185-189.
284. Nishimaru, T.; Sano, M.; Yamaguchi, Y.; Wakamiya, T., Syntheses and biological activities of fluorescent-labeled analogs of acylpolyamine toxin NPTX-594 isolated from the venom of Madagascar Joro spider. *Bioorganic & Medicinal Chemistry* **2009**, 17 (1), 57-63.
285. Aramaki, Y.; Yasuhara, T.; Higashijima, T.; Miwa, A.; Nobufumi, K.; Nakajima, T., Chemical characterization of spider toxin, NSTX. *Biomedical Research* **1987**, 8 (3), 167-173.
286. Aramaki, Y.; Yasuhara, T.; Higashijima, T.; Yoshioka, M.; Miwa, A.; Kawai, N.; Nakajima, T., Chemical characterization of spider toxin, JSTX and NSTX. *Proceedings of the Japan Academy* **1986**, 62 (9), 359-362.

287. Teshima, T.; Wakamiya, T.; Aramaki, Y.; Nakajima, T.; Kawai, N.; Shiba, T., Synthesis of a new neurotoxin NSTX-3 of Papua New Guinean spider. *Tetrahedron Letters* **1987**, 28 (30), 3509-3510.
288. Palma, M. S.; Nakajima, T., A natural combinatorial chemistry strategy in acylpolyamine toxins from nephilinae orb-web spiders. *Toxin Reviews* **2005**, 24 (2), 209-234.
289. Shimazaki, K.; Hagiwara, K.; Hirata, Y.; Nakajima, T.; Kawai, N., An autoradiographic study of binding of iodinated spider toxin to lobster muscle. *Neuroscience Letters* **1988**, 84 (2), 173-177.
290. Choi, S.-K.; Kalivretenos, A. G.; Usherwood, P. N.; Nakanishi, K., Labeling studies of photolabile philanthotoxins with nicotinic acetylcholine receptors: mode of interaction between toxin and receptor. *Chemistry & Biology* **1995**, 2 (1), 23-32.
291. Fang, K.; Hashimoto, M.; Jockusch, S.; Turro, N. J.; Nakanishi, K., A bifunctional photoaffinity probe for ligand/receptor interaction studies. *Journal of the American Chemical Society* **1998**, 120 (33), 8543-8544.
292. Grishin, E.; Volkova, T.; Arsen'Ev, A.; Reshetova, O.; Onoprienko, V. J. B. k., Structural-functional characteristics of argiopine--the ion channel blockers from the spider *Argiope lobata* venom. *Bioorganicheskaja Khimiia* **1986**, 12 (8), 1121-1124.
293. Hashimoto, Y.; Endo, Y.; Shudo, K.; Aramaki, Y.; Kawai, N.; Nakajima, T., Synthesis of spider toxin (JSTX-3) and its analogs. *Tetrahedron Letters* **1987**, 28 (30), 3511-3514.
294. Fujita, T.; Itagaki, Y.; Hisaka, M.; Naoki, H.; Nakajima, T.; Andriantsiferana, M., Application of Liquid Matrix-assisted Laser Desorption/Ionization 4-Sector Tandem Mass Spectrometry for the Analysis of Spider Toxin Acylpolyamines. *Rapid Communications in Mass Spectrometry* **1997**, 11 (10), 1115-1119.
295. Fujita, T.; Itagaki, Y.; Naoki, H.; Nakajima, T.; Hagiwara, K. i., Structural characterization of glutaminergic blocker spider toxins by high-energy collision charge-remote fragmentations. *Rapid Communications in Mass Spectrometry* **1995**, 9 (5), 365-371.
296. Itagaki, Y.; Naoki, H.; Fujita, T.; Hisada, M.; Nakajima, T., Characterization of spider venom by mass spectrometry, construction of analytical system. *Journal of Pharmaceutical Society of Japan* **1997**, 117 (10-11), 715-728.
297. Jasys, V. J.; Kelbaugh, P. R.; Nason, D. M.; Phillips, D.; Rosnack, K. J.; Saccomano, N. A.; Stroh, J. G.; Volkmann, R. A., Isolation, structure elucidation, and synthesis of novel hydroxylamine-containing polyamines from the venom of the *Agelenopsis aperta* spider. *Journal of the American Chemical Society* **1990**, 112 (18), 6696-6704.
298. Quistad, G. B.; Suwanrumpha, S.; Jarema, M. A.; Shapiro, M. J.; Skinner, W. S.; Jamieson, G. C.; Lui, A.; Fu, E. W., Structure of paralytic acylpolyamines from the spider *Agelenopsis aperta*. *Biochemical Biophysical Research Communications* **1990**, 169 (1), 51-56.
299. Jasys, V. J.; Kelbaugh, P. R.; Nason, D. M.; Phillips, D.; Rosnack, K. J.; Saccomano, N. A.; Stroh, J. G.; Volkmann, R. A.; Forman, J. T., Novel quaternary ammonium salt-containing polyamines from the *Agelenopsis aperta* funnel-web spider. *The Journal of Organic Chemistry* **1992**, 57 (6), 1814-1820.

300. Palma, M. S.; Itagaki, Y.; Fujita, T.; Naoki, H.; Nakajima, T., Structural characterization of a new acylpolyaminetoxin from the venom of Brazilian garden spider *Nephilengys cruentata*. *Toxicon* **1998**, 36 (3), 485-493.
301. Tzouros, M.; Chesnov, S.; Bigler, L.; Bienz, S., A template approach for the characterization of linear polyamines and derivatives in spider venom. *European Journal of Mass Spectrometry* **2013**, 19 (1), 57-69.
302. Manov, N.; Tzouros, M.; Chesnov, S.; Bigler, L.; Bienz, S., Solid-phase synthesis of polyamine spider toxins and correlation with the natural products by HPLC-MS/MS. *Helvetica Chimica Acta* **2002**, 85 (9), 2827-2846.
303. Wang, F.; Manku, S.; Hall, D. G., Solid phase syntheses of polyamine toxins HO-416b and PHTX-433. Use of an efficient polyamide reduction strategy that facilitates access to branched analogues. *Organic Letters* **2000**, 2 (11), 1581-1583.
304. Taggi, A. E.; Meinwald, J.; Schroeder, F. C., A new approach to natural products discovery exemplified by the identification of sulfated nucleosides in spider venom. *Journal of the American Chemical Society* **2004**, 126 (33), 10364-10369.
305. McCormick, J.; Li, Y.; McCormick, K.; Duynstee, H. I.; van Engen, A. K.; van der Marel, G. A.; Ganem, B.; van Boom, J. H.; Meinwald, J., Structure and total synthesis of HF-7, a neuroactive glyconucleoside disulfate from the funnel-web spider *Hololena curta*. *Journal of the American Chemical Society* **1999**, 121 (24), 5661-5665.
306. McCormick, K. D.; Meinwald, J., Neurotoxic acylpolyamines from spider venoms. *Journal of Chemical Ecology* **1993**, 19 (10), 2411-2451.
307. Schulz, S., The chemistry of spider toxins and spider silk. *Angewandte Chemie International Edition* **1997**, 36 (4), 314-326.
308. Schroeder, F. C.; Taggi, A. E.; Gronquist, M.; Malik, R. U.; Grant, J. B.; Eisner, T.; Meinwald, J. J., NMR-spectroscopic screening of spider venom reveals sulfated nucleosides as major components for the brown recluse and related species. *Proceedings of the National Academy of Sciences* **2008**, 105 (38), 14283-14287.
309. Lacey, M. E.; Subramanian, R.; Olson, D. L.; Webb, A. G.; Sweedler, J. V., High-resolution NMR spectroscopy of sample volumes from 1 nL to 10 μ L. *Chemical Reviews* **1999**, 99 (10), 3133-3152.
310. Green, B.; Olivera, B., Venom peptides from cone snails: Pharmacological probes for voltage-gated sodium channels. *Current Topics in Membranes*, Elsevier: **2016**; Vol. 78, pp 65-86.
311. Alexander, K.; Niforatos, W.; Bianchi, B.; Burgard, E. C.; Lynch, K. J.; Kowaluk, E. A.; Jarvis, M. F.; van Biesen, T., Allosteric modulation and accelerated resensitization of human P2X3 receptors by cibacron blue. *Journal of Pharmacology Experimental Therapeutics* **1999**, 291 (3), 1135-1142.
312. Ferreira, F. R. B.; da Silva, P. M.; Soares, T.; Machado, L. G.; de Araújo, L. C. C.; da Silva, T. G.; de Mello, G. S. V.; da Rocha Pitta, M. G.; de Melo Rego, M. J. B.; Pontual, E. V., Evaluation of antimicrobial, cytotoxic, and hemolytic activities from venom of the spider *Lasiadora* sp. *Toxicon* **2016**, 122, 119-126.

313. Corzo, G.; Diego-García, E.; Clement, H.; Peigneur, S.; Odell, G.; Tytgat, J.; Possani, L. D.; Alagón, A., An insecticidal peptide from the therapsid *Brachypelma smithi* spider venom reveals common molecular features among spider species from different genera. *Peptides* **2008**, 29 (11), 1901-1908.
314. Tang, X.; Zhang, Y.; Hu, W.; Xu, D.; Tao, H.; Yang, X.; Li, Y.; Jiang, L.; Liang, S., Molecular diversification of peptide toxins from the tarantula *Haplopelma hainanum* (*Ornithoctonus hainana*) venom based on transcriptomic, peptidomic, and genomic analyses. *Journal of Proteome Research* **2010**, 9 (5), 2550-2564.
315. Escoubas, P.; Corzo, G.; Whiteley, B. J.; Célérier, M. L.; Nakajima, T., Matrix-assisted laser desorption/ionization time-of-flight mass spectrometry and high-performance liquid chromatography study of quantitative and qualitative variation in tarantula spider venoms. *Rapid Communications in Mass Spectrometry* **2002**, 16 (5), 403-413.
316. Laustsen, A. H., Toxin synergism in snake venoms. *Toxin Reviews* **2016**, 35 (3-4), 165-170.
317. Kuhn-Nentwig, L.; Schaller, J.; Nentwig, W., Biochemistry, toxicology and ecology of the venom of the spider *Cupiennius salei* (Ctenidae). *Toxicon* **2004**, 43 (5), 543-553.
318. Nikai, T.; Mori, N.; Kishida, M.; Sugihara, H.; Tu, A. T., Isolation and biochemical characterization of hemorrhagic toxin f from the venom of *Crotalus atrox* (western diamondback rattlesnake). *Biochemistry Biophysics* **1984**, 231 (2), 309-319.
319. Strydom, D. J., Snake Venom Toxins: Purification and Properties of Low-Molecular-Weight Polypeptides of *Dendroaspis polylepis polylepis* (Black Mamba) Venom. *European Journal of Biochemistry* **1976**, 69 (1), 169-176.
320. Jaki, B. U.; Franzblau, S. G.; Chadwick, L. R.; Lankin, D. C.; Zhang, F.; Wang, Y.; Pauli, G. F., Purity- activity relationships of natural products: the case of anti-TB active ursolic acid. *Journal of Natural Products* **2008**, 71 (10), 1742-1748.
321. Polyakova, Y.; Koo, Y. M.; Row, K. H., Application of ionic liquids as mobile phase modifier in HPLC. *Biotechnology Bioprocess Engineering* **2006**, 11 (1), 1.
322. Itagaki, Y.; Nakajima, T., Acylpolyamines: mass spectrometric analytical methods for Araneidae spider acylpolyamines. *Journal of Toxicology: Toxin Reviews* **2000**, 19 (1), 23-52.
323. Rocha-e-Silva, T. A.; Rostelato-Ferreira, S.; Leite, G. B.; da Silva Jr, P. I.; Hyslop, S.; Rodrigues-Simioni, L., VdTX-1, a reversible nicotinic receptor antagonist isolated from venom of the spider *Vitalius dubius* (Theraphosidae). *Toxicon* **2013**, 70, 135-141.
324. Scheubert, K.; Hufsky, F.; Böcker, S., Computational mass spectrometry for small molecules. *Journal of Cheminformatics* **2013**, 5 (1), 12.
325. Chesnov, S.; Bigler, L.; Hesse, M., The acylpolyamines from the venom of the spider *Agelenopsis aperta*. *Helvetica Chimica Acta* **2001**, 84 (8), 2178-2197.
326. Chesnov, S.; Bigler, L.; Hesse, M., The Spider *Paracoelotes birulai*: Detection and Structure Elucidation of New Acylpolyamines by On-Line Coupled HPLC-APCI-MS and HPLC-APCI-MS/MS. *Helvetica Chimica Acta* **2000**, 83 (12), 3295-3305.

327. Fitzgerald, B. L.; Mahapatra, S.; Farmer, D. K.; McNeil, M. R.; Casero Jr, R. A.; Belisle, J. T., Elucidating the Structure of N 1-Acetylispoptreanine: A Novel Polyamine Catabolite in Human Urine. *ACS Omega* **2017**, 2 (7), 3921-3930.
328. Manov, N.; Tzouros, M.; Bigler, L.; Bienz, S., Solid-phase synthesis of ¹⁵N-labeled acylpentamines as reference compounds for the MS/MS investigation of spider toxins. *Tetrahedron* **2004**, 60 (10), 2387-2391.
329. Shek, P. I.; Zhao, J.; Ke, Y.; Siu, K. M.; Hopkinson, A. C. J., Fragmentations of protonated arginine, lysine and their methylated derivatives: concomitant losses of carbon monoxide or carbon dioxide and an amine. *The Journal of Physical Chemistry* **2006**, 110 (27), 8282-8296.
330. Skinner, W. S.; Dennis, P. A.; Lui, A.; Carney, R. L.; Quistad, G. B., Chemical characterization of acylpolyamine toxins from venom of a trap-door spider and two tarantulas. *Toxicon* **1990**, 28 (5), 541-546.
331. Tsugawa, H.; Kind, T.; Nakabayashi, R.; Yukihiro, D.; Tanaka, W.; Cajka, T.; Saito, K.; Fiehn, O.; Arita, M., Hydrogen rearrangement rules: computational MS/MS fragmentation and structure elucidation using MS-FINDER software. *Analytical Chemistry* **2016**, 88 (16), 7946-7958.
332. Vaniya, A.; Samra, S. N.; Palazoglu, M.; Tsugawa, H.; Fiehn, O., Using MS-FINDER for identifying 19 natural products in the CASMI 2016 contest. *Phytochemistry Letters* **2017**, 21, 306-312.
333. Lai, Z.; Tsugawa, H.; Wohlgemuth, G.; Mehta, S.; Mueller, M.; Zheng, Y.; Ogiwara, A.; Meissen, J.; Showalter, M.; Takeuchi, K., Identifying metabolites by integrating metabolome databases with mass spectrometry cheminformatics. *Nature Methods* **2018**, 15 (1), 53.
334. Blaženović, I.; Kind, T.; Ji, J.; Fiehn, O., Software tools and approaches for compound identification of LC-MS/MS data in metabolomics. *Metabolites* **2018**, 8 (2), 31.
335. Gilbert, D. F.; Islam, R.; Lynagh, T. P.; Lynch, J.; Webb, T. I., High throughput techniques for discovering new glycine receptor modulators and their binding sites. *Frontiers in Molecular Neuroscience* **2009**, 2, 17.
336. Wirkner, K.; Sperlagh, B.; Illes, P., P2X₃ receptor involvement in pain states. *Molecular Neurobiology* **2007**, 36 (2), 165-183.
337. Burnstock, G., Purinergic mechanisms and pain. *Advances in Pharmacology*, Elsevier: **2016**; Vol. 75, 91-137.
338. Tsuda, M.; Mizokoshi, A.; Shigemoto-Mogami, Y.; Koizumi, S.; Inoue, K., Activation of p38 mitogen-activated protein kinase in spinal hyperactive microglia contributes to pain hypersensitivity following peripheral nerve injury. *Glia* **2004**, 45 (1), 89-95.
339. Masuda, T.; Iwamoto, S.; Yoshinaga, R.; Tozaki-Saitoh, H.; Nishiyama, A.; Mak, T. W.; Tamura, T.; Tsuda, M.; Inoue, K., Transcription factor IRF5 drives P2X₄⁺-reactive microglia gating neuropathic pain. *Nature Communications* **2014**, 5, 3771.
340. Asatryan, L.; Ostrovskaya, O.; Lieu, D.; Davies, D. L. J., Ethanol differentially modulates P2X₄ and P2X₇ receptor activity and function in BV2 microglial cells. *Neuropharmacology* **2018**, 128, 11-21.

341. Gilbert, D. F.; Stebbing, M. J.; Kuenzel, K.; Murphy, R. M.; Zacharewicz, E.; Buttgereit, A.; Stokes, L.; Adams, D. J.; Friedrich, O., Store-operated Ca²⁺ entry (SOCE) and purinergic receptor-mediated Ca²⁺ homeostasis in murine bv2 microglia cells: early cellular responses to ATP-mediated microglia activation. *Frontiers in Molecular Neuroscience* **2016**, 9, 111.
342. Fountain, S. J.; Burnstock, G., An evolutionary history of P2X receptors. *Purinergic Signalling* **2009**, 5 (3), 269-272.
343. Mintz, I. M.; Venema, V. J.; Swiderek, K. M.; Lee, T. D.; Bean, B. P.; Adams, M. E., P-type calcium channels blocked by the spider toxin ω -Aga-IVA. *Nature* **1992**, 355 (6363), 827.
344. Kitaguchi, T.; Swartz, K., An inhibitor of TRPV1 channels isolated from funnel Web spider venom. *Biochemistry* **2005**, 44 (47), 15544-15549.
345. Lu, Z., Mechanism of rectification in inward-rectifier K⁺ channels. *Annual Review of Physiology* **2004**, 66, 103-129.
346. Lopatin, A. N.; Makhina, E. N.; Nichols, C. G., Potassium channel block by cytoplasmic polyamines as the mechanism of intrinsic rectification. *Nature* **1994**, 372 (6504), 366.
347. Guo, D.; Lu, Z., Mechanism of cGMP-gated channel block by intracellular polyamines. *The Journal of General Physiology* **2000**, 115 (6), 783-798.
348. Lin, J.; Rudy, B.; Llinas, R., Funnel-web spider venom and a toxin fraction block calcium current expressed from rat brain mRNA in *Xenopus* oocytes. *Proceedings of the National Academy of Sciences* **1990**, 87 (12), 4538.
349. Usherwood, P.; Duce, I.; Boden, P., Slowly-reversible block of glutamate receptor-channels by venoms of the spiders, *Argiope trifasciata* and *Araneus gemma*. *Journal de Physiologie* **1984**, 79 (4), 241-245.
350. Michaelis, E.; Galton, N.; Early, S., Spider venoms inhibit L-glutamate binding to brain synaptic membrane receptors. *Proceedings of the National Academy of Sciences* **1984**, 81 (17), 5571-5574.
351. Panchenko, V. A.; Glasser, C. R.; Mayer, M. L., Structural similarities between glutamate receptor channels and K⁺ channels examined by scanning mutagenesis. *The Journal of General Physiology* **2001**, 117 (4), 345-360.
352. Liu, M.; Nakazawa, K.; Inou, K.; Ohno, Y., Potent and voltage-dependent block by philanthotoxin-343 of neuronal nicotinic receptor/channels in PC12 cells. *British Journal of Pharmacology* **1997**, 122 (2), 379-385.
353. Nilius, B.; Prenen, J.; Voets, T.; Droogmans, G., Intracellular nucleotides and polyamines inhibit the Ca²⁺-activated cation channel TRPM4b. *Pflugers Archiv* **2004**, 448 (1), 70-75.
354. Kerschbaum, H. H.; Kozak, J. A.; Cahalan, M. D., Polyvalent cations as permeant probes of MIC and TRPM7 pores. *Biophysical Journal* **2003**, 84 (4), 2293-2305.
355. Blaschke, M.; Keller, B. U.; Rivosecchi, R.; Hollmann, M.; Heinemann, S.; Konnerth, A., A single amino acid determines the subunit-specific spider toxin block of alpha-amino-3-hydroxy-5-methylisoxazole-4-propionate/kainate receptor channels. *Proceedings of the National Academy of Sciences* **1993**, 90 (14), 6528-6532.

356. Liang, X.; Luo, D.; Luesch, H., Advances in Exploring the Therapeutic Potential of Marine Natural Products. *Pharmacological Research* **2019**, 104373.
357. Logan, T. M.; Murali, N.; Wang, G.; Jolivet, C., Application of a high-resolution superconducting NMR probe in natural product structure determination. *Magnetic Resonance in Chemistry* **1999**, 37 (10), 762-765.
358. Paterson, I.; Anderson, E. A., Chemistry. The renaissance of natural products as drug candidates. *Science* **2005**, 310 (5747), 451-3.
359. Koehn, F. E.; Carter, G. T., The evolving role of natural products in drug discovery. *Nature Reviews Drug Discovery* **2005**, 4 (3), 206.
360. Smith, J. J.; Lau, C. H. Y.; Herzig, V.; Ikonopoulou, M. P.; Rash, L. D.; King, G. F., *Venoms to Drugs: Venom as a Source for the Development of Human Therapeutics* **2015**, 221-244.
361. Melchiorre, C.; Bolognesi, M. L.; Minarini, A.; Rosini, M.; Tumiatti, V., Polyamines in drug discovery: from the universal template approach to the multitarget-directed ligand design strategy. *Journal of Medicinal Chemistry* **2010**, 53 (16), 5906-5914.
362. Melchiorre, C.; Angeli, P.; Brasili, L.; Giardinà, D.; Gulini, U.; Pigni, M.; Quaglia, W. *Polyamines: a possible "passe-partout" for receptor characterization Actualités de Chimie Therapeutique, Societe Chimie Therapeutique*: **1988**, 149.
363. Bolognesi, M. L.; Minarini, A.; Budriesi, R.; Cacciaguerra, S.; Chiarini, A.; Spampinato, S.; Tumiatti, V.; Melchiorre, C., Universal template approach to drug design: polyamines as selective muscarinic receptor antagonists. *Journal of Medicinal Chemistry* **1998**, 41 (21), 4150-4160.
364. Rosini, M.; Bixel, M. G.; Marucci, G.; Budriesi, R.; Krauss, M.; Bolognesi, M. L.; Minarini, A.; Tumiatti, V.; Hucho, F.; Melchiorre, C., Structure- activity relationships of methoctramine-related polyamines as muscular nicotinic receptor noncompetitive antagonists. 2. Role of polymethylene chain lengths separating amine functions and of substituents on the terminal nitrogen atoms. *Journal of Medicinal Chemistry* **2002**, 45 (9), 1860-1878.
365. Kuska, V.; Buchan, R.; Lin, P. K. T., Synthesis of polyamines, their derivatives, analogues and conjugates. *Synthesis* **2000**, 2000 (09), 1189-1207.
366. Bycroft, B.; Chan, W.; Hone, N.; Millington, S.; Nash, I., Synthesis of the spider toxins nephilatoxin-9 and-11 by a novel solid-phase strategy. *Journal of the American Chemical Society* **1994**, 116 (16), 7415-7416.
367. Olsen, C. A.; Franzyk, H.; Jaroszewski, J. W., N-Alkylation reactions and indirect formation of amino functionalities in solid-phase synthesis. *Synthesis* **2005**, 2005 (16), 2631-2653.
368. Kromann, H.; Krikstolaityte, S.; Andersen, A. J.; Andersen, K.; Krogsgaard-Larsen, P.; Jaroszewski, J. W.; Egebjerg, J.; Strømgaard, K., Solid-phase synthesis of polyamine toxin analogues: potent and selective antagonists of Ca²⁺-permeable AMPA receptors. *Journal of Medicinal Chemistry* **2002**, 45 (26), 5745-5754.
369. Andersen, T. F.; Tikhonov, D. B.; Bølcho, U.; Bolshakov, K.; Nelson, J. K.; Pluteanu, F.; Mellor, I. R.; Egebjerg, J.; Strømgaard, K., Uncompetitive antagonism of AMPA receptors: Mechanistic insights

from studies of polyamine toxin derivatives. *Journal of Medicinal Chemistry* **2006**, 49 (18), 5414-5423.

370. Jensen, L. S.; Bølcho, U.; Egebjerg, J.; Strømgaard, K., Design, Synthesis, and Pharmacological Characterization of Polyamine Toxin Derivatives: Potent Ligands for the Pore-Forming Region of AMPA Receptors. *ChemMedChem: Chemistry Enabling Drug Discovery* **2006**, 1 (4), 419-428.

371. Chhabra, S. R.; Khan, A. N.; Bycroft, B. W., Solid-phase synthesis of polyamines using a Dde-linker: philanthotoxin-4.3. 3 via an on-resin Mitsunobu reaction. *Tetrahedron Letters* **2000**, 41 (7), 1099-1102.

372. Hone, N. D.; Payne, L. J., Solid-phase synthesis of Agel 416; a novel approach to modified polyamines. *Tetrahedron Letters* **2000**, 41 (32), 6149-6152.

373. Méret, M.; Bienz, S., Efficient and flexible solid-phase synthesis of N-hydroxypolyamine derivatives. *European Journal of Organic Chemistry* **2008**, 2008 (33), 5518-5525.

374. Hidai, Y.; Kan, T.; Fukuyama, T., Total synthesis of polyamine toxin HO-416b and Agel-489 using a 2-nitrobenzenesulfonamide strategy. *Chemical and Pharmaceutical Bulletin* **2000**, 48 (10), 1570-1576.

375. Brown, H. C.; Heim, P., Diborane as a mild reducing agent for the conversion of primary, secondary, and tertiary amides into the corresponding amines. *Journal of the American Chemical Society* **1964**, 86 (17), 3566-3567.

376. Paikoff, S. J.; Wilson, T. E.; Cho, C. Y.; Schultz, P. G., The solid phase synthesis of N-alkylcarbamate oligomers. *Tetrahedron Letters* **1996**, 37 (32), 5653-5656.

377. Manov, N.; Bienz, S., A new approach in the solid-phase synthesis of polyamine derivatives: construction of polyamine backbones from the center. *Tetrahedron* **2001**, 57 (37), 7893-7898.

378. Nelson, J. K.; Frølund, S. U.; Tikhonov, D. B.; Kristensen, A. S.; Strømgaard, K., Synthesis and biological activity of argiotoxin 636 and analogues: selective antagonists for ionotropic glutamate receptors. *Angewandte Chemie International Edition* **2009**, 48 (17), 3087-3091.

379. Lucas, S.; Poulsen, M. H.; Nørager, N. G.; Barslund, A. F.; Bach, T. B.; Kristensen, A. S.; Strømgaard, K., General synthesis of β -alanine-containing spider polyamine toxins and discovery of Nephila polyamine toxins 1 and 8 as highly potent inhibitors of ionotropic glutamate receptors. *Journal of Medicinal Chemistry* **2012**, 55 (22), 10297-10301.

380. Burns, M. R.; Carlson, C. L.; Vanderwerf, S. M.; Ziemer, J. R.; Weeks, R. S.; Cai, F.; Webb, H. K.; Graminski, G. F., Amino acid/spermine conjugates: polyamine amides as potent spermidine uptake inhibitors. *Journal of Medicinal Chemistry* **2001**, 44 (22), 3632-3644.

381. Blagbrough, I. S.; Geall, A. J., Practical synthesis of unsymmetrical polyamine amides. *Tetrahedron Letters* **1998**, 39 (5-6), 439-442.

382. Pegg, A. E., Functions of polyamines in mammals. *Journal of Biological Chemistry* **2016**, 291 (29), 14904-14912.

383. Jackson, A. C.; Milstein, A. D.; Soto, D.; Farrant, M.; Cull-Candy, S. G.; Nicoll, R. A., Probing TARP modulation of AMPA receptor conductance with polyamine toxins. *Journal of Neuroscience* **2011**, *31* (20), 7511-7520.
384. Rock, D. M.; Macdonald, R. L., Polyamine regulation of N-methyl-D-aspartate receptor channels. *Annual Review of Pharmacology and Toxicology* **1995**, *35* (1), 463-482.
385. Benveniste, M.; Mayer, M. L., Multiple effects of spermine on N-methyl-D-aspartic acid receptor responses of rat cultured hippocampal neurones. *The Journal of Physiology* **1993**, *464* (1), 131-163.
386. Rock, D. M.; MacDonald, R. L., Spermine and related polyamines produce a voltage-dependent reduction of N-methyl-D-aspartate receptor single-channel conductance. *Molecular Pharmacology* **1992**, *42* (1), 157-164.
387. McGurk, J. F.; Bennett, M.; Zukin, R. S., Polyamines potentiate responses of N-methyl-D-aspartate receptors expressed in *Xenopus* oocytes. *Proceedings of the National Academy of Sciences* **1990**, *87* (24), 9971-9974.
388. Williams, K.; Zappia, A. M.; Pritchett, D. B.; Shen, Y. M.; Molinoff, P. B., Sensitivity of the N-methyl-D-aspartate receptor to polyamines is controlled by NR2 subunits. *Molecular Pharmacology* **1994**, *45* (5), 803-809.
389. Traynelis, S. F.; Hartley, M.; Heinemann, S. F., Control of proton sensitivity of the NMDA receptor by RNA splicing and polyamines. *Science* **1995**, *268* (5212), 873-876.
390. Mony, L.; Zhu, S.; Carvalho, S.; Paoletti, P., Molecular basis of positive allosteric modulation of GluN2B NMDA receptors by polyamines. *The EMBO Journal* **2011**, *30* (15), 3134-3146.
391. Kim, S. K.; Hayashi, H.; Ishikawa, T.; Shibata, K.; Shigetomi, E.; Shinozaki, Y.; Inada, H.; Roh, S. E.; Kim, S. J.; Lee, G., Cortical astrocytes rewire somatosensory cortical circuits for peripheral neuropathic pain. *The Journal of Clinical Investigation* **2016**, *126* (5), 1983-1997.
392. Quintana, P.; Alberi, S.; Hakkoum, D.; Muller, D., Glutamate receptor changes associated with transient anoxia/hypoglycaemia in hippocampal slice cultures. *European Journal of Neuroscience* **2006**, *23* (4), 975-983.
393. Gogas, K. R., Glutamate-based therapeutic approaches: NR2B receptor antagonists. *Current Opinion in Pharmacology* **2006**, *6* (1), 68-74.
394. Tikhonov, D. B., Ion channels of glutamate receptors: structural modeling. *Molecular Membrane Biology* **2007**, *24* (2), 135-147.
395. Gu, J.; Albuquerque, C.; Lee, C.; MacDermott, A., Synaptic strengthening through activation of Ca²⁺-permeable AMPA receptors. *Nature* **1996**, *381* (6585), 793.
396. Metzger, F.; Wiese, S.; Sendtner, M., Effect of glutamate on dendritic growth in embryonic rat motoneurons. *Journal of Neuroscience* **1998**, *18* (5), 1735-1742.
397. Roy, J.; Minotti, S.; Dong, L.; Figlewicz, D. A.; Durham, H. D., Glutamate potentiates the toxicity of mutant Cu/Zn-superoxide dismutase in motor neurons by postsynaptic calcium-dependent mechanisms. *Journal of Neuroscience* **1998**, *18* (23), 9673-9684.

398. Sorkin, L. S.; Yaksh, T. L.; Doom, C. M., Mechanical allodynia in rats is blocked by a Ca²⁺-permeable AMPA receptor antagonist. *Neuroreport* **1999**, 10 (17), 3523-3526.
399. Pogatzki, E. M.; Niemeier, J. S.; Sorkin, L. S.; Brennan, T. J., Spinal glutamate receptor antagonists differentiate primary and secondary mechanical hyperalgesia caused by incision. *Pain* **2003**, 105 (1-2), 97-107.
400. Strømgaard, K.; Mellor, I., AMPA receptor ligands: synthetic and pharmacological studies of polyamines and polyamine toxins. *Medicinal Research Reviews* **2004**, 24 (5), 589-620.
401. Olsen, C. A.; Mellor, I. R.; Wellendorph, P.; Usherwood, P. N.; Witt, M.; Franzyk, H.; Jaroszewski, J. W., Tuning Wasp Toxin Structure for Nicotinic Receptor Antagonism: Cyclohexylalanine-Containing Analogues as Potent and Voltage-Dependent Blockers. *ChemMedChem: Chemistry Enabling Drug Discovery* **2006**, 1 (3), 303-305.
402. Pothineni, V. R.; Wagh, D.; Babar, M. M.; Inayathullah, M.; Watts, R. E.; Kim, K.-M.; Parekh, M. B.; Gurjarpadhye, A. A.; Solow-Cordero, D.; Tayebi, L., Screening of NCI-DTP library to identify new drug candidates for *Borrelia burgdorferi*. *The Journal of Antibiotics* **2017**, 70 (3), 308.
403. Hughes, J. P.; Rees, S.; Kalindjian, S. B.; Philpott, K. L., Principles of early drug discovery. *British Journal of Pharmacology* **2011**, 162 (6), 1239-1249.
404. Olsen, C. A.; Witt, M.; Hansen, S. H.; Jaroszewski, J. W.; Franzyk, H., Fukuyama–Mitsunobu alkylation in amine synthesis on solid phase revisited: N-alkylation with secondary alcohols and synthesis of curtatoxins. *Tetrahedron* **2005**, 61 (25), 6046-6055.
405. Olsen, C. A.; Witt, M.; Jaroszewski, J. W.; Franzyk, H., Solid-Phase Synthesis of Rigid Acylpolyamines Using Temporary N-4, 4'-Dimethoxytrityl Protection in the Presence of Trityl Linkers. *The Journal of Organic Chemistry* **2004**, 69 (18), 6149-6152.
406. Krapcho, A. P.; Kuell, C. S., Mono-Protected Diamines. N-tert-Butoxycarbonyl- α , ω -Alkanediamines from α , ω -Alkanediamines. *Synthetic Communications* **1990**, 20 (16), 2559-2564.
407. Ganem, B., New chemistry of naturally occurring polyamines. *Accounts of Chemical Research* **1982**, 15 (9), 290-298.
408. Ase, A. R.; Therrien, E.; Séguéla, P., An allosteric inhibitory site conserved in the ectodomain of P2X receptor channels. *Frontiers in Cellular Neuroscience* **2019**, 13, 121.
409. Hajduk, P. J.; Greer, J., A decade of fragment-based drug design: strategic advances and lessons learned. *Nature Reviews Drug discovery* **2007**, 6 (3), 211.
410. Li, J.; Fountain, S. J., Fluvastatin suppresses native and recombinant human P2X₄ receptor function. *Purinergic Signalling* **2012**, 8 (2), 311-316.
411. Serrano, A.; Mo, G.; Grant, R.; Paré, M.; O'Donnell, D.; Yu, X. H.; Tomaszewski, M. J.; Perkins, M. N.; Séguéla, P.; Cao, C. Q., Differential expression and pharmacology of native P2X receptors in rat and primate sensory neurons. *Journal of Neuroscience* **2012**, 32 (34), 11890-11896.
412. Garcia-Guzman, M.; Soto, F.; Gomez-Hernandez, J. M.; Lund, P.-E.; Stühmer, W., Characterization of recombinant human P2X₄ receptor reveals pharmacological differences to the rat homologue. *Molecular Pharmacology* **1997**, 51 (1), 109-118.

413. Michel, A. D.; Ng, S. W.; Roman, S.; Clay, W. C.; Dean, D. K.; Walter, D. S., Mechanism of action of species-selective P2X7 receptor antagonists. *British Journal of Pharmacology* **2009**, 156 (8), 1312-1325.
414. Dietz, T., Bringing values and deliberation to science communication. *Proceedings of the National Academy of Sciences* **2013**, 110 (3), 14081-7.
415. Waltz, E., *After theranos*. Nature Publishing Group: **2017**.
416. Davies, S. R., Constructing communication: Talking to scientists about talking to the public. *Science Communication* **2008**, 29 (4), 413-434.
417. Jensen, P.; Rouquier, J.-B.; Kreimer, P.; Croissant, Y., Scientists who engage with society perform better academically. *Science Public Policy* **2008**, 35 (7), 527-541.
418. Jensen, P., A statistical picture of popularization activities and their evolutions in France. *Public Understanding of Science* **2011**, 20 (1), 26-36.
419. Rees, M. J. L., UK: Royal Society, Science Communication: Survey of Factors Affecting Science Communication by Scientists and Engineers. **2006**.
420. Leshner, A. I., Public engagement with science. American Association for the Advancement of Science: **2003**.
421. Fischhoff, B., Evaluating science communication. *Proceedings of the National Academy of Sciences* **2019**, 116 (16), 7670-7675.
422. Haerlin, B.; Parr, D., How to restore public trust in science. *Nature* **1999**, 400 (6744), 499.
423. Varner, J., Scientific outreach: toward effective public engagement with biological science. *BioScience* **2014**, 64 (4), 333-340.
424. Wu, J. S.; Lee, J. J., Climate change games as tools for education and engagement. *Nature Climate Change* **2015**, 5 (5), 413.
425. Tapscott, D., *Growing up digital*. McGraw-Hill Companies San Francisco. **1998**; Vol. 302.
426. Prensky, M., Digital game-based learning. *Computers in Entertainment* **2003**, 1 (1), 21-21.
427. Beck, J. C.; Wade, M., *Got game*. Harvard Business: **2004**.
428. Csikszentmihalyi, M.; Csikszentmihalyi, I. S., *Optimal experience: Psychological studies of flow in consciousness*. Cambridge university press: **1992**.
429. Beeken, M.; Budke, M., "PubScience—The Long Night of Experiments": Students Present Chemical Experiments in Dining Facilities. *Journal of Chemical Education* **2018**.
430. Griep, M. A.; Mikasen, M. L., *ReAction!: chemistry in the movies*. Oxford University Press: **2009**.
431. Frey, C. A.; Mikasen, M. L.; Griep, M. A., Put some movie wow! in your chemistry teaching. *Journal of Chemical Education* **2012**, 89 (9), 1138-1143.
432. Burks, R.; Deards, K.; DeFrain, E., Where Science Intersects Pop Culture: An Informal Science Education Outreach Program. *Journal of Chemical Education* **2017**, 94 (12), 1918-1924.

433. Dubeck, L. W.; Moshier, S. E.; Boss, J. E., Fantastic voyages: Learning science through science fiction films. Springer Science & Business Media: **2006**.
434. Mayo, M. J., Video games: A route to large-scale STEM education? *Science* **2009**, 323 (5910), 79-82.
435. Papastergiou, M., Digital game-based learning in high school computer science education: Impact on educational effectiveness and student motivation. *Computers in Education* **2009**, 52 (1), 1-12.
436. Zyda, M., From visual simulation to virtual reality to games. *Computer* **2005**, 38 (9), 25-32.
437. Gros, B., Digital games in education: The design of games-based learning environments. *Journal of Research on Technology in Education* **2007**, 40 (1), 23-38.
438. Winter, J.; Wentzel, M.; Ahluwalia, S., Chairs!: A mobile game for organic chemistry students to learn the ring flip of cyclohexane. *Journal of Chemical Education* **2016**.
439. Jones, O. A.; Spichkova, M.; Spencer, M. J., Chirality-2: Development of a Multilevel Mobile Gaming App To Support the Teaching of Introductory Undergraduate-Level Organic Chemistry. *Journal of Chemical Education* **2018**.
440. da Silva Júnior, J. N.; Nobre, D. J.; do Nascimento, R. S.; Torres Jr, G. S.; Leite Jr, A. J. M.; Monteiro, A. J.; Alexandre, F. S. O.; Rodríguez, M. T.; Rojo, M. J., Interactive Computer Game That Engages Students in Reviewing Organic Compound Nomenclature. *Journal of Chemical Education* **2018**.
441. Annetta, L. A., Video games in education: Why they should be used and how they are being used. *Theory Into Practice* **2008**, 47 (3), 229-239.
442. Jayaram, S.; Connacher, H. I.; Lyons, K. W., Virtual assembly using virtual reality techniques. *Computer-Aided Design* **1997**, 29 (8), 575-584.
443. Feng, Z.; Gonzalez, V.; Amor, R.; Lovreglio, R.; Cabrera, G., Immersive Virtual Reality Serious Games for Evacuation Training and Research: A Systematic Literature Review. *Computers & Education* **2018** 127, 252-266.
444. Ibáñez, M.-B.; Delgado-Kloos, C., Augmented reality for STEM learning: A systematic review. *Computers & Education* **2018**, 123, 109-123.
445. Bailenson, J., Experience on Demand: What Virtual Reality Is, how it Works, and what it Can Do. WW Norton & Company: **2018**.
446. Illes, J.; Moser, M. A.; McCormick, J. B.; Racine, E.; Blakeslee, S.; Caplan, A.; Hayden, E. C.; Ingram, J.; Lohwater, T.; McKnight, P., Neurotalk: improving the communication of neuroscience research. *Nature Reviews Neuroscience* **2010**, 11 (1), 61.
447. Pham, D., Public engagement is key for the future of science research. *NPJ Science of Learning* **2016**, 1, 16010.
448. Virvou, M.; Katsionis, G., On the usability and likeability of virtual reality games for education: The case of VR-ENGAGE. *Computers Education* **2008**, 50 (1), 154-178.

449. Tee, N. Y. K.; Gan, H. S.; Li, J.; Cheong, B. H.-P.; Tan, H. Y.; Liew, O. W.; Ng, T. W., Developing and demonstrating an augmented reality colorimetric titration tool. *Journal of Chemical Education* **2018**, 95 (3), 393-399.
450. Barrett, R.; Gandhi, H. A.; Naganathan, A.; Daniels, D.; Zhang, Y.; Onwunaka, C.; Luehmann, A.; White, A. D., Social and Tactile Mixed Reality Increases Student Engagement in Undergraduate Lab Activities. *Journal of Chemical Education* **2018**, 95 (10), 1755-1762.
451. Regan, C., An investigation into nausea and other side-effects of head-coupled immersive virtual reality. *Virtual Reality* **1995**, 1 (1), 17-31.
452. Price, S.; Rogers, Y.; Scaife, M.; Stanton, D.; Neale, H., Using 'tangibles' to promote novel forms of playful learning. *Interacting with Computers* **2003**, 15 (2), 169-185.
453. Dawes, J., Do data characteristics change according to the number of scale points used? An experiment using 5-point, 7-point and 10-point scales. *International Journal of Market Research* **2008**, 50 (1), 61-104.
454. Bishop, P. A.; Herron, R. L., Use and misuse of the likert item responses and other ordinal measures. *International Journal of Exercise Science* **2015**, 8 (3), 297.
455. Lee, E. A.-L.; Wong, K. W.; Fung, C. C., How does desktop virtual reality enhance learning outcomes? A structural equation modeling approach. *Computers Education* **2010**, 55 (4), 1424-1442.
456. Alavi, M.; Leidner, D. E., Research commentary: Technology-mediated learning—A call for greater depth and breadth of research. *Information Systems Research* **2001**, 12 (1), 1-10.
457. Kolb, D. A., *Experiential learning: Experience as the source of learning and development*. Englewood Cliffs, NJ: Prentice-Hal: **1984**.
458. Gardner, H., *Frames of mind: The theory of multiple intelligences*. Hachette UK: **2011**.
459. Yang, Y.-T. C., Building virtual cities, inspiring intelligent citizens: Digital games for developing students' problem solving and learning motivation. *Computers Education* **2012**, 59 (2), 365-377.
460. Telner, D.; Bujas-Bobanovic, M.; Chan, D.; Chester, B.; Marlow, B.; Meuser, J.; Rothman, A.; Harvey, B., Game-based versus traditional case-based learning: comparing effectiveness in stroke continuing medical education. *Canadian Family Physician* **2010**, 56 (9), 345-351.
461. Furió, D.; González-Gancedo, S.; Juan, M.-C.; Seguí, I.; Rando, N., Evaluation of learning outcomes using an educational iPhone game vs. traditional game. *Computers Education* **2013**, 64, 1-23.
462. Tobin, K.; Tippins, D. J.; Gallard, A. J., Research on instructional strategies for teaching science. *Handbook of Research on Science Teaching Learning* **1994**, 45, 93.
463. Connolly, T. M.; Stansfield, M.; Hailey, T., An application of games-based learning within software engineering. *British Journal of Educational Technology* **2007**, 38 (3), 416-428.
464. Cohen, J., *Statistical power analysis for the behaviour science* (2nd). New Jersey: Laurence Erlbaum Associates **1988**.

465. Lim, C. P.; Nonis, D.; Hedberg, J., Gaming in a 3D multiuser virtual environment: Engaging students in science lessons. *British Journal of Educational Technology* **2006**, 37 (2), 211-231.
466. Merchant, Z.; Goetz, E. T.; Cifuentes, L.; Keeney-Kennicutt, W.; Davis, T. J., Effectiveness of virtual reality-based instruction on students' learning outcomes in K-12 and higher education: A meta-analysis. *Computers Education* **2014**, 70, 29-40.
467. Amin, A.; Gromala, D.; Tong, X.; Shaw, C. In Immersion in cardboard VR compared to a traditional head-mounted display, International Conference on Virtual, Augmented and Mixed Reality, Springer: **2016**, 269-276.
468. Lee, S. H.; Sergueeva, K.; Catangui, M.; Kandaurova, M., Assessing Google Cardboard virtual reality as a content delivery system in business classrooms. *Journal of Education for Business* **2017**, 92 (4), 153-160.
469. Wrzesien, M.; Raya, M. A., Learning in serious virtual worlds: Evaluation of learning effectiveness and appeal to students in the E-Junior project. *Computers Education* **2010**, 55 (1), 178-187.
470. Malone, T. W., Toward a theory of intrinsically motivating instruction. *Cognitive Science* **1981**, 5 (4), 333-369.
471. Provenzo Jr, E. F., Video kids: Making sense of Nintendo. Harvard University Press: **1991**.
472. Rieber, L. P., Seriously considering play: Designing interactive learning environments based on the blending of microworlds, simulations, and games. *Educational Technology Research Development* **1996**, 44 (2), 43-58.
473. Gee, J. P., What video games have to teach us about learning and literacy. *Computers in Entertainment* **2003**, 1 (1), 20-20.
474. Conle, C., An anatomy of narrative curricula. *Educational Researcher* **2003**, 32 (3), 3-15.
475. McLellan, H., Hypertextual tales: Story models for hypertext design. *Journal of Educational Multimedia Hypermedia* **1993**, 2 (3), 239-60.
476. Schank, R. C.; Fano, A.; Bell, B.; Jona, M., The design of goal-based scenarios. *The Journal of Learning Sciences* **1994**, 3 (4), 305-345.
477. Virvou, M.; Katsionis, G.; Manos, K., Combining software games with education: Evaluation of its educational effectiveness. *Journal of Educational Technology Society* **2005**, 8 (2), 54-65.
478. Navarrete, C. C., Creative thinking in digital game design and development: A case study. *Computers Education* **2013**, 69, 320-331.
479. de Souza Sombrio, G.; Ulbricht, V. R.; Haeming, W. K., Games and gamification: A proposal for a creative learning process in education. *Journal of Education Human Development* **2014**, 3 (4), 117-129.
480. Soares-Bezerra, R. J.; da Silva Ferreira, N. C.; Alberto, A. V. P.; Bonavita, A. G.; Fidalgo-Neto, A. A.; Calheiros, A. S.; da Silva Frutuoso, V.; Alves, L. A., An improved method for P2X7R antagonist screening. *PloS One* **2015**, 10 (5), e0123089.

481. Tay, B.; Stewart, T. A.; Davis, F. M.; Deuis, J. R.; Vetter, I., Development of a high-throughput fluorescent no-wash sodium influx assay. *PLoS One* **2019**, 14 (3), e0213751.
482. Wilm, M.; Shevchenko, A.; Houthaeve, T.; Breit, S.; Schweigerer, L.; Fotsis, T.; Mann, M., Femtomole sequencing of proteins from polyacrylamide gels by nano-electrospray mass spectrometry. *Nature* **1996**, 379 (6564), 466.
483. Tsuda, M.; Shigemoto-Mogami, Y.; Koizumi, S.; Mizokoshi, A.; Kohsaka, S.; Salter, M. W.; Inoue, K., P2X 4 receptors induced in spinal microglia gate tactile allodynia after nerve injury. *Nature* **2003**, 424 (6950), 778.
484. Schmidtko, A.; Lötsch, J.; Freynhagen, R.; Geisslinger, G., Ziconotide for treatment of severe chronic pain. *The Lancet* **2010**, 375 (9725), 1569-1577.
485. Kuhn-Nentwig, L.; Stöcklin, R.; Nentwig, W., Venom composition and strategies in spiders: is everything possible? *Advances in insect physiology*, Elsevier: **2011**; Vol. 40, 1-86.

Supporting Information

Table S1. Retention times of the spider venom fractions (RP-HPLC)

<i>Lasiadora klugi</i>	
Fraction	Retention time (min)
F1	4.507
F2	5.205
F3	6.056
F4	7.140
F5	11.366
F6	11.730
F7	14.215
F8	14.360
F9	15.989
F10	16.168
F11	16.381
F12	16.581
F13	17.000
F14	17.500
F15	18.080
F16	18.224
F17	18.645
F18	19.163
F19	19.943
F20	24.904
F21	25.860
F22	27.648
F23	30.127
F24	35.945
F25	58.800

<i>Lasiadora parahybana</i>	
F1	4.462
F2	4.792
F3	5.108
F4	13.052
F5	15.657
F6	15.931
F7	16.220
F8	16.581
F9	16.852
F10	16.999
F11	17.128
F12	17.923
F13	18.510
F14	18.720
F15	19.919

F16	20.740
F17	25.773
F18	26.776
F19	28.301
F20	57.099
F21	58.124
F22	58.531
F23	58.865
F24	59.080
F25	59.589

Nhandu chromatus

F1	3.849
F2	4.135
F3	4.208
F4	4.613
F5	5.847
F6	6.341
F7	6.624
F8	6.578
F9	15.402
F10	16.522
F11	17.068
F12	18.719
F13	19.666
F14	19.963
F15	27.236
F16	27.845
F17	28.086
F18	29.060
F19	29.337
F20	31.052
F21	31.438
F22	31.666
F23	32.515
F24	32.782
F25	33.542
F26	34.052
F27	35.129
F28	35.463
F29	35.990
F30	36.931
F31	37.369
F32	38.253
F33	41.622
F34	42.101
F35	43.818
F36	44.529
F37	45.570
F38	46.243

F39	46.688
F40	46.883
F41	47.323
F42	47.689
F43	48.367
F44	49.076
F45	49.502
F46	50.370
F47	50.752
F48	51.539
F49	52.279
F50	52.765
F51	53.152
F52	53.568
F53	53.981
F54	54.367
F55	55.102
F56	55.855
F57	56.466
F58	56.823
F59	57.187
F60	57.849
F61	58.170
F62	58.573
F63	58.684
F64	58.851
F65	59.334
F66	59.603
F67	59.851
F68	60.143
F69	78.474

Acanthoscurria geniculata

F1	3.731
F2	4.263
F3	5.625
F4	6.820
F5	7.321
F6	12.298
F7	13.062
F8	13.720
F9	14.474
F10	15.543
F11	16.402
F12	16.544
F13	16.814
F14	16.901
F15	17.183
F16	17.506
F17	18.306

F18	19.040
F19	31.600
F20	32.330
F21	33.421
F22	34.309
F23	37.530
F24	38.100
F25	49.519
F26	56.163
F27	57.268
F28	58.620
F29	59.011
F30	59.478
F31	60.490
F32	60.971
F33	78.472

Acanthoscurria cordubensis

F1	3.620
F2	3.872
F3	4.117
F4	4.704
F5	5.019
F6	9.237
F7	10.046
F8	11.785
F9	12.282
F10	13.137
F11	13.569
F12	14.265
F13	14.670
F14	15.785
F15	16.082
F16	16.137
F17	16.569
F18	16.665
F19	16.670
F20	28.435
F21	39.575
F22	48.371
F23	49.737
F24	50.568
F25	51.660
F26	52.273
F27	52.739
F28	53.226
F29	55.120
F30	56.374
F31	57.778

F32	58.302
F33	58.721
F34	59.250
F35	59.500
F36	59.643
F37	60.200
F38	60.400
F39	60.850
F40	63.800
F41	64.000
F42	64.867
F43	78.726

Ephebopus murinus

F1	3.675
F2	4.523
F3	4.716
F4	7.974
F5	8.694
F6	12.507
F7	14.880
F8	15.180
F9	15.851
F10	16.467
F11	16.661
F12	17.098
F13	17.327
F14	17.763
F15	18.202
F16	18.630
F17	19.123
F18	19.384
F19	20.416
F20	20.589
F21	20.930
F22	21.675
F23	22.314
F24	23.973
F25	24.563
F26	24.836
F27	25.170
F28	25.683
F29	26.490
F30	27.113
F31	28.819
F32	29.249
F33	30.676
F34	32.861
F35	34.111

F36	37.499
F37	38.726
F38	39.872
F39	40.728
F40	42.316
F41	43.958
F42	44.877
F43	45.461
F44	51.445
F45	53.445
F46	58.205
F47	78.464

Phormictopus cancerides

F1	3.479
F2	3.759
F3	4.963
F4	4.077
F5	5.265
F6	11.980
F7	12.387
F8	16.387
F9	16.689
F10	16.902
F11	17.980
F12	18.387
F13	19.387
F14	19.689
F15	19.902
F16	20.113
F17	21.509
F18	26.132
F19	27.846
F20	28.321
F21	28.813
F22	29.053
F23	29.512
F24	29.769
F25	30.257
F26	30.992
F27	31.706
F28	32.789
F29	33.539
F30	34.152
F31	34.869
F32	35.176
F33	35.638
F34	36.870
F35	37.519
F36	38.111

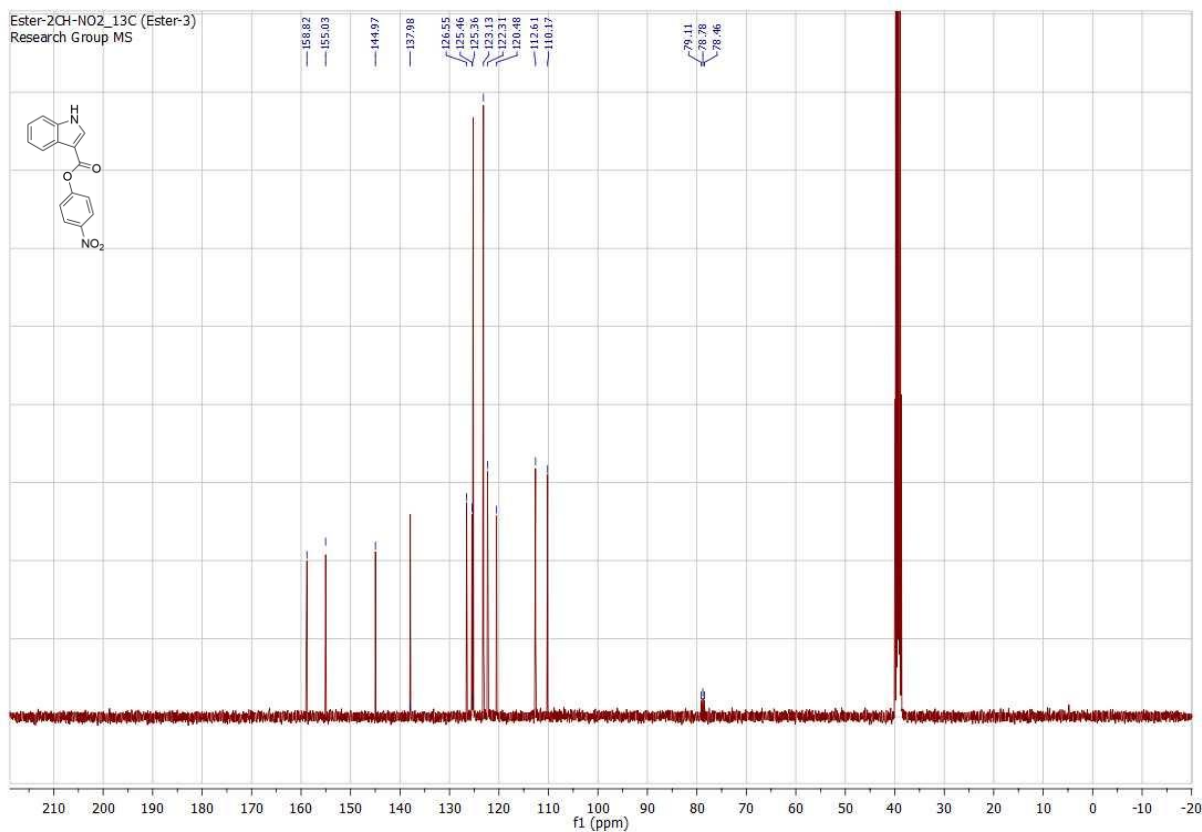
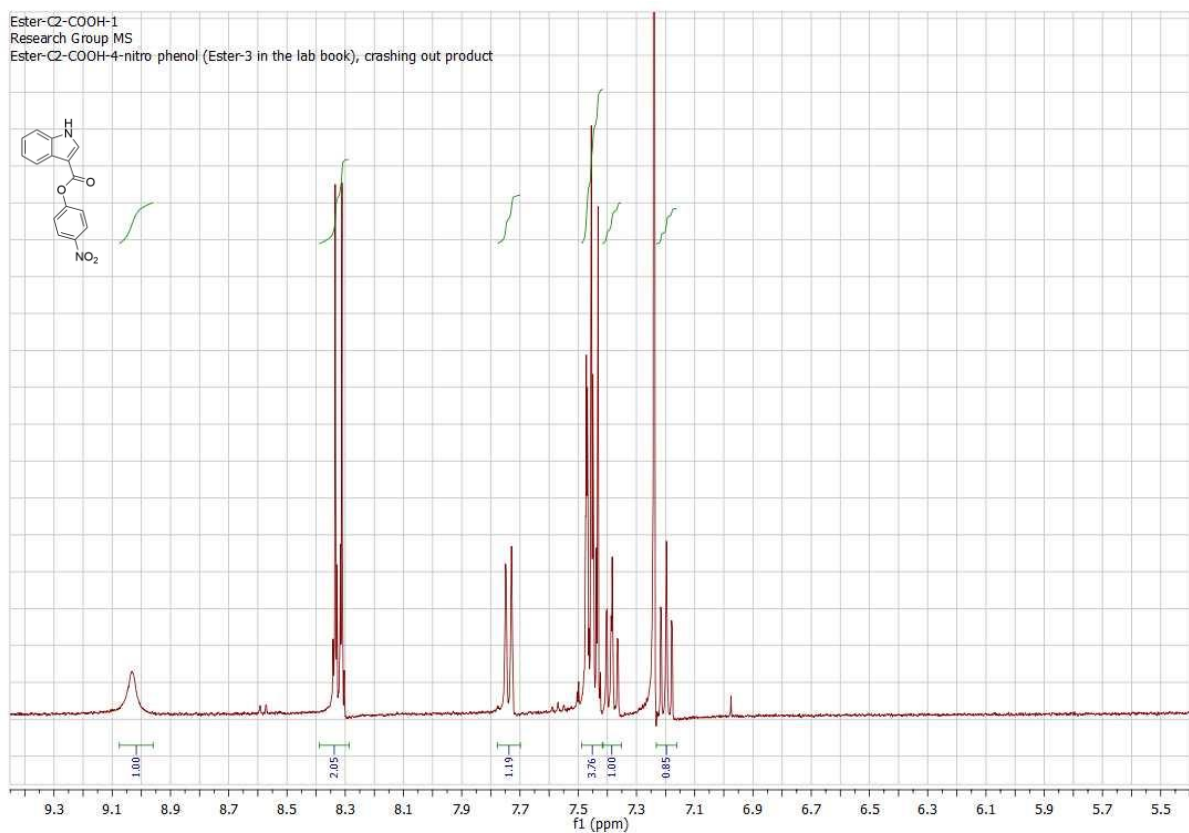
F37	38.549
F38	39.449
F39	41.974
F40	42.319
F41	44.943
F42	45.386
F43	46.176
F44	46.424
F45	47.199
F46	47.624
F47	48.913
F48	49.937
F49	50.611
F50	51.555
F51	52.456
F52	53.074
F53	54.562
F54	55.366
F55	56.121
F56	57.094
F57	58.277
F58	58.772
F59	59.065
F60	59.616
F61	60.204

Haploelma albostriatum

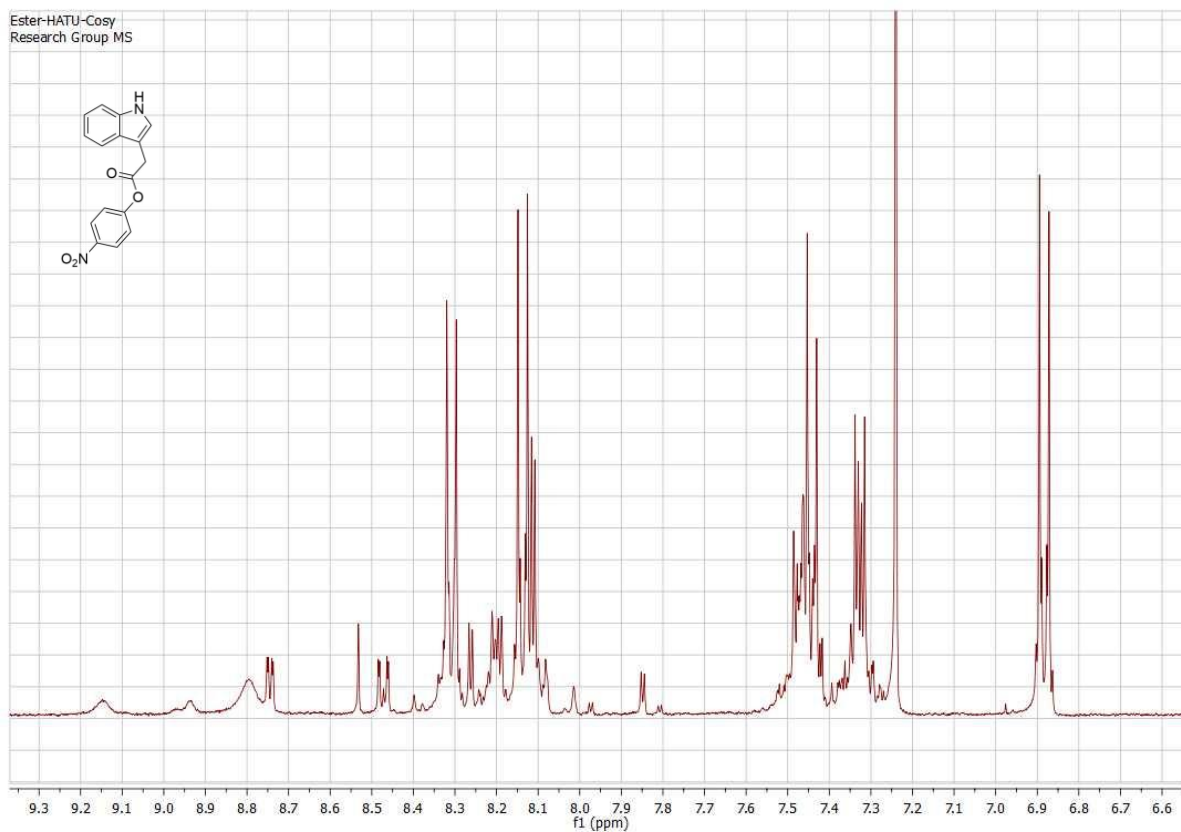
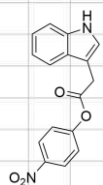
F1	3.537
F2	6.526
F3	6.668
F4	7.107
F5	7.853
F6	11.943
F7	15.342
F8	15.731
F9	15.898
F10	16.251
F11	16.346
F12	16.729
F13	17.101
F14	17.438
F15	17.536
F16	18.242
F17	18.700
F18	20.904
F19	21.266
F20	23.236
F21	23.623
F22	24.097
F23	24.628

F24	25.278
F25	25.990
F26	27.788
F27	29.222
F28	29.541
F29	29.996
F30	30.430
F31	31.274
F32	31.768
F33	32.805
F34	33.374
F35	34.719
F36	35.783
F37	36.286
F38	38.546
F39	39.261
F40	40.060
F41	41.862
F42	46.139
F43	58.465
F44	59.074
F45	59.394
F46	59.568
F47	60.332

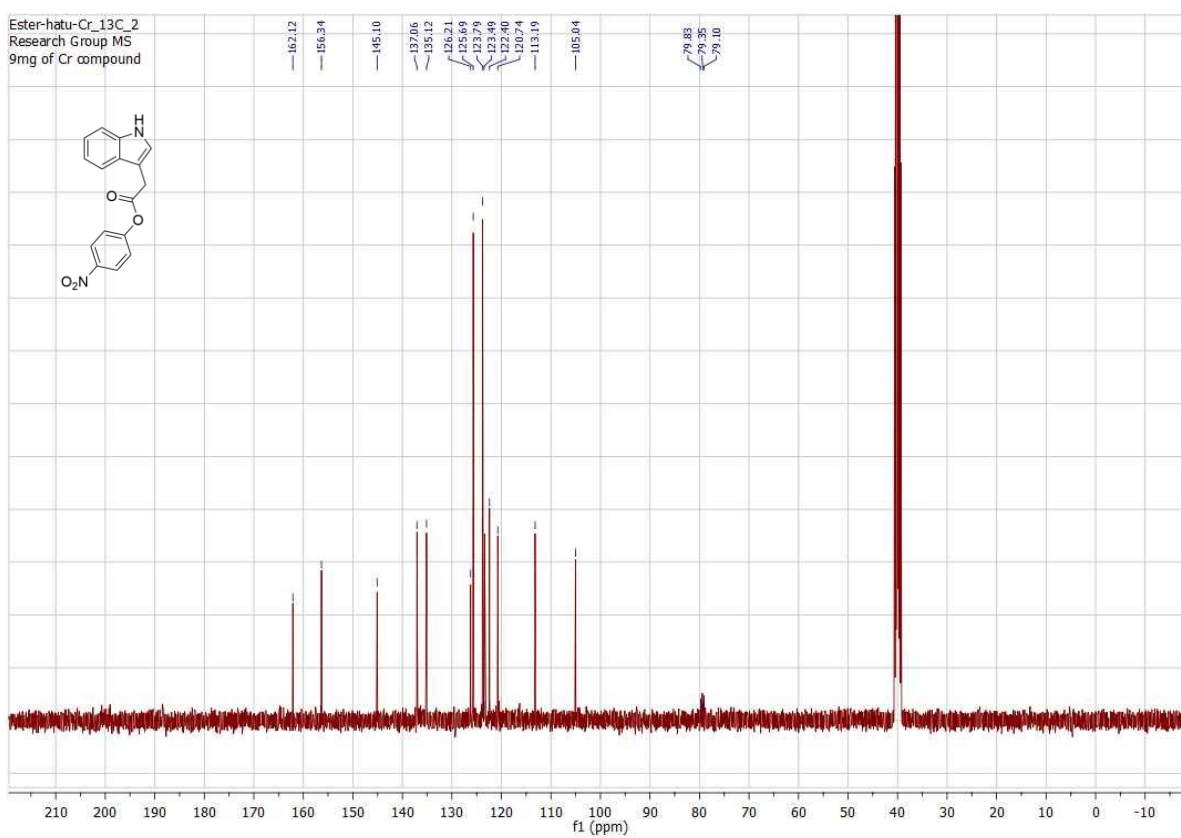
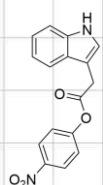
Figure S1. NMR Spectra of the activated esters (intermediates) and the final products (LK-601 analogues). ¹H and ¹³C NMR spectra were recorded at 400 MHz on a Bruker Avance III spectrometer.



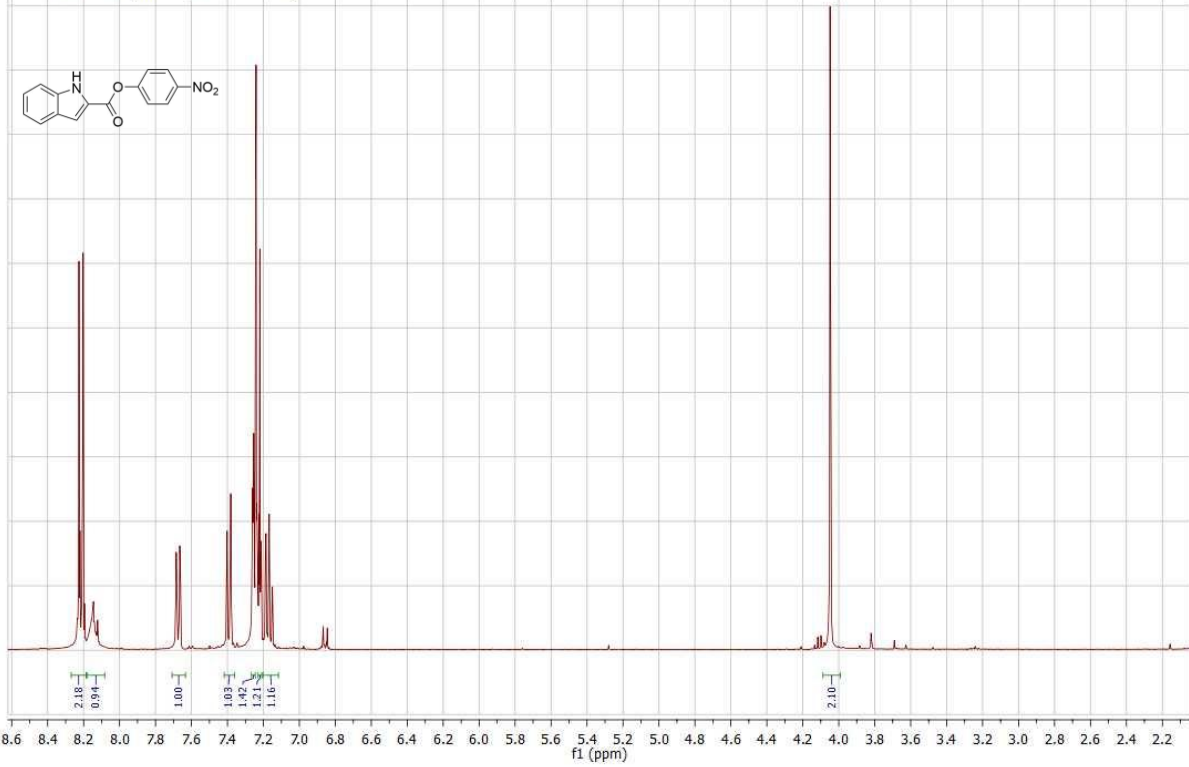
Ester-HATU-Cosy
Research Group MS



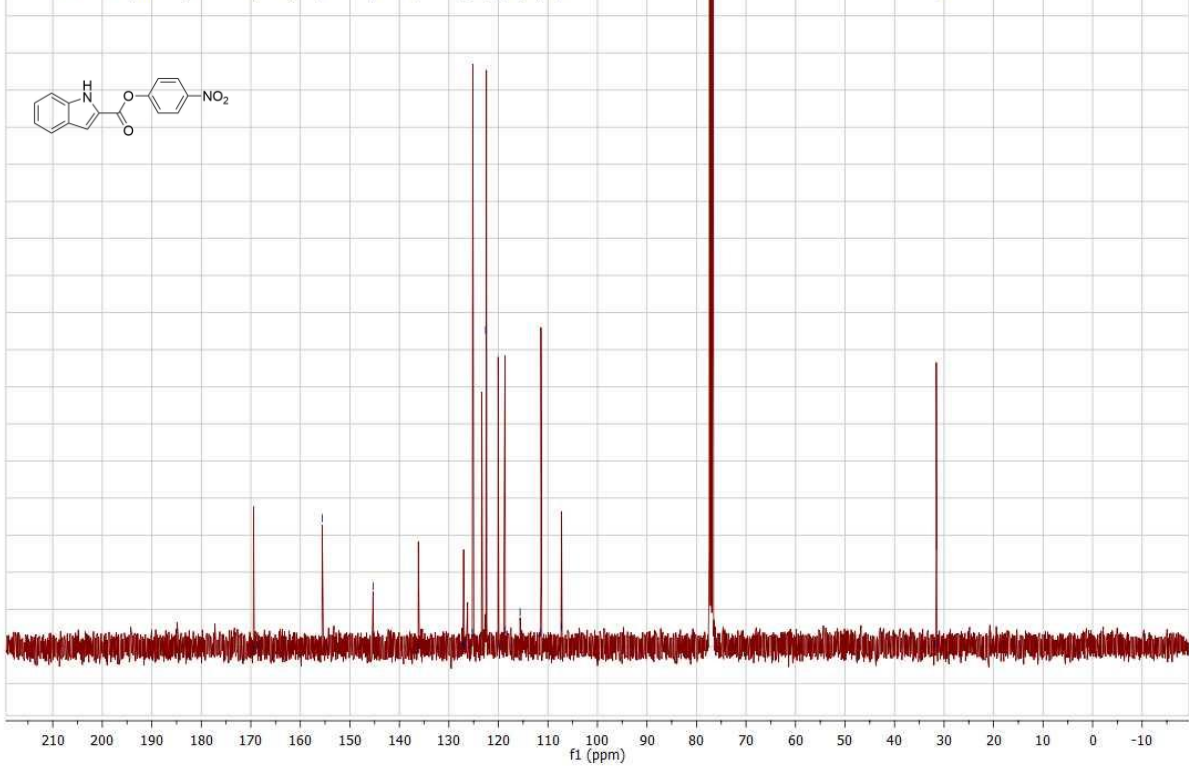
Ester-hatu-Cr_13C_2
Research Group MS
9mg of Cr compound



Ester-2-CH2COOH
Research Group MS
Second in-between product (indol-CH2-COOH)

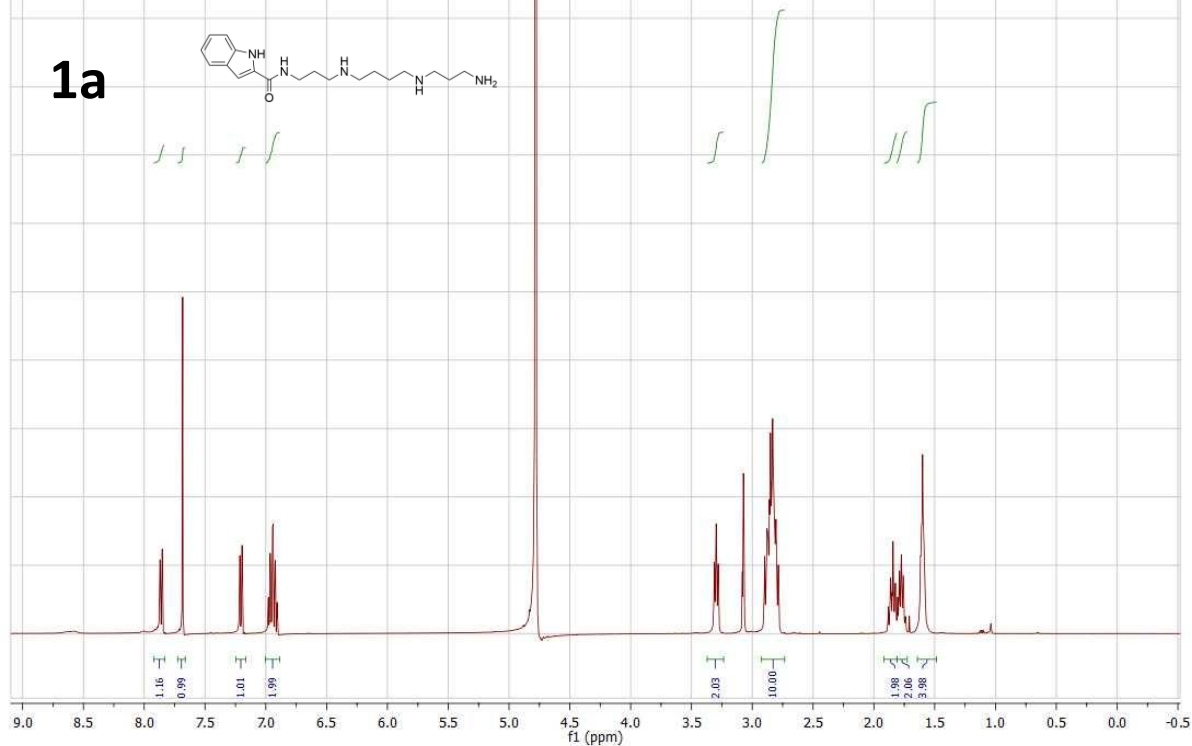
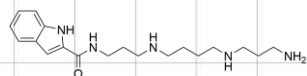


Ester-2-CH2COOH
Research Group MS
Second in-between product (indol-CH2-COOH)



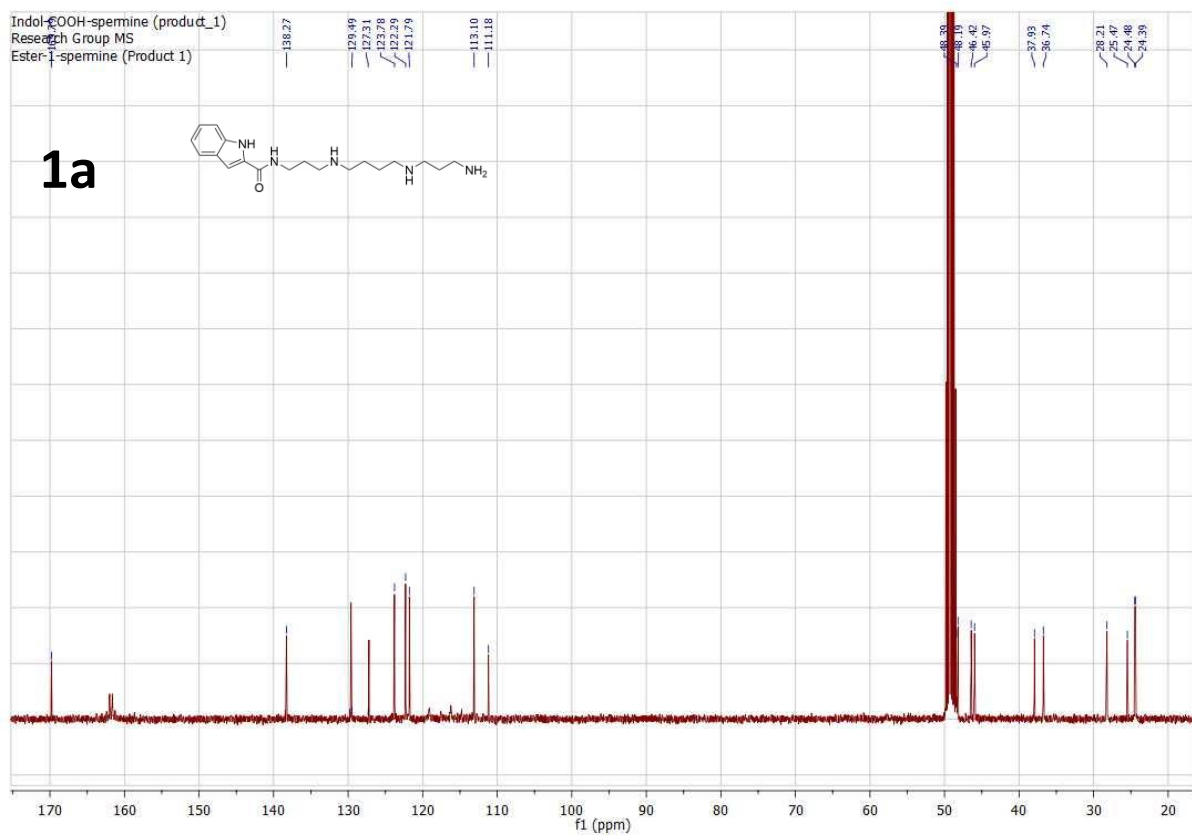
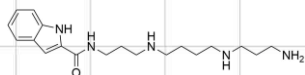
Indol-COOH-spermine (product_1)
Research Group MS
Ester-1-spermine (Product 1)

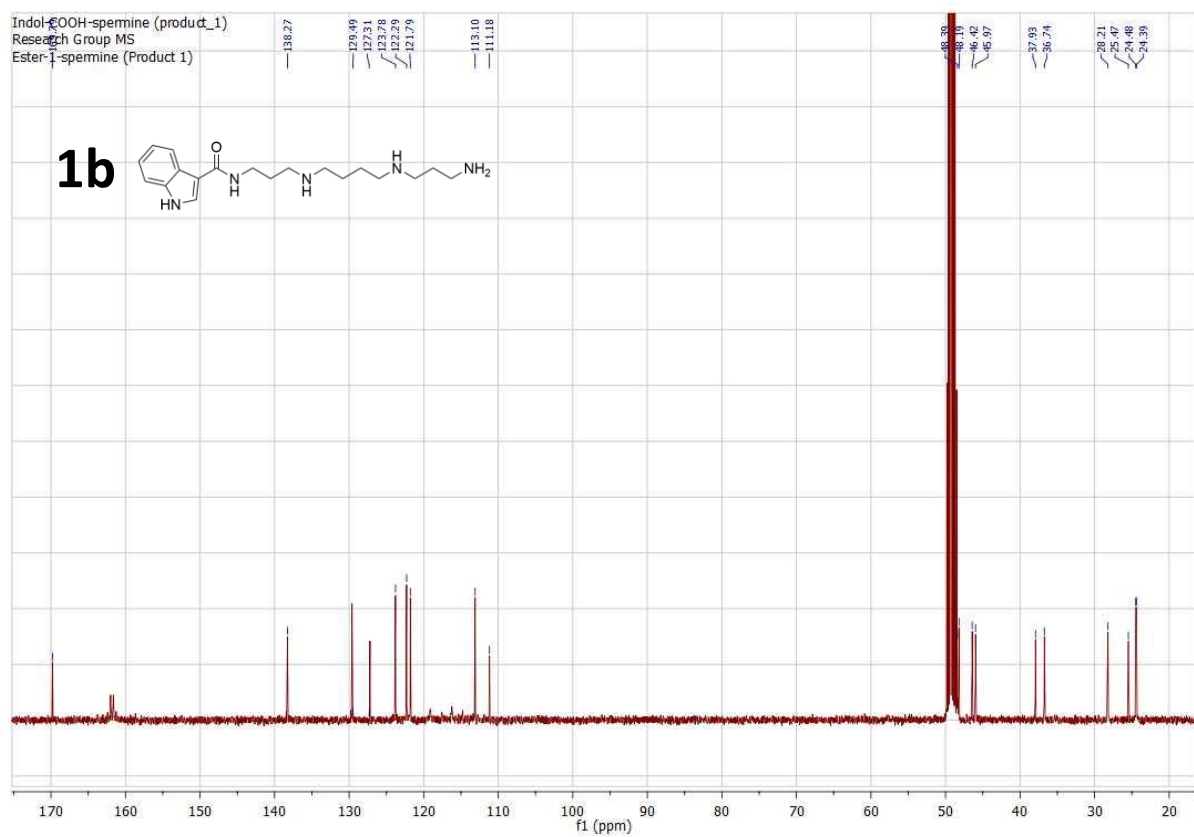
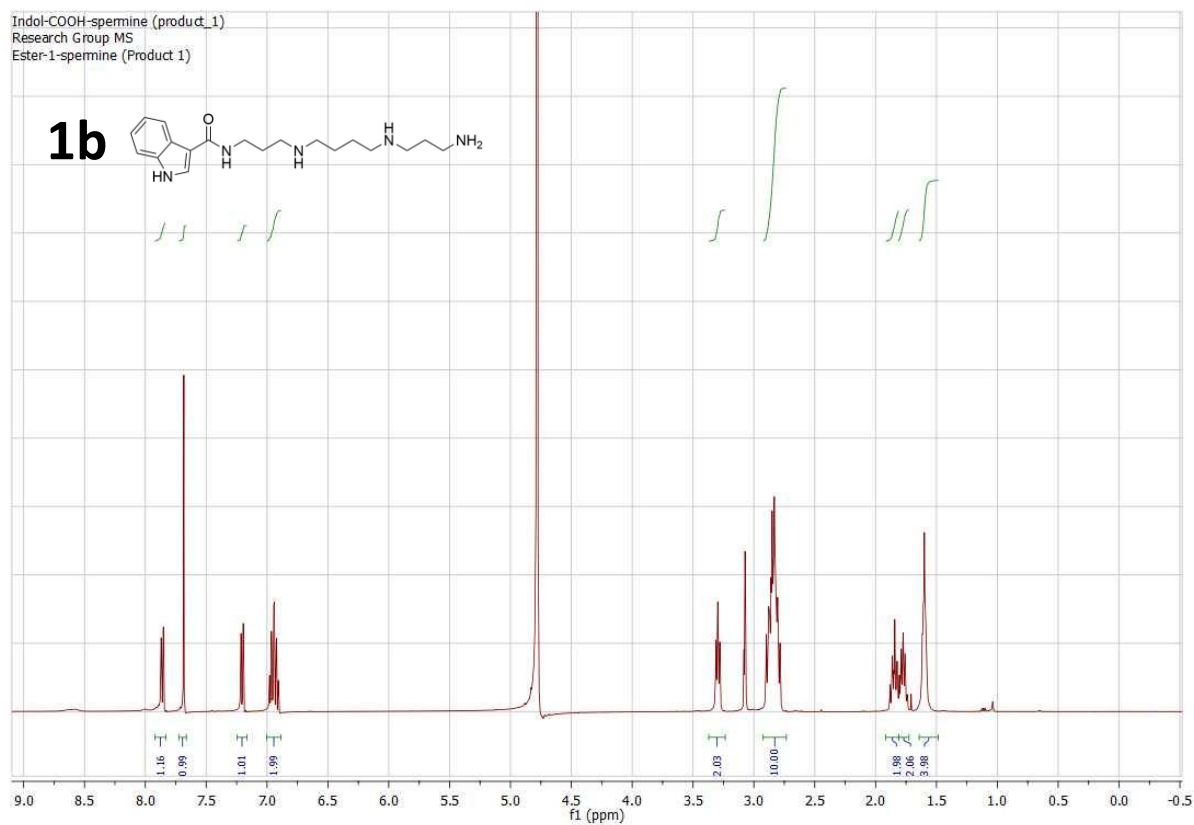
1a



Indol-COOH-spermine (product_1)
Research Group MS
Ester-1-spermine (Product 1)

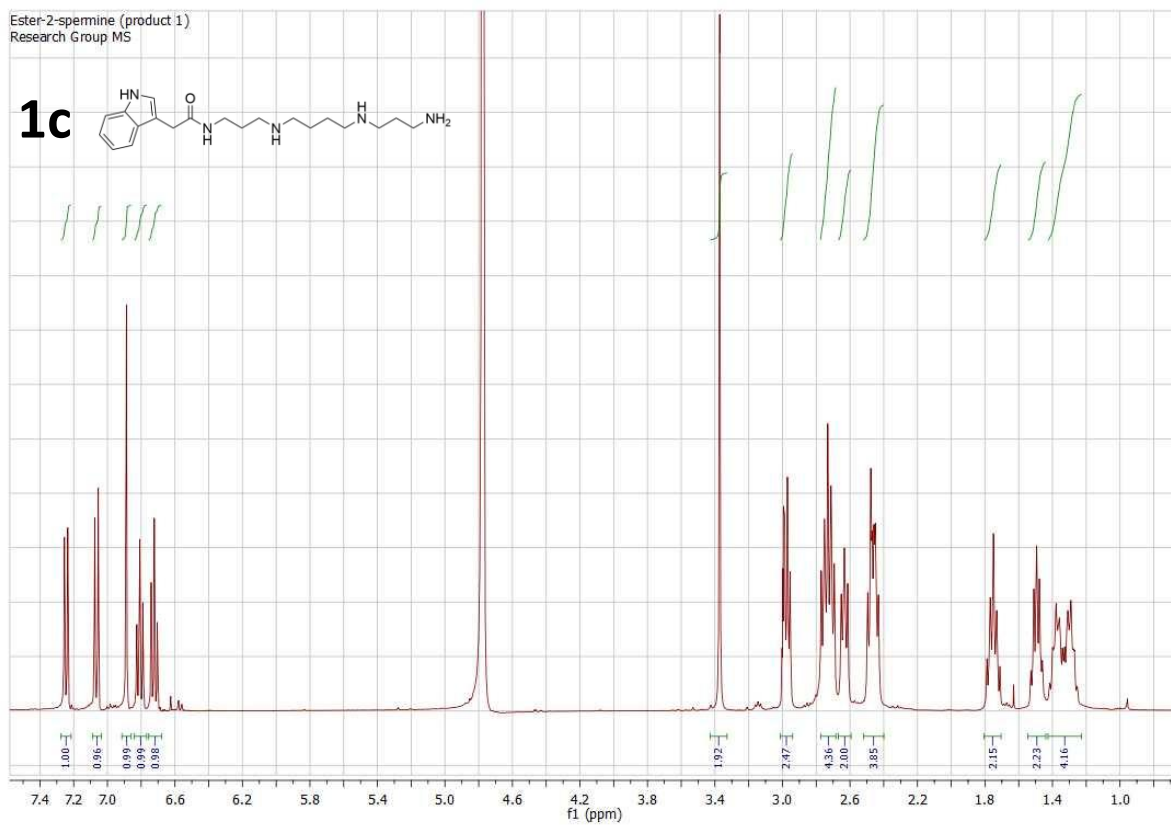
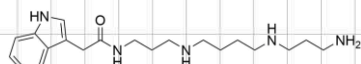
1a





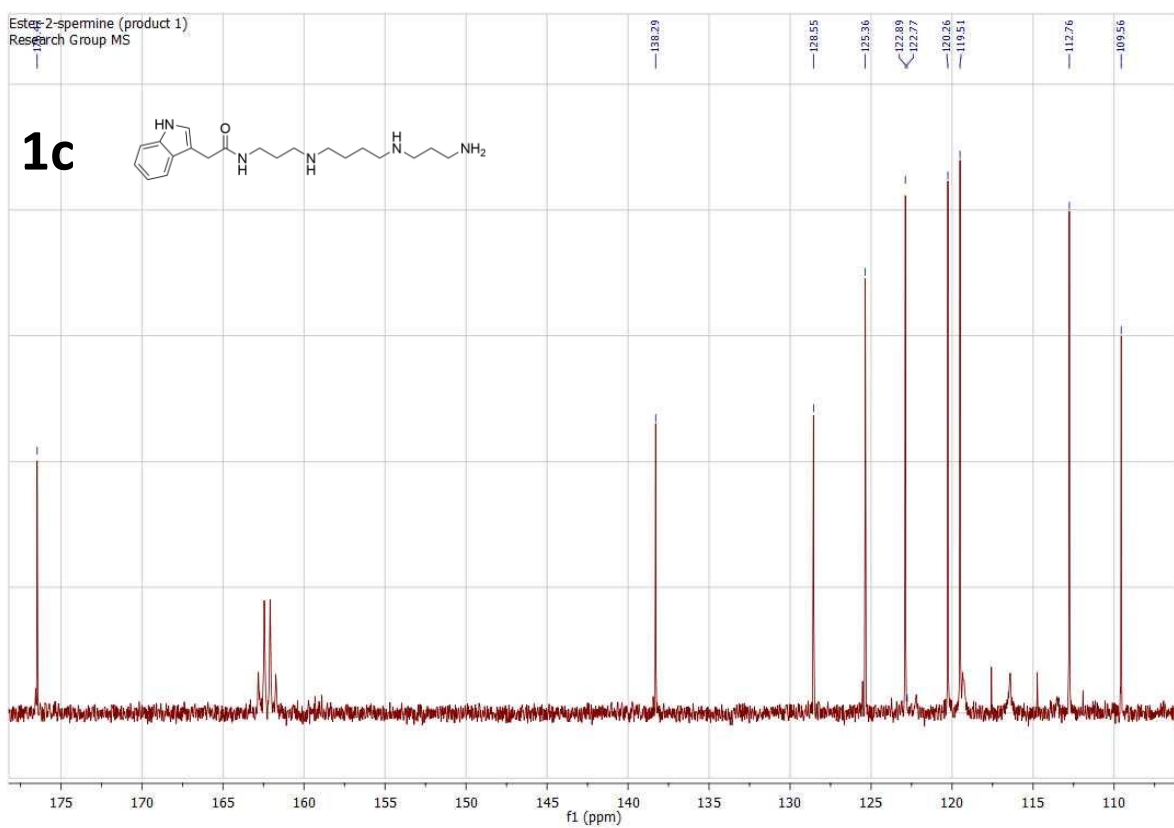
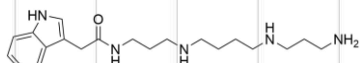
Ester-2-spermine (product 1)
Research Group MS

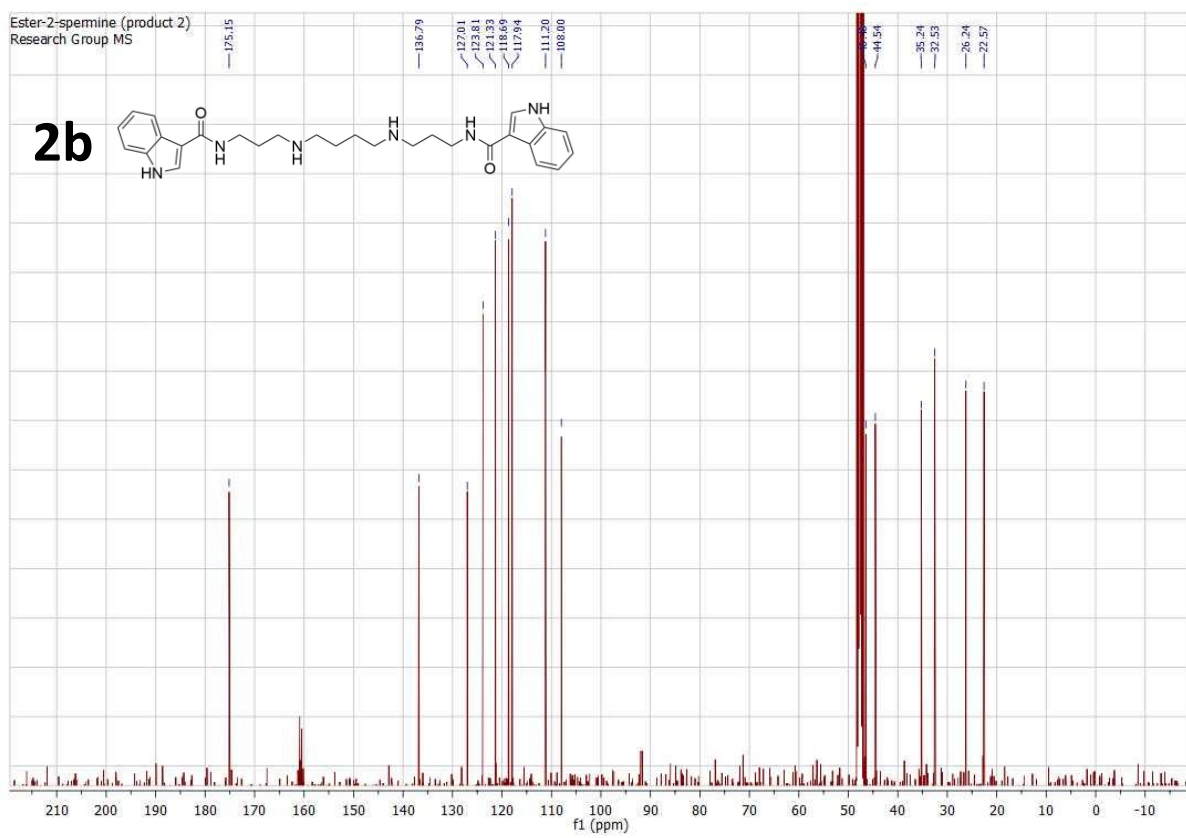
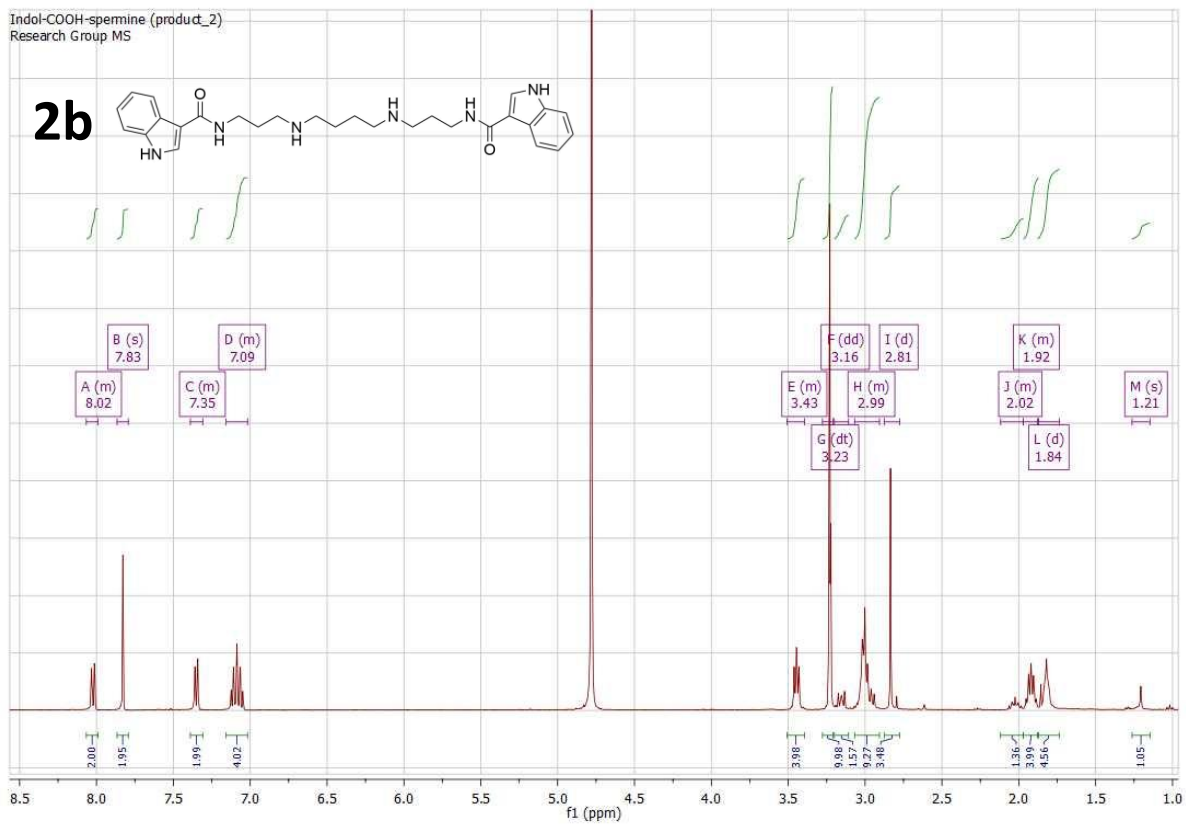
1c



Ester-2-spermine (product 1)
Research Group MS

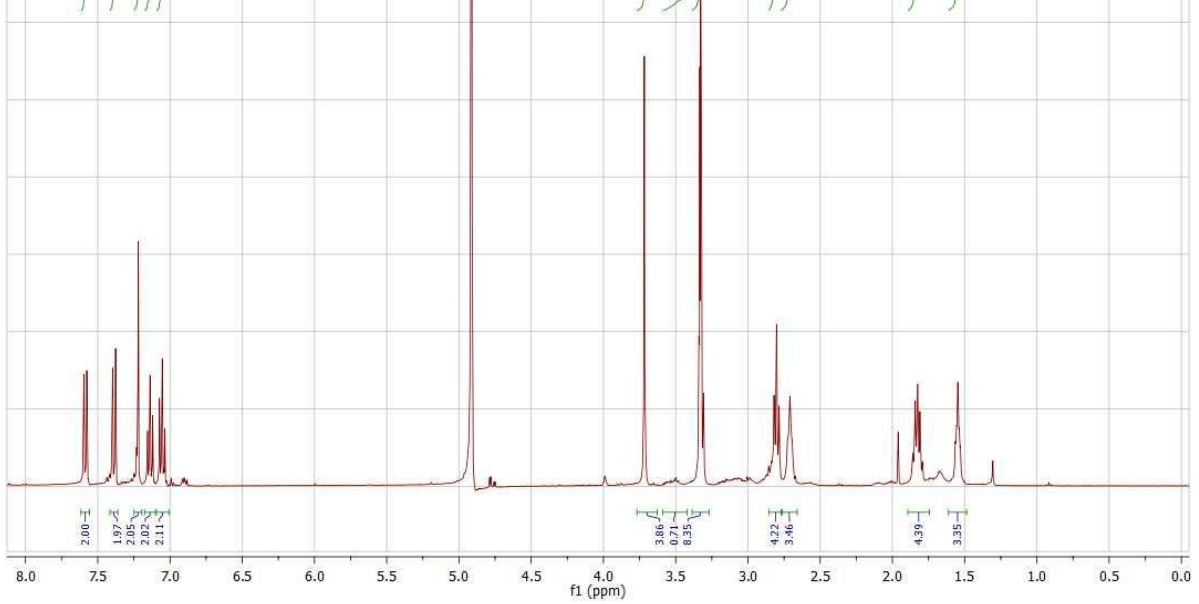
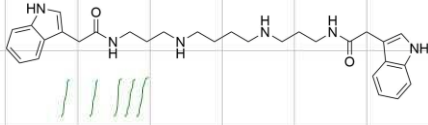
1c





Ester-2-spermine (product 2)
Research Group MS

2c



Ester-2-spermine (product 2)
Research Group MS

2c

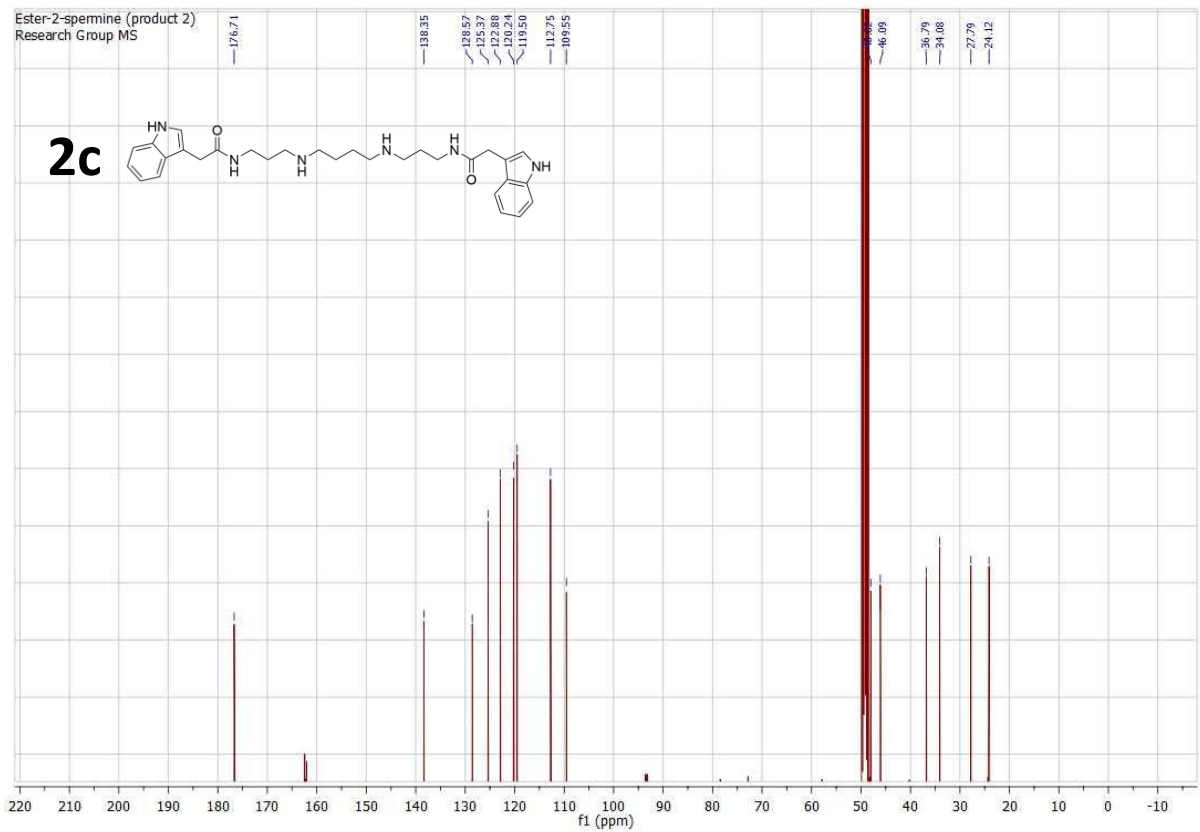
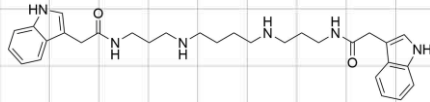
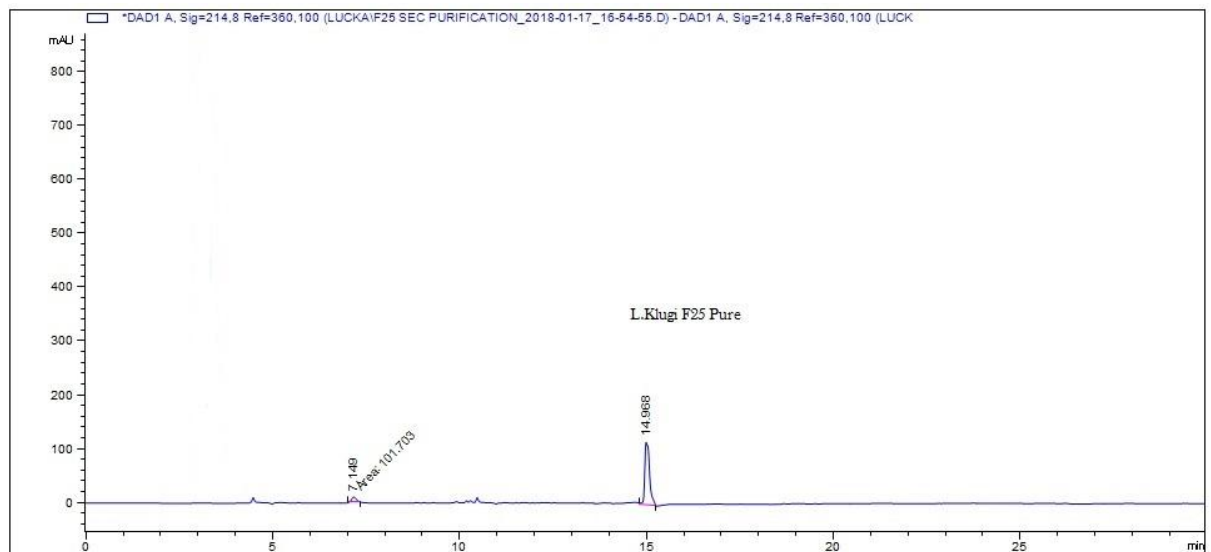
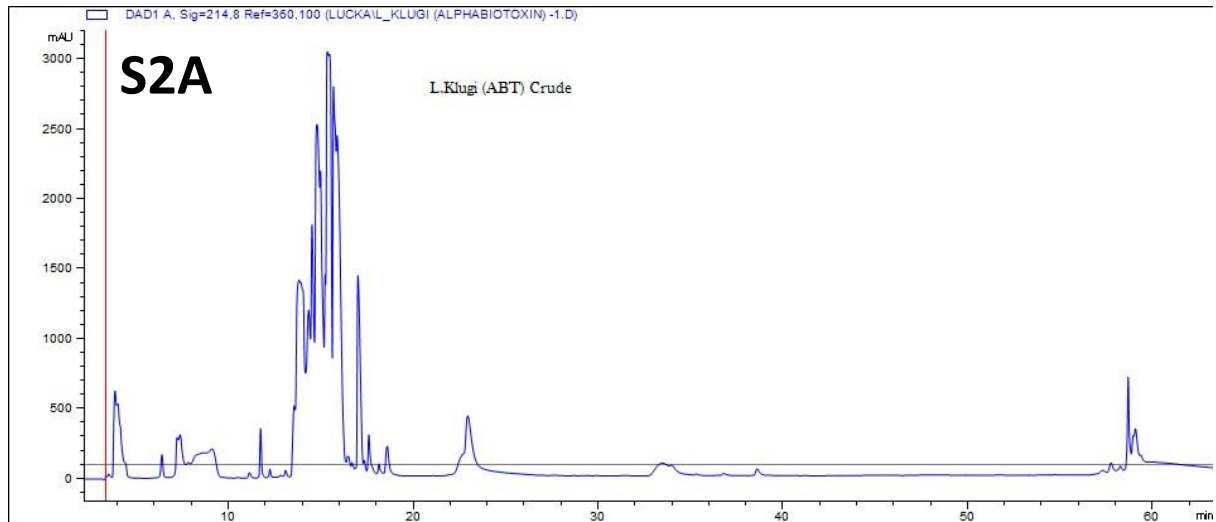


Figure S2. Peptide F25 Purification and Mass Estimation. **A:** RP-HPLC Chromatograms of crude venom (*Lasidora klugi*) and the purified F25 (purity was estimated to be 91.2 %). **B:** MALDI-TOF estimation of the peptide mass (two peaks were found at m/z 3.8 and 7.7 kDa with 7.7 kDa being the dimer of the 3.8 kDa one).



#	Time	Area	Height	Width	Area%	Symmetry
1	7.149	101.7	10.3	0.1651	8.737	0.758
2	14.968	1062.3	117.7	0.1193	91.263	0.436

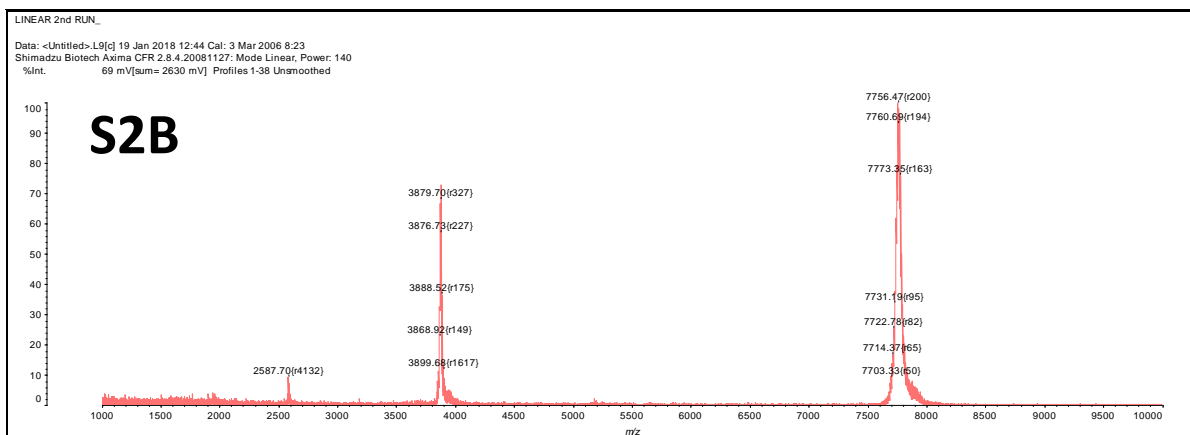
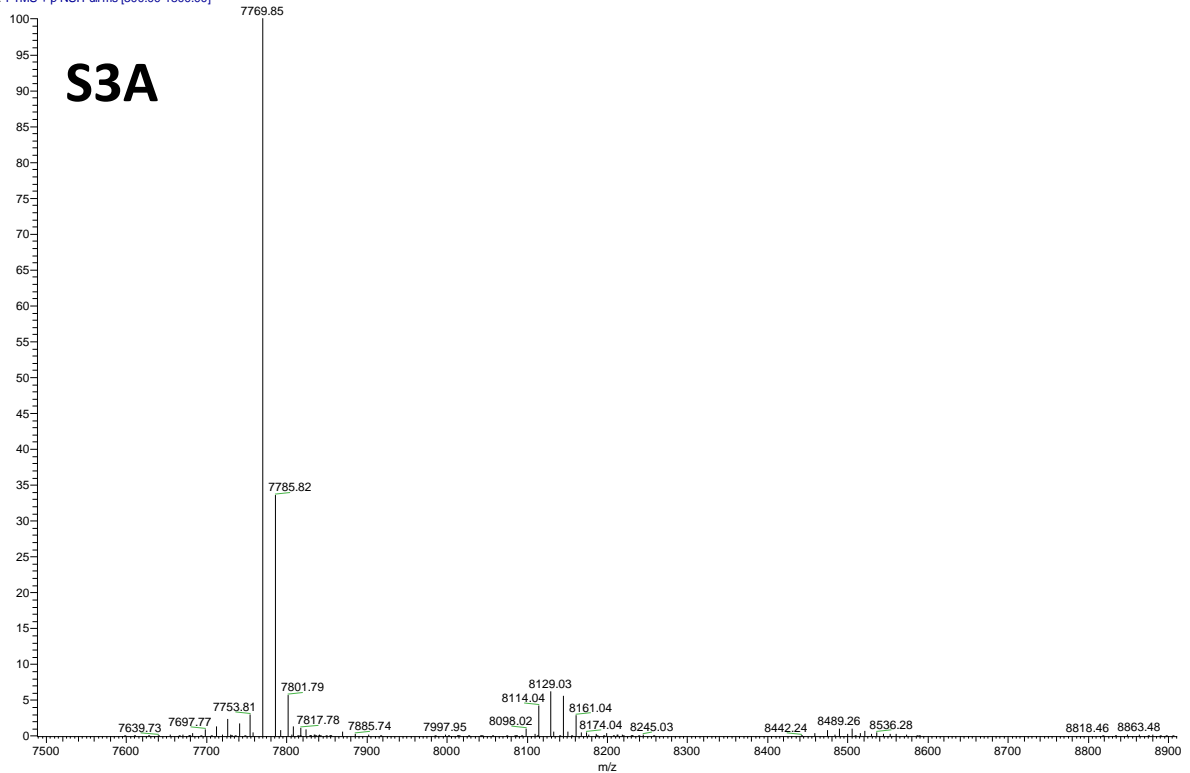
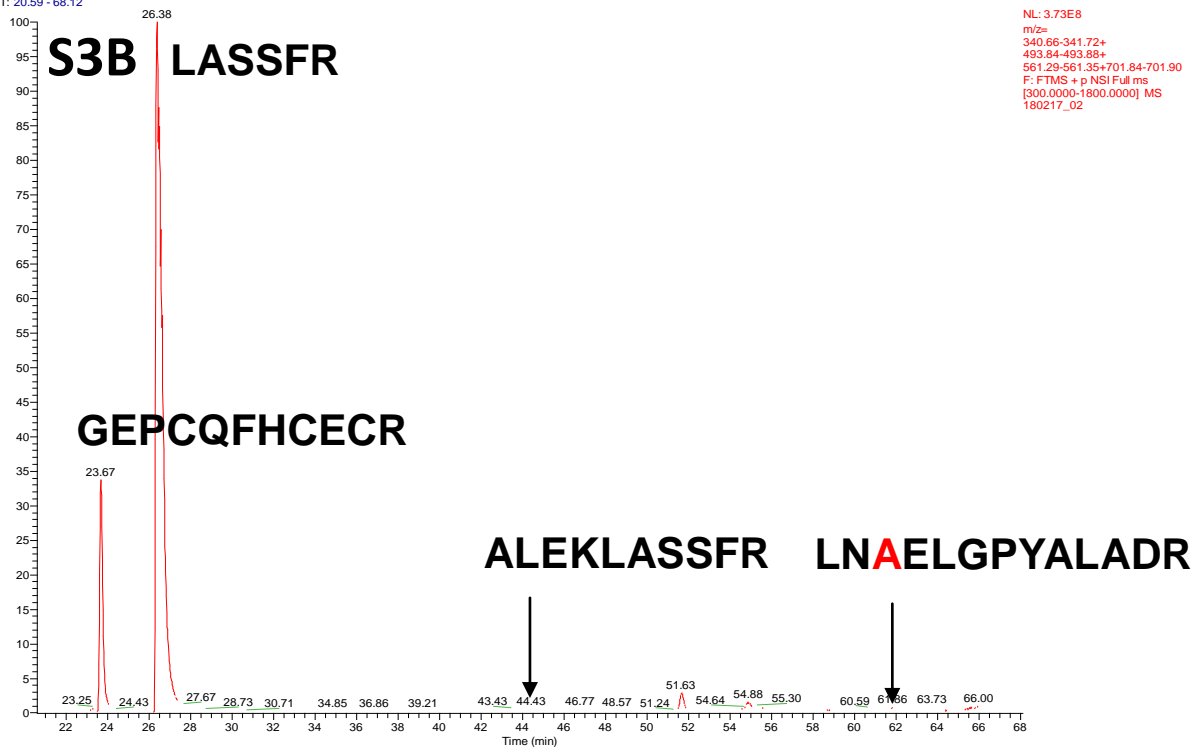


Figure S3. Peptide F25 Mass Determination and Identification. **A:** LC-MS Orbitrap determination of the exact peptide mass (one peak was found with the accurate molecular weight of 7769.85 Da). **B:** Trypsin digestion (peptide mass was 150 µg) was carried out and the peptide fragments identified. **C:** Zoom in on two later fragments is presented in greater detail. **D:** The identified peptide fragments were subjected to the protein database to match any already identified peptides. **E:** The N terminal portion of F25 was sequenced (Cambridge Peptides Inc.) and first five amino residues (N-terminal end) identified.

180217_03_XT_00001_M_#2 RT: 2.00 AV: 1 NL: 7.28E8
T: FTMS + p NSI Full ms [300.00-1800.00]



RT: 20.59 - 68.12



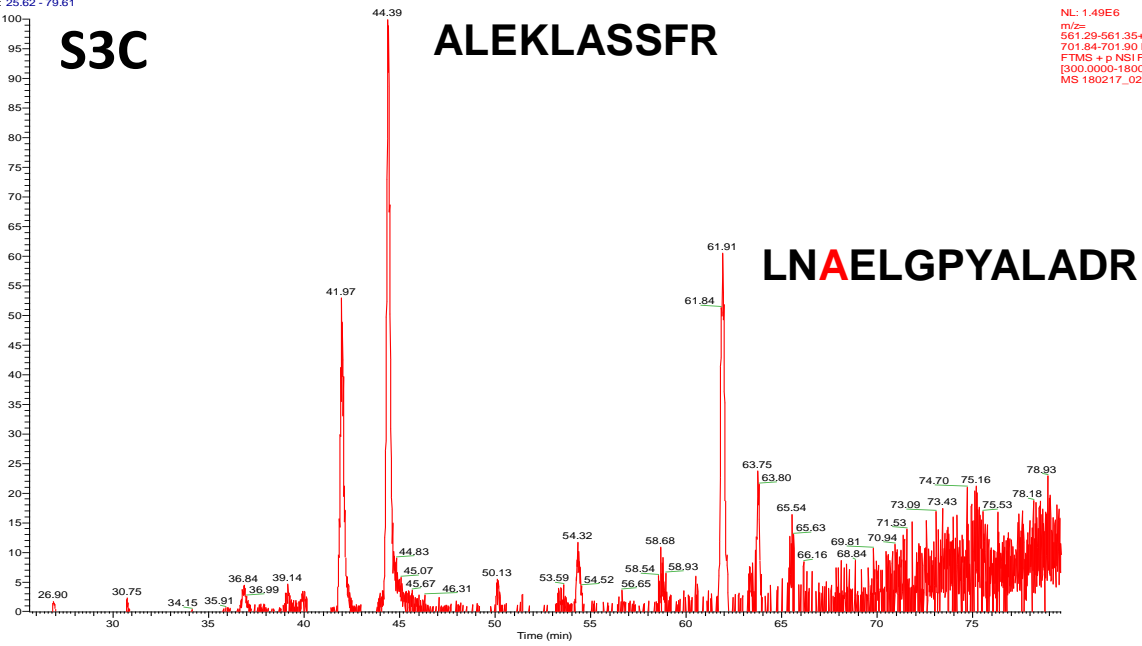
NL: 3.73E8
m/z:
340.66-341.72+
493.84-493.88+
561.29-561.35+701.84-701.90
F: FTMS + p NSI Full ms
[300.0000-1800.0000] MS
180217_02

RT: 25.62 - 79.61

S3C

ALEKLASSFR

NL: 1.49E6
 m/z=
 561.29-561.35+
 701.84-701.90 F-
 FTMS + p NSI Full ms
 [300.000-1800.0000]
 MS 180217_02



S3D

as:U3-theraphotoxin-Lsp1a|sp:A3F7X2|719 (100%), 12,908.4 Da
 Toxin with unknown activity from venom of the spider Lasiodora sp.
 5 exclusive unique peptides, 13 exclusive unique spectra, 25 total spectra, 36/116 amino acids (31% coverage)

MKLSTFIIMI SLAVLATWP SEHIEGSDSE TKLNVELOPY ALADRAEKVK DDSLNLKGEPC QFHSELR GAS VLCEAVYGTR SPYKCMIKR
 LPI SVLDIMY QAERALEKLA SSFRCE

S3E



Protein sequence report

Cambridge Peptides Order: CPO32580
 Customer sample code: peptide
 Created on: 12th February 2018

N terminus

Residue				
1	A			
2	E			
3	F			
4	G			
5	F			
6				
7				
8				
9				
10				
11				
12				
13				
14				
15				

Figure S4. A concentration-response curve of F25 on 1321N1-hP2X4 (Fura-2) cell line. Normalized concentration-response curves of two commercially available hP2X4 antagonist (n=3) 5-BDBD (10 μ M), and BX430 (10 μ M), together with F25 (5 μ M) using the ATP concentration of 1.6 μ M (EC_{50}).

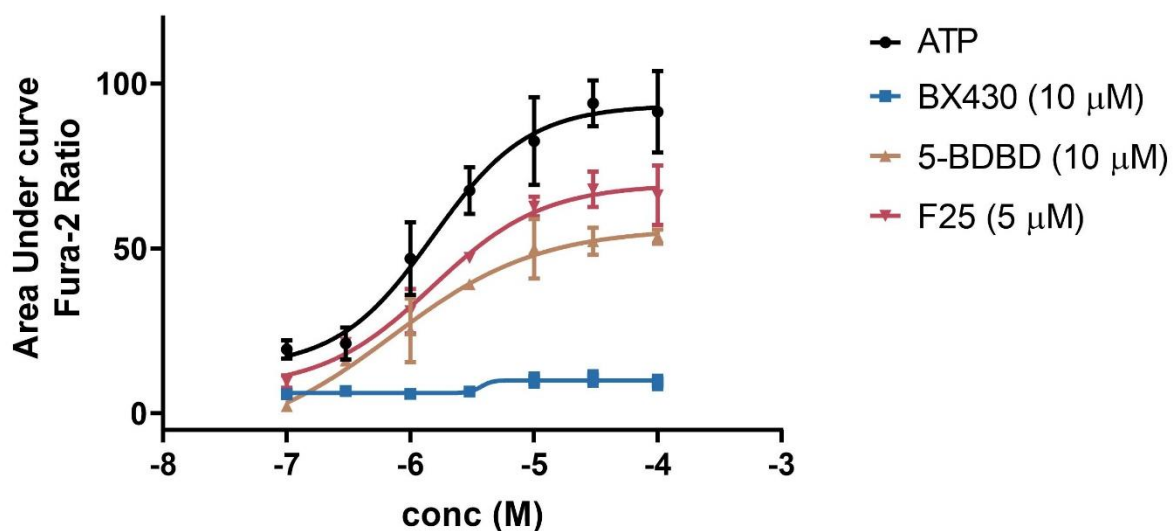


Figure S5. ESI-MS for 1H-Indole-3-carboxylic acid, 4-nitrophenyl ester. m/z calcd for $C_{15}H_{10}N_2O_4$ (M+H) 283.25, found 283.0535.

fragmentor voltage 130									
Comment	130 V	Count	4688	Data Type	MS	Date	2019-03-14	File Name	E:\190225 HRMS\Ester 1.d
Instrument	Instrument 1	Ion Mode	ESI+	Plot Type	Stick	Retention Time	3.738	Sample	Ester 1
Scan Type	Scan	Spectrum Type	MS	TIC	1184.97	Total Signal	2624382.4571	Scan	88

Ester 1_1_0283.0535.rcted_Scan_3.74_88

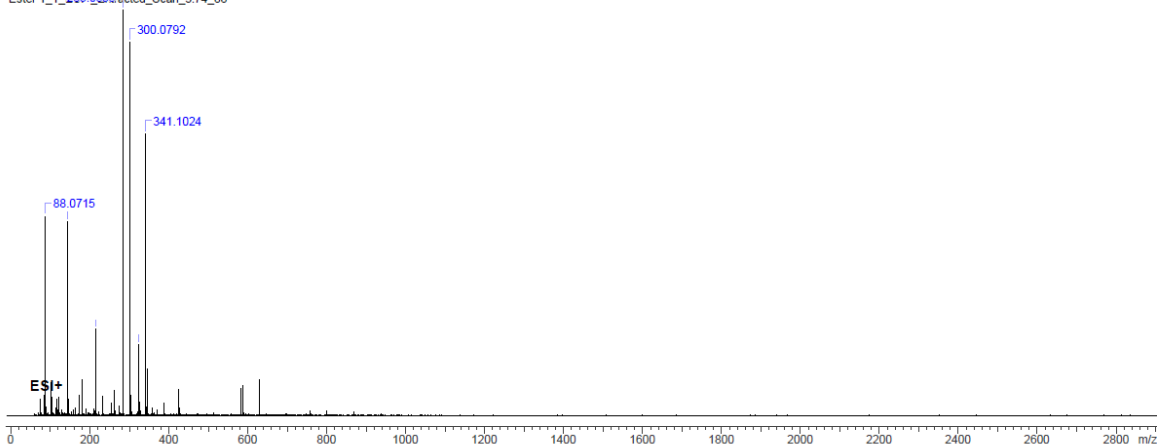


Figure S6. ESI-MS for 1H-Indole-3-carboxamide, N-[3-[[4-[(3-aminopropyl) amino]butyl] amino] propyl]- and its dimer. m/z calcd for C₁₉H₃₁N₅O (M+H) 346.49, found 346.2355. For the dimer, m/z calcd for C₂₈H₃₆N₆O₂ (M+H) 489.63, found 489.2634.

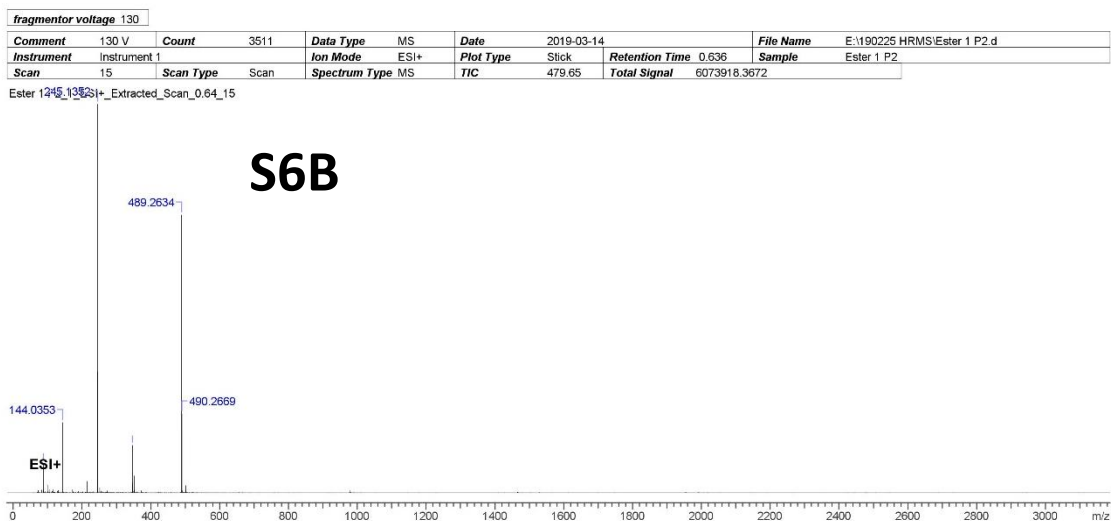
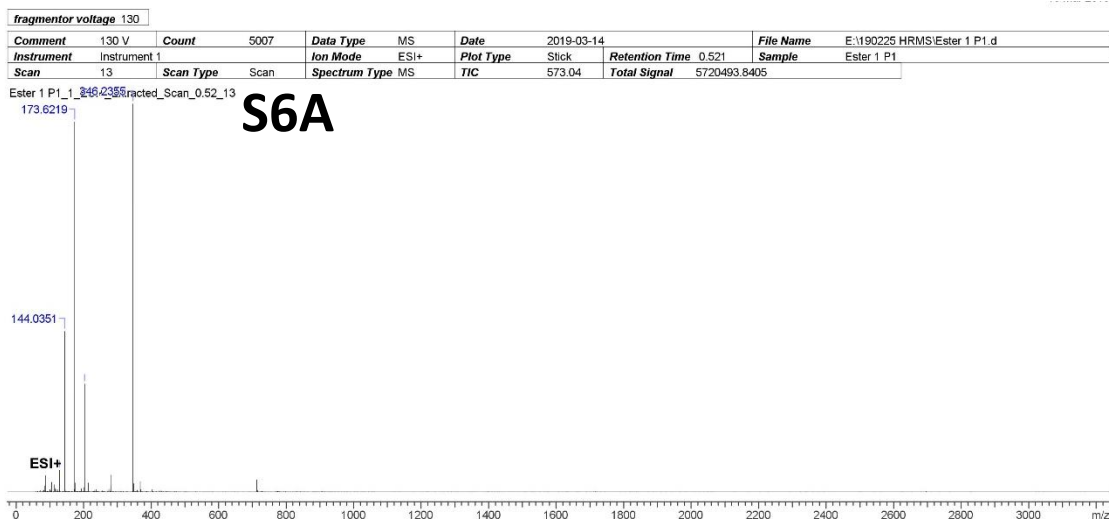


Figure S7. ESI-MS for 1H-Indole-3-acetic acid, 4-nitrophenyl ester. ESI: m/z calcd for C₁₆H₁₂N₂O₄ (M-H) 295.28, found 295.0985

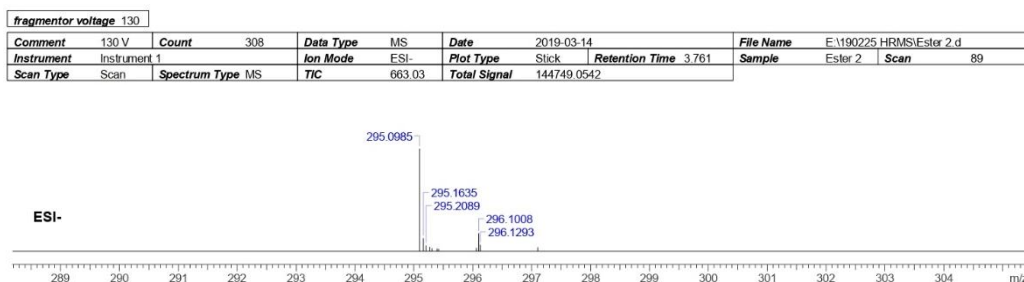


Figure S8. ESI-MS for 1H-Indole-3-acetamide, N-[3-[[4-[(3-aminopropyl)amino]butyl]amino]propyl]- and its dimer. m/z calcd for C₂₀H₃₃N₅O (M+H) 360.52, found 360.2506. For the dimer: m/z calcd for C₃₀H₄₀N₆O₂ (M+H) 517.69, found 517.2922

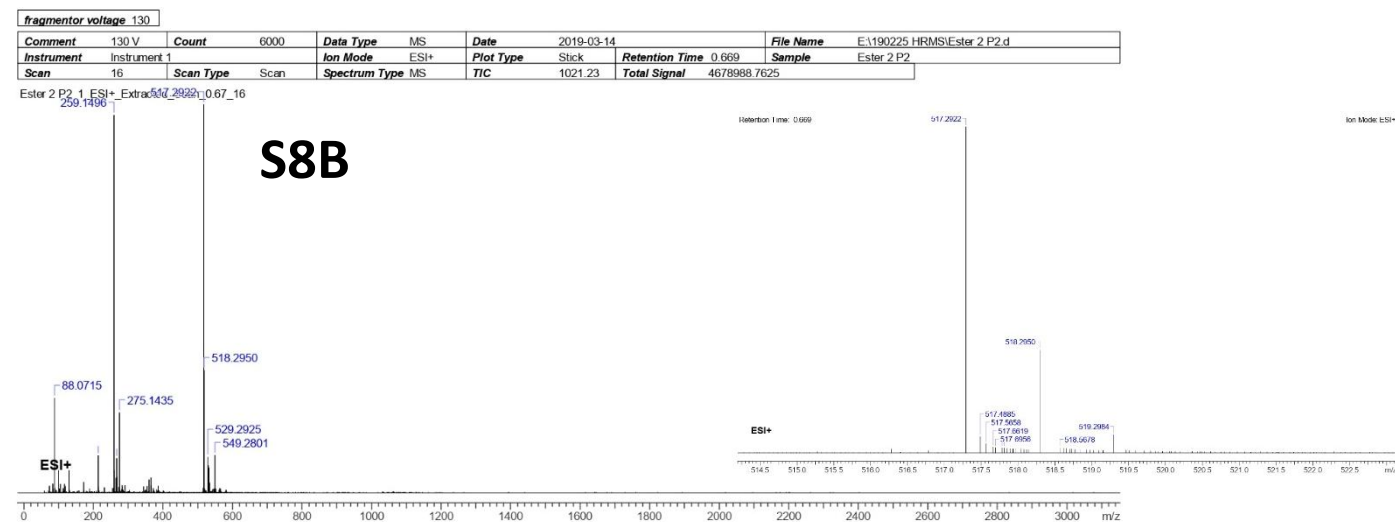
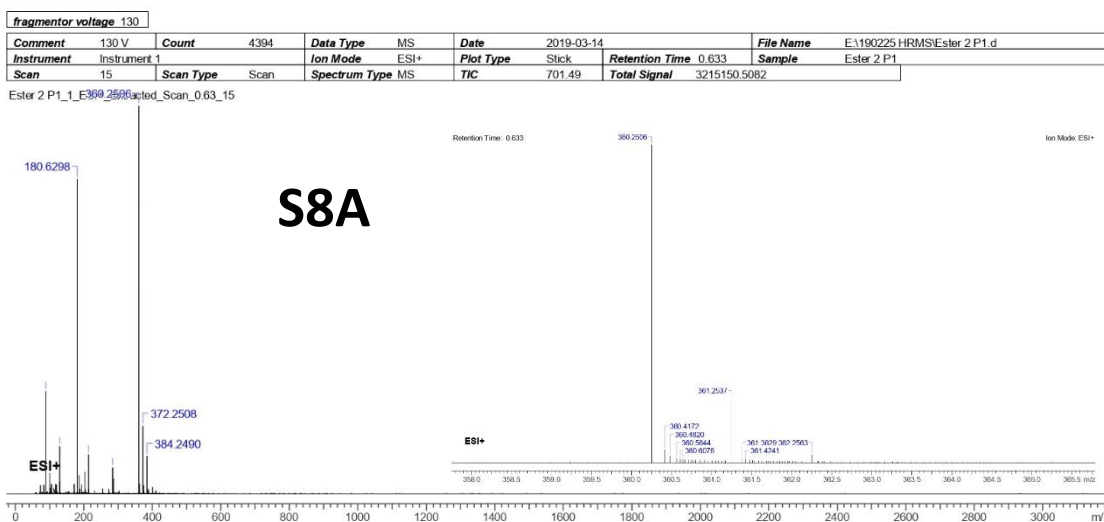


Figure S9. ESI-MS for 1H-Indole-2-carboxylic acid, 4-nitrophenyl ester. m/z calcd for C₁₅H₁₀N₂O₄ (M-H) 281.26, found 281.0846.

fragmentor voltage 130									
Comment	130 V	Count	246	Data Type	MS	Date	2019-03-14	File Name	E:\190225 HRMS\Ester 3.2.d
Instrument	Instrument 1	Ion Mode	ESI-	Plot Type	Slick	Retention Time	3.976	Sample	Ester 3.2
Scan Type	Scan	Spectrum Type	MS	TIC	515.51	Total Signal	107489.4658	Scan	94

Retention Time: 3.976

Ion Mode: ESI-

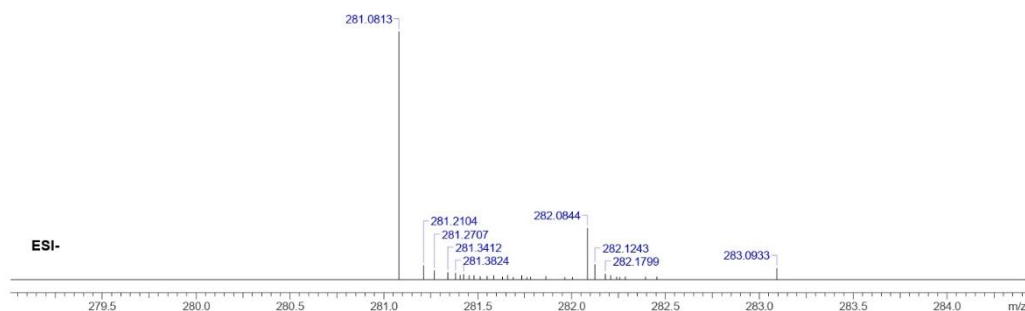


Figure S10. ESI-MS for 1H-Indole-2-carboxamide, N-[3-[[4-[(3-aminopropyl)amino]butyl] amino] propyl]-. m/z calcd for C₁₉H₃₁N₅O (M-H) 344.49, found 344.2810.

fragmentor voltage 130									
Comment	130 V	Count	7	Data Type	MS	Date	2019-03-14	File Name	E:\190225 HRMS\Ester 1 P1.d
Instrument	Instrument 1	Ion Mode	ESI-	Plot Type	Slick	Retention Time	0.500	Sample	Ester 1 P1
Scan	12	Scan Type	Scan	Spectrum Type	MS	TIC	546.95	Total Signal	849.6332

Retention Time: 0.500

Ion Mode: ESI-

